

# **Factors regulating cell shedding in mouse and rat small intestine**

**Thesis submitted in accordance with the  
requirements of the University of Liverpool  
for the degree of Doctor in philosophy**

**Ahmed Hamed Elramli**

**August 2018**

## **Acknowledgements**

I am truly grateful and thankful to Professor D Mark Pritchard who has supported me throughout my PhD studies, and without his patience, guidance and immense knowledge, this doctoral thesis would not have been completed.

I would like to thank him for teaching me scientific writing and for the opportunity to participate in the British Society of Gastroenterology meeting (2016).

I am also grateful to my second supervisors, Professor Barry J Campbell and Dr Carrie Duckworth for their supervision, advice and valuable support throughout all my PhD studies and thesis preparation.

I gratefully acknowledge Dr Jonathan Williams for his help at the start of my PhD studies. I am also grateful to Dr Stamatia Papoutsopoulou, Dr Felix Ikuomola and Dr Esam Shahout from the Department of Cellular and Molecular Physiology and Juan Hernandez-Fernaud from the University of Warwick for their help with proteomics and Mrs Alison Beckett from EM unit, Department of Cellular and molecular physiology for the help in tissue preparation for EM. Thanks also to all members of the Henry Wellcome Laboratories at the University of Liverpool for their help.

I would like to acknowledge the University of Benghazi via the Ministry of Education in Libya for my PhD funding.

Last but not the least, I would like to thank my father, mother, wife and kids for their sincere encouragement and inspiration throughout this study.

# **Factors regulating apoptosis and shedding in mouse and rat small intestine**

**Ahmed Hamed Elramli**

The gut barrier is composed of a single layer of intestinal epithelial cells which are connected together by junctional complexes and are covered by a layer of glycocalyx. Its function is to prevent the passage of harmful and toxic substances from the gut lumen into the blood circulation. Structural homeostasis in the small intestine is maintained by the shedding of intestinal epithelial cells at the villus tip and generation of new cells within the crypt compartment. Increased gut permeability can result when the rate of intestinal epithelial cell shedding is greater than the rate of generation of new crypt cells, and this phenomenon is associated with several gastrointestinal diseases including inflammatory bowel disease (IBD).

Lipopolysaccharide (LPS) is an integral cell wall component of Gram negative bacteria and following intraperitoneal administration induces the pathological shedding of murine small intestinal epithelial cells (SIEC). This thesis characterises the pathological apoptosis and shedding of SIECs induced by systemic LPS administration in wild-type mouse strains of different genetic background including C57BL/6J, Balb/C, CD1, FVB/N and DBA/2. We have also determined whether murine age and LPS derived from different bacterial species are factors that modulate the severity of SIEC apoptosis and shedding in C57BL/6J mice. Comparative studies were also conducted in Ludwig Olac Wistar rats following to determine whether this phenomenon occurred to the same extent within another species.

SIEC apoptosis and shedding was additionally induced by the administration of other systemic stimuli to C57BL/6J mice including anti-CD3 antibody (to activate T cells), polyinosinic:polycytidylic acid (to mimic viral infection) and the putative downstream effector tumour necrosis factor (TNF). The roles of NF $\kappa$ B transcription factor subunits in regulating SIEC apoptosis and shedding in villi and crypts induced by all stimuli at 1.5 and 24 hours were assessed and compared with the responses to LPS. SIEC apoptosis and shedding was assessed morphologically and quantified by immunohistochemistry for active caspase-3.

Ultrastructural analysis of SIEC apoptosis and shedding following LPS administration was conducted using transmission electron microscopy to determine the action of LPS on the intracellular components and how they may contribute to the breakdown of barrier function associated with this stimulus by modulating NF $\kappa$ B signalling. A broad spectrum proteomic analysis was also conducted to determine how LPS alters the small intestinal mucosal proteome to modulate susceptibility to SIEC apoptosis and shedding.

Conclusion: In conclusion, this study has described the SIEC apoptosis and shedding that are induced by different stimuli including LPS, anti-CD3, poly I:C and TNF. Particularly it has indicated that LPS from different bacterial sources induces SIEC apoptosis and shedding in different mouse strains, at different ages and in both mouse and rats, but with different degrees of effectiveness. It has also indicated the role of the NF $\kappa$ B signalling pathway in regulating this process.

## Table of contents

Acknowledgement.....	1
Abstract .....	2
List of figures.....	7
List of tables.....	11
Abbreviation.....	14
<b>1. Introduction.....</b>	<b>17</b>
1.1 Anatomy and histology of the small intestine.....	17
1.2 Disease of the intestinal tract.....	19
1.2.1 Inflammatory bowel disease (IBD).....	19
1.2.2 Cancer of the intestine.....	20
1.2.3 Sepsis.....	22
1.3 Intestinal mucosal epithelium.....	23
1.4 Cell types in the intestinal epithelium.....	24
1.4.1 Intestinal epithelial stem cells.....	25
1.4.2 Absorptive cells (mature enterocytes).....	26
1.4.3 Goblet cells.....	27
1.4.4 Paneth cells.....	27
1.4.5 Enteroendocrine cells.....	28
1.4.6 Tuft cells.....	28
1.5 Proliferation and differentiation of the small intestinal epithelium.....	29
1.5.1 Wnt signalling pathway.....	31
1.5.2 Notch signalling pathway.....	32
1.6 Cell death.....	34
1.6.1 Necrosis.....	34
1.6.2 Apoptosis.....	35
1.6.3 Necroptosis.....	36
1.6.4 Pyroptosis.....	37
1.6.5 Autophagy.....	37
1.7 Cell death in the small intestine.....	38
1.7.1 Mechanism of the IEC shedding during homeostasis.....	39
1.8 Genetic regulation of apoptosis in the gastrointestinal tract.....	44
1.8.1 Bcl2 and related genes.....	45
1.8.2 p53.....	46
1.8.3 Tumour necrosis factor family.....	47

1.8.4 C-myc proto-oncogene.....	48
1.9 Stimuli that cause pathological intestinal epithelial cell apoptosis and shedding.....	48
1.9.1 Bacterial lipopolysaccharide (LPS).....	49
1.9.2 Anti-mouse CD3e antibody.....	51
1.9.3 Polyinosinic:polycytidylic acid (poly I:C).....	52
1.9.4 Tumour necrosis factor (TNF).....	53
1.10 Nuclear factor kappa B (NFκB) signalling.....	55
1.10.1 Canonical NFκB signalling pathway.....	56
1.10.2 Non-canonical NFκB signalling pathway.....	56
1.11 proteomics approaches in the intestine.....	58
1.12 Aims of the study.....	61
<b>2. Materials and methods.....</b>	<b>63</b>
2.1 Animals.....	63
2.1.1 Mice.....	63
2.1.1.1 C57BL/6J mice.....	63
2.1.1.2 Balb/C mice.....	65
2.1.1.3 CD1 mice.....	65
2.1.1.4 FVB/N mice.....	65
2.1.1.5 DBA/2 mice.....	66
2.1.2 Ludwig Olac Wistar Rats.....	66
2.2 Animal procedures.....	66
2.3 Induction of Apoptosis and Shedding.....	66
2.3.1 Bacterial Lipopolysaccharide (LPS).....	67
2.3.2 Anti-CD3 antibody ( Clone 145:2C11).....	67
2.3.3 Polyinosinic:polycytidylic acid (Poly i:C).....	68
2.3.4 Recombinant Tumour necrosis factor (TNF).....	68
2.4 Tissue collection and processing.....	68
2.5 ABES slide coating for immunohistopathology.....	69
2.6 Active caspase-3 immunohistochemistry.....	69
2.7 Scoring of Active caspase-3 positively labelled cells.....	70
2.8 Haematoxylin and Eosin (H&E) staining protocol.....	71
2.9 Transmission Electron Microscopy (TEM).....	72
2.10 Preparation of tissue for Proteomic analysis.....	73
2.11 Data and Statistic.....	75
<b>3. Characterisation of the effects of lipopolysaccharide on proximal small intestinal epithelial cell apoptosis and shedding.....</b>	<b>76</b>
3.1 Introduction.....	76
3.2 LPS caused apoptosis and shedding of proximal small intestinal epithelial cells in different mouse strains.....	79

3.3 No age related differences in small intestinal cell shedding or apoptosis were observed between six, ten and twenty eight week old C57BL/6J mice following administration of LPS.....	82
3.4 LPS from different bacterial sources induced pathological apoptosis and shedding of small intestinal epithelial cells to different extents.....	84
3.5 Do rats and mice respond differently to systemically induced bacterial LPS?.....	86
3.6 RelB does not regulates LPS induced SIEC apoptosis and shedding.....	89
3.7 At 24 hours post administration of LPS, significant apoptosis was observed in the small intestinal crypts of Nfκb1 <sup>-/-</sup> and c-Rel <sup>-/-</sup> mice but not in wild-type and Nfκb2 mice .....	90
3.8 Discussion.....	93
<b>4. Ultrastructural changes within the small intestinal epithelial cells of wild-type and transgenic mice treated with bacterial lipopolysaccharide.....</b>	<b>98</b>
4.1 Ultrastructural comparison of proximal small intestinal epithelium of untreated wild-type C57BL/6J and various transgenic Nfκb subunit global knockout mice.....	99
4.2 Examination of the action of LPS on SIEC ultrastructural morphology.....	105
4.2.1 Inter- and intra-cellular vacuolisation was a key feature observed in wild-type C57BL/6J mice after LPS treatment.....	105
4.2.2 Nfκb1 <sup>-/-</sup> mouse proximal small intestine was more sensitive to LPS than other strains as demonstrated by multiple, distinct morphological changes.....	106
4.2.3 No morphological changes were identified in the SIECs of LPS treated Nfκb2 <sup>-/-</sup> mice.....	109
4.2.4 c-Rel <sup>-/-</sup> mice show an intermediate response to LPS treatment.....	109
4.3 Transmission electron microscopy highlights key morphological changes and dynamic events of cellular apoptosis and shedding induced by LPS in murine small intestinal epithelium.....	112
4.4 Discussion.....	118
<b>5. Proteomic analysis of murine small intestinal tissue pre- and post-administration of LPS.....</b>	<b>122</b>
5.1 Nfκb transgenic mice exhibit differences in the small intestinal mucosal proteome.....	125
5.1.1 Nfκb1 <sup>-/-</sup> .....	126
5.1.2 Nfκb2 <sup>-/-</sup> .....	127
5.1.3 c-Rel <sup>-/-</sup> .....	128
5.1.4 Summary of the previously investigated biological roles of the identified proteins in intestinal mucosa.....	132
5.2 Does systemic LPS cause any changes in the intestinal mucosal proteome?.....	134
5.2.1 LPS resulted in 884 changes in the small intestinal mucosal proteome of C57BL/6J mice.....	134
5.2.2 LPS did not induce any significant changes in the small intestinal mucosal	

proteome of Nfκb1 <sup>-/-</sup> mice.....	137
5.2.3 The small intestinal mucosal proteome of Nfκb2 <sup>-/-</sup> and c-Rel <sup>-/-</sup> mice showed minimal changes in response to LPS.....	138
5.3 LPS exclusively induces 298 proteomic changes in Nfκb1 <sup>-/-</sup> small intestinal mucosa compared with C57BL/6J mice .....	140
5.4 118 significant small intestinal mucosal proteomic changes were identified exclusively in LPS-treated Nfκb2 <sup>-/-</sup> mice compared to LPS-treated C57BL/6J mice....	144
5.5 Small intestinal mucosal proteomic analysis of c-Rel <sup>-/-</sup> mice identified 176 changes in comparison to C57BL/6J .....	148
5.6 Discussion.....	151
<b>6. Investigation of stimuli other than LPS that induce small intestinal epithelial cell apoptosis and shedding .....</b>	<b>155</b>
6.1 Introduction .....	155
6.2 Anti-CD3 antibody induces T-cell mediated apoptosis and shedding in murine small intestinal epithelial cells .....	157
6.2.1 Maximal induction of small intestinal epithelial cell apoptosis and shedding occurred 1.5 hours post intraperitoneal administration of anti-CD3 antibody .....	157
6.2.2 A direct relationship was observed between anti-CD3 antibody dose and the percentage of small intestinal epithelial cell apoptosis and shedding in female C57BL/6J mice 1.5 post administration .....	159
6.2.3 Members of the NFκB family of proteins regulate the pathological small intestinal epithelial apoptosis and shedding induced by anti-CD3 antibody .....	162
6.2.4 Anti-CD3 antibody also significantly induced apoptosis in murine small intestinal crypt epithelial cells 24 hours post IP administration .....	165
6.3 Polyinosinic:polycytidylic acid (Poly I:C) induces murine small intestinal epithelial cell apoptosis and shedding mimicking the viral activation of shedding .....	167
6.3.1 Poly I:C induces pathological apoptosis and shedding of murine small intestinal epithelial cells .....	168
6.3.2 Nfκb2 <sup>-/-</sup> mice were more resistant to poly I:C induced small intestinal epithelial cell apoptosis and shedding .....	171
6.3.3 Poly I:C has no effect on small intestinal crypt epithelial cell apoptosis and shedding at 24 hours post intraperitoneal administration .....	173
6.4 TNF caused significant apoptosis and cell shedding in proximal segment of murine small intestine .....	175
6.4.1 0.33mg/kg TNF caused pathological apoptosis and shedding in proximal small intestinal villi at 1.5 hours equivalent to that caused by administration of 10mg/kg LPS .....	175

6.4.2 TNF at 24 hours post intraperitoneal administration induced small intestinal crypt apoptosis more in Nfκb1 and c-Rel knockout mice than wild-type C57BL/6J mice, while Nfκb2 null mice showed no significant change .....	179
6.5 Discussion .....	181
<b>7. Discussion .....</b>	<b>186</b>
7.1 Major findings and subsequent concepts .....	186
7.2 Limitations of the study .....	188
7.3 Future research plans .....	191
7.4 Translational impact .....	194
7.5 Conclusions .....	195
8. Bibliography .....	196
9. Appendix .....	221

## List of Figures

<b>Figure 1.1:</b> Schematic diagram of the small intestinal crypts and villi showing different cell types of lining epithelium .....	24
<b>Figure 1.2:</b> Schematic diagram illustrating the differentiation of stem cell into different types of intestinal epithelial lineage.....	30
<b>Figure 1.3:</b> schematic diagram illustrating the events of epithelial cell shedding and redistribution of tight junction to maintain the epithelial barrier integrity.....	42
<b>Figure 1.4:</b> Schematic representation of the main molecular pathways leading to apoptosis.....	45
<b>Figure 1.5:</b> The components of LPS molecules.....	50
<b>Figure 1.6:</b> Diagram summarising the putative mechanism by which LPS induces apoptosis in SIECs .....	51
<b>Figure 1.7:</b> Schematic diagram summarising NFκB signalling pathways .....	58
<b>Figure 3.1:</b> Active caspase-3 IHC in sections of proximal segment of small intestine of different tested mouse strains demonstrating the location of positively labelled SIEC along the villus axis .....	80
<b>Figure 3.2:</b> Bar chart representing the percentage of IECs undergoing apoptosis and shedding in LPS treated versus untreated mice of different strains .....	80
<b>Figure 3.3:</b> Cell positional graphs showing quantification of positively immuno-labelled IECs along the villus axis of treated mice compared to untreated mice for each mouse strain .....	81
<b>Figure 3.4:</b> Active caspase-3 IHC in sections of proximal segment of small intestine demonstrating the location of positively labelled SIEC along the villus axis in small intestine of 3 different age groups .....	83
<b>Figure 3.5:</b> Bar chart representing the percentage of intestinal epithelial cell shedding in LPS-treated versus untreated control C57BL/6J mice at different age groups.....	83

<b>Figure 3.6:</b> Cell positional graphs showing quantification of positively immuno-labelled IECs along the villus axis of LPS-treated mice compared to untreated C57BL/6J mice for each age group of mice.....	84
<b>Figure 3.7:</b> Active caspase-3 IHC in sections of proximal segment of small intestine demonstrating the location of positively labelled SIEC along the villus axis in the small intestine of C57BL/6J mice treated with LPS purified from different bacterial species.....	85
<b>Figure 3.8:</b> Bar chart demonstrating a comparison between the percentage of intestinal epithelial cell apoptosis and shedding in C57BL/6J mice treated with LPS purified from different bacterial sources against an untreated group.....	85
<b>Figure 3.9:</b> Cell positional graphs indicating the quantification of positively immuno-labelled IECs along the villus axis of C57BL/6J mice treated with different types of bacterial LPS versus an untreated group .....	86
<b>Figure 3.10:</b> Active caspase-3 IHC in sections of proximal small intestinal segment of C57BL/6J mice versus Ludwig Olac Wistar rats demonstrating the location of positively labelled SIEC along the villus axis .....	87
<b>Figure 3.11:</b> Bar chart and cell positional graph demonstrating a comparison between the percentage of intestinal epithelial cell apoptosis and shedding in C57BL/6J mice and Ludwig Olac Wistar rats pre and post LPs administration .....	88
<b>Figure 3.12:</b> Active caspase-3 IHC in sections of proximal segment of small intestine of RelB mice (of different genotypes) demonstrating the location of positively labelled SIEC along the villus axis .....	89
<b>Figure 3.13:</b> Bar chart and cell positional graph representing the percentage of SIEC apoptosis and shedding in different RelB genotypes 1.5 hours post injection LPS injection.....	90
<b>Figure 3.14:</b> Active caspase-3 IHC in sections of proximal segment of small intestine of C57BL6J mice (different genotypes) injected with 0.125mg/kg LPS for 24 hours demonstrating the location of positively labelled SIEC along the crypt axis .....	92
<b>Figure 3.15:</b> Quantification of apoptotic (active caspase-3 positive and negative) proximal small intestinal crypt epithelial cells 24 hours after IP injection of 0.125mg/kg LPS .....	92
<b>Figure 3.16:</b> Cell positional graph indicating the apoptotic cell positions (based on modified median test) in different C57BL/6J mice genotypes 24 hours post administration of 0.125mg/kg LPS .....	93
<b>Figure 4.1:</b> Transmission electron microscopy (TEM) of proximal SIECs from untreated wild-type C57BL/6J mice .....	101
<b>Figure 4.2:</b> TEM of normal proximal SIECs from untreated Nfκb1 <sup>-/-</sup> mice .....	102
<b>Figure 4.3:</b> TEM of normal proximal SIECs from untreated Nfκb2 <sup>-/-</sup> mice .....	103
<b>Figure 4.4:</b> TEM of normal proximal SIECs from untreated c-Rel <sup>-/-</sup> mice .....	104

<b>Figure 4.5:</b> TEM of proximal SIECs treated with 0.125 mg/kg LPS versus untreated wild-type C57BL/6J mice .....	107
<b>Figure 4.6:</b> TEM of proximal SIECs of 0.125 mg/kg LPS treated versus untreated Nfκb1 mice.....	108
<b>Figure 4.7:</b> TEM of proximal SIECs of 0.125 mg/kg LPS treated versus untreated Nfκb2 <sup>-/-</sup> mice .....	110
<b>Figure 4.8:</b> TEM of proximal SIECs of 0.0125 mg/kg LPS treated versus untreated c-Rel <sup>-/-</sup> mice .....	111
<b>Figure 4.9:</b> Higher magnification TEM of SIECs from wild-type C57BL/6J mouse treated with 0.125 mg/kg LPS highlights the large intracellular vacuoles and intercellular spaces .....	113
<b>Figure 4.10:</b> Small intestinal TEM of LPS-treated Nfκb1 <sup>-/-</sup> mouse showing epithelial cell extrusion and nuclear fragmentation .....	114
<b>Figure 4.11:</b> Small intestinal TEM of LPS-treated Nfκb1 mouse showing mitochondrial vacuolation and loss of cisternae .....	115
<b>Figure 4.12:</b> Small intestinal TEM of LPS-treated Nfκb1 <sup>-/-</sup> mouse showing intracellular vacuolation and intercellular space formation .....	115
<b>Figure 4.13:</b> Small intestinal TEM of LPS-treated Nfκb1 <sup>-/-</sup> mouse showing an intraepithelial lymphocyte underlying the small intestinal epithelial cell layer.....	116
<b>Figure 4.14:</b> Small intestinal TEM showing disruption of intestinal microvilli in a c-Rel <sup>-/-</sup> mouse injected with 0.125 mg/kg IP LPS for 1.5 hours.....	117
<b>Figure 4.15:</b> Small intestinal TEM showing a funnel shaped epithelial cell and vacuolation in a c-Rel <sup>-/-</sup> mouse after LPS administration.....	117
<b>Figure 5.1:</b> Pie chart showing the total number of statistically significantly unregulated and downregulated proteins in Nfκb1 <sup>-/-</sup> , Nfκb2 <sup>-/-</sup> and c-Rel <sup>-/-</sup> small intestinal mucosa compared to C57BL/6J.....	126
<b>Figure 5.2:</b> Pie charts representing the total significant up and downregulated changes in small intestinal mucosal proteome of Nfκb1 <sup>-/-</sup> , Nfκb2 <sup>-/-</sup> and c-Rel <sup>-/-</sup> mice 1.5 hours post intraperitoneal administration of bacterial LPS compared with untreated mice of the same strain .....	135
<b>Figure 5.3:</b> Venn graph indicating a comparison of significant proteomic changes between Nfκb1 <sup>-/-</sup> and C57BL/6J mice before and after IP injection of 0.125 mg/kg LPS.....	141
<b>Figure 5.4:</b> Venn graph indicating a comparison of significant proteomic changes between Nfκb2 <sup>-/-</sup> and C57BL/6J mice before and after IP injection of 0.125mg/kg LPS.....	145
<b>Figure 5.5:</b> Venn graph indicating a comparison of significant protein changes between c-Rel <sup>-/-</sup> and C57BL/6J mice before and after IP injection of 0.125mg/kg LPS.....	148
<b>Figure 6.1:</b> Active caspase-3 IHC in sections of proximal segments of small intestine of female C57BL/6J mice injected with 1mg/kg anti-CD3 antibody at different time-	

points.....	158
<b>Figure 6.2:</b> Bar chart representing the percentage of IEC apoptosis and shedding in female C57BL/6J mice treated with 1mg/kg anti-CD3 antibody at different time-points.....	158
<b>Figure 6.3:</b> Cell positional graphs showing quantification of positively immuno-labelled IECs along the villus axis of C57BL/6J mice treated with 1mg/kg anti-CD3 antibody at different time-points.....	159
<b>Figure 6.4:</b> Active caspase-3 IHC in sections of proximal segments of small intestine of female C57BL/6J mice injected with increasing doses of anti-CD3 antibody at 1.5 hours.....	160
<b>Figure 6.5:</b> Percentage of active caspase 3 positively labelled IECs in C57BL/6J mice injected with differing doses of anti-CD3 antibody for 1.5 hours.....	161
<b>Figure 6.6:</b> Cell positional graphs showing quantification of positively immuno-labelled IECs along the villus axis of C57BL/6J mice injected with differing doses of anti-CD3 antibody for 1.5 hours.....	161
<b>Figure 6.7:</b> Bar chart and cell positional plot representing the percentage and distribution of SIEC apoptosis and shedding in C57BL/6J mice injected with differing doses of anti-CD3 isotope control for 1.5 hours compared to untreated mice.....	162
<b>Figure 6.8:</b> Active caspase-3 IHC in sections of proximal segments of small intestine of transgenic and wild-type C57BL/6J mice injected with 2mg/kg anti-CD3 antibody at 1.5 hours.....	163
<b>Figure 6.9:</b> Comparison between the percentage of active caspase 3 positively labelled SIECs in <i>Nfκb1<sup>-/-</sup></i> , <i>Nfκb2<sup>-/-</sup></i> , <i>c-Rel<sup>-/-</sup></i> and wild-type C57BL/6J mice.....	164
<b>Figure 6.10:</b> Cell positional graphs showing quantification of positively immuno-labelled IECs along the villus axis of transgenic mice compared to wild-type C57BL/6J mice, all treated with 2mg/kg anti-CD3 antibody for 1.5 hours.....	164
<b>Figure 6.11:</b> Active caspase-3 IHC demonstrating apoptotic small intestinal crypt epithelial cells in transgenic and wild-type C57BL/6J mice injected with 2mg/kg anti-CD3 antibody for 24 hours.....	166
<b>Figure 6.12:</b> Bar chart and cell positional graph indicating the percentage and distribution of apoptotic small intestinal crypt epithelial cells in transgenic and wild-type C57BL/6J mice injected with anti-CD3 antibody for 24 hours.....	167
<b>Figure 6.13:</b> Active caspase-3 IHC showing proximal small intestinal epithelial apoptosis and cell shedding in female C57BL/6J mice injected intraperitoneally with 30mg/kg poly I:C for different periods of time.....	169
<b>Figure 6.14:</b> Bar chart indicating the percentage of apoptotic and shedding IECs in the duodenal villi of C57BL/6J mice injected with 30mg/kg Poly I:C at different time-points.....	170
<b>Figure 6.15:</b> Cell positional graphs indicating the quantification of positively immuno-labelled IECs along the villus axis of C57BL/6J mice injected with 30mg/kg	

Poly I:C at different time points in comparison to untreated group.....	170
<b>Figure 6.16:</b> Active caspase-3 IHC in sections of proximal segments of small intestine of transgenic and wild-type female C57BL/6J mice injected with 30mg/kg poly I:C for different periods of time.....	171
<b>Figure 6.17:</b> Bar chart showing percentage of apoptotic and shedding SIECs in the duodenal villi of wild-type and transgenic C57BL/6J mice at 1.5h post IP injection of 30mg/kg Poly I:C.....	172
<b>Figure 6.18:</b> Cell positional graphs showing quantification of positively immunolabelled IECs along the villus axis of transgenic mice (Nfκb1, Nfκb2 and c-Rel) compared to wild-type C57BL/6J mice.....	172
<b>Figure 6.19:</b> Active caspase-3 IHC (A and B) and H&E (C) in sections of proximal segments of small intestine of transgenic and wild-type C57BL/6J mice injected with 30mg/kg poly I:C for 24 hours.....	174
<b>Figure 6.20:</b> Bar chart cell positional graph indicating the percentage and distribution of apoptotic small intestinal crypt epithelial cells in transgenic and wild type C57BL/6J mice injected with 30mg/kg poly I:C for 24 hours.....	174
<b>Figure 6.21:</b> Active caspase-3 IHC in sections of proximal segments of small intestine of different mice groups injected with 0.33mg/kg TNF for 1.5 hours.....	177
<b>Figure 6.22:</b> Bar charts and cell positional graph showing percentage and distribution of apoptotic and shedding SIECs in the duodenal villi of wild- and transgenic C57BL/6J mice 1.5h post IP injection of 0.33mg/kg TNF.....	178
<b>Figure 4.23:</b> Cell positional graph indicating the distribution of apoptotic SIECs along the villus length of TNF treated wild-type and transgenic C57BL/6J mice .....	178
<b>Figure 6.24:</b> Active caspase-3 IHC indicating the apoptosis of small intestinal crypt epithelial cells of wild-type and transgenic C57BL/6J mice at 24 hours post administration of 0.33mg/kg recombinant TNF.....	180
<b>Figure 6.25:</b> Bar chart representing the percentage of small intestinal crypt epithelial cell apoptosis in adult female wild-type C57BL/6J and transgenic mice injected with 0.33mg/kg TNF for 24 hours.....	180
<b>Figure 6.26:</b> Cell positional graph indicating the position of apoptotic small intestinal crypt epithelial cell along the crypt axis of TNF treated wild-type and transgenic C57BL/6J mice.....	181

**List of tables**

<b>Table 5.1.A:</b> indicates the top upregulated proteins in Nfκb1-/-small intestinal mucosa and their expression in Nfκb2-/- and c-Rel-/- mice all in comparison to wild-type C57BL/6J mice.....	129
<b>Table 5.1.B:</b> indicates the top downregulated proteins in Nfκb1-/- small intestinal mucosa and their expression in Nfκb2-/- and c-Rel-/- mice all in comparison to wild-type C57BL/6J mice .....	129

<b>Table 5.2.A:</b> indicates the top upregulated proteins in Nfκb2 small intestinal mucosa and their expression in Nfκb1 and c-Rel mice all in comparison to wild-type C57BL/6J mice.....	130
<b>Table 5.2.B:</b> indicates the top downregulated proteins in Nfκb2 <sup>-/-</sup> small intestinal mucosa and their expression in Nfκb1 <sup>-/-</sup> and c-Rel <sup>-/-</sup> mice all in comparison to wild-type C57BL/6J mice.....	130
<b>Table 5.3.A:</b> indicates the top upregulated proteins in c-Rel <sup>-/-</sup> small intestinal mucosa and their expression in Nfκb1 <sup>-/-</sup> and Nfκb2 <sup>-/-</sup> mice all in comparison to wild-type C57BL/6J mice.....	131
<b>Table 5.3.B:</b> indicates the top downregulated proteins in c-Rel <sup>-/-</sup> small intestinal mucosa and their expression in Nfκb1 <sup>-/-</sup> and Nfκb2 <sup>-/-</sup> mice all in comparison to wild-type C57BL/6J mice .....	131
<b>Table 5.4-A:</b> The top 10 proteins showing the greatest difference in log <sub>2</sub> fold change that were significantly upregulated in C57BL/6J small intestinal mucosa after intraperitoneal administration of 0.125 mg/kg LPS .....	136
<b>Table 5.4.B:</b> The top proteins showing the greatest difference in log <sub>2</sub> fold change that were significantly downregulated in the small intestinal mucosa of C57BL/6J mice following 0.125 mg/kg LPS .....	136
<b>Table 5.5:</b> indicating the changes in small intestinal mucosal proteome of Nfκb2 <sup>-/-</sup> mice following LPS administration compared to untreated mice of the same genotype .....	139
<b>Table 5.6:</b> Upregulation of proteins in the small intestinal mucosal proteome in c-Rel <sup>-/-</sup> mice following LPS administration compared with untreated c-Rel <sup>-/-</sup> .....	139
<b>Table 5.7:</b> The top 10 upregulated proteins with greatest log <sub>2</sub> differences in Nfκb1 <sup>-/-</sup> small intestinal mucosa in comparison to C57BL/6J post LPS administration and the log <sub>2</sub> differences at baseline (untreated) between Nfκb1 <sup>-/-</sup> and C57BL/6 small intestinal mucosa for these proteins .....	143
<b>Table 5.8:</b> The top 10 downregulated proteins with greatest log <sub>2</sub> differences in Nfκb1 <sup>-/-</sup> small intestinal mucosa in comparison to C57BL/6J post LPS administration and log <sub>2</sub> differences at baseline (untreated) between Nfκb1 <sup>-/-</sup> and C57BL/6 small intestinal mucosa for these proteins .....	143
<b>Table 5.9:</b> The top 10 upregulated proteins with greatest log <sub>2</sub> differences in Nfκb2 <sup>-/-</sup> small intestinal mucosa in comparison to C57BL/6J post LPS administration and log <sub>2</sub> differences at baseline (untreated) between Nfκb2 <sup>-/-</sup> and C57BL/6 small intestinal mucosa for these proteins .....	147
<b>Table 5.10:</b> The top 10 downregulated proteins with greatest log <sub>2</sub> differences in Nfκb2 <sup>-/-</sup> small intestinal mucosa in comparison to C57BL/6J post LPS administration and log <sub>2</sub> differences at baseline (untreated) between Nfκb2 <sup>-/-</sup> and C57BL/6 small intestinal mucosa for these proteins .....	147

**Table 5.11:** The top 10 upregulated proteins with greatest log2 differences in c-Rel<sup>-/-</sup> small intestinal mucosa in comparison to C57BL/6J post LPS administration and log2 differences at baseline (untreated) between c-Rel<sup>-/-</sup> and C57BL/6 small intestinal mucosa for these proteins .....150

**Table 5.12:** The top 10 downregulated proteins with greatest log2 differences in c-Rel<sup>-/-</sup> small intestinal mucosa in comparison to C57BL/6J post LPS administration and log2 differences at baseline (untreated) between c-Rel<sup>-/-</sup> and C57BL/6 small intestinal mucosa for these proteins .....155

## Abbreviations:

ANOVA: Analysis of variance  
Anti-CD3: anti mouse CD3 antibody  
AP-1: Activator protein 1  
APAF1: Apoptotic peptidase activating factor 1  
APC: Adenomatous polyposis coli gene  
APES: 3-aminopropyltriethoxysilane  
A-Raf-1: A-Raf proto-oncogene, serine/threonine kinase  
ATP: Adenosine triphosphate  
bad: Bcl-2 associated agonist of cell death  
BAFFR: B-cell activating factor receptor  
bag-1: Bcl-2 associated athanogene 1  
Bak: Bcl-2 antagonist/killer 1  
Bax: Bcl-2 associated X  
Bcl-2: B cell lymphoma/leukaemia 2 oncogene  
bcl-w: Bcl-2 like 2  
BclxL and BclxS: Bcl-2 like 1  
bfl-1: Bcl-2 related protein A 1  
bfl1: Bcl-2 related protein A1  
BH-3: Bcl-2 homology domain  
Bik: Bcl-2 interacting killer  
Bim: Bcl-2 like 11  
Bmi-1: B-cell lymphoma Mo-MLV insertion region 1 homolog  
brag-1: IQ motif and Sec7 domain 2  
CD: Crohn's disease  
CXCL10: C-X-C motif chemokine 10  
DCAMKL1: Doublecortin-like kinase 1  
DISC: Death initiation signalling complex  
DKK1: Dickkopf-related protein 1  
DNA: Deoxyribonucleic acid  
EDTA: Ethylenediaminetetraacetic acid  
ELISA: Enzyme-linked immunosorbent assay  
EM: Electron microscope  
ETEC: Enterotoxigenic Escherichia coli  
FADD: Fas-associated death domain protein  
Fas: Fas cell surface death receptor  
FasL: Fas ligand (TNF superfamily, member 6)  
Gfi1: SSXT family protein  
GIT: Gastrointestinal tract  
H & E: Haematoxylin and eosin

Hes1: Hes family bHLH transcription factor 1  
HIV: Human immunodeficiency virus  
IBD: Inflammatory bowel disease  
ICD: Intracellular domain  
IECs: Intestinal epithelial cells  
IFN $\gamma$ : Interferon Gamma  
IHC: Immunohistochemistry  
IL: Interleukin  
INF $\beta$ : Interferon beta  
IP: Int; raperitoneal  
IRF3: Interferon regulatory factor 3  
Lgr5: Leucine-rich repeat containing G-protein coupled receptor 5  
LPS: Lipopolysaccharide  
LRP: Lipoprotein related protein  
LT $\beta$ R: Lymphotoxin  $\beta$  receptor  
MAPKs: Mitogen-activated protein kinase  
Math1: Atonal bHLH transcription factor 1  
mcl1: Bcl-2 family apoptosis regulator  
MDA5: Melanoma Differentiation-Associated protein 5  
Mo-MLV: Moloney murine leukaemia virus  
mRNA: Messenger ribonucleic acid  
MyD88: Innate immune signal transduction adaptor  
NEMO: NF $\kappa$ B essential modulator  
NF $\kappa$ B and Nf $\kappa$ b: Nuclear factor Kappa B  
Ngn3: Neurogenin 3  
NK: Natural killer cell  
PAMPs: Pathogen associated molecular patterns  
PBS: Phosphate buffered saline  
PGK: Phosphoglycerate kinase  
Poly I:C: polyinosinic:polycytidylic acid  
PRRS: Pattern recognition receptors  
RANK: Receptor activator of NF $\kappa$ B  
RBP-J: Recombination signal binding protein for immunoglobulin kappa J region  
Reg I and Reg II: Regenerative proteins I and II  
rER: Rough endoplasmic reticulum  
RIG-I: Retinoic Acid-Inducible Gene-I-like receptor  
RIP: Receptor interacting protein  
RIP1: Receptor interacting protein 1  
RIPK1-RIPK3: Receptor-interacting protein kinase 1 and 3  
SDS: Sodium dodecyl sulphate  
SEM: Standard error of mean

SIEC: Small intestinal epithelial cell  
SMAC/DIABLO: Second mitochondria-derived activator of caspases/ Direct IAP binding protein with low pI  
SPF: Specific pathogen free  
TAD: Transcription associated domain  
TBST: Tris-buffered saline, 0.1% Tween®20  
Tcf: T-cell factor  
TCR-CD3: T cell receptor-CD3 complex  
TEAB: Triethylammonium bicarbonate  
TEM: Transmission electron microscopy  
TIR: Toll-IL1 receptor  
TLR3: Toll like receptor 3  
TLR4: Toll like receptor 4  
TLRs: Toll like receptors  
TNF: Tumour necrosis factor  
TNFR1: Tumour necrosis factor receptor 1  
TNFR2: Tumour necrosis factor receptor 2  
TNFRSF13C: Tumour necrosis factor receptor superfamily member 13C  
TNFSF: Tumour necrosis factor superfamily  
TRADD: Tumour necrosis factor-associated death domain protein  
TRAF6: TNF receptor associated factor 6  
TRAIL: TNF-related apoptosis inducing ligand  
UC: Ulcerative colitis

## **1. Introduction**

The gut barrier is composed of a single layer of epithelial cells that are connected together by junctional complexes and a layer of glycocalyx. Its function is to prevent the passage of harmful and toxic substances from the gut lumen into the blood circulation. This structural homeostasis is maintained in a state of equilibrium by the shedding of intestinal epithelial cells at the villus tips and the generation of new cells within the intestinal crypt compartment. Increased gut permeability and gut barrier dysfunction can result when the rate of intestinal epithelial cell shedding is greater than the rate of generation of new crypt cells, and this phenomenon can be associated with several gastrointestinal diseases.

### **1.1 Anatomy and histology of the small intestine**

The small intestine is a specialised convoluted tube contained within the abdominal cavity. It is in continuity with the pylorus of the stomach proximally and the colon distally via the ileocaecal valve. The large bowel surrounds it superiorly and laterally. Anteriorly it is related to the greater omentum and abdominal parities and it is connected posteriorly to the vertebral column by a fold of membranous tissue that arises from posterior wall of the peritoneal cavity. These membranous folds represent the mesentery (Standring *et al.*, 2005). The mesentery contains the arteries and veins that supply the intestine, the superior and inferior mesenteric arteries and veins. The mesentery divides the small intestine into three segments. The C shaped duodenum is the first part of the small bowel and is connected to the pylorus via the pyloroduodenal junction and is surrounded by the head of the pancreas. It is about

20-25 cm in length in man and 7cm in mouse. It is considered to be the shortest part of the small intestine. The midsection of the small intestine is known as the jejunum; it is about 2.5 meters long in man and 32 cm in mouse. It connects the duodenum to the ileum. The ileum is the last part of the small intestine and joins to the caecum of the large intestine by the ileocecal junction and measures about 3 m in man and 4.3 cm in mouse (Standring *et al.*, 2005, Casteleyn *et al.*, 2010).

The small intestine increases 20 times in length during life from 200 cm in new-born infants to approximately 6 meters in the adult human (Feldman *et al.*, 2015). Histologically the small intestine is a hollow tube composed of 4 main structures, including from the interior to the exterior; the mucosa, submucosa, muscularis externa and serosa (with the exception being the beginning of the duodenum which is retroperitoneal and possesses adventitia). The mucosa is further divided into 3 parts from interior to exterior, including; the epithelium, lamina propria and muscularis mucosa. Three kinds of luminal surface modification increase the absorptive surface area of the luminal surface of small intestine. The first is plicae circulares (valve of Kerkring); permanent transverse folds of the submucosa and mucosa which are more numerous in the distal part of the duodenum and the beginning of the jejunum which become reduced in size in the middle of the ileum. The second type of intestinal luminal surface modification is the presence of villi which are finger-like mucosal projections covering the whole surface of the small bowel. They are larger, broader, taller and more numerous in the duodenum than in the jejunum and ileum and are almost absent over the Peyer's patches. The villi have a core of loose connective tissue (lamina propria) and are covered by a layer of simple columnar epithelium. The third

type of luminal modification is the presence of microvilli; cylindrical extensions of the plasma membrane of the enterocyte (Mescher, 2010).

## **1.2 Diseases of the intestinal tract**

### **1.2.1 Inflammatory bowel disease (IBD)**

Inflammatory bowel diseases (IBD) are immune-mediated chronic intestinal conditions that are identified histologically by inflammation in the gastrointestinal tract. Ulcerative colitis (UC) and Crohn's disease (CD) are the two major types of IBD. In addition, there are rarer forms termed microscopic (collagenous or lymphocytic) colitis. As with other chronic diseases, a person with IBD will generally run a waxing and waning course in which the disease flares up and causes symptoms, followed by periods in which symptoms decrease or disappear and the disease is said to be in remission. Symptoms range from mild to severe and generally depend upon which region of the intestinal tract is involved. CD is commonly seen in the small intestine and colon but can affect any part of gastrointestinal tract from mouth to anus (Freeman, 2014) while ulcerative colitis involves only the colon and rectum (Whitlow, 2004). The exact causes of IBD are unknown. However, a genetic component, dysregulated immune system in response to pathogen, increased epithelial barrier permeability, infectious microbes, and environmental factors (ethnic origin, cigarette smoking) have been associated with IBD (Baumgart and Carding, 2007, Xavier and Podolsky, 2007, Goyette *et al.*, 2007). In addition to the previously described factors, impairment of the intestinal mucosal barrier that consists of outer mucosal barrier elements (commensal bacteria, mucus layer and immunoglobulin A), IECs and subepithelial immune cell, plays an important role in

intestinal inflammation and pathogenesis of IBD (Ukabam *et al.*, 1983, Bjarnason *et al.*, 1995). Various studies have indicated the role of intestinal microbiota in inducing inflammation in IBD (Guarner, 2008, Manichanh *et al.*, 2012). Disruption of the intestinal epithelium has been characterised as a hallmark of IBD and is associated with increased IEC apoptosis (Salim and Soderholm, 2011). Increased IEC apoptosis is seen in bacterial enteric infections but is also seen in UC and CD due to release of proinflammatory cytokines including TNF (Paesold *et al.*, 2002, Di Sabatino *et al.*, 2003). By using confocal laser endoscopy Kiesslich and colleagues identified three related determinants to predict relapse in IBD. These determinants included intestinal epithelial cell shedding, flow of fluorescein into the gut lumen and formation of microerosions. These three criteria collectively indicated loss of gut barrier function that play a major role in pathogenesis of IBD (Kiesslich *et al.*, 2011). Increased permeability of the gut barrier in IBD is largely related to dysregulation of tight junctions and increased IEC apoptosis. This disruption is functionally related to an uncontrolled immune response due to increased bacterial translocation and high expression of inflammatory cytokines such as TNF and IFN $\gamma$  in CD and IL-13 in UC (Hindrycks and Laukens, 2012).

### **1.2.2 Cancer of the intestine**

Many studies have indicated that chronic intestinal inflammation in IBD increases the risk of GIT cancer development and that includes colorectal cancer, small bowel adenocarcinoma, intestinal lymphoma and cholangiocarcinoma (Axelrad *et al.*, 2016). Small intestinal cancer is a rare disease in which cancer cells form in the tissue of the small intestine. Specifically, there are five types of small bowel cancer including

adenocarcinoma that is recognised as the most common type of small intestinal cancer. Adenocarcinoma is most commonly found in the duodenum and affects small intestinal crypt epithelial cells. The other types include neuroendocrine tumours (also called carcinoid tumour), lymphoma (in lymphoid tissue of small intestine) and leiomyosarcoma that affects the smooth muscle of the small bowel wall and is mostly found in the ileum (Vagholkar and Mathew, 2009).

Colorectal cancer is one of the most serious complications of IBD, however, the mechanism of developing cancer in relation to IBD is generally unclear (Vagefi and Longo, 2005). Experimental studies in IBD-related carcinogenesis have indicated that this cancer occurs in a multistep process including clonal growth that is characterised by genetic instability, clonal expansion, progressive accumulation of genetic abnormalities including abnormalities of tumour suppressor genes (such as p53, adenomatous polyposis coli gene (APC)) and development of dysplasia and carcinoma (Redston *et al.*, 1995, Willenbacher *et al.*, 1997). The tumour growth is significantly related to the disturbance of the balance between cell proliferation and cell apoptosis, however, decreased cell proliferation alone is not enough to reduce or prevent growth of tumour cells (Kulkarni *et al.*, 1992, Holmgren *et al.*, 1995). In contrast Sinicrope and colleagues in 1996 studied the proliferative and apoptosis indices in of human colonic adenocarcinoma and found a direct relationship between progression of the tumour and reduced apoptosis of colonic epithelial cells.

### 1.2.3 Sepsis

Sepsis is a potentially life-threatening complication of an infection of any part of the body that has entered the blood stream resulting in the release of cytokines from the immune system. The most common sites of infection leading to sepsis are the lungs, urinary tract, peritoneal cavity, pelvis and skin (Jacob, 2012). One of the first organs to be affected by excessive cytokine release during sepsis is the gastrointestinal tract (Rowlands *et al.*, 1999). The number of people dying from sepsis has increased in the last 20 years. The number of patients who develop sepsis has increased for many reasons. For example, an increased aging population with a weakened immune system, increased antibiotic use resulting in many more resistant strains of bacteria, increased use of medications that weaken the body's defence mechanism during cancer treatment and organ transplantation (Deustchman and Tracey, 2014). The most common causes of infection resulting in sepsis are bacterial, mainly Gram-positive staphylococcal strains, but they can also be viral or fungal (Munford and Suffredini, 2014). These bacteria create a wide range of virulence factors that enable them to avoid the immune system and spread to remote organs (Ramachandran, 2014). The most potent bacterial virulence factors are toxins including lipopolysaccharide (LPS), which is found in the outer membrane of the cell wall of Gram-negative bacteria and elicits a strong immune response from the host defence mechanism. LPS is important for bacterial survival as it provides protection from their surrounding environment (Merrell and Flakow, 2004, Rosenfeld and Shai, 2006). Once inside the body, natural defence cells such as macrophages and monocytes recognise the bacteria as a foreign substance. This recognition process is mediated by the

antigens in bacteria which include the O-antigen of LPS. LPS are recognised as pathogen associated molecular patterns (PAMPs) by the pattern recognition receptors (PRRs), among them toll like receptors (TLRs) that are expressed on monocytes and macrophages to increase their phagocytic activity and cause secretion of proinflammatory cytokines such as TNF, IL-6, IFN- $\beta$  (Ulevitch and Tobias, 1999). LPS is then released into the blood circulation and binds to LPS binding molecules to exert deleterious effects, for example, small intestinal epithelial cell (SIEC) shedding.

### **1.3 Intestinal mucosal epithelium**

The epithelium lining the small intestine is a simple columnar epithelium and consists of a number of cells of different types and functions. These cells are connected tightly together by intercellular junctional complexes which are the zonula occludens, zonula adherens, desmosomes and gap junctions, and are also connected to the underlying basement membrane via hemidesmosomes. These junctional complexes play an important role in maintaining intestinal homeostasis and prevent subsequent intestinal leakage (Lai *et al.*, 2013). The lamina propria of the intestinal mucosa consists of vascular and lymph vessels, nerve fibres, smooth muscle cells and diffuse lymphoid tissue which all form the core of intestinal villi (Mescher, 2010). The submucosa has larger blood and lymph vessels, and a plexus of neurons known as a Meissner's plexus, while the distal part of the duodenum contains branched tubular glands called Brunner's glands that secrete an alkaline mucus to neutralise the acidity of the chyme that comes from the stomach (Mescher, 2010). The well-developed

muscularis in the small intestine is composed of an inner circular and outer longitudinal smooth muscle layer with the myenteric or Auerbach's nerve plexus in between. This plexus of nerves is responsible for producing peristaltic movements of the bowel. The small intestine is covered on its exterior surface by a thin layer of connective tissue known as the serosa (Mescher, 2010).

### 1.4 Cell types in the intestinal epithelium

Intestinal integrity is maintained by the self-renewal activity of intestinal epithelia. The intestinal epithelium consists of various cell types (Figure 1.1). They are held together by intercellular junctions forming a structural unity of one cell thickness that is folded to produce villi and crypts (Bjerknes and Cheng, 1999).

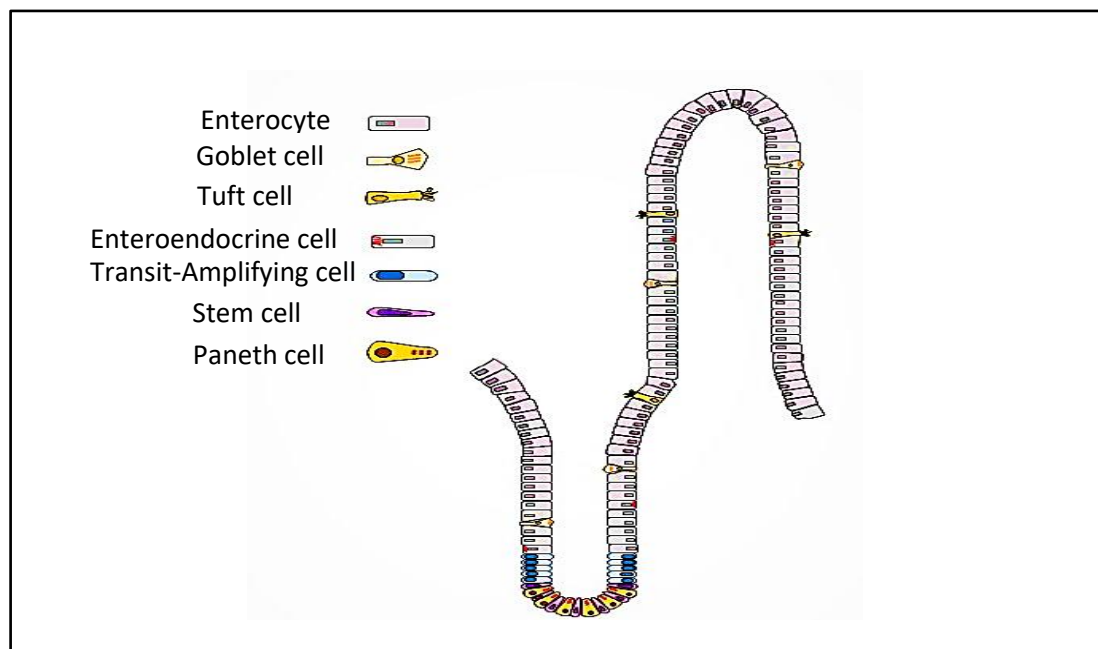


Figure 1.1: Schematic diagram of the small intestinal crypts and villi showing different cell types of lining epithelium.

### 1.4.1 Intestinal epithelial stem cells

Intestinal epithelial stem cells are pluripotential cells that are located in the basal part of the small intestinal crypt. They are undifferentiated cells with few intracellular organelles and little microvilli. These cells have a capability to proliferate for self-maintenance and differentiation into the various different cell lineages (Bach *et al.*, 2000). The basal compartment of the intestinal crypts (proliferative compartment) contains undifferentiated and rapidly cycling cells that are responsible for cell turnover and protective niche for the epithelial stem cells (Umar, 2010). Several experimental studies have used methods to identify the location of stem cells in intestinal crypts. However, the true nature of their position still remains unclear. Two different hypotheses have suggested the position of intestinal stem cells among the epithelial lining of the crypts of Lieberkühn. The +4 hypothesis was proposed by Potten and colleagues in 1974 and 1977, and suggested that stem cells are located at cell position +4 in the crypt axis from the crypt base with the lower three positions occupied by mature Paneth cells. These cells were subsequently shown to be positively labelled for Bmi-1 (B-cell lymphoma Mo-MLV insertion region 1 homolog), but were only noted among the epithelial lining of proximal small intestinal crypts suggesting the existence of Bmi-1 negative stem cell in the other parts of the small intestine (Sangiorgi and Capecchi, 2008, Potten *et al.*, 2009). The crypt base columnar cell hypothesis suggested the presence of undifferentiated columnar epithelial stem cells between the Paneth cells below position 4 from the crypt base (Cheng and Leblond, 1974, Bjerknes and Cheng, 1999). These crypt base columnar cells expressed the stem cell marker Lgr5 (Leucine-rich repeat containing G-protein coupled receptor 5) and are characterised by their ability for self-renewal and capability to produce all

types of differentiated intestinal epithelial cells found along the crypt-villus axis (Barker *et al.*, 2007).

#### **1.4.2 Absorptive cells (mature enterocytes)**

Enterocytes are absorptive cells that are specialised for nutrient transport from the intestinal lumen into the blood circulation. They are tall columnar cells with basally positioned nuclei. The apical surface of these cells is folded into finger-like projections called microvilli that appear under the light microscope as a brush border toward the intestinal lumen. The microvilli increase the absorptive surface area of enterocytes. Each microvillus consists of an actin microfilament core that extends vertically from the tips of microvilli into the apical cytoplasm and inserts into the terminal web playing a part in forming the cytoskeleton that stabilises the apical cell membrane. In addition to their absorptive function, enterocytes also have a secretory function. They secrete glycoproteins that are found in vesicles in the apical part of the cells just below the terminal web (Ross *et al.*, 2007). The brush borders of enterocytes are covered with a layer of glycocalyx that contains the secretion from enterocytes (glycoproteins and carbohydrates) mixed with the mucopolysaccharides and trefoil factors that are secreted by goblet cells (Herdt, 1997). By electron microscopy (EM) the absorptive cells show heterochromatic nuclei, supra-nuclear Golgi complex, mitochondria, ribosomes, rough endoplasmic reticulum (rER), secretory granules and lysosomal bodies (Shoma, 1983).

### **1.4.3 Goblet cells**

Goblet cells are found in both the intestinal crypts and intestinal villi and increase in number from the duodenum to ileum. They produce mucus and trefoil factors that play a role in the maintenance of cell surface integrity and improve healing of the gastrointestinal mucosa by restitution (Barrera and Tortolero, 2016). The apical part of goblet cells appears to be empty in routine haematoxylin and eosin stained sections due to the loss of water soluble mucinogen that accumulates in this cellular region during section preparation. EM examination of goblet cells shows accumulation of mucinogen granules in the broad apical part of the cell while the narrow basal part that appears basophilic in histological sections contains a heterochromatic nucleus, Golgi complex, rER, free ribosomes and mitochondria (Ross *et al.*, 2007).

### **1.4.4 Paneth cells**

Paneth cells are found at the base of intestinal crypts and do not migrate along the crypt-villus axis. They have a basophilic basal cytoplasm containing the nucleus and supranuclear Golgi complex. These cells are easily recognised in routine histological sections as their apical portion contains large intensely eosinophilic granules that contain antibacterial enzymes, lysosyme, and other substances such as phospholipase, ribonuclease and tumour necrosis factor (TNF). Lysosyme breaks down the cell wall of some bacteria giving the cells a phagocytic activity. The action of antibacterial enzymes and the phagocytic activity of Paneth cells against certain bacteria suggest that these cells play a role in regulating the normal bacterial flora of the small intestine (Ross *et al.*, 2007).

#### **1.4.5 Enteroendocrine cells**

Enteroendocrine cells are found in the lower portion of intestinal crypts and migrate slowly along the crypt-villus axis, therefore they can be seen at all levels of the villi. They are considered to be part of the gut neuroendocrine system and produce hormones such as somatostatin, gastrin, secretin, cholecystokinin and enteroglucagon that regulate the physiological activities of the gastrointestinal tract (Strader and Woods 2005).

#### **1.4.6 Tuft cells**

Tuft cells are scattered throughout intestinal crypt and villi and represent about 0.4% of all epithelial cells. In intestinal crypts they are located just above the level of stem cells; they are sometimes described as inactive stem cells with a slower proliferation rate (Gerbe and Jay, 2016). Tuft cells are characterised by a thick brush border of microvilli that project from their apical surface and by a well-developed tubulovascular system in the apical cytoplasm. These cells can be seen in different epithelial tissues but little is known about their function due to the lack of Tuft cell specific markers. However their specific morphological structure expresses signalling constituents typical of chemosensory cell types (Gerbe *et al.*, 2012). Gerbe *et al.* in 2011 described various proteins that are specifically expressed by Tuft cells including DCAMKL 1 (doublecortin-like kinase 1). They also found that Tuft cells secrete opioids and produce enzymes used for prostaglandin synthesis (Grebe *et al.*, 2011).

## **1.5 Proliferation and differentiation of the small intestinal epithelium**

The small intestinal epithelium renews itself continuously by the processes of proliferation and differentiation. This renewing system serves to populate two main compartments, the crypts and villi. The proliferative (stem) cells are located in the lower part of the crypt compartment and give rise to the other types of cells that line the crypt-villus axis (Wright, 2000). The stem cells proliferate and show gradual characteristic changes from undifferentiated cells in the crypt base to partially differentiated cells at higher crypt levels. At the top of the crypts, they stop dividing but continue to differentiate to become fully differentiated cells within the villus compartment (Cheng and Leblond, 1974). The stem cells at the crypt base start to divide symmetrically producing identical stem cells that maintain the stem cell compartment and asymmetrically producing transit-amplifying cells that continue to divide and differentiate while they migrate from the crypt along the crypt villus axis into enterocytes, goblet cells and enteroendocrine cells (Kolf *et al.*, 2007). Also, a small number of transit-amplifying cells migrate downwards and differentiate into Paneth cells (Garabedian *et al.*, 1997).

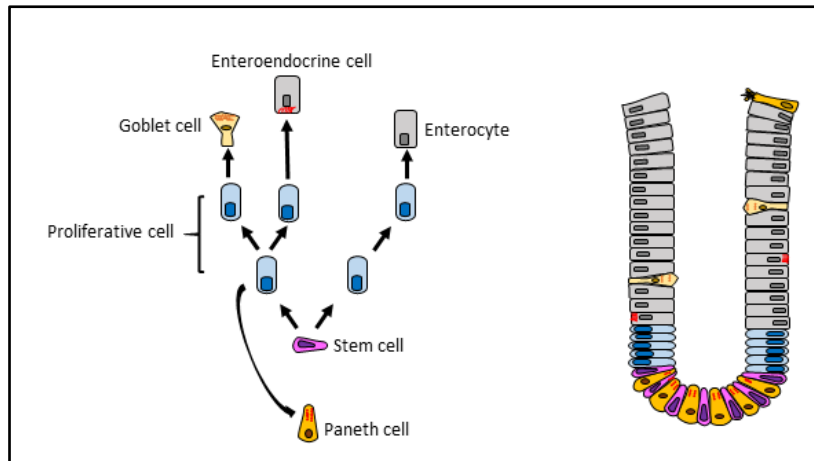


Figure 1.2: Schematic diagram illustrating the differentiation of stem cell into different types of intestinal epithelial lineage.

Proliferation and differentiation of the small intestinal epithelium is crucial for maintaining tissue homeostasis. This means that the percentage of stem cell proliferation and differentiation is directly related to the number of cells that die at small intestinal villus apices (Booth and Potten, 2001).

Parker and colleagues (2017) established a cell-tracking mathematical scheme to calculate the rate of small intestinal stem cell proliferation and migration under normal conditions including the time when proliferation starts to slowdown and when it is completely stopped. They found a direct relationship between the proliferation of stem cells in the intestinal crypt and the velocities of migration of differentiated cells along the villus axis, concluding that the proliferation of stem cells in intestinal crypts is the primary force that initiates and determines the migration rate of cells along the villus length (Parker *et al.*, 2007).

There are two different major signalling pathways controlling intestinal stem cell proliferation and differentiation, Wnt signalling and Notch signalling (Vanuystel *et al.*, 2013 and vanDussen *et al.*, 2012).

### **1.5.1 Wnt signalling pathway**

The Wnt signalling pathway depends on the autocrine and paracrine interaction of secreted cysteine-rich Wnt-glycoprotein with the transmembrane receptor Frizzled and the co-receptor lipoprotein related protein (LRP) (Vanuystel *et al.*, 2013). Binding of Wnt to its receptor activates the canonical pathway that increases cell proliferation by regulating progression through the cell cycle. Activation of Wnt/ $\beta$ -catenin signalling preserves the proliferative state of transit amplifying progenitors at the bottom of intestinal crypts. Inactivation of the Wnt signalling pathway by over expression of the inhibitor DKK1 leads to loss of crypt cell proliferation (Pinto *et al.*, 2003 and Kuhnert *et al.*, 2004). On the contrary, activation of the Wnt/ $\beta$ -catenin/T-cell factor (Tcf) pathway principally maintains the intestinal epithelial cells in a proliferative condition and suppresses differentiation (van de Wetering *et al.*, 2002). Cytosolic  $\beta$ -catenin is the key mediator of the Wnt signalling pathway. It translocates into the nucleus and stimulates the subsequent transcriptional regulation of Wnt target genes such as the *c-myc* oncogene. Therefore, nuclear accumulation of  $\beta$ -catenin is considered to be an indicator of an activated canonical Wnt signalling pathway. In the absence of binding of Wnt to its receptor, the free cytoplasmic  $\beta$ -catenin is efficiently degraded by the tumour suppressor gene product adenomatous polyposis coli (APC) that is considered to act as a suppressor of the Wnt signalling pathway (Pinto and Clevers, 2005).

The role of Wnt signalling in inducing cell proliferation is thought to be mediated by down regulation of the cell cycle inhibitor p21<sup>CIP1/WAF1</sup> that is mediated by upregulation of the C-myc proto-oncogene (Nakamura *et al.*, 2007 and Furriols and Bray, 2001).

### 1.5.2 Notch signalling pathway

Both Wnt and Notch signalling pathways play important roles in maintaining a proliferative state in the intestinal crypt; many studies have suggested that the key element of cell fate and differentiation in the intestinal epithelium is the Notch signalling pathway. The Notch signalling pathway is based on the direct contact between Notch receptors and ligands of adjacent cells (Morimoto *et al.*, 2012). This Notch receptor-ligand interaction leads to cleavage of an intracellular domain (ICD) from the transmembrane domain of the receptor and the subsequent translocation of ICD into the nucleus, where it binds to the DNA binding protein RBP-J (recombination signal binding protein for immunoglobulin kappa J region). Afterward this complex activates the transcription of Notch target genes such as *Hes1* (Artavanis-Tsakonas *et al.*, 1999 and Furriols and Bray, 2001). These Notch signalling pathway elements, ligands, receptors and the target gene *Hes1*, are expressed in the proliferative cell compartment of the intestinal crypt (Zecchini *et al.*, 2005). Inhibition of the Notch signalling pathway by deletion of RBP-J leads to an increase in the expression of *Math1* (which is usually suppressed by active Notch signalling), and the replacement of the transit amplifying (proliferative) compartment by goblet cells. This was associated with suppression of all epithelial cell division whilst the Wnt signalling pathway remained active (van Es *et al.*, 2005 and van Es and Clevers, 2005). Disruption of the

Notch signalling pathway also caused an increase in the population of goblet cells within the gut epithelium (Zecchini *et al.*, 2005 and Crosnier *et al.*, 2005). Murine intestinal epithelium deficient in *Hes1* revealed an increase in the number of secretory cell types (goblet cells, enteroendocrine cells and Paneth cells) and a decrease in enterocytes. This indicated the role of *Hes1* as a negative regulator of secretory cell type differentiation (Jensen *et al.*, 2000). Moreover, *Hes1* inhibits *Math1* that is recognised as a positive regulator of secretory cell lineage differentiation. Additionally, deletion of *Math1* noticeably indicated a reduction in intestinal epithelial goblet cells, enteroendocrine cells and Paneth cells without affecting the enterocyte population (Yang *et al.*, 2001). Consequently, the equilibrium between expression of *Hes1* and *Math1* regulates the differentiation of progenitor cells into either absorptive or secretory cell types. Nevertheless, additional downstream regulation of *Math1*-specified secretory cell lineages is crucial for the differentiation of individual secretory cell lineages. This downstream choice involves the zinc-finger transcriptional repressor *Gfi1* which is absent in *Math1*-null embryonic intestines. The intestine of *Gfi1*-knockout mice showed loss of Paneth cells and a drop in the number of goblet cells and by contrast indicated an increase in the number of enteroendocrine cells. This suggests a role of *Gfi1* in regulating the differentiation of Paneth and goblet cells and not the differentiation of enteroendocrine cells (Shroyer *et al.*, 2005). On the other hand, deletion of neurogenin 3 (*Ngn3*) in mice lead to the complete loss of enteroendocrine cells, however, the other three cell lineages (enterocytes, goblet cells and Paneth cells) developed normally indicating a specific role of *Ngn3* in development of enteroendocrine cells (Jenny *et al.*, 2002).

## 1.6 Cell death

Cell death is defined as the point at which a cell fails to perform its vital functions. Some previous reviews defined cell death as an irreversible loss of cell membrane integrity (Kromer *et al.*, 2009 and Alvarez *et al.*, 2010). Historically cell death has been classified into regulated apoptosis and unregulated necrosis, but more recent research suggests that necrosis may also be implemented through another pathway termed necroptosis (Degterev *et al.*, 2005). In addition to these three types of cell death, recent investigators have proposed another type of programmed cell death categorised as an inflammatory type of cell death that results from infections with intracellular pathogens (*Salmonella* and *Shigella* species) and is known as pyroptosis (Fink and Cookson, 2005).

### 1.6.1 Necrosis

The term necrosis describes the uncontrolled irreversible damage to a cell or tissue. It is a form of non-specific, unregulated, non-programmed cell death that is often associated with inflammation. Necrosis is frequently associated with pathological conditions and is prominent in ischaemia, trauma, and exposure to toxins or invasion by viruses or bacteria (Alvarez *et al.*, 2010). Necrotic cells are characterised by numerous morphological changes including an increase in the size of the cell itself (swelling) and the size of its organelles with subsequent rupture of the cell membrane followed by dissolution and lysis of nuclear and cellular components. It usually occurs in groups of neighbouring cells (Kerr *et al.*, 1972).

### 1.6.2 Apoptosis

Apoptosis is a regulated form of cell suicide that is tightly controlled by a genetic mechanism (Yuan and Horvitz, 2004). Apoptosis is achieved through either the extrinsic pathway via ligand binding receptor or via the intrinsic pathway involving the mitochondria as discussed in more detail below (Figure 1.3). Early apoptosis research focused on the important role of apoptosis or programmed cell death in development and the maintenance of normal tissue homeostasis (Yuan and Kroemer, 2010). As a mode of cell death, apoptosis has always shown a series of morphological and biochemical changes to cell architecture, including shrinkage of cells, chromatin condensation, blebbing of the nucleus and cytoplasm and breakdown of DNA (Majno and Joris, 1995). Apoptotic cells are recognised by phagocytes and are engulfed before they leak their contents (Martin and Henry, 2013). Programmed cell death removes aged, unwanted and injured cells with a reduced level of disturbance to neighbouring cells (Martin *et al.*, 2012). Apoptosis complements mitosis as a means of regulating cell numbers in multicellular organisms and for this reason it is under molecular control by a dedicated set of enzymes and their regulators. Caspases, members of the family of cysteine proteases, become activated during apoptosis and regulate the events that take place to ensure the immediate recognition and removal of apoptotic cells (Riedl and Salvesen, 2007).

The structural and functional efficiency of the gut barrier is only maintained if there is equilibrium between cell mitosis within the intestinal crypt and cell shedding at the tips of intestinal villi (Günther *et al.*, 2013). Epithelial cells migrate from the crypt base to the villus tip in the small intestine where they undergo cell death and shedding. A

number of studies have shown that this process is actively regulated, and that it involves a subset of the caspase family of proteases including Caspase-3, -6, -7, -8, and -9 (Tylor *et al.*, 2008 and Martin and Henry, 2013).

Caspase-3 activation is often accompanied by morphological changes that are associated with cell shedding. On the other hand, no morphological changes were observed during gastrointestinal tract development in mice that were deficient for caspase 3, supporting the suggestion that caspase 3 may not play an important role in gut tissue homeostasis (Günther *et al.*, 2013) or that there is functional redundancy with other proteins such as other caspases.

### **1.6.3 Necroptosis**

Recently the term necroptosis has been used to describe a process of regulated necrosis that occurs in certain types of cells such as neurones (Degterve *et al.*, 2005). It can be defined as a form of cell death that is negatively regulated by caspase 8. It is dependent on the receptor-interacting protein kinase 1 and 3 (RIPK1-RIPK3) complex, and this process can be inhibited by necrostatin-1 (Kaczmarek *et al.*, 2013). Necroptotic cell death *in vitro* is confirmed by plasma membrane rupture and lacks apoptotic markers such as caspase activation and chromatin condensation (Kaczmarek *et al.*, 2013). Necroptosis may be stimulated by TNF, Fas ligand and TNF-related apoptosis inducing ligand; the same ligands that can activate apoptosis (Alvarez *et al.*, 2010). Günther and colleagues in 2013 demonstrated that necroptosis is an alternative mode of cell death in the intestine which can drive intestinal inflammation. They described that intestinal inflammation in inflammatory bowel

disease patients can be evoked by an undesirable mechanism through dysregulation of the immune response and epithelial cell death due to strong inflammatory mediators such as TNF that are recognised as potent inducers of necroptosis.

#### **1.6.4 Pyroptosis**

Pyroptosis is a special type of programmed cell death that is considered as pro-inflammatory and is induced by an infection with *Salmonella* and *Shigella* species (Cookson and Brennan, 2001). This type of cell death is uniquely dependent on caspase 1 (which is not involved in the apoptotic type of cell death). Activation of caspase 1 in bacterially infected macrophages causes activation of inflammatory cytokines (IL-1 $\beta$  and IL-18), leading to cell death that is distinctly different from apoptosis (cell death without inflammation). This type of cell death can be recognised in a variety of biological systems including the immune system, nervous system and cardiovascular system (Fink and Cookson, 2005).

#### **1.6.5 Autophagy**

Autophagy is a physiological self-destructive process that takes place within autophagy vacuoles of dying cells. It is a non-inflammatory mechanism that is regulated by GTPases and phosphatidylinositol kinases through the ubiquitin-like conjugation system and is characterised by the segregation of cytoplasmic components in double-membrane vacuoles forming autophagosomes that later fuse with cellular lysosomes to be destroyed by the action of lysosomal proteolytic

enzymes. *In vivo*, autophagic cells can be phagocytosed by adjacent cells (Fink and Cookson, 2005 and Glick *et al.*, 2010).

## **1.7 Cell death in the small intestine**

Structural and functional integrity of the gut barrier are maintained by the equilibrium between cell death and cell proliferation. Continuation of this equilibrium results in maintaining cellular functional efficiency and prevents the accumulation of damaged cells (Delgado *et al.*, 2016). Under normal homeostatic conditions the majority of cell death occurs at the villus tip, however it can also be observed at the crypt base in the region where stem cells are located (Watson and Pritchard, 2000). The process of cell death was originally recognised based on morphological changes, but recently a number of studies have distinguished the cell death process based on the activity of biochemical pathways. The activation of more than one biochemical pathway can result in the same morphological endpoint while activation of an individual pathway may lead to different morphological features (Hacker and Karin, 2000). Programmed cell death in the intestine was described as apoptosis that was dependent on a family of aspartic-acid specific proteases called caspases and necroptosis which involves caspase independent cell death mechanisms and is dependent on activity of receptor-interacting protein (RIP) kinases (Delgado *et al.*, 20016). The first programmed cell death response due to cellular stress is apoptosis. However, if the mechanism of apoptosis is impaired or blocked the alternative pathway will be necroptosis which causes rupture of the cell membrane, the release of cytoplasmic components and induction of inflammation (Delgado *et al.*, 2016).

### **1.7.1 Mechanism of SIEC shedding during homeostasis**

An increase in the loss of SIECs or a decrease in the regenerative capacity of the intestine results in loss of epithelial layer integrity and increased gut barrier permeability, leading to the passage of harmful materials and microorganisms into the body. Despite the very high mitotic activity of the small intestine, a healthy intestinal mucosa has the ability to preserve its epithelial integrity and maintain intestinal barrier function by generating new epithelial cells to compensate for the loss of mature cells at the villus tip by shedding. Previously, shedding or the loss of mature epithelial cells was recognised to be a result of continuous cell maturation, possibly due to crowding of the epithelial cells at the tip of the villi. Nonetheless, the continuity of this process indicates that it is a complex sequence of coordinated events that seem to be important to maintain the integrity of the epithelium and gut barrier function. For this reason, the mechanism by which epithelial cells are shed from the tip of the villus into the lumen is crucial for understanding intestinal homeostasis in health and disease (Williams *et al.*, 2015).

The intestinal epithelium represents part of a renewing system that undergoes a series of active mitotic divisions throughout life (Leblond and Stevens, 1948). Generally intestinal epithelial cells arise from stem cells located at the base of intestinal crypts. These cells undergo three or four mitotic divisions before they start to migrate up through the crypt-villus axis to eventually be shed at the villus tips into the gut lumen (Watson *et al.*, 2009).

The early description of cell shedding in the intestinal epithelium was made by Leblond and Stevens, 1948. They studied the mitotic activity of rat intestinal epithelial cells as

a powerful regulatory process following the damage that resulted from the action of bacterial enzymes (Leblond and Stevens, 1948). In the mouse, the process of cell migration to the villus tip takes two to three days and approximately 1400 cells per villus are shed every day (Yuan and Kroemer, 2010). Different morphological features have been observed during the shedding of intestinal epithelial cells in different animals. In mice, extrusion of whole cells into the lumen has been noted, whereas in guinea pigs the epithelial cells undergo a series of events leading to cell fragmentation and these fragments are pinched off leaving intact junctional complexes between the neighbouring cells (Mayhew *et al.*, 1999). In humans the type of cell shedding is by whole cell extrusion which is similar to the intestinal epithelial cell shedding process observed in mice and rats, suggesting that these species are the appropriate models to study the regulation of human cell shedding (Williams *et al.*, 2015).

The equilibrium between the production of newly synthesised cells in intestinal crypts and the shedding of epithelial cells from the villus tip should be matched. Many factors may affect this balance, either by inhibiting cell proliferation such as by chaperones such as bone morphogenic proteins (van der Flier and Clevers, 2009) or by increasing the rate of cell shedding at villus tips by factors including growth factors and the intestinal microbiota (Dong *et al.*, 2014).

Although shedding of intestinal epithelial cells at villus tips occurs in all living species, variations in the morphological features of epithelial cell shedding were clearly noted between different species. A whole cell extrusion type of shedding was noted in mice and rats, while in guinea pigs the epithelial apoptotic bodies are pinched out from the shedding cells leaving intact junctional complexes between the adjacent cells (Mayhew *et al.*, 1999). Recently, various studies have shown that the shedding of small

intestinal epithelial cells (SIECs) in humans has whole cell extrusion features (Bullen *et al.*, 2006). However, several different SIEC shedding mechanisms may be present with different degrees of abundance within each species to maintain intestinal barrier function as effectively as possible.

Maintenance of the intestinal barrier following shedding of epithelial cells is a complicated process that involves the integration of microtubules, microfilaments and membrane components to remove the apoptotic cells. This process is complemented by redistribution of junctional proteins including zonula occludens 1 (ZO-1) to the lateral membrane of the shedding cells (Figure 1.3). This protein eventually forms a funnel around the shedding cell that preserves the integrity of the gut barrier. In addition other junctional proteins including claudin, E-cadherin, F-actin, myosin II, Rho-associated kinase (ROCK) and myosin light chain kinase (MLCK) are also redistributed to the lateral membrane (Marchiando *et al.*, 2012). Guan *et al.*, 2011 demonstrated that the primary indicator of cell shedding was ZO-1 redistribution which also appears as a marker of tight junction movement to maintain the intestinal barrier function during cell extrusion. Furthermore, they suggested that ZO-1 may bind to both the basolateral membrane and cell cytoskeleton that when contracts produces a force causing extrusion of the shedding cell and ZO-1 redistribution to the apical tight junction complex (Guan *et al.*, 2011). Additionally, Kiesslich and colleagues in 2012 using intravenous fluorescein, found that in the healthy human intestine, fluorescein filled the intercellular spaces up to the apical border and did not leak into the lumen suggesting that these spaces were occluded by tight junctions.

In patients with active IBD or patients around to undergo relapse of their IBD, fluorescein was observed leaking through paracellular spaces into the lumen

indicating that they had increased intestinal permeability. This leakage across tight junctions may predict the onset of IBD relapse (Kiesslich *et al.*, 2012).

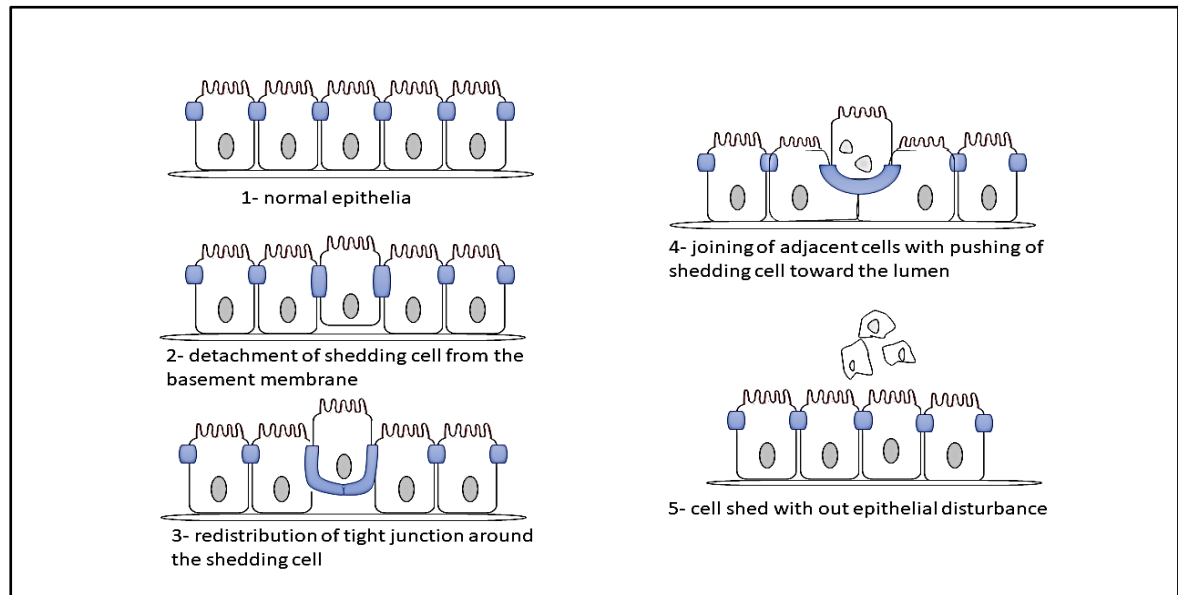


Figure 1.3: Schematic diagram illustrating the events of epithelial cell shedding and redistribution of tight junction to maintain the epithelial barrier integrity.

Shedding of intestinal epithelial cells either at the villus tip or crypt base leads to activation of the main initiators of apoptosis, the caspase family of proteins (Bullen *et al.*, 2006, Günther *et al.*, 2013, Williams *et al.*, 2015, Delgado *et al.*, 2015). Various recent studies have indicated differences in the apoptotic response in crypts and villi between different wild type mouse strains after exposure to different stimuli. Pritchard *et al.*, in 2000 found that Balb/c mice displayed more ralitrexed induced intestinal apoptosis than DBA/2 mice, they also demonstrate greater histopathological damage in the colon associated with diarrhoea and loss of body weight. Similar results were generated by Clarke *et al.* in 2000 who noted villus atrophy in the murine small

intestine 24 hours after ralitrexed injection which was more pronounced in Balb/c mice than in DBA/2 mice. Furthermore in 2012 Browne *et al.* investigated the effect of LPS on the hippocampus of two different mouse strains and they found that LPS administration significantly increased TNF mRNA expression in the hippocampus of Balb/c mice but not in C57BL/6J mice, however, significantly increased the mRNA expression of IL-1 $\beta$  in both mouse strains suggesting that LPS administration affects various tissues and that cytokines released by these tissues (such as TNF) may have systemic effects including on the gastrointestinal tract.

The small intestinal flora consists of many microorganisms. In the duodenum and jejunum there are about  $10^3$ - $10^4$  bacteria/ml of intestinal contents, mostly acid-tolerant lactobacilli and streptococci. The microflora of the ileum is more similar to that of the colon compared with other regions of the small intestine and consists of around  $10^7$ - $10^8$  bacteria/ml of the intestinal contents (Hao and Lee, 2004). Gram negative bacteria are a constituent of the commensal microorganisms that form the intestinal microbiota. Lipopolysaccharide (LPS) is an integral cell wall component of Gram negative bacteria and has the ability to evoke the host immune system. The LPS molecule is composed of three different domains that include a lipid A domain, an oligosaccharide core and an O-antigen (Figure 1.5). The lipid A domain is the part responsible for the toxicity of LPS whereas the O- antigen gives antigenic specificity to the bacterial LPS (Van Amersfoort *et al.*, 2003, Williams *et al.*, 2013).

In many previous studies the LPS used to induce endotoxic shock and clearly induce pathological SIEC apoptosis and shedding in mice has been the LPS derived from *Escherichia coli* serotype O111:B4 given its reported relationship to the occurrence of infant gastroenteritis (Campos *et al.*, 1994, Williams *et al.*, 2013).

Mathiak *et al.* in 2003 investigated the stimulatory effect of purified LPS from various different bacterial sources on the production of cytokines and chemokines that measured in whole blood assay by enzyme-linked immunosorbent assay (ELISA) and indicated that LPS originating from different bacterial sources demonstrated different effects upon the production of inflammatory mediators. However, there is currently no previous literature indicating the role of LPS from different bacterial species in inducing apoptosis and shedding of murine SIECs.

### **1.8 Genetic regulation of apoptosis in the gastrointestinal tract**

Apoptosis is considered to be a genetically controlled self-destruction process. The failure of cells to undergo apoptosis may lead to neoplastic transformation (Pritchard and Watson, 1996 and Potten *et al.*, 1997). Although apoptosis can be initiated by numerous stimuli, it involves one of two main cellular pathways; the mitochondrial pathway (intrinsic) and the membrane pathway (extrinsic) (Zhang and Fang, 2007). Extrinsic apoptosis is induced by extracellular stimuli that bind to specific transmembrane receptors termed death receptors, leading to the assembly of the death initiation signalling complex (DISC) that subsequently activates the caspase cascade. The intrinsic pathway is activated as a result of internal cellular stimuli such as DNA damage that affect the mitochondrial outer membrane causing cessation of ATP production and the release of a group of proteins that contribute to caspase activation (Favaloro *et al.*, 2012 and Figure 1.4).

Zhang and Fang in 2007 demonstrated that the modulation of different proteins, some pro-apoptotic and others anti-apoptotic, determine whether a cell will live or die by regulating activity of the apoptotic pathway.

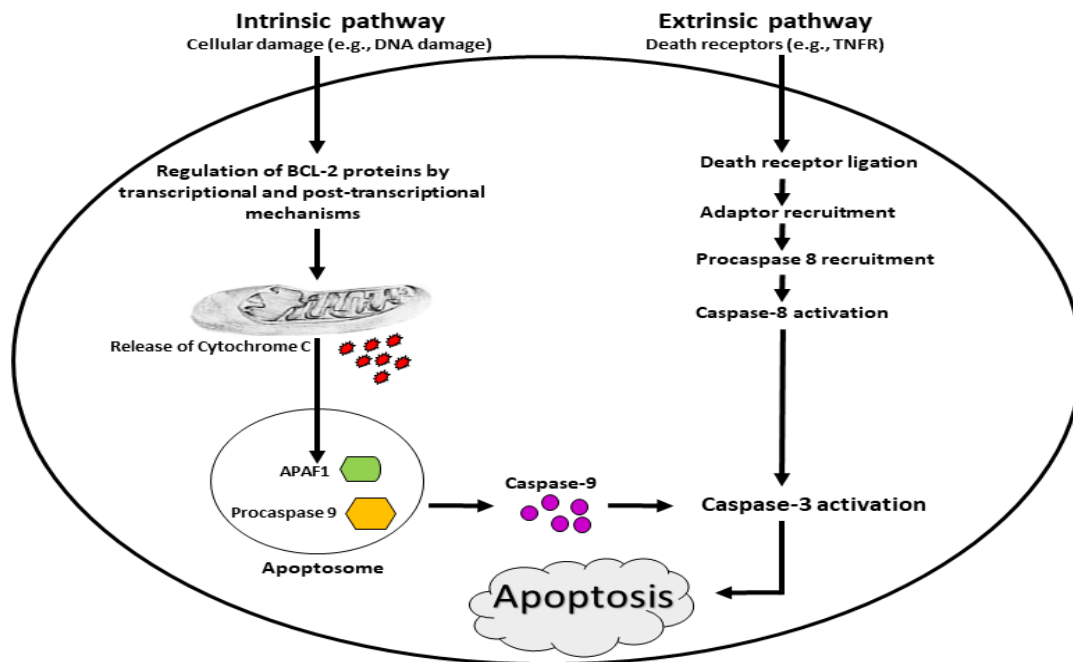


Figure 1.4: Schematic representation of the main molecular pathways leading to apoptosis.

### 1.8.1 Bcl-2 and related genes

The B cell Lymphoma/Leukaemia 2 (Bcl-2) oncogene has an important role in regulating apoptosis through the mitochondrial cascade (Edelblum *et al.*, 2006 and Zhang and Fang, 2007). There are two groups of Bcl-2 family members that have opposite cellular effects on apoptosis; some are involved in suppressing apoptosis and these include Bcl-2, bcl-x<sub>L</sub>, mcl1, bag-1, bfl-1, brag-1 and bcl-w. Conversely, bax, bad, bcl-x<sub>s</sub>, bak and bik are members that promote the process of apoptosis (Pritchard and Watson, 1996 and Potten *et al.*, 1997).

In response to apoptotic signals, Bax (a pro-apoptotic protein) accumulates inside the mitochondria resulting in the release of two important apoptotic factors which are cytochrome C and SMAC/DIABLO into the cell cytosol. Cytochrome C binds to APAF1,

causing activation of caspases 3, 7 and 9 while SMAC/DIABLO prevents the apoptotic inhibitory action of the apoptosis inhibitors by masking them (Zhang and Fang, 2007). In 2000, Pritchard and colleagues described the roles of Bcl-2 in the gastrointestinal tract (GIT) and found that Bcl-2 has a role in regulation of colonic epithelial cell apoptosis but did not appear to have the same anti-apoptotic action on small intestinal epithelial cells. However, Bcl-w was shown to play a crucial role in regulating apoptosis in the small intestinal epithelium.

There are other Bcl-2 family members that play roles in the inhibition or promotion of apoptosis. Bcl-x<sub>L</sub> and bcl-w are apoptosis inhibitors as they inhibit the Fas signalling pathway while Bax and Bak promote cell death. Bax is one of the principal promoters of apoptosis in the intestinal epithelium (Pritchard *et al.*, 2000, Bowen *et al.*, 2006). Duckworth and Pritchard in 2009 found that the proapoptotic protein Bak plays a major role in regulating colonic epithelial cell homeostasis, but it does not appear to have the same effect in the murine small intestine. Bim is a BH-3-domain only protein, the only such member of the Bcl-2 family that is expressed through the intestine and its role is relatively similar to Bax as its expression is seen at the base of colonic crypts and in intestinal villi (Bowen *et al.*, 2006).

### **1.8.2 p53**

p53 is a tumour suppressor protein that has two different roles. It has been recognised as an apoptosis mediator and also functions as a transcription factor to promote the activation of a variety of genes that are necessary for normal cell cycle regulation. It is responsible for the up-regulation of Fas and TNFR1 signalling in several cell types (Edelblum *et al.*, 2006). Many studies have shown that p53 deficient transgenic mice

develop normally, indicating that this gene has little involvement in controlling developmental processes or basal amounts of apoptosis (Potten *et al.*, 1997). However, examination of the changes that occur in p53 expression in the small intestine following exposure to ionising radiation indicate a role for p53 in this tissue. Ionising radiation can induce apoptosis in the position of intestinal stem cells with the peak of apoptosis being noted 3-6 hours following radiation exposure indicating the role of p53 either in initiating apoptosis or in holding the cells in the G1 or G2 phase of the cell cycle until repair of DNA damage has occurred (Potten *et al.*, 1997, Potten and Grant, 1998).

### **1.8.3 Tumour necrosis factor family**

TNF, FasL, and TNF-related apoptosis inducing ligand (TRAIL) are members of the TNF superfamily. All of these three mediators are known to have a role in promoting cell death by activation of a death receptor pathway (extrinsic pathway). Briefly, activation of the death receptor pathway by TNF will activate FADD (Fas-associated death domain protein) and TRADD (Tumour necrosis factor-associated death domain protein) that subsequently activate the caspases which initiate the apoptosis of intestinal epithelial cells (Zhang and Fang, 2007). TNF is a strong stimulator for intestinal epithelial cell shedding in mice. Sixty minutes after intraperitoneal administration of TNF, marked atrophy of duodenal villi is observed (Williams *et al.*, 2013). The cellular interleukin 1B (IL-1B) as well as bacterial lipopolysaccharide (LPS) and other bacterial products can strongly regulate the action of TNF on intestinal epithelial cells by stimulating two TNF receptors, TNFR1 (which contains a death domain) and TNFR2 that does not have a death domain (Slebioda and Kmiec, 2014).

#### **1.8.4 C-myc proto-oncogene**

C-myc is a proto-oncogene which has high expression in many tumours. It has two functional properties as it can induce uncontrolled cell proliferation as a result of preventing the cell from leaving the cell cycle, however it can also induce apoptosis (Pritchard and Watson, 1996). C-myc is a crucial regulator for a number of cellular processes that include apoptosis, cell cycle regulation, metabolism, ribosome biogenesis, protein synthesis and mitochondrial function. By contrast it can suppress many genes that are involved in cell adhesion and cellular growth (Wilkins and Sansom, 2008).

C-myc has an ability to make cells sensitive to many apoptotic stimuli including DNA damaging agents which are triggered through p53 activation and are mediated by BH3. C-myc also induces apoptosis by increasing the effectiveness of the death receptors Fas and TRAIL (Watson, 2004).

### **1.9 Stimuli that cause pathological intestinal epithelial cell apoptosis and shedding**

Spontaneous apoptosis occurs at a low rate in intestinal crypts and is usually observed at position 4 and 5 from the crypt base. This type of apoptosis is not related to any known stimuli (Potten, 1992). Correspondingly, physiological apoptosis and shedding of SIECs from intestinal villi are also seen on rare occasions (Bullen *et al.*, 2006). This suggests that physiological apoptosis and shedding does not affect gut barrier function.

Pathological apoptosis and shedding of SIECs have previously been induced by administration of different stimuli including TNF (Piguet *et al.*, 1998, Marchiando *et al.*, 2011, Watson and Hughes, 2012), bacterial LPS (Williams *et al.*, 2013, Yue *et al.*, 2013, Guo *et al.*, 2013), anti-CD3 antibody (Miura *et al.*, 2005), Polyinosinic:polycytidylic acid (McAllister *et al.*, 2013, Zhao *et al.*, 2017) and indomethacin (Shi *et al.*, 2014).

### **1.9.1 Bacterial lipopolysaccharide (LPS)**

LPS is an integral cell wall component of Gram negative bacteria and has the ability to evoke the host immune system. The LPS molecule is composed of three different domains that include a lipid A domain, an oligosaccharide core and an O-antigen (Figure 1.5). The lipid A domain is responsible for the toxicity of LPS whereas the O-antigen gives antigenic specificity to the bacterial LPS (Van Amersfoort *et al.*, 2003, Williams *et al.*, 2013). The LPS molecule is a complex amphiphilic molecule and consists of two structural components, a hydrophobic component termed lipid A and a hydrophilic component which consists of both an oligosaccharide core region and an O-specific antigen chain (Guo *et al.*, 2013). The highest concentration of LPS was noted in the intestinal lumen due to the residency of huge number of commensal bacteria. However, under normal physiologic conditions LPS cannot penetrate through the healthy gut barrier (Benoit *et al.*, 1998, Ge *et al.*, 2000).

Toll like receptor 4 (TLR 4) is expressed on myeloid-derived cells such as macrophages and dendritic cells as well as in some epithelial and endothelial cells and is considered to be a crucial component of the innate immune response (Kawai and Akira, 2010).

LPS signalling via TLR4 ligation was found to be dependent on several other molecules including lipopolysaccharide-binding protein and myeloid differentiation protein. This co-receptor mediates the ligation and transfer of LPS to TLR4 (Poltorak *et al.*, 2000, van der Mark *et al.*, 2017). Ligation induces the dimerisation of TLR4 and causes activation of the MyD88-independent signalling pathway that leads to production of proinflammatory cytokines such as TNF, interleukin 1(IL-1) and interleukin 6 (IL-6) (Lee *et al.*, 2012).

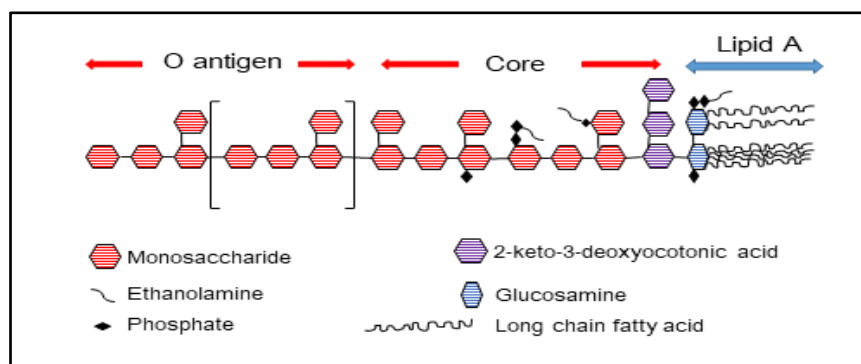


Figure 1.5: The components of LPS molecules, modified from: James and Hurley; 2013.Toxins, 5(12), 2589-2620

LPS represents a pathogen-associated molecular pattern. When administered systemically it is recognised by TLR4 on the wall of mononuclear phagocytic cells initiating a systemic inflammatory response involving nuclear factor kappa B (NFκB). This inflammatory response evokes mononuclear phagocytic cells to release TNF into the circulation. TNF subsequently binds to tumour necrosis factor receptor 1 (TNFR1) on the basolateral membrane of intestinal epithelial cells stimulates apoptosis and shedding of intestinal epithelial cells if NFκB2 signalling dominates, or cell survival if NFκB1 signalling dominates (Williams *et al.*, 2013).

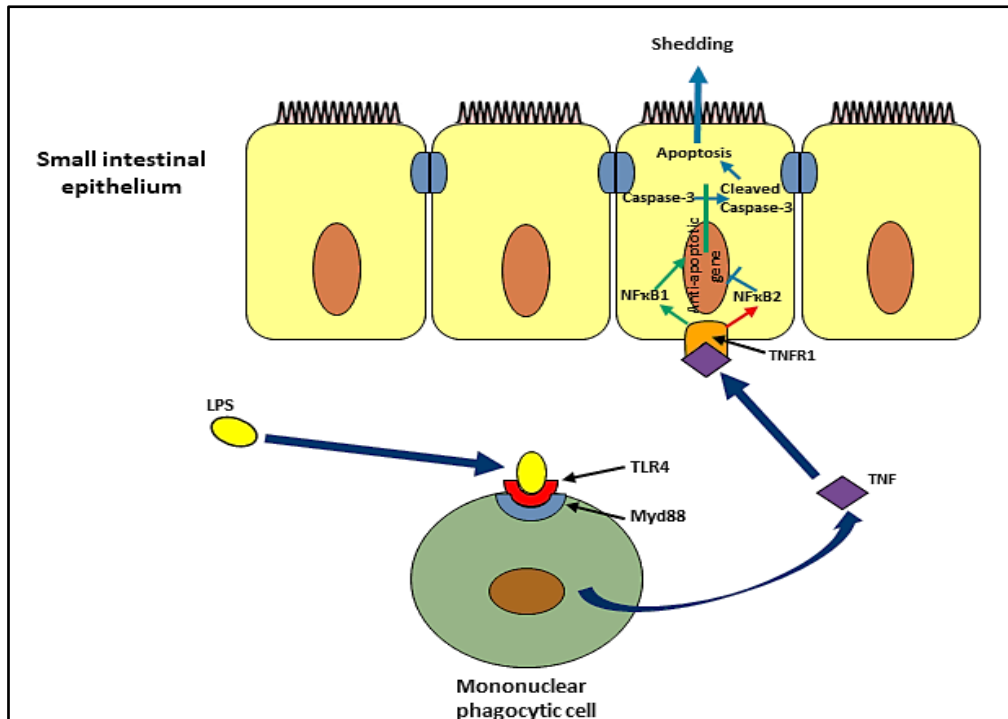


Figure 1.6: Diagram summarising the putative mechanism by which LPS induces apoptosis in SIECs. Modified from Williams *et al.*, 2013. *Dis Mod Mech* 6(6):1388-99

### 1.9.2 Anti-mouse CD3e antibody

The anti-mouse CD3 antibody is widely used for prevention and treatment of clinical organ allograft rejection because of its immunosuppressive properties. However, the clinical use of this antibody is accompanied by a number of symptoms including fever, nausea, vomiting, headache and diarrhoea due to a release of numerous cytokines including interleukin 2 (IL-2), TNF, interferon- $\gamma$  (IFN- $\gamma$ ) and IL-6 (Bloemena *et al.*, 1990, Vossen *et al.*, 1995). Anti-CD3e antibody targets the T cell receptor-CD3 (TCR-CD3) complex on the surface of circulating T-lymphocytes leading to activation of T-cells. This activation of T- cells results in the release of the proinflammatory cytokines described above (Carpenter *et al.*, 2000). *In vivo* activation of T-lymphocytes has been demonstrated to be the cause of intestinal damage that is characterised by increased

gut permeability, loss of intestinal villi and increased crypt apoptosis (Zhou *et al.*, 2004).

Miura and colleagues in 2005 investigated the effect of anti-CD3 antibody in the activation of T-lymphocytes and interestingly they found that an IP administration of anti-CD3 antibody induced a biphasic apoptosis and cell shedding of murine SIECs at both villus and crypt levels. The first phase consisted of apoptosis at the villus tip which was observed 2 hours post IP injection of 12.5mg/kg anti-CD3 antibody and reached a peak 4 hours post administration with a decline thereafter. The second observed phase was crypt epithelial cell apoptosis that increased gradually to reach a peak amount 24 hours post administration. The authors also noted an inflammatory infiltration of mononuclear phagocytic cells and indicated that all of these pathological features returned to normal by 4 days post administration (Miura *et al.*, 2005).

### **1.9.3 Polyinosinic: polycytidylic acid (Poly I:C)**

Poly I:C is a synthetic analogue of double stranded RNA (dsRNA), a virus associated molecular pattern. Injection of poly I:C into mice markedly induced rapid but reversible damage of the intestinal mucosa with significant villus shortening and increased enterocyte apoptosis (McAllister *et al.*, 2013).

Araya and colleagues, 2014 showed that intramural administration of poly I:C into C57BL/6J mice resulted in a severe enteropathy characterised by blunting of intestinal villi and oedema, with increased cell infiltration in the underlying lamina propria. These features were clearly observed 12 hours post poly I:C injection with decreased

villus/crypt ratio in comparison to PBS-treated C57Bl/6J mice. Full recovery was observed 72 hours post poly I:C treatment. The small intestine of poly I:C treated mice showed increased IFN $\beta$  expression 2 hours post injection whereas C-X-C motif chemokine 10 (CXCL10) and TNF peaked 6 hours following poly I:C treatment. The authors also indicated that MDA5 (Melanoma Differentiation-Associated protein 5), RIG-I (Retinoic acid-Inducible Gene-I-like receptor) and TLR3 mRNA were equally upregulated in the small intestine following poly I:C injection, furthermore the highest expression of these three receptors was observed 6 hours post intraluminal administration.

Recognition of poly I:C by TLR3 activates the transcription factor interferon regulatory factor 3 (IRF3) through the adapter protein Toll-IL1 receptor (TIR) domain- containing adapter inducing INF $\beta$ . Activation of IRF3 leads to increased production of IFN $\beta$  (Yamamoto *et al.*, 2003). On the contrary, involvement of TNF receptor associated factor 6 (TRAF6) or receptor interacting protein 1 (RIP1) with the subsequent activation of the transcription factors NF- $\kappa$ B and AP-1 triggers the production of inflammatory cytokines and chemokines such as TNF, IL-6 and CXCL10 (Kawai and Akira, 2008).

#### **1.9.4 Tumour necrosis factor (TNF)**

TNF was historically known as TNF and tumour necrosis factor superfamily 2 (TNFSF2). It is a member of a family that consist of 19 ligands and 29 receptors identified as the tumour necrosis factor superfamily (TNFSF) (Aggarwal *et al.*, 2012). The expression, form and structural characteristics of these constituents allows these family members

to activate various signalling pathways that control different cellular mechanisms including cell proliferation, cell differentiation, cell survival and apoptosis (Aggarwal *et al.*, 2003). TNF is expressed by different cells including macrophages, T-lymphocytes, B-lymphocytes, natural killer (NK) cells, mast cells, endothelial cells, fibroblasts and neurons. This expression is strongly up-regulated through a number of proinflammatory components such as LPS and IL-1 $\beta$  (Locksley *et al.*, 2001, Wajant *et al.*, 2003, Aggarwal *et al.*, 2012). Two types of TNF receptors have been identified, TNF receptor 1 (TNFR1 or p55 or TNFRSF1A) that contains the death domain and is essentially expressed on almost all mammalian cells and activated by both soluble and transmembrane forms of TNF. The second receptor is TNFR2 (p75 or TNFRSF1B) which does not contain the death domain and is only activated by the transmembrane form of TNF. The expression of TNFR2 is strictly regulated and found in T-lymphocytes, endothelial cells, microglia, neurons, oligodendrocytes, cardiac myocytes, thymocytes and mesenchymal stem cells (Wajant *et al.*, 2003, Aggarwal *et al.*, 2012, Faustman *et al.*, 2013).

Marchiando *et al.* in 2011 indicated that administration of TNF leads to shedding of intestinal epithelial cells due to activation of caspase-3 through TNF induced activation of the NF $\kappa$ B signalling pathway and proapoptotic pathway. Many previous studies have indicated the role of TNF in intestinal inflammation due to intestinal penetration of luminal materials as a result of intestinal epithelial barrier disruption (Ma *et al.*, 2004, Watson *et al.*, 2009).

Various studies have indicated the presence of TNFR1 in the intestinal epithelium (Song *et al.*, 2005, Lau *et al.*, 2011). Lau and colleagues in 2011 found that the

responses to systemic TNF were variable in the different parts of the small intestine. The percentage of TNF induced apoptosis was much higher in the duodenum and decreased toward the ileum. The authors also related this variation to higher expression of TNFR1 in duodenum that decreased in the ileum.

### **1.10 Nuclear factor kappa B (NFκB) signalling**

NFκB epitomises a family of highly evolutionarily preserved cytosolic proteins that regulates a large spectrum of genes implicated in various processes of the immune responses and inflammation (Oeckinghaus and Ghosh, 2009). The NFκB family consists of five members that are structurally related. They are NFκB1 (p50 and its precursor p105), NFκB2 (p52 and its precursor p100), RelA (p65), RelB and c-Rel. All these proteins share an N-terminal Rel homology domain that mediates homo- and heterodimerisation as well as being responsible for sequence-binding. Furthermore, the precursor protein of NFκB1 (p105) and NFκB2 (p100) act as an IκB-like protein as their C-terminal portion resembles the structure of IκB and has a NFκB inhibitory function. RelA, RelB and c-Rel also contain a C-terminal transcription activation domain (TAD) that facilitates gene transcription. Most of these members (with the exception of RelB) can homodimerise but also have the ability to form heterodimers with each other (Tak and Firestein, 2001). Generally, NF-κB proteins are impounded in the cytoplasm by an action of a family of inhibitory proteins (IκB family members and related proteins) that are characterized by the presence of ankyrin repeats (Sun, 2011).

Activation of the NF $\kappa$ B family of proteins occurs through two major signalling pathways, the canonical (classical) and non-canonical (alternative) pathways (Figure 1.7). Each of these two pathways plays a critical role in the regulation of immune and inflammatory responses despite their differences in signalling mechanism (Sun, 2011 and Vallabhapurapu and Karin, 2009).

### **1.10.1 Canonical NF $\kappa$ B signalling pathway**

The canonical pathway responds to various stimuli including ligands of different cytokine receptors, pattern recognition receptors (PPRs), TNFR, also T- and B- cell receptors (Zhang and Sun, 2015). Activation of the canonical pathway results from phosphorylation of I $\kappa$ B $\alpha$  through the action of multi-subunit I $\kappa$ B kinase (IKK) that is composed of two catalytic subunits, IKK $\alpha$  and IKK $\beta$  and regulatory subunit known as NF $\kappa$ B essential modulator (NEMO) or IKK $\gamma$  (Karin and Delhase, 2000, Sun and Ley, 2008 and Oeckinghaus and Ghosh, 2009). Activation of IKK is triggered through different stimuli such as cytokines, stress agents and microbial components leading to phosphorylation of I $\kappa$ B $\alpha$  which is targeted through ubiquitin-dependent degradation to the proteasome resulting in release of NF $\kappa$ B members p50/relA and p50/c-Rel dimers in the cytoplasm that afterwards undergo nuclear translocation to bind to the DNA binding sites and regulate target gene transcription (Karin and Delhase, 2000, Neinke and Ley, 2004 and Hayden and Ghosh, 2008).

### **1.10.2 Non-canonical NF $\kappa$ B signalling pathway**

In contrast to the canonical pathway, the non-canonical pathway specifically responds to a particular group of stimuli such as ligands of TNFR including lymphotoxin  $\beta$

receptor (LT $\beta$ R), B-cell activating factor receptor (BAFFR, also known as tumour necrosis factor receptor superfamily member 13C (TNFRSF13C)), CD40 and receptor activator of NF $\kappa$ B (RANK). Furthermore, the non-canonical pathway does not involve I $\kappa$ B $\alpha$  degradation but depends on processing of NF $\kappa$ B2 precursor protein, p100 (Su, 2011 and Su and Liu, 2012). One of the main signalling molecules in the non-canonical pathway is NF $\kappa$ B inducing kinase (NIK) which is responsible for activation of IKK $\alpha$  that mediates phosphorylation of p100 which in turn causes NF $\kappa$ B2 ubiquitination and processing (Xiao *et al.*, 2001 and Senftleben *et al.*, 2001). Processing NF $\kappa$ B2 involves degradation of the C-terminal I $\kappa$ B like structure and the formation of mature NF $\kappa$ B2 p52 followed by nuclear translocation of the NF $\kappa$ B complex p52/RelB (Su, 2011 and Zhang and Su, 2015). In general, activation of the non-canonical NF $\kappa$ B signalling pathway is slower than the canonical pathway and appears to have evolved as a complementary signalling axis that cooperates with the canonical pathway to induce a coordinated and continuous immunological response (Merga *et al.*, 2016).

In 2011 Guma and colleagues indicated that the activation of NF $\kappa$ B canonical pathway signalling in the intestine does not generate an acute inflammation in small intestinal tissue accompanied with apoptosis of SIECs and disruption of gut barrier function unless there is a concurrent activation of mitogen-activated protein kinase (MAPKs).

Williams *et al.*, 2013 interestingly demonstrated that NF $\kappa$ B1<sup>-/-</sup> mice (mice that lack the NF $\kappa$ B family member that signals through the canonical pathway) develop more SIEC apoptosis and shedding in response to TNF than wild-type mice and by contrast, NF $\kappa$ B2<sup>-/-</sup> mice (mice deficient in an NF $\kappa$ B family member that signals via the non-canonical pathway) were more resistant to SIEC apoptosis and shedding in response

to TNF suggesting an important role of non-canonical NFκB signalling in intestinal epithelial cell apoptosis and shedding.

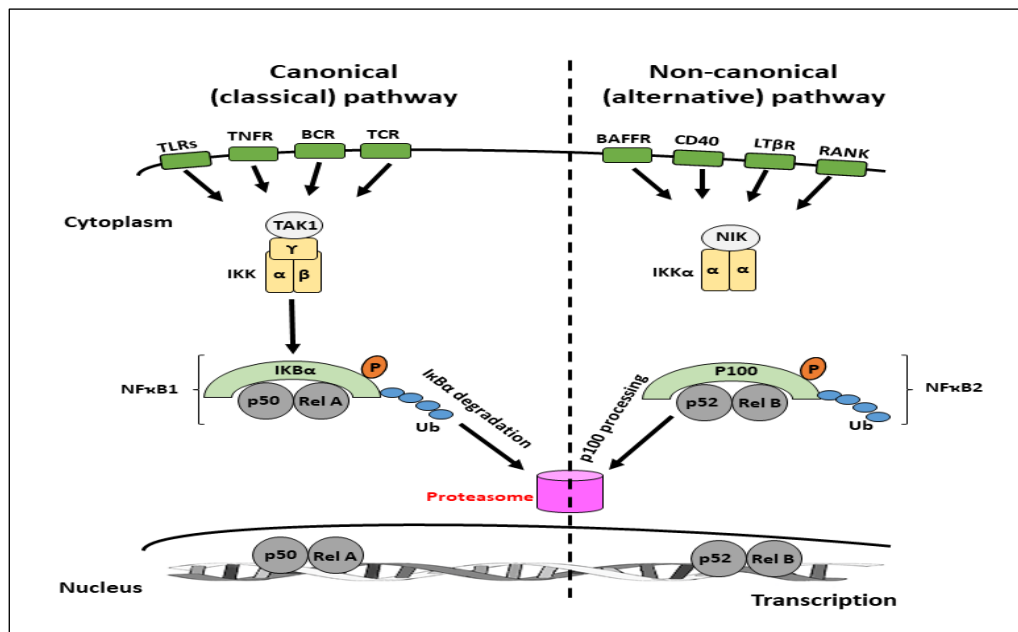


Figure 1.7: Schematic diagram summarising NFκB signalling pathways. Modified from Sun, 2011, Cell Research 21:71-85. Doi:10.1038/cr.2010.177

### 1.11 Proteomics approaches in the intestine

Proteomic analysis is the complete study of proteins that are produced and expressed in a biological system at a particular point in time. The term proteomics was first described in 1997 after Marc Wilkins (while he was a PhD student at University of Macquarie) used the term proteome to describe an entire set of proteins that were produced by an organism in response to an effector (Parker *et al.*, 2010). Proteomics relies on three basic technologies including methods of protein complex fractionation, mass spectrometry to identify individual proteins, and bioinformatics to analyse and collect the mass spectrometry data (Yu *et al.*, 2010). Specific disease biomarkers in body fluids (such as serum, plasma, and urine), tissues, and other biologic samples

have been highly investigated using proteomic analysis (Sahab *et al.*, 2007, Ahram *et al.*, 2008). Proteins are characterised by hundreds of various posttranslational modifications whose functional state differs based on their particular modifications, structural alteration, transport, and translocation (Duan and Walther, 2015). Moreover, the challenging aspect in proteomics is not only presented by the techniques that need precise protein fractionation, identification, quantification and proteome-bioinformatics, but also by the need for careful selection and reproducible processing of tissues/samples to be analysed (Titz *et al.*, 2014). This continuous evolution in protein technologies in association with data collection and analysis will enhance our capability to recognise the intestinal inflammatory proteomes that play a critical role in IBD pathogenesis (Alex *et al.*, 2009). Recently abundant research has focused on proteomic studies to identify IBD biomarkers in order to investigate disease aetiology and help establish an accurate diagnosis of IBD (Bennike *et al.*, 2014).

Apoptosis is known to be induced by various chemical compounds such as chemotherapeutic agents and pollutants due to their effect on the caspase cascade (Riedl and Shi, 2004). Apoptotic failure plays a major role in cancer development and resistance to cancer treatment. Proteomic analysis has been used to identify the substrates for proteases and protein kinases which play an important role for apoptosis and inflammation (Wang and Chen, 2011). Using proteomic analysis to analyse and identify crucial immune function related proteins and the detection of their modifications can widen our knowledge, not only to understand the clear difference in pathogenesis of IBD but also to fully understand the causes of intestinal

mucosal injuries and help in detection of medications to ameliorate IBD and other intestinal diseases related to loss of intestinal barrier function (Berndt *et al.*, 2007).

## 1.12 Aims

The intestinal epithelium exhibits a high turnover rate with a balance between shedding and generation of epithelial cells. Increased epithelial cell apoptosis over generation of new cells from intestinal crypts is one of the main causes of gut barrier dysfunction. It has been previously shown that pathological shedding of small intestinal villi epithelial cells takes place in mice injected with bacterial LPS indicating the role of NFκB Transcription proteins in regulating this phenomenon.

The main objectives of this study were to determine whether a panel of different stimuli that cause or mimic human systemic disease result in increased SIEC apoptosis and shedding along the murine crypt-villus axis and to assess how this process was altered by NFκB signaling in order to elucidate potential therapeutic approaches for diseases associated with intestinal barrier dysfunction.

The specific aims during this study were:

- 1- To investigate whether systemic LPS from different bacterial species induces pathological SIEC apoptosis and shedding in wild-type mouse and rat strains from different genetic backgrounds and of different ages.
- 2- To assess the role of the alternative NFκB signalling pathway subunit RelB in the regulation of murine SIEC apoptosis and shedding induced by LPS.
- 3- To determine whether the administration of anti-CD3 antibody, poly I:C and TNF induces pathological small intestinal epithelial apoptosis and cell shedding in C57BL/6J mice and how the NFκB signaling pathway regulates the response of small intestinal villi and crypts to these stimuli in comparison to LPS.

- 4- To evaluate the ultrastructural features of SIEC apoptosis and shedding after administration of LPS to wild-type C57BL/6J, *Nfκb1*<sup>-/-</sup>, *Nfκb2*<sup>-/-</sup> and *c-Rel*<sup>-/-</sup> mice.
- 5- To investigate how LPS alters the murine small intestinal mucosal proteome to modulate susceptibility to SIEC apoptosis and shedding and the ways in which this proteome is altered following the deletion of individual members of the NFκB family of transcription factors.

## **2. Materials and Methods:**

### **2.1 Animals**

#### **2.1.1 Mice**

Unless otherwise stated, all animals used in this work were adult female mice aged between 9-11 weeks.

Mice from five different strains were purchased from Charles River laboratory (Margate, UK) or Harlan laboratories, UK limited (Bicester, UK) and were transferred to the biomedical services unit at the University of Liverpool. Mice were housed in groups of 3 mice per GR500 cage in the Techniplast Green Line System which is comprised of individually ventilated cages each provided with an individually heap filtered air supply and extraction. In addition to the mice, 6 *Ludwig Olac Wistar rats* (4 males and 2 females) were used in one experiment. These rats were also from Charles River laboratories (Margate, UK) and were housed in group of 2 per GR1800 Double Decker cages in the Techniplast Green Line System. All rodents were provided with reverse osmosis water through an automatic watering system and maintained in a conventional specific pathogen free (SPF) unit with ad libitum food on a 12 hour light-dark cycle at University of Liverpool's Biomedical Services Unit.

##### **2.1.1.1 C57BL/6J mice**

**In-bred, wild-type C57BL/6J mice** were purchased from Charles River Laboratories (Margate, UK), kept for a one week acclimatisation period under standard animal house conditions before being used in various experiments.

**Transgenic mice, including NFκB1<sup>-/-</sup>, NFκB2<sup>-/-</sup>, cREL<sup>-/-</sup> and RelB mice** were bred at the Biomedical Services Unit (Prof. DM Pritchard team) at University of Liverpool in SPF conditions.

NFκB1<sup>-/-</sup> mice were originally produced on a C57BL/6J genetic background by Sha et al. in 1995. The targeted disruption of NFκB1<sup>-/-</sup> gene was achieved by insertion of a linearised pp50KO construct with a phosphoglycerate kinase (PGK) neo cassette into exon 6 of the NFκB1 gene that encodes residues 134-187 that lie within the Rel homology domain that extends from residues 30-330. This disruption was shown to inhibit the synthesis of functional p105 and p50 due to production of inactive protein that failed to dimerise with other NFκB proteins or bind to DNA, but did not affect the production of IκBγ from an internally promoted mRNA (Sha *et al.*, 1995). This null colony does not demonstrate abnormal development, but shows nonspecific responses to infection and defective humoral immunity due to failure of B lymphocytes to proliferate in response to bacterial lipopolysaccharides. Additionally, studies regarding the function of macrophages in this colony have indicated normality of phagocytic activity and production of TNF and IL-1 while there was reduction in production of IL-6.

NFκB2<sup>-/-</sup> mice were generated on a C57BL/6J mice background by insertion of a PGK neo cassette into exon 4 to disrupt production of p100 or p52 (Caamano *et al.*, 1998). This colony shows abnormalities in lymphoid organs with defective T- cell responses and low proliferative responses of B cells to LPS, CD40 and anti-IgD-dextran.

c-Rel<sup>-/-</sup> mice were also generated on the C57BL/6J mice genetic background. Exons 4-9 of the cREL gene encoding amino acids 145-588 of the c-Rel protein were replaced with a PGK-neo cassette. This disruption causes truncation of c-Rel proteins by

removing a sequence required for DNA binding and protein dimerisation (Kontgen *et al.*, 1995). Although c-Rel null mice show normal haematopoiesis, they show impairment in activation of T and B lymphocytes.

RelB<sup>-/-</sup> mice were also generated on the C57BL/6J mice background by Wieh *et al.*, 1995. Exons 2-7 of the Rel gene were targeted resulting in deletion of a 500bp in exon 4 at the beginning of the DNA subdomain of the Rel homology domain followed by insertion of PGK-neo cassette. These mice show reduced κB-binding activity in the lymphoid tissue with multifocal lesions, infiltration of lymphatic tissue in several organs, myeloid hyperplasia and splenomegaly due to extra-medullary haematopoiesis (Wieh *et al.*, 1995).

#### **2.1.1.2 Balb/c mice**

Inbred, wild-type Balb/c mice were purchased from Charles River Laboratories (Margate, UK), kept for a one week acclimatisation period under standard animal house conditions before being used in experiment.

#### **2.1.1.3 CD1 mice**

Outbred wild-type CD1 mice were purchased from Charles River Laboratories (Margate, UK), kept for a one week acclimatisation period under standard animal house conditions before being used in experiment.

#### **2.1.1.4 FVB/N mice**

Inbred, wild-type FVB/N mice were purchased from Charles River Laboratories (Margate, UK), kept for a one week acclimatisation period under standard animal house conditions before being used in experiment.

#### **2.1.1.5 DBA/2 mice**

Inbred, wild-type DBA/2 mice were purchased from Harlan Laboratories, UK Limited (Bicester, UK), kept for a one week acclimatisation period under standard animal house conditions before being used in experiment.

#### **2.1.2 Ludwig Olac Wistar Rats**

Adult Ludwig Olac Wistar rats aged 10-11 weeks were purchased from Charles River Laboratories (Margate, UK), kept for a one week acclimatisation period under standard animal house conditions before being used in experiment.

### **2.2 Animal procedures**

All animal procedures were performed under UK home office approval on project licences 40-3392 and 70-8457 as specified by the animals (Scientific Procedures) act 1986. All experiments were conducted by the author as a UK home office personal licensee and undertaken within the University of Liverpool in specified rooms for animal procedures.

### **2.3 Induction of Apoptosis and Shedding**

Based on previous literature, 4 different stimuli were used to induce small intestinal epithelial cell apoptosis and shedding. These included bacterial lipopolysaccharide (LPS), anti-CD3e antibody, polyinosinic:polycytidylic acid (Poly I:C) and tumor necrosis factor (TNF).

### **2.3.1 Bacterial Lipopolysaccharide (LPS)**

LPS was used from different bacterial species. This included *Escherichia coli* serotype O111:B4 as this was previously used in our laboratories to induce apoptosis and shedding of small intestinal epithelial cells (Williams *et al.*, 2013). LPS from *Salmonella enterica* serotype *enteritidis* and *Klebsiella pneumoniae* was also used. 10 mg/kg was the dose administered in the majority of experiments, but 0.125 mg/kg LPS from *Escherichia coli* was injected into C57BL/6J mice for electron microscopy and proteomic analysis studies. All LPS used was purified by phenol-extraction and was purchased from Sigma Aldrich, UK, in the form of lyophilised powder. It was then dissolved in sterile phosphate buffered saline (PBS) in a biosafety cabinet at 2 different concentrations, 1 mg/ml and 12.5 µg/ml to prepare the used doses of 10 mg/kg and 0.125 mg/kg body weight respectively. After reconstitution to a working concentration, the solution were filtered through a 0.2 µm syringe filter then aliquoted and frozen at -20°C before use. Before administration of LPS to experimental mice, it was thawed, vortexed and warmed to room temperature.

### **2.3.2 Anti-mouse-CD3e antibody (145:2C11)**

Anti-mouse-CD3e functional grade purified antibody was obtained from eBioscience™, Thermo-Fisher Scientific, UK in liquid form at a concentration of 1 mg/ml in sterile PBS and was stored at 4°C. It was then diluted in a biosafety cabinet prior to use into 50µg, 100µg, 200µg and 400µg/1 ml sterile PBS to make different concentrations of 0.5, 1, 2 and 4 mg/kg body weight that were administered via the intraperitoneal route to C57BL/6J mice.

### **2.3.3 Polyinosinic:polycytidylic acid sodium salt**

Poly I:C sodium salt-TLR tested from Sigma Aldrich, UK was obtained in the form of a lyophilised powder. It was dissolved in normal saline in a biosafety cabinet to preserve its ionic strength. The solution was heated to 50°C and then left to cool to room temperature to achieve annealing. It was administered at a concentration of 30 mg/kg body weight into C57BL/6J mice by intraperitoneal injection.

### **2.3.4 Recombinant Tumour Necrosis Factor alpha (TNF $\alpha$ )**

Murine recombinant TNF from *Escherichia coli* was purchased from PeproTech Ltd., UK. It was dissolved in sterile water in a biosafety cabinet to a concentration of 200  $\mu$ g/ml, and then it was diluted to 0.33 mg/kg body weight prior to being injected intraperitoneally into C57BL/6J mice.

## **2.4 Tissue collection and processing**

Following cervical dislocation, the entire small intestine was collected. The intestinal contents were flushed out using PBS followed by immersion of the small intestine in 10% neutral buffered formalin for 24 hours for fixation. The small intestine was then divided into 3 parts representing the proximal, middle and distal segments. These segments were bundled with 3M micropore surgical tape separately then cut into small pieces of 0.5 cm length and then stored in histological cassettes in 70% ethanol. These cassettes containing the bundled pieces of small intestine were then transferred into a Thermo Shandon Pathcentre tissue processor to be dehydrated through increased concentrations of ethanol (70%, 90% and 3 changes of 100% ethanol) followed by clearing with 3 changes of xylene then infiltrated with 2 changes of soft

paraffin wax and finally embedded in paraffin wax using a Shandon histocentre embedder. Sections of 3-5µm were cut using a microtome then transferred into a waterbath containing water heated to 40°C before placement onto glass slides for haematoxylin and eosin staining or onto 3-aminopropyltriethoxysilane (APES) coated slides for immunohistochemistry.

## **2.5 APES slide coating for Immunohistochemistry**

To increase the adhesiveness of tissue sections onto the glass slides used for immunohistochemistry, these slides were cleaned by immersion in 1% acid alcohol (1% concentrated hydrochloric acid, 70% ethanol and 29% H<sub>2</sub>O) for 30 minutes. The slides were then washed under running tap water for 5 minutes and immersed in distilled water for another 5 minutes, before removing them and leaving them to dry. After they had dried, the slides were immersed in 2 changes of acetone (2 minutes each) then in freshly prepared 2% (v/v) APES in acetone for 5 minutes followed by 2 changes of distilled water (2 minutes each) and finally were left to dry at 37°C in a fan assisted drying oven overnight before storage in dust free containers.

## **2.6 Active caspase-3 Immunohistochemistry**

Human/Mouse active caspase-3 primary antibody (rabbit polyclonal) from R&D Systems Inc., UK, was reconstituted at 0.2 mg/ml in sterile PBS, aliquoted and stored at -20°C. This antibody was first titrated to determine the optimal dilution for staining procedures. After de-waxing of the tissue sections in xylene for 10 minutes, tissue rehydration was started by immersion of the sections in decreasing concentrations of

ethanol (from 100% to 70%). Endogenous peroxidase activity was blocked by dipping the sections in 3% hydrogen peroxide-methanol solution (9 ml hydrogen peroxide in 300 ml methanol) for 5 minutes. Following washing in distilled water, tissue sections were microwaved for 20 minutes in antigen retrieval buffer (0.01M citrate buffer pH 6.0). Sections were left to cool down for 20 minutes then were washed in tris-buffered saline, 0.1% Tween<sup>®</sup>20 (TBST) for 5 minutes. Afterwards the primary antibody was applied onto the tissue sections and this was incubated in a moist dark chamber for 2 hours at room temperature. The slides were washed in TBST and incubated for 30 minutes with the secondary antibody, Envision™ HRP labelled polymer anti-rabbit (Dako), for 30minutes at room temperature. Sections were washed twice with TBST then incubated with DAB chromogen and substrate liquid solution in the dark for 6 minutes. Following washing with water, sections were counterstained with Gill no. 1 haematoxylin for 2.5 minutes, then dehydrated and mounted with DPX mountant.

## **2.7 Scoring of Active caspase-3 positively labelled cells**

Scoring of apoptotic and shedding small intestinal epithelial cells that positively labelled with active caspase-3 antibody was done based on the criteria that have been set out in Williams *et al.*, in 2013. Small intestinal epithelial cells were attributed to one of three categories:

Normal cells: if they had basophilic, basally located nuclei with no or weak non-specific brown staining cytoplasm.

Apoptotic cells: if they had basophilic, basally located nuclei with defined, clearly brown stained cytoplasm.

Shedding cells: if they had defined, clearly brown stained cytoplasm with apically

positioned nuclei or apically protruded cytoplasmic membranes.

Scoring of intestinal epithelial cells based on these features was performed on 20 well oriented hemivilli or 50 hemicrypts per mouse using a light microscope at 400x magnification. Scoring of hemivilli started at the level of crypt-villus junction and proceeded to the mid-point of the villus tip and scoring of crypts was from the crypt base to the crypt-villus junction.

Counting of positively immunolabelled cells was done by using SCORE software (Version 1, Beta 1, established by Stave Roberts, at the Paterson Institute for Cancer Research, Manchester, UK 1996) that facilitates quantification of the epithelial cells according to the previously mentioned criteria.

Scored data were saved as individual files that were later analysed with WinCrypt© software version 1.00, Release 1.9, Cancer Research Campaign 1999. This software was also used to compare the cell positional data by adjusting the villus length to a fixed length of 100 cells that allowed expressing the percentage of villus length with 0% representing the villus base and 100% indicating the villus tip.

## **2.8 Haematoxylin and Eosin (H&E) staining protocol**

After de-waxing and rehydration of tissue sections, they were stained with Gill no. 1 haematoxylin for 2.5 minutes. Following bluing of the sections under running tap water for 5-7 minutes, the sections were stained with eosin for 3.5 minutes. The excess of eosin was removed by rapid dipping of sections in water for a few seconds then sections were dehydrated with 2 changes of 90% ethanol for 1 minute each followed by 2 changes of 100% ethanol for a few seconds. Afterwards sections were cleared with xylene followed by mounting with DPX and they were left to dry prior to being

examined under the light microscope.

## **2.9 Transmission Electron Microscopy (TEM)**

Following animal dissection a small segments measuring about 3 cm in length from the proximal small intestine were directly moved to small bottles containing a solution of 4% paraformaldehyde and 2% glutaraldehyde in 0.1 M phosphate buffer pH 7.4. They were then transferred to the TEM Unit in the Department of Cellular and Molecular Physiology at the University of Liverpool where the samples were further dissected before placing them in 2.5% glutaraldehyde in 0.1M phosphate buffer pH7.4 on a rotator overnight at room temperature for fixation. The samples were then washed 3 times for 1 minute each in phosphate buffer pH 7.4 at room temperature before post-fixation with 1.5% potassium ferrocyanide reduced osmium tetroxide in 0.1M phosphate buffer. The tissue was then rinsed 3 times for 5 minutes each in double distilled water at room temperature. Post-fixation was followed by *en bloc* staining for 1 hour in 1% uranyl acetate in double distilled water at room temperature followed by Walton lead aspartate in double distilled water for 30 minutes at room temperature then washed overnight in a rotator. The samples were then dehydrated through a graded ethanol concentration series: 30%, 50%, 70% and 90 % followed by 2 changes of 100 % ethanol then 2 changes of 100 % acetone, each for 10 minutes. Afterwards the samples were infiltrated and embedded in TAAB hard cure resin overnight at 60°C. Thin sections of 0.5µm were cut and mounted on copper grids and viewed with a Tecani G2 20 S TEM for imaging.

## 2.10 Preparation of tissue for proteomic analysis

Following dissection of the proximal thirds of small intestine from control mice and mice injected with 0.125 mg/kg LPS; they were flushed several times with PBS and opened longitudinally and cut transversely into small pieces of 1 cm length, then washed thoroughly with PBS several times before harvesting into PBS on ice. Washing of these samples in PBS was continued several times by pipetting them up and down until a clear supernatant was produced. Subsequently, 20 ml of ice cold chelation buffer (2mM ethylenediaminetetraacetic acid [EDTA] stock in 500 ml PBS) was added to each sample and these were then left for 30 minutes on a roller in the cold room at 4°C. Afterwards the chelation buffer was removed and the samples were placed in a shaking buffer (43.3mM sucrose, 59.4mM sorbitol in 500ml PBS) with continuous hand shaking until the crypts were released. Remnants of the intestinal wall were removed while the other contents were centrifuged for 4 minutes to precipitate the tissue pellet. Later, 0.25 ml of 0.1M triethylammonium bicarbonate (TEAB) in 0.1 % sodium dodecyl sulphate (SDS) was added with pipetting up and down to disrupt the tissue pellet, this was then left on ice for 30 minutes to lyse the cells. The lysed cells then were centrifuged at 13,000 rpm for 15 minutes at 4°C. Following spinning of the cells, the supernatant was transferred carefully into a new eppendorf tube clearly labelled with the mouse strain, mouse number and treatment. To determine the concentration of proteins in the extracted supernatant, the samples were assessed using an ultra-violet spectrophotometer. 300 µg protein in 100 µl buffer was measured and stored in well labelled self-lock eppendorf tubes at -80°C. These were then posted in a package containing dry ice to the Proteomics Research Technology Platform at the University of Warwick for proteomic analysis. This proteomic experiment were designed to

compare the protein levels between the various tested mouse strains (C57BL/6J *Nfκb1*<sup>-/-</sup>, *Nfκb2*<sup>-/-</sup> and *c-Rel*<sup>-/-</sup>), and also before and after LPS administration (C57BL/6J vs LPS-treated C57BL/6J, *Nfκb1*<sup>-/-</sup> vs LPS-treated *Nfκb1*<sup>-/-</sup>, *Nfκb2*<sup>-/-</sup> vs LPS-treated *Nfκb2*<sup>-/-</sup> and *c-Rel*<sup>-/-</sup> vs LPS-treated *c-Rel*<sup>-/-</sup> mice).

Protein extracts were further fractionated to reduce their complexity using sodium dodecyl sulfate–polyacrylamide gel (SDS-PAGE) electrophoresis followed by in-gel trypsin digestion to produce peptides that allow the identification and quantification of proteins by mass spectrometry using Tandem mass tags (TMT-10 plex assay that assayed 10 samples at once in a single mass spec experiment by labelling each sample with a different tag) (Plubell *et al.*, 2017). Mass spectrometry started with chromatography of the peptides by reverse phase C<sub>18</sub> attached to an electrospray ionisation source to calculate the mass of peptides and their fragments. Afterwards, matching of calculated protein digests and peptide fragments with the real peptide fragments acquired in the mass spectrometer was performed using protein and peptide identification search engine software and known protein sequences (Plubell *et al.*, 2017). These searches used a reversed sequence decoy strategy to control the peptide false discovery rate and identifications were validated using Percolator software (an algorithm for improving the rate of confident peptide identification, Kall *et al.*, 2007). Only peptides with a q score (adjusted p value using an optimised false discovery rate) ≤0.05 were accepted and only one peptide was required to match the protein record for identification (Plubell *et al.*, 2017). After identification, a common combined internal standard was used to normalise the data across different TMT experiments. This enabled proteins to be presented with their individual intensity scale measurements rather than their relative intensities. Three reference values for

each protein were generated and were averaged to find the geometric mean from which a scaling factor was calculated (known as internal reference scaling (IRS)). Finally, protein abundances were determined and compared using IRS normalised total reporter ion intensities between different groups using the Bioconductor package edgeR that normalises, tests and calculates the false discovery rate to identify and quantify proteins and their modifications during the process of LPS induced SIEC apoptosis and shedding (Plubell et al., 2017).

## **2.11 Data and Statistics**

Data are expressed as mean  $\pm$  standard error of the mean (SEM). Statistical analysis was performed using one-way ANOVA with Dunnett *post-hoc* test for multiple comparisons with control for normally distributed data while non-parametric data were tested by ANOVA on ranks (Kruskal-Wallis). Differences were considered to be significant where  $p < 0.05$ . Data sets consisting of 2 groups were assessed by Student's t-test. In some situations, the modified median test was used to evaluate the significant differences at individual cell positions.

### **3. Characterisation of the effects of lipopolysaccharide on proximal small intestinal epithelial cell apoptosis and shedding**

#### **3.1 Introduction**

Maintenance of gut barrier haemostasis is determined by the equilibrium between the number of cells that are shed at the villus tips and the number of cells that are newly formed in intestinal crypts (Ikeda *et al.*, 1997). The process of active programmed cell death termed apoptosis is characterised by various alterations in cell morphology including nuclear chromatin condensation, compaction of cytoplasmic organelles, membrane blebbing and fragmentation of the cell into apoptotic bodies (Kerr *et al.*, 1972).

LPS has been previously shown to induce pathological SIEC apoptosis and shedding in adult C57BL/6J mice (10-11 weeks old). This phenomenon is observed 1 hour after IP injection of LPS from *Escherichia coli* serotype O111:B4 then increases to reach the peak amount at 1.5 hours and resolves approximately 3 hours post LPS administration. These findings were characterised by marked villus atrophy with presence of large numbers of shedding cells detached into the small intestinal lumen (Williams *et al.*, 2013).

Various different inbred mouse strains have previously been shown to respond differently to similar stimuli due to inherent genetic differences (Pritchard *et al.*, 2000 and Sellers *et al.*, 2012). To establish the role of genetic differences in regulating LPS induced SIEC apoptosis and shedding, five different mouse strains were used to

investigate pathological small intestinal apoptosis and shedding 1.5 hours after IP injection of 10mg/kg LPS from *Escherichia coli* serotype O111:B4.

IBD is a chronic disease that primarily starts in young adults and in elderly people. The majority of patients diagnosed with IBD are adults (between 20-40 years old), but lower incidence rates are also seen in elderly and young people (about 20% in children and 16% in adult over age of 65 years) (Prelicpean *et al.*, 2013). To investigate whether any age related factors affect the process of SIEC apoptosis and shedding, three different age groups of C57BL/6J mice were studied representing three different periods of life (puberty, adulthood and old age). These groups were injected IP with 10 mg/kg *Escherichia coli* serotype O111:B4 LPS and SIEC apoptosis and shedding was assessed after 1.5 hours.

Mathiak and colleagues in 2003 tested the stimulatory effect of purified LPS from various different bacterial sources (*E. coli*, *S. typhosa*, *P. aeruginosa*, and *K. pneumoniae*) on the production of cytokines and chemokines. They found that LPS originating from different bacterial sources exhibited different effects upon the production of inflammatory mediators. We therefore investigated whether C57BL/6J female mice exhibited similar or different amount of SIEC apoptosis and shedding at 1.5 hours post IP administration of 10 mg/kg LPS extracted from three different bacterial species namely *Escherichia coli* serotype O111:B4, *Salmonella enterica* serotype *enteritidis* and *Klebsiella pneumoniae*.

Many previous studies have indicated morphological similarities between small intestinal apoptosis and shedding in humans, mice and rats (whole cell extrusion) and have suggested that these rodents can be used as reliable models for studying the

regulation of human SIEC apoptosis and shedding (Bullen *et al.*, 2006 and Williams *et al.*, 2015). Based on this suggestion, we compared SIEC apoptosis and shedding in mice and rats treated with 10 mg/kg of *Escherichia coli* LPS serotype O111:B4 at 1.5 hours post IP administration.

The NFκB family of transcription factors regulate various different biological processes including the immune response and inflammation via two different signalling pathways. NFκB1, RelA and cRel signal via the canonical (classical) activation pathway, whereas NFκB2 and RelB signal via the non-canonical (alternative) activation pathway. A previous study in our laboratory described the role of three of these transcription factors in regulating SIEC apoptosis and shedding (NFκB1, c-Rel and NFκB2) and suggested an important role for the alternative NFκB2 signalling pathway in enhancing LPS induced small intestinal injury, while NFκB1 and c-Rel played important roles in suppressing LPS induced SIEC apoptosis and shedding (Williams *et al.*, 2013). To further investigate the role of the alternative NFκB activation pathway in regulating LPS induced SIEC apoptosis and cell shedding we injected *RelB* null mice (*RelB*<sup>+/+</sup>, *RelB*<sup>+/-</sup> and *RelB*<sup>-/-</sup>) IP with 0.125 mg/kg *Escherichia coli* LPS serotype O111:B4 for 1.5 hours.

Having established the role of LPS in inducing SIEC apoptosis and shedding in the villus and recognising the role of the NFκB family of proteins in regulating this phenomenon we tested the role of these transcription factors in regulating LPS induced small intestinal crypt epithelial cell apoptosis 24 hours post administration of 0.125 mg/kg *Escherichia coli* LPS serotype O111:B4.

### **3.2 LPS caused apoptosis and shedding of proximal small intestinal epithelial cells in different mouse strains**

Our first investigation indicated increased numbers of apoptotic cells on the apical half of intestinal villi of all mouse strains treated with LPS (Figure 3.1). IP injection of LPS at 10 mg/kg, caused significant increases in the percentage of active caspase-3 positively labelled intestinal epithelial cells (Figure 3.2) from  $1.0 \pm 0.03$ ,  $0.8 \pm 0.103$ ,  $0.6 \pm 0.07$ ,  $0.3 \pm 0.03$  and  $0.8 \pm 0.07$  % to  $9.2 \pm 0.05$ ,  $6.4 \pm 0.58$ ,  $6.9 \pm 0.096$ ,  $6.6 \pm 0.03$  and  $6.9 \pm 0.12$  % in C57BL/6J, Balb/C, CD1, FVB/N and DBA/2 mouse strains respectively (all  $P < 0.0001$ ,  $N = 6$ ; ANOVA). This indicates that LPS increases the amount of pathological intestinal epithelial cell shedding in all mouse strains tested. There were no significant differences observed in the intestinal epithelial response to LPS between C57BL/6J, CD1 and DBA/2 mice and also between Balb/C, CD1, and FVB/N strains. However we observed minor differences between C57BL/6J and FVB/N mice ( $p < 0.05$ ) and between C57BL/6J and Balb/C mice ( $p < 0.01$ ). Based on cell positional plots (Figure 3.3), the effect of LPS appeared to occur predominantly in the apical portion of small intestinal villi in all mouse strains examined.

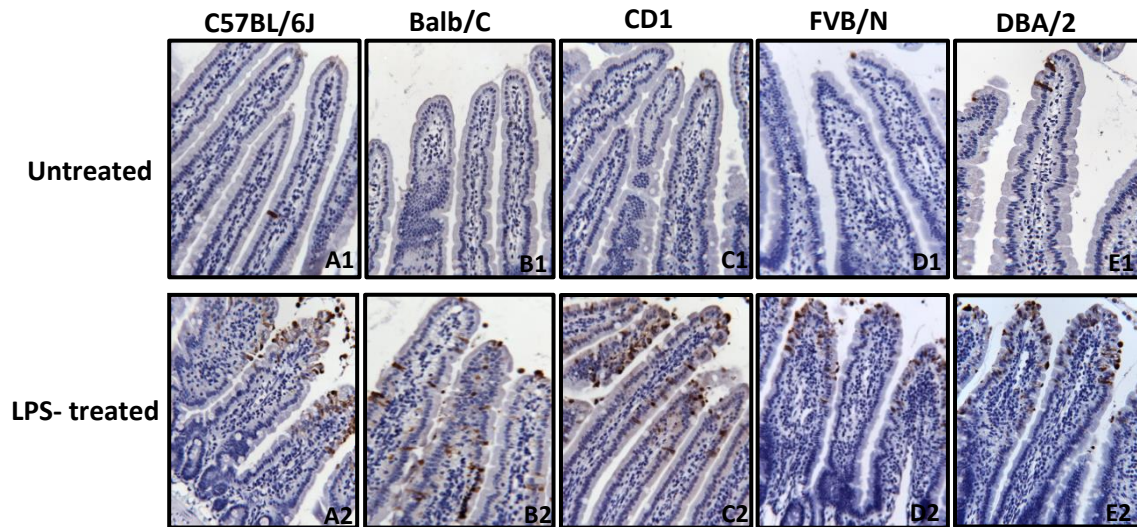


Figure 3.1: Active caspase-3 IHC in sections of proximal segment of small intestine of different tested mouse strains demonstrating the location of positively labelled SIEC along the villus axis (X40).

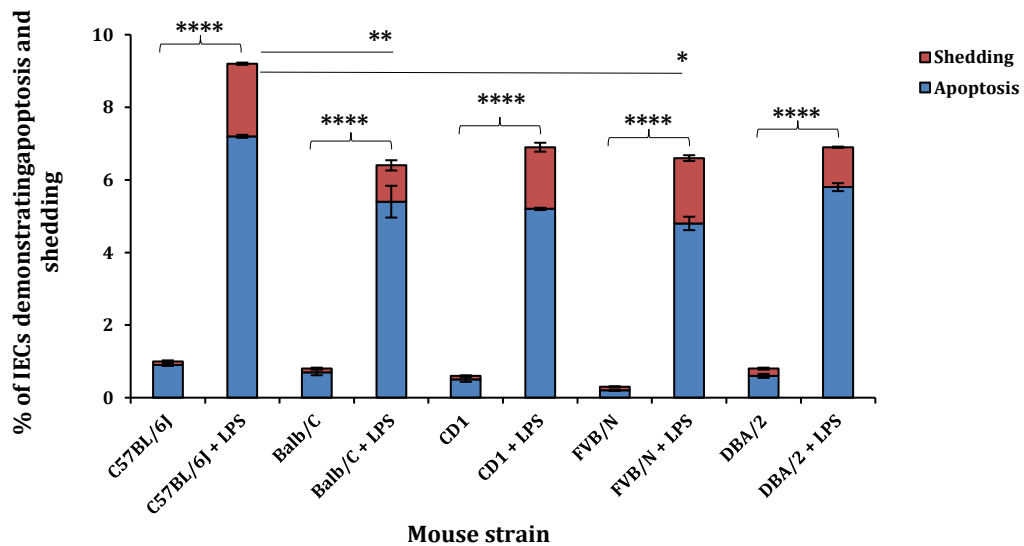


Figure 3.2: Bar chart representing the percentage of IECs undergoing apoptosis and shedding in LPS treated versus untreated mice of different strains, LPS-treated groups vs. untreated groups (N=6); \*\*\*\*P<0.0001, \*\*P<0.01, \*P<0.05, ANOVA.

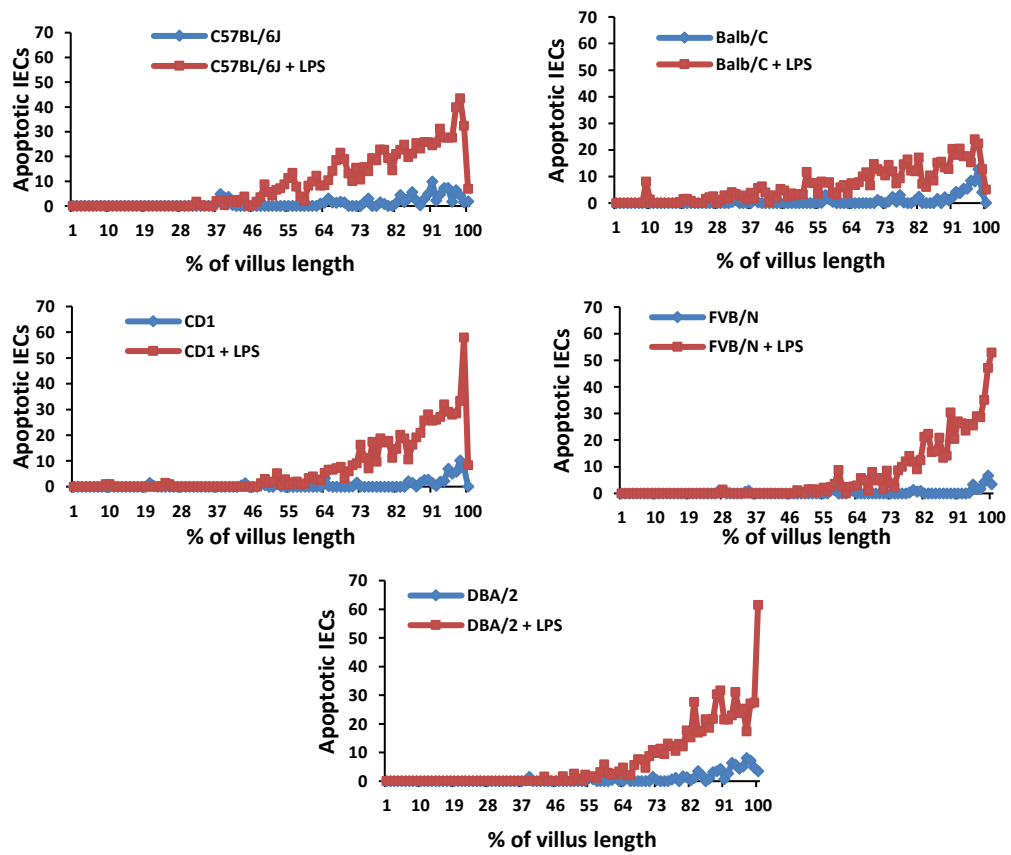


Figure 3.3: Cell positional graphs showing quantification of positively immuno-labelled IECs along the villus axis of treated mice compared to untreated mice for each mouse strain (N=6 mice per group).

### **3.3 No age related differences in small intestinal cell shedding or apoptosis were observed between six, ten and twenty eight week old C57BL/6J mice following administration of LPS**

We noted that in all age groups, active caspase-3 labelled cells were positioned in the upper half of intestinal villi 1.5 hours following LPS administration. There was also a significant increase in the percentage of intestinal epithelial cells undergoing shedding and apoptosis following administration of 10 mg/kg body weight of *Escherichia coli* LPS in all tested age groups of mice (Figure 3.4). The percentages of cell shedding and apoptosis were increased from  $0.4 \pm 0.04$ ,  $1 \pm 0.03$  and  $1.1 \pm 0.06\%$  to  $8.2 \pm 0.20$ ,  $9.2 \pm 0.05$  and  $8.8 \pm 0.17\%$  in 6 week, 10 week and 28 week old mice respectively (all  $P < 0.0001$ ,  $N=6$ ; ANOVA. Figure 3.5). This indicates that LPS at 10 mg/kg has the ability to cause an equal amount of pathological cell shedding and apoptosis in the small intestinal epithelia of C57BL/6J mice in all tested age groups (representing puberty, young adulthood and mature periods of life). Again the cell positional plots (Figure 3.6) indicated that LPS appeared to cause greater effects at the villus tip than in the basal region of small intestinal villi in all three tested ages of mice.

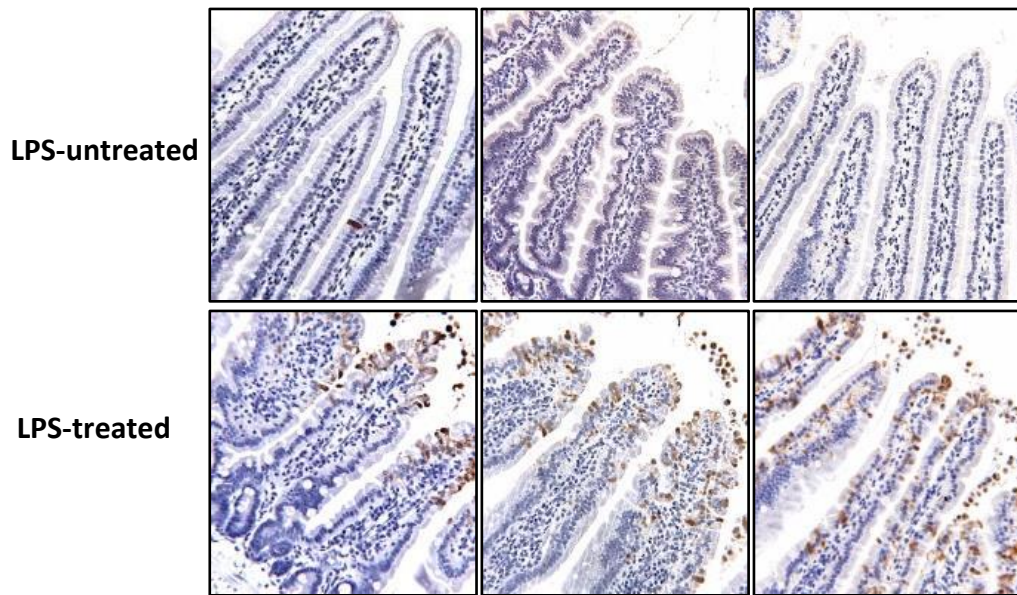


Figure 3.4: Active caspase-3 IHC in sections of proximal segment of small intestine demonstrating the location of positively labelled SIEC along the villus axis in small intestine of 3 different age groups. (X40).

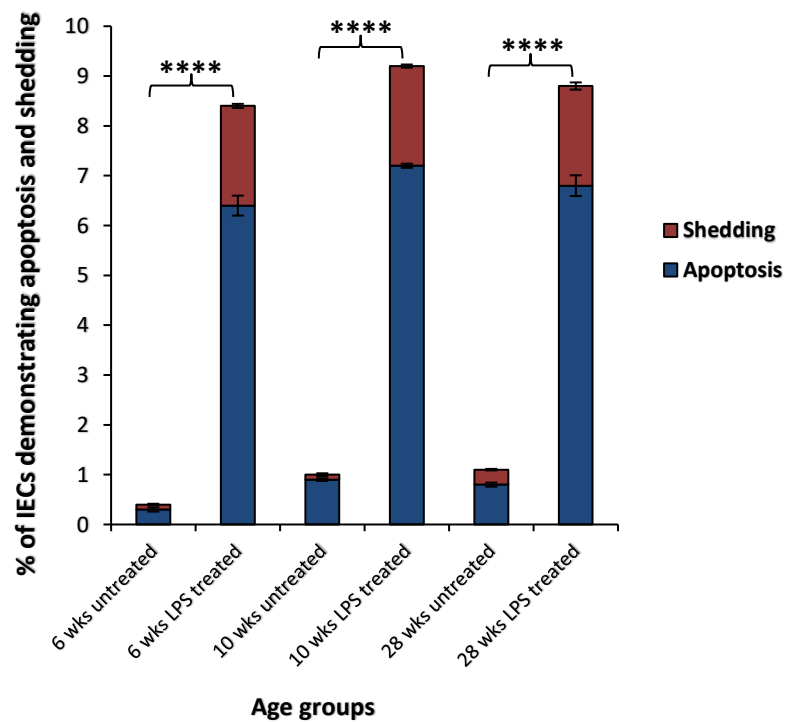


Figure 3.5: Bar chart representing the percentage of intestinal epithelial cell shedding in LPS-treated versus untreated control C57BL/6J mice at different age groups, (N=6); \*\*\*\*P<0.0001, ANOVA.

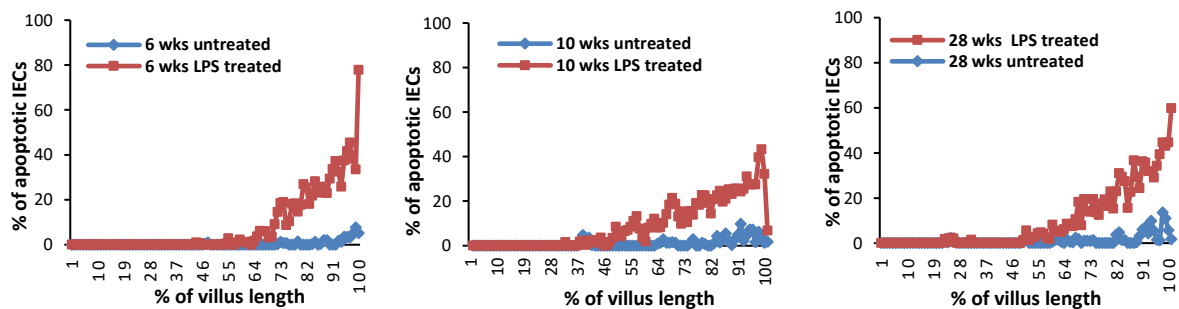


Figure 3.6: Cell positional graphs showing quantification of positively immuno-labelled IECs along the villus axis of LPS-treated mice compared to untreated C57BL/6J mice for each age group of mice (N=6 mice per group).

### 3.4 LPS from different bacterial sources induced pathological apoptosis and shedding of small intestinal epithelial cells to different extents

Interestingly we observed that LPS purified from three different bacterial species had the ability to induce apoptosis and shedding of small intestinal epithelial cells in C57BL/6J mice in the apical half of small intestinal villi (Figure 3.7). The percentage of pathological shedding and apoptosis was significantly increased from  $1.1 \pm 0.03\%$  in untreated mice to  $9.2 \pm 0.06\%$ ,  $6.7 \pm 0.13\%$  and  $6.5 \pm 0.096\%$  in mice injected with LPS from *E. coli*, *Klebsiella pneumonia* and *Salmonella enterica* respectively (all  $P < 0.0001$ ,  $N = 6$ ; ANOVA). On other hand, there was a significant difference in the percentage of small intestinal epithelial cell shedding between the 3 different LPS types used in this experiment ( $P < 0.0001$ ). The LPS from *E. coli* caused a higher degree of pathological SIEC apoptosis and shedding than the LPS from *Klebsiella pneumonia* and *Salmonella enterica* (Figure 3.8). Based on cell positional plots (Figure 3.9), LPS from all the

bacterial species used in this experiment again caused effects predominantly at the villus tips rather than in the basal parts of the intestinal villi.

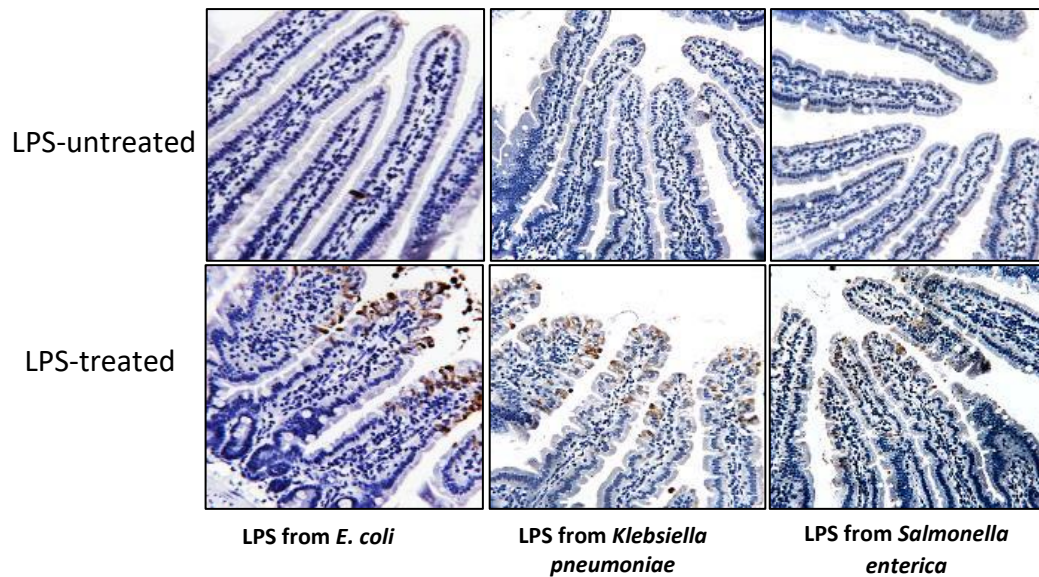


Figure 3.7: Active caspase-3 IHC in sections of proximal segment of small intestine demonstrating the location of positively labelled SIEC along the villus axis in the small intestine of C57BL/6J mice treated with LPS purified from different bacterial species. (X40).

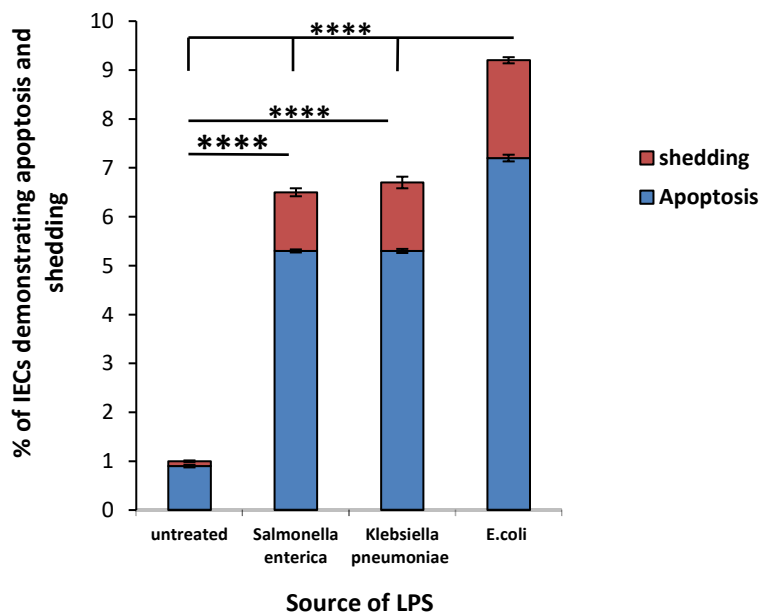


Figure 3.8: Bar chart demonstrating a comparison between the percentage of intestinal epithelial cell apoptosis and shedding in C57BL/6J mice treated with LPS purified from different bacterial sources against an untreated group, (N=6); \*\*\*\*P<0.0001, ANOVA.

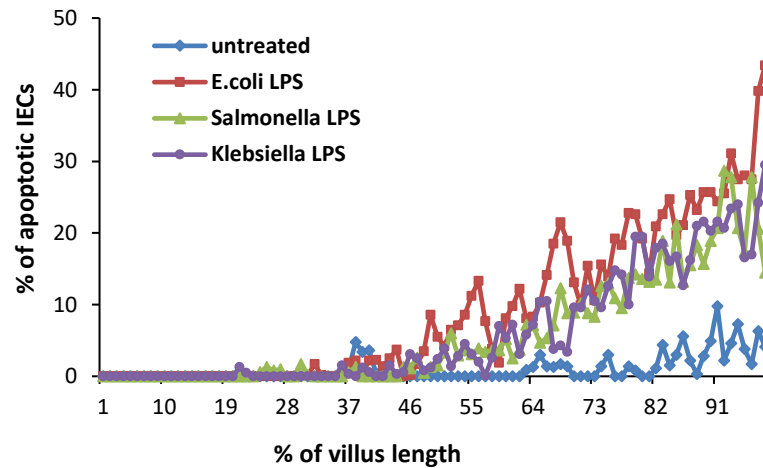


Figure 3.9: Cell positional graphs indicating the quantification of positively immunolabelled IECs along the villus axis of C57BL/6J mice treated with different types of bacterial LPS versus an untreated group (N=6 mice per group).

### 3.5: Do rats and mice respond differently to systemically induced bacterial LPS?

After finding that LPS induced murine small intestinal epithelial cell apoptosis and shedding, we tested whether LPS induced similar effects on rat small intestinal epithelial cells. *Ludwig Olac Wistar* rats were injected IP with 10 mg/kg LPS purified from *Escherichia coli* serotype O111:B4 and were euthanased after 1.5 hours. Interestingly, active caspase-3 immunohistochemistry clearly indicated positively labelled apoptotic and shedding epithelial cells in the rat small intestine (Figure 3.10). Following 10 mg/kg LPS, C57BL/6J mice revealed a percentage of  $9.2 \pm 0.05\%$  apoptotic and shedding small intestinal epithelial cells compared to  $1.0 \pm 0.03\%$  in untreated mice. *Ludwig Olac Wistar* rats similarly exhibited a significant increase in small intestinal epithelial cell apoptosis and shedding from  $1.1 \pm 0.07\%$  in untreated rats to  $4.0 \pm 0.22\%$  in rats injected with 10 mg/kg LPS for 1.5 hours ( $P < 0.001$ , one way ANOVA).

However, there was a significant difference between the percentage of SIEC apoptosis and shedding in C57BL/6J mice and *Ludwig Olac Wistar* rats ( $9.2\pm 0.05\%$  and  $4.0\pm 0.22\%$  respectively,  $P<0.0001$ , one way ANOVA). Nonetheless, we demonstrated that LPS has an ability to induce SIEC apoptosis and shedding in rats in the same way as in mice (Figure 3.11-A). In spite of the significant difference in the degree of response between mice and rats, the cell positional plots (Figure 3.11-B) showed similar patterns of apoptosis and shedding of SIECs in LPS treated groups of mice and rats.

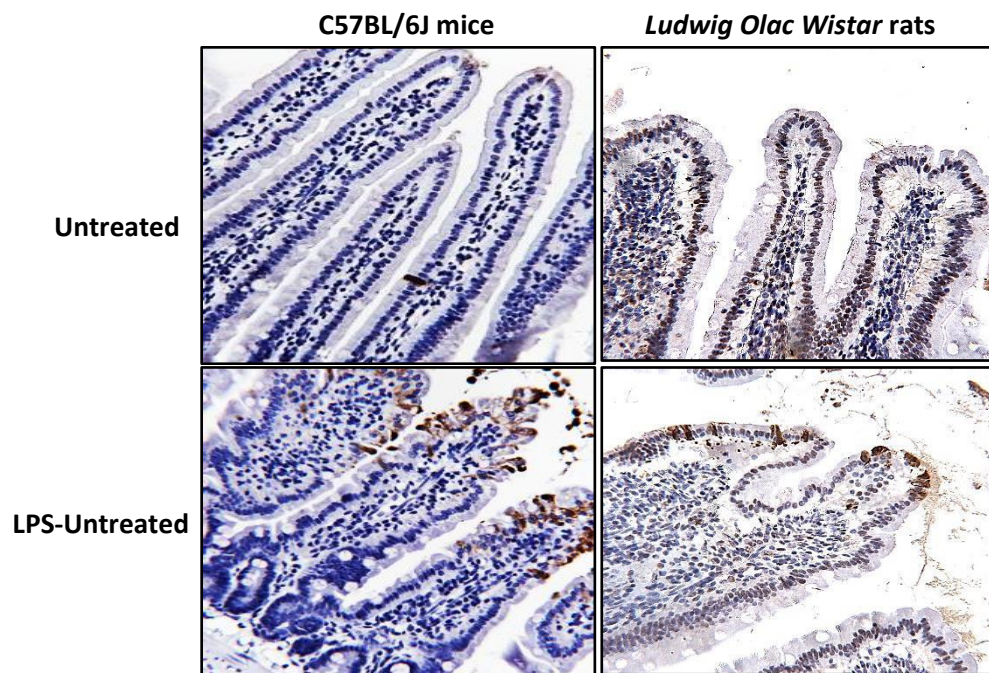


Figure 3.10: Active caspase-3 IHC in sections of proximal small intestinal segment of C57BL/6J mice versus *Ludwig Olac Wistar* rats demonstrating the location of positively labelled SIEC along the villus axis. (X40)

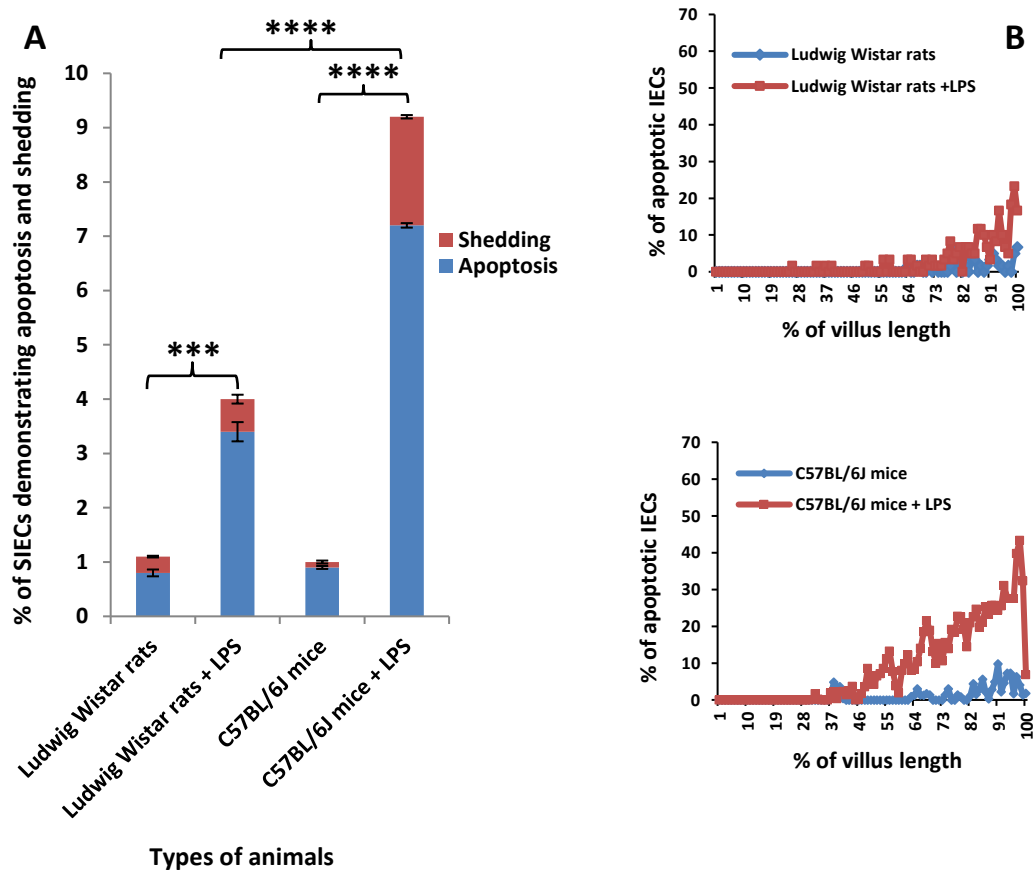


Figure 3.11: **A**: Bar chart demonstrating a comparison between the percentage of intestinal epithelial cell apoptosis and shedding in C57BL/6J mice and Ludwig Wistar rats pre and 1.5 hours post 10mg/kg LPS administration. (N=6); \*\*\*P<0.001, \*\*\*\*P<0.0001, ANOVA. **B**: Cell positional graphs showing quantification of active caspase-3 positive IECs along the villus axis of LPS treated vs untreated mice in comparison to LPS treated vs untreated rats (N=3).

### 3.6 RelB does not regulate LPS induced SIEC apoptosis and shedding:

Previous studies had indicated that LPS induced SIEC apoptosis and shedding were regulated by the NF $\kappa$ B signaling pathways. However this was only apparent using the lower LPS dose of 0.125 mg/kg. The RelB transcription factor is another member of the NF $\kappa$ B family that signals via the non-canonical activation pathway. After injecting 3 genotypes of RelB mice (*RelB*<sup>+/+</sup>, *RelB*<sup>+/-</sup> and *RelB*<sup>-/-</sup>), with 0.125 mg/kg LPS we found the percentage of SIEC apoptosis and shedding after 1.5 hours was increased from 0.6 $\pm$ 0.09, 0.3 $\pm$ 0.04 and 0.4 $\pm$ 0.05% to 5.4 $\pm$ 0.66, 5.2 $\pm$ 0.66 and 5.5 $\pm$ 0.63% in *RelB*<sup>+/+</sup>, *RelB*<sup>+/-</sup> and *RelB*<sup>-/-</sup> respectively (see Figure 3.13-A). The cell positional graph (Figure 3.13-B) again showed similar features with more apoptotic and shedding cells being observed on the apical half of small intestinal villi in all tested *RelB* genotypes. These findings suggesting that the RelB transcription factor does not play a significant role in the regulation of LPS induced apoptosis and shedding.

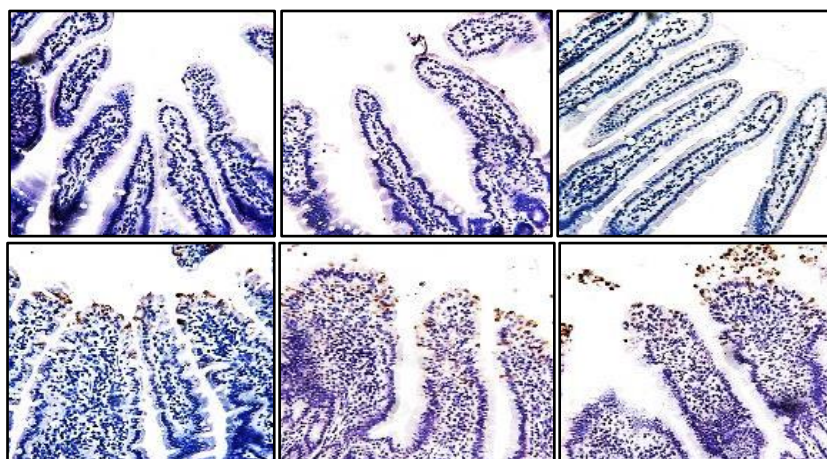


Figure 3.12: Active caspase-3 IHC in sections of proximal segment of small intestine of *RelB* mice (of different genotypes) demonstrating the location of positively labelled SIEC along the villus axis. (X40).

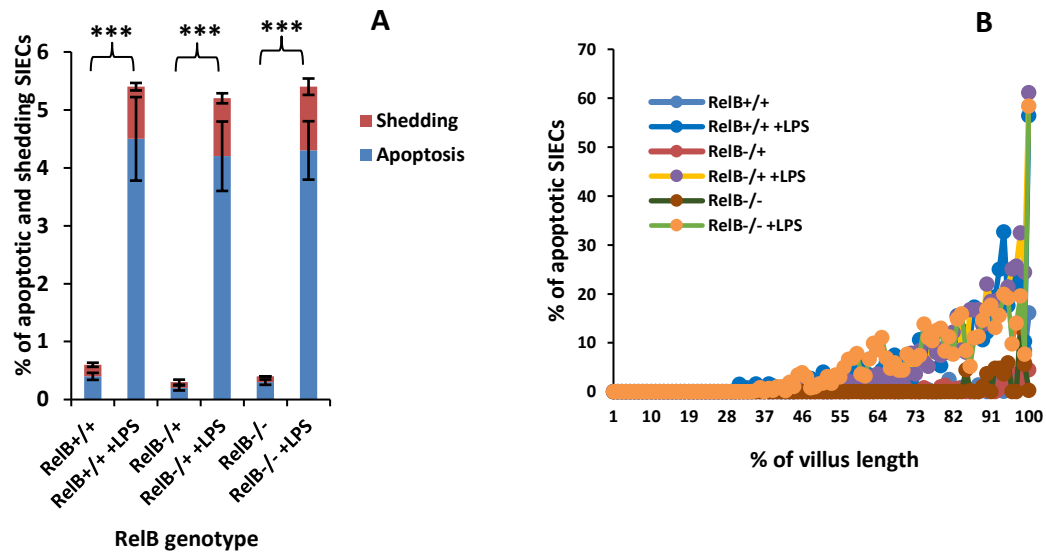


Figure 3.13: **A**: Bar chart representing the percentage of SIEC apoptosis and shedding in different *RelB* genotypes 1.5 hours post injection of 0.125 mg/kg LPS (N=5, \*\*\*P<0.001, ANOVA). **B**: Cell positional graph demonstrating quantification of active caspase-3 positively labelled cells along the villus axis of *RelB*<sup>+/+</sup>, *RelB*<sup>+/-</sup> and *RelB*<sup>-/-</sup> mice 1.5 hours after 0.125 mg/kg LPS.

### 3.7 At 24 hours post administration of LPS, significant apoptosis was observed in the small intestinal crypts of *Nfκb1*<sup>-/-</sup> and *c-Rel*<sup>-/-</sup> mice but not in wild-type and *Nfκb2*<sup>-/-</sup> mice

Various previous studies of the small intestinal injury caused by LPS have focused on its effects on crypt cells at 4 hours' time onwards. A previous study in our laboratory studied small intestinal crypt apoptosis in wild-type C57BL/6J mice treated with LPS at different time points ranging from 1 hour to 6 hours and showed that no significant changes were seen throughout the time course studied. However, when *Nfκb1*<sup>-/-</sup>, *Nfκb2*<sup>-/-</sup> *c-Rel*<sup>-/-</sup> in addition to wild-type C57BL/6J mice were injected with 0.125 mg/kg

LPS for 24 hours, we observed an increase in the number of active caspase-3 positively labelled crypt epithelial cells (accompanied by some non-stained cells which had cell death characteristics that represent non-apoptotic cell death) in *Nfκb1*<sup>-/-</sup> and *c-Rel*<sup>-/-</sup> mice but not in wild-type and *Nfκb2*<sup>-/-</sup> mice (Figure 3.14). Quantification of apoptotic cells (Figure 3.15) showed that the percentage of apoptotic small intestinal crypt epithelial cells (caspase-3 positive cells) was 0.2±0.09% in *Nfκb1*<sup>-/-</sup> whereas it was 0.1±0.03%, 0.1±0.03% and 0.1±0.05% in wild-type C57BL/6J, *Nfκb2*<sup>-/-</sup> and *c-Rel*<sup>-/-</sup> mice respectively. Furthermore, percentage of the cells with non-apoptotic cell death was significantly increased in *Nfκb1*<sup>-/-</sup> and *c-Rel*<sup>-/-</sup> mice representing 0.5±0.05% and 0.04±0.07% respectively (P<0.01 and P<0.05, ANOVA, Kruskal-Wallis test for non-parametric data) while it was 0.2±0.03% and 0.3±0.03% in C57BL/6J and *Nfκb2*<sup>-/-</sup> mice respectively. Moreover, the cell positional graphs (Figure 3.16) did not show an obvious pattern in all tested groups. In order to determine the position of the crypt cells that contributed to the significant alteration in *Nfκb1*<sup>-/-</sup> and *c-Rel*<sup>-/-</sup> mice we used the modified median test and this indicated that the majority of cell death seen was between cell position 6 and 12 from the base of the small intestinal crypts.

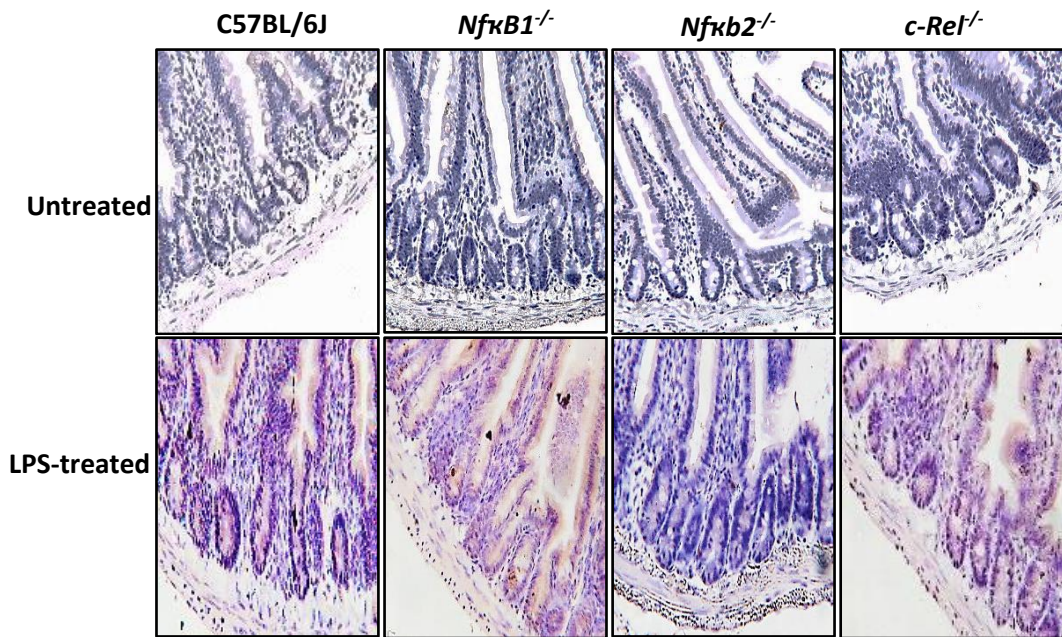


Figure 3.14: Active caspase-3 IHC in sections of proximal segment of small intestine of C57BL6J mice (different genotypes) injected with 0.125mg/kg LPS for 24 hours demonstrating the location of positively labelled SIEC along the crypt axis. (X40).

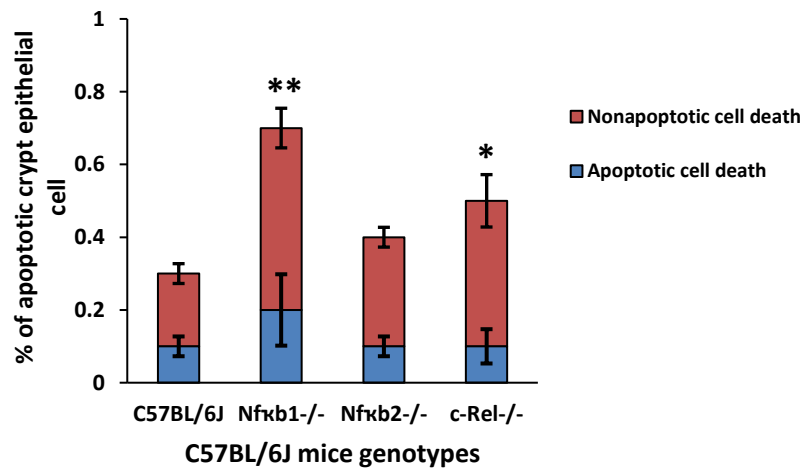


Figure 3.15: Quantification of apoptotic (positive active caspase-3) and non-apoptotic (negative active caspase-3) cells in proximal small intestinal crypt epithelial cells 24 hours after IP injection of 0.125 mg/kg LPS, (N=6, \*P<0.05, \*\*P<0.01).

(Position of significant apoptosis, Modified median test)

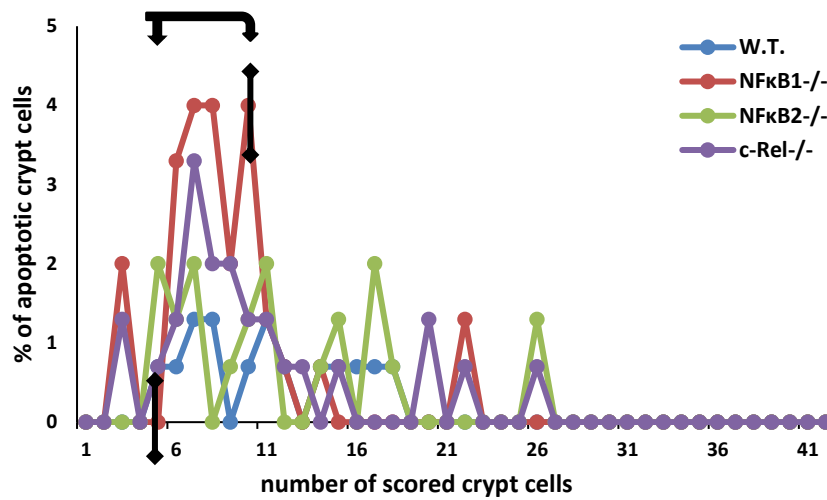


Figure 3.16: Cell positional graph indicating the apoptotic cell positions (based on modified median test) in different C57BL/6J mice genotypes (wild-type, *Nfκb1*<sup>-/-</sup>, *Nfκb2*<sup>-/-</sup> and *c-Rel*<sup>-/-</sup>) 24 hours post administration of 0.125 mg/kg LPS, (N=6).

### 3.8 Discussion

The data provided in this chapter provide more detailed information on the effect of LPS on murine and rat proximal small intestinal epithelial cells. We firstly investigated whether LPS induced the pathological shedding of small intestinal epithelial cells in five different mouse strains. Our results showed that 10 mg/kg LPS significantly induced pathological cell shedding and apoptosis in murine small intestinal epithelial cells in all tested mouse strains. However, the highest amount of cell shedding and apoptosis was observed in C57BL/6J mice (Williams *et al.*, 2013), whereas Balb/C mice showed lower amounts (see Figure 3.2). Various mouse strains have also previously been shown to respond differently to other drugs and chemicals (Pritchard *et al.*,

2000) and this may explain the difference in the degree of response among the tested strains.

Xiao *et al.*, 2001 examined age related changes in the proliferation and apoptosis of intestinal epithelial cells and found that the number of apoptotic cells decreased with age. Other studies have indicated that inflammatory bowel disease occurs most commonly in young adulthood, but also sometimes presents in childhood and elderly people (Duricova *et al.*, 2014). To clarify the role of age in influencing LPS induced small intestinal epithelial cell apoptosis and shedding, we tested three different age groups of mice representing puberty, young adulthood and the older periods of life. Our results indicated that there were no age related changes in response to LPS as the three age groups responded similarly to the administered dose of LPS.

One of the most interesting results shown in this chapter was obtained when we tested LPS from 3 different bacteria (*Escherichia coli*, *Klebsiella pneumonia* and *Salmonella enterica*). We found that the *E. coli* LPS more strongly induced the shedding and apoptosis of intestinal epithelial cells than the other two types of bacterial LPS. The LPS purified from *Escherichia coli* is the most commonly utilised serotype for inducing endotoxic shock responses in mice (Compos *et al.*, 1994) and this difference may be due to the antigenic specificity of the LPS molecule (Van Amersfoort *et al.*, 2003). However, LPS from all three bacterial sources significantly induced pathological cell shedding in the murine small intestinal epithelium. The cell positional distribution of apoptosis and cell shedding had similar patterns in all strains and all ages of mice with all bacterial sources of LPS tested, with the exception that in

Balb/C mice the distribution tended to be more basal whereas pathological cell shedding occurred more often in the apical part of intestinal villi in all other cases.

Most of the previous studies describing the mechanism and morphology of intestinal epithelial cell apoptosis and shedding have used mice due to the similarity between the physiological process of apoptosis and cell shedding between mice and humans (Bullen *et al.*, 2006 and Williams *et al.*, 2015). To investigate whether another rodent species, the rat, responded similarly, we tested whether LPS induced small intestinal epithelial cell apoptosis and shedding after administration of 10 mg/kg LPS. The number of apoptotic small intestinal epithelial cells was dramatically increased in both mice and rats (see Figure 3.11 A & B), although there was a significant difference between species. In a previous study to explore the sepsis induced by LPS in rats and mice, Thomas RC *et al.*, 2014 assessed the responses to different doses of LPS in mice and rats and found that the dose that resulted in an inflammatory response in C57BL/6J mice might or might not elicit a similar response in Wistar rats. This may explain the difference in the degree of response between C57BL/6J mice and Ludwig Wistar rats that we used in the current assessment of LPS induced small intestinal epithelial cell apoptosis and shedding.

Previous studies have demonstrated an important role of the non-canonical NF $\kappa$ B signalling pathway in activation of pathological apoptosis and shedding of small intestinal epithelial cells (Williams *et al.*, 2013). We therefore assessed the role of the RelB subunit. Unexpectedly *RelB*<sup>+/+</sup>, *RelB*<sup>+/-</sup> and *RelB*<sup>-/-</sup> mice treated with 10 mg/kg LPS for 1.5 hours showed no differences in the response to LPS suggesting that the RelB protein has no major role in preventing or enhancing the process of SIEC apoptosis.

Most previous studies describing the small intestinal injury associated with sepsis and endotoxic shock have focused on the intestinal pathology that occurs at time points later than 4 hours. (Alscher *et al.*, 2001, Mura *et al.*, 2005, Guma *et al.*, 2011). These late phase effects were observed on small intestinal crypt epithelial cells. Previous work in our laboratory quantifying apoptosis in small intestinal crypt epithelial cells using active caspase-3 immunohistochemistry indicated non-significant changes during the time course from 1.5 hours up to 6 hours post administration of LPS (Williams *et al.*, 2013). This result was however based on quantifying active caspase-3 positively labelled crypt cells only and ignored any morphological signs in non-labelled crypt epithelial cells. In the study described in this chapter we injected the different C57BL/6J mice genotypes with 0.125 mg/kg LPS and 24 hours later we prepared the proximal small intestine for active caspase-3 immunohistochemistry. We counted the cells that undergo programmed cell death based on two criteria; active caspase-3 positively labelled cell (apoptotic cell death) and active caspase-3 negatively labelled cells (non-apoptotic cell death). Based on active caspase-3 IHC, positively labelled crypt epithelial cells were slightly increased in *Nfκb1*<sup>-/-</sup> mice but not in *Nfκb2*<sup>-/-</sup> and *c-Rel*<sup>-/-</sup> mice in comparison to wild-type C57BL/6J mice. This result supports the previous result in our laboratory, by Williams *et al.*, 2013, which indicated that LPS did not significantly cause an increase in the percentage of apoptotic cells in small intestinal crypts. However, when we counted the cells based on morphological features of cell death, the percentage of cell death (including positive and negative caspase-3 labelled cells) was found to be significantly increased in *Nfκb1*<sup>-/-</sup> and *c-Rel*<sup>-/-</sup> mice but not in *Nfκb2*<sup>-/-</sup> mice relative to wild-type C57BL/6J mice (see Figure 3.15). Some cells which had morphological features of cell death were

immunohistochemically negative for active caspase-3. These could represent cells at the later stages of apoptosis, when processes such as DNA fragmentation are taking place and the cells no longer express active caspase-3 (Glamočlija *et al.*, 2005). Alternatively they could represent cells which are dying via a non-caspase-3 associated apoptotic process such as necroptosis (Kaczmarek *et al.*, 2013) or pyroptosis (Fink and Cookson, 2005).

In summary, the studies presented in this chapter confirm that LPS induces pathological small intestinal epithelial cell apoptosis and shedding in all tested mouse strains and ages and also in *Ludwig Olac Wistar* rats, but with different degree of effectiveness. Different sources of LPS caused different effects and RelB did not appear to be an important regulator of this process. However, NFκB family members were shown to regulate crypt apoptosis 24 hours after LPS administration in a similar manner to that observed in the villus after 1.5 hours.

#### **4. Ultrastructural changes within the small intestinal epithelial cells of wild-type and transgenic mice treated with bacterial lipopolysaccharide (LPS).**

##### **Introduction**

The features of LPS-induced SIEC apoptosis have been well described in many previous studies, particularly at the light microscope level and based on morphological criteria using H&E staining and immunohistochemistry (Williams *et al.*, 2013, Guo *et al.*, 2013, Nighot *et al.*, 2017). However, to our knowledge there has been no previous study describing the morphological features within SIECs after IP administration of bacterial LPS using transmission electron microscopy (TEM). A number of previous publications have however, evaluated the ultrastructure of SIECs in certain conditions or diseases using TEM (Sohma 1983, Miura *et al.*, 2005 Leite *et al.*, 2013). The ultrastructure of enterocytes under normal physiological conditions was described by Sohma and colleagues, where they reported well developed apical microvilli, numerous mitochondria scattered in the apical and basal cytoplasm, rough endoplasmic reticulum and free ribosomes, lysosome-like bodies and a well-developed Golgi apparatus located apical to the basally positioned oval nucleus (Sohma *et al.*, 1983). Leite and colleagues have reported ultrastructural changes in SIECs in children who were infected with HIV, describing frequent structural changes that include cell extrusion toward the intestinal lumen, vacuolation of mitochondria, disruption and loss of microvilli, intensive intracytoplasmic vacuolation with well-defined intercellular spaces and a large number of vesicular bodies found within all areas of the cell cytoplasm (Leite *et al.*, 2013). He *et al.*, in 2015 studied the role of heat stress-induced small intestinal injury and showed desquamation of intestinal epithelial cells, and

destruction of both intestinal microvilli and mitochondria. They also observed that NFκB signalling pathway regulated such intestinal injury (He *et al.*, 2015).

Marchiando *et al.*, in 2011 have indicated the role of junctional proteins in barrier maintenance using TEM. They showed that redistribution of ZO-1 and occludin from the tight junction to basolateral membranes along with the recruitment of claudins, E-cadherin, tubulin, F-actin, Rho-associated protein kinase (ROCK) and Myosin light-chain kinase (MLCK) to basolateral membranes caused contraction of the cell and the development of a funnel that ejected the apoptotic cell (Marchiando *et al.*, 2011).

In this chapter, we aimed to evaluate the ultrastructure of proximal SIECs from wild-type C57BL/6J mice and various transgenic strains on a C57BL/6J background, including *Nfκb1*<sup>-/-</sup>, *Nfκb2*<sup>-/-</sup> and *c-Rel*<sup>-/-</sup> mice, housed under normal conditions and 1.5h post administration of 0.125 mg/kg LPS from *Escherichia coli* serotype O111:B4.

#### **4.1 Ultrastructural comparison of proximal small intestinal epithelium of untreated wild-type C57BL/6J and various transgenic Nfκb subunit global knockout mice.**

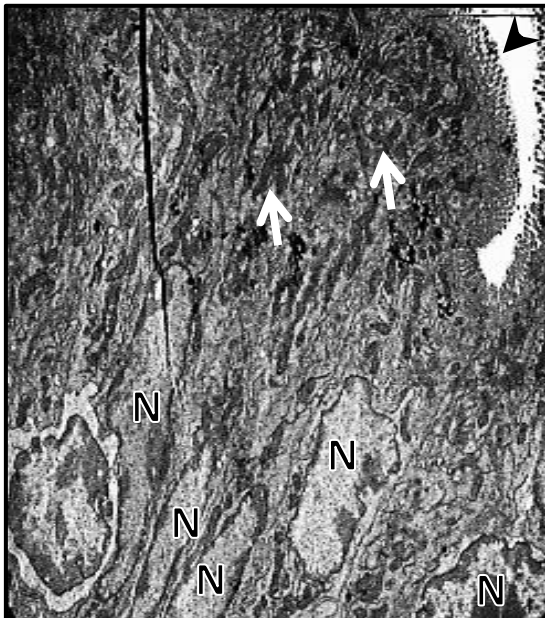
Previous immunohistochemistry results in our laboratory of LPS induced SIEC apoptosis and shedding showed differences in the degree of responsiveness of wild-type C57BL/6J mice and transgenic mice (*Nfκb1*<sup>-/-</sup>, *Nfκb2*<sup>-/-</sup> and *c-Rel*<sup>-/-</sup>) to intraperitoneal LPS (Williams *et al.*, 2013). Ultrastructural analysis of small intestinal epithelium in wild-type C57BL/6J mice showed well-defined microvilli on the apical surface of enterocytes oriented toward the intestinal lumen, elongated tubular

mitochondria that were scattered throughout the cytoplasm and a basally located, well-defined nucleus surrounded by a clear nuclear membrane (Figure 4.1). The cell boundaries appeared very clear, indicating the unity of the epithelium by different junctional components. The morphological structure of SIECs in *Nfκb1*<sup>-/-</sup> mice appeared similar to wild-type SIECs, with TEM again revealing a normal brush border, normally distributed cytoplasmic organelles, mitochondria aggregated in both the apical and basal aspect of cells, and the basal nuclei again surrounded by a well-defined nuclear envelope with clear eccentric nucleoli and well distributed heterochromatin and euchromatin material. The only exception was that numerous paracellular spaces were noted close to the lateral membranes (Figure 4.2). Likewise, small intestine of *Nfκb2*<sup>-/-</sup> mice (Figure 4.3) were also morphologically indistinct from wild-type C57BL/6J mice SIECs, as was the morphology observed in the proximal segment of *c-Rel*<sup>-/-</sup> mouse small intestine (Figure 4.4). The only noted minor difference was the appearance of dark opaque vesicular bodies in the apical cytoplasm of *c-Rel*<sup>-/-</sup> SIECs (Figure 4.4).

X 2,550



X 4,200



X 6,000



X 8,200

**Figure 4.1: Transmission electron microscopy (TEM) of proximal SIECs from untreated wild-type C57BL/6J mice.** Arrowheads indicate a well distributed brush border microvilli; N is the nucleus, white arrows indicate mitochondria. Representative images from N=3 mice. Magnification from X 2,550 to 8,200.

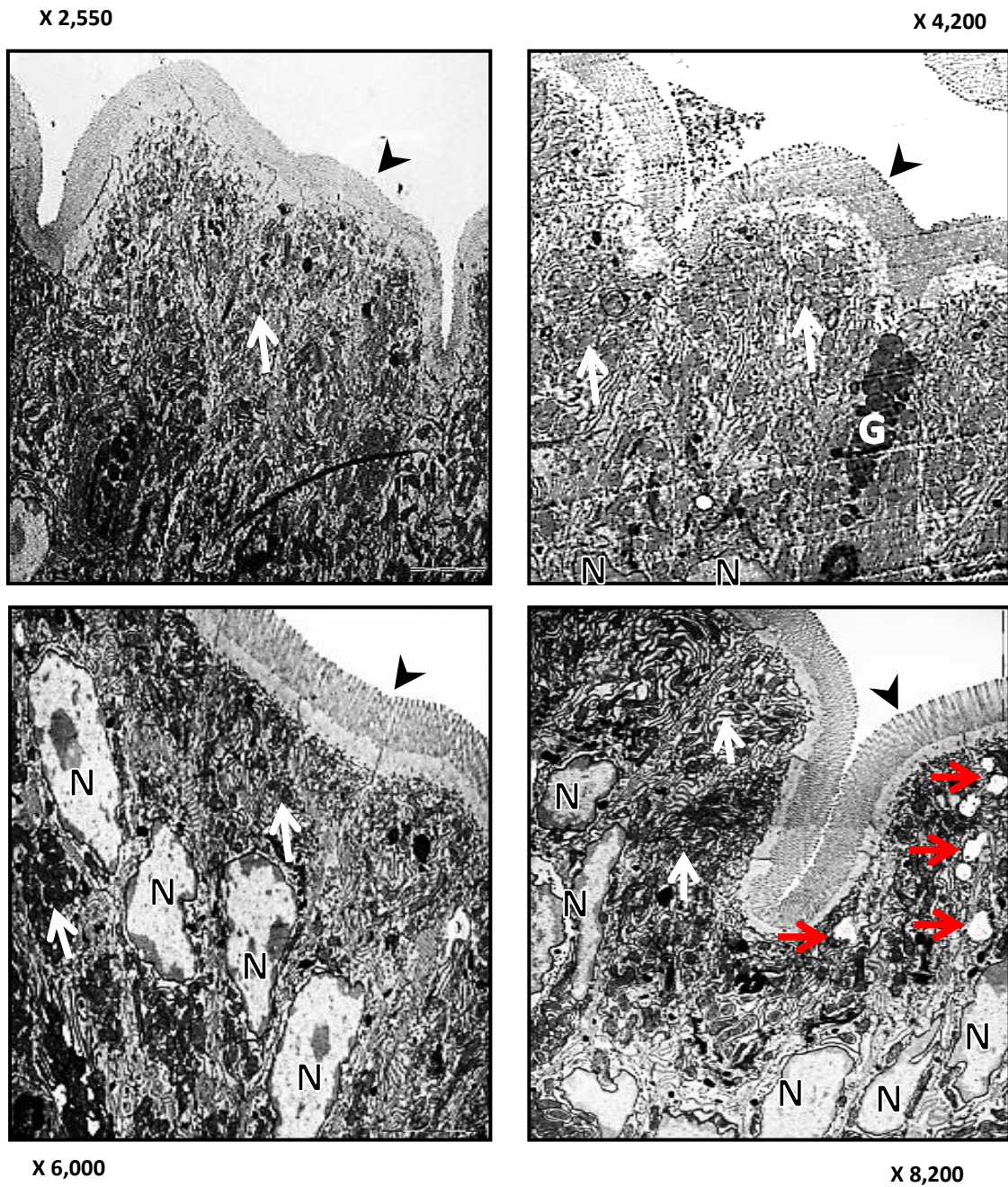
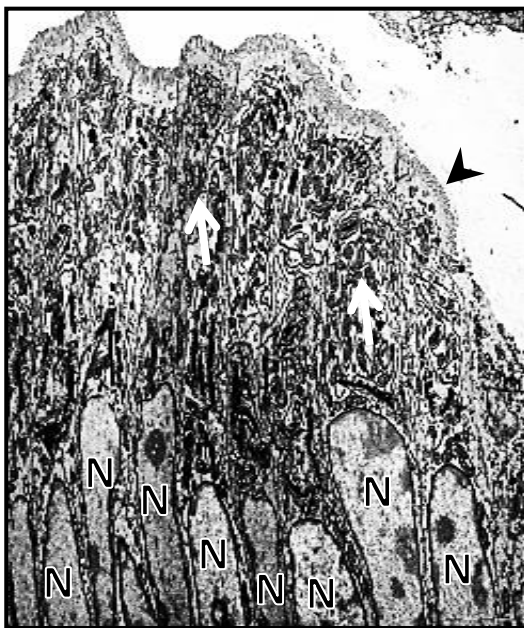
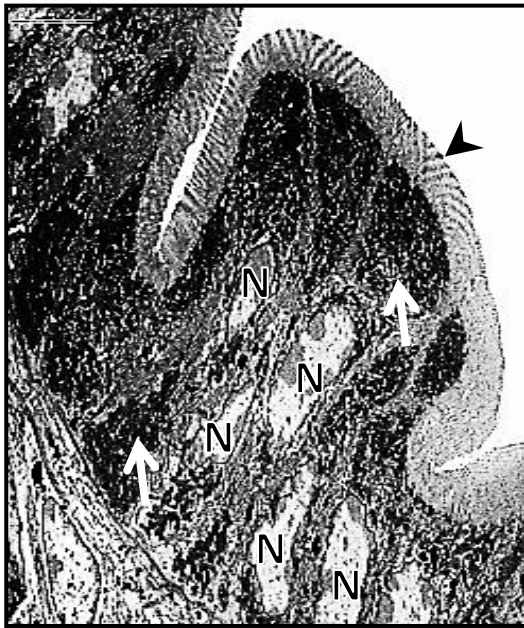


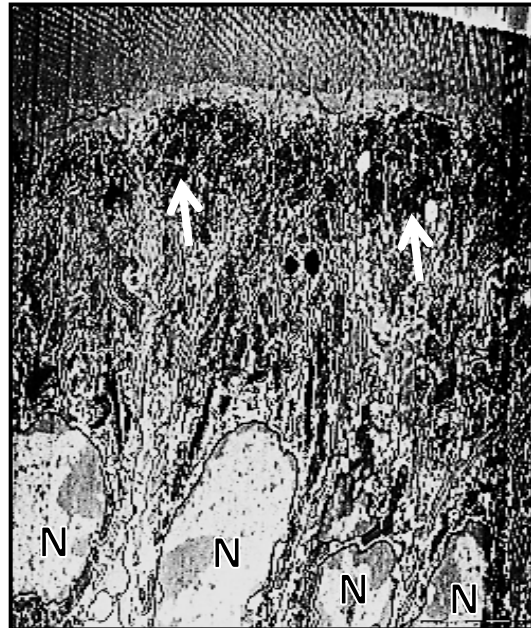
**Figure 4.2: TEM of normal proximal SIECs from untreated *Nfkb1*<sup>-/-</sup> mice.** Black arrowheads indicate well distributed brush border microvilli; N is the nucleus; white arrows indicate the mitochondria; red arrows indicate presence of paracellular spaces; G is a goblet cell. Representative images from N=3 mice. Magnification from X 2,550 to 8,200.

X 2,550

X 4,200



X 6,000



X 8,200

**Figure 4.3: TEM of normal proximal SIECs from untreated *Nfkb2*<sup>-/-</sup> mice.** Black arrowheads indicate well distributed brush border microvilli; N is the nucleus; white arrows indicate the mitochondria. Representative images from N=3 mice. Magnification from X 2,550 to 8,200.

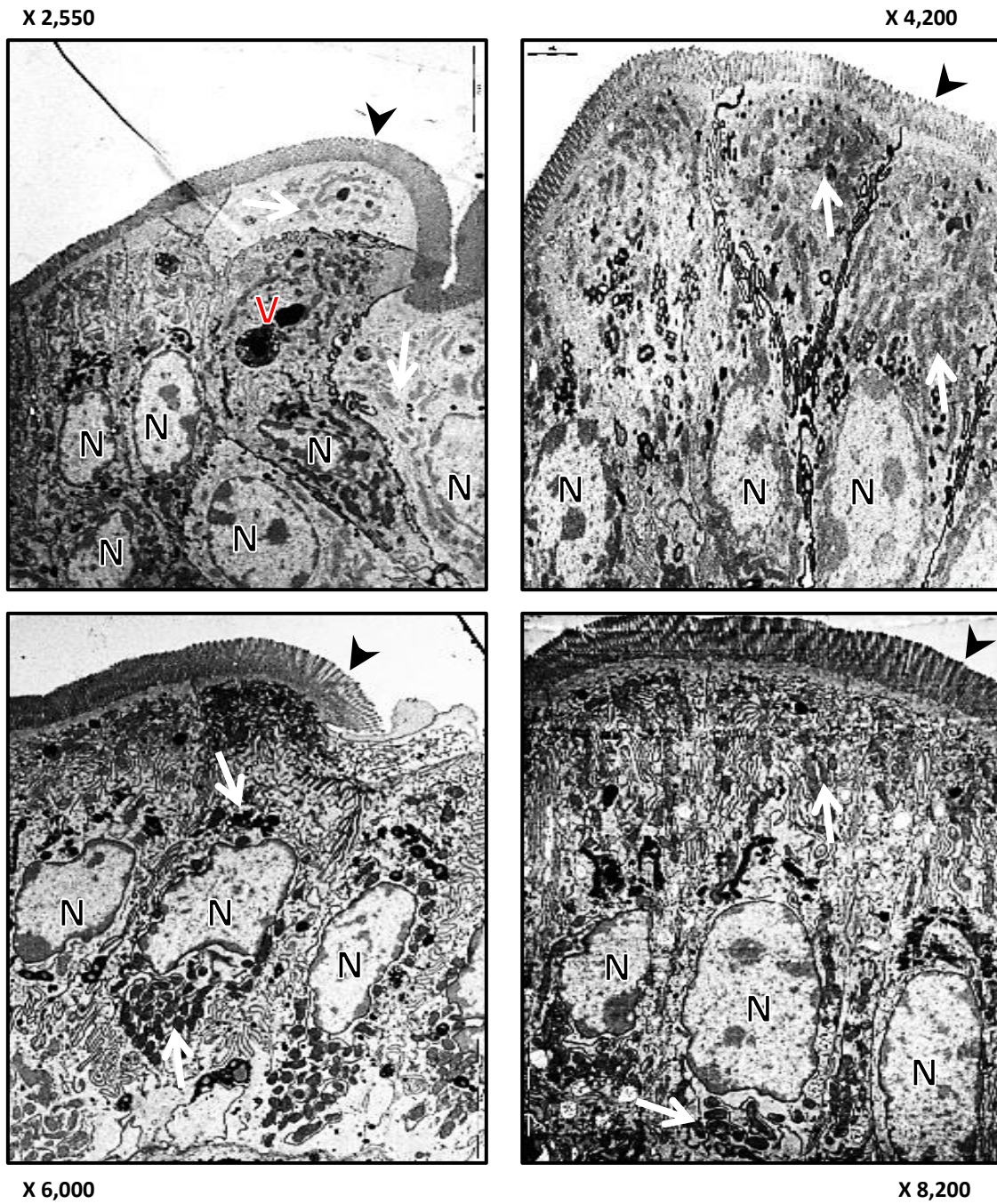


**Figure 4.4: TEM of normal proximal SIECs from untreated *c-Rel*<sup>-/-</sup> mice.** Black arrowheads indicate well distributed brush border microvilli; N is the heterochromatic nucleus; white arrows indicate the mitochondria; V indicates a dark opaque vesicular body. Representative images from N=3 mice. Magnification from X 2,550 to 8,200.

## **4.2 Examination of the action of LPS on SIEC ultrastructural morphology**

Intraperitoneal administration of LPS is known to induce pathological apoptosis and shedding of murine small intestinal epithelial cells in wild-type C57BL/6J mice, with *Nfκb2<sup>-/-</sup>* mice showing resistance to shedding (Williams *et al.*, 2013). However, the ultrastructural characteristic features of apoptosis and shedding have not previously been described. In this section, the ultrastructural changes that were observed in different transgenic Nfκb subunit global knockout mouse strains treated with low dose (0.125 mg/kg) IP injection of LPS for 1.5 h will be described.

### **4.2.1 Inter- and intra-cellular vacuolisation was a key feature observed in wild-type C57BL/6J mice after LPS treatment**

TEM of the proximal segments of small intestine from C57BL/6J mice showed some key ultrastructural changes 1.5h following IP administration of 0.125 mg/kg LPS. The most obvious features noted were the appearance of marked amounts of intracellular vacuolisation and the appearance of intercellular spaces (red arrows) in LPS treated wild-type mice (Figure 4.5). In addition, dark (opaque) vesicular bodies (black arrows) were also observed in the apical portions of the SIECs in all treated wild-type mice (Figure 4.5). Remarkably however, despite these perceptible morphological changes, normal cell shape and distribution of brush border microvilli were preserved, with nuclei (N) of normal appearance and that remained positioned basally, and mitochondria which also retained a normal shape and orientation throughout all the sections examined.

#### **4.2.2 *Nfκb1*<sup>-/-</sup> mouse proximal small intestine was more sensitive to LPS than other strains as demonstrated by multiple, distinct morphological changes**

Following intraperitoneal injection of 0.125 mg/kg LPS to *Nfκb1*<sup>-/-</sup> mice, multiple distinct morphological structural changes were observed 1.5h post-administration that affected almost all cellular components (Figure 4.6). The brush border microvilli, whilst appearing to be preserved in some areas, were markedly disrupted or lost in some areas of the cell surface membrane (black arrowheads; Figure 4.6). Intracytoplasmic vacuoles and intercellular spaces (red arrows) were large in size and increased in number compared to those observed in wild-type C57BL/6J mice. Obvious whole cell extrusions (black arrows; Figure 4.6) were seen in all LPS-treated *Nfκb1*<sup>-/-</sup> mice indicating the presence of shedding SIECs. Vesicular bodies (blue arrows) appeared in the apical cytoplasm in some cells (Figure 4.6). Vacuolated and expanded mitochondria (green arrowheads), with loss of their characteristic cristae, were also noted in all LPS treated *Nfκb1*<sup>-/-</sup> mice. The nuclei appeared to retain a normal shape (N) in some cells but were fragmented with loss of their usual chromatin distribution (white arrowheads) within exfoliated cells (Figure 4.6).

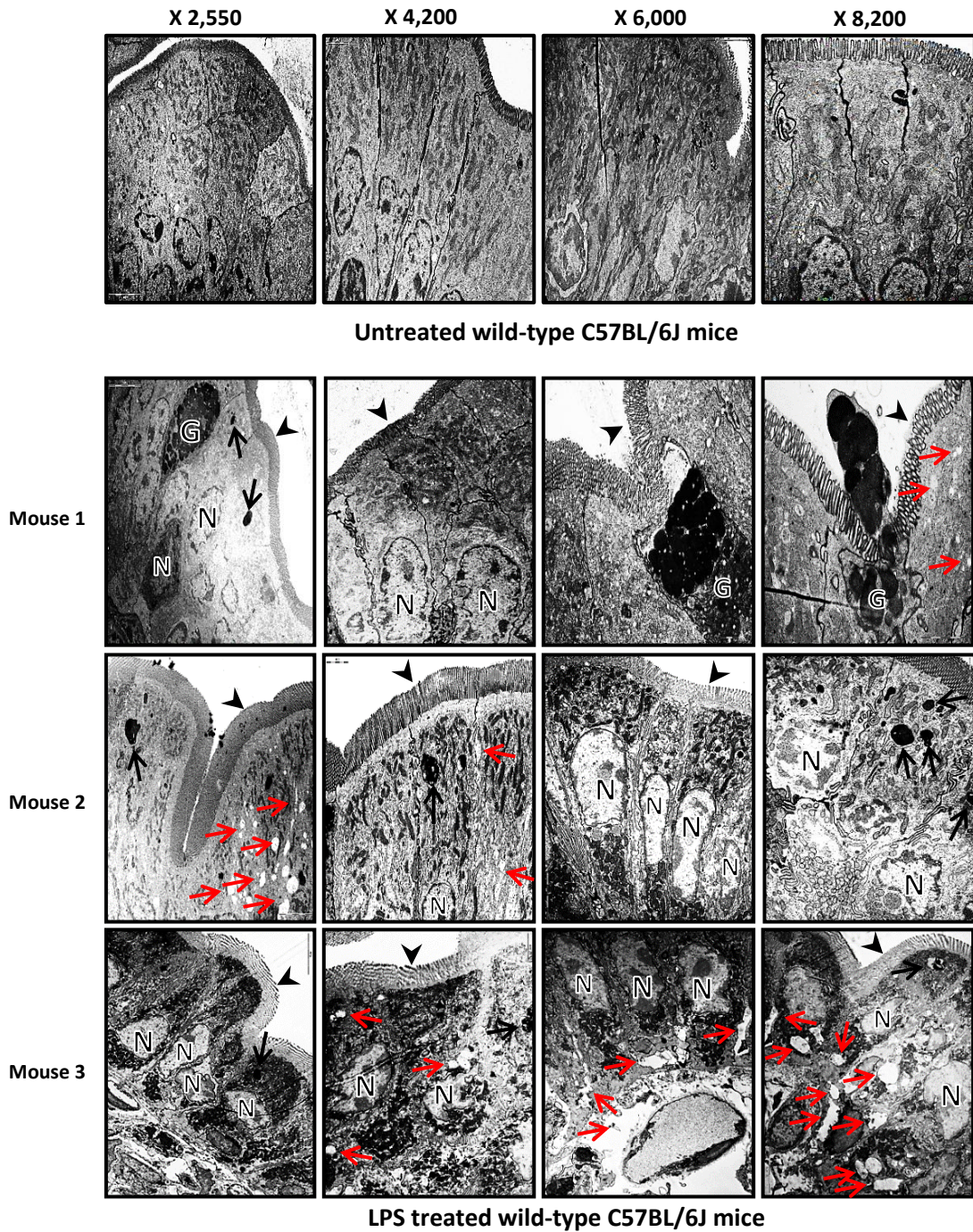


**Figure 4.5: TEM of proximal SIECs treated with 0.125 mg/kg LPS versus untreated wild-type C57BL/6J mice.** Morphological changes include appearance of inter- and intracellular vacuoles and numerous opaque vesicular bodies. (Black arrowheads: microvilli, N: nucleus, black arrows: vesicular bodies, red arrows: vacuolation, and G: goblet cells). Representative images from N=3 mice. Magnification X 2,550 to 8,200.

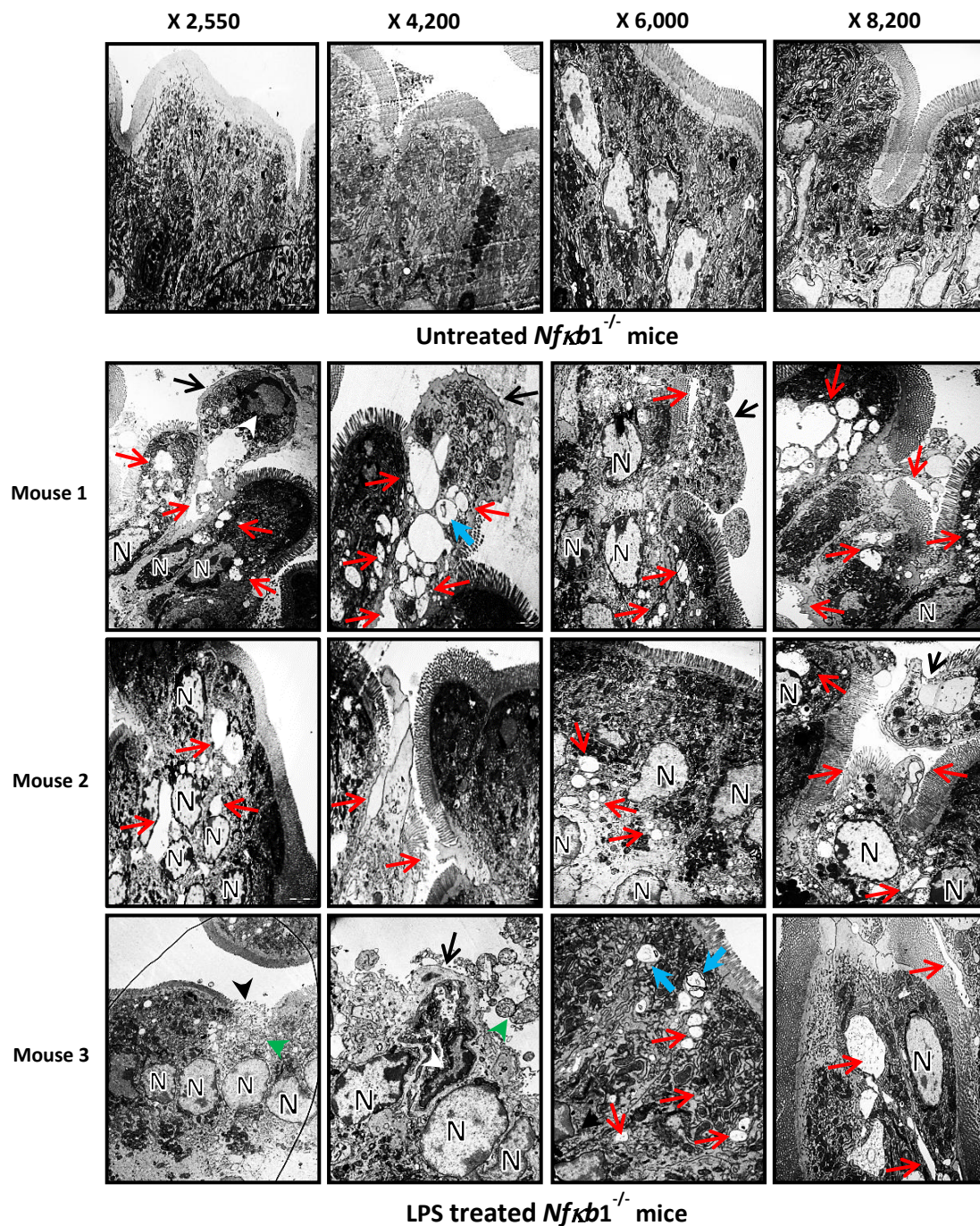


**Figure 4.6: TEM of proximal SIECs of 0.125 mg/kg LPS treated versus untreated *Nfkb1*<sup>-/-</sup> mice, (N=3). Gross morphological changes include: loss of microvilli (black arrowheads), shedding cells (black arrows), inter- and intra-cellular vacuoles (red arrows), indented nuclei (white arrows), vacuolated mitochondria (green arrows), and vesicular bodies (blue arrows), N is the normal nuclei. Representative images from N=3 mice. Magnification X 2,550 to 8,200.**

#### **4.2.3 No morphological changes were identified in the SIECs of LPS treated *Nfκb2*<sup>-/-</sup> mice**

No obvious morphological changes were observed 1.5h post IP injection of 0.125 mg/kg LPS into *Nfκb2*<sup>-/-</sup> mice compared to untreated mice of same strain, excepting for the appearance of some small vesicular bodies (red arrows) that may represent increased levels of endocytic activity (see Figure 4.7). All other cellular structures, including the brush border microvilli, nuclei and cytoplasmic organelles appeared normal, retaining their shape and distribution (Figure 4.7). These observations further confirm the ability of *Nfκb2* null mice to resist LPS-induced apoptosis and shedding of SIECs.

#### **4.2.4 *c-Rel*<sup>-/-</sup> mice show an intermediate response to LPS treatment**

Administration of 0.125 mg/kg LPS to *c-Rel*<sup>-/-</sup> mice for 1.5 hours resulted in only subtle morphological changes within SIECs (Figure 5.8). These changes included focal areas of cell surface microvilli disruption (B), along with increased presence of well-defined intercellular spaces and intracellular vacuoles (red arrows) and the appearance of some funnel shaped cells (F) within the epithelial layer of small intestine (see Figure 4.8). The latter were characterised by a narrow base and wide apex, with a darker cytoplasm in comparison to adjacent epithelial cells. The appearance of large vesicular bodies (black arrows) within the apical zone of SIECs was one of the most noticeable changes seen 1.5h post IP administration of low dose LPS. Other than these small but distinct ultrastructural changes, all other cellular components seemed to be normal in

size, location and appearance, including nuclei (N), retaining an intact nuclear envelope surrounded by normally distributed chromatin.

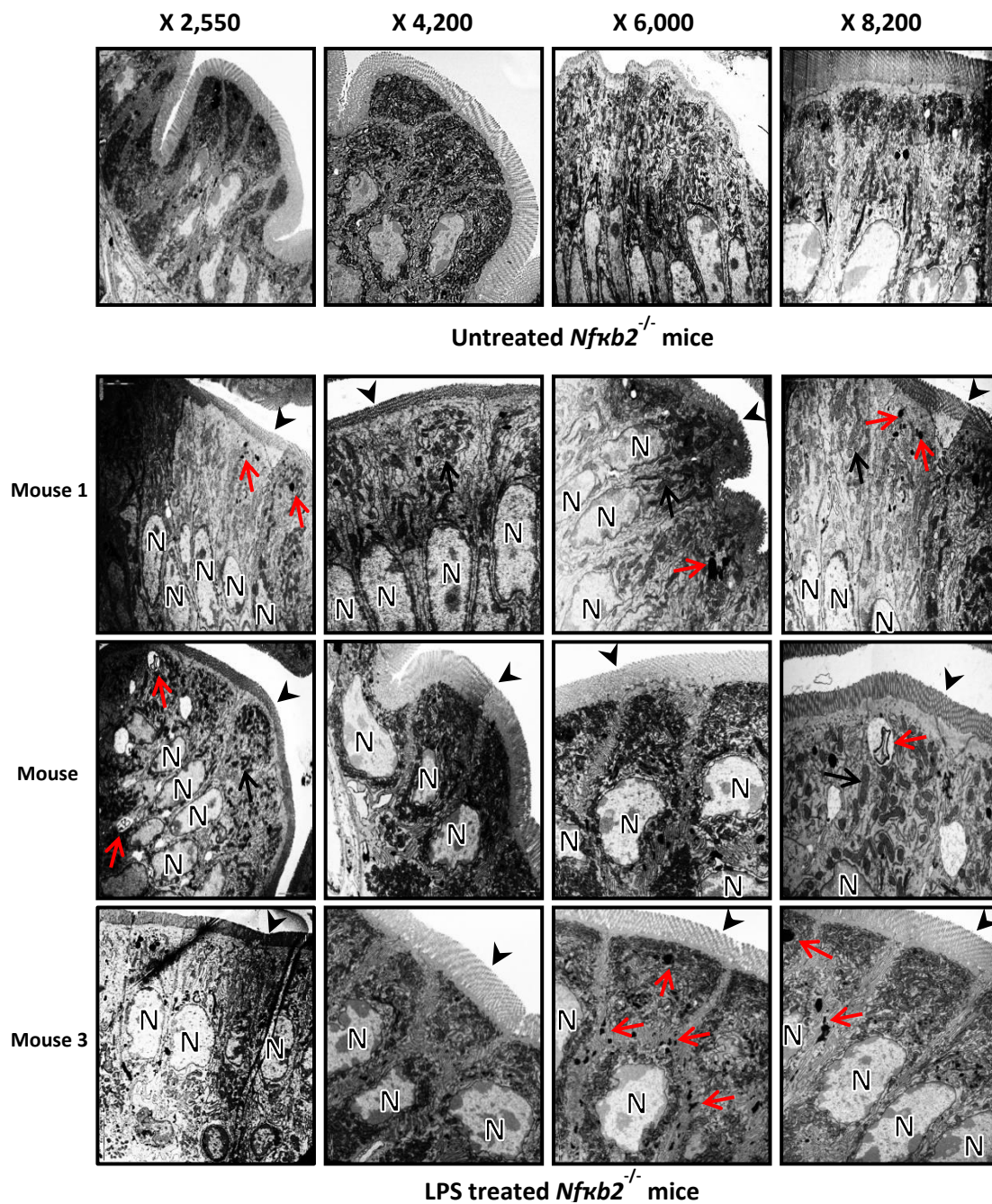


**Figure 4.7: TEM of proximal SIECs from 0.125 mg/kg LPS treated versus untreated *Nfkb2*<sup>-/-</sup> mice.** No morphological changes were observed indicating that the *Nfkb2*<sup>-/-</sup> strain was resistant to the actions of LPS. Microvilli (black arrowheads) and vesicular bodies (red arrows) were of normal shape and distribution. Nuclei (N) and mitochondria (black arrows) were of normal shape and position. Representative images from 3 mice. Magnification from X 2,550 to 8,200.

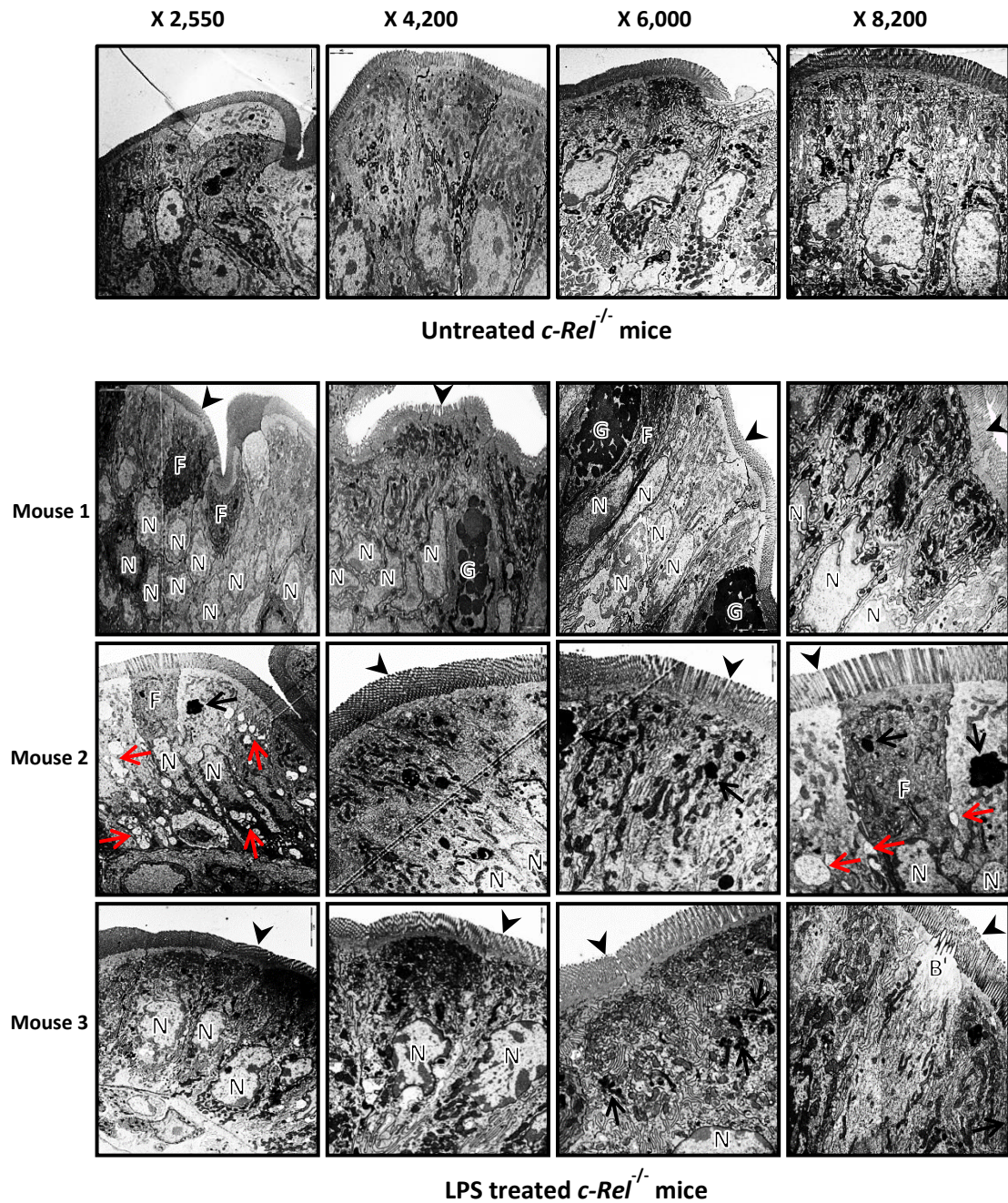


**Figure 4.8: TEM of proximal SIECs of 0.0125 mg/kg LPS treated versus untreated *c-Rel*<sup>-/-</sup> mice.** Subtle morphological changes include increased number of vacuoles (red arrows), vesicular bodies (black arrows), appearance of funnel shaped cells (F) and disrupted cell surface microvilli (B). Nuclei appear of normal shape and position (N). G indicate goblet cells, and black arrowheads indicate microvilli of normal shape and distribution. Representative images from three mice. Magnification from X 2,550 to 8,200.

### **4.3 Transmission electron microscopy highlights key morphological changes and dynamic events of cellular apoptosis and shedding induced by LPS in murine small intestinal epithelium.**

The light microscopic features of LPS induced apoptosis and shedding have been presented in a previous report (Williams *et al.*, 2013). In this study, a series of TEM images highlight the major features of small intestinal epithelial apoptosis and shedding in mice following injection of 0.125 mg/kg IP injection of *E. coli* LPS.

Increased intracellular vacuolisation and intercellular spaces are clearly seen in the epithelial cells of wild-type C57BL/6J mice following injection of bacterial LPS (Figure 4.9). At higher magnification (X 9,900 and X 16,500) the vacuolisation and spaces noted may indicate an increase in autophagocytic/phagocytic activity (to support degradation of proteins, other macromolecules and organelles), and detachment from adjacent cells. However, the mitochondria surrounding these spaces still appeared to retain a normal ultrastructure.

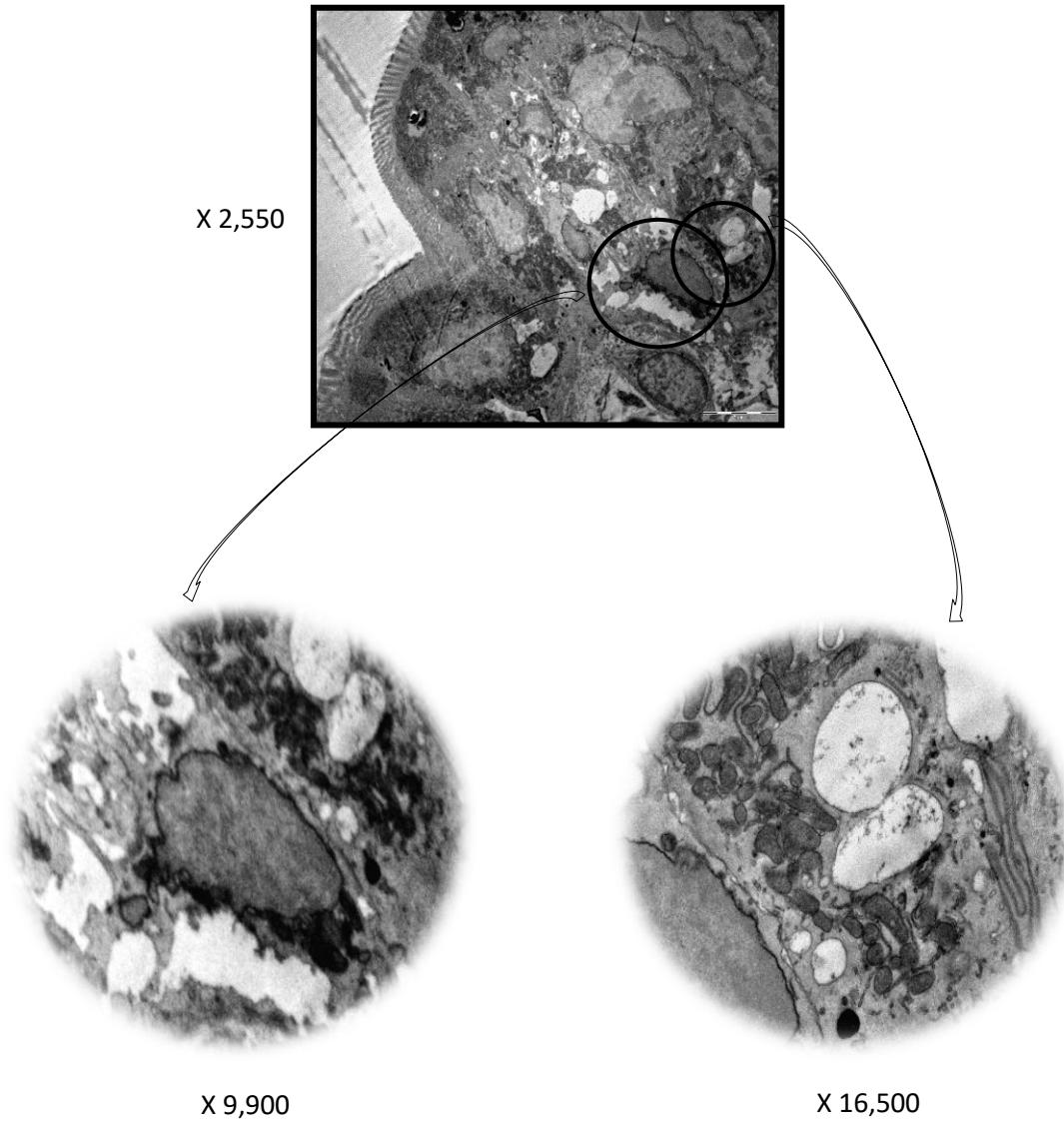


Figure 4.9: Higher magnification TEM of SIECs from wild-type C57BL/6J mouse treated with 0.125 mg/kg LPS highlights the large intracellular vacuoles and intercellular spaces.

Gross morphological changes were seen in LPS-treated *Nfκb1*<sup>-/-</sup> mice (Figures 4.10, 4.11 and 4.12). At higher magnification (X 4,200, X 6,000, X 8,200 and X 9,900), these ultrastructural changes included extrusion of epithelial cells toward the intestinal lumen, with loss of microvilli from their apical surfaces (black arrowhead), nuclear fragmentation (white arrowhead), increased vacuolation and loss of mitochondria (Figure 4.10 and 4.11). Intracellular vacuolisation and the appearance of intercellular spaces were also noted in other LPS treated mouse groups (Figure 4.9 and 4.12). Intraepithelial lymphocytes (Figure 4.13) were also observed to be located basal to the intestinal epithelial cells.

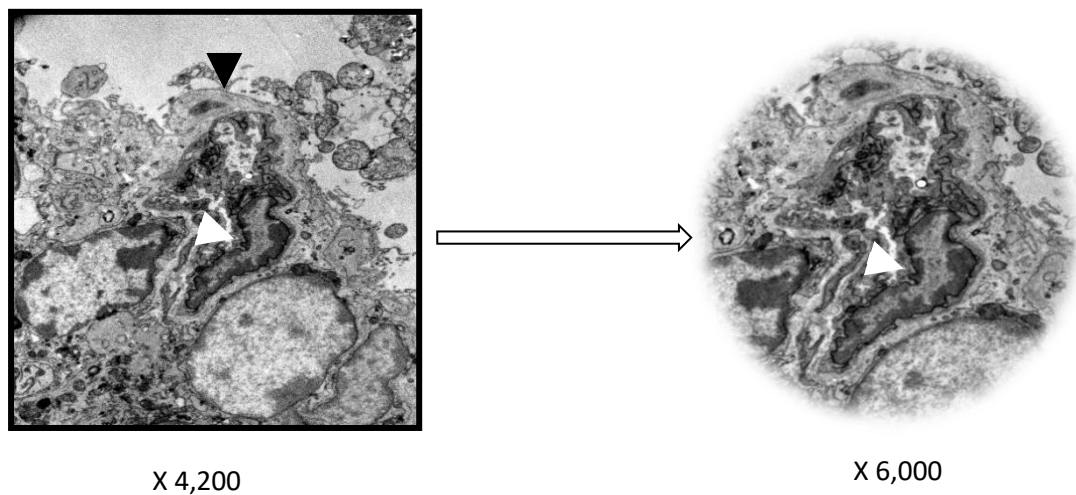


Figure 4.10: Small intestinal TEM of LPS-treated *Nfκb1*<sup>-/-</sup> mouse showing epithelial cell extrusion (black arrowhead), nuclear fragmentation (white arrowheads).

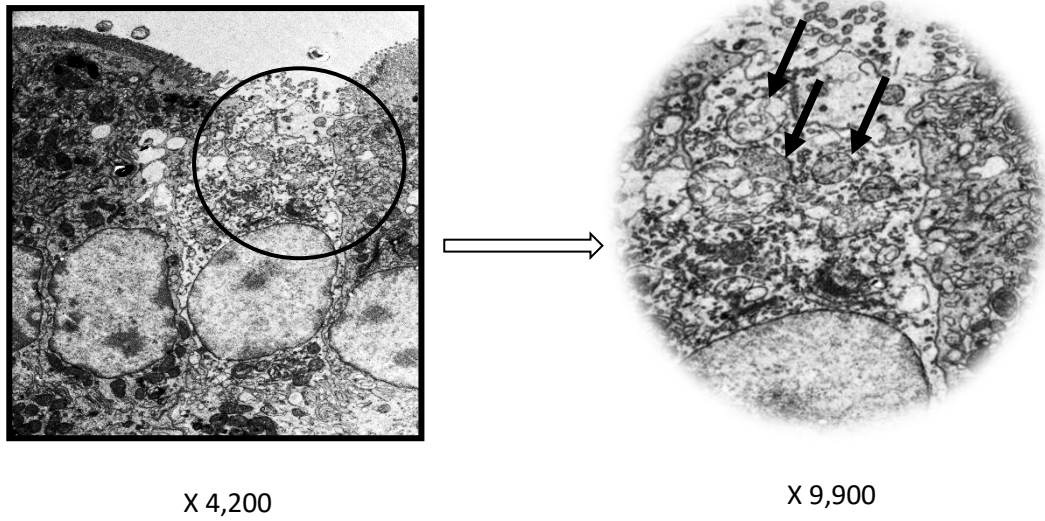


Figure 4.11: Small intestinal TEM of LPS-treated *Nfκb1*<sup>-/-</sup> mouse showing mitochondrial vacuolation and loss of cisternae (black arrows).

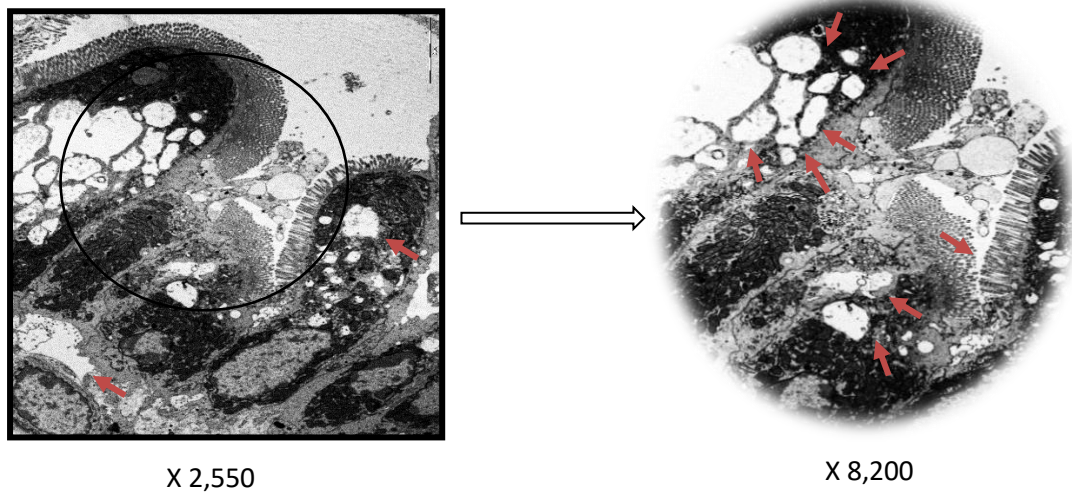
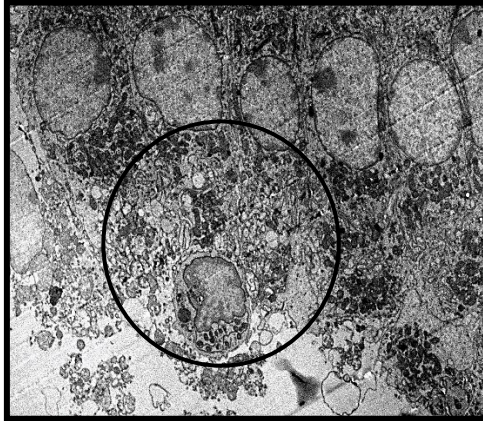


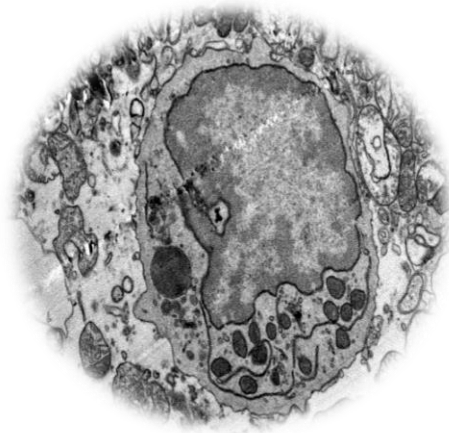
Figure 4.12: Small intestinal TEM of LPS-treated *Nfκb1*<sup>-/-</sup> mouse showing intracellular vacuolation and intercellular space formation.



X 2,550



X 4,200



X 8,200

Figure 4.13: Small intestinal TEM of LPS-treated *Nfkb1*<sup>-/-</sup> mouse showing an intraepithelial lymphocyte underlying the small intestinal epithelial cell layer.

In *c-Rel*<sup>-/-</sup> mice, the most obvious morphological changes seen after low dose IP injection of LPS were disruption of microvilli (Figure 4.14), the appearance of funnel shaped cells (Figure 4.15) and the development of intra- and inter-cellular vacuolation.

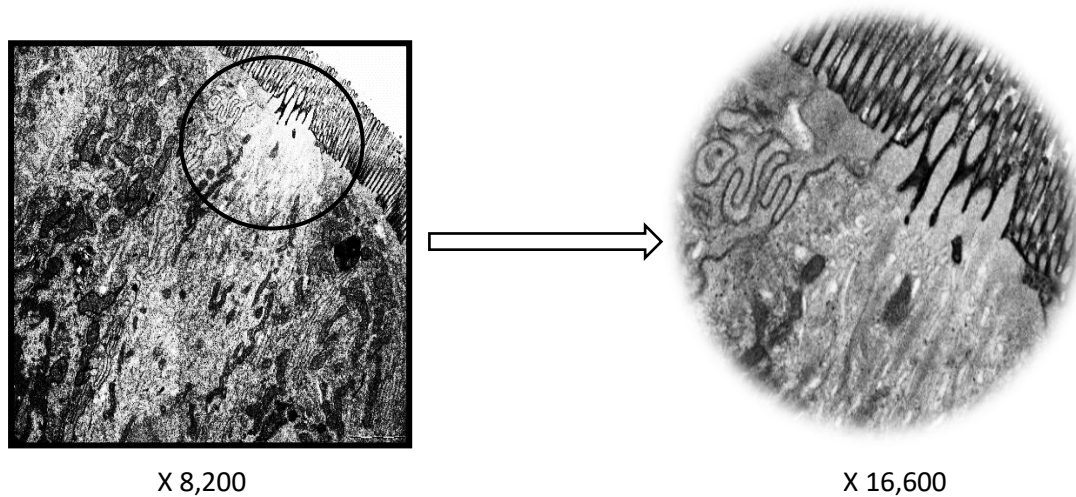


Figure 4.14: Small intestinal TEM showing disruption of intestinal microvilli in a *c-Rel*<sup>-/-</sup> mouse injected with 0.125 mg/kg IP LPS for 1.5 hours.

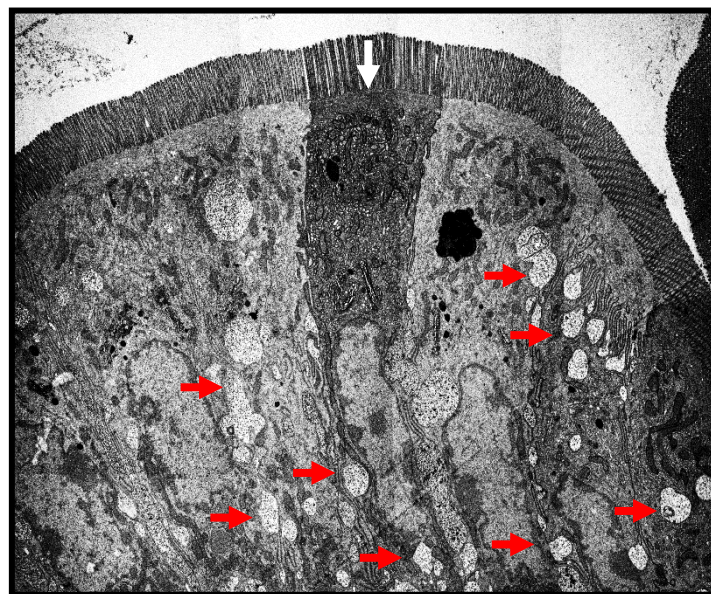


Figure 4.15: Small intestinal TEM showing a funnel shaped epithelial cell (white arrow) and vacuolation (red arrows) in a *c-Rel*<sup>-/-</sup> mouse after LPS administration (X 4,200).

## 5.4 Discussion

The data presented in this chapter provide further characterisation of LPS-induced apoptosis and shedding in the murine small intestinal epithelium. Work described earlier in this thesis and previous light microscopy studies undertaken by Williams and colleagues (Williams *et al.*, 2013) have indicated that pathological SIEC apoptosis and shedding is induced by bacterial LPS in wild-type C57BL/6J mice. Maximal SIEC apoptosis and shedding post intraperitoneal administration of low dose (0.125 mg/kg) LPS was seen at 1.5 hours and was more pronounced in *Nfκb 1<sup>-/-</sup>* mice, as also seen by Williams and colleagues (Williams *et al.*, 2013). *c-Rel<sup>-/-</sup>* mice showed an intermediate response to LPS relative to wild-type and *Nfκb1<sup>-/-</sup>* mice, whilst *Nfκb2<sup>-/-</sup>* mice appeared to be more resistant to LPS-induced SIEC apoptosis and shedding, again as previously observed (Williams *et al.*, 2013).

To date, there have been no previous reports describing the characteristic features of LPS-induced apoptosis and shedding of murine SIECs using TEM, although a few studies have described ultrastructural changes in the small intestinal epithelium under other conditions, including starvation (Sohma, 1983), following injection of mice with anti-CD3e antibody (Miura *et al.*, 2005), and also in African children infected with HIV (Leite *et al.*, 2013)

In our study, the ultrastructural features of normal murine intestinal absorptive cells included well-developed brush border microvilli and numerous mitochondria within the apical zone surface, just below the terminal web and around the basal zone below the level of the nucleus. Nuclei located in the basal zone of the cell contained prominent nucleoli, peripherally arranged heterochromatin just beneath the nuclear

envelope and normal centrally distributed euchromatin. Other cytoplasmic organelles, such as rough endoplasmic reticulum, the Golgi complex, ribosomes and lysosomes, were also observed to be of normal appearance (size, shape and position) within the cell cytoplasm. These features were similar to those described for duodenal absorptive cells in a previous study (Sohma, 1983).

After administration of LPS, the SIECs of wild-type C57BL/6J mice showed increased intra- and inter-cellular vacuolation, with the appearance of dark (opaque) vesicular bodies in the apical cell compartment. The appearance of vesicular bodies of different size was also previously highlighted by Sohma, and described as lysosome-like bodies (Sohma, 1983) potentially indicating an increase in the endocytic and/or autophagocytic activity of epithelial cells (Luzio *et al.*, 2014).

The most interesting ultrastructural features were noted in *Nfκb1*<sup>-/-</sup> mice following LPS administration. We observed shedding or extrusion of enterocytes that were detached from adjacent cells toward the intestinal lumen as whole cells containing their nuclei and without rupturing their cell membranes. This type of apoptosis is similar to that seen in both human and mouse small intestine (Bullen *et al.*, 2006, Williams *et al.*, 2013). Moreover, a large number of intracellular vacuoles and intercellular spaces were noted in all LPS-treated *Nfκb1*<sup>-/-</sup> mice suggesting detachment of apoptotic cells from their neighbouring cells and an increase in cell endocytic activity. Similar vacuolation and spaces were also seen in wild-type C57BL/6J and *c-Rel*<sup>-/-</sup> mice, but to a lower extent.

In 2005, Mura and colleagues described electron microscopic findings of murine small intestinal epithelial cells 24 hours following anti-CD3 antibody injection (Mura *et al.*,

2005). They described that the nuclei of the intestinal epithelial cells showed a significant degree of condensation and fragmentation, and that the mitochondria showed marked expansion and vacuolation, with accompanying loss of their characteristic cisternae. Similar features were observed in our study, especially in *Nfκb1*<sup>-/-</sup> mice 1.5 hours after IP injection of *E. coli* LPS. Additionally, that epithelial microvilli were lost or disrupted in association with the formation of multivesicular bodies, again perhaps indicative of endocytic activity as had been previously suggested (Sohma, 1983).

The most remarkable finding seen in *c-Rel*<sup>-/-</sup> mice, in addition to increased levels of intra- and inter-cellular vacuolation, was the appearance of funnel shaped cells with characteristic narrow bases and a wider apical cell surface membrane. This distinctive cellular morphology may be due to repositioning/re-localisation of cytoskeletal elements (including microtubules and microfilaments), resulting in contraction of the shedding cell, and the role played by junctional complexes in the lateral membrane of the cell, so as to maintain integrity of the barrier between shedding and adjacent healthy epithelial cells (Marchiando *et al.*, 2012).

*Nfκb2*<sup>-/-</sup> mice showed no ultrastructural differences between LPS treated and untreated groups, supporting our previous finding of the resistance of this genotype to pathological apoptosis and shedding induced by LPS.

In conclusion the ultrastructural morphological changes observed in mouse SIECs following LPS injection can be summarised as follows:

- i. Extrusion of shedding cells toward the intestinal lumen

- ii. Fragmentation and condensation of nuclei
- iii. Appearance of intracellular vacuolation and intercellular spaces
- iv. Vacuolation and expansion of mitochondria
- v. Formation of multivesicular bodies
- vi. Appearance of funnel shaped cells

In summary, the data described in this chapter support our previous results from immunohistochemistry which have indicated the role of bacterial LPS in inducing pathological SIEC apoptosis and shedding.

Our results support previous observations that *Nfκb1*<sup>-/-</sup> mice were more susceptible and *Nfκb2*<sup>-/-</sup> mice were more resistant to LPS induced SIEC apoptosis and shedding. Furthermore, our results indicate that wild-type C57BL/6J and *c-Rel*<sup>-/-</sup> mice showed an intermediate response to LPS relative to *Nfκb1*<sup>-/-</sup> and *Nfκb2*<sup>-/-</sup> mice.

## **5. Proteomic analysis of murine small intestinal tissue pre- and post-administration of LPS**

Previous studies in our laboratory and my current work presented in chapter 3 of this thesis indicated that LPS induces maximal small intestinal epithelial cell apoptosis and shedding in C57BL/6J mice at 1.5 hours post LPS administration. We have also shown that apoptosis and shedding of murine SIECs following LPS administration was dependent on the expression of the NF $\kappa$ B family of proteins with signalling via NF $\kappa$ B1 transcription favouring cell survival and signalling via NF $\kappa$ B2 activation favouring cell apoptosis (Williams *et al.*, 2013).

To the best of our knowledge there have been no prior studies using large scale analyses of the mouse small intestinal mucosal proteome in responses to LPS. However, there have been several studies that have identified proteins that are differentially expressed in the whole murine small intestine in response to starvation or dietary supplementation. For instance, Lenaerts and colleagues used a 2 dimensional electrophoresis proteomic approach to determine starvation-induced adaptations at the molecular level in mouse small intestine. From a total of around 1500 proteins identified, they found that several proteins involved in glycolysis were down regulated in early starvation and this resulted in a decrease in activity of glycolysis and citric acid cycle enzymes in the intestine. They also noted a strong upregulation of regenerative proteins I and II (reg I and reg II) that are expressed in crypt epithelial cells but not villus epithelial cells, suggesting that these proteins play a role in growth and the early differentiation states of the intestinal epithelium (Lenaerts *et al.*, 2006). We have similarly used a combination of proteomic data

analysis and literature searches to identify whether proteins are present in crypt or villus epithelial cells, in order to suggest the likely regions of the crypt-villus axis that respond to LPS.

Wang *et al.*, in 2009 tested the effect of zinc supplementation on the expression of proteins related to glutathione metabolism and apoptosis in the jejunum of piglets. They indicated from a total of 22 significantly upregulated and 19 significantly downregulated proteins that zinc oxide supplementation increased the expression of A-Raf-1 (Serine/threonine-protein kinase A-Raf) and calregulin (also called calreticulin) that are known to activate cell proliferation and inhibit apoptosis in small intestinal epithelium. Furthermore, they also found that zinc oxide supplementation reduced the expression of active caspase-3 that plays a crucial role in cell apoptosis. A proteomic approach is therefore suitable for the detection of apoptosis related proteins such as caspases within the intestine.

Inhibition of the intestinal immune response has been seen as a result of enterotoxigenic *Escherichia coli* induced diarrhoea in piglet jejunum (Ren *et al.*, 2016). In this study Ren and colleagues demonstrated that downregulation of the NFκB transcription factor p65 subunit and other proteins from the mitogen-activated protein kinase (MAPK) family (including serine/threonine protein kinase 4, serine/threonine phosphatase, caspase-3, protein phosphatase 1B, calcineurin homologous protein 1, and ribosomal protein S6 kinase) inhibited the NFκB and MAPK pathways in piglet jejunum. Also, they found that ETEC-infected piglets had low mRNA expression of Toll-like receptors on the epithelial cell surface including TLR4, 5, 2, 6

and 10 suggesting the role of ETEC-induced diarrhoea in suppression of immune responses in the jejunum (Ren *et al.*, 2016).

In this chapter I aimed to identify the proteomic changes related to LPS induced small intestinal apoptosis and shedding in C57BL/6J mice 1.5 hours post intraperitoneal administration of LPS and to understand whether there are any differences in the small intestinal proteome between wild type C57BL/6J and their counterpart transgenic mice (*Nfκb1*<sup>-/-</sup>, *Nfκb2*<sup>-/-</sup> and *c-Rel*<sup>-/-</sup>) that may explain the different degrees of responses of these strains to LPS induced small intestinal epithelial cell apoptosis and shedding and therefore identify future targets to ameliorate intestinal disease.

## 5.1 *Nfκb* transgenic mice exhibit differences in the small intestinal mucosal proteome

*Nfκb1*<sup>-/-</sup>, *Nfκb2*<sup>-/-</sup> and *c-Rel*<sup>-/-</sup> mice were all previously generated on a C57BL/6J wild-type background. Following a comparative analysis of the small intestinal protein profile for the transgenic mouse strains with the proteome of C57BL/6J mice, we determined multiple proteomic changes that resulted from the deletion of individual *Nfκb* subunits (Figure 5.1). 499 significant proteomic changes were detected in *Nfκb1*<sup>-/-</sup> small intestinal mucosa in comparison to the comparable wild-type C57BL/6J mouse proteome. Among these changes, 250 proteins (representing 50.1% of the total changes) were upregulated while the remaining 249 proteins (49.9%) were downregulated in expression. In contrast, 2173 significant changes were seen in the protein profile of *Nfκb2*<sup>-/-</sup> compared to wild-type C57BL/6J small intestinal mucosa. The total number of upregulated proteins was 1036 (47.7% of the total changes) and 1137 proteins were downregulated in expression. We identified 363 significant protein changes in the small intestinal mucosa of *c-Rel*<sup>-/-</sup> mice, 220 (60.6%) proteins of which were upregulated and 143 (39.4%) proteins were downregulated in comparison to C57BL/6 wild type control mice.

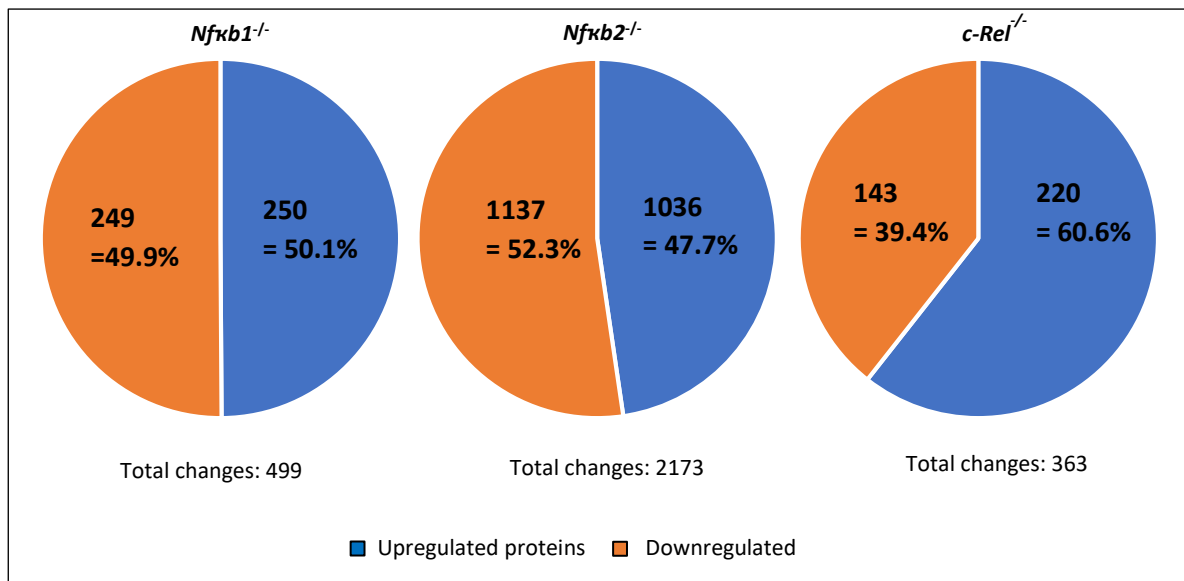


Figure 5.1: Pie chart showing the total number of statistically significantly upregulated and downregulated proteins in *Nfkb1*<sup>-/-</sup>, *Nfkb2*<sup>-/-</sup> and *c-Rel*<sup>-/-</sup> small intestinal mucosa compared to C57BL/6J, comparison of multiple means tested by Student's *t*-test. N=4

### 5.1.1 *Nfkb1*<sup>-/-</sup>

Tables 5.1-A and 1-B show the greatest fold changes of 10 significantly upregulated and downregulated proteins in the small intestinal mucosa of *Nfkb1*<sup>-/-</sup> mice compared with C57BL/6 at baseline in addition to their corresponding expressions in *Nfkb2*<sup>-/-</sup> and *c-Rel*<sup>-/-</sup> mice. Data are expressed as a log<sub>2</sub> fold changes and were tested following logarithmic transformation by student *t*-test and p values are displayed as -log<sub>10</sub> (p-value). We found that proteins that were significantly upregulated in the small intestinal mucosa of *Nfkb1*<sup>-/-</sup> mice also appeared to be significantly upregulated in *Nfkb2*<sup>-/-</sup> mice with the exception of nucleoplasmin-3 and gastrotropin which were not significantly expressed and downregulated respectively (Table 5.1-A). Similarly, *c-Rel*<sup>-/-</sup> mouse small intestinal mucosa showed upregulated expression of the top 10 upregulated *Nfkb1*<sup>-/-</sup> proteins with the exception of RNA-binding protein 3 that was

not significantly expressed and *RIKEN cDNA 2200002D01*, a 28kDa heat-and acid-stable phosphoprotein that was downregulated.

Table 5.11.B indicates the top 10 downregulated proteins in the *Nfκb1*<sup>-/-</sup> mouse small intestinal mucosal proteome compared with C57BL/6 at baseline. These proteins also appeared to be either downregulated or showed no significantly altered regulation in *Nfκb2*<sup>-/-</sup> and *c-Rel*<sup>-/-</sup> small intestinal mucosa compared with C57BL/6 wild type mice as indicated.

### **5.1.2 *Nfκb2*<sup>-/-</sup>**

There were a large number of proteins identified in *Nfκb2*<sup>-/-</sup> small intestinal mucosal samples that were differentially expressed compared with C57BL/6 mice (2173 total changes as shown in appendix A). The majority of the top 10 up- and downregulated proteins of this genotype appeared not to be significantly expressed in *c-Rel*<sup>-/-</sup> mice, while *Nfκb1*<sup>-/-</sup> mice exhibited a similar proteomic profile with the exception of pyridine nucleotide-disulphide oxidoreductase domain 2, adenosine deaminase and proteasome subunit beta type-5 that were not significantly expressed in the *Nfκb1*<sup>-/-</sup> small intestinal mucosa in comparison to C57BL/6 (Tables 5.2.A and 5.2.B).

### 5.1.3 *c-Rel*<sup>-/-</sup>

There were a smaller number of differentially expressed proteins observed in *c-Rel*<sup>-/-</sup> small intestinal mucosa in comparison to C57BL/6 mice compared with the proteomic differences observed between C57BL/6 and *Nfκb1*<sup>-/-</sup> and *Nfκb2*<sup>-/-</sup> transgenic mice, indicating that the small intestinal mucosa of *c-Rel*<sup>-/-</sup> mice may function more normally compared to the other transgenic strains. The top 10 up- or downregulated proteins within the *c-Rel*<sup>-/-</sup> small intestinal mucosa exhibited either reverse or non-significant expression in *Nfκb1*<sup>-/-</sup> and *Nfκb2*<sup>-/-</sup> mice (Tables 5.3-A and B).

<i>Nfkb1</i> <sup>-/-</sup>				Expression in other genotypes	
Protein names	Gene names	Regulation fold change	P value	<i>Nfkb2</i> <sup>-/-</sup>	<i>c-Rel</i> <sup>-/-</sup>
Nucleoplasmin-3	<i>Npm3</i>	10.99	0.0078	None	Up
Tubulin-specific chaperone A	<i>Tbca</i>	7.926	0.0002	Up	None
Calcium-regulated heat stable protein 1	<i>Carhsp1</i>	6.542	0.0002	Up	Up
Gastrotropin	<i>Fabp6</i>	6.458	0.0012	Down	Up
Copper transport protein ATOX1	<i>Atox1</i>	5.072	0.0093	Up	Up
RNA-binding protein 3	<i>Rbm3</i>	4.864	0.0041	Up	None
RIKEN cDNA 2200002D01 gene	<i>2200002D01</i> <i>Rik</i>	4.831	0.0013	Up	Down
Cysteine-rich with EGF-like domain protein 2	<i>Creld2</i>	4.392	0.0076	Up	Up
Regenerating islet-derived protein 3-beta	<i>Reg3b</i>	4.312	0.0024	Up	Up
28kDa heat-and acid-stable phosphoprotein	<i>Pdap1</i>	3.58	0.0216	Up	Down

Table 5.1.A: indicates the top upregulated proteins in *Nfkb1*<sup>-/-</sup> small intestinal mucosa and their expression in *Nfkb2*<sup>-/-</sup> and *c-Rel*<sup>-/-</sup> mice all in comparison to wild-type C57BL/6J mice, N=4 (Up: significant upregulation, Down: significant downregulation, None: non-significant expression).

<i>Nfkb1</i> <sup>-/-</sup>				Expression in other genotypes	
Protein name	Gene name	Regulation fold change	P value	<i>Nfkb2</i> <sup>-/-</sup>	<i>c-Rel</i> <sup>-/-</sup>
Reticulon-3	<i>Rtn3</i>	-11.26	0.0376	None	None
Defensin, alpha, 27	<i>Gm15299 (Defa 27)</i>	-9.762	0.0004	Down	Down
Lysozyme C-1;Lysozyme C-2	<i>Lyz1;Lyz2</i>	-6.755	0.0018	Down	None
Alpha-defensin 20	<i>Defcr20;Defa20</i>	-5.563	0.0341	Down	None
Protein FAM83F	<i>Fam83f</i>	-4.679	0.0014	Down	Down
Cysteine dioxygenase type 1	<i>Cdo1</i>	-4.138	0.001	Down	None
Intelectin-1a	<i>Itln1</i>	-4.132	0.0013	Down	None
Lactase-like protein	<i>Lctf</i>	-4.106	0.0386	Down	Down
Ig alpha chain C region	<i>Igha</i>	-3.978	0.0001	Down	None
Alpha-defensin 23	<i>Defa23</i>	-3.968	0.0037	Down	Down

Table 5.1.B: indicates the top downregulated proteins in *Nfkb1*<sup>-/-</sup> small intestinal mucosa and their expression in *Nfkb2*<sup>-/-</sup> and *c-Rel*<sup>-/-</sup> mice all in comparison to wild-type C57BL/6J mice, N=4 (Down: Downregulation, None: non-significant expression).

<i>Nfkb2</i> <sup>-/-</sup>				Expression in other genotypes	
Protein names	Gene names	Regulation fold change	P value	<i>Nfkb1</i> <sup>-/-</sup>	<i>c-Rel</i> <sup>-/-</sup>
Cytochrome b	<i>Mt-Cyb</i>	6.3045	0.0006	Up	None
Tubulin-specific chaperone A	<i>Tbca</i>	6.2372	0.0001	Up	None
Calumenin	<i>Calu</i>	4.5687	0.0006	Up	None
Histocompatibility 2, class II antigen,A, alpha	<i>H2-Aa</i>	4.4762	0.0082	Up	Up
Copper transport protein ATOX1	<i>Atox1</i>	4.4345	0.0005	Up	Up
Pyridine nucleotide-disulfide oxidoreductase domain 2	<i>Pyroxd2</i>	4.3738	0.0001	None	None
40S ribosomal protein S28	<i>Rps28;Gm10263</i>	4.1087	0.0001	Up	None
Guanine nucleotide-binding protein subunit beta-2-like 1	<i>Gnb2l1</i>	3.8836	0.0005	Up	Up
Adenosine deaminase	<i>Ada</i>	3.8046	0.0018	None	Down
Cysteine-rich with EGF-like domain protein 2	<i>Crel2</i>	3.5998	0.0001	Up	Up

Table 5.2.A: indicates the top upregulated proteins in *Nfkb2*<sup>-/-</sup> small intestinal mucosa and their expression in *Nfkb1*<sup>-/-</sup> and *c-Rel*<sup>-/-</sup> mice all in comparison to wild-type C57BL/6J mice, N=4 (Up: upregulation, Down: downregulation, None: non-significant expression).

<i>Nfkb2</i> <sup>-/-</sup>				Expression in other genotypes	
Protein names	Gene names	Regulation fold change)	P value	<i>Nfkb1</i> <sup>-/-</sup>	<i>c-Rel</i> <sup>-/-</sup>
Ig alpha chain C region	<i>Igha</i>	-11.05	0.0007	Down	None
Ig kappa chain C region	<i>Igkc</i>	-7.942	0.0007	Down	None
Alpha-defensin 20	<i>Defcr20;Defa20</i>	-6.753	0.0049	Down	None
Protein disulfide-isomerase A2	<i>Pdia2</i>	-6.4	0.001	Down	None
Lysozyme C-1;Lysozyme C-2	<i>Lyz1;Lyz2</i>	-5.614	0.0014	Down	None
predicted gene 7849	<i>Gm7849</i>	-5.596	0.0011	Down	None
Histone H2B type 1-C/E/G;Histone H2B type 1-M;Histone H2B type 2-B;Histone H2B type 1-H	<i>Hist1h2bc;Hist1h2bm;Hist2h2bb;Hist1h2bh</i>	-5.554	0.001	Down	None
Proteasome subunit beta type-5	<i>Psm5</i>	-5.379	0.0004	None	None
Alpha-defensin-related sequence 1	<i>Gm14851;Defa-rs1</i>	-5.286	0.001	Down	None
Zymogen granule membrane protein 16	<i>Zg16</i>	-5.125	0.0005	Down	None

Table 5.2.B: indicates the top downregulated proteins in *Nfkb2*<sup>-/-</sup> small intestinal mucosa and their expression in *Nfkb1*<sup>-/-</sup> and *c-Rel*<sup>-/-</sup> mice all in comparison to wild-type C57BL/6J mice, N=4 (Up: upregulation, Down: downregulation, None: non-significant expression).

<i>c-Rel</i> <sup>-/-</sup>				Expression in other genotypes	
Protein names	Gene names	Regulation fold change	P value	<i>Nfκb1</i> <sup>-/-</sup>	<i>Nfκb2</i> <sup>-/-</sup>
Solute carrier family 35 member A4	<i>Slc35a4</i>	16.79	0.0001	None	None
Glutathione peroxidase 2	<i>Gpx2</i>	4.246	0.0002	Up	Up
Unconventional myosin-IXb	<i>Myo9b</i>	2.89	0.0001	Down	Down
Transformation/transcription domain-associated protein	<i>Trrap</i>	2.793	0.0065	None	Noe
MAU2 chromatid cohesion factor homolog	<i>Mau2</i>	2.42	0.0119	Down	Down
Dual oxidase 2	<i>Duox2</i>	2.293	0.029	Noe	Down
Mucosal pentraxin 2	<i>Mptx2</i>	2.154	0.0237	Down	Down
Lactase-like protein	<i>Lct1</i>	2.126	0.0037	Down	Down
Uncharacterized protein KIAA0556	<i>D430042O09Rik;</i> <i>Kiaa0556</i>	2.079	0.0289	None	Up
1,4-alpha-glucan-branching enzyme	<i>Gbe1</i>	2.074	0.0022	None	None

Table 5.3.A: indicates the top upregulated proteins in *c-Rel*<sup>-/-</sup> small intestinal mucosa and their expression in *Nfκb1*<sup>-/-</sup> and *Nfκb2*<sup>-/-</sup> mice all in comparison to wild-type C57BL/6J mice, N=4 (Up: upregulation, Down: downregulation, None: non-significant expression).

<i>c-Rel</i> <sup>-/-</sup>				Expression in other genotypes	
Protein names	Gene names	Regulation fold change	P value	<i>Nfκb1</i> <sup>-/-</sup>	<i>Nfκb2</i> <sup>-/-</sup>
E3 ubiquitin-protein ligase AMFR	<i>Amfr</i>	-2.17	0.0227	None	Down
Galactokinase	<i>Galk1</i>	-2.31	0.0302	None	None
Guanine deaminase	<i>Gda</i>	-2.33	0.0369	Up	Up
Proteasome subunit alpha type-1	<i>Psm1</i>	-2.4	0.0014	None	Up
6-pyruvoyl tetrahydrobiopterin synthase	<i>Pts</i>	-2.45	0.0012	Up	Up
Semaphorin-4G	<i>Sema4g</i>	-2.49	0.0113	Up	Up
Mitochondrial import inner membrane translocase subunit Tim8 A	<i>Timm8a1</i>	-2.67	0.011	Up	Up
Proteasome subunit alpha type-7	<i>Psm7</i>	-2.82	0.0132	None	Up
Proteasome subunit alpha type-5	<i>Psm5</i>	-3.23	0.0427	Up	Up
Serine/threonine-protein kinase 25	<i>Stk25</i>	-10.9	0.0106	Down	Down

Table 5.3.B: indicates the top downregulated proteins in *c-Rel*<sup>-/-</sup> small intestinal mucosa and their expression in *Nfκb1*<sup>-/-</sup> and *Nfκb2*<sup>-/-</sup> mice all in comparison to wild-type C57BL/6J mice, N=4 (Up: upregulation, Down: downregulation, None: not-significant expression).

#### 5.1.4 Summary of the previously investigated biological roles of the identified proteins in intestinal mucosa

The changes in protein expression in the small intestinal mucosa of *Nfkb* transgenic mice in comparison to wild-type C57BL/6J mice indicated some similar differences in *Nfkb1*<sup>-/-</sup> and *Nfkb2*<sup>-/-</sup> mucosal proteins when the proteins which showed the greatest upregulations and downregulations were compared. However, *c-Rel*<sup>-/-</sup> mice showed the least variation from C57BL/6 mice and had different profiles within the 10 proteins which showed the greatest upregulations and downregulations compared with *Nfkb1*<sup>-/-</sup> and *Nfkb2*<sup>-/-</sup> mice. Some of these proteins have previously been shown to play roles in regulating intestinal cellular processes.

Tbca was significantly upregulated in the small intestinal mucosa of *Nfkb1*<sup>-/-</sup> and *Nfkb2*<sup>-/-</sup> mice and has previously been shown to play an essential role in regulating cell viability with loss of this protein leading to cell cycle arrest and cell death (Nolasco *et al.*, 2005). Similarly, Carhsp1 was previously indicated to be an important enhancer required for TNF production (Pfeiffer *et al.*, 2011); this protein showed significantly upregulated expression in all transgenic mice used in our study. Downregulation of gastrotrypin (*Fabp6*) has been shown to cause a disturbance in enterohepatic bile acid circulation and lipid metabolism (Collado-Romero *et al.*, 2015) and transcription of this protein is controlled by NFκB signalling (Fang *et al.*, 2007). We observed an upregulation of gastrotrypin in *Nfkb1*<sup>-/-</sup> and *c-Rel*<sup>-/-</sup> small intestinal mucosa, however, this protein was downregulated at baseline in *Nfkb2*<sup>-/-</sup> mice. Rbm3 was upregulated in *Nfkb1*<sup>-/-</sup> and *Nfkb2*<sup>-/-</sup> mice but was unaltered in *c-Rel*<sup>-/-</sup> small intestinal mucosa and this protein has previously been shown to promote cell proliferation and inhibit apoptosis (Al-Astal *et al.*, 2016). Reg3b was upregulated in the small intestinal mucosa

of all transgenic mouse strains and has previously been shown to inhibit cell proliferation and induce cell apoptosis in the colon (Liu *et al.*, 2017). Lysozyme and various defensins were also significantly downregulated within the small intestinal mucosa of *Nfκb1*<sup>-/-</sup> and *Nfκb2*<sup>-/-</sup> but not *c-Rel*<sup>-/-</sup> mice at baseline. These components are secreted by Paneth cells in small intestinal crypts and have important roles as mediators of enteric innate immunity (Mastroianni and Ouellette., 2009). Defensins also induce the secretion of inflammatory cytokines by activating NFκB signalling pathways (Lin *et al.*, 2004). Psmb5 protein was downregulated in *Nfκb2*<sup>-/-</sup> small intestinal mucosa at baseline but this was not observed in *Nfκb1*<sup>-/-</sup> and *c-Rel*<sup>-/-</sup> strains. Psmb5 was previously identified as activating NFκB signalling pathways leading to the regulation of various pro-inflammatory cytokines including TNF and also regulating cell differentiation and apoptosis (Goldberg *et al.*, 1995). Gpx2 was up-regulated in the small intestinal mucosa of all *Nfκb* transgenic strains and has previously been shown to have a role in reducing colonic crypt epithelial cell apoptosis (Florian *et al.*, 2010). Myo9b was upregulated in *c-Rel*<sup>-/-</sup> but downregulated in *Nfκb1*<sup>-/-</sup> and *Nfκb2*<sup>-/-</sup> small intestinal mucosa and has been reported to be involved in the regulation of epithelial barrier function and to cause increased intestinal permeability in Crohn's disease (Prager *et al.*, 2014 and Wang *et al.*, 2016). Mau2 was upregulated in *c-Rel*<sup>-/-</sup> but downregulated in *Nfκb1*<sup>-/-</sup> and *Nfκb2*<sup>-/-</sup> small intestinal mucosa and previous reports suggest that it maintains immune homeostasis in mice by regulating the interaction between intestinal microbiota and the mucosa and its overexpression increases susceptibility to IBD (Grasberger *et al.*, 2015). Finally, the expression of Stk25 was downregulated in the small intestinal mucosa of all *Nfκb* transgenic mice and this protein has previously been shown to elicit apoptotic cell death by activating the

intrinsic apoptosis pathway (Nogueria *et al.*, 2008). The remaining proteins have not yet been investigated or identified to have any biological role in the small intestinal mucosa.

## **5.2 Does systemic LPS cause any changes in the intestinal mucosal proteome?**

### **5.2.1 LPS resulted in 884 changes in the small intestinal mucosal proteome of C57BL/6J mice**

The total number of proteins that were detected in the small intestinal mucosa of untreated wild type C57BL/6J mice was 5845 and this number was similar in *Nfκb1*<sup>-/-</sup> (5678 proteins), *Nfκb2*<sup>-/-</sup> (5686 proteins) and *c-Rel*<sup>-/-</sup> (5750 proteins) mice suggesting standardisation and validity across all data sets. Following intraperitoneal administration of 0.125 mg/kg LPS into wild-type C57BL/6J mice for 1.5 hours we recorded 884 protein expression changes. 255 (28.85%) of the proteins were upregulated while 629 proteins (71.15%) were downregulated in expression (Figure 5.2). The top 10 proteins with the greatest fold changes that were significantly up- or downregulated in expression in C57BL/6J mice following intraperitoneal injection of LPS are shown below in tables 5.4.A and 5.4.B.

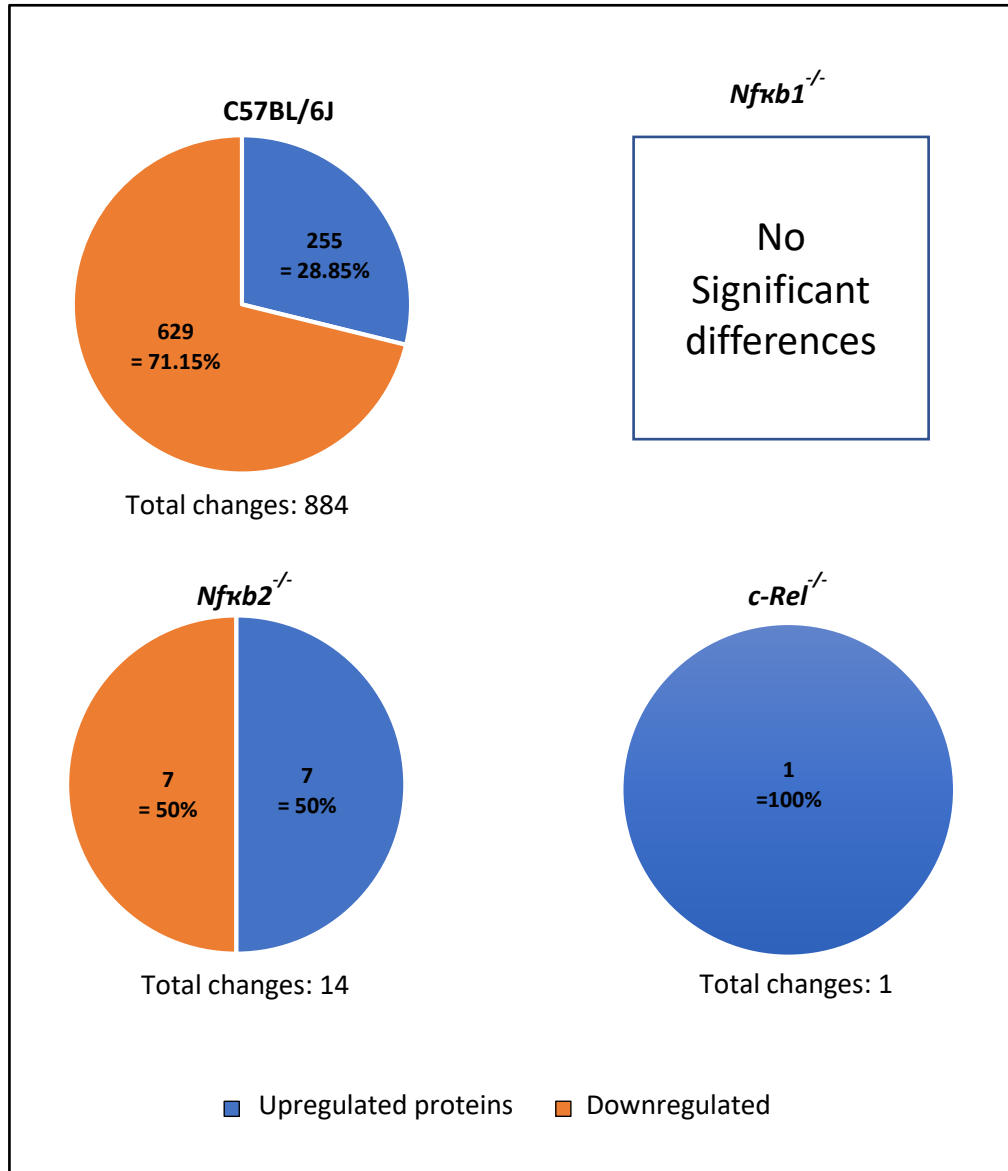


Figure 5.2: Pie charts representing the total significant up and downregulated changes in small intestinal mucosal proteome of *Nfκb1*<sup>-/-</sup>, *Nfκb2*<sup>-/-</sup> and *c-Rel*<sup>-/-</sup> mice 1.5 hours post intraperitoneal administration of bacterial LPS compared with untreated mice of the same strain (N=4).

Protein names	Gene names	Regulation fold change	P value
PHD finger protein 10	<i>Phf10</i>	10.67	0.0017
THAP domain-containing protein 4	<i>Thap4</i>	5.444	0.0004
Lactase-like protein	<i>Lctl</i>	5.103	0.0354
Nucleolar protein 9	<i>Nop9</i>	5.018	0.0181
Reticulon;Reticulon-1	<i>Rtn1</i>	2.785	0.0189
Metastasis-associated protein MTA1	<i>Mta1</i>	2.602	0.0057
Catenin alpha-3	<i>Ctnna3</i>	2.396	0.0041
Proto-oncogene c-Fos	<i>Fos</i>	2.192	0.0009
Acyl-CoA-binding protein	<i>Dbi</i>	1.967	0.0207
Clathrin light chain B	<i>Cltb</i>	1.914	0.0354

Table 5.4-A: The top 10 proteins showing the greatest difference in log<sub>2</sub> fold change that were significantly upregulated in C57BL/6J small intestinal mucosa after intraperitoneal administration of 0.125 mg/kg LPS.

Protein names	Gene names	Regulation fold change	P value
Otolin-1	<i>Otol1</i>	-4.16	0.0162
Carboxypeptidase A1	<i>Cpa1</i>	-3.4	0.0141
Myosin heavy chain 11	<i>Myh11</i>	-2.58	0.005
Tropomodulin-1	<i>Tmod1</i>	-2.55	0.0198
collagen type VI alpha 3 chain	<i>Col6a3</i>	-2.55	0.007
Tubulointerstitial nephritis antigen-like	<i>Tinagl1</i>	-2.4	0.0418
Protein disulfide-isomerase A2	<i>Pdia2</i>	-2.29	0.0133
Tropomyosin alpha-1 chain	<i>Tpm1</i>	-2.22	0.0309
carboxypeptidase B1	<i>Cpb1</i>	-2.17	0.0204
Peptidyl-prolyl cis-trans isomerase FKBP11	<i>Fkbp11</i>	-2.16	0.0001

Table 5.4.B: The top proteins showing the greatest difference in log<sub>2</sub> fold change that were significantly downregulated in the small intestinal mucosa of C57BL/6J mice following 0.125 mg/kg LPS.

Some proteins that showed significant up- or downregulation expression post LPS injection into C57BL/6J mice have previously been demonstrated to play roles in regulating cellular adhesion and apoptosis. For example, reduced expression of Phf10 caused suppression of caspase-3 and inhibited apoptosis in human gastric cancer (Wei

*et al.*, 2010) suggesting that it may be partially responsible for LPS-induced apoptosis within the small intestinal epithelium. Despite the well-known role of *Ctnna3* as a cell-cell adhesion gene, it has also been shown to have a central role in the inhibition of cell proliferation, migration and invasion in hepatocellular carcinoma (He *et al.*, 2016). Additionally, upregulation of *Cpb1* in breast cancer patients caused activation of NFκB and increased a cell survival mechanism (Bouchal *et al.*, 2015).

### **5.2.2 LPS did not induce any significant changes in the small intestinal mucosal proteome of *Nfκb1*<sup>-/-</sup> mice**

Although we identified a total of 5678 proteins contributing to the small intestinal mucosal proteome of untreated *Nfκb1*<sup>-/-</sup> mice, surprisingly none of these proteins showed significant differences in protein expression between untreated and LPS treated *Nfκb1*<sup>-/-</sup> mice (Figure 5.2). This suggests that the 884 protein changes identified in C57BL/6 small intestinal mucosal samples following LPS are in some way (directly or indirectly) either a result of *Nfκb1* activation or that *Nfκb1*<sup>-/-</sup> mice already express many of these 884 proteins at similar levels at baseline to those observed following LPS administration to C57BL/6 mice and they are not further altered by LPS administration. This may at least partly account for the increased susceptibility of *Nfκb1*<sup>-/-</sup> mice to LPS-induced SIEC apoptosis and shedding.

### 5.2.3 The small intestinal mucosal proteome of *Nfκb2<sup>-/-</sup>* and *c-Rel<sup>-/-</sup>* mice showed minimal changes in response to LPS

Only 14 proteins from a total of 5686 proteins identified in the small intestinal mucosa of *Nfκb2<sup>-/-</sup>* mice were shown to have significant differences in expression following administration of 0.125 mg/kg LPS. Seven proteins were upregulated, and 7 proteins were downregulated in expression (Figure 5.2 and Table 5.5).

Myob9 was significantly upregulated in *Nfκb2<sup>-/-</sup>* small intestinal mucosa following LPS treatment, however, this protein was downregulated at baseline when compared with C57BL/6 wild-type mucosa. Myob9 plays a role in the regulation of epithelial barrier function and has been shown to increase gut permeability in Crohn's disease (Preger *et al.*, 2014 and Wang *et al.*, 2016). Additionally, Klhdc4 and Irf8 were significantly downregulated post LPS injection. Decreased expression of Klhdc4 was previously demonstrated to induce spontaneous apoptosis in nasopharyngeal carcinoma cells due to an increase in cleaved caspase-3 (Lian *et al.*, 2016), while Irf8 has been considered to be an essential regulator in Fas-mediated apoptosis and disruption of its function inhibited the activation of cytochrome C, caspase-9 and caspase-3 in a human colon carcinoma cell line *in vitro* and in murine primary mammary carcinoma and lung metastases *in vivo* (Yang *et al.*, 2007 and Yang *et al.*, 2009). These proteins may therefore contribute to the reduced susceptibility of *Nfκb2<sup>-/-</sup>* mice to LPS-induced SIEC apoptosis and shedding.

Following LPS administration into *c-Rel<sup>-/-</sup>* mice, we only identified a significant change in a single protein (Ig heavy chain V region VH558 A1/A4) from 5750 proteins analysed. This protein showed a significant upregulation in expression following LPS treatment in comparison to untreated *c-Rel<sup>-/-</sup>* mice (Table 5.6). This protein has not been

previously shown to play any biological role in the small intestinal mucosa, although as it is an immunoglobulin, it may have a role in humoral immunity.

Protein names	Gene names	Regulation fold change	P value
Protein FAM50A	<i>Fam50a</i>	2.567	0.0049
NADH dehydrogenase [ubiquinone] 1 alpha subcomplex assembly factor 5	<i>Ndufaf5</i>	2.549	0.0155
Snf2 related CREBBP activator protein	<i>Srcap</i>	1.892	0.0001
Pre-B-cell leukemia transcription factor 1;Pre-B-cell leukemia transcription factor 2	<i>Pbx1;Pbx2</i>	1.765	0.0003
Translation factor Guf1, mitochondrial	<i>Guf1</i>	1.682	0.0011
Transmembrane protein 253	<i>Tmem253</i>	1.602	0.0036
Unconventional myosin-IXb	<i>Myo9b</i>	1.376	0.0003
L-lactate dehydrogenase;L-lactate dehydrogenase B chain	<i>Ldhb</i>	-2.549	0.0047
60S ribosomal protein L18	<i>Rpl18</i>	-1.972	0.0025
Solute carrier family 35 member E2	<i>Slc35e2</i>	-1.505	0.0014
Peptidyl-prolyl cis-trans isomerase-like 3;Peptidyl-prolyl cis-trans isomerase	<i>Ppil3</i>	-1.434	0.0003
Kelch domain-containing protein 4	<i>Klhdc4</i>	-1.424	0.0012
Interferon regulatory factor 8	<i>Irf8</i>	-1.357	0.0005
F-box only protein 25	<i>Fbxo25</i>	-1.329	0.0005

Table 5.5: indicating the changes in small intestinal mucosal proteome of *Nfkb2<sup>-/-</sup>* mice following LPS administration compared to untreated mice of the same genotype. The top half shows the significantly upregulated proteins (blue) while the lower section shows significantly downregulated proteins (orange) (N=4).

Protein names	Gene names	Regulation fold change	P value
Ig heavy chain V region VH558 A1/A4	<i>Ighv1-23;Ighv1-81;Ighv1-77;Ighv1-78;Ighv1-62-2;Ighv1-80;Ighv1-63;Ighv1-54;Ighv1-7;Ighv1-4;Gm5629</i>	5.242	0.0017

Table 5.6: Upregulation of proteins in the small intestinal mucosal proteome in *c-Rel<sup>-/-</sup>* mice following LPS administration compared with untreated *c-Rel<sup>-/-</sup>* (N=4).

### **5.3 LPS exclusively induces 298 proteomic changes in *Nfκb1*<sup>-/-</sup> small intestinal mucosa compared with C57BL/6J mice**

We have described the differences in baseline protein expression changes between transgenic mice with different deletions in *Nfκb* subunits (section 5.1) and have identified the protein changes within the mucosa in response to LPS within each genotype (section 5.2). We now aim to characterise the differences in small intestinal mucosal protein expression between LPS treated transgenic mice of each genotype and LPS treated C57BL/6 mice whilst taking into consideration the baseline differences in small intestinal mucosal proteome between transgenic and C57BL/6 wild-type mice. To identify the specific changes in small intestinal mucosal proteome of *Nfκb1*<sup>-/-</sup> mice in comparison to the proteome of wild type C57BL/6J mice following LPS treatment we made a comparison between two different comparisons (untreated *Nfκb1*<sup>-/-</sup> vs untreated C57BL/6J against LPS-treated *Nfκb1*<sup>-/-</sup> vs LPS-treated C57BL/6J). Based on this comparison we identified 797 total significant differences between the small intestinal mucosal proteome of *Nfκb1*<sup>-/-</sup> mice and C57BL/6J mice. 49.4% of these changes appeared to be significantly upregulated proteins while 50.6% represented proteins with downregulated expression (Figure 5.3).

Interestingly, 208 proteins representing 83.2% from a total of 250 proteins with significant upregulation differences were exclusively seen between untreated *Nfκb1*<sup>-/-</sup> and untreated C57BL/6J mice. By contrast, from a total of 144 upregulated proteins with significant differences between LPS-treated *Nfκb1*<sup>-/-</sup> and LPS-treated C57BL/6J mice, only 102 proteins were exclusively noted in the LPS treated comparison. The remaining 42 proteins were seen significantly upregulated in both LPS-treated and untreated comparison groups. (Figure 5.3-A).

Correspondingly, we found 403 proteins which showed significant downregulation between *Nfkb1*<sup>-/-</sup> and C57BL/6J small intestinal mucosa (Figure 5.3-B). 178 proteins (representing 71.5% of the total 249 proteins) that were downregulated between untreated *Nfkb1*<sup>-/-</sup> and untreated C57BL/6J small intestinal mucosa exclusively appeared in the untreated comparison group. 83 proteins were exclusively identified between LPS treated *Nfkb1*<sup>-/-</sup> and C57BL/6J mice. A further 71 proteins were significantly down regulated in both LPS-treated and untreated comparisons between *Nfkb1*<sup>-/-</sup> and C57BL/6J small intestinal mucosa (Figure 5.3-B).

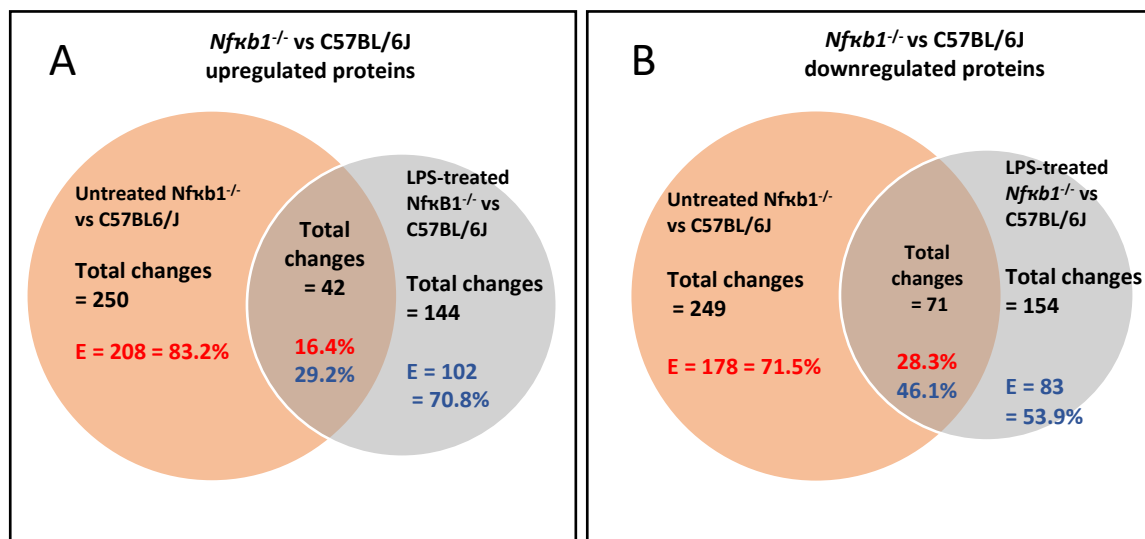


Figure 5.3: Venn graph indicating a comparison of significant proteomic changes between *Nfkb1*<sup>-/-</sup> and C57BL/6J mice before and after IP injection of 0.125 mg/kg LPS (N=4). A) shows upregulated and B) shows downregulated protein numbers. E= proteomic changes that exclusively seen in the corresponding comparison.

In summary, the total significant proteomic changes that were exclusively noted between *Nfkb1*<sup>-/-</sup> and C57BL/6J mice following administration of LPS at 0.125mg/kg were 102 proteins that were significantly upregulated and 83 proteins which showed significant downregulation.

Tables 5.7 and 5.8 describe the top 10 up- and downregulated proteins with the greatest differences in fold change between LPS-treated *Nfκb1*<sup>-/-</sup> and LPS-treated C57BL/6J small intestinal mucosa excluding the protein differences that were observed at baseline between these genotypes. We identified that some proteins were downregulated between untreated *Nfκb1*<sup>-/-</sup> and C57BL/6J mice but were upregulated after administration of LPS between the same genotypes and vice versa. Among the top 10 upregulated proteins only one protein has previously been indicated to have a biological role in the small intestinal mucosa. Pla2g6 is an enzyme that catalyses the release of fatty acids from phospholipids. It was previously shown to promote intestinal epithelial cell apoptosis and inhibit crypt cell regeneration causing damage to the intestinal barrier and exacerbating colitis (Jialo *et al.*, 2015). Overexpression of Pla2g6 may therefore contribute to the increased susceptibility of *Nfκb1*<sup>-/-</sup> mice to LPS-induced SIEC apoptosis and shedding.

Phf10 and Stx3 were significantly downregulated in *Nfκb1*<sup>-/-</sup> versus C57BL/6 small intestinal mucosa following LPS administration and both proteins have been previously investigated. Phf10 suppressed caspase-3 activation and inhibited apoptosis in a gastric cancer cell line (Wei *et al.*, 2010), while loss of Stx3 caused the variant microvillus inclusion disease “congenital enteropathy of apical microvilli” (Wiegerinck *et al.*, 2014 and Hong *et al.*, 2016) suggesting that these proteins may modulate susceptibility to LPS-induced SIEC apoptosis and shedding. The remaining proteins listed in tables 5.7 and 5.8 have not previously been investigated or identified to have a biological role in the small intestinal mucosa.

Proteomics comparison		LPS-treated ( <i>Nfκb1</i> <sup>-/-</sup> vs C57BL/6J)		untreated ( <i>Nfκb1</i> <sup>-/-</sup> vs C57BL/6J)	
Protein names	Gene names	Regulation fold change	P value	Regulation fold change	P value
Solute carrier family 35 member B1	<i>Slc35b1</i>	7.642	0.0034	1.659	0.537
NADH-ubiquinone oxidoreductase chain 5	<i>Mtnd5</i>	3.766	0.0301	1.31	0.7079
NADH:ubiquinone oxidoreductase core subunit S1	<i>Ndufs1</i>	3.546	0.0005	1.84	0.123
85/88 kDa calcium-independent phospholipase A2	<i>Pla2g6</i>	3.246	0.0002	1.485	0.0741
Protein transport protein Sec61 subunit gamma	<i>Sec61g</i>	3.158	0.0007	1.495	0.2344
Oligosaccharyltransferase complex subunit OSTC	<i>Ostc</i>	3.012	0.0442	-1.29	0.7943
Apolipoprotein C-I;Truncated apolipoprotein C-I	<i>Apoc1</i>	2.749	0.0042	1.05	0.6761
ATP synthase subunit e, mitochondrial	<i>Atp5i;Atp5k</i>	2.615	0.0005	1.659	0.0257
interferon gamma induced GTPase	<i>lgtp</i>	2.526	0.0014	1.58	0.123
DNA-dependent protein kinase catalytic subunit	<i>Prkdc</i>	2.488	0.0005	1.165	0.5012

Table 5.7: The top 10 upregulated proteins with greatest log<sub>2</sub> differences in *Nfκb1*<sup>-/-</sup> small intestinal mucosa in comparison to C57BL/6J post LPS administration and the log<sub>2</sub> differences at baseline (untreated) between *Nfκb1*<sup>-/-</sup> and C57BL/6 small intestinal mucosa for these proteins. (N=4)

Proteomics comparison		LPS-treated ( <i>Nfκb1</i> <sup>-/-</sup> vs C57BL/6J)		Untreated ( <i>Nfκb1</i> <sup>-/-</sup> vs C57BL/6J)	
Protein names	Gene names	Regulation fold change	P value	Regulation fold change	P value
PHD finger protein 10	<i>Phf10</i>	-7.91	0.0005	1.39	0.5129
THAP domain-containing protein 4	<i>Thap4</i>	-7.04	0.0003	-1.1	0.6166
Serine (or cysteine) peptidase inhibitor, clade B, member 9b and 9c	<i>Serpib9b;Serpib9c</i>	-3.5	0.001	-1.8	0.1549
Aminoacylase-1	<i>Acy1</i>	-3.39	0.0401	-1.6	0.0214
Reticulon;Reticulon-1	<i>Rtn1</i>	-3.36	0.0022	-1.5	0.2455
Liver carboxylesterase 1	<i>Ces1</i>	-2.99	0.0016	-1.5	0.302
Syntaxin-3	<i>Stx3</i>	-2.77	0.0003	-1.4	0.2138
Solute carrier family 15 member 1	<i>Slc15a1</i>	-2.68	0.0006	-1.5	0.0813
Ectonucleotide pyrophosphatase/phosphodiesterase 3	<i>Enpp3</i>	-2.61	0.0078	-1.3	0.166
ADP-ribosyl cyclase/cyclic ADP-ribose hydrolase 2	<i>Bst1</i>	-2.55	0.0008	-1.3	0.4266

Table 5.8: The top 10 downregulated proteins with greatest log<sub>2</sub> differences in *Nfκb1*<sup>-/-</sup> small intestinal mucosa in comparison to C57BL/6J post LPS administration and log<sub>2</sub> differences at baseline (untreated) between *Nfκb1*<sup>-/-</sup> and C57BL/6 small intestinal mucosa for these proteins. (N=4)

#### **5.4 118 significant small intestinal mucosal proteomic changes were identified exclusively in LPS-treated *Nfκb2<sup>-/-</sup>* mice compared to LPS-treated C57BL/6J mice**

Following the administration of LPS we found 915 significant changes in the small intestinal mucosal proteome of *Nfκb2<sup>-/-</sup>* mice in comparison to LPS-treated C57BL/6J mice. 419 proteins were significantly upregulated (representing 45.8% of the total proteomic changes) while the remaining 496 proteins (54.2%) were downregulated. To determine the significant proteomic changes that arose exclusively following LPS administration (i.e. excluding baseline differences between *Nfκb2<sup>-/-</sup>* and C57BL/6J mice from the analysis) we compared all significant changes that were observed between these two genotypes before and after LPS administration. Interestingly we found that only 46 proteins (representing 11% from the total upregulation changes post LPS injection) were upregulated in LPS-treated *Nfκb2<sup>-/-</sup>* mice compared to LPS-treated C57BL/6J mice when baseline differences in the small intestinal mucosal proteome of *Nfκb2<sup>-/-</sup>* and C57BL/6J mice were excluded (Figure 5.4-A). We also found that only 72 proteins (14.5%) (from a total of 496 significantly downregulated proteins) in LPS-treated *Nfκb2<sup>-/-</sup>* compared to LPS-treated C57BL/6J mice showed significant changes as a result of LPS administration (Figure 5.4-B). The majority of up- and downregulated proteins (89% and 85.5% respectively) observed between *Nfκb2<sup>-/-</sup>* and C57BL/6J small intestinal mucosa were identified both before and after IP administration of LPS (Figure 5.4).

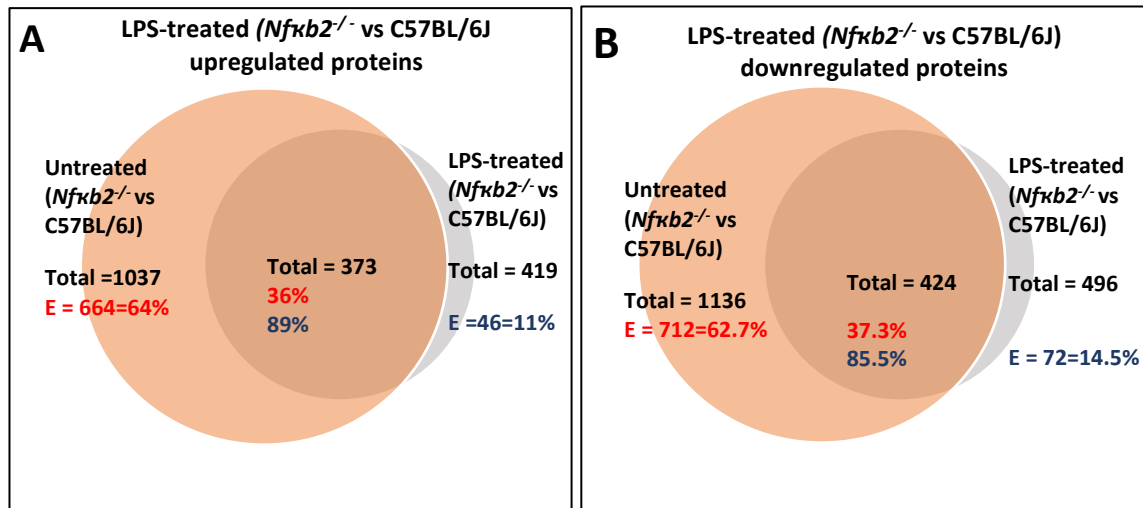


Figure 5.4: Venn graph indicating a comparison of significant proteomic changes between *Nfκb2*<sup>-/-</sup> and C57BL/6J mice before and after IP injection of 0.125mg/kg LPS (N=4). A) shows upregulated and B) shows downregulated protein numbers. E= proteomic changes that were exclusively seen in the corresponding comparison.

Tables 5.9 and 5.10 show the top 10 log<sub>2</sub> fold up- and downregulations in protein expression in the small intestinal mucosa of LPS-treated *Nfκb2*<sup>-/-</sup> versus C57BL/6J mouse groups and the expression of these proteins in the *Nfκb2*<sup>-/-</sup> versus C57BL/6J untreated groups comparison. The majority of these proteins have not previously been investigated or identified as having a biological role in the small intestinal mucosa.

We identified some proteins that were significantly downregulated in untreated *Nfκb2*<sup>-/-</sup> mouse small intestinal mucosa that were significantly upregulated in LPS treated *Nfκb2*<sup>-/-</sup> mice when compared against untreated and LPS treated C57BL/6 small intestinal mucosa respectively; these were Guf1 and Cdc42bpa. Guf1 has not previously been shown to play any role in small intestinal mucosal homeostasis, but Cdc42bpa has been shown to be downregulated in jejunal epithelial cells of enterotoxigenic *E. coli* (ETEC)-infected piglets resulting in NFκB and MAPK pathway

inhibition (Ren *et al.*, 2016). We also identified proteins that were upregulated at baseline such as Mrpl21 (not previously identified to have a biological role in the small intestine) and Phf10 (described above; knockdown of Phf10 activated caspase-3 and induced apoptosis in gastric cancer cells; Wei *et al.*, 2010) and these exhibited downregulation after LPS injection (Table 5.9 and 5.10).

Proteomics comparison		LPS-treated ( <i>Nfkb2</i> <sup>-/-</sup> vs C57BL/6J)		Untreated ( <i>Nfkb2</i> <sup>-/-</sup> vs C57BL/6J)	
Protein names	Gene names	Log2 (Differences)	-Log10 (p-value)	Log2 (Differences)	-Log10 (p-value)
NADH dehydrogenase [ubiquinone] 1 alpha subcomplex assembly factor 5	<i>Ndufaf5</i>	2.962	0.0019	1.21	0.389
Peripherin	<i>Prph</i>	2.149	0.0033	1.09	0.8318
Interferon-induced guanylate-binding protein 2	<i>Gbp2</i>	1.809	0.0065	1.16	0.389
Ras-related protein Rab-8B	<i>Rab8b</i>	1.795	0.0004	1.23	0.0759
Volume-regulated anion channel subunit LRRC8A	<i>Lrrc8a</i>	1.672	0.0003	1.14	0.0363
Translation factor Guf1, mitochondrial	<i>Guf1</i>	1.596	0.0016	-1.1	0.1047
Annexin	<i>Anxa6</i>	1.595	0.0161	1.21	0.2042
Serine/threonine-protein kinase MRCK alpha	<i>Cdc42bpa</i>	1.586	0.0019	-1.1	0.6457
Disheveled-associated activator of morphogenesis 1	<i>Daam1</i>	1.582	0.0112	1.17	0.263
Ufm1-specific protease 2	<i>Ufsp2</i>	1.566	0.0012	1.24	0.0661

Table 5.9: The top 10 upregulated proteins with greatest log<sub>2</sub> differences in *Nfkb2*<sup>-/-</sup> small intestinal mucosa in comparison to C57BL/6J post LPS administration and log<sub>2</sub> differences at baseline (untreated) between *Nfkb2*<sup>-/-</sup> and C57BL/6 small intestinal mucosa for these proteins. (N=4)

Proteomics comparison		LPS-treated ( <i>Nfkb2</i> <sup>-/-</sup> vs C57BL/6J)		Untreated ( <i>Nfkb2</i> <sup>-/-</sup> vs C57BL/6J)	
Protein names	Gene names	Regulation fold change	P value	Regulation fold change	P value
PHD finger protein 10	<i>Phf10</i>	-9.49	0.0004	1.18	0.6761
Ly6/PLAUR domain-containing protein 8	<i>Lypd8</i>	-1.84	0.0122	-1.09	0.871
39S ribosomal protein L21, mitochondrial	<i>Mrpl21</i>	-1.75	0.0016	1.14	0.3162
Hepatoma-derived growth factor-related protein 2	<i>Hdgfrp2</i>	-1.69	0.0025	-1.16	0.1585
Protein phosphatase 1 regulatory subunit 12C	<i>Ppp1r12c</i>	-1.68	0.0001	-1.03	0.8318
Bcl-2-like protein 15	<i>Bcl2l15</i>	-1.67	0.0314	-1.24	0.1122
ER lumen protein-retaining receptor 1, receptor 2 and receptor 3	<i>Kdelr1, Kdelr2, Kdelr3</i>	-1.67	0.0353	-1.02	0.912
Kinesin-like protein KIF11	<i>Kif11</i>	-1.66	0.0003	-1.19	0.0182
Essential MCU regulator, mitochondrial	<i>Smdt1</i>	-1.66	0.0067	-1.21	0.2042
Cell division cycle protein 23 homolog	<i>Cdc23</i>	-1.64	0.0076	-1.01	0.912

Table 5.10: The top 10 downregulated proteins with greatest log<sub>2</sub> differences in *Nfkb2*<sup>-/-</sup> small intestinal mucosa in comparison to C57BL/6J post LPS administration and log<sub>2</sub> differences at baseline (untreated) between *Nfkb2*<sup>-/-</sup> and C57BL/6 small intestinal mucosa for these proteins (N=4).

## 5.5 Small intestinal mucosal proteomic analysis of *c-Rel*<sup>-/-</sup> mice identified 176 changes in comparison to C57BL/6J

Comparison of the *c-Rel*<sup>-/-</sup> small intestinal mucosal proteome with C57BL/6J after IP administration of 0.125mg/kg LPS indicated 176 significant protein changes. 83 proteins (47.16% of the total proteins) were significantly upregulated while the remaining 93 proteins (52.84%) were significantly downregulated. 57 upregulated proteins (68.7% of total proteins with upregulated expression) and 63 down regulated proteins (67.7% of total downregulated proteins) were expressed exclusively in *c-Rel*<sup>-/-</sup> versus C57BL/6J LPS treated mouse small intestinal mucosae and showed no significant differences at baseline between *c-Rel*<sup>-/-</sup> and C57BL/6 strains. (Figure 5.5)

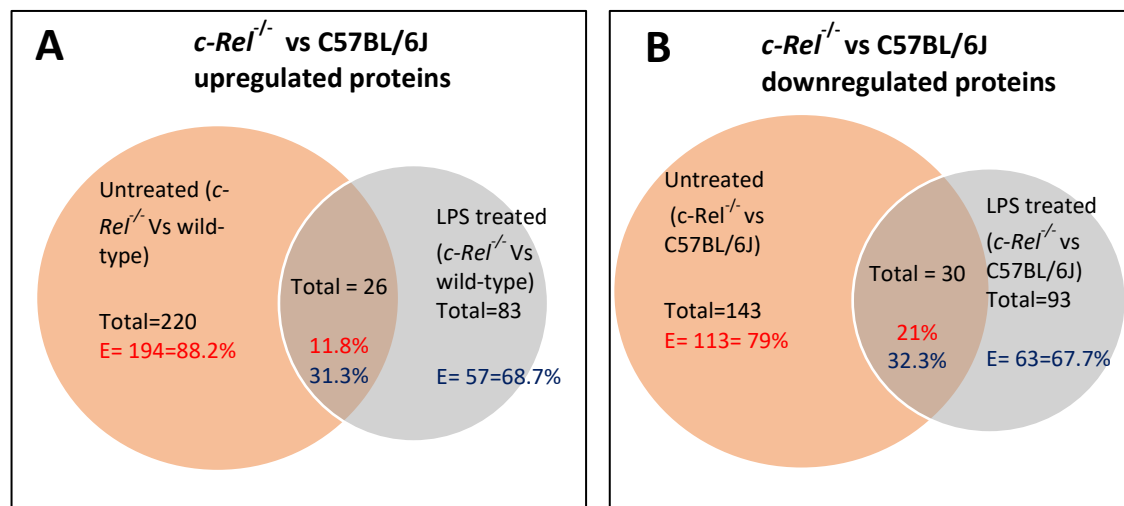


Figure 5.5: Venn graph indicating a comparison of significant protein changes between *c-Rel*<sup>-/-</sup> and C57BL/6J mice before and after IP injection of 0.125mg/kg LPS (N=4) A) shows upregulated and B) shows downregulated protein numbers. E= proteomic changes that exclusively seen in the corresponding comparison.

Tables 5.11 and 5.12 show the proteins with the greatest up- and downregulation  $\log_2$  fold changes in the *c-Rel*<sup>-/-</sup> small intestinal mucosal proteome compared with C57BL/6J following IP injection of 0.125mg/kg LPS that showed non-significant proteomic changes in the untreated *c-Rel*<sup>-/-</sup> vs C57BL/6J comparison.

Myo9b (associated with increased gut permeability in Crohn's disease, Prager *et al.*, 2014, Wang *et al.*, 2016), Mpx2 (newly identified as a Paneth cell marker but its function is unknown, Haber *et al.*, 2017) and Piger (which is downregulated in the colonic mucosa in ulcerative colitis, Bruno *et al.*, 2015) were upregulated in *c-Rel*<sup>-/-</sup> small intestinal mucosa in comparison to C57BL/6J mice following LPS injection. By contrast Klf5, which is involved in the regulation of various biological processes including cell proliferation, differentiation, development and apoptosis and which is normally expressed in proliferating epithelial cells at the base of intestinal crypts, was significantly downregulated in LPS-treated *c-Rel*<sup>-/-</sup> mice in comparison to LPS-treated C57BL/6J small intestinal mucosa.

Proteomics comparison		LPS-treated ( <i>c-Rel</i> <sup>-/-</sup> vs C57BL/6J)		untreated ( <i>c-Rel</i> <sup>-/-</sup> vs C57BL/6J)	
Protein names	Gene names	Regulation fold change	P value	Regulation fold change	P value
Unconventional myosin-IXb	<i>Myo9b</i>	3.99	0.0018	1.61	0.4169
Transformation/transcription domain-associated protein	<i>Trrap</i>	3.88	0.0495	2.13	0.2042
Mucosal pentraxin 2	<i>Mptx2</i>	3.25	0.0493	0.91	0.8318
Uncharacterized protein KIAA0556	<i>D430042O09Rik</i> ; <i>Kiaa0556</i>	3.00	0.019	1.43	0.3467
1,4-alpha-glucan-branching enzyme	<i>Gbe1</i>	2.71	0.0387	1.61	0.2399
Regenerating islet-derived protein 3-gamma	<i>Reg3g</i>	2.49	0.0003	1.31	0.5248
Sorting nexin-3	<i>Snx3</i>	2.22	0.0002	1.33	0.182
Polymeric immunoglobulin receptor	<i>Pigr</i>	2.20	0.0003	1.4	0.1995
MLV-related proviral Env polyprotein	Transmembrane protein	1.97	0.0102	1.14	0.0363
Nectin-2	<i>Pvrl2</i>	1.85	0.0007	1.18	0.0912

Table 5.11: The top 10 upregulated proteins with greatest log<sub>2</sub> differences in *c-Rel*<sup>-/-</sup> small intestinal mucosa in comparison to C57BL/6J post LPS administration and log<sub>2</sub> differences at baseline (untreated) between *c-Rel*<sup>-/-</sup> and C57BL/6 small intestinal mucosa for these proteins. (N=4)

Proteomics comparison		LPS-treated ( <i>c-Rel</i> <sup>-/-</sup> vs C57BL/6J)		untreated ( <i>c-Rel</i> <sup>-/-</sup> vs C57BL/6J)	
Protein names	Gene names	Regulation fold change	P value	Regulation fold change	P value
Kruppel-like factor 5	<i>Klf5</i>	-8.69	0.0005	1.04	0.9333
Solute carrier family 2, facilitated glucose transporter member 5	<i>Slc2a5</i>	-4.38	0.0006	-1.59	0.0955
Sodium/potassium-transporting ATPase subunit alpha-4	<i>Atp1a4</i>	-3.79	0.0019	1.18	0.1862
Replication factor C subunit 2		-3.26	0.0013	-1.75	0.1175
Acyl-coenzyme A thioesterase 2, mitochondrial	<i>Acot2</i>	-2.24	0.0005	-1.2	0.257
39S ribosomal protein L17, mitochondrial	<i>Mrpl17</i>	-2	0.0004	-1.03	0.8318
39S ribosomal protein L21, mitochondrial	<i>Mrpl21</i>	-1.93	0.0002	-1.59	0.0676
H/ACA ribonucleoprotein complex subunit 2	<i>Nhp2</i>	-1.87	0.0281	-1.47	0.2089
Trafficking protein particle complex subunit 5	<i>Trappc5</i>	-1.85	0.0283	-1.39	0.1862
Dehydrogenase/reductase SDR family member 4	<i>Dhrs4</i>	-1.82	0.0046	1.06	0.7413

Table 5.12: The top 10 downregulated proteins with greatest log<sub>2</sub> differences in *c-Rel*<sup>-/-</sup> small intestinal mucosa in comparison to C57BL/6J post LPS administration and log<sub>2</sub> differences at baseline (untreated) between *c-Rel*<sup>-/-</sup> and C57BL/6 small intestinal mucosa for these proteins. (N=4)

## 5.6 Discussion

In this chapter we have studied the small intestinal mucosal proteome of C57BL/6J mice and how the proteome changed following the germline deletion of *Nfκb1*, *Nfκb2* and *c-Rel*. We have also investigated the role of LPS in inducing changes in the small intestinal mucosal proteome in C57BL/6J mice. Using *Nfκb1*<sup>-/-</sup>, *Nfκb2*<sup>-/-</sup> and *c-Rel*<sup>-/-</sup> genotypes, we have identified proteins that may play important roles in the induction and resistance of pathological apoptosis and shedding of murine SIECs following systemic administration of bacterial LPS. Furthermore, we studied these protein regulation changes to try to understand why *Nfκb2*<sup>-/-</sup> mice were more resistant and *Nfκb1*<sup>-/-</sup> mice were more susceptible to LPS- induced SIEC apoptosis and shedding.

To date, there have been no studies discussing changes in the small intestinal proteome of *Nfκb1*<sup>-/-</sup>, *NfκB2*<sup>-/-</sup> and *c-Rel*<sup>-/-</sup> mice in comparison to C57BL/6J mice before and after the administration of bacterial LPS. The small intestinal proteome of these mice indicated differences in upregulated and downregulated proteins. For example, gastrotropin (also known as fatty acid binding protein 6) is regulated by NFκB activation (Fang *et al.*, 2007) and was upregulated in *NfκB1*<sup>-/-</sup> and *c-Rel*<sup>-/-</sup> small intestinal mucosa and downregulated in *Nfκb2*<sup>-/-</sup> mice compared to C57BL/6J and has previously been reported to be overexpressed in colorectal cancer and adenomas compared with normal colonic epithelium (Ohmachi *et al.*, 2006). Gastrotropin may therefore contribute to the increased susceptibility of *c-Rel*<sup>-/-</sup> and reduced susceptibility of *Nfκb2*<sup>-/-</sup> mice to Dextran sulphate sodium/azoxymethane induced colon tumours as previously observed in our laboratory (Burkitt *et al.*, 2015) in addition to regulating how the small intestinal mucosa responds to damage-inducing stimuli such as LPS. Proteasome subunit beta type-5 (Psm5) has a role in activation

of NFκB and regulates the expression of pro-inflammatory cytokines such as TNF and interleukins (Goldberg *et al.*, 1995). Psm5 was downregulated in *Nfκb2<sup>-/-</sup>* mice but non-significantly expressed in *Nfκb1<sup>-/-</sup>* and *c-Rel<sup>-/-</sup>* mice (see more differences in tables 5.1, 5.2 and 5.3). These baseline differences in proteome may contribute to why these genotypes respond with different susceptibilities to induced SIEC apoptosis and shedding in response to bacterial LPS.

Comparing the small intestinal proteomes of *NfκB1<sup>-/-</sup>*, *NfκB2<sup>-/-</sup>* and *c-Rel<sup>-/-</sup>* genotypes before and after LPS administration also indicated differences (see Figure 5.2, tables 5.5 and 5.6). A previous study by Huang and colleagues in 2002 described the proteomic analysis of LPS induced apoptosis in rat pheochromocytoma cells (PC12 cells) and found that LPS induced apoptosis was characterised by changes in proteins associated with endoplasmic reticulum, mitochondria and cell membrane including an increase in the level of calreticulin, calcium binding protein 50, endoplasmic reticulum protein 60, heat shock protein 60 and a decrease in the levels of amphoterin, cytochrome c oxidase poly peptide VIa-liver or endoplasmic reticulum protein 29 (ERP29) (Huang *et al.*, 2002). In our proteomic analysis we found that calreticulin protein (*Calr*) was upregulated in untreated *Nfκb1<sup>-/-</sup>* and *c-Rel<sup>-/-</sup>* mice and downregulated after administration of LPS to these genotypes, whereas it was upregulated pre- and post LPS administration in *Nfκb2<sup>-/-</sup>* small intestinal mucosa. Plant homeodomain finger protein 10 (Phf10) was downregulated in the small intestinal mucosa of LPS-treated *NfκB1<sup>-/-</sup>* and *NfκB2<sup>-/-</sup>* mice compared with LPS-treated C57BL/6J mice. Proteins from this family are well documented to be capable of translocating to the nucleus and regulating transcription (see table 5.8 and 5.10). Phf10 protein expression was previously shown to suppress active caspase 3 expression

and led to impaired apoptosis in gastric cancer cells (Wei *et al.*, 2010). However, Phf10 is likely to have many more functions as it is capable of modulating the transactivating capacity of several common NFκB dimers (both classical and alternative NFκB signalling pathways) in response to TNF (Ishizaka *et al.*, 2012). As Phf10 is one of the proteins that has been consistently identified as having one of the greatest fold changes within our analysis, this transcription factor/co-factor warrants further investigation into how important it is in regulating SIEC apoptosis and shedding in response to LPS and TNF. Furthermore, Bcl-2-like protein 15 contains the BH2 and BH3 domains of the Bcl-2 family and is pro-apoptotic (Zhang *et al.*, 2007). Members of this family of proteins can be pro- or anti-apoptotic and have previously been shown to play important roles in regulating spontaneous and induced apoptosis along the intestinal epithelium (Pritchard *et al.*, 2000, Duckworth and Pritchard, 2009). In our study Bcl-2-like protein 15 was significantly downregulated in LPS-treated *Nfκb2<sup>-/-</sup>* small intestinal mucosa and upregulated in LPS-treated C57BL/6J and *Nfκb1<sup>-/-</sup>* mice (see table 5.10 and appendices 4 and 5), suggesting that the reduced expression of this pro-apoptotic Bcl-2 family member in the *Nfκb2<sup>-/-</sup>* small intestinal mucosa may prevent LPS-induced epithelial cell apoptosis and consequential cell shedding.

In summary, the proteomic analysis of the small intestinal mucosal proteome of *Nfκb1<sup>-/-</sup>*, *Nfκb2<sup>-/-</sup>* and *c-Rel<sup>-/-</sup>* mice indicated significant alterations with different regulatory expressions in comparison to the C57BL/6J small intestinal mucosal proteome. LPS caused various changes in protein expression in each *Nfκb* transgenic mouse group reflecting the differences in response of these mice to pathological apoptosis and shedding induced by administration of bacterial LPS. The data presented in this chapter have identified several targets that need further and deeper

investigation by techniques such as western blot and immunohistochemistry, and by genetic knockdown/overexpression in small intestinal organoids or *in vivo* to identify the importance and localisation of these proteins in regulating the response to LPS induced SIEC apoptosis and shedding.

## 6. Investigation of stimuli other than LPS that induce small intestinal epithelial cell apoptosis and shedding

### 6.1 Introduction

Small intestinal epithelial cell apoptosis and shedding can be induced by agents other than bacterial lipopolysaccharide (LPS). Among these agents are anti-CD3 antibody, polyinosinic:polycytidylic (poly I:C) acid and tumour necrosis factor (TNF).

Intraperitoneal administration of anti-CD3 antibody (clone 145-2C11) *in vivo* activates the T-lymphocytes that play a crucial role in gut epithelial cell inflammatory responses and results in increased small intestinal epithelial cell apoptosis and shedding (Merger *et al.*, 2002 and Miura *et al.*, 2005) and an increase in intestinal epithelial barrier permeability (Zhou *et al.*, 2004). Yamamoto *et al.*, 1998 showed that stimulation of intraepithelial T lymphocytes via the TCR-CD3 complex caused a high proliferation index in the intestinal mucosa with increased cytokine synthesis. Intestinal epithelial cells express toll-like receptors (TLRs) and when these are stimulated this leads to an increase in pathological apoptosis and shedding with loss of intestinal barrier function.

Previous studies have indicated that stimulation of TLR4 by bacterial lipopolysaccharide and of TLR3 by poly I:C (a synthetic analogue of double-stranded RNA virus) induces the apoptosis and shedding of small intestinal epithelial cells. This subsequently influences mucosal homeostasis and increases gut barrier permeability (Williams *et al.*, 2013 and McAllister *et al.*, 2012).

Binding of anti-CD3 antibody to the TCR-CD3 complex on the outer membrane of T-Cells and poly I:C to TLR3 on the outer membrane of mononuclear phagocytic cells

respectively activates these immune cells to produce numerous cytokines including TNF (Merger *et al.*, 2002 and Williams *et al.*, 2013).

A number of previous studies have described the role of TNF as a potent stimulus of pathological apoptosis and shedding in murine small intestinal epithelial cells through its binding to TNFR1 (Pfeffer *et al.*, 1993 and Williams *et al.*, 2013). Gut barrier function is disrupted in mice treated with TNF due to an increase in cell shedding and a failure of tight junction proteins to seal up the resulting barrier discontinuity (Watson and Hughes, 2012).

In this chapter, we aimed to compare the small intestinal epithelial cell apoptosis and shedding that are induced by anti-CD3 antibody (T-cell mediated shedding), poly I:C (viral activation of shedding), TNF (expressed by macrophages, T-cells, B-cells, NK cells, mast cells, endothelial cells, fibroblasts and neurons) and LPS (macrophage mediated shedding) in terms of time of peak effect, the effective dose and genetic regulation by members of the NF $\kappa$ B family of proteins.

## **6.2 Anti-CD3 antibody induces T-cell mediated apoptosis and shedding in murine small intestinal epithelial cells**

### **6.2.1 Maximal induction of small intestinal epithelial cell apoptosis and shedding occurred 1.5 hours post intraperitoneal administration of anti-CD3 antibody**

The monoclonal anti-CD3 antibody, at a dose of 1mg/kg induced small intestinal apoptosis and cell shedding in female C57BL/6J mice (Figure 6.1). This effect was initially observed 1 hour post IP administration ( $1.3 \pm 0.08\%$ ,  $P=0.696$ ,  $N=3$ , ANOVA) but with no significant difference compared to untreated animals ( $1 \pm 0.05\%$ ). After 1.5 hours, the effect had reached its peak with the percentage of apoptosis and cell shedding having increased to  $2.3 \pm 0.09\%$  ( $P < 0.01$ ,  $N=3$ ; ANOVA). This significant effect continued at 2 hours ( $2.1 \pm 0.098\%$ ) then slightly declined at 4 hours ( $2 \pm 0.23\%$ ,  $P < 0.05$ ,  $N=3$ , ANOVA). It continued to decline to reach  $1.3 \pm 0.07\%$  at 6 hours post administration of anti-CD3 antibody ( $P=0.775$ ,  $N=3$ , ANOVA) (Figure 6.2). Based on the cell positional graph (Figure 6.3), the effect of anti-CD3 antibody appeared to be more pronounced at the villus tips rather than in the basal parts of small intestinal villi.

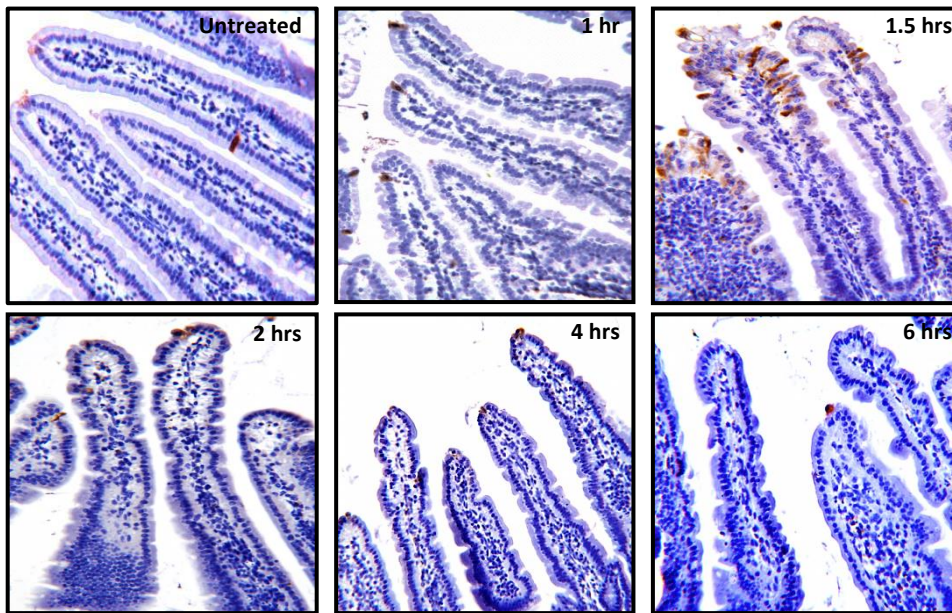


Figure 6.1: Active caspase-3 IHC in sections of proximal segments of small intestine of female C57BL/6J mice injected with 1mg/kg anti-CD3 antibody at different time points.

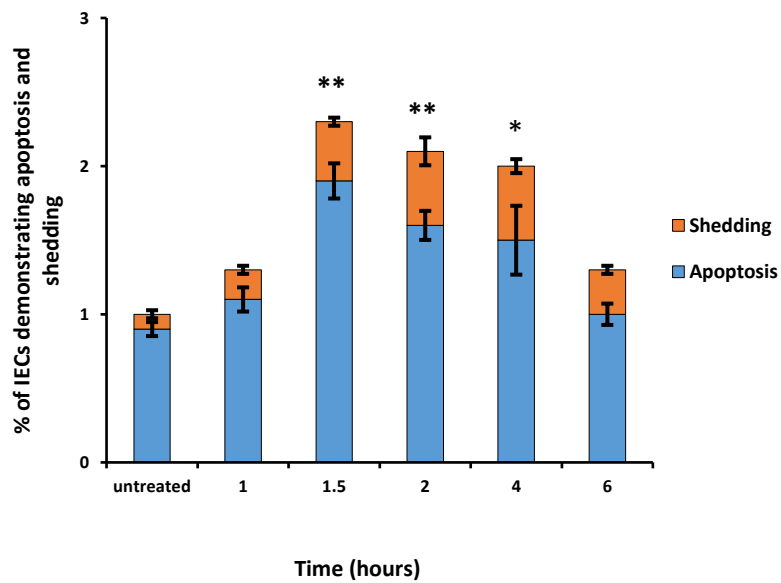


Figure 6.2: Bar chart representing the percentage of IEC apoptosis and shedding in female C57BL/6J mice treated with 1mg/kg anti-CD3 antibody at different time points, N=3; ANOVA, Dunnett post-hoc test for multiple comparisons with control \*\*P<0.01 and \*P<0.05.

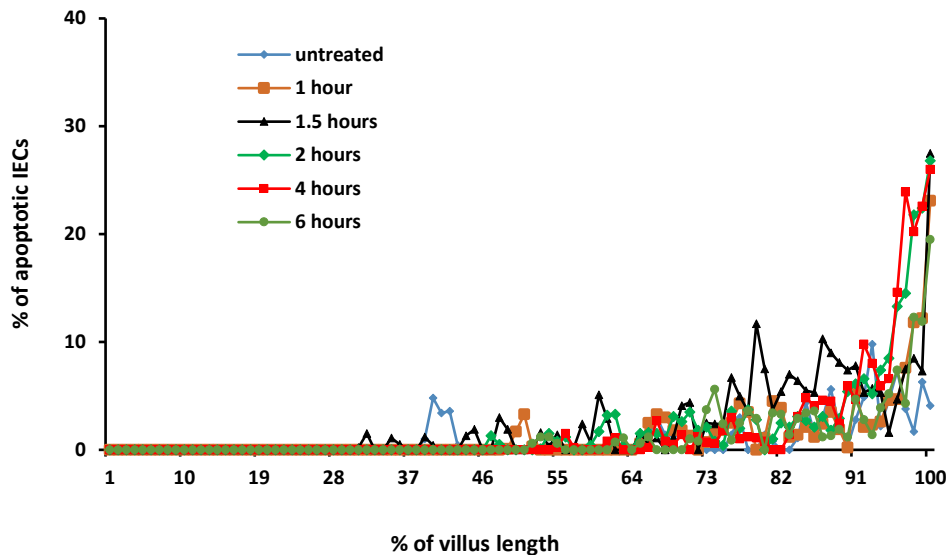


Figure 6.3: Cell positional graphs showing quantification of positively immuno-labelled IECs along the villus axis of C57BL/6J mice treated with 1mg/kg anti-CD3 antibody at different time points.

**6.2.2 A direct relationship was observed between anti-CD3 antibody dose and the percentage of small intestinal epithelial cell apoptosis and shedding in female C57BL/6J mice 1.5 post administration**

Interestingly we observed that mice which were treated with increasing doses of anti-CD3 antibody for 1.5 hours showed increases in the percentage of small intestinal epithelial cell apoptosis and shedding (Figure 6.4). No significant increase was observed in mice treated with 0.5 mg/kg anti-CD3 antibody in comparison to untreated mice ( $1.8 \pm 0.33\%$  and  $1 \pm 0.05\%$  respectively,  $P=0.217$ ,  $N=3$ ; ANOVA). However significant increases were observed following the administration of higher anti-CD3 doses reaching  $2.3 \pm 0.09\%$ ,  $3.4 \pm 0.33\%$  and  $5.6 \pm 0.19\%$  in mice treated with

1 mg/kg, 2 mg/kg and 4 mg/kg ( $P < 0.05$ ,  $< 0.001$  and  $< 0.0001$  respectively,  $N=3$ ; ANOVA) (Figure 6.5). On the other hand, mice that were treated with the anti-CD3 isotype control (Figure 6.7-A) actually showed a lower percentage of apoptosis and shedding than untreated mice ( $0.4 \pm 0.03\%$  for mice injected with 1mg/kg isotype control and  $0.3 \pm 0.05\%$  for mice treated with 4 mg/kg isotype control). Furthermore, the cell positional plots again indicated that the greatest effect of anti-CD3 antibody occurred in the apical part rather than in the basal region of small intestinal villi in all groups (Figure 6.6 and 6.7-B).

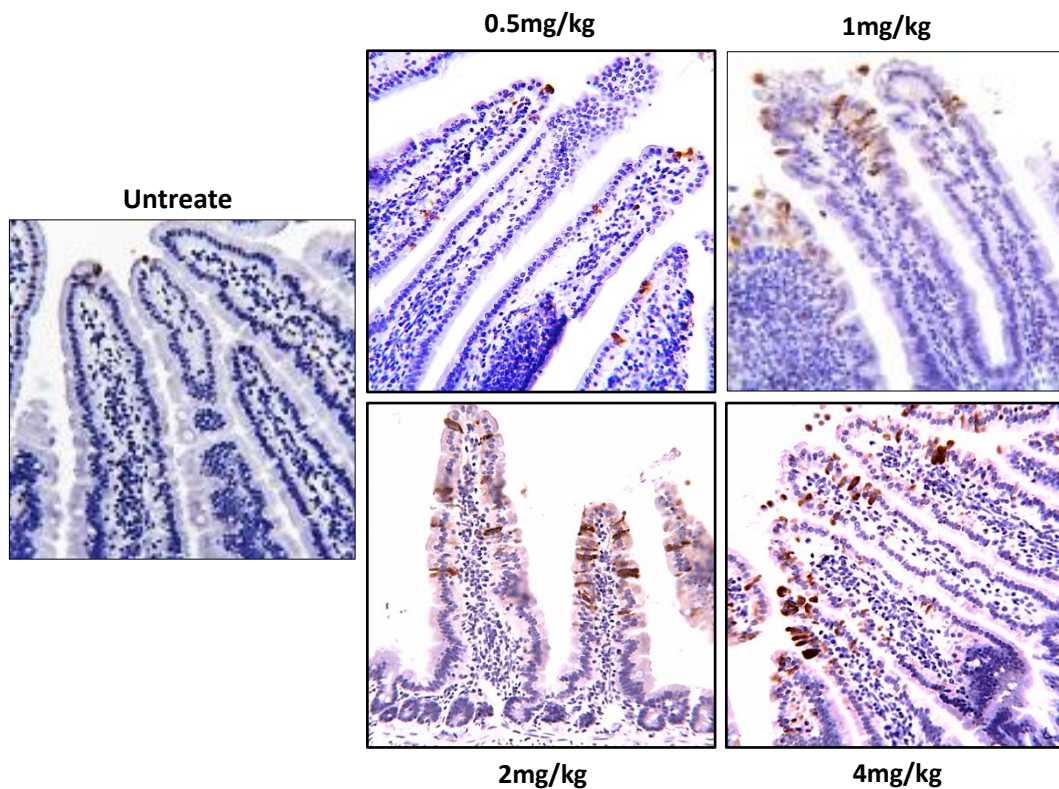


Figure 6.4: Active caspase-3 IHC in sections of proximal segments of small intestine of female C57BL/6J mice injected with increasing doses of anti-CD3 antibody at 1.5 hours. X40

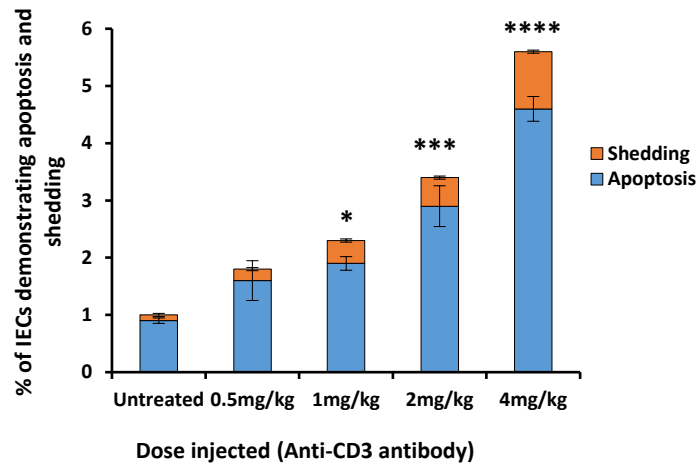


Figure 6.5: Percentage of active caspase 3 positively labelled IECs in C57BL/6J mice injected with differing doses of anti-CD3 antibody for 1.5 hours. N=3; ANOVA, Dunnett post-hoc test for multiple comparisons with control, \*P<0.05, \*\*\*P<0.001, \*\*\*\*P<0.0001

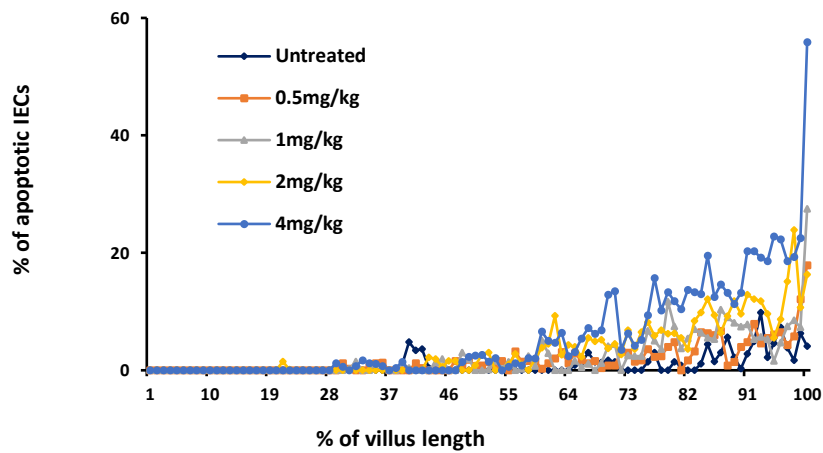


Figure 6.6: Cell positional graphs showing quantification of positively immunolabelled IECs along the villus axis of C57BL/6J mice injected with differing doses of anti-CD3 antibody for 1.5 hours.

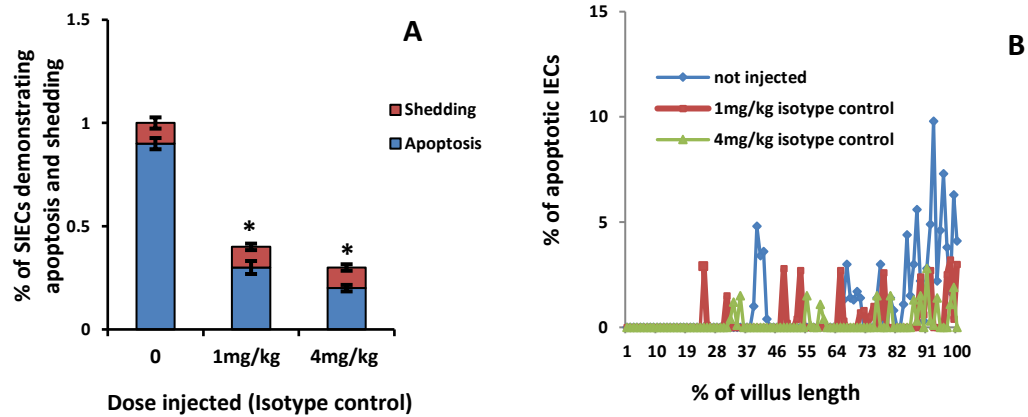


Figure 6.7: Bar chart and cell positional plot representing the percentage (A) and distribution (B) of SIEC apoptosis and shedding in C57BL/6J mice injected with differing doses of anti-CD3 isotype control for 1.5 hours compared to untreated mice (N=3, \*P<0.05, \*\*P<0.01).

### 6.2.3 Members of the NFκB family of proteins regulate the pathological small intestinal epithelial apoptosis and shedding induced by anti-CD3 antibody:

To further investigate the role of NFκB transcription factors in regulating anti-CD3 antibody induced SIEC apoptosis and cell shedding, active caspase-3 stained sections were analysed (Figure 6.8). These indicated increases in the number of apoptotic small intestinal epithelial cells in *Nfκb1*<sup>-/-</sup> and *c-Rel*<sup>-/-</sup> mice and an obvious decrease in *Nfκb2*<sup>-/-</sup> mice. The percentage of SIEC apoptosis and cell shedding (Figure 6.9) was significantly increased from 3.6±0.25% in wild-type mice treated with 2mg/kg anti-CD3 antibody for 1.5 hours to 5.1±0.29% (P<0.05) in *Nfκb1*<sup>-/-</sup> mice treated with the same dose. In contrast, *Nfκb2*<sup>-/-</sup> mice appeared to be more resistant to anti-CD3 antibody induced apoptosis and shedding, as the percentage of small intestinal

epithelial cell apoptosis and shedding was only  $0.8 \pm 0.09\%$  ( $P < 0.001$ ). An increase in the percentage of pathological small intestinal apoptosis and shedding was also observed in *c-Rel*<sup>-/-</sup> mice ( $4.8 \pm 0.62\%$ ), but this increase was not significantly different ( $P = 0.093$ ) from the percentage of apoptosis and shedding that was seen in wild-type C57BL/6J mice (all  $N = 6$ ; ANOVA). The cell positional graph (Figure 6.10) again indicated that the apoptosis and shedding of small intestinal epithelial cells in all strains of transgenic mice as well as in the wild-type group was more pronounced in the upper half of intestinal villi.

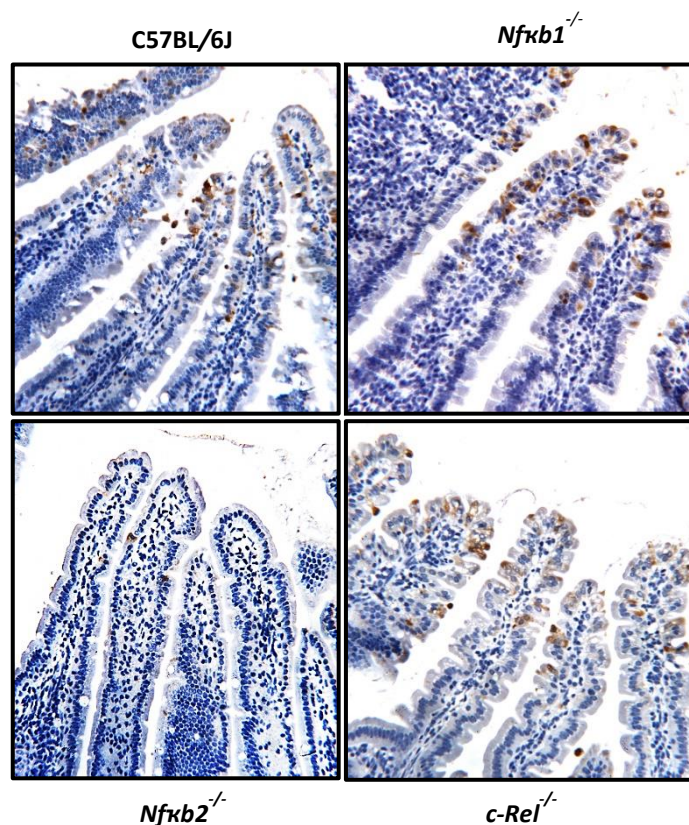


Figure 6.8: Active caspase-3 IHC in sections of proximal segments of small intestine of transgenic and wild-type C57BL/6J mice injected with 2 mg/kg anti-CD3 antibody at 1.5 hours.

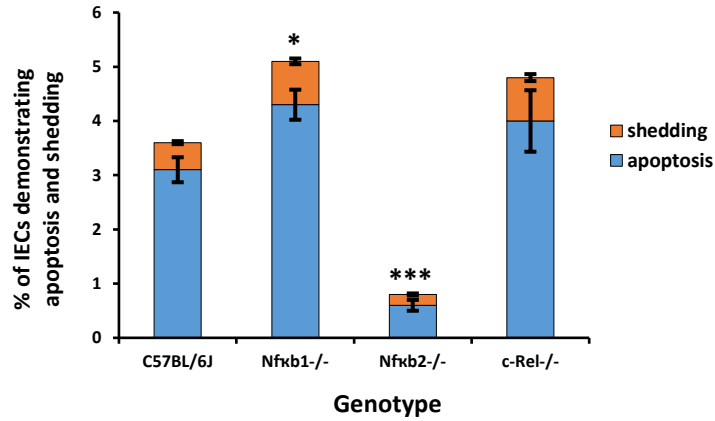


Figure 6.9: Comparison between the percentage of active caspase 3 positively labelled IECs in *Nfκb1*<sup>-/-</sup>, *Nfκb2*<sup>-/-</sup>, *c-Rel*<sup>-/-</sup> and wild-type C57BL/6J mice. N=6; ANOVA, Dunnett post-hoc test for multiple comparison with control, \*P<0.05, \*\*\*P<0.001.

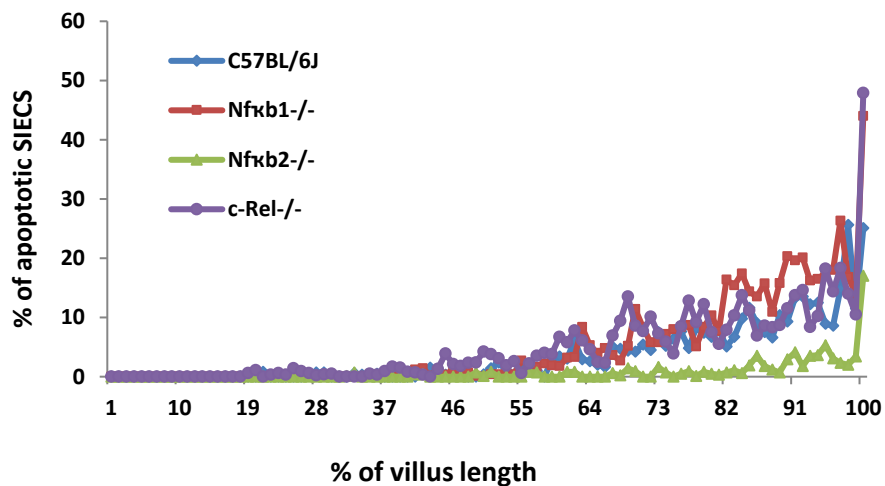


Figure 6.10: Cell positional graphs showing quantification of positively immunolabelled IECs along the villus axis of transgenic mice (*Nfκb1*<sup>-/-</sup>, *Nfκb2*<sup>-/-</sup> and *c-Rel*<sup>-/-</sup>) compared to wild-type C57BL/6J mice, all treated with 2mg/kg anti-CD3 antibody for 1.5 hours.

#### **6.2.4 Anti-CD3 antibody also significantly induced apoptosis in murine small intestinal crypt epithelial cells 24 hours post IP administration**

A previous study by Miura *et al*; 2005 indicated that anti-CD3 antibody induces T-cell mediated bi-phasic apoptosis and shedding in murine small intestinal epithelial cells. Villus apoptosis was observed up to 4 hours, but apoptosis of intestinal crypt cells was also seen up to 24 hours post injection. Our results showed that after IP injection of 2 mg/kg anti-CD3 antibody to wild-type C57BL/6J, *Nfκb1*<sup>-/-</sup>, *Nfκb2*<sup>-/-</sup> and *c-Rel*<sup>-/-</sup> mice for 24 hours, we observed a marked increase in the number of apoptotic small intestinal crypt epithelial cells in *Nfκb1* and *c-Rel* knockout mice, whereas we noted small rise in the number of apoptotic crypt cells in *Nfκb2*<sup>-/-</sup> mice (Figure 6.11). Statistically, there was a significant increase in the percentage of apoptotic small intestinal crypt epithelial cells from 0.4±0.03% in wild-type C57BL/6J mice to 1.2±0.21% and 0.8±0.08% (P<0.001 and P<0.05 respectively, ANOVA) in *Nfκb1*<sup>-/-</sup> and *c-Rel*<sup>-/-</sup> mice. Although there was also an increase in the number of apoptotic crypt epithelial cells noted in *Nfκb2*<sup>-/-</sup> mice (0.5±0.08%), this was not statistically significant (P=0.327, ANOVA). On the other hand, following addition of caspase-3 negatively labelled cells that representing non-apoptotic cell death, the percentage of cell death in small intestinal crypt epithelial cells was increased to 3.9±1.02% (P<0.05) and 2.7±0.26% (P=0.268) in *Nfκb1*<sup>-/-</sup> and *c-Rel*<sup>-/-</sup> whereas *Nfκb2*<sup>-/-</sup> mice showed a non-significant slightly decreased percentage of apoptotic crypt epithelial cells (1.2±0.13%, P=0.974, ANOVA) compared to 1.4±0.14% in treated wild-type C57BL/6J mice (Figure 6.12-A). Although the cell

positional graph (Figure 6.12-B) showed that apoptotic cells were more pronounced in the lower half of small intestinal crypts in all strains, the modified median test indicated that the apoptotic cells were significantly different between cell position 3 and 20 in *Nfκb1*<sup>-/-</sup> mice compared to wild-type C57BL/6J.

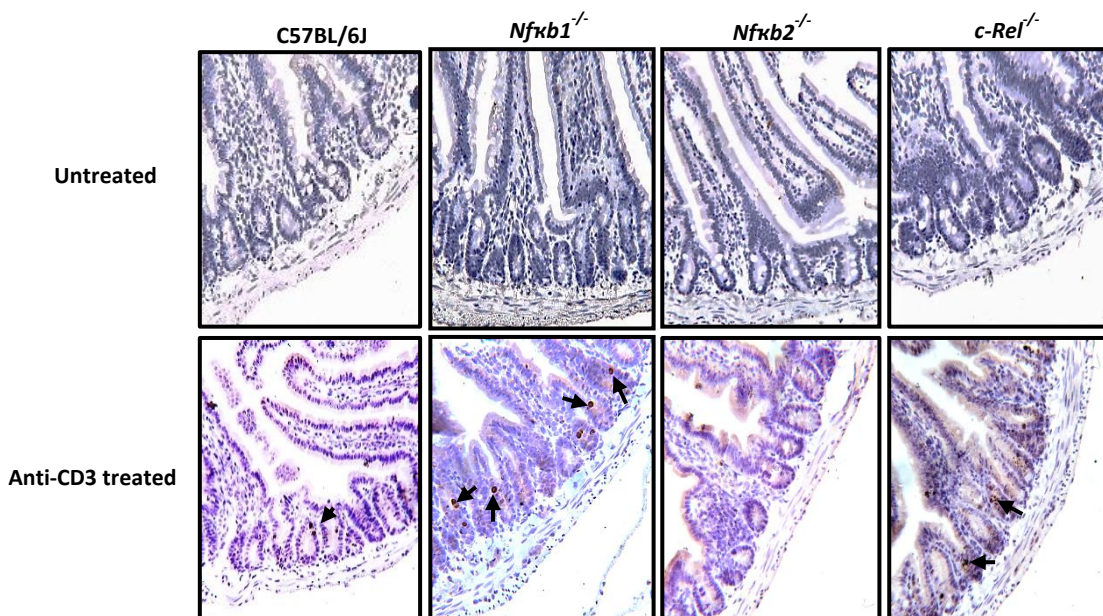


Figure 6.11: Active caspase-3 IHC demonstrating apoptotic small intestinal crypt epithelial cells (black arrows) in transgenic and wild-type C57BL/6J mice injected with 2 mg/kg anti-CD3 antibody for 24 hours. (X40).

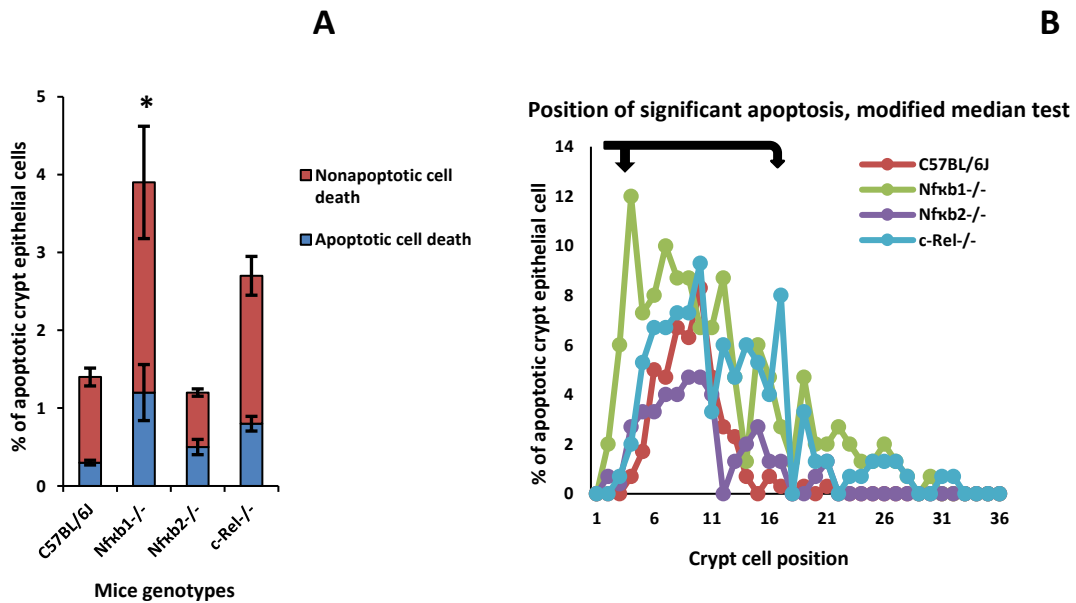


Figure 6.12: (A) Bar chart indicating the percentage of apoptotic small intestinal crypt epithelial cells in transgenic and wild-type C57BL/6J mice injected with anti-CD3 antibody for 24 hours, N=6; ANOVA, Dunnett post-hoc test for multiple comparison with control, \*P<0.05. (B) Cell positional graph demonstrating the position of apoptotic small intestinal crypt epithelial cells.

### 6.3 Polyinosinic:polycytidylic acid (Poly I:C) induces murine small intestinal epithelial cell apoptosis and shedding mimicking the viral activation of shedding

Poly I:C is a synthetic analogue of the ds-RNA that is found in some viruses. It is used experimentally to induce apoptosis and cell shedding that mimics the viral activation of cell shedding through its binding to TLR3 expressed on the surface of B-cells, macrophages and dendritic cells. In this chapter we have evaluated the peak time-point of SIEC apoptosis and shedding following IP administration of 30 mg/kg poly I:C and have investigated the

role of the NF $\kappa$ B family of proteins in regulating this response in both small intestinal villus and crypt cells.

### **6.3.1 Poly I:C induces pathological apoptosis and shedding of murine small intestinal epithelial cells**

After IP administration of 30mg/kg poly I:C we found an increase in the number of apoptotic and shedding SIECs (Figure 6.13). The percentage of apoptotic and shedding cells was significantly increased from  $1.1\pm 0.05\%$  in untreated mice to  $1.9\pm 0.07\%$  after 1 hour ( $P<0.01$ ,  $N=6$ ; ANOVA) (Figure 4.14). This increase in the percentage of SIEC apoptosis and shedding continued at 1.5 hours ( $5.4\pm 0.64\%$ ) and reached its peak of  $5.9\pm 0.79\%$  at 2 hours post administration of poly I:C ( $P<0.0001$  for both time-points,  $N=6$ ; ANOVA). A marked decrease in the percentage of pathological apoptosis and shedding was then noted 3 hours post intraperitoneal injection of poly I:C ( $1.2\pm 0.05\%$ ). Although the highest amount of apoptosis and shedding was observed 2 hours post poly I:C administration, there was no significant difference between the percentage of pathological apoptosis and cell shedding observed at 2 hours and 1.5 hours ( $P=0.2557$ ,  $N=6$ ; ANOVA). The cell positional data (Figure 6.15) showed similar distributions of apoptotic and shedding epithelial cells along the villus axis of the proximal segment of the small intestine to other inducing stimuli. The distribution again appeared to be most pronounced towards the villus tips.

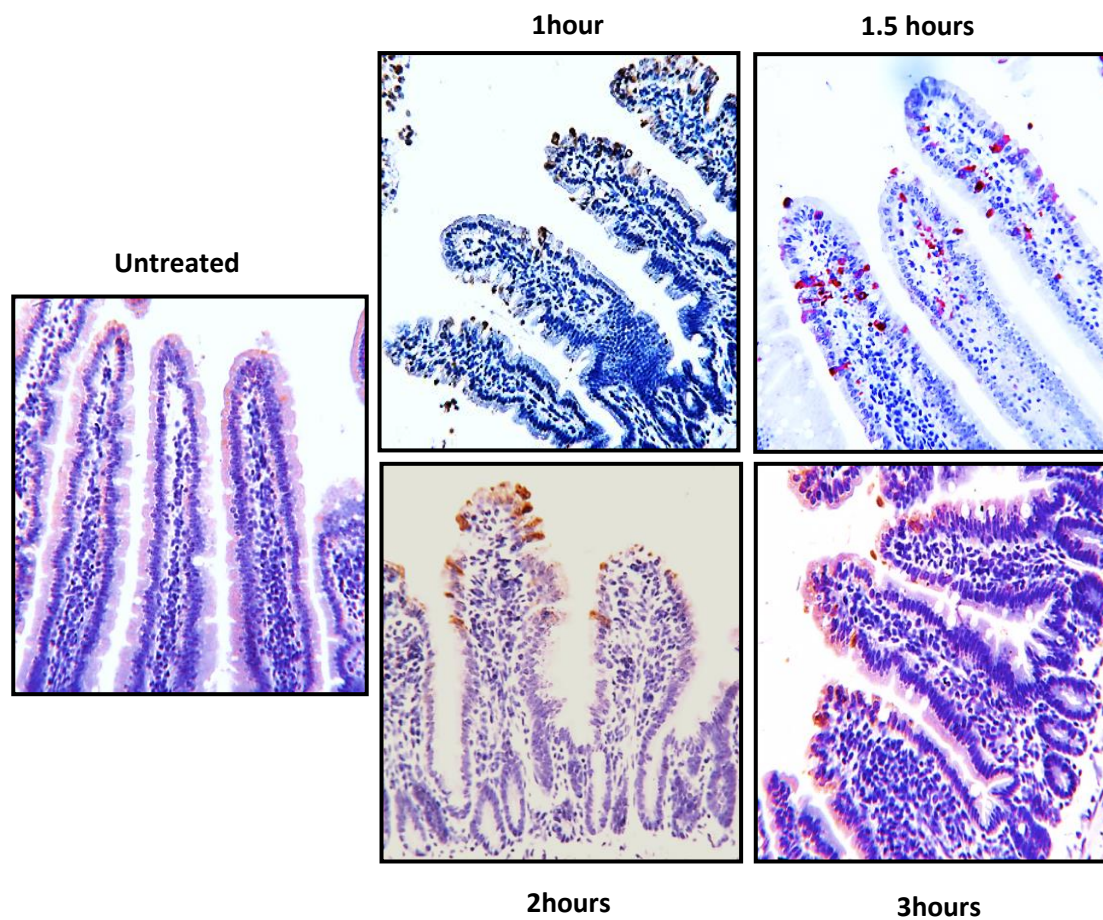


Figure 6.13: Active caspase-3 IHC showing proximal small intestinal epithelial apoptosis and cell shedding in female C57BL/6J mice injected intraperitoneally with 30 mg/kg poly I:C for different periods of time.

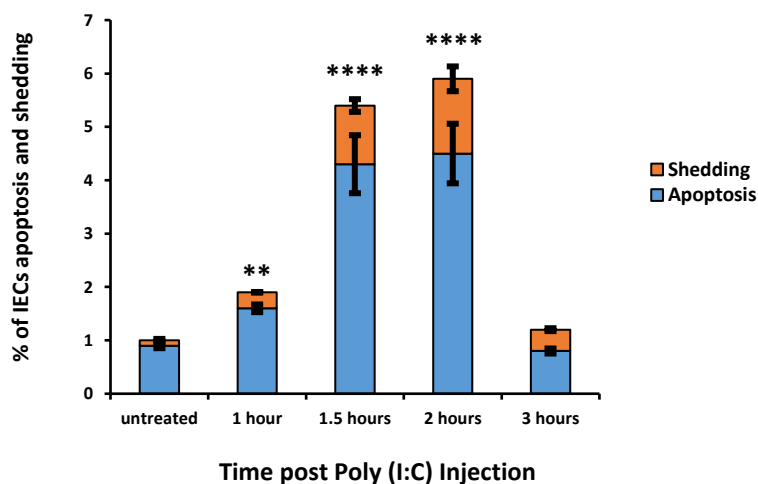


Figure 6.14: Bar chart indicating the percentage of apoptotic and shedding IECs in the duodenal villi of *C57BL/6J* mice injected with 30mg/kg Poly I:C at different time points, N=3; ANOVA (Kruskal-Wallis test), \*\* P<0.01, \*\*\*\* P<0.0001.

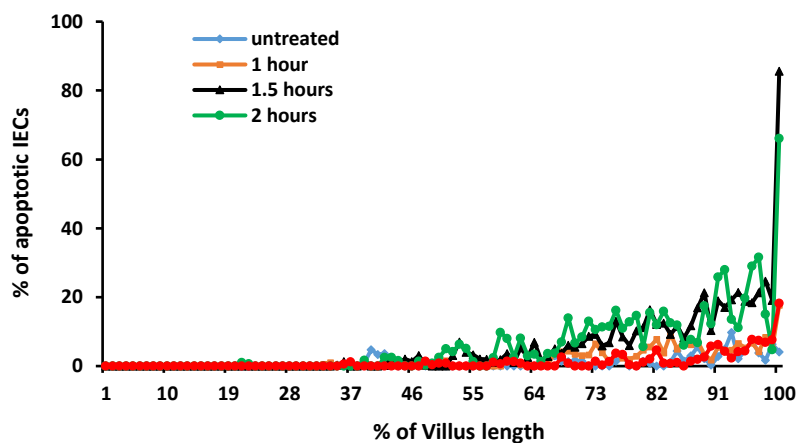


Figure 6.15: Cell positional graphs indicating the quantification of positively immunolabelled IECs along the villus axis of *C57BL/6J* mice injected with 30mg/kg Poly I:C at different time points in comparison to untreated group.

### 6.3.2 *Nfκb2*<sup>-/-</sup> mice were more resistant to poly I:C induced small intestinal epithelial cell apoptosis and shedding

Following 30mg/kg poly I:C for 1.5 hours, *Nfκb1*<sup>-/-</sup> and *c-Rel*<sup>-/-</sup> mice exhibited significant increases (Figures 6.16 and 6.17) in the percentage of small intestinal epithelial cell apoptosis and shedding ( $8.8\pm 0.39\%$  and  $8.4\pm 0.29\%$  respectively,  $P<0.01$ ,  $N=6$ ; ANOVA) compared to similarly treated wild-type C57BL/6J mice ( $5.4\pm 0.64\%$ ). However, *Nfκb2*<sup>-/-</sup> mice given 30mg/kg poly I:C exhibited a significant reduction in the amount of small intestinal epithelial cell apoptosis and shedding at  $3.4\pm 0.39\%$  ( $P<0.05$ ,  $N=6$ ; ANOVA). Based on the cell positional plots (Figure 6.17), poly I:C induced small intestinal epithelial cell apoptosis and shedding again occurred more obviously toward the villus tips rather than toward the villus bases.

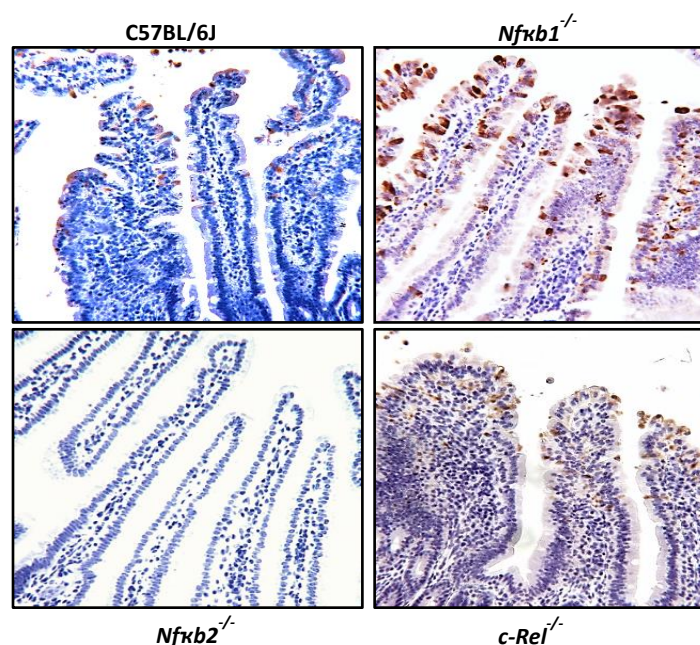


Figure 6.16: Active caspase-3 IHC in sections of proximal segments of small intestine of transgenic and wild-type female C57BL/6J mice injected with 30mg/kg poly I:C for different periods of time.

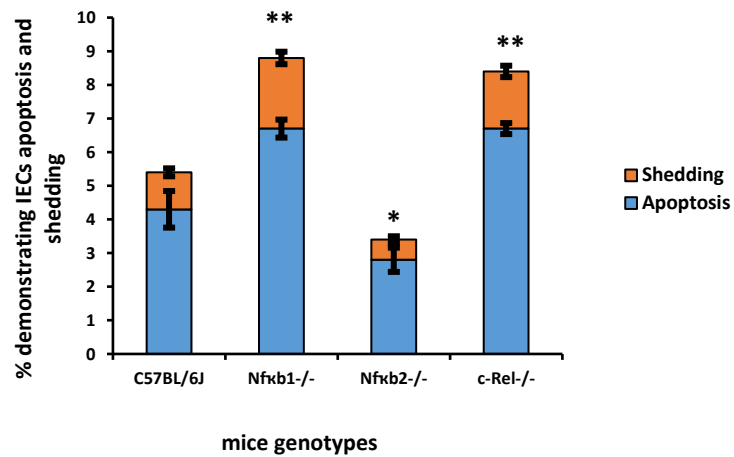


Figure 6.17: Bar chart showing percentage of apoptotic and shedding SIECs in the duodenal villi of *wild-type* and transgenic C57BL/6J mice at 1.5h post IP injection of 30mg/kg Poly I:C. N=6; ANOVA, Dunnett multiple comparison with control, \* = $P < 0.05$ , \*\*= $P < 0.01$ .

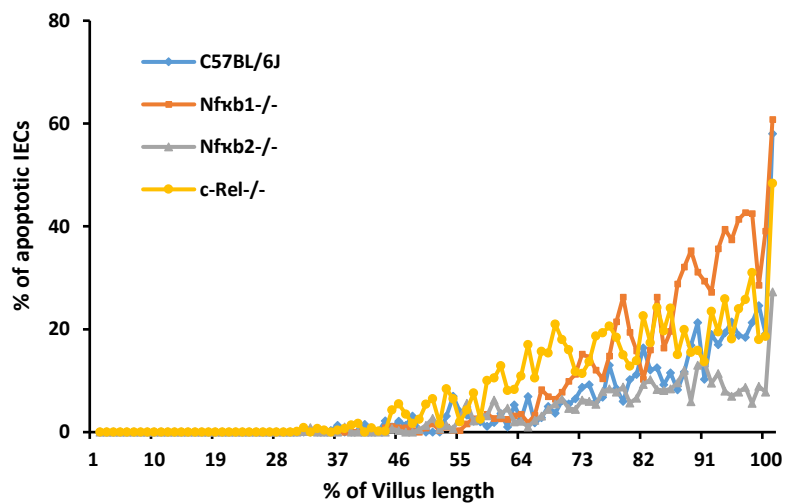


Figure 6.18: Cell positional graphs showing quantification of positively immunolabelled IECs along the villus axis of transgenic mice (*Nfκb1-/-*, *Nfκb2-/-* and *c-Rel-/-*) compared to wild-type C57BL/6J mice.

### 6.3.3 Poly I:C has no effect on small intestinal crypt epithelial cell apoptosis and shedding at 24 hours post intraperitoneal administration

We investigated whether 30mg/kg poly I:C induced small intestinal crypt epithelial cell apoptosis 24 hours post intraperitoneal administration. Apoptosis of small intestinal crypt epithelial cells based on active caspase-3 IHC was not observed in wild-type C57BL/6J and *c-Rel*<sup>-/-</sup> mice, while very few active caspase-3 positively labelled cells were seen in *Nfκb2*<sup>-/-</sup> mice with a percentage of 0.2±0.046% (Figure 6.19). Based on the morphological characteristics of apoptosis the percentages were 0.9±0.05%, 0.3±0.03% and 0.3±0.54% in wild-type C57BL/6J, *c-Rel*<sup>-/-</sup> and *Nfκb2*<sup>-/-</sup> mice respectively (Figure 6.20-A). Unexpectedly, *Nfκb1*<sup>-/-</sup> mice died 5 hours post administration of poly I:C, therefore we have no data on the effect of poly I:C on crypt intestinal epithelial cell apoptosis 24 hours post IP administration. From the cell positional graph (Figure 6.20-B) the crypt apoptosis did not show an obvious cell positional pattern along the crypt axis.

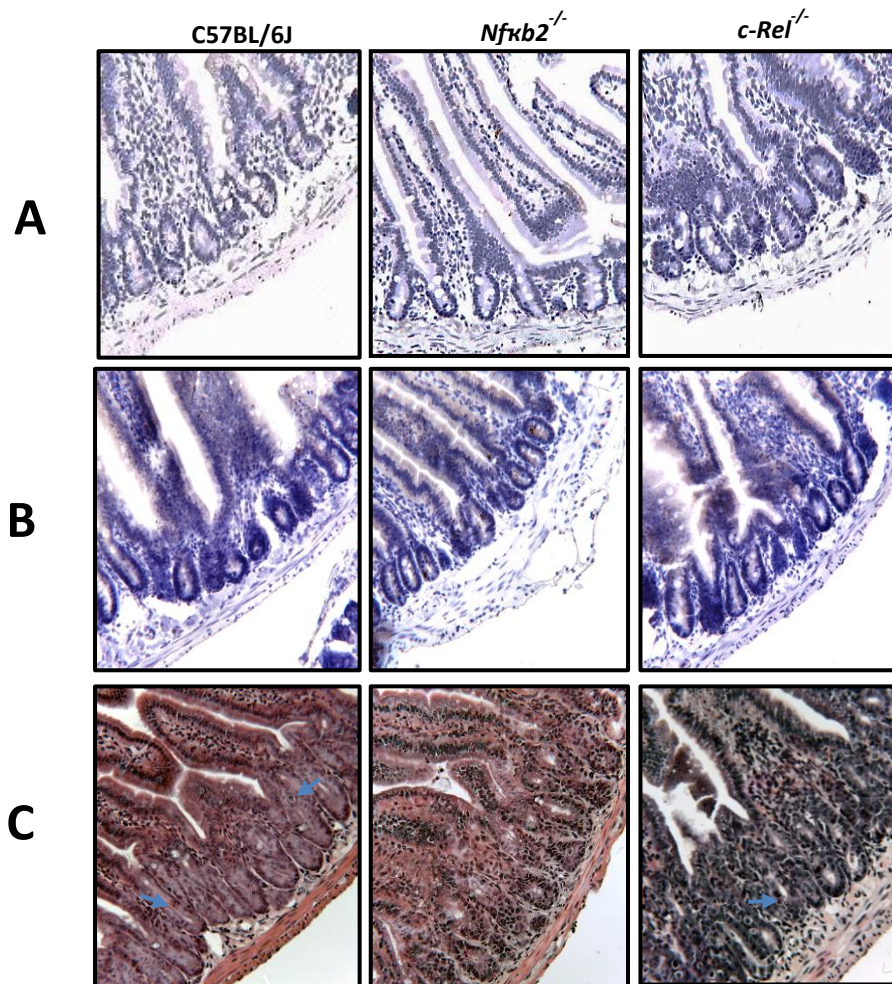


Figure 6.19: Active caspase-3 IHC in sections of proximal segments of small intestine of transgenic and wild-type C57BL/6J mice injected with 30mg/kg poly I:C for 24 hours. (Blue arrows indicating apoptotic cells in H&E stained section) X40

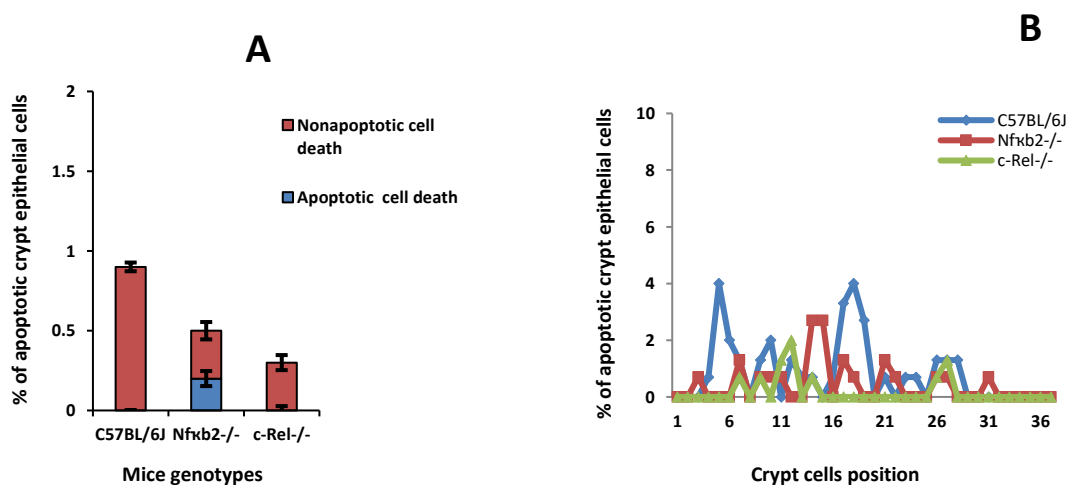


Figure 6.20: (A) Bar chart indicating the percentage of apoptotic small intestinal crypt epithelial cells in transgenic and wild type C57BL/6J mice injected with 30mg/kg poly I:C for 24 hours, (B) Cell positional graph indicated no obvious pattern of crypt apoptosis in all tested genotypes, N=6.

## **6.4 TNF caused significant apoptosis and cell shedding in proximal segment of murine small intestine**

TNF is an important cytokine that plays an important role in regulating gut barrier permeability. Its systemic administration results in a SIEC pathological apoptosis and shedding (Watson and Hughes; 2012, Ślebioda and Kmiec; 2014). A previous study in our laboratory indicated that TNF caused a similar effect in the proximal part of the murine small intestine as LPS and suggested that TNF is a crucial key mediator of LPS-induced intestinal injury in wild-type C57BL/6J mice (Williams *et al*; 2013). In this study we have investigated the role of TNF as a key mediator of small intestinal apoptosis and cells shedding in wild-type C57BL/6J mice in both villus and crypt compartments and have examined the role of the NFκB family of transcription factors in regulating TNF-induced SIEC apoptosis and shedding.

### **6.4.1 0.33mg/kg TNF caused pathological apoptosis and shedding in proximal small intestinal villi at 1.5 hours equivalent to that caused by administration of 10 mg/kg LPS**

Active caspase-3 IHC sections showed that an intraperitoneal administration of 0.33mg/kg TNF into adult female C57BL/6J mice caused an increase in the number of apoptotic and shedding cells in small intestinal villi at 1.5 hours (Figure 6.21). Quantification of active caspase-3 positively labelled cells (Figure 6.22-B) indicated a significant increase in the percentage of apoptotic and shedding cells from  $1.0 \pm 0.05\%$  in untreated wild-type C57BL/6J mice to  $6.0 \pm 0.92\%$  in TNF-treated wild-type C57BL/6J mice ( $P < 0.0001$ , ANOVA-Kruskal-Wallis multiple comparison). A further increase in

percentage of SIEC apoptosis and shedding to  $11.4 \pm 0.34\%$  were seen in TNF-treated *Nfκb1*<sup>-/-</sup> ( $P < 0.0001$ , ANOVA-Kruskal-Wallis multiple comparison) whereas *c-Rel*<sup>-/-</sup> mice showed non-significant reduction in percentage of SIEC apoptosis and shedding ( $4.2 \pm 0.37\%$ ,  $P = 0.2432$ , ANOVA-Kruskal-Wallis multiple comparison) in compare to TNF-treated wild-type C57BL/6J (Figure 6.22-A). Similar to the other tested stimuli, *Nfκb2*<sup>-/-</sup> mice appeared to be significantly resistant to TNF induced SIEC apoptosis and shedding in compare to TNF-treated C57BL/6J mice presenting a percentage of  $1.6 \pm 0.16\%$  apoptotic SIECs ( $P < 0.0001$ , ANOVA-Kruskal-Wallis multiple comparison). Although of this substantial reduction in the number of apoptotic and shedding SIECs, *Nfκb2*<sup>-/-</sup> mice indicated a slight increase in the percentage of SIEC apoptosis and shedding in compare to untreated wild-type C57BL/6J mice ( $1.6 \pm 0.16\%$  and  $1.0 \pm 0.05\%$  respectively) but this increase did not reach statistical significance ( $P = 0.2757$ , ANOVA-Kruskal-Wallis multiple comparison). The cell positional plots again indicated that TNF caused greater effects at the villus tip than in the basal region of small intestinal villi in all treated groups (Figure 6.23-A and B).

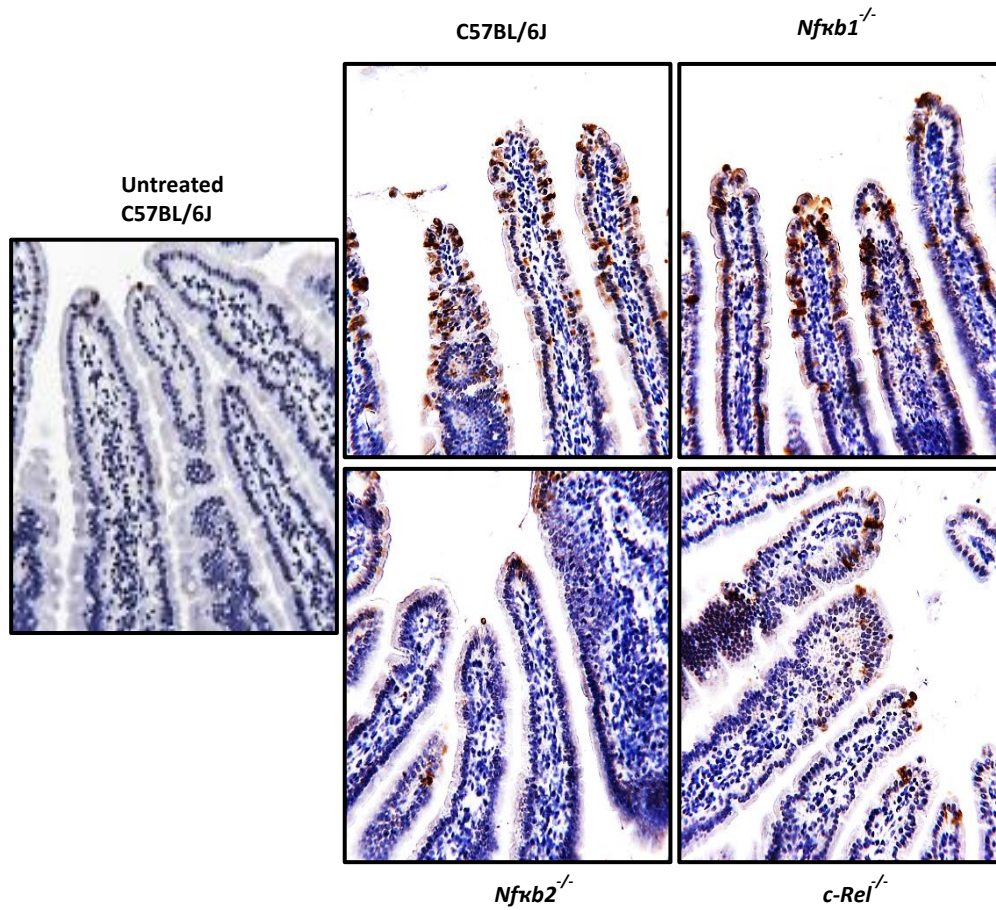


Figure 6.21: Active caspase-3 IHC in sections of proximal segments of small intestine of different mice groups injected with 0.33mg/kg TNF for 1.5 hours.

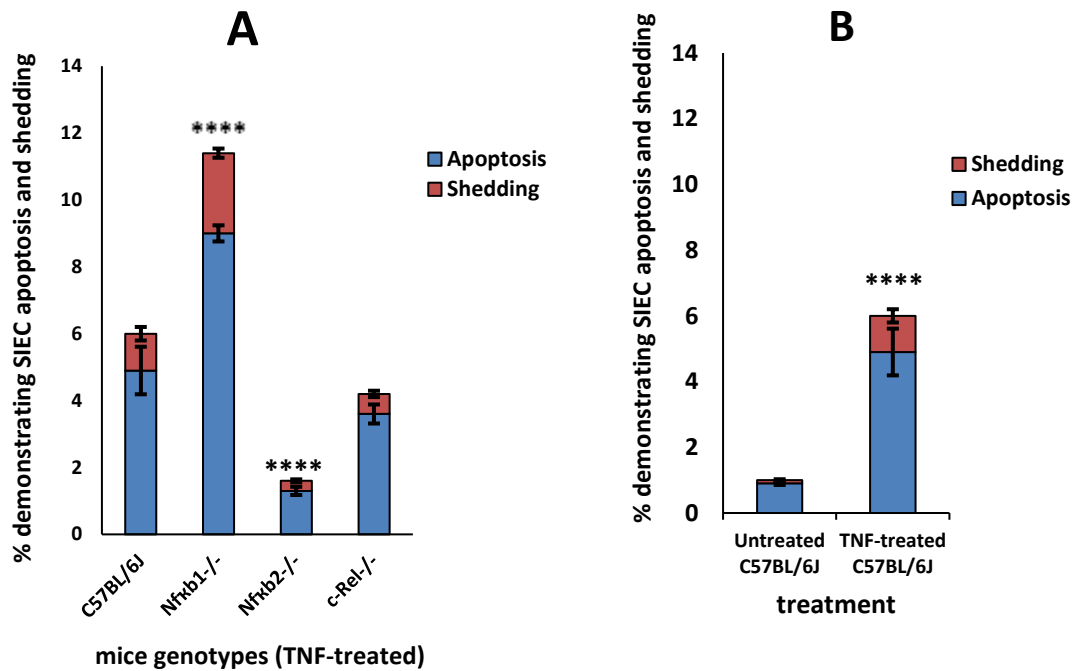


Figure 6.22: Bar charts (A) showing percentage of apoptotic and shedding SIECs in the duodenal villi of wild- and transgenic C57BL/6J mice 1.5h post IP injection of 0.33mg/kg TNF and (B) showing percentage of apoptotic and shedding SIECs in TNF-treated versus untreated C57BL/6J mice, N=6; ANOVA, Kruskal-Wallis multiple comparisons, \*\*\*\* =  $P < 0.0001$ .

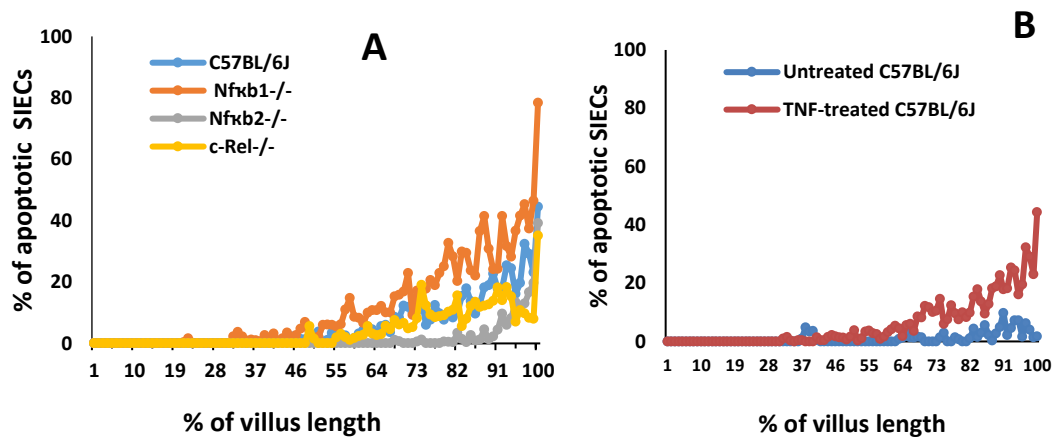


Figure 4.23: Cell positional graph indicating the distribution of apoptotic SIECs along the villus length of TNF treated wild-type and transgenic C57BL/6J mice (A) and a comparison of TNF-treated to untreated C57BL/6J mice (B). N=6.

#### **6.4.2 TNF at 24 hours post intraperitoneal administration induced small intestinal crypt apoptosis more in *Nfκb1* and *c-Rel* knockout mice than wild-type C57BL/6J mice, while *Nfκb2* null mice showed no significant change**

To identify the effect of TNF on small intestinal crypt apoptosis 24 hours post intraperitoneal injection of 0.33mg/kg recombinant TNF, we injected 6 wild-type adult female C57BL/6J mice together with the various transgenic groups (*Nfκb1*<sup>-/-</sup>, *Nfκb2*<sup>-/-</sup> and *c-Rel*<sup>-/-</sup>, all consisting of 6 mice). The small intestine was then processed for active caspase-3 IHC. Quantification of positively labelled active caspase-3 crypt cells indicated that the number of apoptotic cells was markedly increased in *Nfκb1*<sup>-/-</sup> mice and to a lesser extent *c-Rel*<sup>-/-</sup> mice compared to wild-type C57BL/6J mice (Figure 6.24). The percentage of apoptotic crypt cells in wild-type C57BL/6J mice (0.7±0.26%) was significantly increased to 7.3±0.66% in *Nfκb1*<sup>-/-</sup> mice (P<0.0001, N=6, ANOVA-Kruskal-Wallis multiple comparison) and 1.2±0.19% in *c-Rel*<sup>-/-</sup> mice (P<0.05, N=6). On the other hand, there was a significant decrease in the percentage of apoptotic crypt cells in *Nfκb2*<sup>-/-</sup> mice (0.3±0.08%, P<0.05, N=6) in comparison to wild-type C57BL/6J mice (Figure 6.25). Furthermore, following addition of caspase-3 negatively labelled cells (cells that indicate non-apoptotic cell death), the percentage of cell death in crypt epithelial cells slightly increased in all tested genotypes to 0.9±0.32%, 7.8±0.79%, 0.5±0.07% and 1.4±0.20% in C57BL/6J, *Nfκb1*<sup>-/-</sup>, *Nfκb2*<sup>-/-</sup> and *c-Rel*<sup>-/-</sup> mice respectively. The cell positional plot (Figure 6.26) showed that the small intestinal crypt apoptosis was more obvious in the lower part of the intestinal crypt especially in *Nfκb1*<sup>-/-</sup> mice. The modified median test showed that apoptotic cells were significantly different between cell positions 3 and 14 in *Nfκb1*<sup>-/-</sup> mice and between cell positions 7 and 12 in *c-Rel*<sup>-/-</sup> mice compared to wild-type.

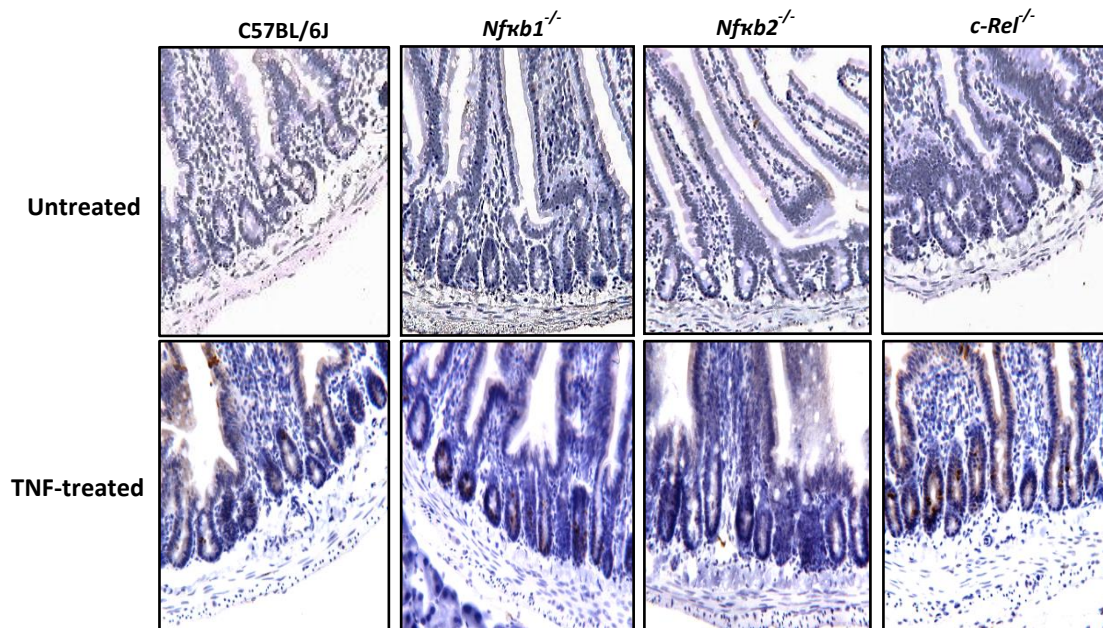


Figure 6.24: Active caspase-3 IHC indicating the apoptosis of small intestinal crypt epithelial cells of wild-type and transgenic C57BL/6J mice at 24 hours post administration of 0.33mg/kg recombinant TNF.

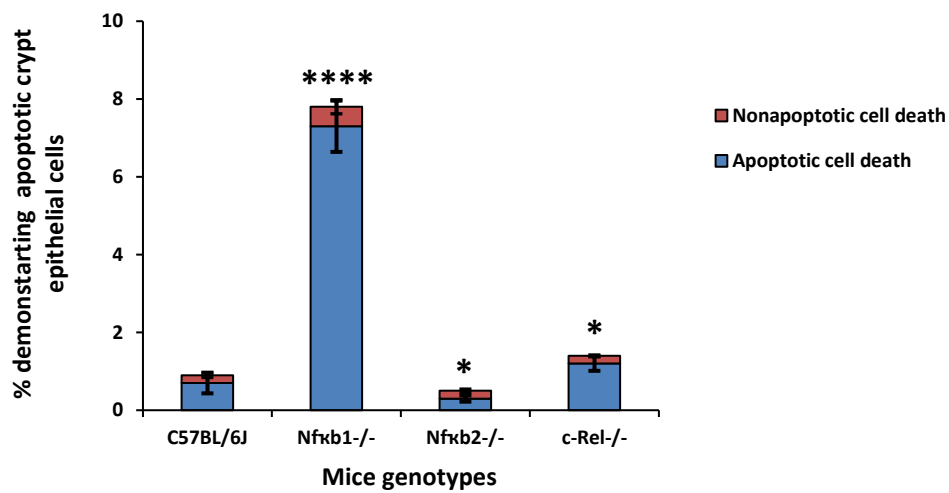


Figure 6.25: Bar chart representing the percentage of small intestinal crypt epithelial cell apoptosis in adult female wild-type C57BL/6J and transgenic mice injected with 0.33mg/kg TNF for 24 hours. \* $P < 0.05$ , \*\*\*\* $P < 0.0001$ , ANOVA-Kruskal-Wallis test for multiple comparison,  $N = 6$ .

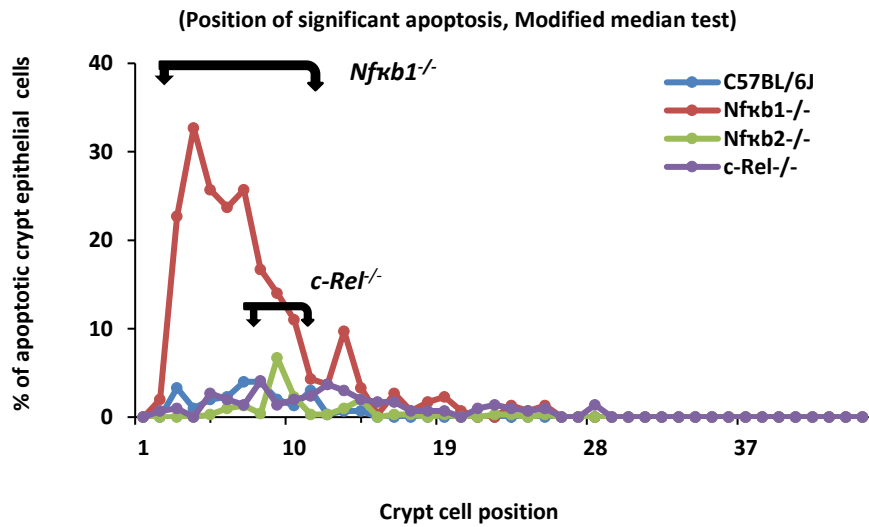


Figure 6.26: Cell positional graph indicating the position of apoptotic small intestinal crypt epithelial cell along the crypt axis of TNF treated wild-type and transgenic C57BL/6J mice. N=6.

#### 4.5 Discussion:

In this chapter we have investigated the roles of substances other than LPS that have been shown to induce murine small intestinal apoptosis and cell shedding by activating receptors other than TLR4. We have tested these substances based on the time of peak effect, the dose needed to cause a maximal effect and the role of the NFκB family of proteins in regulating these responses. We have compared responses to our previous results using LPS.

Miura *et al*; 2005 investigated the role of anti-CD3 antibody in inducing SIEC apoptosis and shedding by administering 12.5 μg of anti-CD3 antibody into *C3H/HeN* mice. They found that anti-CD3 antibody induced villus apoptosis starting 2 hours post intraperitoneal administration, this reached a peak at 4 hours and then started to decline thereafter. They also reported marked small intestinal crypt epithelial cell

apoptosis at 24 hours post injection. This continued up to 48 hours, then completely recovered 4 days post anti-CD3 antibody injection. Activation of T-lymphocytes by administration of anti-CD3 antibody was also shown to increase the number of apoptotic cells and cause shortening of intestinal villi in C57BL/6J mice at 2 hours and 24-48 hours post administration of anti-CD3 antibody respectively. This was associated with increased serum concentrations of TNF (Zhou *et al.*; 2004).

Our current results indicated that an IP administration of 1 mg/kg anti-CD3 antibody into adult female C57BL/6J mice slightly increased the percentage of apoptosis and cell shedding in small intestinal villi after 1 hour. This response reached its peak at 1.5 hours, continued until 2 hours post IP administration, started to slightly decline at 4 hours, then the small intestine was recovered at 6 hours post injection. We also demonstrated a direct relationship between the dose of anti-CD3 antibody injected and the percentage of apoptotic and shedding SIECs (see Figure 6.5) as previously documented by Mura *et al.* in 2005. Moreover our results of investigating the role of the NFκB family of proteins in regulating the process of apoptosis and shedding induced by anti-CD3 antibody indicated similar patterns to those following administration of LPS. However the degree of response was a little less than that seen after LPS treatment. We found that expression the NFκB2 transcription protein was associated with an increased percentage of apoptosis and shedding in C57BL/6J mice treated with 2 mg/kg anti-CD3 antibody for 1.5 hours, while NFκB1 expression was associated with cell survival as previously reported by Williams *et al.*, in 2013. A similar pattern of response was seen in the small intestinal crypt compartments at 24 hours, but the response was more pronounced after anti-CD3 antibody than LPS. These results suggest that both LPS and anti-CD3 antibody cause similar effects even though

they stimulate different immune cells namely macrophage-mediated apoptosis and T-cell mediated apoptosis. It is likely that both stimuli eventually lead to a common pathway largely involving TNF.

Poly I:C is another apoptosis stimulating substance that signals through TLR3 and which has previously been described to induce small intestinal injury in mice (Zhao *et al*; 2017 and McAllister *et al*; 2012). Günther *et al*; 2012 previously reported that activation of TLR3 by poly I:C and of TLR4 by LPS induced excessive intestinal epithelial cell death. Intraperitoneal administration of 30 mg/kg poly I:C increased the apoptotic activity of SIECs and this resulted in blunting of proximal small intestinal villi with a reduction in number of SIECs per villus that reached a peak 2 hours after poly I:C injection. Apoptosis was mainly localised at the upper half of the small intestinal villi, in contrast there were no increases in the number of apoptotic cells seen in the crypt region (McAllister *et al*; 2012). Our time course study after administration of 30mg/kg poly I:C into adult female C57BL/6J mice indicated a significant increase in the number of apoptotic and shedding cells after 1 hour that markedly increased at 1.5 hours and continued to reach its peak at 2 hours. This was followed by a sudden drop to nearly the level observed in untreated mice 3 hours post injection. These data support the previous data by McAllister *et al.*, 2012. However our results also indicated no significant difference between the percentage of SIECs undergoing apoptosis and shedding at 1.5 and 2 hours. To examine the role of the NFκB family of proteins in regulating poly I:C induced small intestinal apoptosis and shedding and because no significant difference was seen in the percentage of apoptosis and shedding of SIECs at 1.5 and 2 hours, we injected wild-type C57BL/6J, *Nfκb1*<sup>-/-</sup>, *Nfκb2*<sup>-/-</sup> and *c-Rel*<sup>-/-</sup> mice with 30 mg/kg poly I:C for 1.5 hours and 24 hours to compare these data with the data

obtained following LPS treatment at similar time points. Interestingly we observed similar patterns of changes in the percentage of apoptosis and shedding in the villus compartment after 1.5 hours as those reported by Williams *et al.*, in 2013 after injecting 0.125 mg/kg LPS. This result suggests that the NFκB1 and NFκB2 transcription factors regulate cell death and cell survival respectively following IP injection of both LPS and poly I:C. However we observed very little apoptosis in the crypt compartment of C57BL/6J, *c-Rel*<sup>-/-</sup> and *Nfκb2*<sup>-/-</sup> mice following injection of poly I:C. This agrees with the previous result by McAllister *et al.*, in 2012 who also observed no increase in the percentage of crypt apoptosis after poly I:C injection. Unfortunately *Nfκb1*<sup>-/-</sup> mice died due to extensive fluid accumulation in the proximal small intestine and diarrhoea at 4-6 hours post poly I:C injection. This is likely to be due to extensive loss of SIECs by apoptosis and shedding from the villus compartment. It was therefore not possible to test the effect of NFκB1 deletion on poly I:C induced crypt apoptosis at 24 hours.

A previous study in our laboratory indicated that exogenous TNF at 0.33 mg/kg caused murine small intestinal damage equivalent to that caused by 10 mg/kg LPS at 1.5 hours post IP administration. It also reported that the pathological process of apoptosis and shedding that was induced by both LPS and TNF was regulated in the same way by the NFκB signalling pathway (Williams *et al.*, 2013). Our result confirmed that 0.33 mg/kg recombinant TNF induced apoptosis and shedding in the upper half of proximal small intestinal villi at 1.5 hours and that this was equivalent to that caused by LPS at the same time point. This effect was regulated by the NFκB signalling pathway and once again the NFκB1 transcription protein suppressed while the NFκB2 transcription protein promoted pathological apoptosis and shedding of villus SIECs. The data reported in this chapter also indicated that *Nfκb1*<sup>-/-</sup> mice were much more sensitive to TNF

induced crypt apoptosis than to the other stimuli that were used to induce small intestinal crypt apoptosis. This may be due to the accumulation of endogenous and exogenous TNF that may exaggerate the response of gut epithelial cells thus exhibiting a more potent response.

As previously indicated in LPS induced small intestinal crypt epithelial cells (chapter 3), some intestinal crypt epithelial cells were not labelled by antibodies against active caspase-3 but could be in the process of undergoing non-caspase-3-dependent cell death following administration of anti-CD3 antibody, poly I:C and TNF. Some of these cells appeared to be undergoing cell death by analysis of their morphology and may represent cells at a later stage of apoptosis due to fragmentation of the DNA (Glamočlija *et al.*, 2005) or represent other types of non-caspase-3 dependent cell death such as pyroptosis (Fink and Cookson, 2005) and necroptosis (Kaczmarek *et al.*, 2013).

In summary, the data reported in this chapter indicate that T-cell mediated, viral induced and exogenous TNF-induced SIEC apoptosis and shedding occur in similar ways to that seen following the administration of LPS. All of the stimuli that we used caused similar patterns of response in both villus and crypt epithelial cells (with the exception of poly I:C which did not induce small intestinal crypt apoptosis). All of these stimuli may result in an increase in the amount of TNF that binds to TNFR1 on the basolateral surfaces of SIECs, leading to pathological apoptosis and cell shedding. These processes seem to be consistently regulated by the expression of both NFκB1 and NFκB2.

## 7. Discussion

### 7.1 Major findings and subsequent concepts

The primary aims of this project were to further improve our understanding of the processes of pathological apoptosis and cell shedding in murine small intestinal epithelial cells and their relationship to gut barrier dysfunction. As previously indicated in our laboratory by Williams *et al.*, in 2013, systemic administration of *Escherichia coli* LPS (serotype O111:B4) induced pathological apoptosis and shedding of cells from the murine small intestinal epithelium at 1.5 hours post intraperitoneal administration and this phenomenon was regulated via NFκB signalling pathways with NFκB1 (p105/p50) and c-Rel promoting cell survival and NFκB2 (p100/p52) promoting cell apoptosis (Williams *et al.*, 2013).

It was previously demonstrated that LPS induced small intestinal epithelial apoptosis and cell shedding in C57BL/6J mice that peaked at 1.5 hours post IP administration (Williams *et al.*, 2013). In the present study we have established that LPS-induced SIEC apoptosis and shedding occurred in different mouse strains and also in rats with a similar phenotype, but with different degrees of responsiveness. Also, we demonstrated that LPS-induced SIEC apoptosis and cell shedding occurred in all tested age groups of mice representing puberty, young adulthood and maturity. It was further demonstrated that LPS from different bacterial species induced apoptosis and shedding in C57BL/6J mice at 1.5 hours post IP injection. Testing of the role of the RelB transcription factor in LPS-induced SIEC apoptosis and shedding indicated no major role for this alternative pathway NFκB subunit in regulating this phenomenon. We also showed that LPS induced apoptosis in small intestinal crypt epithelial cells at 24 hours

post IP administration of 0.125 mg/kg and similarly our data indicated that this phenomenon was regulated by NFκB signalling pathways with NFκB1 (p105/p50) signalling suppressing apoptosis and shedding of small intestinal villus and crypt epithelial cells while NFκB2 signalling promoted apoptosis and cell shedding. The apoptosis that is observed within the crypt compartment within the stem cell zone at this later time point following LPS administration could impact on the regenerative capacity of the epithelium.

Additionally, we confirmed that anti-CD3 antibody and TNF also induced SIEC apoptosis and shedding in small intestinal villi and crypts with similar patterns to that which occurred in LPS-treated mice. This suggests that TNF released by different circulating cell types (i.e. LPS acts mainly on monocytes and macrophages via TLR4, anti-CD3 stimulates T cells, poly I:C mimics viral infection and acts via TLR3) is able to exert effects on SIEC apoptosis and shedding. Furthermore, our results from mice treated with poly I:C indicated that the maximal degree of small intestinal epithelial apoptosis and cell shedding occurred 2 hours post IP injection in intestinal villi and was regulated by NFκB signalling pathways similarly to the regulation by LPS. However, our data did not indicate a role of NFκB transcription factors in regulating crypt epithelial cell apoptosis in response to this stimulus.

The ultrastructural changes that were observed in the small intestinal epithelium within this study supported the previous immunohistochemical observations for LPS-induced small intestinal epithelial cells. Ultrastructural changes were most marked in *Nfκb1*<sup>-/-</sup> mice treated with 0.125 mg/kg LPS while no changes were observed in

*Nfκb2*<sup>-/-</sup> mice before and after LPS IP administration suggesting that signalling via NFκB2 was necessary for these ultrastructural changes to occur.

Proteomic analysis of the small intestinal mucosal proteome of C57BL/6 mice before and after the administration of LPS revealed several changes in protein expression within the small intestinal mucosa which were further modified by *Nfκb1*, *Nfκb2* and *c-Rel* deletion. Some of these proteins may account for the different susceptibilities of the different mouse groups to LPS-induced small intestinal epithelial apoptosis and cell shedding.

## **7.2 Limitations of the study**

Although the morphological features of small intestinal epithelial apoptosis and cell shedding in this study were obtained from mice and rats, the phenotypic changes associated with these phenomena were similar to those previously reported in human small intestinal epithelia (Mayhew *et al.*, 1999 and Bullen *et al.*, 2006). However, there are functional and anatomical variations between human and rodent intestines. Copeland *et al.*, in 2005 indicated that humans are much more sensitive than mice and rats in terms of their immune responses, hence the doses of the various stimuli that were used in this study to induce SIEC apoptosis and shedding may be larger than those that would be needed to induce similar effects in the human small intestine.

In this study we used the immunohistological and scoring procedures for active caspase-3 that had previously been used in our laboratory by Williams and colleagues to obtain a consistent dataset that could be compared with previous results described

for LPS-induced SIEC apoptosis and shedding (Williams *et al.*, 2013). The anti-active caspase-3 primary antibody has previously been validated and each new batch of antibody purchased was re-assessed for activity during this study. However, these data rely on the specificity of a single polyclonal antibody. Active caspase-3 positive cells were however commonly associated with apoptotic morphology which further validated the antibody specificity.

The ultrastructural changes that were observed by EM following the administration of 0.125 mg/kg of bacterial LPS suggested similar sensitivities of *Nfkb1*<sup>-/-</sup>, *Nfkb2*<sup>-/-</sup> and *c-Rel*<sup>-/-</sup> mice to small intestinal epithelial apoptosis and cell shedding to that obtained by immunohistochemical analysis. However, both of these techniques did not indicate any discontinuity of the gut barrier as a result of cell loss from small intestinal epithelia which may have been more detectable using the higher dose of 10 mg/kg that has previously been shown to induce maximal rates of SIEC apoptosis and shedding. Histology and transmission electron microscopy are techniques that only capture the snapshot in time at which the tissue was fixed and consider a thin cross section through a tissue, which makes these techniques unreliable to assess intestinal barrier function. More dynamic assays that are more technically challenging and which were beyond the scope of this thesis would be needed to assess loss of intestinal barrier function and potential gap formation upon treatment with LPS, anti-CD3 or poly I:C.

Assays could include the oral gavage of a fluorescent probe/sugars such as FITC-dextran and analysis of the concentration of this dye in the peripheral circulation (Williams *et al.*, 2013), real-time confocal microscopy of small intestinal epithelia *en face* following topical or intravenous injection of dyes (Kiesslich *et al.*, 2011) or the

establishment of permeability assays using microinjection techniques in enteroid culture (Thompson and Duckworth, unpublished methods).

Proteomic analysis of the murine proximal small intestinal mucosa indicated a very large number of proteins that were altered in expression in C57BL/6 and NF $\kappa$ B transgenic mice 1.5 hours post administration of bacterial LPS. Initial interpretation of this dataset has involved determining the functional roles of proteins that were shown to have the largest fold up and down regulations from group sizes of 4 mice per group. Several of these proteins will be interesting to follow up and potentially validate in order to establish the extent to which they contribute towards the mechanisms responsible for pathological SIEC apoptosis and shedding. However, there were many more proteins identified which showed significantly altered expressions following LPS administration that may also be important regulators of SIEC apoptosis and shedding and which also warrant full validation. In depth analysis and validation of these proteins by western blot and immunohistochemistry has been beyond the scope of this thesis, but is now needed to determine the importance of these small intestinal mucosal proteome changes in contributing to pathological small intestinal apoptosis and cell shedding. Further in depth analysis is also warranted to determine whether these proteomic changes are a cause or a consequence of SIEC apoptosis and shedding in order to identify potential therapeutic targets for conditions known to result from excessive epithelial cell death and loss of intestinal barrier function such as inflammatory bowel disease.

### 7.3 Future research plans

Several possible future plans have already been discussed above and performing these experiments could help to answer several crucial questions and explain the molecular mechanisms associated with pathological apoptosis and cell shedding in regulating gut barrier function and subsequent intestinal pathology.

Although the results of this study have indicated essential roles of NF $\kappa$ B signalling pathways in the regulation of pathological SIEC apoptosis and shedding following different damage-inducing stimuli and have identified numerous proteins that show altered expression due to the deletion of individual NF $\kappa$ B subunits, it would be fascinating to determine which of these proteins are drivers of intestinal epithelial apoptosis and cell shedding. A selection of identified proteins (see chapter 5) should next be validated in a repeat experiment to confirm their altered expressions using immunohistochemistry for location and western blotting for quantitation. Genetic manipulation using 3D small intestinal enteroid cultures could also be conducted to knockdown or overexpress these targets and modified enteroids would be compared against control enteroids following treatment with a stimulus such as TNF (which is believed to be the main mediator of small intestinal villus enterocyte apoptosis and shedding) to determine whether they are protected or sensitised to apoptosis and cell shedding.

The small intestinal epithelium has a remarkable capacity to prevent breaches in barrier function. There are likely to be several mechanisms in place to prevent the invasion of abundant inflammation-causing luminal microorganisms. Understanding how these organisms gain entry across the intestinal epithelium (via bacterial-derived

and host factors which may be organism-dependent) and how NFκB signalling in the host epithelium contributes to this would help to further elucidate how the small intestine is homeostatically regulated. We would therefore like to further investigate the translocation of bacteria through discontinuities and gaps that may develop in the intestinal epithelium as a result of pathological apoptosis and shedding of SIECs. This would be achievable using microinjection of enteroids *in vitro* and assessment via confocal microscopy in the first instance and translating these findings *in vivo* to identify how other cellular compartments such as the intestinal immune system may contribute to the regulation of these processes. These experiments would improve our knowledge of the onset of gut barrier dysfunction in acute and chronic inflammatory diseases.

Anti-CD3 antibody, poly I:C and recombinant TNF administration all resulted in SIEC apoptosis and cell shedding at the villus tip although the peak time of maximal apoptosis and cell shedding post administration was different between stimuli. All mouse genotypes treated with these stimuli responded with similar sensitivities to those that resulted post administration of LPS (i.e. *Nfkb1*<sup>-/-</sup> were more sensitive and *Nfkb2*<sup>-/-</sup> were less sensitive than C57BL/6 controls) however, the mechanisms that ultimately resulted in apoptosis and cell shedding were different. Accordingly, it would be interesting to investigate the ultrastructural and proteomic changes of the small intestinal mucosal proteomes for different mouse groups treated with these stimuli to compare the similarities and differences to apoptosis and cell shedding induced by LPS to determine whether there is a single mechanism or multiple mechanisms responsible for epithelial damage in different intestinal diseases.

The ultimate aim of our studies was to improve understanding of pathological small intestinal epithelial apoptosis and cell shedding and how these processes affect gut barrier function and the development of inflammatory bowel disease. Therefore, it is now necessary to extend these studies into humans by using antibodies to characterise specific NFκB signalling-related proteins in human small intestinal epithelial cells and to derive small intestinal enteroids from human biopsies followed by their genetic manipulation to modulate NFκB signalling components and other targets identified from our proteomic analysis as contributing to apoptosis and cell shedding regulation. Human enteroids will be stimulated with TNF and assessed by confocal microscopy and histology.

Once targets have been validated by the experiments proposed above, a pharmacological or dietary approach could then be applied to modulate the small intestinal epithelial proteome to make the small intestinal epithelium less sensitive to the induction of apoptosis and cell shedding induced by genetic (e.g. susceptibility genes for IBD) or environmental (e.g. diet or chemotherapy) factors to preserve intestinal homeostasis and intestinal barrier function.

## 7.4 Translational impact

Results obtained from these studies have indicated that pathological apoptosis and shedding of murine small intestinal epithelial cells may play an important role in the development of acute inflammation in the small intestine. This phenomenon may lead to increased gut barrier permeability and loss of tissue homeostasis. Increased gut barrier permeability due to increased intestinal epithelial cell shedding has previously been demonstrated in IBDs such as Crohn's disease and ulcerative colitis which affect 145 and 243 per 100,000 of the UK population respectively. Additionally, an increased percentage of apoptotic and shedding cells may also lead to the formation of discontinuities and gaps that allow the penetration of luminal bacteria into the blood circulation and contribute to the severity of systemic conditions such as metabolic endotoxaemia and sepsis which affect 260,000 of the UK population annually at a cost of £7.76 billion to the NHS (Hex *et al.*, 2017).

The data described in this work have also demonstrated a role of NFκB signalling pathways in regulating small intestinal epithelial apoptosis and cell shedding and have described several proteins that changed in abundance as a result of systemic LPS administration. With the follow up experiments described above, these findings could potentially be used to modulate the processes of pathological apoptosis and shedding in the gut and help in the early diagnosis and prevention of inflammatory gastrointestinal diseases.

## 7.5 Conclusions

This study has described in detail the process of SIEC apoptosis and shedding induced by different stimuli including LPS, anti-CD3, poly I:C and TNF. In particular, it has demonstrated that LPS induces SIEC apoptosis and shedding in different mouse strains and also in rats. We have also determined that this phenomenon is not affected by age but is affected by mouse genotype. The alternative NF $\kappa$ B signalling pathway is a particularly important regulator of this process. We have described the effects of LPS on SIEC ultrastructure in detail and have proposed several proteins that may contribute to the SIEC apoptosis and shedding process. These now warrant further investigation as potential targets to ameliorate intestinal disease in humans.

## 8. Bibliography:

1. Aggarwal BB. Signalling pathways of the TNF superfamily: a double-edged sword. *Nat Rev Immunol.* 2003;3(9):745-56.
2. Aggarwal BB, Gupta SC, Kim JH. Historical perspectives on tumor necrosis factor and its superfamily: 25 years later, a golden journey. *Blood.* 2012;119(3):651-65.
3. Ahram M, Petricoin EF. Proteomics Discovery of Disease Biomarkers. *Biomark Insights.* 2008;3:325-33.
4. Al-Astal HI, Massad M, AlMatar M, Ekal H. Cellular Functions of RNA-Binding Motif Protein 3 (RBM3): Clues in Hypothermia, Cancer Biology and Apoptosis. *Protein Pept Lett.* 2016;23(9):828-35.
5. Alex P, Gucek M, Li X. Applications of proteomics in the study of inflammatory bowel diseases: Current status and future directions with available technologies. *Inflamm Bowel Dis.* 2009;15(4):616-29.
6. Alscher KT, Phang PT, McDonald TE, Walley KR. Enteral feeding decreases gut apoptosis, permeability, and lung inflammation during murine endotoxemia. *Am J Physiol Gastrointest Liver Physiol.* 2001;281(2):G569-76.
7. Alvarez A, Lacalle J, Canavate M, Alonso-Alconada D, Lara-Celador I, Alvarez F, et al. Cell death. A comprehensive approximation. *Necrosis. Microscopy: Science, Technology, Application and Education.* 2010;3:1017-24.
8. Araya RE, Jury J, Bondar C, Verdu EF, Chirido FG. Intraluminal Administration of Poly I:C Causes an Enteropathy That Is Exacerbated by Administration of Oral Dietary Antigen. *Plos One.* 2014;9(6).
9. Arntzen MO, Thiede B. ApoptoProteomics: An integrated database for analysis of proteomics data obtained from apoptotic cells. *Molecular & Cellular Proteomics.* 2011:mcp. M111. 010447.
10. Artavanis-Tsakonas S, Rand MD, Lake RJ. Notch signaling: Cell fate control and signal integration in development. *Science.* 1999;284(5415):770-6.
11. Axelrad JE, Lichtiger S, Yajnik V. Inflammatory bowel disease and cancer: The role of inflammation, immunosuppression, and cancer treatment. *World J Gastroentero.* 2016;22(20):4794-801.

12. Bach SP, Renehan AG, Potten CS. Stem cells: the intestinal stem cell as a paradigm. *Carcinogenesis*. 2000;21(3):469-76.
13. Barceló-Batllori S, André M, Servis C, Lévy N, Takikawa O, Michetti P, et al. Proteomic analysis of cytokine induced proteins in human intestinal epithelial cells: implications for inflammatory bowel diseases. *Proteomics*. 2002;2(5):551-60.
14. Barker N, van Es JH, Kuipers J, Kujala P, van den Born M, Cozijnsen M, et al. Identification of stem cells in small intestine and colon by marker gene *Lgr5*. *Nature*. 2007;449(7165):1003-7.
15. Baumgart DC, Carding SR. Inflammatory bowel disease: cause and immunobiology. *The Lancet*. 2007;369(9573):1627-40.
16. Baumgart DC, Sandborn WJ. Inflammatory bowel disease: clinical aspects and established and evolving therapies. *Lancet*. 2007;369(9573):1641-57.
17. Beaulieu J-F. Differential expression of the VLA family of integrins along the crypt-villus axis in the human small intestine. *J Cell Sci*. 1992;102(3):427-36.
18. Beinke S, Ley SC. Functions of NF-kappaB1 and NF-kappaB2 in immune cell biology. *Biochem J*. 2004;382(Pt 2):393-409.
19. Bennike T, Birkelund S, Stensballe A, Andersen V. Biomarkers in inflammatory bowel diseases: current status and proteomics identification strategies. *World J Gastroenterol*. 2014;20(12):3231-44.
20. Benoit R, Rowe S, Watkins SC, Boyle P, Garrett M, Alber S, et al. Pure endotoxin does not pass across the intestinal epithelium in vitro. *Shock (Augusta, Ga)*. 1998;10(1):43-8.
21. Berndt U, Bartsch S, Philipsen L, Danese S, Wiedenmann B, Dignass AU, et al. Proteomic analysis of the inflamed intestinal mucosa reveals distinctive immune response profiles in Crohn's disease and ulcerative colitis. *J Immunol*. 2007;179(1):295-304.
22. Berndt U, Bartsch S, Philipsen L, Danese S, Wiedenmann B, Dignass AU, et al. Proteomic analysis of the inflamed intestinal mucosa reveals distinctive immune response profiles in Crohn's disease and ulcerative colitis. *The Journal of Immunology*. 2007;179(1):295-304.
23. Bischoff SC, Barbara G, Buurman W, Ockhuizen T, Schulzke J-D, Serino M, et al. Intestinal permeability—a new target for disease prevention and therapy. *Bmc*

Gastroenterol. 2014;14(1):189.

24. Bjarnason I, Macpherson A, Hollander D. Intestinal Permeability - an Overview. *Gastroenterology*. 1995;108(5):1566-81.

25. Bjerknes M, Cheng H. Clonal analysis of mouse intestinal epithelial progenitors. *Gastroenterology*. 1999;116(1):7-14.

26. Bloemena E, ten Berge I, Surachno J, Wilmink J. Kinetics of interleukin 6 during OKT3 treatment in renal allograft recipients. *Transplantation*. 1990;50(2):330.

27. Booth D, Potten CS. Protection against mucosal injury by growth factors and cytokines. *JNCI Monographs*. 2001;2001(29):16-20.

28. Boshuizen JA, Reimerink JH, Korteland-van Male AM, van Ham VJ, Koopmans MP, Büller HA, et al. Changes in small intestinal homeostasis, morphology, and gene expression during rotavirus infection of infant mice. *J Virol*. 2003;77(24):13005-16.

29. Bouchal P, Dvorakova M, Roumeliotis T, Bortlicek Z, Ihnatova I, Prochazkova I, et al. Combined Proteomics and Transcriptomics Identifies Carboxypeptidase B1 and Nuclear Factor kappaB (NF-kappaB) Associated Proteins as Putative Biomarkers of Metastasis in Low Grade Breast Cancer. *Mol Cell Proteomics*. 2015;14(7):1814-30.

30. Bowen JM, Gibson RJ, Cummins AG, Keefe DMK. Intestinal mucositis: the role of the Bcl-2 family, p53 and caspases in chemotherapy-induced damage. *Support Care Cancer*. 2006;14(7):713-31.

31. Bren GD, Solan NJ, Miyoshi H, Pennington KN, Pobst LJ, Paya CV. Transcription of the RelB gene is regulated by NF-κB. *Oncogene*. 2001;20(53):7722.

32. Browne CA, O'Brien FE, Connor TJ, Dinan TG, Cryan JF. Differential Lipopolysaccharide-Induced Immune Alterations in the Hippocampus of Two Mouse Strains: Effects of Stress. *Neuroscience*. 2012;225:237-48.

33. Bruewer M, Samarin S, Nusrat A. Inflammatory bowel disease and the apical junctional complex. *Inflammatory Bowel Disease: Genetics, Barrier Function, Immunologic Mechanisms, and Microbial Pathways*. 2006;1072:242-52.

34. Bruno MEC, Rogier EW, Arsenescu RI, Flomenhoft DR, Kurkjian CJ, Ellis GI, et al. Correlation of Biomarker Expression in Colonic Mucosa with Disease Phenotype in Crohn's Disease and Ulcerative Colitis. *Digest Dis Sci*. 2015;60(10):2976-84.

35. Bullen TF, Forrest S, Campbell F, Dodson AR, Hershman MJ, Pritchard DM, et al. Characterization of epithelial cell shedding from human small intestine. *Lab Invest*.

2006;86(10):1052-63.

36. Burkitt MD, Hanedi AF, Duckworth CA, Williams JM, Tang JM, O'reilly LA, et al. NF- $\kappa$ B1, NF- $\kappa$ B2 and c-Rel differentially regulate susceptibility to colitis-associated adenoma development in C57BL/6 mice. *The Journal of pathology*. 2015;236(3):326-36.
37. Caamano JH, Rizzo CA, Durham SK, Barton DS, Raventos-Suarez C, Snapper CM, et al. Nuclear factor (NF)-kappa B2 (p100/p52) is required for normal splenic microarchitecture and B cell-mediated immune responses. *J Exp Med*. 1998;187(2):185-96.
38. Campos LC, Whittam TS, Gomes T, Andrade J, Trabulsi LR. Escherichia coli serogroup O111 includes several clones of diarrheagenic strains with different virulence properties. *Infection and immunity*. 1994;62(8):3282-8.
39. Cario E. Toll-like receptors in inflammatory bowel diseases: a decade later. *Inflamm Bowel Dis*. 2010;16(9):1583-97.
40. Carpenter PA, Pavlovic S, Tso JY, Press OW, Gooley T, Yu XZ, et al. Non-Fc receptor-binding humanized anti-CD3 antibodies induce apoptosis of activated human T cells. *Journal of Immunology*. 2000;165(11):6205-13.
41. Carulli AJ, Samuelson LC, Schnell S. Unraveling intestinal stem cell behavior with models of crypt dynamics. *Integr Biol-Uk*. 2014;6(3):243-57.
42. Casteleyn C, Rekecki A, Van der Aa A, Simoens P, Van den Broeck W. Surface area assessment of the murine intestinal tract as a prerequisite for oral dose translation from mouse to man. *Lab Anim-Uk*. 2010;44(3):176-83.
43. Cheng H, Leblond C. Origin, differentiation and renewal of the four main epithelial cell types in the mouse small intestine V. Unitarian theory of the origin of the four epithelial cell types. *American Journal of Anatomy*. 1974;141(4):537-61.
44. Ciccocioppo R, Di Sabatino A, Parroni R, Muzi P, D'Alo S, Ventura T, et al. Increased enterocyte apoptosis and Fas-Fas ligand system in celiac disease. *Am J Clin Pathol*. 2001;115(4):494-503.
45. Clarke SJ, Farrugia DC, Aherne GW, Pritchard DM, Benstead J, Jackman AL. Balb/c mice as a preclinical model for raltitrexed-induced gastrointestinal toxicity. *Clinical Cancer Research*. 2000;6(1):285-96.

46. Collado-Romero M, Aguilar C, Arce C, Lucena C, Codrea MC, Morera L, et al. Quantitative proteomics and bioinformatic analysis provide new insight into the dynamic response of porcine intestine to Salmonella Typhimurium. *Front Cell Infect Mi.* 2015;5.
47. Cookson BT, Brennan MA. Pro-inflammatory programmed cell death. *Trends Microbiol.* 2001;9(3):113-4.
48. Copeland S, Warren HS, Lowry SF, Clavano SE, Remic D, et al. Acute inflammatory response to endotoxin in mice and humans. *Clin. Diagn. Lab immunol.* 2005; 12(1):60-67
49. Crosnier C, Vargesson N, Gschmeissner S, Ariza-McNaughton L, Morrison A, Lewis J. Delta-Notch signalling controls commitment to a secretory fate in the zebrafish intestine. *Development.* 2005;132(5):1093-104.
50. Dagenais M, Douglas T, Saleh M. Role of programmed necrosis and cell death in intestinal inflammation. *Curr Opin Gastroenterol.* 2014;30(6):566-75.
51. Daniele B, D'Agostino L. Proliferation and differentiation of the small intestinal epithelium: from Petri dish to bedside. *The Italian journal of gastroenterology.* 1994;26(9):459-70.
52. Degterev A, Huang ZH, Boyce M, Li YQ, Jagtap P, Mizushima N, et al. Chemical inhibitor of nonapoptotic cell death with therapeutic potential for ischemic brain injury (vol 1, pg 112, 2005). *Nat Chem Biol.* 2005;1(3).
53. Delgado ME, Grabinger T, Brunner T. Cell death at the intestinal epithelial front line. *Febs J.* 2016;283(14):2701-19.
54. Deutschman CS, Tracey KJ. Sepsis: Current Dogma and New Perspectives. *Immunity.* 2014;40(4):464-76.
55. Di Sabatino A, Ciccocioppo R, D'alò S, Parroni R, Millimaggi D, Cifone M, et al. Intraepithelial and lamina propria lymphocytes show distinct patterns of apoptosis whereas both populations are active in Fas based cytotoxicity in coeliac disease. *Gut.* 2001;49(3):380-6.
56. Dong CX, Zhao W, Solomon C, Rowland KJ, Ackerley C, Robine S, et al. The Intestinal Epithelial Insulin-Like Growth Factor-1 Receptor Links Glucagon-Like Peptide-2 Action to Gut Barrier Function. *Endocrinology.* 2014;155(2):370-9.

57. Duan GY, Walther D. The Roles of Post-translational Modifications in the Context of Protein Interaction Networks. *Plos Comput Biol*. 2015;11(2).
58. Duckworth CA, Pritchard DM. Suppression of apoptosis, crypt hyperplasia, and altered differentiation in the colonic epithelia of bak-null mice. *Gastroenterology*. 2009;136(3):943-52.
59. Duricova D, Burisch J, Jess T, Gower-Rousseau C, Lakatos PL, EpiCom E. Age-related differences in presentation and course of inflammatory bowel disease: an update on the population-based literature. *J Crohns Colitis*. 2014;8(11):1351-61.
60. Edelblum KL, Yan F, Yamaoka T, Polk DB. Regulation of apoptosis during homeostasis and disease in the intestinal epithelium. *Inflamm Bowel Dis*. 2006;12(5):413-24.
61. Eisenhoffer GT, Loftus PD, Yoshigi M, Otsuna H, Chien CB, Morcos PA, et al. Crowding induces live cell extrusion to maintain homeostatic cell numbers in epithelia. *Nature*. 2012;484(7395):546-9.
62. Fang C, Dean J, Smith JW. A novel variant of ileal bile acid binding protein is up-regulated through nuclear factor-kappaB activation in colorectal adenocarcinoma. *Cancer Res*. 2007;67(19):9039-46.
63. Favaloro B, Allocati N, Graziano V, Di Ilio C, De Laurenzi V. Role of Apoptosis in disease. *Aging-U.S.* 2012;4(5):330-49.
64. Feist P, Hummon AB. Proteomic challenges: sample preparation techniques for microgram-quantity protein analysis from biological samples. *International journal of molecular sciences*. 2015;16(2):3537-63.
65. Feldman M, Friedman LS, Brandt LJ. *Sleisenger and Fordtran's gastrointestinal and liver disease: pathophysiology, diagnosis, management*: Elsevier Health Sciences; 2015.
66. Fink SL, Cookson BT. Apoptosis, pyroptosis, and necrosis: mechanistic description of dead and dying eukaryotic cells. *Infection and immunity*. 2005;73(4):1907-16.
67. Florian S, Krehl S, Loewinger M, Kipp A, Banning A, Esworthy S, et al. Loss of GPx2 increases apoptosis, mitosis, and GPx1 expression in the intestine of mice. *Free Radic Biol Med*. 2010;49(11):1694-702.
68. Ford AC, Moayyedi P, Hanauer SB. Ulcerative colitis. *Bmj-Brit Med J*. 2013;346.

69. Freeman HJ. Natural history and long-term clinical course of Crohn's disease. *World Journal of Gastroenterology: WJG*. 2014;20(1):31.
70. Furriols M, Bray S. A model Notch response element detects Suppressor of Hairless-dependent molecular switch. *Curr Biol*. 2001;11(1):60-4.
71. Garabedian EM, Roberts LJJ, McNevin MS, Gordon JI. Examining the role of Paneth cells in the small intestine by lineage ablation in transgenic mice. *J Biol Chem*. 1997;272(38):23729-40.
72. Garner CD, Antonopoulos DA, Wagner B, Duhamel GE, Keresztes I, Ross DA, et al. Perturbation of the small intestine microbial ecology by streptomycin alters pathology in a *Salmonella enterica* serovar typhimurium murine model of infection. *Infection and immunity*. 2009;77(7):2691-702.
73. Gasparini C, Foxwell BM, Feldmann M. RelB/p50 regulates TNF production in LPS-stimulated dendritic cells and macrophages. *Cytokine*. 2013;61(3):736-40.
74. Ge YM, Ezzell RM, Warren HS. Localization of endotoxin in the rat intestinal epithelium. *J Infect Dis*. 2000;182(3):873-81.
75. Gerbe F, Jay P. Intestinal tuft cells: epithelial sentinels linking luminal cues to the immune system. *Mucosal immunology*. 2016;9(6):1353.
76. Gerbe F, Legraverend C, Jay P, et al. The intestinal epithelium tuft cells: specification and function. *Cell Mol Life Sci*. 2012; 69(17): 2907–2917
77. Gerbe F, van Es JH, Makrini L, Brulin B, Mellitzer G, Robine S, et al. Distinct ATOH1 and Neurog3 requirements define tuft cells as a new secretory cell type in the intestinal epithelium. *The Journal of cell biology*. 2011;192(5):767-80.
78. Gilmore AP. Anoikis. *Cell Death Differ*. 2005;12 Suppl 2:1473-7.
79. Gilmore TD. Introduction to NF- $\kappa$ B: players, pathways, perspectives. *Oncogene*. 2006;25(51):6680.
80. Glamočlija, V., Vilović, K., Saraga-Babić, M., Baranović, A. and Sapunar, D., 2005. Apoptosis and active caspase-3 expression in human granulosa cells. *Fertility and sterility*, 83(2), pp.426-431.
81. Glick D, Barth S, Macleod KF. Autophagy: cellular and molecular mechanisms. *J Pathol*. 2010;221(1):3-12.
82. Goldberg AL. New Insights into Proteasome Function - from Archaeobacteria to Drug Development. *Chemistry & Biology*. 1995;2(8):503-8.

83. Gonzalez LM, Williamson I, Piedrahita JA, Blikslager AT, Magness ST. Cell Lineage Identification and Stem Cell Culture in a Porcine Model for the Study of Intestinal Epithelial Regeneration. *Plos One*. 2013;8(6).
84. Goyette P, Labbe C, Trinh TT, Xavier RJ, Rioux JD. Molecular pathogenesis of inflammatory bowel disease: Genotypes, phenotypes and personalized medicine. *Ann Med*. 2007;39(3):177-99.
85. Grasberger H, Gao J, Nagao-Kitamoto H, Kitamoto S, Zhang M, Kamada N, et al. Increased Expression of DUOX2 Is an Epithelial Response to Mucosal Dysbiosis Required for Immune Homeostasis in Mouse Intestine. *Gastroenterology*. 2015;149(7):1849-59.
86. Groschwitz KR, Hogan SP. Intestinal barrier function: molecular regulation and disease pathogenesis. *J Allergy Clin Immunol*. 2009;124(1):3-20.
87. Grosse AS, Pressprich MF, Curley LB, Hamilton KL, Margolis B, Hildebrand JD, et al. Cell dynamics in fetal intestinal epithelium: implications for intestinal growth and morphogenesis. *Development*. 2011;138(20):4423-32.
88. Guan YF, Watson AJM, Marchiando AM, Bradford E, Shen L, Turner JR, et al. Redistribution of the tight junction protein ZO-1 during physiological shedding of mouse intestinal epithelial cells. *American Journal of Physiology-Cell Physiology*. 2011;300(6):C1404-C14.
89. Guarino MP, Altomare A, Barera S, Locato V, Cocca S, Franchin C, et al. Effect of Inulin on Proteome Changes Induced by Pathogenic Lipopolysaccharide in Human Colon. *Plos One*. 2017;12(1):e0169481.
90. Guma M, Stepniak D, Shaked H, Spehlmann ME, Shenouda S, Cheroutre H, et al. Constitutive intestinal NF- $\kappa$ B does not trigger destructive inflammation unless accompanied by MAPK activation. *Journal of Experimental Medicine*. 2011;208(9):1889-900.
91. Gunther C, Buchen B, He GW, Hornef M, Torow N, Neumann H, et al. Caspase-8 controls the gut response to microbial challenges by Tnf-alpha-dependent and independent pathways. *Gut*. 2015;64(4):601-10.
92. Gunther C, Martini E, Wittkopf N, Amann K, Weigmann B, Neumann H, et al. Caspase-8 regulates TNF-alpha-induced epithelial necroptosis and terminal ileitis. *Nature*. 2011;477(7364):335-U108.

93. Gunther C, Neumann H, Neurath MF, Becker C. Apoptosis, necrosis and necroptosis: cell death regulation in the intestinal epithelium. *Gut*. 2013;62(7):1062-71.
94. Guo S, Al-Sadi R, Said HM, Ma TY. Lipopolysaccharide causes an increase in intestinal tight junction permeability in vitro and in vivo by inducing enterocyte membrane expression and localization of TLR-4 and CD14. *The American journal of pathology*. 2013;182(2):375-87.
95. Guy-Grand D, DiSanto JP, Henchoz P, Malassis-Seris M, Vassalli P. Small bowel enteropathy: role of intraepithelial lymphocytes and of cytokines (IL-12, IFN-gamma, TNF) in the induction of epithelial cell death and renewal. *European Journal of Immunology*. 1998;28(2):730-44.
96. Haber AL, Biton M, Rogel N, Herbst RH, Shekhar K, Smillie C, et al. A single-cell survey of the small intestinal epithelium. *Nature*. 2017;551(7680):333-+.
97. Hacker H, Karin M. Regulation and function of IKK and IKK-related kinases. *Sci STKE*. 2006;2006(357):re13.
98. Haller D, Bode C, Hammes W, Pfeifer A, Schiffrin E, Blum S. Non-pathogenic bacteria elicit a differential cytokine response by intestinal epithelial cell/leucocyte co-cultures. *Gut*. 2000;47(1):79-87.
99. Hammoudi A, Song F, Reed KR, Jenkins RE, Meniel VS, Watson AJ, et al. Proteomic profiling of a mouse model of acute intestinal Apc deletion leads to identification of potential novel biomarkers of human colorectal cancer (CRC). *Biochem Biophys Res Commun*. 2013;440(3):364-70.
100. Han JH, Zhong CQ, Zhang DW. Programmed necrosis: backup to and competitor with apoptosis in the immune system. *Nature Immunology*. 2011;12(12):1143-9.
101. Hao WL, Lee YK. Microflora of the gastrointestinal tract: a review. *Methods Mol Biol*. 2004;268:491-502.
102. Hayden MS, Ghosh S. Shared principles in NF-kappaB signaling. *Cell*. 2008;132(3):344-62.
103. He B, Li T, Guan L, Liu FE, Chen XM, Zhao J, et al. CTNNA3 is a tumor suppressor in hepatocellular carcinomas and is inhibited by miR-425. *Oncotarget*. 2016;7(7):8078-89.
104. He S, Hou X, Xu X, Wan C, Yin P, Liu X, et al. Quantitative proteomic analysis

reveals heat stress-induced injury in rat small intestine via activation of the MAPK and NF- $\kappa$ B signaling pathways. *Molecular BioSystems*. 2015;11(3):826-34.

105. Himmel ME, Hardenberg G, Piccirillo CA, Steiner TS, Levings MK. The role of T-regulatory cells and Toll-like receptors in the pathogenesis of human inflammatory bowel disease. *Immunology*. 2008;125(2):145-53.

106. Hindryckx P, Laukens D. Intestinal barrier dysfunction: the primary driver of IBD? *Inflammatory Bowel Disease-Advances in Pathogenesis and Management*: InTech; 2012.

107. Holmgren L, O'Reilly MS, Folkman J. Dormancy of Micrometastases - Balanced Proliferation and Apoptosis in the Presence of Angiogenesis Suppression. *Nat Med*. 1995;1(2):149-53.

108. Honda K, Takeda K. Regulatory mechanisms of immune responses to intestinal bacteria. *Mucosal Immunology*. 2009;2(3):187.

109. Huang YH, Chang AY, Huang CM, Huang SW, Chan SH. Proteomic analysis of lipopolysaccharide-induced apoptosis in PC12 cells. *Proteomics*. 2002;2(9):1220-8.

110. Hurley JC. Towards Clinical Applications of Anti-endotoxin Antibodies; A Re-appraisal of the Disconnect. *Toxins*. 2013;5(12):2589-620.

111. Ikeda H, Suzuki Y, Suzuki M, Koike M, Tamura J, Tong J, et al. Apoptosis is a major mode of cell death caused by ischaemia and ischaemia/reperfusion injury to the rat intestinal epithelium. *Gut*. 1998;42(4):530-7.

112. Ishizaka A, Mizutani T, Kobayashi K, Tando T, Sakurai K, Fujiwara T, et al. Double PHD finger proteins DPF3a and 3b are required as transcriptional coactivators in the SWI/SNF complex-dependent activation of the NF- $\kappa$ B RelA/p50 heterodimer. *J Biol Chem*. 2012;287(15):11924-33.

113. Ishizaka A, Mizutani T, Kobayashi K, Tando T, Sakurai K, Fujiwara T, et al. Double plant homeodomain (PHD) finger proteins DPF3a and -3b are required as transcriptional co-activators in SWI/SNF complex-dependent activation of NF-kappaB RelA/p50 heterodimer. *J Biol Chem*. 2012;287(15):11924-33.

114. Iwamura T, Yoneyama M, Yamaguchi K, Suhara W, Mori W, Shiota K, et al. Induction of IRF-3/-7 kinase and NF- $\kappa$ B in response to double-stranded RNA and virus infection: common and unique pathways. *Genes to Cells*. 2001;6(4):375-88.

115. Jacob A. A comprehensive textbook of midwifery and gynecological nursing.

Third edition. ed. New Delhi: Jaypee Brothers Medical Publishers (P) Ltd.; 2012. xxii, 806 pages, 8 pages of plates p.

116. Jaramillo S, Zador AM. Mice and rats achieve similar levels of performance in an adaptive decision-making task. *Frontiers in systems neuroscience*. 2014;8:173.
117. Jenny M, Uhl C, Roche C, Duluc I, Guillermin V, Guillemot F, et al. Neurogenin3 is differentially required for endocrine cell fate specification in the intestinal and gastric epithelium. *Embo J*. 2002;21(23):6338-47.
118. Jensen J, Pedersen EE, Galante P, Hald J, Heller RS, Ishibashi M, et al. Control of endodermal endocrine development by Hes-1. *Nat Genet*. 2000;24(1):36-44.
119. Jiao L, Inhoffen J, Gan-Schreier H, Tuma-Kellner S, Stremmel W, Sun Z, et al. Deficiency of Group VIA Phospholipase A2 (iPLA2beta) Renders Susceptibility for Chemical-Induced Colitis. *Dig Dis Sci*. 2015;60(12):3590-602.
120. John LJ, Fromm M, Schulzke JD. Epithelial Barriers in Intestinal Inflammation. *Antioxid Redox Sign*. 2011;15(5):1255-70.
121. Johnson LR, Ray RM. Programmed Cell Death in the Gastrointestinal Tract. *Physiology of the Gastrointestinal Tract (Fifth Edition)*: Elsevier; 2012. p. 379-414.
122. Jui J. Septic shock. *Tintinalli's Emergency Medicine: A Comprehensive Study Guide*. 2011.
123. Kaczmarek A, Vandenabeele P, Krysko DV. Necroptosis: The Release of Damage-Associated Molecular Patterns and Its Physiological Relevance. *Immunity*. 2013;38(2):209-23.
124. Käll, L., Canterbury, J.D., Weston, J., Noble, W.S. and MacCoss, M.J., Semi-supervised learning for peptide identification from shotgun proteomics datasets. *Nature methods*, 2007, 4(11), p.923.
125. Karin M, Delhase M. The I kappa B kinase (IKK) and NF-kappa B: key elements of proinflammatory signalling. *Semin Immunol*. 2000;12(1):85-98.
126. Karnatovskaia LV, Festic E. Sepsis: a review for the neurohospitalist. *Neurohospitalist*. 2012;2(4):144-53.
127. Kawai T, Akira S. Toll-like receptor and RIG-1-like receptor signaling. *Annals of the New York Academy of Sciences*. 2008;1143(1):1-20.
128. Kawai T, Akira S. The role of pattern-recognition receptors in innate immunity: update on Toll-like receptors. *Nature immunology*. 2010;11(5):373.

129. Kerr JFR, Wyllie AH, Currie AR. Apoptosis - Basic Biological Phenomenon with Wide-Ranging Implications in Tissue Kinetics. *Brit J Cancer*. 1972;26(4):239-&.
130. Kiesslich R, Duckworth CA, Moussata D, Gloeckner A, Lim LG, Goetz M, et al. Local barrier dysfunction identified by confocal laser endomicroscopy predicts relapse in inflammatory bowel disease. *Gut*. 2012;61(8):1146-53.
131. Kolf CM, Cho E, Tuan RS. Mesenchymal stromal cells - Biology of adult mesenchymal stem cells: regulation of niche, self-renewal and differentiation. *Arthritis Res Ther*. 2007;9(1).
132. Kontgen F, Grumont RJ, Strasser A, Metcalf D, Li R, Tarlinton D, et al. Mice lacking the c-rel proto-oncogene exhibit defects in lymphocyte proliferation, humoral immunity, and interleukin-2 expression. *Genes Dev*. 1995;9(16):1965-77.
133. Kroemer G, Galluzzi L, Vandenabeele P, Abrams J, Alnemri ES, Baehrecke EH, et al. Classification of cell death: recommendations of the Nomenclature Committee on Cell Death 2009. *Cell Death Differ*. 2009;16(1):3-11.
134. Kuhnert F, Davis CR, Wang HT, Chu P, Lee M, Yuan J, et al. Essential requirement for Wnt signaling in proliferation of adult small intestine and colon revealed by adenoviral expression of Dickkopf-1. *P Natl Acad Sci USA*. 2004;101(1):266-71.
135. Kulkarni N, Zang E, Kelloff G, Reddy BS. Effect of the Chemopreventive Agents Piroxicam and D,L-Alpha-Difluoromethylornithine on Intermediate Biomarkers of Colon Carcinogenesis. *Carcinogenesis*. 1992;13(6):995-1000.
136. Kuriyan J, Thanos D. Structure of the NF- $\kappa$ B transcription factor: a holistic interaction with DNA. *Structure*. 1995;3(2):135-41.
137. Labbé K, Saleh M. Pyroptosis: a caspase-1-dependent programmed cell death and a barrier to infection. *The Inflammasomes*: Springer; 2011. p. 17-36.
138. Lai C-W, Sun T-L, Lo W, Tang Z-H, Wu S, Chang Y-J, et al. Shedding-induced gap formation contributes to gut barrier dysfunction in endotoxemia. *Journal of Trauma and Acute Care Surgery*. 2013;74(1):203-13.
139. Lau KS, Juchheim AM, Cavaliere KR, Philips SR, Lauffenburger DA, Haigis KM. In Vivo Systems Analysis Identifies Spatial and Temporal Aspects of the Modulation of TNF-alpha-Induced Apoptosis and Proliferation by MAPKs. *Sci Signal*. 2011;4(165).
140. Lawrence T. The nuclear factor NF- $\kappa$ B pathway in inflammation. *Cold Spring Harbor perspectives in biology*. 2009:a001651.

141. Leblond C, Stevens C. The constant renewal of the intestinal epithelium in the albino rat. *The Anatomical Record*. 1948;100(3):357-77.
142. Lee CC, Avalos AM, Ploegh HL. Accessory molecules for Toll-like receptors and their function. *Nat Rev Immunol*. 2012;12(3):168-79.
143. Leite CA, Fagundes-Neto U, Haapalainen EF. Evaluation of the ultrastructure of the small intestine of hiv infected children by transmission and scanning electronic microscopy. *Arq Gastroenterol*. 2013;50(1):70-7.
144. Lenaerts K, Sokolovic M, Bouwman FG, Lamers WH, Mariman EC, Renes J. Starvation induces phase-specific changes in the proteome of mouse small intestine. *J Proteome Res*. 2006;5(9):2113-22.
145. Lian YF, Yuan J, Cui Q, Feng QS, Xu M, Bei JX, et al. Upregulation of KLHDC4 Predicts a Poor Prognosis in Human Nasopharyngeal Carcinoma. *Plos One*. 2016;11(3):e0152820.
146. Lin PW, Simon PO, Gewirtz AT, Neish AS, Ouellette AJ, Madara JL, et al. Paneth cell cryptdins act in vitro as apical paracrine regulators of the innate inflammatory response. *J Biol Chem*. 2004;279(19):19902-7.
147. Liu T, Zhang L, Joo D, Sun S-C. NF- $\kappa$ B signaling in inflammation. *Signal transduction and targeted therapy*. 2017;2:17023.
148. Liu X, Wei W, Li X, Shen P, Ju D, Wang Z, et al. BMI1 and MEL18 Promote Colitis-Associated Cancer in Mice via REG3B and STAT3. *Gastroenterology*. 2017;153(6):1607-20.
149. Locksley RM, Killeen N, Lenardo MJ. The TNF and TNF receptor superfamilies: Integrating mammalian biology. *Cell*. 2001;104(4):487-501.
150. Luzio JP, Hackmann Y, Dieckmann NM, Griffiths GM. The biogenesis of lysosomes and lysosome-related organelles. *Cold Spring Harb Perspect Biol*. 2014;6(9):a016840.
151. Madara JL. Maintenance of the Macromolecular Barrier at Cell Extrusion Sites in Intestinal Epithelium - Physiological Rearrangement of Tight Junctions. *J Membrane Biol*. 1990;116(2):177-84.
152. Majno G, Joris I. Apoptosis, oncosis, and necrosis. An overview of cell death. *The American journal of pathology*. 1995;146(1):3.
153. Manichanh C, Borrueal N, Casellas F, Guarner F. The gut microbiota in IBD. *Nat*

Rev Gastro Hepat. 2012;9(10):599-608.

154. Marchiando AM, Shen L, Graham WV, Edelblum KL, Duckworth CA, Guan Y, et al. The epithelial barrier is maintained by in vivo tight junction expansion during pathologic intestinal epithelial shedding. *Gastroenterology*. 2011;140(4):1208-18. e2.

155. Marshall KD, Edwards MA, Krenz M, Davis JW, Baines CP. Proteomic mapping of proteins released during necrosis and apoptosis from cultured neonatal cardiac myocytes. *American Journal of Physiology-Cell Physiology*. 2014;306(7):C639-C47.

156. Marshman E, Ottewell PD, Potten CS, Watson AJ. Caspase activation during spontaneous and radiation-induced apoptosis in the murine intestine. *The Journal of Pathology: A Journal of the Pathological Society of Great Britain and Ireland*. 2001;195(3):285-92.

157. Martin SJ, Henry CM. Distinguishing between apoptosis, necrosis, necroptosis and other cell death modalities. *Methods*. 2013;61(2):87-9.

158. Martin SJ, Henry CM, Cullen SP. A Perspective on Mammalian Caspases as Positive and Negative Regulators of Inflammation. *Mol Cell*. 2012;46(4):387-97.

159. Mastroianni JR, Ouellette AJ. Alpha-defensins in enteric innate immunity: functional Paneth cell alpha-defensins in mouse colonic lumen. *J Biol Chem*. 2009;284(41):27848-56.

160. Mathiak G, Kabir K, Grass G, Keller H, Steinringer E, Minor T, et al. Lipopolysaccharides from different bacterial sources elicit disparate cytokine responses in whole blood assays. *International journal of molecular medicine*. 2003;11(1):41-4.

161. Mayhew TM, Myklebust R, Whybrow A, Jenkins R. Epithelial integrity, cell death and cell loss in mammalian small intestine. *Histology and Histopathology*. 1999;14(1):257-67.

162. McAllister CS, Lakhdari O, de Chambrun GP, Gareau MG, Broquet A, Lee GH, et al. TLR3, TRIF, and Caspase 8 Determine Double-Stranded RNA-Induced Epithelial Cell Death and Survival In Vivo. *Journal of Immunology*. 2013;190(1):418-27.

163. Merga YJ, O'Hara A, Burkitt MD, Duckworth CA, Probert CS, Campbell BJ, et al. Importance of the alternative NF- $\kappa$ B activation pathway in inflammation-associated gastrointestinal carcinogenesis. *Am J Physiol-Gastr L*. 2016;310(11):G1081-G90.

164. Merger M, Viney JL, Borojevic R, Steele-Norwood D, Zhou P, Clark DA, et al.

Defining the roles of perforin, Fas/FasL, and tumour necrosis factor alpha in T cell induced mucosal damage in the mouse intestine. *Gut*. 2002;51(2):155-63.

165. Merrell DS, Falkow S. Frontal and stealth attack strategies in microbial pathogenesis. *Nature*. 2004;430(6996):250-6.

166. Mescher AL. Junqueira's basic histology: text & atlas: McGraw-Hill Medical New York; 2010.

167. Millet P, McCall C, Yoza B. RelB: an outlier in leukocyte biology. *J Leukoc Biol*. 2013;94(5):941-51.

168. Miura N, Yamamoto M, Fukutake M, Ohtake N, Iizuka S, Ishige A, et al. Anti-CD3 induces bi-phasic apoptosis in murine intestinal epithelial cells: possible involvement of the Fas/Fas ligand system in different T cell compartments. *International Immunology*. 2005;17(5):513-22.

169. Morimoto M, Nishinakamura R, Saga Y, Kopan R. Different assemblies of Notch receptors coordinate the distribution of the major bronchial Clara, ciliated and neuroendocrine cells. *Development*. 2012;139(23):4365-73.

170. Munford RS, Suffredini AF. Sepsis, severe sepsis, and septic shock. Mandell, Douglas, and Bennett's Principles and Practice of Infectious Diseases (Eighth Edition): Elsevier; 2015. p. 914-34. e6.

171. Nakamura T, Tsuchiya K, Watanabe M. Crosstalk between Wnt and Notch signaling in intestinal epithelial cell fate decision. *J Gastroenterol*. 2007;42(9):705-10.

172. Nighot M, Al-Sadi R, Guo SH, Rawat M, Nighot P, Watterson MD, et al. Lipopolysaccharide-Induced Increase in Intestinal Epithelial Tight Permeability Is Mediated by Toll-Like Receptor 4/Myeloid Differentiation Primary Response 88 (MyD88) Activation of Myosin Light Chain Kinase Expression. *Am J Pathol*. 2017;187(12):2698-710.

173. Nogueira E, Fidalgo M, Molnar A, Kyriakis J, Force T, Zalvide J, et al. SOK1 translocates from the Golgi to the nucleus upon chemical anoxia and induces apoptotic cell death. *J Biol Chem*. 2008;283(23):16248-58.

174. Nolasco S, Bellido J, Goncalves J, Zabala JC, Soares H. Tubulin cofactor A gene silencing in mammalian cells induces changes in microtubule cytoskeleton, cell cycle arrest and cell death. *FEBS Lett*. 2005;579(17):3515-24.

175. Nunes T, Bernardazzi C, de Souza HS. Cell death and inflammatory bowel

diseases: apoptosis, necrosis, and autophagy in the intestinal epithelium. *Biomed Res Int.* 2014;2014:218493.

176. Oeckinghaus A, Ghosh S. The NF- $\kappa$ B family of transcription factors and its regulation. *Cold Spring Harbor perspectives in biology.* 2009:a000034.

177. Ohmachi T, Inoue H, Mimori K, Tanaka F, Sasaki A, Kanda T, et al. Fatty acid binding protein 6 is overexpressed in colorectal cancer. *Clinical Cancer Research.* 2006;12(17):5090-5.

178. Paesold G, Guiney DG, Eckmann L, Kagnoff MF. Genes in the Salmonella pathogenicity island 2 and the Salmonella virulence plasmid are essential for Salmonella-induced apoptosis in intestinal epithelial cells. *Cell Microbiol.* 2002;4(11):771-81.

179. Parker A, Maclaren OJ, Fletcher AG, Muraro D, Kreuzaler PA, Byrne HM, et al. Cell proliferation within small intestinal crypts is the principal driving force for cell migration on villi. *Faseb J.* 2017;31(2):636-49.

180. Parker CE, Warren MR, Mocanu V. Mass Spectrometry for Proteomics. In: Alzate O, editor. *Neuroproteomics. Frontiers in Neuroscience.* Boca Raton (FL)2010.

181. Pelaseyed T, Bergstrom JH, Gustafsson JK, Ermund A, Birchenough GMH, Schutte A, et al. The mucus and mucins of the goblet cells and enterocytes provide the first defense line of the gastrointestinal tract and interact with the immune system. *Immunol Rev.* 2014;260(1):8-20.

182. Pfeiffer K, Matsuyama T, Kundig TM, Wakeham A, Kishihara K, Shahinian A, et al. Mice deficient for the 55 kd tumor necrosis factor receptor are resistant to endotoxic shock, yet succumb to *L. monocytogenes* infection. *Cell.* 1993;73(3):457-67.

183. Pfeiffer JR, McAvoy BL, Fecteau RE, Deleault KM, Brooks SA. CARHSP1 Is Required for Effective Tumor Necrosis Factor Alpha mRNA Stabilization and Localizes to Processing Bodies and Exosomes. *Molecular and Cellular Biology.* 2011;31(2):277-86.

184. Piguet PF, Vesin C, Guo J, Donati Y, Barazzone C. TNF-induced enterocyte apoptosis in mice is mediated by the TNF receptor 1 and does not require p53. *European journal of immunology.* 1998;28(11):3499-505.

185. Pinto D, Clevers H. Wnt control of stem cells and differentiation in the intestinal epithelium. *Exp Cell Res.* 2005;306(2):357-63.

186. Pinto D, Gregorieff A, Begthel H, Clevers H. Canonical Wnt signals are essential for homeostasis of the intestinal epithelium. *Gene Dev.* 2003;17(14):1709-13.
187. Plubell, D.L., Wilmarth, P.A., Zhao, Y., Fenton, A.M., Minnier, J., Reddy, A.P., Klimek, J., Yang, X., David, L.L. and Pamir, N., 2017. Extended multiplexing of TMT labeling reveals age and high fat diet specific proteome changes in mouse epididymal adipose tissue. *Molecular & Cellular Proteomics*, pp.mcp-M116.
188. Poltorak A, Ricciardi-Castagnoli P, Citterio S, Beutler B. Physical contact between lipopolysaccharide and toll-like receptor 4 revealed by genetic complementation. *Proceedings of the National Academy of Sciences.* 2000;97(5):2163-7.
189. Potten CS. Extreme Sensitivity of Some Intestinal Crypt Cells to X and Gamma-Irradiation. *Nature.* 1977;269(5628):518-21.
190. Potten CS. The Significance of Spontaneous and Induced Apoptosis in the Gastrointestinal-Tract of Mice. *Cancer Metast Rev.* 1992;11(2):179-95.
191. Potten CS. Stem cells in gastrointestinal epithelium: numbers, characteristics and death. *Philos T R Soc B.* 1998;353(1370):821-30.
192. Potten CS, Booth C, Pritchard DM. The intestinal epithelial stem cell: the mucosal governor. *Int J Exp Pathol.* 1997;78(4):219-43.
193. Potten CS, Gandara R, Mahida YR, Loeffler M, Wright NA. The stem cells of small intestinal crypts: where are they? *Cell Proliferat.* 2009;42(6):731-50.
194. Potten CS, Grant HH. The relationship between ionizing radiation-induced apoptosis and stem cells in the small and large intestine. *Brit J Cancer.* 1998;78(8):993-1003.
195. Potten CS, Kovacs L, Hamilton E. Continuous Labeling Studies on Mouse Skin and Intestine. *Cell Tissue Kinet.* 1974;7(3):271-83.
196. Potten CS, Wilson JW, Booth C. Regulation and significance of apoptosis in the stem cells of the gastrointestinal epithelium. *Stem Cells.* 1997;15(2):82-93.
197. Prager M, Durmus T, Buttner J, Molnar T, de Jong DJ, Drenth JPH, et al. Myosin IXb variants and their pivotal role in maintaining the intestinal barrier: A study in Crohn's disease. *Scand J Gastroentero.* 2014;49(10):1191-200.
198. Prelipcean CC, Mihai C, Gogalniceanu P, Mihai B. What is the impact of age on adult patients with inflammatory bowel disease? *Clujul Med.* 2013;86(1):3-9.

199. Pritchard DM, Bower L, Potten CS, Jackman AL, Hickman JA. The importance of p53-independent apoptosis in the intestinal toxicity induced by raltitrexed (ZD1694, Tomudex): Genetic differences between BALB/c and DBA/2 mice. *Clinical Cancer Research*. 2000;6(11):4389-95.
200. Pritchard DM, Watson AJM. Apoptosis and gastrointestinal pharmacology. *Pharmacol Therapeut*. 1996;72(2):149-69.
201. Qin CF, Qiu K, Sun WJ, Jiao N, Zhang X, Che LQ, et al. A proteomic adaptation of small intestinal mucosa in response to dietary protein limitation. *Sci Rep-Uk*. 2016;6.
202. Quaroni A, Beaulieu JF. Cell dynamics and differentiation of conditionally immortalized human intestinal epithelial cells. *Gastroenterology*. 1997;113(4):1198-213.
203. Que FG, Gores GJ. Cell death by apoptosis: basic concepts and disease relevance for the gastroenterologist. *Gastroenterology*. 1996;110(4):1238-43.
204. Radtke F, Clevers H. Self-renewal and cancer of the gut: two sides of a coin. *Science*. 2005;307(5717):1904-9.
205. Ramachandran G. Gram-positive and gram-negative bacterial toxins in sepsis: a brief review. *Virulence*. 2014;5(1):213-8.
206. Ramig RF. Pathogenesis of intestinal and systemic rotavirus infection. *J Virol*. 2004;78(19):10213-20.
207. Redston MS, Papadopoulos N, Caldas C, Kinzler KW, Kern SE. Common Occurrence of Apc and K-Ras Gene-Mutations in the Spectrum of Colitis-Associated Neoplasias. *Gastroenterology*. 1995;108(2):383-92.
208. Ren W, Yin J, Chen S, Duan J, Liu G, Li T, et al. Proteome analysis for the global proteins in the jejunum tissues of enterotoxigenic Escherichia coli-infected piglets. *Sci Rep-Uk*. 2016;6:25640.
209. Rezaee F, Meednu N, Emo JA, Saatian B, Chapman TJ, Naydenov NG, et al. Polyinosinic:polycytidylic acid induces protein kinase D-dependent disassembly of apical junctions and barrier dysfunction in airway epithelial cells. *J Allergy Clin Immun*. 2011;128(6):1216-U546.
210. Riedl SJ, Salvesen GS. The apoptosome: signalling platform of cell death. *Nat Rev Mol Cell Bio*. 2007;8(5):405-13.

211. Riedl SJ, Shi YG. Molecular mechanisms of caspase regulation during apoptosis. *Nat Rev Mol Cell Bio.* 2004;5(11):897-907.
212. Roa B, Tortolero S. Trefoil factor 3 (TFF3) from human breast milk activates PAR-2 receptors, of the intestinal epithelial cells HT-29, regulating cytokines and defensins. *Bratisl Med J.* 2016;117(6):332-9.
213. Rosenfeld Y, Shai Y. Lipopolysaccharide (Endotoxin)-host defense antibacterial peptides interactions: role in bacterial resistance and prevention of sepsis. *Biochim Biophys Acta.* 2006;1758(9):1513-22.
214. Ross MH, Pawlina W. *Histology: Interactive Atlas to Accompany Histology: a Text and Atlas; with Correlated Cell and Molecular Biology.* CD-ROM: Lippincott, Williams & Wilkins; 2007.
215. Rowlands BJ, Soong CV, Gardiner KR. The gastrointestinal tract as a barrier in sepsis. *Brit Med Bull.* 1999;55(1):196-211.
216. Ruemmele FM, Seidman EG, Lentze MJ. Regulation of intestinal epithelial cell apoptosis and the pathogenesis of inflammatory bowel disorders. *J Pediatr Gastr Nutr.* 2002;34(3):254-60.
217. Sahab ZJ, Semaan SM, Sang QX. Methodology and applications of disease biomarker identification in human serum. *Biomark Insights.* 2007;2:21-43.
218. Salim SY, Soderholm JD. Importance of Disrupted Intestinal Barrier in Inflammatory Bowel Diseases. *Inflamm Bowel Dis.* 2011;17(1):362-81.
219. Sangiorgi E, Capecchi MR. Bmi1 is expressed in vivo in intestinal stem cells. *Nat Genet.* 2008;40(7):915-20.
220. Sellers RS, Clifford CB, Treuting PM, Brayton C. Immunological Variation Between Inbred Laboratory Mouse Strains: Points to Consider in Phenotyping Genetically Immunomodified Mice. *Vet Pathol.* 2012;49(1):32-43.
221. Sha WC, Liou HC, Tuomanen EI, Baltimore D. Targeted Disruption of the P50 Subunit of Nf-Kappa-B Leads to Multifocal Defects in Immune-Responses. *Cell.* 1995;80(2):321-30.
222. Shen Z-Y, Zhang J, Song H-L, Zheng W-P. Bone-marrow mesenchymal stem cells reduce rat intestinal ischemia-reperfusion injury, ZO-1 downregulation and tight junction disruption via a TNF- $\alpha$ -regulated mechanism. *World Journal of Gastroenterology: WJG.* 2013;19(23):3583.

223. Shi S, Wang H, Gao H, Li Z, Chen FX, Zuo XL, et al. Increased Gap Density Predicts Weakness of the Epithelial Barrier In Vivo by Confocal Laser Endomicroscopy in Indomethacin-Induced Enteropathy. *Digest Dis Sci.* 2014;59(7):1398-405.
224. Shih RH, Wang CY, Yang CM. NF-kappaB Signaling Pathways in Neurological Inflammation: A Mini Review. *Front Mol Neurosci.* 2015;8:77.
225. Shroyer NF, Wallis D, Venken KJT, Bellen HJ, Zoghbi HY. Gfi1 functions downstream of Math1 to control intestinal secretory cell subtype allocation and differentiation. *Gene Dev.* 2005;19(20):2412-7.
226. Simpson EM, Linder CC, Sargent EE, Davisson MT, Mobraaten LE, Sharp JJ. Genetic variation among 129 substrains and its importance for targeted mutagenesis in mice. *Nat Genet.* 1997;16(1):19-27.
227. Sinicrope FA, Roddey G, McDonnell TJ, Shen Y, Cleary KR, Stephens LC. Increased apoptosis accompanies neoplastic development in the human colorectum. *Clinical Cancer Research.* 1996;2(12):1999-2006.
228. Ślebioda TJ, Kmiec Z. Tumour necrosis factor superfamily members in the pathogenesis of inflammatory bowel disease. *Mediat Inflamm.* 2014;2014.
229. Sohma M. Ultrastructure of the Absorptive Cells in the Small-Intestine of the Rat during Starvation. *Anat Embryol.* 1983;168(3):331-9.
230. Song HL, Lu S, Liu P. Tumor necrosis factor-alpha induces apoptosis of enterocytes in mice with fulminant hepatic failure. *World J Gastroenterol.* 2005;11(24):3701-9.
231. Standring S, Ellis H, Healy J, Johnson D, Williams A, Collins P, et al. Gray's anatomy: the anatomical basis of clinical practice. *American Journal of Neuroradiology.* 2005;26(10):2703.
232. Stenson WF, Ciorba MA. Cell Death. *Physiology of the Gastrointestinal Tract (Sixth Edition)*: Elsevier; 2018. p. 221-34.
233. Strader AD, Woods SC. Gastrointestinal hormones and food intake. *Gastroenterology.* 2005;128(1):175-91.
234. Sun R, Zhang Y, Lv Q, Liu B, Jin M, Zhang W, et al. Toll-like receptor 3 (TLR3) induces apoptosis via death receptors and mitochondria by up-regulating the transactivating p63 isoform  $\alpha$  (TAP63 $\alpha$ ). *J Biol Chem.* 2011;286(18):15918-28.
235. Sun S-C. Non-canonical NF- $\kappa$ B signaling pathway. *Cell research.* 2011;21(1):71.

236. Tak PP, Firestein GS. NF- $\kappa$ B: a key role in inflammatory diseases. *The Journal of clinical investigation*. 2001;107(1):7-11.
237. Taura M, Fukuda R, Suico MA, Eguma A, Koga T, Shuto T, et al. TLR3 induction by anticancer drugs potentiates poly I:C-induced tumor cell apoptosis. *Cancer Sci*. 2010;101(7):1610-7.
238. Thiede B, Rudel T. Proteome analysis of apoptotic cells. *Mass spectrometry reviews*. 2004;23(5):333-49.
239. Thomas RC, Bath MF, Stover CM, Lambert DG, Thompson JP. Exploring LPS-induced sepsis in rats and mice as a model to study potential protective effects of the nociceptin/orphanin FQ system. *Peptides*. 2014;61:56-60.
240. Titz B, Elamin A, Martin F, Schneider T, Dijon S, Ivanov NV, et al. Proteomics for systems toxicology. *Comput Struct Biotechnol J*. 2014;11(18):73-90.
241. Tremaine W, Timmons L, Loftus Jr E, Pardi D, Sandborn W, Harmsen W, et al. Age at onset of inflammatory bowel disease and the risk of surgery for non-neoplastic bowel disease. *Alimentary pharmacology & therapeutics*. 2007;25(12):1435-41.
242. Ukabam S, Clamp J, Cooper B. Abnormal small intestinal permeability to sugars in patients with Crohn's disease of the terminal ileum and colon. *Digestion*. 1983;27(2):70-4.
243. Ulevitch RJ, Tobias PS. Recognition of gram-negative bacteria and endotoxin by the innate immune system. *Curr Opin Immunol*. 1999;11(1):19-22.
244. Umar S. Intestinal stem cells. *Current gastroenterology reports*. 2010;12(5):340-8.
245. Vagefi PA, Longo WE. Colorectal cancer in patients with inflammatory bowel disease. *Clinical colorectal cancer*. 2005;4(5):313-9.
246. Vagholkar K, Mathew T. Adenocarcinoma of the small bowel: a surgical dilemma. *Saudi J Gastroenterol*. 2009;15(4):264-7.
247. Vallabhapurapu S, Karin M. Regulation and function of NF-kappaB transcription factors in the immune system. *Annu Rev Immunol*. 2009;27:693-733.
248. Van Amersfoort ES, Van Berkel TJC, Kuiper J. Receptors, mediators, and mechanisms involved in bacterial sepsis and septic shock. *Clin Microbiol Rev*. 2003;16(3):379-+.
249. Van De Wetering M, Sancho E, Verweij C, De Lau W, Oving I, Hurlstone A, et al.

The  $\beta$ -catenin/TCF-4 complex imposes a crypt progenitor phenotype on colorectal cancer cells. *Cell*. 2002;111(2):241-50.

250. van der Flier LG, Clevers H. Stem cells, self-renewal, and differentiation in the intestinal epithelium. *Annual review of physiology*. 2009;71:241-60.

251. van der Mark VA, Ghiboub M, Marsman C, Zhao J, van Dijk R, Hiralall JK, et al. Phospholipid flippases attenuate LPS-induced TLR4 signaling by mediating endocytic retrieval of Toll-like receptor 4. *Cellular and molecular life sciences*. 2017;74(4):715-30.

252. van Es JH, Clevers H. Notch and Wnt inhibitors as potential new drugs for intestinal neoplastic disease. *Trends in molecular medicine*. 2005;11(11):496-502.

253. van Es JH, van Gijn ME, Riccio O, van den Born M, Vooijs M, Begthel H, et al. Notch/ $\gamma$ -secretase inhibition turns proliferative cells in intestinal crypts and adenomas into goblet cells. *Nature*. 2005;435(7044):959.

254. VanDussen KL, Carulli AJ, Keeley TM, Patel SR, Puthoff BJ, Magness ST, et al. Notch signaling modulates proliferation and differentiation of intestinal crypt base columnar stem cells. *Development*. 2012;139(3):488-97.

255. Vanuytsel T, Senger S, Fasano A, Shea-Donohue T. Major signaling pathways in intestinal stem cells. *Bba-Gen Subjects*. 2013;1830(2):2410-26.

256. Vossen AC, Tibbe GJM, Kroos MJ, van de Winkel JG, Benner R, Savelkoul HF. Fc receptor binding of anti-CD3 monoclonal antibodies is not essential for immunosuppression, but triggers cytokine-related side effects. *European journal of immunology*. 1995;25(6):1492-6.

257. Wajant H, Pfizenmaier K, Scheurich P. Tumor necrosis factor signaling. *Cell Death Differ*. 2003;10(1):45-65.

258. Wang C, Xi R. Keeping intestinal stem cell differentiation on the Tramtrack. *Fly*. 2015;9(3):110-4.

259. Wang L, Chen G. Current advances in the application of proteomics in apoptosis research. *Science China Life Sciences*. 2011;54(3):209-19.

260. Wang MJ, Xu XL, Yao GL, Yu Q, Zhu CF, Kong ZJ, et al. MYO9B gene polymorphisms are associated with the risk of inflammatory bowel diseases. *Oncotarget*. 2016;7(37):58862-75.

261. Wang X, Ou D, Yin J, Wu G, Wang J. Proteomic analysis reveals altered

- expression of proteins related to glutathione metabolism and apoptosis in the small intestine of zinc oxide-supplemented piglets. *Amino Acids*. 2009;37(1):209-18.
262. Watson AJ, Hughes KR. TNF- $\alpha$ -induced intestinal epithelial cell shedding: implications for intestinal barrier function. *Annals of the new York Academy of Sciences*. 2012;1258(1):1-8.
263. Watson AJM. Apoptosis and colorectal cancer. *Gut*. 2004;53(11):1701-9.
264. Watson AJM, Duckworth CA, Guan YF, Montrose MH. Mechanisms of Epithelial Cell Shedding in the Mammalian Intestine and Maintenance of Barrier Function. *Ann Ny Acad Sci*. 2009;1165:135-42.
265. Watson AJM, Pritchard DM. Lessons from genetically engineered animal models VII. Apoptosis in intestinal epithelium: lessons from transgenic and knockout mice. *Am J Physiol-Gastr L*. 2000;278(1):G1-G5.
266. Wei M, Liu B, Su L, Li J, Zhang J, Yu Y, et al. A novel plant homeodomain finger 10-mediated antiapoptotic mechanism involving repression of caspase-3 in gastric cancer cells. *Mol Cancer Ther*. 2010;9(6):1764-74.
267. Weih F, Carrasco D, Durham SK, Barton DS, Rizzo CA, Ryseck RP, et al. Multiorgan inflammation and hematopoietic abnormalities in mice with a targeted disruption of RelB, a member of the NF-kappa B/Rel family. *Cell*. 1995;80(2):331-40.
268. Weih F, Carrasco D, Durham SK, Barton DS, Rizzo CA, Ryseck R-P, et al. Multiorgan inflammation and hematopoietic abnormalities in mice with a targeted disruption of RelB, a member of the NF-kB/Rel family. *Cell*. 1995;80(2):331-40.
269. Wiegerinck CL, Janecke AR, Schneeberger K, Vogel GF, van Haaften-Visser DY, Escher JC, et al. Loss of syntaxin 3 causes variant microvillus inclusion disease. *Gastroenterology*. 2014;147(1):65-8 e10.
270. Wilkins JA, Sansom OJ. C-Myc is a critical mediator of the phenotypes of Apc loss in the intestine. *Cancer research*. 2008;68(13):4963-6.
271. Willenbacher RF, Zelman SJ, Ferrell LD, Moore DH, Waldman FM. Chromosomal alterations in ulcerative colitis-related neoplastic progression. *Gastroenterology*. 1997;113(3):791-801.
272. Williams JM, Duckworth CA, Burkitt MD, Watson AJM, Campbell BJ, Pritchard DM. Epithelial Cell Shedding and Barrier Function: A Matter of Life and Death at the Small Intestinal Villus Tip. *Vet Pathol*. 2015;52(3):445-55.

273. Williams JM, Duckworth CA, Watson AJ, Frey MR, Miguel JC, Burkitt MD, et al. A mouse model of pathological small intestinal epithelial cell apoptosis and shedding induced by systemic administration of lipopolysaccharide. *Disease models & mechanisms*. 2013;dmm. 013284.
274. Wood MB, Rios D, Williams IR. TNF-alpha augments RANKL-dependent intestinal M cell differentiation in enteroid cultures. *Am J Physiol Cell Physiol*. 2016;311(3):C498-507.
275. Wright NA. Epithelial stem cell repertoire in the gut: clues to the origin of cell lineages, proliferative units and cancer. *Int J Exp Pathol*. 2000;81(2):117-43.
276. Xavier RJ, Podolsky DK. Unravelling the pathogenesis of inflammatory bowel disease. *Nature*. 2007;448(7152):427-34.
277. Xiao G, Harhaj EW, Sun SC. NF-kappaB-inducing kinase regulates the processing of NF-kappaB2 p100. *Mol Cell*. 2001;7(2):401-9.
278. Xiao ZQ, Moragoda L, Jaszewski R, Hatfield JA, Fligiel SEG, Majumdar APN. Aging is associated with increased proliferation and decreased apoptosis in the colonic mucosa. *Mech Ageing Dev*. 2001;122(15):1849-64.
279. Yamamoto M, Fujihashi K, Kawabata K, McGhee JR, Kiyono H. A mucosal intranet: intestinal epithelial cells down-regulate intraepithelial, but not peripheral, T lymphocytes. *The Journal of Immunology*. 1998;160(5):2188-96.
280. Yamamoto M, Sato S, Hemmi H, Hoshino K, Kaisho T, Sanjo H, et al. Role of adaptor TRIF in the MyD88-independent toll-like receptor signaling pathway. *Science*. 2003;301(5633):640-3.
281. Yang D, Wang S, Brooks C, Dong Z, Schoenlein PV, Kumar V, et al. IFN regulatory factor 8 sensitizes soft tissue sarcoma cells to death receptor-initiated apoptosis via repression of FLICE-like protein expression. *Cancer Res*. 2009;69(3):1080-8.
282. Yang DF, Thangaraju M, Greeneltch K, Browning DD, Schoenlein PV, Tamura T, et al. Repression of IFN regulatory factor 8 by DNA methylation is a molecular determinant of apoptotic resistance and metastatic phenotype in metastatic tumor cells. *Cancer Research*. 2007;67(7):3301-9.
283. Yang Q, Bermingham NA, Finegold MJ, Zoghbi HY. Requirement of Math1 for secretory cell lineage commitment in the mouse intestine. *Science*. 2001;294(5549):2155-8.

284. Yu LR, Stewart NA, Veenstra TD. Proteomics: The Deciphering of the Functional Genome. *Essentials of Genomic and Personalized Medicine*. 2010:89-96.
285. Yuan J, Horvitz HR. A first insight into the molecular mechanisms of apoptosis. *Cell*. 2004;116:S53-S6.
286. Yuan JY, Kroemer G. Alternative cell death mechanisms in development and beyond. *Gene Dev*. 2010;24(23):2592-602.
287. Yue C, Wang W, Tian WL, Huang Q, Zhao RS, Zhao YZ, et al. Lipopolysaccharide-induced failure of the gut barrier is site-specific and inhibitable by growth hormone. *Inflamm Res*. 2013;62(4):407-15.
288. Zecchini V, Domaschek R, Winton D, Jones P. Notch signaling regulates the differentiation of post-mitotic intestinal epithelial cells. *Gene Dev*. 2005;19(14):1686-91.
289. Zhang L, Fang B. *Oncogenes, Tumor Suppressor Genes and Apoptosis-Inducing Genes Utilized in Cancer Gene Therapy*. *Gene Therapy for Cancer*: Springer; 2007. p. 173-84.
290. Zhang H, Sun SC. NF $\kappa$ B in inflammation and renal diseases. *Cell and Biosciences* 2015;5(1):63
291. Zhao HW, Yue YH, Han H, Chen XL, Lu YG, Zheng JM, et al. Effect of toll-like receptor 3 agonist poly I:C on intestinal mucosa and epithelial barrier function in mouse models of acute colitis. *World J Gastroentero*. 2017;23(6):999-1009.
292. Zhou PF, Streutker C, Borojevic R, Wang YF, Croitoru K. IL-10 modulates intestinal damage and epithelial cell apoptosis in T cell-mediated enteropathy. *Am J Physiol-Gastr L*. 2004;287(3):G599-G604.

## Appendix:

### Appendix 1: significant proteomic changes in *Nfkb1*<sup>-/-</sup> small intestinal mucosa in comparison to C57BL/6J mice

Protein names	Gene names	Regulation fold change	P value
Nucleoplasmin-3	<i>Npm3</i>	10.99	0.0078
Tubulin-specific chaperone A	<i>Tbca</i>	7.926	0.0002
Calcium-regulated heat stable protein 1	<i>Carhsp1</i>	6.542	0.0002
Gastrotropin	<i>Fabp6</i>	6.458	0.0012
Copper transport protein ATOX1	<i>Atox1</i>	5.072	0.0093
RNA-binding protein 3	<i>Rbm3</i>	4.864	0.0041
RIKEN cDNA 2200002D01 gene	<i>2200002D01Rik</i>	4.831	0.0013
Cysteine-rich with EGF-like domain protein 2	<i>Creld2</i>	4.392	0.0076
Regenerating islet-derived protein 3-beta	<i>Reg3b</i>	4.312	0.0024
28 kDa heat- and acid-stable phosphoprotein	<i>Pdap1</i>	3.58	0.0216
60S acidic ribosomal protein P2	<i>Rplp2</i>	3.465	0.0152
	<i>Calu</i>	3.335	0.0074
40S ribosomal protein S28	<i>Rps28;Gm10263</i>	3.227	0.0003
40S ribosomal protein S21	<i>Rps21</i>	3.113	0.0003
D-dopachrome decarboxylase	<i>Ddt</i>	3.077	0.0145
LIM and SH3 domain protein 1	<i>Lasp1</i>	3.065	0.0095
Prothymosin alpha;Prothymosin alpha, N-terminally processed;Thymosin alpha	<i>Ptma</i>	2.949	0.0197
Cystatin-B	<i>Cstb</i>	2.93	0.0139
Acidic leucine-rich nuclear phosphoprotein 32 family member E	<i>Anp32e</i>	2.921	0.0097
Cellular nucleic acid-binding protein	<i>Cnbp</i>	2.907	0.0378
Fatty acid-binding protein, liver	<i>Fabp1</i>	2.902	0.0092
Transthyretin	<i>Ttr</i>	2.852	0.0052
	<i>Gm20441</i>	2.785	0.0347
Cathepsin L1;Cathepsin L1 heavy chain;Cathepsin L1 light chain	<i>Ctsl</i>	2.781	0.0141
Parathymosin	<i>Ptms</i>	2.768	0.0218
Chromatin modification-related protein MEAF6	<i>Meaf6</i>	2.735	0.0412
Prefoldin subunit 4	<i>Pfdn4</i>	2.721	0.027
Craniofacial development protein 1	<i>Cfdp1</i>	2.701	0.0149
Caprin-1	<i>Caprin1</i>	2.695	0.0246
Interferon alpha-inducible protein 27-like protein 2B	<i>Ifi27l2b</i>	2.68	0.0007
Translationally-controlled tumor protein	<i>Tpt1</i>	2.669	0.0068
Protein phosphatase 1 regulatory subunit 1B	<i>Ppp1r1b</i>	2.651	0.0182
UV excision repair protein RAD23 homolog A	<i>Rad23a</i>	2.635	0.0174
Guanine nucleotide-binding protein subunit beta-2-like 1	<i>Gnb2l1</i>	2.626	0.0133
Thioredoxin	<i>Txn</i>	2.623	0.0268

H-2 class II histocompatibility antigen gamma chain	<i>Cd74</i>	2.615	0.131
Z-DNA-binding protein 1	<i>Zbp1</i>	2.614	0.0096
60S acidic ribosomal protein P1	<i>Rplp1;Gm10073</i>	2.608	0.0136
Thioredoxin domain-containing protein 17	<i>Txndc17</i>	2.569	0.0274
Thioredoxin, mitochondrial	<i>Txn2</i>	2.494	0.043
Mesencephalic astrocyte-derived neurotrophic factor	<i>Manf</i>	2.491	0.0262
Protein SET	<i>Set</i>	2.49	0.0267
Calumenin	<i>Calu</i>	2.459	0.0115
Prefoldin subunit 2	<i>Pfdn2</i>	2.45	0.0361
Phospholysine phosphohistidine inorganic pyrophosphate phosphatase	<i>Lhpp</i>	2.41	0.0135
Mth938 domain-containing protein	<i>Aamdc</i>	2.409	0.0097
Huntingtin-interacting protein K	<i>Hypk</i>	2.398	0.022
CD2-associated protein	<i>Cd2ap</i>	2.394	0.0531
40S ribosomal protein SA	<i>Rpsa</i>	2.375	0.0066
Protein FAM192A	<i>Fam192a</i>	2.372	0.0888
Stress-induced-phosphoprotein 1	<i>Stip1</i>	2.357	0.0056
Ran-specific GTPase-activating protein	<i>Ranbp1</i>	2.344	0.0085
Acidic leucine-rich nuclear phosphoprotein 32 family member A	<i>Anp32a</i>	2.318	0.0154
Retinol-binding protein 2	<i>Rbp2</i>	2.306	0.0028
Small glutamine-rich tetratricopeptide repeat-containing protein alpha	<i>Sgta</i>	2.292	0.0247
Protein S100-A11	<i>S100a11</i>	2.287	0.0157
GDP-mannose 4,6 dehydratase	<i>Gmds</i>	2.274	0.005
Programmed cell death protein 5	<i>Pdcd5</i>	2.246	0.0435
Cathepsin Z	<i>Ctsz</i>	2.24	0.0012
Transcription elongation factor A protein 1	<i>Tcea1</i>	2.239	0.0194
Probable ATP-dependent RNA helicase DHX58	<i>Dhx58</i>	2.217	0.0025
Galectin-3-binding protein	<i>Lgals3bp</i>	2.204	0.0037
WAS/WASL-interacting protein family member 3	<i>Wipf3</i>	2.202	0.0417
Alcohol dehydrogenase class-3	<i>Adh5</i>	2.2	0.0058
Peroxisome oxidoreductin-6	<i>Prdx6</i>	2.187	0.0037
C-Myc-binding protein	<i>Mycbp</i>	2.187	0.0042
Eukaryotic translation initiation factor 3 subunit J-A;Eukaryotic translation initiation factor 3 subunit J-B	<i>Eif3j1;Eif3j2</i>	2.16	0.0121
Serum albumin	<i>Alb</i>	2.153	0.0024
SH3 domain-binding glutamic acid-rich-like protein	<i>Sh3bgrl</i>	2.148	0.093
Heterogeneous nuclear ribonucleoprotein D-like	<i>Hnrnpdl</i>	2.137	0.0182
Protein-glutamine gamma-glutamyltransferase 2	<i>Tgm2</i>	2.134	0.0008
Protein PRRC2A	<i>Prrc2a</i>	2.128	0.0396
Eukaryotic translation initiation factor 5A-1;Eukaryotic translation initiation factor 5A	<i>Eif5a</i>	2.126	0.004
Proteasome subunit beta type-8;Proteasome subunit beta type	<i>Psm8</i>	2.114	0.0015

UPF0587 protein C1orf123 homolog	<i>0610037L13Rik</i>	2.098	0.0157
U6 snRNA-associated Sm-like protein LSM3	<i>Lsm3</i>	2.088	0.007
Glutathione reductase, mitochondrial	<i>Gsr</i>	2.086	0.0029
Adapter molecule crk	<i>Crk</i>	2.067	0.0087
Protein archease	<i>Zbtb8os</i>	2.066	0.032
Apoptosis-associated speck-like protein containing a CARD	<i>Pycard</i>	2.057	0.0052
Phosphatidylethanolamine-binding protein 1	<i>Pebp1</i>	2.03	0.0153
U6 snRNA-associated Sm-like protein LSM7	<i>Lsm7</i>	2.03	0.0004
L-lactate dehydrogenase;L-lactate dehydrogenase A chain	<i>Ldha</i>	2.018	0.0234
Creatine kinase B-type	<i>Ckb</i>	2.011	0.0215
Acylphosphatase;Acylphosphatase-1	<i>Acyp1</i>	2.01	0.0292
Sperm-associated antigen 7	<i>Spag7</i>	2.007	0.0426
Xanthine dehydrogenase/oxidase;Xanthine dehydrogenase;Xanthine oxidase	<i>Xdh</i>	2.007	0.014
Selenoprotein P	<i>Sepp1</i>	2.007	0.0393
MIP18 family protein FAM96A	<i>Fam96a</i>	2.003	0.0437
Aspartate aminotransferase, cytoplasmic	<i>Got1</i>	2.002	0.0249
Neuron-specific calcium-binding protein hippocalcin	<i>Hpca</i>	1.993	0.0152
Nardilysin	<i>Nrd1</i>	1.992	0.0144
Caspase-3	<i>Casp3</i>	1.983	0.0036
Chromobox protein homolog 1	<i>Cbx1</i>	1.981	0.0239
Cytosolic acyl coenzyme A thioester hydrolase	<i>Acot7</i>	1.977	0.0054
NEDD8	<i>Nedd8</i>	1.975	0.0172
Phosphorylated adapter RNA export protein	<i>Phax</i>	1.966	0.0324
Hsc70-interacting protein	<i>St13</i>	1.965	0.0022
Pterin-4-alpha-carbinolamine dehydratase	<i>Pcbd1</i>	1.961	0.0321
Protein deglycase DJ-1	<i>Park7</i>	1.959	0.0029
DAZ-associated protein 1	<i>Dazap1</i>	1.948	0.0008
E3 ubiquitin-protein ligase UBR2	<i>Ubr2</i>	1.944	0.0063
Protein S100-A10	<i>S100a10</i>	1.938	0.0155
Prosaposin	<i>Psap</i>	1.935	0.0313
Proteasome subunit beta type-9	<i>Psmb9</i>	1.934	0.0089
Fucose mutarotase	<i>Fuom</i>	1.932	0.012
Serine/threonine-protein phosphatase 4 catalytic subunit	<i>Ppp4c</i>	1.93	0.0125
Drebrin-like protein	<i>Dbnl</i>	1.926	0.0241
Adenosylhomocysteinase	<i>Ahcy</i>	1.919	0.0367
Caspase-6;Caspase-6 subunit p18;Caspase-6 subunit p11	<i>Casp6</i>	1.918	0.026
DNA methyltransferase 1-associated protein 1	<i>Dmap1</i>	1.907	0.0325
Mitochondrial import inner membrane translocase subunit Tim8 A	<i>Timm8a1</i>	1.905	0.0123
Cysteine and glycine-rich protein 1	<i>Csrp1</i>	1.905	0.0096
Elongation factor 1-beta	<i>Eef1b;Eef1b2</i>	1.904	0.0337
Heterogeneous nuclear ribonucleoprotein A/B	<i>Hnrnpab</i>	1.892	0.0172
Filamin-binding LIM protein 1	<i>Fblim1</i>	1.884	0.0176

Prefoldin subunit 6	<i>Pfdn6</i>	1.872	0.0105
Thioredoxin reductase 1, cytoplasmic	<i>Txnrd1</i>	1.871	0.026
High mobility group protein B2	<i>Hmgb2</i>	1.866	0.0445
Myeloid-derived growth factor	<i>Mydgf</i>	1.863	0.0111
Transaldolase	<i>Taldo1</i>	1.86	0.0262
Peptidyl-prolyl cis-trans isomerase NIMA-interacting 1	<i>Pin1;Pin1rt1</i>	1.859	0.0142
Heat shock protein 105 kDa	<i>Hsph1</i>	1.858	0.0023
Cytochrome c oxidase assembly factor 7	<i>Coa7</i>	1.849	0.0359
Interferon-induced protein with tetratricopeptide repeats 1	<i>Ifit1</i>	1.846	0.003
Semaphorin-4G	<i>Sema4g</i>	1.84	0.0002
High mobility group protein B1	<i>Hmgb1</i>	1.837	0.0159
Far upstream element-binding protein 1	<i>Fubp1</i>	1.837	0.0257
Coiled-coil domain-containing protein 6	<i>Ccdc6</i>	1.829	0.029
Growth factor receptor-bound protein 2	<i>Grb2</i>	1.82	0.0001
Elongation factor 1-delta	<i>Eef1d</i>	1.818	0.0021
Polymeric immunoglobulin receptor;Secretory component	<i>Pigr</i>	1.817	0.0058
Mitochondrial import inner membrane translocase subunit Tim8 B	<i>Timm8b</i>	1.817	0.0359
14-3-3 protein sigma	<i>Sfn</i>	1.812	0.0142
Glutathione peroxidase 2	<i>Gpx2</i>	1.811	0.0099
Myotrophin	<i>Mtpn</i>	1.81	0.05
Protein TSSC1	<i>Tssc1</i>	1.809	0.003
Gamma-interferon-inducible lysosomal thiol reductase	<i>Ifi30</i>	1.808	0.004
Proteasome subunit alpha type-5	<i>Pma5</i>	1.795	0.0156
Steroid receptor RNA activator 1	<i>Sra1</i>	1.788	0.0813
Glucosidase 2 subunit beta	<i>Prkcsh</i>	1.787	0.049
Signal peptide peptidase-like 2A	<i>Sppl2a</i>	1.785	0.035
2-5-oligoadenylate synthase-like protein 2	<i>Oasl2</i>	1.784	0.006
Lysosome-associated membrane glycoprotein 2	<i>Lamp2</i>	1.778	0.0082
Serine/arginine-rich splicing factor 4	<i>Srsf4</i>	1.769	0.0189
Crk-like protein	<i>Crkl</i>	1.766	0.0266
Cofilin-1	<i>Cfl1</i>	1.765	0.0011
Mannose-1-phosphate guanylyltransferase beta	<i>Gmppb</i>	1.759	0.0068
Thioredoxin domain-containing protein 12	<i>Txndc12</i>	1.758	0.0738
Uridine phosphorylase 1	<i>Upp1</i>	1.757	0.0163
6-phosphogluconate dehydrogenase, decarboxylating	<i>Pgd</i>	1.755	0.037
Heterogeneous nuclear ribonucleoprotein D0	<i>Hnrnpd</i>	1.754	0.0015
Ketohexokinase	<i>Khk</i>	1.754	0.0074
Biotinidase	<i>Btd</i>	1.749	0.0235
6-pyruvoyl tetrahydrobiopterin synthase	<i>Pts</i>	1.746	0.0419
Copper chaperone for superoxide dismutase	<i>Ccs</i>	1.744	0.0325
BUB3-interacting and GLEBS motif-containing protein ZNF207	<i>Znf207;Zfp207</i>	1.744	0.0044
Major vault protein	<i>Mvp</i>	1.743	0.0286

Hippocalcin-like protein 1	<i>Hpcal1</i>	1.733	0.0155
	<i>Gm14446</i>	1.728	0.0395
Acylamino-acid-releasing enzyme	<i>Apeh</i>	1.725	0.0427
Ribose-5-phosphate isomerase	<i>Rpia</i>	1.725	0.0037
Ubiquitin-conjugating enzyme E2 A	<i>Ube2a</i>	1.725	0.0055
Serine/arginine-rich splicing factor 3	<i>Srsf3;Gm12355</i>	1.724	0.0033
Adenosylhomocysteinase;Putative adenosylhomocysteinase 3	<i>Ahcyl2</i>	1.723	0.014
N-acetyl-D-glucosamine kinase	<i>Nagk</i>	1.721	0.0349
Proteasomal ubiquitin receptor ADRM1	<i>Gm9774;Adrm1</i>	1.721	0.0335
Serine/threonine-protein phosphatase 5;Serine/threonine-protein phosphatase	<i>Ppp5c</i>	1.713	0.0237
Aminopeptidase B	<i>Rnpep</i>	1.711	0.033
Splicing factor 3B subunit 4	<i>Sf3b4</i>	1.711	0.0315
Leukotriene A-4 hydrolase	<i>Lta4h</i>	1.709	0.0382
Succinate dehydrogenase assembly factor 2, mitochondrial	<i>Sdhaf2</i>	1.708	0.0366
Ribulose-phosphate 3-epimerase	<i>Rpe</i>	1.705	0.002
Ribonuclease inhibitor	<i>Rnh1</i>	1.705	0.036
Proteasome subunit alpha type-6	<i>Psm6</i>	1.702	0.0283
Cytosolic 10-formyltetrahydrofolate dehydrogenase	<i>Aldh1l1</i>	1.702	0.0357
Peptidyl-prolyl cis-trans isomerase A;Peptidyl-prolyl cis-trans isomerase A, N-terminally processed;Peptidyl-prolyl cis-trans isomerase	<i>Ppia;Gm5160</i>	1.7	0.0219
Heat shock 70 kDa protein 4	<i>Hspa4</i>	1.699	0.0063
Calmodulin-like protein 4	<i>Calml4</i>	1.699	0.0282
Heterogeneous nuclear ribonucleoproteins C1/C2	<i>Hnrnpc</i>	1.697	0.0034
Transketolase	<i>Tkt</i>	1.695	0.024
Transducin-like enhancer protein 4;Transducin-like enhancer protein 1	<i>Tle4;Tle1</i>	1.693	0.0021
Costars family protein ABRACL	<i>Abracl</i>	1.691	0.0007
Nicotinamide phosphoribosyltransferase	<i>Nampt</i>	1.689	0.0317
2-5-oligoadenylate synthase 1A	<i>Oas1a;Oas1g</i>	1.688	0.0283
Enhancer of rudimentary homolog	<i>Erh</i>	1.684	0.0014
Thiamin pyrophosphokinase 1	<i>Tpk1</i>	1.679	0.0126
Small ubiquitin-related modifier 2	<i>Sumo2;Sumo3</i>	1.671	0.0034
Vacuolar protein sorting-associated protein 26A	<i>Vps26a</i>	1.669	0.0148
Methylosome subunit pICln	<i>Clns1a</i>	1.657	0.0212
Xaa-Pro dipeptidase	<i>Pepd</i>	1.654	0.0142
39S ribosomal protein L15, mitochondrial	<i>Mrpl15</i>	1.649	0.0012
Protein PML	<i>Pml</i>	1.647	0.0143
Protein farnesyltransferase subunit beta	<i>Fntb</i>	1.64	0.0097
Fatty acid-binding protein, epidermal	<i>Fabp5</i>	1.635	0.0014
Proteasome activator complex subunit 1	<i>Psme1</i>	1.629	0.0035
	<i>Hnrnpd</i>	1.626	0.0084
PHD finger-like domain-containing protein 5A	<i>Phf5a</i>	1.625	0.0043
Transcription elongation factor B polypeptide 2	<i>Tceb2</i>	1.624	0.0026

Carboxypeptidase;Lysosomal protective protein;Lysosomal protective protein 32 kDa chain;Lysosomal protective protein 20 kDa chain	<i>Ctsa</i>	1.612	0.0066
Transgelin-2	<i>Tagln2</i>	1.611	0.0042
	<i>Hnrnp3</i>	1.608	0.0002
28S ribosomal protein S36, mitochondrial	<i>Mrps36</i>	1.599	0.0036
	<i>Arhgef5</i>	-1.556	0.0002
RNA polymerase-associated protein RTF1 homolog	<i>Rtf1</i>	-1.564	0.0004
Cell division cycle protein 27 homolog	<i>Cdc27</i>	-1.568	0.0005
Sorting nexin-6;Sorting nexin-6, N-terminally processed	<i>Snx6</i>	-1.592	0.0021
Serine/threonine-protein kinase 25	<i>Stk25</i>	-1.594	0.0021
Peptidyl-prolyl cis-trans isomerase FKBP5;Peptidyl-prolyl cis-trans isomerase FKBP5, N-terminally processed	<i>Fkbp5</i>	-1.601	0.002
Adseverin	<i>Scin</i>	-1.601	0.002
Cyclin-dependent kinase 2	<i>Cdk2</i>	-1.602	0.0025
ATP-binding cassette sub-family F member 3	<i>Abcf3</i>	-1.613	0.0003
AP-3 complex subunit beta-1	<i>Ap3b1</i>	-1.613	0.004
Sorting nexin-4	<i>Snx4</i>	-1.614	0.0005
Dynammin-3	<i>Dnm3</i>	-1.619	0.0042
Serine/threonine-protein kinase 17B	<i>Stk17b</i>	-1.623	0.0043
Rho guanine nucleotide exchange factor 16	<i>Arhgef16</i>	-1.627	0.0018
Glycoprotein-N-acetylgalactosamine 3-beta-galactosyltransferase 1	<i>C1galt1</i>	-1.628	0.0071
Charged multivesicular body protein 7	<i>Chmp7</i>	-1.628	0.0013
Growth hormone-regulated TBC protein 1	<i>Grtp1</i>	-1.629	0.0016
Ras-related protein Ral-A	<i>Rala</i>	-1.629	0.008
Rhotekin	<i>Rtkn</i>	-1.629	0.0004
Casein kinase I isoform alpha	<i>Csk1a1</i>	-1.63	0.0085
Pyrroline-5-carboxylate reductase 2	<i>Pycr2</i>	-1.63	0.0042
	<i>Prdm2</i>	-1.634	0.0002
E3 ubiquitin-protein ligase NEDD4-like	<i>Nedd4l</i>	-1.635	0.0045
ATPase family AAA domain-containing protein 3	<i>Atad3</i>	-1.635	0.0004
E3 ubiquitin-protein ligase RLIM	<i>Rlim</i>	-1.637	0.0108
Tyrosyl-DNA phosphodiesterase 2	<i>Tdp2</i>	-1.64	0.0001
Leucine-rich repeat-containing protein 57	<i>Lrrc57</i>	-1.644	0.0013
	<i>Chn2</i>	-1.644	0.0058
Poly(A) RNA polymerase, mitochondrial	<i>Mtpap</i>	-1.644	0.0038
	<i>Gcn1l1</i>	-1.646	0.0059
Protein KTI12 homolog	<i>Kti12</i>	-1.651	0.0084
Zinc finger protein 512	<i>Znf512</i>	-1.654	0.0146
Rho-related GTP-binding protein RhoG	<i>Rhog</i>	-1.655	0.0027
	<i>Slfn9</i>	-1.656	0.0046
Ras GTPase-activating-like protein IQGAP2	<i>Iqgap2</i>	-1.66	0.0011
Nucleolar GTP-binding protein 2	<i>Gnl2</i>	-1.661	0.0011
Alpha-parvin	<i>Parva</i>	-1.665	0.0028

Endophilin-A1	<i>Sh3gl2</i>	-1.668	0.003
IST1 homolog	<i>Ist1</i>	-1.67	0.0008
DNA mismatch repair protein Msh6	<i>Msh6</i>	-1.671	0.0034
Mortality factor 4-like protein 1	<i>Morf4l1</i>	-1.672	0.0071
Methylsterol monooxygenase 1	<i>Msmo1</i>	-1.672	0.0223
Calmegein	<i>Clgn</i>	-1.673	0.023
Metalloendopeptidase OMA1, mitochondrial	<i>Oma1</i>	-1.68	0.0166
Chromodomain-helicase-DNA-binding protein 2	<i>Chd2</i>	-1.681	0.0182
UPF0505 protein C16orf62 homolog	<i>9030624J02Rik</i>	-1.683	0.0172
GEM-interacting protein	<i>Gmip</i>	-1.683	0.0007
Vacuolar fusion protein MON1 homolog A	<i>Mon1a</i>	-1.683	0.0016
ATP-binding cassette sub-family F member 2	<i>Abcf2</i>	-1.683	0.0048
	<i>Myo6</i>	-1.683	0.0153
Ribosomal protein S6 kinase alpha-5	<i>Rps6ka5</i>	-1.684	0.0113
cAMP-dependent protein kinase catalytic subunit alpha	<i>Prkaca</i>	-1.687	0.0292
DNA ligase;DNA ligase 1	<i>Lig1</i>	-1.688	0.0211
Serine/threonine-protein kinase MARK2	<i>Mark2</i>	-1.691	0.0019
StAR-related lipid transfer protein 4	<i>Stard4</i>	-1.691	0.0006
Mitochondrial import inner membrane translocase subunit TIM50	<i>Timm50</i>	-1.695	0.0198
Calcium-binding mitochondrial carrier protein SCaMC-1	<i>Slc25a24</i>	-1.7	0.0285
Golgi phosphoprotein 3	<i>Golph3</i>	-1.703	0.0035
Mitogen-activated protein kinase 1	<i>Mapk1</i>	-1.703	0.0085
	<i>Pkp2</i>	-1.706	0.001
Ras-related protein Rab-22A	<i>Rab22a</i>	-1.707	0.0123
Cytochrome c oxidase subunit 7A-related protein, mitochondrial	<i>Cox7a2l</i>	-1.708	0.0085
Pinin	<i>Pnn</i>	-1.709	0.0024
Sterol 26-hydroxylase, mitochondrial	<i>Cyp27a1</i>	-1.71	0.0096
Phosphatidylinositol 4,5-bisphosphate 3-kinase catalytic subunit beta isoform	<i>Pik3cb</i>	-1.713	0.0222
Mitogen-activated protein kinase 3;Mitogen-activated protein kinase	<i>Mapk3</i>	-1.714	0.0065
Dolichol-phosphate mannosyltransferase subunit 3	<i>Dpm3</i>	-1.714	0.0498
Transmembrane protein 65	<i>Tmem65</i>	-1.715	0.0462
DNA primase large subunit	<i>Prim2</i>	-1.715	0.0027
Mitochondrial ubiquitin ligase activator of NFKB 1	<i>Mul1</i>	-1.718	0.0201
FERM, RhoGEF and pleckstrin domain-containing protein 1	<i>Farp1</i>	-1.722	0.0009
28S ribosomal protein S33, mitochondrial	<i>Mrps33</i>	-1.722	0.0258
	<i>Ppp2r5d</i>	-1.724	0.0037
5-AMP-activated protein kinase catalytic subunit alpha-2	<i>Prkaa2</i>	-1.724	0.0037
Multifunctional protein ADE2;Phosphoribosylaminoimidazole-succinocarboxamide	<i>Paics</i>	-1.726	0.0211

synthase;Phosphoribosylaminoimidazole carboxylase			
Dedicator of cytokinesis protein 5	<i>Dock5</i>	-1.729	0.0013
Phosphofurin acidic cluster sorting protein 2	<i>Pacs2</i>	-1.734	0.0008
Chromodomain-helicase-DNA-binding protein 8;Chromodomain-helicase-DNA-binding protein 9	<i>Chd8;Chd9</i>	-1.735	0.0019
Trinucleotide repeat-containing gene 6B protein	<i>Tnrc6b</i>	-1.736	0.034
Protein FAM210A	<i>Fam210a</i>	-1.738	0.0444
Cytochrome P450 2J6	<i>Cyp2j6</i>	-1.739	0.0498
Putative hexokinase HKDC1	<i>Hkdc1</i>	-1.74	0.033
Cytochrome b-c1 complex subunit 10	<i>Uqcr11</i>	-1.741	0.0231
Protein disulfide-isomerase A5	<i>Pdia5</i>	-1.746	0.0176
FACT complex subunit SSRP1	<i>Ssrp1</i>	-1.749	0.0033
Synaptobrevin homolog YKT6	<i>Ykt6</i>	-1.749	0.0075
Ras-related C3 botulinum toxin substrate 1;Ras-related C3 botulinum toxin substrate 3	<i>Rac1;Rac3</i>	-1.758	0.01
DENN domain-containing protein 2D	<i>Dennd2d</i>	-1.759	0.0006
cGMP-dependent protein kinase;cGMP-dependent protein kinase 2	<i>Prkg2</i>	-1.76	0.0024
Mitochondrial fission 1 protein	<i>Fis1</i>	-1.767	0.0009
N-alpha-acetyltransferase 40	<i>Naa40</i>	-1.768	0.0039
NADH dehydrogenase [ubiquinone] 1 alpha subcomplex subunit 13	<i>Ndufa13</i>	-1.775	0.023
Niban-like protein 1	<i>Fam129b</i>	-1.777	0.015
ATP synthase subunit epsilon, mitochondrial	<i>Atp5e</i>	-1.779	0.0082
Abhydrolase domain-containing protein 4	<i>Abhd4</i>	-1.78	0.0065
Transforming growth factor-beta-induced protein ig-h3	<i>Tgfb1</i>	-1.789	0.0219
PX domain-containing protein kinase-like protein	<i>Pxk</i>	-1.79	0.0003
Sterol O-acyltransferase 1	<i>Soat1</i>	-1.79	0.0184
MOB kinase activator 2	<i>Mob2</i>	-1.792	0.0175
ATP synthase subunit O, mitochondrial	<i>Atp5o</i>	-1.795	0.0386
Pumilio homolog 1;Pumilio homolog 2	<i>Pum1;Pum2</i>	-1.796	0.0047
Plasminogen receptor (KT)	<i>Plgrkt</i>	-1.797	0.0338
Serine/threonine-protein kinase Nek3	<i>Nek3</i>	-1.798	0.0124
EH domain-containing protein 1	<i>Ehd1</i>	-1.799	0.0033
Integrin-linked protein kinase	<i>Ilk</i>	-1.801	0.0125
Spermatogenesis-defective protein 39 homolog	<i>Vipas39</i>	-1.803	0.0003
Sorting nexin-3	<i>Snx3</i>	-1.808	0.0002
DNA-directed RNA polymerase III subunit RPC3	<i>Polr3c</i>	-1.809	0.0134
Cyclin-dependent kinase 9	<i>Cdk9</i>	-1.809	0.0118
Ribosomal protein S6 kinase;Ribosomal protein S6 kinase alpha-1	<i>Rps6ka1</i>	-1.811	0.0072
Platelet glycoprotein 4	<i>Cd36</i>	-1.811	0.006
Non-syndromic hearing impairment protein 5 homolog	<i>Dfna5</i>	-1.812	0.0116
Transmembrane protein 209	<i>Tmem209</i>	-1.813	0.0203
Cytochrome P450 4B1	<i>Cyp4b1</i>	-1.816	0.0219
Zinc finger CCCH domain-containing protein 18	<i>Zc3h18</i>	-1.818	0.0037

Protein NDRG1	<i>Ndrp1</i>	-1.818	0.0041
Sorting and assembly machinery component 50 homolog	<i>Samm50</i>	-1.818	0.0334
	<i>Spcs3</i>	-1.835	0.0302
Lipoamide acyltransferase component of branched-chain alpha-keto acid dehydrogenase complex, mitochondrial	<i>Dbt</i>	-1.841	0.0002
Sodium/nucleoside cotransporter	<i>Slc28a1</i>	-1.844	0.0135
Phosphatidylcholine transfer protein	<i>Pctp</i>	-1.853	0.0015
EH domain-containing protein 2	<i>Ehd2</i>	-1.855	0.0031
Sorting nexin-9	<i>Snx9</i>	-1.859	0.0026
Nucleolar transcription factor 1	<i>Ubtf</i>	-1.859	0.0039
Sodium/potassium-transporting ATPase subunit alpha-4	<i>Atp1a4</i>	-1.863	0.0031
Signal peptidase complex catalytic subunit SEC11;Signal peptidase complex catalytic subunit SEC11A	<i>Sec11a</i>	-1.867	0.049
Transmembrane protein 109	<i>Tmem109</i>	-1.868	0.013
NADH dehydrogenase [ubiquinone] 1 alpha subcomplex assembly factor 5	<i>Ndufaf5</i>	-1.869	0.0129
Unconventional myosin-Id	<i>Myo1d</i>	-1.87	0.0015
Death-associated protein kinase 3	<i>Dapk3</i>	-1.873	0.0012
Probable ATP-dependent RNA helicase DDX17	<i>Ddx17</i>	-1.875	0.0124
GTP-binding protein 8	<i>Gtpbp8</i>	-1.875	0.0023
Unconventional myosin-VIIb	<i>Myo7b</i>	-1.876	0.0022
Immediate early response 3-interacting protein 1	<i>Hdhd2;Ier3ip1;Gm10784</i>	-1.878	0.0261
	<i>Ak2</i>	-1.881	0.0012
Amino acid transporter;Neutral amino acid transporter B(0)	<i>Slc1a5</i>	-1.893	0.0141
Unconventional myosin-Ie	<i>Myo1e</i>	-1.894	0.004
Ras suppressor protein 1	<i>Rsu1</i>	-1.896	0.0059
Sulfotransferase 1 family member D1	<i>Sult1d1</i>	-1.897	0.0015
Replication factor C subunit 4	<i>Rfc4</i>	-1.9	0.0037
Amine oxidase [flavin-containing] B	<i>Maob</i>	-1.9	0.0345
	<i>Gls</i>	-1.902	0.0042
MOB kinase activator 1A;MOB kinase activator 1B	<i>Mob1b;Mob1a</i>	-1.905	0.0254
Mitochondrial pyruvate carrier 1	<i>Mpc1</i>	-1.907	0.027
ATP-dependent RNA helicase DDX3X;Putative ATP-dependent RNA helicase PI10	<i>Ddx3x;D1Pas1</i>	-1.908	0.0003
Solute carrier family 12 member 2	<i>Slc12a2</i>	-1.909	0.0025
	<i>Dnm1l</i>	-1.924	0.0006
N-acylneuraminase cytidyltransferase	<i>Cmas</i>	-1.927	0.004
Calcium-transporting ATPase;Sarcoplasmic/endoplasmic reticulum calcium ATPase 3	<i>Atp2a3</i>	-1.936	0.0024
Serine/threonine-protein kinase VRK1	<i>Vrk1</i>	-1.943	0.0053
Mitogen-activated protein kinase 13	<i>Mapk13</i>	-1.945	0.0031
Flap endonuclease 1	<i>Fen1</i>	-1.956	0.0049

Redox-regulatory protein FAM213A	<i>Fam213a</i>	-1.96	0.0301
Unconventional myosin-1a	<i>Myo1a</i>	-1.961	0.0067
SUN domain-containing protein 1	<i>Sun1</i>	-1.971	0.0114
Regulator of chromosome condensation	<i>Rcc1</i>	-1.972	0.0023
	<i>Zfp780b</i>	-1.978	0.0139
Ribonucleoside-diphosphate reductase large subunit	<i>Rrm1</i>	-2.003	0.0107
Histidine triad nucleotide-binding protein 3	<i>Hint3</i>	-2.007	0.0034
Cytoplasmic FMR1-interacting protein 2	<i>Cyfp2</i>	-2.008	0.0417
	<i>Mptx2</i>	-2.011	0.0125
Endoplasmic reticulum-Golgi intermediate compartment protein 1	<i>Ergic1</i>	-2.014	0.0063
ATP-dependent RNA helicase DDX3Y	<i>Ddx3y</i>	-2.029	0.0221
ADP-ribosylation factor 6	<i>Arf6</i>	-2.03	0.0031
Histone H2A;Histone H2A type 2-A;Histone H2A type 2-C	<i>Hist1h2al;Hist2h2aa1;Hist2h2ac</i>	-2.041	0.0202
	<i>Cyp2c66</i>	-2.053	0.0365
MAU2 chromatid cohesion factor homolog	<i>Mau2</i>	-2.064	0.0057
Iodotyrosine dehalogenase 1	<i>lyd</i>	-2.068	0.0119
Signal peptidase complex subunit 1	<i>Spcs1</i>	-2.082	0.039
E3 ubiquitin-protein ligase NEDD4	<i>Nedd4</i>	-2.091	0.0012
Cyclin-dependent kinase 1	<i>Cdk1</i>	-2.094	0.0007
	<i>Akr1c14</i>	-2.095	0.0021
GTP-binding protein SAR1b	<i>Sar1b</i>	-2.102	0.0062
Cyclin-dependent kinase 18;Cyclin-dependent kinase 17	<i>Cdk18;Cdk17</i>	-2.104	0.0005
15-hydroxyprostaglandin dehydrogenase [NAD(+)]	<i>Hpgd</i>	-2.107	0.0004
	<i>1700123L14Rik</i>	-2.112	0.0338
pre-mRNA 3 end processing protein WDR33	<i>Wdr33</i>	-2.113	0.0018
Cytochrome P450 3A11	<i>Cyp3a11</i>	-2.115	0.0364
Protein disulfide-isomerase A2	<i>Pdia2</i>	-2.118	0.0489
Estradiol 17-beta-dehydrogenase 2	<i>Hsd17b2</i>	-2.119	0.0039
Adenylate cyclase type 6	<i>Adcy6</i>	-2.122	0.0013
Inactive serine/threonine-protein kinase VRK3	<i>Vrk3</i>	-2.156	0.0002
Unconventional myosin-IXb	<i>Myo9b</i>	-2.158	0.0029
Histone H2B type 1-C/E/G;Histone H2B type 1-M;Histone H2B type 2-B;Histone H2B type 1-H	<i>Hist1h2bc;Hist1h2bm;Hist2h2bb;Hist1h2bh</i>	-2.179	0.0245
FACT complex subunit SPT16	<i>Supt16;Supt16h</i>	-2.196	0.0003
Amine oxidase [flavin-containing] A	<i>Maoa</i>	-2.199	0.0195
Guanine nucleotide-binding protein-like 3-like protein	<i>Gnl3l</i>	-2.229	0.0128
Leiomodin-1	<i>Lmod1</i>	-2.275	0.03
NADH-ubiquinone oxidoreductase chain 3	<i>Mtnd3</i>	-2.289	0.0154
Core histone macro-H2A.1	<i>H2afy</i>	-2.292	0.0074
Histone H2B type 3-B;Histone H2B type 3-A;Histone H2B type 2-E	<i>Hist3h2bb;Hist3h2ba;Hist2h2be</i>	-2.315	0.031
Acylglycerol kinase, mitochondrial	<i>Agk</i>	-2.316	0.0084

	<i>Syne2</i>	-2.353	0.0028
	<i>Col6a3</i>	-2.368	0.0368
Collagen alpha-1(VI) chain	<i>Col6a1</i>	-2.37	0.0495
Peptidyl-prolyl cis-trans isomerase FKBP11	<i>Fkbp11</i>	-2.389	0.0314
Histone H2A type 1-F	<i>Hist1h2af</i>	-2.405	0.0113
Sideroflexin-3	<i>Sfxn3</i>	-2.436	0.0266
Probable ATP-dependent RNA helicase DDX5	<i>Ddx5</i>	-2.446	0.0009
	<i>Sar1a</i>	-2.452	0.0004
Sorting nexin;Sorting nexin-18	<i>Snx18</i>	-2.509	0.0023
Indoleamine 2,3-dioxygenase 1	<i>Ido1</i>	-2.52	0.0115
Histone H2A type 2-B	<i>Hist2h2ab</i>	-2.54	0.0173
	<i>Tns1</i>	-2.546	0.0053
DNA topoisomerase 2-alpha	<i>Top2a</i>	-2.655	0.0052
Histone H3.2	<i>Hist1h3b</i>	-2.76	0.0435
Histone H2A.V;Histone H2A.Z;Histone H2A	<i>H2afv;H2afz</i>	-2.783	0.0033
Syndecan-4	<i>Sdc4</i>	-2.819	0.0017
Histone H2B type 1-F/J/L;Histone H2B;Histone H2B type 1-P;Histone H2B type 1-K;Histone H2B type 1-B;Histone H2B type 1-A	<i>Hist1h2bf;Hist1h2br;Hist1h2bp;Hist1h2bk;Hist1h2bb;Hist1h2ba</i>	-2.823	0.0011
Histone H4	<i>Hist1h4a</i>	-2.842	0.0046
E3 ubiquitin-protein ligase TRIM23	<i>Trim23</i>	-2.876	0.0021
Zymogen granule membrane protein 16	<i>Zg16</i>	-2.895	0.0269
Histone H3.1	<i>Hist1h3a</i>	-2.984	0.0052
Ig kappa chain C region	<i>Igkc</i>	-3.021	0.0008
RNA-binding protein with serine-rich domain 1	<i>Rnps1</i>	-3.022	0.0005
Histone H2A type 1-K	<i>Hist1h2ak</i>	-3.211	0.0052
Alpha-defensin 21;Alpha-defensin 22	<i>Defa22;Defa21</i>	-3.221	0.042
ADP/ATP translocase 1	<i>Slc25a4</i>	-3.238	0.046
Alpha-defensin-related sequence 1	<i>Gm14851;Defa-rs1</i>	-3.273	0.0342
Alpha-defensin 24	<i>Defa24</i>	-3.421	0.0155
Histone H3.3;Histone H3.3C;Histone H3	<i>H3f3a;H3f3c</i>	-3.62	0.0044
Alpha-defensin 23	<i>Defa23</i>	-3.968	0.0037
Ig alpha chain C region	<i>Igha</i>	-3.978	0.0001
Lactase-like protein	<i>Lctf</i>	-4.106	0.0386
Intelectin-1a	<i>Itln1</i>	-4.132	0.0013
Cysteine dioxygenase type 1	<i>Cdo1</i>	-4.138	0.001
Protein FAM83F	<i>Fam83f</i>	-4.679	0.0014
Alpha-defensin 20	<i>Defcr20;Defa20</i>	-5.563	0.0341
Lysozyme C-1;Lysozyme C-2	<i>Lyz1;Lyz2</i>	-6.755	0.0018
Defensin alpha, 27	<i>Gm15299 (Defa 27)</i>	-9.762	0.0004
Reticulon-3	<i>Rtn3</i>	-11.26	0.0376

**Appendix 2: significant proteomic changes in *Nfkb2*<sup>-/-</sup> small intestinal mucosa in comparison to C57BL/6J mice**

Protein names	Gene names	Regulation fold change	P value
Cytochrome b	<i>Mt-Cyb</i>	6.3045	0.0006
Tubulin-specific chaperone A	<i>Tbca</i>	6.2372	0.0001
	<i>Calu</i>	4.5687	0.0006
H-2 class II histocompatibility antigen, A-B alpha chain	<i>H2-Aa</i>	4.4762	0.0082
Copper transport protein ATOX1	<i>Atox1</i>	4.4345	0.0005
Pyridine nucleotide-disulfide oxidoreductase domain-containing protein 2	<i>Pyroxd2</i>	4.3738	0.0001
40S ribosomal protein S28	<i>Rps28;Gm10263</i>	4.1087	0.0001
Guanine nucleotide-binding protein subunit beta-2-like 1	<i>Gnb2l1</i>	3.8836	0.0005
Adenosine deaminase	<i>Ada</i>	3.8046	0.0018
Cysteine-rich with EGF-like domain protein 2	<i>Creld2</i>	3.5998	0.0001
H-2 class II histocompatibility antigen, A beta chain	<i>H2-Ab1</i>	3.5825	0.0058
	<i>Igtp</i>	3.3549	0.0006
Class II histocompatibility antigen, M alpha chain	<i>H2-DMa</i>	3.312	0.0023
RNA-binding protein 3	<i>Rbm3</i>	3.254	0.0001
	<i>2200002D01Rik</i>	3.1907	0.0014
	<i>Gls</i>	3.1068	0.0028
28 kDa heat- and acid-stable phosphoprotein	<i>Pdap1</i>	3.0361	0.0002
LIM and SH3 domain protein 1	<i>Lasp1</i>	2.9755	0.0001
Serum albumin	<i>Alb</i>	2.9712	0.0001
Xanthine dehydrogenase/oxidase	<i>Xdh</i>	2.9589	0.0001
H-2 class II histocompatibility antigen gamma chain	<i>Cd74</i>	2.9379	0.0522
L-lactate dehydrogenase;L-lactate dehydrogenase B chain	<i>Ldhb</i>	2.9315	0.0008
Uridine phosphorylase 1	<i>Upp1</i>	2.8701	0.0001
Proteasome subunit beta type-9	<i>Psmb9</i>	2.7254	0.0001
40S ribosomal protein SA	<i>Rpsa</i>	2.7206	0.0001
Thioredoxin domain-containing protein 17	<i>Txndc17</i>	2.7121	0.0002
Guanine deaminase	<i>Gda</i>	2.6788	0.0016
Aspartate aminotransferase, cytoplasmic	<i>Got1</i>	2.6487	0.0002
Deoxyribonuclease-1	<i>Dnase1</i>	2.6345	0.0003
40S ribosomal protein S21	<i>Rps21</i>	2.6218	0.0003
H-2 class II histocompatibility antigen	<i>H2-Eb1</i>	2.6061	0.0322
Granzyme B(G,H)	<i>Gzmb</i>	2.5922	0.0498
Cathepsin L1;Cathepsin L1 heavy chain;Cathepsin L1 light chain	<i>Ctsl</i>	2.5852	0.0001
Calumenin	<i>Calu</i>	2.5429	0.0001
60S acidic ribosomal protein P2	<i>Rplp2</i>	2.5234	0.0001
Phospholysine phosphohistidine inorganic pyrophosphate phosphatase	<i>Lhpp</i>	2.5142	0.0026
Proteasome subunit beta type-8;Proteasome subunit beta type	<i>Psmb8</i>	2.5091	0.0001
UPF0587 protein C1orf123 homolog	<i>0610037L13Rik</i>	2.5087	0.0011
Cytosolic acyl coenzyme A thioester hydrolase	<i>Acot7</i>	2.4999	0.0001

Retinol-binding protein 2	<i>Rbp2</i>	2.4905	0.0003
Nardilysin	<i>Nrd1</i>	2.4899	0.0003
D-dopachrome decarboxylase	<i>Ddt</i>	2.4853	0.0004
L-lactate dehydrogenase;L-lactate dehydrogenase A chain	<i>Ldha</i>	2.4745	0.0009
Class II histocompatibility antigen, M beta 1 chain	<i>H2-DMb1;H2- DMb2</i>	2.4656	0.0009
	<i>Adh6a</i>	2.4402	0.0017
Cathepsin Z	<i>Ctsz</i>	2.4143	0.0004
Acidic leucine-rich nuclear phosphoprotein 32 family member E	<i>Anp32e</i>	2.4049	0.0002
Proteasome subunit alpha type-6	<i>Psm6</i>	2.4029	0.0001
Cellular nucleic acid-binding protein	<i>Cnbp</i>	2.3924	0.0002
NAD(P)H dehydrogenase [quinone] 1	<i>Nqo1</i>	2.3868	0.0023
Proteasome subunit beta type-2	<i>Psm2</i>	2.3819	0.0001
Alcohol dehydrogenase 1	<i>Adh1</i>	2.3807	0.0087
6-phosphogluconate dehydrogenase, decarboxylating	<i>Pgd</i>	2.3503	0.0002
Creatine kinase B-type	<i>Ckb</i>	2.3401	0.0014
Thiamin pyrophosphokinase 1	<i>Tpk1</i>	2.3284	0.0002
Protein PRRC2A	<i>Prrc2a</i>	2.324	0.0036
Carbonic anhydrase 13	<i>Ca13</i>	2.3035	0.0033
Parathymosin	<i>Ptms</i>	2.2918	0.0039
Tropomyosin beta chain	<i>Tpm2</i>	2.2889	0.0099
Glutathione reductase, mitochondrial	<i>Gsr</i>	2.2736	0.0001
Caspase-3;Caspase-3 subunit p17;Caspase-3 subunit p12	<i>Casp3</i>	2.2734	0.001
Proteasome subunit alpha type-5	<i>Psm5</i>	2.2698	0.0003
Acyl-CoA-binding protein	<i>Dbi</i>	2.2533	0.0071
Protein phosphatase 1 regulatory subunit 1B	<i>Ppp1r1b</i>	2.2473	0.0001
Proteasome subunit beta type-1	<i>Psm1</i>	2.2384	0.0001
Thioredoxin reductase 1, cytoplasmic	<i>Txnrd1</i>	2.2323	0.0011
Peptidyl-prolyl cis-trans isomerase NIMA- interacting 1	<i>Pin1;Pin1rt1</i>	2.2274	0.0006
ATP synthase subunit s, mitochondrial	<i>Atp5s</i>	2.2228	0.1511
Adenosylhomocysteinase	<i>Ahcy</i>	2.2221	0.0009
Leukotriene A-4 hydrolase	<i>Lta4h</i>	2.2188	0.0006
Prothymosin alpha;Prothymosin alpha, N- terminally processed;Thymosin alpha	<i>Ptma</i>	2.1998	0.0013
S-formylglutathione hydrolase	<i>Esd</i>	2.199	0.0007
Death-associated protein 1	<i>Dap</i>	2.1947	0.0066
Caprin-1	<i>Caprin1</i>	2.193	0.0007
Proteasome subunit alpha type-2	<i>Psm2</i>	2.1897	0.0001
Cytoplasmic aconitate hydratase	<i>Aco1</i>	2.1826	0.0012
GRB2-related adaptor protein 2	<i>Grap2</i>	2.1798	0.0074
60S ribosomal protein L35a	<i>Rpl35a</i>	2.1785	0.0012
Cystatin-B	<i>Cstb</i>	2.1764	0.0005
PHD finger-like domain-containing protein 5A	<i>Phf5a</i>	2.1763	0.0001
Protein-glutamine gamma-glutamyltransferase 2	<i>Tgm2</i>	2.1752	0.0001
Polymeric immunoglobulin receptor;Secretory component	<i>Pigr</i>	2.1716	0.0007

WD repeat-containing protein 1	<i>Wdr1</i>	2.1711	0.0003
Mth938 domain-containing protein	<i>Aamdc</i>	2.1711	0.0012
Serine hydroxymethyltransferase;Serine hydroxymethyltransferase, cytosolic	<i>Shmt1</i>	2.1585	0.0037
Acylamino-acid-releasing enzyme	<i>Apeh</i>	2.1502	0.0013
Proteasome subunit alpha type-1	<i>Psm1</i>	2.1497	0.0001
	<i>Gm20441</i>	2.1398	0.0077
Unconventional myosin-Ib	<i>Myo1b</i>	2.1324	0.0222
GDP-mannose 4,6 dehydratase	<i>Gm10073</i>	2.1224	0.0004
Z-DNA-binding protein 1	<i>Zbp1</i>	2.1202	0.0001
60S acidic ribosomal protein P1	<i>Rpl1;Gm10073</i>	2.1126	0.0003
Cysteine and glycine-rich protein 1	<i>Csrp1</i>	2.1125	0.0021
Hyaluronan-binding protein 2;Hyaluronan-binding protein 2	<i>Habp2</i>	2.112	0.0022
Dipeptidyl peptidase 1;Dipeptidyl peptidase 1 exclusion domain chain;Dipeptidyl peptidase 1 heavy chain;Dipeptidyl peptidase 1 light chain	<i>Ctsc</i>	2.1108	0.0001
Huntingtin-interacting protein K	<i>Hypk</i>	2.1084	0.0003
Stress-induced-phosphoprotein 1	<i>Stip1</i>	2.1061	0.0002
Major vault protein	<i>Mvp</i>	2.1054	0.0009
Protein deglycase DJ-1	<i>Park7</i>	2.0976	0.0002
Cofilin-1	<i>Cfl1</i>	2.0862	0.0001
Puromycin-sensitive aminopeptidase	<i>Npepps</i>	2.0857	0.0022
Mesencephalic astrocyte-derived neurotrophic factor	<i>Manf</i>	2.0818	0.0002
Prefoldin subunit 2	<i>Pfdn2</i>	2.079	0.0041
Peroxiredoxin-6	<i>Prdx6</i>	2.0777	0.001
Fucose mutarotase	<i>Fuom</i>	2.0754	0.0032
Aminopeptidase B	<i>Rnpep</i>	2.0649	0.0003
Cytosolic 10-formyltetrahydrofolate dehydrogenase	<i>Aldh11</i>	2.0624	0.0014
U1 small nuclear ribonucleoprotein C	<i>Snrpc</i>	2.0538	0.0002
Alcohol dehydrogenase class-3	<i>Adh5</i>	2.0502	0.0011
	<i>Irgm2</i>	2.047	0.0029
Xaa-Pro dipeptidase	<i>Pepd</i>	2.0455	0.0008
Regenerating islet-derived protein 3-gamma	<i>Reg3g</i>	2.0376	0.0003
Lactoylglutathione lyase	<i>Glo1</i>	2.0332	0.0033
Vacuolar protein sorting-associated protein 29	<i>Vps29</i>	2.0294	0.0001
Peptidyl-prolyl cis-trans isomerase A;Peptidyl-prolyl cis-trans isomerase A, N-terminally processed;Peptidyl-prolyl cis-trans isomerase	<i>Ppia;Gm5160</i>	2.0283	0.0017
Aromatic-L-amino-acid decarboxylase	<i>Ddc</i>	2.0273	0.0049
Prefoldin subunit 4	<i>Pfdn4</i>	2.0254	0.0006
Translationally-controlled tumor protein	<i>Tpt1</i>	2.0223	0.0005
Carbonic anhydrase 2	<i>Ca2</i>	2.0183	0.0033
Ribosylidihydronicotinamide dehydrogenase [quinone]	<i>Nqo2</i>	2.0155	0.0016
Protein-tyrosine kinase 6	<i>Ptk6</i>	2.0151	0.0002
U6 snRNA-associated Sm-like protein LSM7	<i>Lsm7</i>	2.0144	0.0003
Myeloid-derived growth factor	<i>Mydgf</i>	2.0137	0.002
Mannose-1-phosphate guanyltransferase beta	<i>Gmppb</i>	2.0111	0.0001

Serine/threonine-protein phosphatase 6 catalytic subunit	<i>Ppp6c</i>	2.0111	0.0001
Plasminogen activator inhibitor 1 RNA-binding protein	<i>Serbp1</i>	2.0111	0.0077
Protein S100-A11	<i>S100a11</i>	2.0084	0.0029
Low molecular weight phosphotyrosine protein phosphatase	<i>Acp1</i>	2.0011	0.0016
Vacuolar protein sorting-associated protein 26A	<i>Vps26a</i>	1.9969	0.0003
Phosphoglycerate kinase 1;Phosphoglycerate kinase	<i>Pgk1</i>	1.9948	0.0038
Spermine synthase	<i>Sms</i>	1.9931	0.0005
UDP-glucose 4-epimerase	<i>Gale</i>	1.989	0.0001
Dehydrogenase/reductase SDR family member 11	<i>Dhrs11</i>	1.9856	0.0013
40S ribosomal protein S12	<i>Rps12</i>	1.9843	0.0001
Acidic leucine-rich nuclear phosphoprotein 32 family member A	<i>Anp32a</i>	1.9818	0.0039
Ran-specific GTPase-activating protein	<i>Ranbp1</i>	1.9807	0.0048
N-acetyl-D-glucosamine kinase	<i>Nagk</i>	1.9791	0.0041
Aspartoacylase	<i>Aspa</i>	1.9771	0.0022
Macrophage migration inhibitory factor	<i>Mif</i>	1.9759	0.0003
Prolyl endopeptidase	<i>Prep</i>	1.9752	0.0012
Glucose-6-phosphate isomerase	<i>Gpi</i>	1.9752	0.0022
Ubiquitin-like protein 5	<i>Ubl5;Gm16381</i>	1.9748	0.0004
Peroxisomal carnitine O-octanoyltransferase	<i>Crot</i>	1.9737	0.0012
Mitochondrial import inner membrane translocase subunit Tim8 B	<i>Timm8b</i>	1.9732	0.0032
Transaldolase	<i>Taldo1</i>	1.9661	0.0058
	<i>Gbp6;Gbp10</i>	1.9653	0.0009
Proteasome subunit alpha type-3	<i>Psm3</i>	1.9647	0.0002
Alanine aminotransferase 1	<i>Gpt</i>	1.9611	0.0055
Protein FAM50A	<i>Fam50a</i>	1.9603	0.0141
Glutathione peroxidase 2	<i>Gpx2</i>	1.9557	0.0001
Asparagine--tRNA ligase, cytoplasmic	<i>Nars</i>	1.9502	0.0001
Pro-cathepsin H;Cathepsin H mini chain;Cathepsin H;Cathepsin H heavy chain;Cathepsin H light chain	<i>Ctsh</i>	1.9456	0.0003
Bifunctional purine biosynthesis protein PURH;Phosphoribosylaminoimidazolecarboxamide formyltransferase;IMP cyclohydrolase	<i>Atic</i>	1.9453	0.0007
Protein SET	<i>Set</i>	1.9389	0.0037
Adenosylhomocysteinase;Putative adenosylhomocysteinase 3	<i>Ahcyl2</i>	1.9351	0.0001
	<i>Gbp9</i>	1.9296	0.004
U6 snRNA-associated Sm-like protein LSM3	<i>Lsm3</i>	1.9283	0.007
CD2-associated protein	<i>Cd2ap</i>	1.9267	0.0029
Small glutamine-rich tetratricopeptide repeat-containing protein alpha	<i>Sgta</i>	1.9263	0.001
F-box only protein 3	<i>Fbxo3</i>	1.9254	0.0002
O-phosphoserine-tRNA(Sec) selenium transferase	<i>Sepsecs</i>	1.9247	0.0072
Calpastatin	<i>Cast</i>	1.9196	0.0025
Nicotinamide phosphoribosyltransferase	<i>Nampt</i>	1.919	0.0033
Triosephosphate isomerase	<i>Tpi1</i>	1.9174	0.0035

Malate dehydrogenase, cytoplasmic	<i>Mdh1</i>	1.9171	0.0031
Acetyl-CoA acetyltransferase, cytosolic	<i>Acat2;Acat3</i>	1.9158	0.0007
DAZ-associated protein 1	<i>Dazap1</i>	1.9139	0.0002
Serine/arginine-rich splicing factor 4	<i>Srsf4</i>	1.9129	0.0076
Acetoacetyl-CoA synthetase	<i>Aacs</i>	1.9124	0.0001
Transketolase	<i>Tkt</i>	1.9091	0.0008
	<i>Gimap9</i>	1.9003	0.0686
6-pyruvoyl tetrahydrobiopterin synthase	<i>Pts</i>	1.8997	0.0065
Pro-interleukin-16;Interleukin-16	<i>Il16</i>	1.8978	0.0058
Sperm-associated antigen 7	<i>Spag7</i>	1.8967	0.0014
Protein farnesyltransferase subunit beta	<i>Fntb</i>	1.8922	0.0007
Proteasome subunit beta type-10	<i>Psmb10</i>	1.888	0.0001
Nuclease-sensitive element-binding protein 1	<i>Ybx1</i>	1.8878	0.0004
Serine--tRNA ligase, cytoplasmic	<i>Sars</i>	1.8874	0.0007
Superoxide dismutase [Cu-Zn]	<i>Sod1</i>	1.8874	0.0156
Lambda-crystallin homolog	<i>Cryl1</i>	1.884	0.0049
Signal transducer and activator of transcription 1	<i>Stat1</i>	1.8825	0.0024
Proteasome subunit alpha type-4	<i>Psm4</i>	1.88	0.0002
Nitrilase homolog 1	<i>Nit1</i>	1.8791	0.0006
Protein archease	<i>Zbtb8os</i>	1.8736	0.0037
Calcium-regulated heat stable protein 1	<i>Carhsp1</i>	1.872	0.0001
Xaa-Pro aminopeptidase 1	<i>Xpnpep1</i>	1.8712	0.0006
Protein phosphatase 1 regulatory subunit 14D	<i>Ppp1r14d</i>	1.8701	0.0006
Tyrosine-protein kinase ZAP-70	<i>Zap70</i>	1.8621	0.0443
Transcription elongation factor A protein 1	<i>Tcea1</i>	1.8602	0.0015
Aldose 1-epimerase	<i>Galm</i>	1.8577	0.0032
Ketohexokinase	<i>Khk</i>	1.857	0.0011
Serine/threonine-protein phosphatase 2A catalytic subunit alpha isoform	<i>Ppp2ca</i>	1.857	0.0001
ADP-sugar pyrophosphatase	<i>Nudt5</i>	1.856	0.0008
Eukaryotic translation initiation factor 1A, X-chromosomal	<i>Eif1ax;Eif1a;Gm5039;Gm5662;Gm8300;Gm2016;Gm21936;Gm2056;Gm6803;Gm2035;Gm2075</i>	1.8466	0.0002
4-trimethylaminobutyraldehyde dehydrogenase	<i>Aldh9a1</i>	1.8458	0.0003
Carboxylic ester hydrolase	<i>Ces1f</i>	1.8455	0.0477
Zyxin	<i>Zyx</i>	1.8432	0.0001
Carboxypeptidase;Lysosomal protective protein;Lysosomal protective protein 32 kDa chain;Lysosomal protective protein 20 kDa chain	<i>Ctsa</i>	1.8421	0.0016
MIP18 family protein FAM96A	<i>Fam96a</i>	1.8418	0.0224
Craniofacial development protein 1	<i>Cfdp1</i>	1.8398	0.0034
60S ribosomal protein L34	<i>Rpl34</i>	1.839	0.0103
Proteasome subunit beta type-3	<i>Psmb3</i>	1.8361	0.0001
Serine/threonine-protein phosphatase 2A catalytic subunit beta isoform	<i>Ppp2cb</i>	1.8357	0.0001
Heterogeneous nuclear ribonucleoprotein D0	<i>Hnrnpd</i>	1.8334	0.0001

Eukaryotic translation initiation factor 3 subunit J-A;Eukaryotic translation initiation factor 3 subunit J-B	<i>Eif3j1;Eif3j2</i>	1.8307	0.0025
Ribose-5-phosphate isomerase	<i>Rpia</i>	1.8273	0.0006
1,5-anhydro-D-fructose reductase	<i>Akr1e2;Akr1e1</i>	1.8267	0.0102
Caspase-6;Caspase-6 subunit p18;Caspase-6 subunit p11	<i>Casp6</i>	1.8238	0.0014
Gamma-glutamylaminocyclotransferase	<i>Ggact</i>	1.8236	0.0005
Transthyretin	<i>Ttr</i>	1.8223	0.0047
NADP-dependent malic enzyme;Malic enzyme	<i>Me1</i>	1.8219	0.0479
Antigen peptide transporter 1	<i>Tap1</i>	1.8199	0.0046
Heterogeneous nuclear ribonucleoprotein A/B	<i>Hnrnpab</i>	1.8196	0.0012
Calcium channel flower homolog	<i>Cacfd1</i>	1.8195	0.0001
Histidine--tRNA ligase, cytoplasmic	<i>Hars</i>	1.8187	0.0013
U1 small nuclear ribonucleoprotein 70 kDa	<i>Snrnp70</i>	1.816	0.0006
Ribulose-phosphate 3-epimerase	<i>Rpe</i>	1.8125	0.0002
Serine/threonine-protein phosphatase 5;Serine/threonine-protein phosphatase	<i>Ppp5c</i>	1.8108	0.0016
Adenylosuccinate lyase	<i>Adsl</i>	1.807	0.0013
Heterogeneous nuclear ribonucleoprotein U-like protein 1	<i>Hnrnpul1</i>	1.8066	0.0001
Exosome complex component CSL4	<i>Exosc1</i>	1.8062	0.0065
E3 ubiquitin-protein ligase XIAP	<i>Xiap</i>	1.8043	0.0001
MOB-like protein phocein	<i>Mob4</i>	1.8039	0.0001
Alpha-enolase	<i>Eno1</i>	1.8035	0.0009
Aldose reductase-related protein 2	<i>Akr1b8</i>	1.8028	0.0179
SH3 domain-binding glutamic acid-rich-like protein	<i>Sh3bgrl</i>	1.8001	0.0034
Biotinidase	<i>Btd</i>	1.7998	0.0036
Cytochrome c, somatic	<i>Cycs</i>	1.7955	0.0167
RNA-binding protein EWS	<i>Ewsr1</i>	1.7955	0.0004
Glutathione synthetase	<i>Gss</i>	1.7915	0.0054
Gamma-interferon-inducible lysosomal thiol reductase	<i>Ifi30</i>	1.7909	0.0016
Protein LZIC	<i>Lzic</i>	1.7888	0.0061
UPF0160 protein MYG1, mitochondrial	<i>Myg1</i>	1.7884	0.0003
Eukaryotic translation initiation factor 4B	<i>Eif4b</i>	1.7851	0.0008
Secernin-2	<i>Scrn2</i>	1.7815	0.0022
Protein MEMO1	<i>Memo1</i>	1.7799	0.003
Phosphoglycolate phosphatase	<i>Pgp</i>	1.7799	0.0011
Eukaryotic translation initiation factor 5A-1;Eukaryotic translation initiation factor 5A	<i>Eif5a</i>	1.7789	0.0005
Purine nucleoside phosphorylase	<i>Pnp</i>	1.7782	0.0001
Fructose-bisphosphate aldolase A;Fructose-bisphosphate aldolase	<i>Aldoa;Aldoat1</i>	1.7764	0.0001
Programmed cell death protein 5	<i>Pdcd5</i>	1.776	0.0014
Fatty acid-binding protein, liver	<i>Fabp1</i>	1.774	0.0018
Drebrin-like protein	<i>Dbnl</i>	1.7714	0.0005
Interferon alpha-inducible protein 27-like protein 2B	<i>Ifi27l2b</i>	1.7695	0.0009
Hsc70-interacting protein	<i>St13</i>	1.7655	0.0012
28S ribosomal protein S36, mitochondrial	<i>Mrps36</i>	1.7651	0.001

N-acyl-aromatic-L-amino acid amidohydrolase (carboxylate-forming)	<i>Acy3</i>	1.7617	0.0041
Stathmin	<i>Stmn1</i>	1.7596	0.0101
Polyadenylate-binding protein 2	<i>Gm20521;Pabpn1</i>	1.7592	0.0023
BUB3-interacting and GLEBS motif-containing protein ZNF207	<i>Znf207;Zfp207</i>	1.759	0.0008
Proteasome subunit alpha type-7	<i>PsmA7</i>	1.7579	0.0002
Alcohol dehydrogenase [NADP(+)]	<i>Akr1a1</i>	1.755	0.0093
Isocitrate dehydrogenase [NADP] cytoplasmic	<i>Idh1</i>	1.7544	0.0345
60S ribosomal protein L28	<i>Rpl28</i>	1.7515	0.0074
Geranylgeranyl pyrophosphate synthase	<i>Ggps1</i>	1.7506	0.0027
Threonine--tRNA ligase, cytoplasmic	<i>Tars</i>	1.7506	0.0013
Dipeptidyl peptidase 3	<i>Dpp3</i>	1.7502	0.0023
Phosphatidylethanolamine-binding protein 1;Hippocampal cholinergic neurostimulating peptide	<i>Pebp1</i>	1.7453	0.0011
Nucleoside diphosphate kinase A;Nucleoside diphosphate kinase	<i>Nme1</i>	1.7452	0.0024
60S ribosomal protein L13a	<i>Rpl13a</i>	1.745	0.001
S-adenosylmethionine synthase isoform type-2	<i>Mat2a</i>	1.7444	0.0005
Thioredoxin, mitochondrial	<i>Txn2</i>	1.7431	0.0109
Uncharacterized protein C1orf43 homolog	<i>4933434E20Rik</i>	1.7426	0.0294
Tetratricopeptide repeat protein 38	<i>Ttc38</i>	1.742	0.0003
Microsomal triglyceride transfer protein large subunit	<i>Mttp</i>	1.7418	0.0026
Rab GDP dissociation inhibitor alpha	<i>Gdi1</i>	1.7391	0.003
Protein canopy homolog 2	<i>Cnpy2</i>	1.7377	0.0029
Epididymal secretory protein E1	<i>Npc2</i>	1.7374	0.0068
Delta-1-pyrroline-5-carboxylate dehydrogenase, mitochondrial	<i>Aldh4a1</i>	1.736	0.0007
Glucosamine-6-phosphate isomerase 1	<i>Gnpda1</i>	1.7302	0.0002
Small integral membrane protein 24	<i>Smim24</i>	1.7301	0.0094
Protein FAM192A	<i>Fam192a</i>	1.7292	0.0134
Cathepsin D	<i>Ctsd</i>	1.7286	0.0005
Selenium-binding protein 1;Selenium-binding protein 2	<i>Selenbp1;Selenbp2</i>	1.7286	0.0041
Apoptosis-associated speck-like protein containing a CARD	<i>Pycard</i>	1.7255	0.0007
Heat shock 70 kDa protein 4	<i>Hspa4</i>	1.7248	0.0004
Small ubiquitin-related modifier 2	<i>Sumo2;Sumo3</i>	1.7218	0.0021
Cytochrome c oxidase assembly factor 7	<i>Coa7</i>	1.7201	0.007
Delta-aminolevulinic acid dehydratase	<i>Alad</i>	1.7199	0.0039
	<i>Parp4</i>	1.7198	0.0005
WAS/WASL-interacting protein family member 3	<i>Wipf3</i>	1.7197	0.0038
Proliferation-associated protein 2G4	<i>Pa2g4</i>	1.7167	0.0007
	<i>Tpm3</i>	1.7155	0.0106
Retinoid-inducible serine carboxypeptidase	<i>Scpep1</i>	1.7146	0.0002
Sialate O-acetyltransferase;Sialate O-acetyltransferase small subunit;Sialate O-acetyltransferase large subunit	<i>Siae</i>	1.7121	0.0006
Purine nucleoside phosphorylase	<i>Pnp2</i>	1.7119	0.0001

Arylamine N-acetyltransferase 2	<i>Nat2</i>	1.7093	0.0075
Aspartyl aminopeptidase	<i>Dnpep</i>	1.7085	0.0004
Enhancer of rudimentary homolog	<i>Erh</i>	1.7067	0.0014
Creatine kinase U-type, mitochondrial	<i>Ckmt1</i>	1.7053	0.0071
Peptidyl-prolyl cis-trans isomerase G	<i>Ppig</i>	1.7045	0.0253
Glutathione S-transferase P 1	<i>Gstp1</i>	1.7044	0.0022
Serine/arginine-rich splicing factor 7	<i>Srsf7</i>	1.7043	0.0202
Cystathionine gamma-lyase	<i>Cth</i>	1.7035	0.0059
Heterogeneous nuclear ribonucleoprotein D-like	<i>Hnrnpdl</i>	1.7034	0.0018
60S ribosomal protein L29	<i>Gm17669;Rpl29;Gm3550</i>	1.7003	0.0026
Serine/threonine-protein phosphatase 4 catalytic subunit	<i>Ppp4c</i>	1.697	0.0021
Probable aminopeptidase NPEPL1	<i>Npepl1</i>	1.6965	0.0003
Tyrosine--tRNA ligase;Tyrosine--tRNA ligase, cytoplasmic;Tyrosine--tRNA ligase, cytoplasmic, N-terminally processed	<i>Yars</i>	1.6931	0.0053
Small nuclear ribonucleoprotein Sm D3	<i>Snrpd3</i>	1.693	0.0015
Small nuclear ribonucleoprotein Sm D2	<i>Snrpd2;Gm5449</i>	1.6929	0.0003
60S ribosomal protein L14	<i>Rpl14</i>	1.6922	0.0316
Fructose-1,6-bisphosphatase isozyme 2	<i>Fbp2</i>	1.6901	0.0023
	<i>Acy1</i>	1.6901	0.0082
Elongation factor 2	<i>Eef2</i>	1.6895	0.0001
Coiled-coil domain-containing protein 58	<i>Ccdc58</i>	1.6863	0.0268
DNA-(apurinic or apyrimidinic site) lyase	<i>Apex1</i>	1.6838	0.0016
RNA-binding protein FUS	<i>Fus</i>	1.6822	0.0018
Aldose reductase-related protein 1	<i>Akr1b7</i>	1.6814	0.0049
Ribonuclease inhibitor	<i>Rnh1</i>	1.6805	0.0024
Beta-enolase;Enolase	<i>Eno3</i>	1.6774	0.0132
Isopentenyl-diphosphate Delta-isomerase 1	<i>Idi1</i>	1.6748	0.002
Heat shock protein 105 kDa	<i>Hsph1</i>	1.674	0.0001
Platelet-activating factor acetylhydrolase IB subunit alpha	<i>Pafah1b1</i>	1.6726	0.0003
Filamin-binding LIM protein 1	<i>Fblim1</i>	1.6717	0.0001
Serine/arginine-rich splicing factor 2	<i>Srsf2</i>	1.6706	0.029
Hepatoma-derived growth factor	<i>Hdgf</i>	1.6702	0.0061
Peroxiredoxin-5, mitochondrial	<i>Prdx5</i>	1.6699	0.0026
Peptidyl-prolyl cis-trans isomerase FKBP2	<i>Fkbp2</i>	1.6688	0.0001
Thioredoxin	<i>Txn</i>	1.6663	0.0006
N-acetylglucosamine-6-sulfatase	<i>Gns</i>	1.6661	0.0018
60S ribosomal protein L36a	<i>Rpl36a</i>	1.6649	0.0023
Chloride intracellular channel protein 1	<i>Clic1</i>	1.6635	0.0001
Adapter molecule crk	<i>Crk</i>	1.6632	0.0018
Prostaglandin reductase 2	<i>Ptgr2</i>	1.6631	0.0015
RNA polymerase II subunit A C-terminal domain phosphatase SSU72	<i>Ssu72</i>	1.6576	0.0063
Bleomycin hydrolase	<i>Blmh</i>	1.6572	0.0013
Serine-threonine kinase receptor-associated protein	<i>Strap</i>	1.6537	0.0001
Glutathione peroxidase 1;Glutathione peroxidase	<i>Gpx1</i>	1.6535	0.0007
Mannose-1-phosphate guanyltransferase alpha	<i>Gmppa</i>	1.6494	0.0006

Fatty acid-binding protein, intestinal	<i>Fabp2</i>	1.6469	0.045
Elongation factor 1-delta	<i>Eef1d</i>	1.6436	0.0003
Guanylate cyclase activator 2B;Uroguanylin	<i>Guca2b</i>	1.6419	0.0211
Ubiquitin-conjugating enzyme E2 A	<i>Ube2a</i>	1.6403	0.002
Serine/arginine-rich splicing factor 6	<i>Srsf6</i>	1.6381	0.0018
Calreticulin	<i>Calr</i>	1.6377	0.0027
Transcription elongation factor B polypeptide 2	<i>Tceb2</i>	1.6358	0.0001
	<i>Hnrnpd</i>	1.6351	0.0009
High mobility group nucleosome-binding domain-containing protein 5	<i>Hmgn5</i>	1.6324	0.0131
Inorganic pyrophosphatase	<i>Ppa1</i>	1.6322	0.0004
Negative elongation factor A	<i>Nelfa</i>	1.6318	0.0165
Coiled-coil domain-containing protein 6	<i>Ccdc6</i>	1.6299	0.0033
Protein FAM136A	<i>Fam136a</i>	1.6271	0.0138
Interferon-induced protein with tetratricopeptide repeats 1	<i>Ifit1</i>	1.6263	0.0002
Microtubule-associated protein 4;Microtubule-associated protein	<i>Map4</i>	1.6252	0.0003
26S proteasome non-ATPase regulatory subunit 9	<i>Psmc9</i>	1.6239	0.0043
ATP synthase subunit e, mitochondrial	<i>Atp5i;Atp5k</i>	1.6209	0.0163
	<i>Rabgap1l</i>	1.6207	0.0016
Aldehyde dehydrogenase family 16 member A1	<i>Aldh16a1</i>	1.6185	0.0002
Carboxymethylenebutenolidase homolog	<i>Cmb1</i>	1.6167	0.0134
Uncharacterized protein KIAA0556	<i>D430042O09Rik;Kiaa0556</i>	1.616	0.0087
Serine/arginine-rich splicing factor 9	<i>Srsf9</i>	1.6159	0.0071
3-oxoacyl-[acyl-carrier-protein] synthase, mitochondrial	<i>Oxsm</i>	1.6151	0.0049
NEDD8	<i>Nedd8</i>	1.6055	0.0014
Semaphorin-4B	<i>Sema4b</i>	1.6032	0.0022
Prostaglandin reductase 1	<i>Ptgr1</i>	1.6016	0.0348
UV excision repair protein RAD23 homolog A	<i>Rad23a</i>	1.5988	0.0002
MAP/microtubule affinity-regulating kinase 3	<i>Mark3</i>	1.5978	0.0001
Aldose reductase	<i>Akr1b1</i>	1.5976	0.0036
Tapasin	<i>Tapbp</i>	1.5942	0.0016
Dihydropteridine reductase	<i>Qdpr</i>	1.5936	0.0113
GMP reductase 2	<i>Gmpr2</i>	1.593	0.003
Carboxypeptidase Q	<i>Cpq</i>	1.5927	0.0001
60S ribosomal protein L12	<i>Rpl12</i>	1.5895	0.0011
Tropomyosin alpha-4 chain	<i>Tpm4</i>	1.5884	0.0256
Protein canopy homolog 3	<i>Cnpy3</i>	1.5882	0.0122
Hydroxyacylglutathione hydrolase, mitochondrial	<i>Hagh</i>	1.5882	0.0106
Protein disulfide-isomerase A3	<i>Pdia3</i>	1.5857	0.0064
40S ribosomal protein S17	<i>Rps17</i>	1.5844	0.0085
Epithelial discoidin domain-containing receptor 1	<i>Ddr1</i>	1.5843	0.0004
FYN-binding protein	<i>Fyb</i>	1.5833	0.0417
Cytosolic non-specific dipeptidase	<i>Cndp2</i>	1.5825	0.0246
Phenazine biosynthesis-like domain-containing protein 2	<i>Pbl2</i>	1.5808	0.0362
Beta-glucuronidase	<i>Gusb</i>	1.5805	0.0021
GDP-fucose transporter 1	<i>Slc35c1</i>	1.5801	0.0172

Signal transducer and activator of transcription	<i>Stat1</i>	1.5767	0.0311
Thioredoxin domain-containing protein 12	<i>Txndc12</i>	1.5752	0.0027
Rab9 effector protein with kelch motifs	<i>Rabepk</i>	1.5732	0.0009
Deoxyribose-phosphate aldolase	<i>Dera</i>	1.5722	0.0014
E3 ubiquitin-protein ligase RNF126	<i>Rnf126</i>	1.5721	0.0026
Nucleoside diphosphate kinase;Nucleoside diphosphate kinase B	<i>Gm20390;Nme2</i>	1.5716	0.0043
Eukaryotic translation initiation factor 4H	<i>Eif4h</i>	1.5715	0.0007
Glycogen phosphorylase, brain form	<i>Pygb</i>	1.5693	0.0003
Glutathione S-transferase Mu 5	<i>Gstm5</i>	1.5684	0.0007
Gamma-parvin	<i>Parvg</i>	1.5668	0.0273
C-1-tetrahydrofolate synthase, cytoplasmic;Methylenetetrahydrofolate dehydrogenase;Methenyltetrahydrofolate cyclohydrolase;Formyltetrahydrofolate synthetase;C-1-tetrahydrofolate synthase, cytoplasmic, N-terminally processed	<i>Mthfd1</i>	1.5668	0.0016
60S ribosomal protein L4	<i>Rpl4</i>	1.5658	0.0037
60S ribosomal protein L26	<i>Rpl26</i>	1.5658	0.041
Guanylate kinase	<i>Guk1</i>	1.561	0.0009
Antigen peptide transporter 2	<i>Tap2</i>	1.5608	0.0088
Protein phosphatase 1 regulatory subunit 14B	<i>Ppp1r14b</i>	1.5601	0.003
Small nuclear ribonucleoprotein-associated protein B;Small nuclear ribonucleoprotein-associated protein N	<i>Snrpb;Snrpn</i>	1.5599	0.0006
Leucine-rich repeat flightless-interacting protein 1	<i>Lrrfip1</i>	1.5594	0.0158
Steroid receptor RNA activator 1	<i>Sra1</i>	1.5589	0.0076
Succinyl-CoA:3-ketoacid coenzyme A transferase 1, mitochondrial;Succinyl-CoA:3-ketoacid-coenzyme A transferase	<i>Oxct1</i>	1.5576	0.004
Echinoderm microtubule-associated protein-like 2	<i>Eml2</i>	1.5575	0.0003
Galactose-1-phosphate uridylyltransferase	<i>Galt</i>	1.5559	0.0007
	<i>Taf15</i>	1.5543	0.0097
Haloacid dehalogenase-like hydrolase domain-containing protein 2	<i>Hdhd2</i>	1.5542	0.0066
Exosome complex component MTR3	<i>Exosc6</i>	1.5536	0.0003
Aftiphilin	<i>Aftph</i>	1.5501	0.001
Dnal homolog subfamily C member 8	<i>Dnajc8</i>	1.5486	0.0003
Protein RCC2	<i>Rcc2</i>	1.5477	0.0077
U6 snRNA-associated Sm-like protein LSM4	<i>Lsm4</i>	1.5476	0.0001
Tissue alpha-L-fucosidase	<i>Fuca1</i>	1.547	0.0001
Transducin-like enhancer protein 4;Transducin-like enhancer protein 1	<i>Tle4;Tle1</i>	1.5466	0.0011
39S ribosomal protein L30, mitochondrial	<i>Mrpl30</i>	1.5462	0.0014
Phosphorylated adapter RNA export protein	<i>Phax</i>	1.5456	0.0376
Putative adenosylhomocysteinase 2	<i>Ahcyl1</i>	1.545	0.0007
Semaphorin-4G	<i>Sema4g</i>	1.5443	0.0002
Mitochondrial import inner membrane translocase subunit Tim13	<i>Timm13</i>	1.5439	0.0033
Group XIIB secretory phospholipase A2-like protein	<i>Pla2g12b</i>	1.5429	0.0201
	<i>Serpib9</i>	1.5428	0.0356

40S ribosomal protein S20	<i>Rps20</i>	1.5425	0.0158
60S ribosomal protein L3	<i>Rpl3</i>	1.5423	0.0053
Mitotic checkpoint protein BUB3	<i>Bub3</i>	1.5415	0.0003
Protein NipSnap homolog 3B	<i>Nipsnap3b</i>	1.5412	0.0002
NAD(P)H-hydrate epimerase	<i>Apoa1bp</i>	1.5394	0.0002
Serine/arginine-rich splicing factor 3	<i>Srsf3;Gm12355</i>	1.5393	0.0152
	<i>Gm8909</i>	1.5391	0.0042
N(4)-(beta-N-acetylglucosaminy)-L-asparaginase;Glycosylasparaginase alpha chain;Glycosylasparaginase beta chain	<i>Aga</i>	1.5383	0.0007
Cyclin-dependent kinase inhibitor 1B	<i>Cdkn1b</i>	1.5378	0.0022
Dynein light chain 1, cytoplasmic	<i>Dynl1;BC048507</i>	1.5374	0.0003
Glyoxylate reductase/hydroxypyruvate reductase	<i>Grhpr</i>	1.5373	0.0218
Arginyl-tRNA--protein transferase 1	<i>Ate1</i>	1.5355	0.0048
Omega-amidase NIT2	<i>Nit2</i>	1.5353	0.0035
High mobility group protein B1	<i>Hmgb1</i>	1.5343	0.0182
WASH complex subunit FAM21	<i>Fam21</i>	1.5339	0.0189
Coiled-coil domain-containing protein 43	<i>Ccdc43</i>	1.5336	0.0035
Heterogeneous nuclear ribonucleoprotein U-like protein 2	<i>Hnrnpul2</i>	1.5324	0.0002
Fructose-bisphosphate aldolase C	<i>Aldoc</i>	1.5324	0.0132
Glycerol-3-phosphate dehydrogenase [NAD(+)];Glycerol-3-phosphate dehydrogenase [NAD(+)], cytoplasmic	<i>Gpd1</i>	1.5315	0.0115
DNA methyltransferase 1-associated protein 1	<i>Dmap1</i>	1.5311	0.0024
Ribonuclease P protein subunit p30	<i>Rpp30</i>	1.531	0.0002
60S ribosomal protein L6	<i>Rpl6;Gm5428</i>	1.5308	0.0128
Protein arginine N-methyltransferase 1	<i>Prmt1</i>	1.5307	0.0001
Chromobox protein homolog 3	<i>Cbx3</i>	1.5276	0.0089
FAD-linked sulfhydryl oxidase ALR	<i>Gfer</i>	1.5264	0.0039
Stromal cell-derived factor 2-like protein 1	<i>Sdf2l1</i>	1.5263	0.0006
60S ribosomal protein L22	<i>Rpl22</i>	1.5262	0.0006
Ribosomal protein L15;60S ribosomal protein L15	<i>Gm10020;Rpl15</i>	1.5257	0.0134
BolA-like protein 1	<i>Bola1</i>	1.5249	0.0181
COX assembly mitochondrial protein homolog	<i>Cmc1</i>	1.5239	0.0236
14-3-3 protein gamma;14-3-3 protein gamma, N-terminally processed	<i>Ywhag</i>	1.5233	0.0117
Proliferating cell nuclear antigen	<i>Pcna</i>	1.5223	0.005
Prefoldin subunit 6	<i>Pfdn6</i>	1.5223	0.0023
Proteasome activator complex subunit 1	<i>Psme1</i>	1.5212	0.0006
Kinetochole-associated protein 1	<i>Kntc1</i>	1.518	0.0079
Myotrophin	<i>Mtpn</i>	1.5175	0.0416
Plasma alpha-L-fucosidase	<i>Fuca2</i>	1.5163	0.0006
Ubiquitin-conjugating enzyme E2 L3	<i>Ube2l3</i>	1.5155	0.0015
Heterogeneous nuclear ribonucleoprotein A3	<i>Hnrnpa3;Gm9242;Gm6793</i>	1.5155	0.0003
U6 snRNA-associated Sm-like protein LSm1	<i>Lsm1</i>	1.5144	0.015
Beta-lactamase-like protein 2	<i>Lactb2</i>	1.5126	0.0031
40S ribosomal protein S19	<i>Rps19</i>	1.5125	0.013
Eukaryotic translation initiation factor 6	<i>Eif6</i>	1.5106	0.0001
Putative helicase MOV-10	<i>Mov10</i>	1.5099	0.0001

Adenylosuccinate synthetase isozyme 2	<i>Adss</i>	1.5096	0.0018
Putative deoxyribonuclease TATDN1	<i>Tatdn1</i>	1.5087	0.0126
Tripeptidyl-peptidase 2	<i>Tpp2</i>	1.5076	0.0001
DnaJ homolog subfamily B member 11	<i>Dnajb11</i>	1.5068	0.0017
GDP-L-fucose synthase	<i>Tsta3</i>	1.5067	0.0101
Far upstream element-binding protein 2	<i>Khsrp</i>	1.5051	0.0065
Growth factor receptor-bound protein 2	<i>Grb2</i>	1.5028	0.0002
Queuine tRNA-ribosyltransferase subunit QTRTD1	<i>Qtrtd1</i>	1.5024	0.0233
Lysine--tRNA ligase	<i>Kars</i>	1.5023	0.0001
Serpin B6	<i>Serpinb6a;Serpinb6</i>	1.5019	0.0006
Small nuclear ribonucleoprotein G	<i>Snrpg</i>	1.5013	0.0001
THO complex subunit 6 homolog	<i>Thoc6</i>	1.5008	0.0005
Serotransferrin	<i>Tf</i>	1.4999	0.0065
Dihydropyrimidine dehydrogenase [NADP(+)]	<i>Dpyd</i>	1.4988	0.001
Malate dehydrogenase, mitochondrial	<i>Mdh2</i>	1.498	0.0052
Selenoprotein P	<i>Sepp1</i>	1.4974	0.0116
PDZ and LIM domain protein 2	<i>Pdlim2</i>	1.497	0.0009
Heterogeneous nuclear ribonucleoproteins C1/C2	<i>Hnrnpc</i>	1.4967	0.0033
Aldo-keto reductase family 1 member C13	<i>Akr1c13</i>	1.4967	0.0162
Nuclear ubiquitous casein and cyclin-dependent kinase substrate 1	<i>Nucks1</i>	1.4961	0.011
60S ribosomal protein L9	<i>Rpl9</i>	1.4961	0.0085
Na(+)/H(+) exchange regulatory cofactor NHE-RF1	<i>Slc9a3r1</i>	1.4943	0.004
Dihydropyrimidinase-related protein 2	<i>Dpysl2</i>	1.4931	0.0008
60S ribosomal protein L7	<i>Rpl7</i>	1.4925	0.0203
Protein-glutamate O-methyltransferase	<i>Armt1</i>	1.4924	0.0042
10 kDa heat shock protein, mitochondrial	<i>Hspe1</i>	1.4914	0.0077
60S ribosomal protein L5	<i>Rpl5</i>	1.4904	0.005
Cleavage stimulation factor subunit 2	<i>Cstf2</i>	1.4898	0.0033
BAG family molecular chaperone regulator 3	<i>Bag3</i>	1.4887	0.0001
Pirin	<i>Pir</i>	1.4874	0.0031
Protein disulfide-isomerase	<i>P4hb</i>	1.4853	0.0343
Proteasome subunit beta type-4	<i>Psmb4</i>	1.4843	0.0003
Phosphoribosyl pyrophosphate synthase-associated protein 1	<i>Prpsap1</i>	1.4813	0.0001
LDLR chaperone MESD	<i>Mesdc2</i>	1.4799	0.0006
Mitochondrial import inner membrane translocase subunit Tim8 A	<i>Timm8a1</i>	1.4784	0.0007
Neutral alpha-glucosidase AB	<i>Ganab</i>	1.4779	0.0004
Glucosidase 2 subunit beta	<i>Prkcsh</i>	1.4775	0.0049
Ubiquitin-like protein 4A	<i>Ubl4a</i>	1.4774	0.0031
THO complex subunit 7 homolog	<i>Thoc7</i>	1.4764	0.0039
182 kDa tankyrase-1-binding protein	<i>Tnks1bp1</i>	1.4752	0.0074
Crk-like protein	<i>Crkl</i>	1.4747	0.0038
Ribose-phosphate pyrophosphokinase 1	<i>Prps1/3;Prps1</i>	1.4739	0.0009
Eukaryotic translation initiation factor 3 subunit D	<i>Eif3d</i>	1.4738	0.0009
TATA element modulatory factor	<i>Tmf1</i>	1.4718	0.013
Serine/threonine-protein phosphatase CPPED1	<i>Cpped1</i>	1.4717	0.0035
60S ribosomal protein L30	<i>Rpl30</i>	1.4696	0.0139
40S ribosomal protein S9	<i>Rps9</i>	1.4688	0.0249

Serine protease inhibitor A3K	<i>Serpina3k</i>	1.4668	0.0112
Geranylgeranyl transferase type-2 subunit beta	<i>Rabggtb</i>	1.4662	0.0091
39S ribosomal protein L41, mitochondrial	<i>Mrpl41</i>	1.4662	0.0222
UV excision repair protein RAD23 homolog B	<i>Rad23b</i>	1.465	0.0015
Glyceraldehyde-3-phosphate dehydrogenase	<i>Gapdh;Gm3839</i>	1.4648	0.0034
H-2 class I histocompatibility antigen, K-B alpha chain	<i>H2-K1</i>	1.4648	0.0009
Acid sphingomyelinase-like phosphodiesterase 3a	<i>Smpdl3a</i>	1.4645	0.0016
Pyruvate kinase PKM	<i>Pkm</i>	1.4644	0.0001
Telomerase protein component 1	<i>Tep1</i>	1.4641	0.0009
Glutaredoxin-related protein 5, mitochondrial	<i>Glrx5</i>	1.4635	0.0335
SUMO-conjugating enzyme UBC9	<i>Ube2i</i>	1.463	0.0001
	<i>Tpm3-rs7</i>	1.4618	0.0073
Protein CREG1	<i>Creg1</i>	1.4616	0.0077
14-3-3 protein zeta/delta	<i>Ywhaz</i>	1.4615	0.0001
60S ribosomal protein L21	<i>Rpl21</i>	1.4597	0.0058
CCR4-NOT transcription complex subunit 3	<i>Cnot3</i>	1.4588	0.0279
Cytosol aminopeptidase	<i>Lap3</i>	1.4584	0.0011
Cyclin-dependent kinase 12	<i>Cdk12</i>	1.4577	0.0054
Galectin-3-binding protein	<i>Lgals3bp</i>	1.4574	0.0032
C-Myc-binding protein	<i>Mycbp</i>	1.457	0.0061
Methionine adenosyltransferase 2 subunit beta	<i>Mat2b</i>	1.4565	0.0002
Peptidyl-prolyl cis-trans isomerase NIMA-interacting 4	<i>Pin4</i>	1.4564	0.0046
Alanyl-tRNA editing protein Aarsd1	<i>Aarsd1;Gm27029</i>	1.4561	0.0123
Prefoldin subunit 5	<i>Pfdn5</i>	1.4559	0.0129
Putative N-acetylglucosamine-6-phosphate deacetylase	<i>Amdhd2</i>	1.4556	0.0008
14-3-3 protein sigma	<i>Sfn</i>	1.4547	0.0002
Rab GDP dissociation inhibitor beta	<i>Gdi2</i>	1.4545	0.0047
Aconitate hydratase, mitochondrial	<i>Aco2</i>	1.4538	0.0061
RNA-binding protein 8A	<i>Rbm8a</i>	1.4535	0.0053
N-myc-interactor	<i>Nmi</i>	1.4522	0.0001
Adenylyl cyclase-associated protein 1	<i>Cap1</i>	1.4513	0.0036
60S ribosomal protein L18a	<i>Rpl18a;Gm17541</i>	1.4512	0.0195
	<i>Pop1</i>	1.4508	0.0011
Aspartate aminotransferase, mitochondrial	<i>Got2</i>	1.4507	0.0062
Quinone oxidoreductase-like protein 1	<i>Cryz1</i>	1.4492	0.0093
Inositol-3-phosphate synthase 1	<i>Isyna1</i>	1.4478	0.0003
Microtubule-associated protein 1S;MAP1S heavy chain;MAP1S light chain	<i>Map1s</i>	1.4478	0.0002
	<i>Aamp</i>	1.4475	0.0026
	<i>Uba7</i>	1.4472	0.0001
Coiled-coil-helix-coiled-coil-helix domain-containing protein 7	<i>Chchd7</i>	1.445	0.0047
60S ribosomal protein L13	<i>Rpl13</i>	1.4449	0.0222
Protein N-terminal asparagine amidohydrolase	<i>Ntan1</i>	1.4448	0.0001
Pterin-4-alpha-carbinolamine dehydratase 2	<i>Pcbd2</i>	1.4433	0.0167
Pyruvate kinase;Pyruvate kinase PKLR	<i>Pklr</i>	1.4432	0.0001
Enoyl-CoA hydratase, mitochondrial	<i>Echs1</i>	1.4431	0.01
Farnesyl pyrophosphate synthase	<i>Fdps</i>	1.4425	0.0027

U6 snRNA-associated Sm-like protein LSM6	<i>Lsm6</i>	1.4418	0.0001
Ribose-phosphate pyrophosphokinase 2	<i>Prps2</i>	1.4406	0.0011
2-amino-3-ketobutyrate coenzyme A ligase, mitochondrial	<i>Gcat</i>	1.4401	0.0017
Cofilin-2	<i>Cfl2</i>	1.4396	0.0042
Alpha-aminoadipic semialdehyde dehydrogenase	<i>Aldh7a1</i>	1.4391	0.0005
Beta-mannosidase	<i>Manba</i>	1.4386	0.0172
Peptidyl-prolyl cis-trans isomerase F, mitochondrial	<i>Ppif</i>	1.4386	0.0109
Proteasomal ubiquitin receptor ADRM1	<i>Gm9774;Adrm1</i>	1.4382	0.0055
Carboxylesterase 1C	<i>Ces1c</i>	1.4381	0.0387
Beta-2-microglobulin	<i>B2m</i>	1.4373	0.0001
Probable cytosolic iron-sulfur protein assembly protein CIAO1	<i>Ciao1</i>	1.4373	0.0064
PDZ and LIM domain protein 1	<i>Pdlim1</i>	1.4373	0.0023
Costars family protein ABRACL	<i>Abracl</i>	1.4361	0.0011
Acidic leucine-rich nuclear phosphoprotein 32 family member B	<i>Anp32b</i>	1.4355	0.0227
Cathepsin S	<i>Ctss</i>	1.4345	0.0028
Protein LSM12 homolog	<i>Lsm12</i>	1.4336	0.0001
Proprotein convertase subtilisin/kexin type 5	<i>Pcsk5</i>	1.4328	0.0063
Peroxiredoxin-2	<i>Prdx2</i>	1.432	0.0001
Phosphomannomutase 2	<i>Pmm2</i>	1.4316	0.0014
Paxillin	<i>Pxn</i>	1.4313	0.0011
Vacuolar protein sorting-associated protein 35	<i>Vps35</i>	1.4308	0.0012
Fatty acid-binding protein, epidermal	<i>Fabp5</i>	1.4307	0.0005
Disks large-associated protein 4	<i>Dlgap4</i>	1.4298	0.01
Toll-interacting protein	<i>Tollip</i>	1.4294	0.002
Histidine triad nucleotide-binding protein 1	<i>Hint1</i>	1.4292	0.0043
Nuclear transport factor 2	<i>Nutf2</i>	1.4285	0.0004
Glucose-6-phosphate 1-dehydrogenase X;Glucose-6-phosphate 1-dehydrogenase	<i>G6pdx</i>	1.4283	0.0002
Protein N-terminal glutamine amidohydrolase	<i>Wdyhv1</i>	1.428	0.0016
Citrate synthase, mitochondrial	<i>Cs</i>	1.4276	0.0066
Calmodulin-like protein 4	<i>Calml4</i>	1.4275	0.0091
Far upstream element-binding protein 1	<i>Fubp1</i>	1.4267	0.0046
Sulfatase-modifying factor 1	<i>Sumf1</i>	1.4241	0.0184
Mesoderm induction early response protein 1	<i>Mier1</i>	1.4234	0.0108
Casein kinase II subunit beta	<i>Csnk2b</i>	1.4233	0.004
Nuclear autoantigenic sperm protein	<i>Nasp</i>	1.4233	0.0058
Nascent polypeptide-associated complex subunit alpha;Nascent polypeptide-associated complex subunit alpha, muscle-specific form	<i>Naca</i>	1.423	0.0034
Derlin-2	<i>Derl2</i>	1.422	0.0001
E3 ubiquitin-protein ligase MYCBP2	<i>Mycbp2</i>	1.4218	0.0369
Osteoclast-stimulating factor 1	<i>Ostf1</i>	1.4212	0.0009
Acylphosphatase;Acylphosphatase-1	<i>Acyp1</i>	1.421	0.0002
S-methyl-5-thioadenosine phosphorylase	<i>Mtap</i>	1.4205	0.0001
N-acetylglucosamine-1-phosphotransferase subunits alpha/beta	<i>Gnptab</i>	1.4196	0.0062
Splicing factor 3B subunit 4	<i>Sf3b4</i>	1.4175	0.0003
Fructose-1,6-bisphosphatase 1	<i>Fbp1</i>	1.4168	0.0207

Protein phosphatase 1 regulatory subunit 12A	<i>Ppp1r12a</i>	1.4167	0.001
Acylpyruvase FAHD1, mitochondrial	<i>Fahd1</i>	1.4162	0.0201
SH3 domain-binding glutamic acid-rich-like protein 3	<i>Sh3bgrl3</i>	1.4138	0.0157
Synapse-associated protein 1	<i>Syap1</i>	1.4135	0.0081
45 kDa calcium-binding protein	<i>Sdf4</i>	1.4133	0.0163
GTP-binding nuclear protein Ran	<i>Ran;1700009N14 Rik</i>	1.413	0.0003
2-aminoethanethiol dioxygenase	<i>Ado</i>	1.4127	0.0021
	<i>Gm14446</i>	1.4124	0.0479
Exosome complex exonuclease RRP42	<i>Exosc7</i>	1.4124	0.0026
Endoplasmic reticulum aminopeptidase 1	<i>Erap1</i>	1.4122	0.0001
Thioredoxin reductase 2, mitochondrial	<i>Txnrd2</i>	1.412	0.0053
Alpha-1-antitrypsin 1-4	<i>Serpina1d</i>	1.4109	0.0106
Y-box-binding protein 3	<i>Ybx3</i>	1.4108	0.0115
Tetratricopeptide repeat protein 1	<i>Ttc1</i>	1.4102	0.0084
40S ribosomal protein S23	<i>Rps23</i>	1.409	0.0336
39S ribosomal protein L2, mitochondrial	<i>Mrp12</i>	1.4088	0.001
40S ribosomal protein S11	<i>Rps11</i>	1.4085	0.0428
Electron transfer flavoprotein subunit beta	<i>Etfb</i>	1.4074	0.015
	<i>Nans</i>	1.4073	0.0126
Copper chaperone for superoxide dismutase	<i>Ccs</i>	1.4067	0.0209
Transmembrane protein 128	<i>Tmem128</i>	1.4054	0.0007
Rootletin	<i>Crocc</i>	1.4053	0.0129
	<i>2210016F16Rik</i>	1.4052	0.0051
Nucleoporin SEH1	<i>Seh1l</i>	1.4051	0.0025
Heterogeneous nuclear ribonucleoprotein Q	<i>Syncrip</i>	1.4041	0.0004
Dynein light chain 2, cytoplasmic	<i>Dynll2</i>	1.4032	0.0012
Ribosomal protein L19;60S ribosomal protein L19	<i>Rpl19</i>	1.4032	0.0125
Zinc phosphodiesterase ELAC protein 2	<i>Elac2</i>	1.4029	0.0012
RING-box protein 2	<i>Gm7075;Rnf7</i>	1.3994	0.0076
Phosphoglucomutase-1	<i>Pgm1;Pgm2</i>	1.3993	0.0226
Ras-related GTP-binding protein D	<i>Rragd</i>	1.3992	0.0005
Palmitoyl-protein thioesterase 1	<i>Ppt1</i>	1.3988	0.0016
Nucleolar MIF4G domain-containing protein 1	<i>Nom1</i>	1.3981	0.0381
PITH domain-containing protein 1	<i>Pithd1</i>	1.397	0.0057
40S ribosomal protein S15a	<i>Rps15a</i>	1.397	0.0353
Tyrosine-protein phosphatase non-receptor type 1	<i>Ptpn1</i>	1.3967	0.0128
Serine/threonine-protein phosphatase PP1-gamma catalytic subunit	<i>Ppp1cc</i>	1.3962	0.0007
2-5-oligoadenylate synthase-like protein 1	<i>Oasl1</i>	1.3962	0.0018
Phosphoribosyl pyrophosphate synthase-associated protein 2	<i>Prpsap2</i>	1.3961	0.0023
FGFR1 oncogene partner 2 homolog	<i>Fgfr1op2</i>	1.396	0.017
Lysosomal alpha-glucosidase	<i>Gaa</i>	1.3956	0.0184
Iron-sulfur cluster assembly 2 homolog, mitochondrial	<i>Isca2</i>	1.3952	0.0125
Hydroxymethylglutaryl-CoA synthase, cytoplasmic	<i>Hmgcs1</i>	1.3949	0.0118
Heterogeneous nuclear ribonucleoprotein A1;Heterogeneous nuclear ribonucleoprotein A1, N-terminally processed	<i>Hnrnpa1</i>	1.393	0.0003

60S ribosomal protein L36	<i>Rpl36;Gm8973</i>	1.3907	0.0156
DNA damage-binding protein 1	<i>Ddb1</i>	1.3905	0.0017
Short-chain specific acyl-CoA dehydrogenase, mitochondrial	<i>Acads</i>	1.3894	0.019
Protein disulfide-isomerase A4	<i>Pdia4</i>	1.3885	0.0031
	<i>Immt</i>	1.3866	0.0259
CAP-Gly domain-containing linker protein 2	<i>Clip2</i>	1.3864	0.0264
Protein transport protein Sec31B	<i>Sec31b</i>	1.3862	0.0357
E3 ubiquitin-protein ligase RNF115	<i>Rnf115</i>	1.3857	0.0078
WD40 repeat-containing protein SMU1;WD40 repeat-containing protein SMU1, N-terminally processed	<i>Smu1</i>	1.3852	0.0037
Transmembrane protein 43	<i>Tmem43</i>	1.3846	0.0052
Espin	<i>Espn</i>	1.3833	0.0038
Glutaredoxin-1	<i>Glrx</i>	1.3828	0.006
Protein PRRC2C	<i>Prrc2c</i>	1.3823	0.0012
NIF3-like protein 1	<i>Nif3l1</i>	1.3812	0.0041
Ribonuclease T2	<i>Rnaset2</i>	1.381	0.0114
Coatomer subunit beta	<i>Copb2</i>	1.3806	0.0001
Optineurin	<i>Optn</i>	1.3801	0.0312
tRNA (adenine(58)-N(1))-methyltransferase non-catalytic subunit TRM6	<i>Trmt6</i>	1.3798	0.0021
Annexin A6	<i>Anxa6</i>	1.3797	0.0275
Nucleoporin Nup37	<i>Nup37</i>	1.3793	0.0157
Pleiotropic regulator 1	<i>Plrg1</i>	1.3787	0.0081
WD repeat-containing protein 61;WD repeat-containing protein 61, N-terminally processed	<i>Wdr61</i>	1.3763	0.0144
Chromobox protein homolog 1	<i>Cbx1</i>	1.3759	0.004
Glia maturation factor beta	<i>Gmfb</i>	1.3737	0.0048
Protein mago nashi homolog 2;Protein mago nashi homolog	<i>Magohb;Magoh</i>	1.3728	0.0013
Lupus La protein homolog	<i>Ssb</i>	1.3727	0.0216
Lipoma-preferred partner homolog	<i>Lpp</i>	1.3721	0.001
39S ribosomal protein L10, mitochondrial	<i>Mrpl10</i>	1.3712	0.0002
	<i>Ifi47</i>	1.3711	0.0451
Signal peptide peptidase-like 2A	<i>Sppl2a</i>	1.3711	0.0022
Oxygen-dependent coproporphyrinogen-III oxidase, mitochondrial	<i>Cpox</i>	1.3699	0.0489
Propionyl-CoA carboxylase beta chain, mitochondrial	<i>Pccb</i>	1.368	0.0066
Small nuclear ribonucleoprotein Sm D1	<i>Snrpd1</i>	1.368	0.0002
Transgelin-2	<i>Tagln2</i>	1.365	0.0014
Protein S100-A13	<i>S100a13</i>	1.365	0.0437
WD repeat-containing protein 37	<i>Wdr37</i>	1.3627	0.0026
Exosome complex component RRP43	<i>Exosc8</i>	1.3626	0.0082
Syntaxin-7	<i>Stx7</i>	1.361	0.0024
Peroxiredoxin-4	<i>Prdx4</i>	1.3599	0.0014
Coactosin-like protein	<i>Cotl1</i>	1.3597	0.0299
Tubulin-folding cofactor B	<i>Tbcf</i>	1.3596	0.0037
UDP-glucose 6-dehydrogenase	<i>Ugdh</i>	1.3594	0.0166
	<i>Gm20425</i>	1.3592	0.0021

Thyroid hormone receptor-associated protein 3	<i>Thrap3</i>	1.3591	0.0338
Ras-related protein Rab-21	<i>Rab21</i>	1.358	0.0001
39S ribosomal protein L32, mitochondrial	<i>Mrpl32</i>	1.3573	0.0009
Peptidyl-prolyl cis-trans isomerase-like 1	<i>Ppil1</i>	1.3571	0.0001
Transcription factor p65	<i>Rela</i>	1.3571	0.0048
Cleavage and polyadenylation specificity factor subunit 6	<i>Cpsf6</i>	1.3566	0.0028
Pre-mRNA-splicing regulator WTAP	<i>Wtap</i>	1.356	0.015
Multiple myeloma tumor-associated protein 2 homolog	<i>Mmtag2</i>	1.355	0.0057
60S ribosomal protein L18	<i>Rpl18</i>	1.3544	0.0312
pre-mRNA 3 end processing protein WDR33	<i>Wdr33</i>	1.3538	0.0029
Lysosomal alpha-mannosidase	<i>Man2b1</i>	1.3537	0.022
Methylosome subunit pICln	<i>Clns1a</i>	1.3531	0.0027
Propionyl-CoA carboxylase alpha chain, mitochondrial	<i>Pcca</i>	1.3529	0.0098
Fumarate hydratase, mitochondrial	<i>Fh</i>	1.3528	0.0382
Protein S100-A10	<i>S100a10</i>	1.3526	0.0422
CTTNBP2 N-terminal-like protein	<i>Cttnbp2nl</i>	1.3523	0.0153
Protein SEC13 homolog	<i>Sec13</i>	1.3522	0.0001
U2 small nuclear ribonucleoprotein B	<i>Snrpb2</i>	1.352	0.0014
Medium-chain specific acyl-CoA dehydrogenase, mitochondrial	<i>Acadm</i>	1.3508	0.0135
WD repeat and HMG-box DNA-binding protein 1	<i>Wdhd1</i>	1.3501	0.0016
Exosome complex component RRP40	<i>Exosc3</i>	1.3499	0.0088
ADP-ribose pyrophosphatase, mitochondrial	<i>Nudt9</i>	1.3499	0.0179
Electron transfer flavoprotein subunit alpha, mitochondrial	<i>Etfa</i>	1.349	0.0276
Phosphoglycerate mutase 1	<i>Pgam1</i>	1.3479	0.0026
Cathepsin B;Cathepsin B light chain;Cathepsin B heavy chain	<i>Ctsb</i>	1.3478	0.0213
CD151 antigen	<i>Cd151</i>	1.3478	0.0465
Cleavage and polyadenylation specificity factor subunit 5	<i>Nudt21</i>	1.3478	0.0024
NEDD8-activating enzyme E1 regulatory subunit	<i>Nae1</i>	1.3475	0.0005
Heterogeneous nuclear ribonucleoprotein H	<i>Hnrnp1</i>	1.3462	0.0001
Tetratricopeptide repeat protein 39B	<i>Ttc39b</i>	1.3457	0.0007
Elongation factor G, mitochondrial	<i>Gfm1</i>	1.3443	0.0015
Protein YIPF;Protein YIPF1	<i>Yipf1</i>	1.3441	0.0001
F-box-like/WD repeat-containing protein TBL1XR1	<i>Tbl1xr1</i>	1.3433	0.0006
Adrenodoxin, mitochondrial	<i>Fdx1</i>	1.3428	0.029
Ribosomal protein;60S ribosomal protein L10a	<i>Rpl10a</i>	1.3427	0.0106
Proteasome activator complex subunit 2	<i>Psme2</i>	1.3425	0.0019
Succinate-semialdehyde dehydrogenase, mitochondrial	<i>Aldh5a1</i>	1.3403	0.0094
Molybdenum cofactor biosynthesis protein 1	<i>Mocs1</i>	1.3402	0.0079
NudC domain-containing protein 2	<i>Nudcd2</i>	1.3401	0.0104
Mannose-6-phosphate isomerase	<i>Mpi</i>	1.3395	0.0005
14-3-3 protein eta	<i>Ywhah</i>	1.3389	0.0001
Thioredoxin-dependent peroxide reductase, mitochondrial	<i>Prdx3</i>	1.3383	0.013

Alpha-N-acetylgalactosaminidase	<i>Naga</i>	1.3378	0.0322
Ubiquitin-associated protein 2-like	<i>Ubap2l</i>	1.3366	0.0011
U3 small nucleolar RNA-interacting protein 2	<i>Rrp9</i>	1.3361	0.0286
Kynurenine--oxoglutarate transaminase 1	<i>Ccbl1</i>	1.336	0.0436
Heat shock cognate 71 kDa protein	<i>Hspa8</i>	1.3357	0.0091
Actin-related protein 2/3 complex subunit 5	<i>Arpc5</i>	1.3351	0.0024
Pyridoxine-5-phosphate oxidase	<i>Pnpo</i>	1.3347	0.0219
Arf-GAP domain and FG repeat-containing protein 1	<i>Agfg1</i>	1.3332	0.0001
Amine oxidase;Amiloride-sensitive amine oxidase [copper-containing]	<i>Aoc1</i>	1.3329	0.0214
Nucleoporin p58/p45	<i>Nupl1</i>	1.3329	0.0363
AMP deaminase 2	<i>Ampd2</i>	1.3329	0.0071
Iron-sulfur cluster co-chaperone protein HscB, mitochondrial	<i>Hscb</i>	1.3328	0.0058
Actin-related protein 2/3 complex subunit 1A	<i>Arpc1a</i>	1.3309	0.0002
Hippocalcin-like protein 1	<i>Hpcal1</i>	1.3305	0.0253
Prefoldin subunit 3	<i>Vbp1</i>	1.3292	0.002
Transcription and mRNA export factor ENY2	<i>Eny2</i>	1.3292	0.0129
Splicing factor 3B subunit 3	<i>Sf3b3</i>	1.329	0.0004
Molybdenum cofactor sulfurase	<i>Mocos</i>	1.3278	0.0005
Vesicle-associated membrane protein 3;Vesicle-associated membrane protein 2	<i>Vamp3;Vamp2</i>	1.3276	0.013
Cat eye syndrome critical region protein 5 homolog	<i>Cecr5</i>	1.3272	0.0098
Transformer-2 protein homolog alpha	<i>Tra2a</i>	1.326	0.0281
Serine/threonine-protein phosphatase 4 regulatory subunit 2	<i>Ppp4r2</i>	1.3256	0.0014
Peptidyl-prolyl cis-trans isomerase FKBP1A;Peptidyl-prolyl cis-trans isomerase	<i>Fkbp1a</i>	1.3255	0.0015
CD2 antigen cytoplasmic tail-binding protein 2	<i>Cd2bp2</i>	1.3245	0.023
		1.3237	0.0019
Lathosterol oxidase	<i>Sc5d</i>	1.3215	0.0043
Eukaryotic translation initiation factor 3 subunit I	<i>Eif3i</i>	1.321	0.0145
Small ubiquitin-related modifier 1	<i>Sumo1</i>	1.3205	0.0109
Lys-63-specific deubiquitinase BRCC36	<i>Brcc3</i>	1.3199	0.0002
39S ribosomal protein L19, mitochondrial	<i>Mrpl19</i>	1.3197	0.0007
Ral GTPase-activating protein subunit alpha-2	<i>Ralgapa2</i>	1.319	0.028
Survival of motor neuron-related-splicing factor 30	<i>Smndc1</i>	1.3188	0.0275
Polyadenylate-binding protein-interacting protein 1	<i>Paip1</i>	1.3185	0.0041
Masparidin	<i>Spg21</i>	1.3185	0.0035
Peroxisomal sarcosine oxidase	<i>Pipox</i>	1.3182	0.007
V-type proton ATPase subunit G 1	<i>Atp6v1g1</i>	1.3174	0.0164
Nucleolar protein 4-like	<i>Nol4l</i>	1.3168	0.0368
Bis(5-nucleosyl)-tetraphosphatase [asymmetrical]	<i>Nudt2</i>	1.3166	0.0065
Dynein light chain roadblock-type 1	<i>Dynlrb1</i>	1.3165	0.0017
78 kDa glucose-regulated protein	<i>Hspa5</i>	1.316	0.0281
Nucleophosmin	<i>Npm1</i>	1.3156	0.0193
28S ribosomal protein S18a, mitochondrial	<i>Mrps18a</i>	1.3152	0.0121
Ribosome-recycling factor, mitochondrial	<i>Mrrf</i>	1.3148	0.0177
39S ribosomal protein L1, mitochondrial	<i>Mrpl1</i>	1.314	0.0029

14 kDa phosphohistidine phosphatase	<i>Phpt1</i>	1.314	0.0068
Kunitz-type protease inhibitor 1	<i>Spint1</i>	1.3119	0.0006
Protein BUD31 homolog	<i>Bud31</i>	1.3119	0.0001
17-beta-hydroxysteroid dehydrogenase type 6	<i>Hsd17b6</i>	1.3115	0.0392
Nuclear autoantigen Sp-100	<i>Sp100</i>	1.3114	0.0266
Beta-hexosaminidase subunit beta	<i>Hexb</i>	1.3114	0.0279
Splicing factor 1	<i>Sf1</i>	1.3107	0.0076
Acyl-coenzyme A thioesterase 4	<i>Acot4</i>	1.309	0.0494
Carnitine O-acetyltransferase	<i>Crat</i>	1.3084	0.019
Cleavage stimulation factor subunit 1	<i>Cstf1</i>	1.3074	0.0027
U5 small nuclear ribonucleoprotein 200 kDa helicase	<i>Snrnp200</i>	1.3071	0.0057
39S ribosomal protein L45, mitochondrial	<i>Mrpl45</i>	1.3067	0.0002
Chloride intracellular channel protein 6	<i>Clic6</i>	1.305	0.044
Heterogeneous nuclear ribonucleoprotein F;Heterogeneous nuclear ribonucleoprotein F, N-terminally processed	<i>Hnrnpf</i>	1.3046	0.0308
Pyrroline-5-carboxylate reductase 3	<i>Pycrl</i>	1.3042	0.017
60S ribosomal protein L37a	<i>Rpl37a</i>	1.3038	0.0446
	<i>Aim1</i>	1.3036	0.0023
39S ribosomal protein L15, mitochondrial	<i>Mrpl15</i>	1.3028	0.0005
	<i>Gbp7</i>	1.3019	0.0105
Kelch repeat and BTB domain-containing protein 11	<i>Kbtbd11</i>	1.3018	0.0071
Apoptotic protease-activating factor 1	<i>Apaf1</i>	1.3005	0.0001
Gamma-aminobutyric acid receptor-associated protein;Gamma-aminobutyric acid receptor-associated protein-like 1	<i>Gabarap;Gabarap1</i>	1.3004	0.0074
Small acidic protein	<i>Smap;1110004F1ORik</i>	1.2989	0.0201
RNA polymerase II-associated protein 3	<i>Rpap3</i>	1.2986	0.0186
RNA-binding protein 4B;RNA-binding protein 4	<i>Gm21992;Rbm14;Rbm4;Rbm4b</i>	1.2985	0.0241
	<i>Hnrnp3</i>	1.298	0.001
39S ribosomal protein L13, mitochondrial	<i>Mrpl13</i>	1.2969	0.0001
40S ribosomal protein S3a	<i>Rps3a</i>	1.2964	0.0471
Protein TSSC1	<i>Tssc1</i>	1.2959	0.017
Phosphatase and actin regulator 4	<i>Phactr4</i>	1.2951	0.0006
Activating signal cointegrator 1 complex subunit 2	<i>Ascc2</i>	1.2934	0.0243
Mitochondrial fission regulator 1-like	<i>Mtfr1l</i>	1.2932	0.0009
Peptidyl-prolyl cis-trans isomerase FKBP4;Peptidyl-prolyl cis-trans isomerase FKBP4, N-terminally processed;Peptidyl-prolyl cis-trans isomerase	<i>Fkbp4</i>	1.2922	0.0019
28S ribosomal protein S30, mitochondrial	<i>Mrps30</i>	1.2921	0.0007
Heterogeneous nuclear ribonucleoproteins A2/B1	<i>Hnrnpa2b1</i>	1.292	0.0056
Elongation factor 1-beta	<i>Eef1b;Eef1b2</i>	1.2917	0.0139
Activated RNA polymerase II transcriptional coactivator p15	<i>Sub1</i>	1.2906	0.0095
Putative transferase CAF17 homolog, mitochondrial	<i>Iba57</i>	1.29	0.0004
Leucine zipper protein 1	<i>Luzp1</i>	1.2899	0.0391

Peptidyl-prolyl cis-trans isomerase D	<i>Ppid</i>	1.2895	0.0061
Glucosamine 6-phosphate N-acetyltransferase	<i>Gnpnat1</i>	1.2891	0.0071
Actin-related protein 2/3 complex subunit 1B	<i>Arpc1b</i>	1.289	0.0024
Sequestosome-1	<i>Sqstm1</i>	1.2877	0.0014
Pre-mRNA-splicing factor ISY1 homolog	<i>Isy1</i>	1.2869	0.0154
26S proteasome non-ATPase regulatory subunit 8	<i>Psm8</i>	1.2869	0.0171
26S proteasome non-ATPase regulatory subunit 10	<i>Psm10</i>	1.2865	0.0016
Serine hydroxymethyltransferase	<i>Shmt2</i>	1.2858	0.0015
	<i>Acad12</i>	1.285	0.0192
Fructose-bisphosphate aldolase B	<i>Aldob</i>	1.2844	0.0015
Probable ATP-dependent RNA helicase DHX58	<i>Dhx58</i>	1.2837	0.0089
Valacyclovir hydrolase	<i>Bphl</i>	1.2834	0.0354
Molybdopterin synthase catalytic subunit	<i>Mocs2</i>	1.2815	0.0146
Trimethyllysine dioxygenase, mitochondrial	<i>Tmlhe</i>	1.2813	0.0198
26S proteasome non-ATPase regulatory subunit 14	<i>Psm14</i>	1.2813	0.0049
TGF-beta-activated kinase 1 and MAP3K7-binding protein 1	<i>Tab1</i>	1.2811	0.0285
28S ribosomal protein S26, mitochondrial	<i>Mrps26</i>	1.2806	0.0007
Gamma-glutamylcyclotransferase	<i>Ggct</i>	1.2805	0.0053
Dipeptidyl peptidase 8	<i>Dpp8</i>	1.2801	0.0365
Flavin reductase (NADPH)	<i>Blvrb</i>	1.2798	0.0001
Prostaglandin E synthase 3	<i>Ptges3</i>	1.2792	0.0003
Anamorsin	<i>Ciapi1</i>	1.2785	0.0385
Choline transporter-like protein 1	<i>Slc44a1</i>	1.2763	0.0159
Splicing factor, arginine/serine-rich 19	<i>Scaf1</i>	1.2752	0.0188
E3 ubiquitin-protein ligase RNF114	<i>Rnf114</i>	1.275	0.0002
Integrator complex subunit 2	<i>Ints2</i>	1.2743	0.0061
mRNA export factor	<i>Rae1</i>	1.2739	0.0042
39S ribosomal protein L3, mitochondrial	<i>Mrpl3</i>	1.2738	0.0015
Isovaleryl-CoA dehydrogenase, mitochondrial	<i>Ivd</i>	1.2718	0.0326
NF-kappa-B essential modulator	<i>Ikbkg</i>	1.2709	0.0031
Splicing factor U2AF 65 kDa subunit	<i>U2af2</i>	1.2708	0.0007
Glutaryl-CoA dehydrogenase, mitochondrial	<i>Gcdh</i>	1.2706	0.0014
High mobility group protein B2	<i>Hmgb2</i>	1.2693	0.0346
CCA tRNA nucleotidyltransferase 1, mitochondrial	<i>Trnt1</i>	1.2685	0.0049
Coiled-coil domain-containing protein 124	<i>Ccdc124</i>	1.2684	0.0365
3-hydroxyisobutyryl-CoA hydrolase, mitochondrial	<i>Hibch</i>	1.2684	0.0264
2-oxoglutarate dehydrogenase, mitochondrial	<i>Ogdh</i>	1.2683	0.0017
60S ribosomal protein L17	<i>Rpl17</i>	1.2676	0.0341
Copper homeostasis protein cutC homolog	<i>Cutc</i>	1.2671	0.0202
Protein canopy homolog 4	<i>Cnpy4</i>	1.2667	0.0225
Selenocysteine lyase	<i>Scly</i>	1.2664	0.0035
	<i>Nbeal1</i>	1.2643	0.0138
p21-activated protein kinase-interacting protein 1	<i>Pak1ip1</i>	1.2643	0.0052
Adenylate kinase 2, mitochondrial;Adenylate kinase 2, mitochondrial, N-terminally processed	<i>Ak2</i>	1.2624	0.0025
SNARE-associated protein Snapin	<i>Snapin</i>	1.2598	0.0221
Interleukin-13 receptor subunit alpha-1	<i>Il13ra1</i>	1.2598	0.0002
Multifunctional methyltransferase subunit TRM112-like protein	<i>Trmt112</i>	1.2592	0.0427
Histone deacetylase 2	<i>Hdac2</i>	1.259	0.0066

Immunity-related GTPase family M protein 1	<i>Irgm1</i>	1.2583	0.0311
Hypoxia-inducible factor 1-alpha inhibitor	<i>Hif1an</i>	1.2578	0.0138
Growth arrest and DNA damage-inducible proteins-interacting protein 1	<i>Gadd45gip1</i>	1.2571	0.0121
14-3-3 protein epsilon	<i>Ywhae</i>	1.2566	0.0006
HIV Tat-specific factor 1 homolog	<i>Htatsf1</i>	1.2561	0.0007
	<i>Sgsh</i>	1.2557	0.0417
	<i>Sptan1</i>	1.2556	0.0367
SNW domain-containing protein 1	<i>Snw1</i>	1.2553	0.0137
Protein angel homolog 2	<i>Angel2</i>	1.2552	0.0044
Pre-mRNA-processing factor 17	<i>Cdc40</i>	1.2535	0.0065
Cytosolic Fe-S cluster assembly factor NUBP1	<i>Nubp1</i>	1.2535	0.0024
Scaffold attachment factor B1	<i>Safb</i>	1.2535	0.0294
	<i>Fuk</i>	1.2527	0.0043
Annexin A5	<i>Anxa5</i>	1.2518	0.0402
H-2 class I histocompatibility antigen, D-B alpha chain	<i>H2-D1</i>	1.2518	0.0101
THO complex subunit 5 homolog	<i>Thoc5</i>	1.2508	0.0202
Nucleoside diphosphate-linked moiety X motif 19, mitochondrial	<i>Nudt19</i>	1.2504	0.0008
Isocitrate dehydrogenase [NAD] subunit alpha, mitochondrial	<i>Idh3a</i>	1.2493	0.0301
Kinase suppressor of Ras 1	<i>Ksr1</i>	1.2489	0.007
Junctional adhesion molecule A	<i>F11r</i>	1.2481	0.0034
THO complex subunit 3	<i>Thoc3</i>	1.2481	0.0121
Chloride channel protein;Chloride channel protein 2	<i>Clcn2</i>	1.2478	0.0074
Signal recognition particle 19 kDa protein	<i>Srp19</i>	1.2474	0.036
DNA-directed RNA polymerases I, II, and III subunit RPABC3	<i>Polr2h</i>	1.2471	0.0266
U6 snRNA-associated Sm-like protein LSM8	<i>Lsm8</i>	1.2466	0.0146
Four and a half LIM domains protein 2	<i>Fhl2</i>	1.2464	0.0109
60S ribosomal protein L11	<i>Gm10036;Rpl11</i>	1.246	0.0195
ATP-dependent (S)-NAD(P)H-hydrate dehydratase	<i>Carkd</i>	1.2449	0.015
FAS-associated death domain protein	<i>Fadd</i>	1.2445	0.0279
ES1 protein homolog, mitochondrial	<i>D10Jhu81e</i>	1.2427	0.0182
RNA-binding protein Raly	<i>Raly</i>	1.2414	0.0061
28S ribosomal protein S11, mitochondrial	<i>Mrps11</i>	1.2402	0.0002
39S ribosomal protein L39, mitochondrial	<i>Mrpl39</i>	1.2402	0.0102
Nuclear export mediator factor Nemf	<i>Nemf</i>	1.2397	0.0022
E3 ubiquitin-protein ligase UBR2	<i>Ubr2</i>	1.2395	0.0163
Peptidyl-prolyl cis-trans isomerase;Peptidyl-prolyl cis-trans isomerase H	<i>Ppih</i>	1.2392	0.0033
High affinity cGMP-specific 3,5-cyclic phosphodiesterase 9A	<i>Pde9a</i>	1.2391	0.0094
Vam6/Vps39-like protein	<i>Vps39</i>	1.2381	0.0217
Macrophage-capping protein	<i>Capg</i>	1.2373	0.0285
Polyadenylate-binding protein 1	<i>Pabpc1</i>	1.2369	0.0017
ELKS/Rab6-interacting/CAST family member 1	<i>Erc1</i>	1.2367	0.0263
Nicotinate phosphoribosyltransferase	<i>Naprt</i>	1.2362	0.0127
Vacuolar protein sorting-associated protein 26B	<i>Vps26b</i>	1.236	0.0052

Pre-mRNA-processing-splicing factor 8	<i>Prpf8</i>	1.235	0.0075
THO complex subunit 1	<i>Thoc1</i>	1.2349	0.0089
	<i>Ankhd1</i>	1.2348	0.0149
39S ribosomal protein L4, mitochondrial	<i>Mrpl4</i>	1.2331	0.006
2-5-oligoadenylate synthase-like protein 2	<i>Oasl2</i>	1.2329	0.0182
	<i>Parp3</i>	1.2326	0.0061
ATP-dependent RNA helicase DDX39A	<i>Ddx39a</i>	1.2326	0.001
Transcription elongation factor B polypeptide 1	<i>Tceb1</i>	1.2325	0.0073
28S ribosomal protein S7, mitochondrial	<i>Mrps7</i>	1.2324	0.004
Glycerol-3-phosphate dehydrogenase 1-like protein	<i>Gpd1l</i>	1.2321	0.009
Glycerol kinase	<i>Gyk;Gk</i>	1.2316	0.0156
Retinoid-binding protein 7	<i>Rbp7</i>	1.2314	0.0124
Sorting nexin-14	<i>Snx14</i>	1.2312	0.0168
Ataxin-2	<i>Atxn2</i>	1.2304	0.0004
Splicing factor, proline- and glutamine-rich	<i>Sfpq</i>	1.2298	0.0105
Small nuclear ribonucleoprotein E	<i>Snrpe</i>	1.2289	0.0011
26S proteasome non-ATPase regulatory subunit 2	<i>Psm2</i>	1.2288	0.0015
V-type proton ATPase subunit B, brain isoform	<i>Atp6v1b2</i>	1.2264	0.0013
F-box only protein 22	<i>Fbxo22</i>	1.226	0.0049
Peroxisomal acyl-coenzyme A oxidase 3;Acyl-coenzyme A oxidase	<i>Acox3</i>	1.2257	0.0009
Succinate dehydrogenase [ubiquinone] flavoprotein subunit, mitochondrial	<i>Sdha</i>	1.2253	0.002
Trafficking protein particle complex subunit 4	<i>Trappc4</i>	1.2238	0.0001
E3 ubiquitin-protein ligase AMFR	<i>Amfr</i>	-1.221	0.0003
TBC1 domain family member 22A	<i>Tbc1d22a</i>	-1.224	0.002
Coiled-coil domain-containing protein 93	<i>Ccdc93</i>	-1.225	0.0028
Serine/threonine-protein kinase OSR1	<i>Oxsr1</i>	-1.225	0.0002
Kinesin-1 heavy chain;Kinesin-like protein	<i>Kif5b</i>	-1.225	0.0024
Stromal interaction molecule 2	<i>Stim2</i>	-1.226	0.0002
Dolichol-phosphate mannosyltransferase subunit 1	<i>Dpm1</i>	-1.226	0.0046
Unconventional myosin-VIIa	<i>Myo7a</i>	-1.227	0.0029
Ras-related protein Rab-43	<i>Rab43</i>	-1.227	0.0004
L-aminoadipate-semialdehyde dehydrogenase-phosphopantetheinyl transferase	<i>Aasdhppt</i>	-1.228	0.0004
Dual specificity mitogen-activated protein kinase kinase 4	<i>Map2k4</i>	-1.228	0.0011
Na(+)/H(+) exchange regulatory cofactor NHE-RF4	<i>Pdzd3</i>	-1.228	0.0047
SRSF protein kinase 1	<i>Srpk1</i>	-1.229	0.0063
Guanylate-binding protein 4	<i>Gbp4</i>	-1.229	0.0006
Sodium/potassium-transporting ATPase subunit beta-3	<i>Atp1b3</i>	-1.229	0.0004
Syntaxin-binding protein 2	<i>Stxbp2</i>	-1.23	0.0022
Oxysterol-binding protein 1	<i>Osbp</i>	-1.23	0.0056
Chloride channel CLIC-like protein 1	<i>Clcc1</i>	-1.231	0.0008
Ras-related protein Rab-17	<i>Rab17</i>	-1.231	0.0021
Mitochondrial import inner membrane translocase subunit TIM44	<i>Timm44</i>	-1.231	0.0042
Ubiquinone biosynthesis protein COQ4 homolog, mitochondrial	<i>Coq4</i>	-1.231	0.0002

Transcription initiation factor TFIID subunit 12	<i>Taf12</i>	-1.231	0.0017
Exocyst complex component 2	<i>Exoc2</i>	-1.232	0.0004
Protein kinase C delta type;Protein kinase C delta type regulatory subunit;Protein kinase C delta type catalytic subunit;Protein kinase C	<i>Prkcd</i>	-1.233	0.0107
SPRY domain-containing protein 7	<i>Spryd7</i>	-1.233	0.0129
Protein FAM98A	<i>Fam98a</i>	-1.233	0.0033
FAS-associated factor 1	<i>Faf1</i>	-1.233	0.0035
Protein disulfide-isomerase TMX3	<i>Tmx3</i>	-1.234	0.0001
Immunoglobulin superfamily member 3	<i>Igsf3</i>	-1.234	0.022
ATP-binding cassette sub-family F member 3	<i>Abcf3</i>	-1.234	0.0149
BRCA1-A complex subunit BRE	<i>Bre</i>	-1.234	0.0003
CLIP-associating protein 1	<i>Clasp1</i>	-1.234	0.003
Probable ATP-dependent RNA helicase YTHDC2	<i>Ythdc2</i>	-1.235	0.0005
Serine/threonine-protein kinase 25	<i>Stk25</i>	-1.235	0.004
Rho guanine nucleotide exchange factor 16	<i>Arhgef16</i>	-1.236	0.0217
Ethylmalonyl-CoA decarboxylase	<i>Echdc1</i>	-1.236	0.0126
Serine/threonine-protein kinase WNK2	<i>Wnk2</i>	-1.236	0.011
Ladinin-1	<i>Lad1</i>	-1.236	0.0277
Methylmalonic aciduria type A homolog, mitochondrial	<i>Mmaa</i>	-1.237	0.0069
Rab5 GDP/GTP exchange factor	<i>Rabgef1</i>	-1.237	0.0016
Hormone-sensitive lipase	<i>Lipe</i>	-1.237	0.0051
Transmembrane emp24 domain-containing protein 4	<i>Tmed4</i>	-1.237	0.0079
Protein FAM114A2	<i>Fam114a2</i>	-1.238	0.01
Evolutionarily conserved signaling intermediate in Toll pathway, mitochondrial	<i>Ecsit</i>	-1.238	0.0065
Probable gluconokinase	<i>Idnk</i>	-1.238	0.0012
RWD domain-containing protein 2B	<i>Rwdd2b</i>	-1.238	0.0007
AP-3 complex subunit sigma-1	<i>Ap3s1</i>	-1.238	0.0202
Uncharacterized protein KIAA2013	<i>Kiaa2013</i>	-1.238	0.0026
Guanine nucleotide-binding protein-like 3	<i>Gnl3</i>	-1.239	0.0065
SRA stem-loop-interacting RNA-binding protein, mitochondrial	<i>Slirp</i>	-1.239	0.0066
Annexin A11;Annexin	<i>Anxa11</i>	-1.24	0.0011
Leucine-rich repeat-containing protein 1	<i>Lrrc1</i>	-1.24	0.0086
3-ketodihydrosphingosine reductase	<i>Kdsr</i>	-1.24	0.0187
Ubiquitin-conjugating enzyme E2 G2	<i>Ube2g2</i>	-1.24	0.005
Ubiquitin-conjugating enzyme E2 E1	<i>Ube2e1;Ube2e2</i>	-1.24	0.0015
Exocyst complex component 1	<i>Exoc1</i>	-1.24	0.0014
Forkhead box protein K1	<i>Foxk1</i>	-1.241	0.0289
Endophilin-B1	<i>Sh3glb1</i>	-1.241	0.0022
FAS-associated factor 2	<i>Faf2</i>	-1.241	0.0023
Protein FAM83H	<i>Fam83h</i>	-1.241	0.0313
Endophilin-B2	<i>Sh3glb2</i>	-1.241	0.0188
Chloride channel protein;H(+)/Cl(-) exchange transporter 3	<i>Clcn3</i>	-1.241	0.001
Inositol hexakisphosphate kinase 1	<i>Ip6k1</i>	-1.242	0.0322
ATP-dependent 6-phosphofructokinase, muscle type	<i>Pfkm</i>	-1.242	0.0194

Fermitin family homolog 1	<i>Fermt1</i>	-1.242	0.0007
		-1.242	0.0131
ATP-dependent RNA helicase SUPV3L1, mitochondrial	<i>Supv3l1</i>	-1.243	0.0069
D-3-phosphoglycerate dehydrogenase	<i>Phgdh</i>	-1.243	0.0076
Microtubule-associated protein RP/EB family member 2	<i>Mapre2</i>	-1.243	0.0009
Coiled-coil domain-containing protein 132	<i>Ccdc132</i>	-1.243	0.0143
ATP synthase subunit alpha, mitochondrial;ATP synthase subunit alpha	<i>Atp5a1</i>	-1.243	0.0059
3-phosphoinositide-dependent protein kinase 1	<i>Pdpk1</i>	-1.243	0.0006
Mitochondrial import receptor subunit TOM70	<i>Tomm70a</i>	-1.243	0.018
SWI/SNF complex subunit SMARCC1	<i>Smarcc1</i>	-1.244	0.0131
Vesicle-associated membrane protein 5	<i>Vamp5</i>	-1.244	0.0012
Replication protein A 70 kDa DNA-binding subunit	<i>Rpa1</i>	-1.244	0.0109
Steroid hormone receptor ERR1	<i>Esrra</i>	-1.245	0.0102
Transmembrane and coiled-coil domains protein 1	<i>Tmcc1</i>	-1.245	0.0152
C2 domain-containing protein 2-like	<i>C2cd2l</i>	-1.246	0.0024
Exocyst complex component 6	<i>Exoc6</i>	-1.246	0.0005
Transportin-1	<i>Tnpo1</i>	-1.246	0.0012
NADH dehydrogenase [ubiquinone] 1 alpha subcomplex subunit 3	<i>Ndufa3</i>	-1.246	0.0118
Aflatoxin B1 aldehyde reductase member 2	<i>Akr7a2</i>	-1.246	0.0025
Mothers against decapentaplegic homolog;Mothers against decapentaplegic homolog 1;Mothers against decapentaplegic homolog 5	<i>Smad1;Smad5</i>	-1.246	0.0281
Polymerase delta-interacting protein 2	<i>Poldip2</i>	-1.247	0.0002
Replication protein A 32 kDa subunit	<i>Rpa2</i>	-1.247	0.0008
Nischarin	<i>Nisch</i>	-1.247	0.0218
DNA replication licensing factor MCM2	<i>Mcm2</i>	-1.247	0.0256
OCIA domain-containing protein 1	<i>Ociad1</i>	-1.247	0.0123
Protein transport protein Sec61 subunit alpha isoform 1	<i>Sec61a1</i>	-1.247	0.0492
Twinfilin-1	<i>Twf1</i>	-1.247	0.0015
Cytochrome c oxidase subunit 7A1, mitochondrial	<i>Cox7a1</i>	-1.248	0.0302
Golgi resident protein GCP60	<i>Acbd3</i>	-1.248	0.0029
Protein C19orf12 homolog	<i>1600014C10Rik</i>	-1.248	0.0066
Bifunctional 3-phosphoadenosine 5-phosphosulfate synthase 1;Sulfate adenylyltransferase;Adenylyl-sulfate kinase	<i>Papss1</i>	-1.249	0.0043
Eukaryotic translation initiation factor 3 subunit A	<i>Eif3a</i>	-1.249	0.0523
LisH domain and HEAT repeat-containing protein KIAA1468	<i>2310035C23Rik;Kiaa1468</i>	-1.249	0.0098
Decaprenyl-diphosphate synthase subunit 1	<i>Pdss1</i>	-1.249	0.0031
	<i>BC030870</i>	-1.249	0.0034
28S ribosomal protein S22, mitochondrial	<i>Mrps22</i>	-1.249	0.0019
Cytochrome c oxidase assembly protein COX15 homolog	<i>Cox15</i>	-1.249	0.0327
MMS19 nucleotide excision repair protein homolog	<i>Mms19</i>	-1.25	0.0037

Transcription activator BRG1	<i>Smarca4</i>	-1.25	0.0346
ATP synthase subunit g, mitochondrial	<i>Atp5l</i>	-1.25	0.02
Uridine 5-monophosphate synthase;Orotate phosphoribosyltransferase;Orotidine 5-phosphate decarboxylase	<i>Umps</i>	-1.25	0.0045
Tensin-3	<i>Tns3</i>	-1.25	0.0077
Calcyclin-binding protein	<i>Cacybp</i>	-1.25	0.0181
Spartin	<i>Spg20</i>	-1.251	0.0118
Calnexin	<i>Canx</i>	-1.251	0.0231
Anoctamin-9	<i>Ano9</i>	-1.251	0.0075
Endophilin-A2	<i>Sh3gl1</i>	-1.252	0.0144
GPI transamidase component PIG-S	<i>Pigs</i>	-1.252	0.0011
Mini-chromosome maintenance complex-binding protein	<i>Mcmbp</i>	-1.252	0.0016
Golgi phosphoprotein 3-like	<i>Golph3l</i>	-1.252	0.0024
	<i>Kidins220</i>	-1.253	0.0011
Solute carrier family 12 member 9	<i>Slc12a9</i>	-1.254	0.0044
Junction plakoglobin	<i>Jup</i>	-1.254	0.0012
Vesicle transport protein USE1	<i>Use1</i>	-1.254	0.0007
	<i>Prdm2</i>	-1.254	0.021
Zinc finger protein 598	<i>Znf598</i>	-1.255	0.0125
DNA (cytosine-5)-methyltransferase 1;DNA (cytosine-5)-methyltransferase	<i>Dnmt1</i>	-1.255	0.0372
28S ribosomal protein S33, mitochondrial	<i>Mrps33</i>	-1.255	0.0124
Integrin beta;Integrin beta-6	<i>Itgb6</i>	-1.255	0.0029
Exocyst complex component 7	<i>Exoc7</i>	-1.255	0.0036
Sorting nexin-12	<i>Snx12</i>	-1.255	0.0008
	<i>Golgb1</i>	-1.255	0.0042
Protein NipSnap homolog 1	<i>Nipsnap1</i>	-1.255	0.0058
Vacuolar protein sorting-associated protein 13A	<i>Vps13a</i>	-1.256	0.0022
Msx2-interacting protein	<i>Spen</i>	-1.256	0.022
Vacuolar protein sorting-associated protein 33A	<i>Vps33a</i>	-1.256	0.0004
Pleckstrin homology domain-containing family A member 8	<i>Plekha8</i>	-1.257	0.0117
Putative methyltransferase C9orf114 homolog	<i>D2Wsu81e</i>	-1.258	0.0258
Protein NDRG3	<i>Ndr3</i>	-1.258	0.0004
Exportin-2	<i>Cse1l</i>	-1.258	0.0021
ER membrane protein complex subunit 4	<i>Emc4</i>	-1.258	0.0018
ATP-dependent RNA helicase DDX19A	<i>Ddx19a</i>	-1.258	0.0136
REST corepressor 1	<i>Rcor1</i>	-1.258	0.009
NADH dehydrogenase [ubiquinone] 1 beta subcomplex subunit 4	<i>Ndufb4</i>	-1.258	0.0469
Anion exchange protein;Electrogenic sodium bicarbonate cotransporter 1	<i>Slc4a4</i>	-1.259	0.0005
Phosphatidylinositol 4-kinase type 2-beta	<i>Pi4k2b</i>	-1.259	0.0047
ADP-ribosylation factor 1	<i>Arf1</i>	-1.26	0.0176
Serine/threonine-protein phosphatase 2A 56 kDa regulatory subunit alpha isoform	<i>Ppp2r5a</i>	-1.26	0.0026
NADH dehydrogenase [ubiquinone] 1 alpha subcomplex subunit 11	<i>Ndufa11</i>	-1.26	0.0069
Saccharopine dehydrogenase-like oxidoreductase	<i>Sccpdh</i>	-1.26	0.006

Apoptosis inhibitor 5	<i>Api5</i>	-1.26	0.0036
Arfaptin-2	<i>Arfp2</i>	-1.261	0.0126
Exocyst complex component 3-like protein 4	<i>Exoc3l4</i>	-1.261	0.0282
MAGUK p55 subfamily member 5	<i>Mpp5</i>	-1.261	0.0035
Polypeptide N-acetylgalactosaminyltransferase 4	<i>Galnt4</i>	-1.262	0.0069
5-AMP-activated protein kinase catalytic subunit alpha-2	<i>Prkaa2</i>	-1.262	0.0041
Copper-transporting ATPase 1	<i>Atp7a</i>	-1.263	0.0083
Signal recognition particle subunit SRP72	<i>Srp72</i>	-1.263	0.0034
Uncharacterized protein KIAA1467	<i>Kiaa1467</i>	-1.263	0.0084
Exportin-5	<i>Xpo5</i>	-1.263	0.0111
Bifunctional coenzyme A synthase;Phosphopantetheine adenylyltransferase;Dephospho-CoA kinase	<i>Coasy</i>	-1.264	0.0001
Dolichol-phosphate mannosyltransferase subunit 3	<i>Dpm3</i>	-1.264	0.0001
Protein diaphanous homolog 1	<i>Diap1;Diaph1</i>	-1.264	0.0005
PDZ domain-containing protein 11	<i>Pdzd11</i>	-1.266	0.0001
	<i>Dnm2</i>	-1.266	0.0005
Protein Shroom2	<i>Shroom2</i>	-1.266	0.0113
Leucyl-cystinyl aminopeptidase	<i>Lnpep</i>	-1.266	0.0011
ATP-binding cassette sub-family B member 7, mitochondrial	<i>Abcb7</i>	-1.266	0.0021
Enoyl-CoA delta isomerase 2, mitochondrial	<i>Eci2</i>	-1.266	0.0148
Retinol dehydrogenase 14	<i>Rdh14</i>	-1.266	0.0035
Serine/threonine-protein kinase A-Raf	<i>Araf</i>	-1.267	0.0305
Translin-associated protein X	<i>Tsnax</i>	-1.267	0.0022
Protein CASP	<i>Cux1</i>	-1.268	0.0162
Rab11 family-interacting protein 1	<i>Rab11fip1</i>	-1.268	0.0224
Niban-like protein 1	<i>Fam129b</i>	-1.268	0.002
Tryptophan--tRNA ligase, mitochondrial	<i>Wars2</i>	-1.269	0.0026
Coiled-coil domain-containing protein 184	<i>Ccdc184</i>	-1.269	0.002
Sister chromatid cohesion protein PDS5 homolog B	<i>Pds5b</i>	-1.27	0.0159
Glycogen synthase kinase-3 beta	<i>Gsk3b</i>	-1.27	0.0177
NADH dehydrogenase [ubiquinone] 1 alpha subcomplex assembly factor 3	<i>Ndufaf3</i>	-1.27	0.0018
Mitochondrial ribonuclease P protein 1	<i>Trmt10c</i>	-1.271	0.0009
Alpha-1,3/1,6-mannosyltransferase ALG2	<i>Alg2</i>	-1.271	0.0032
Vitamin D3 receptor	<i>Vdr</i>	-1.271	0.0107
Sulfhydryl oxidase 2	<i>Qsox2</i>	-1.271	0.0075
Cytochrome P450 2S1	<i>Cyp2s1</i>	-1.271	0.0027
Histone acetyltransferase KAT7	<i>Kat7</i>	-1.271	0.0158
Apoptosis-inducing factor 1, mitochondrial	<i>Aifm1</i>	-1.272	0.001
Eukaryotic translation initiation factor 3 subunit E	<i>Eif3e</i>	-1.272	0.0141
Methyl-CpG-binding domain protein 3	<i>Mbd3</i>	-1.272	0.0257
Max-like protein X	<i>Mlx</i>	-1.273	0.0102
Electron transfer flavoprotein-ubiquinone oxidoreductase, mitochondrial	<i>Etfdh</i>	-1.274	0.0026
Structural maintenance of chromosomes protein 2	<i>Smc2</i>	-1.274	0.0099
28S ribosomal protein S31, mitochondrial	<i>Mrps31</i>	-1.274	0.0006
Calcium-binding mitochondrial carrier protein Aralar2	<i>Slc25a13</i>	-1.274	0.0217

Hepatocyte nuclear factor 4-alpha	<i>Hnf4a</i>	-1.274	0.003
Synaptophysin-like protein 1	<i>Sypl;Sypl1</i>	-1.274	0.0147
Developmentally-regulated GTP-binding protein 2	<i>Drg2</i>	-1.274	0.0107
Coiled-coil domain-containing protein 22	<i>Ccdc22</i>	-1.275	0.0021
U2 snRNP-associated SURP motif-containing protein	<i>U2surp</i>	-1.275	0.0011
Ubiquinol-cytochrome-c reductase complex assembly factor 2	<i>Uqcc2</i>	-1.275	0.02
Telomerase-binding protein EST1A	<i>Smg6</i>	-1.276	0.0064
Cyclin-Y	<i>Ccny</i>	-1.276	0.0023
UPF0505 protein C16orf62 homolog	<i>9030624J02Rik</i>	-1.276	0.0003
Activating signal cointegrator 1	<i>Trip4</i>	-1.276	0.003
Transporter;Sodium- and chloride-dependent transporter XTRP3A;Sodium- and chloride-dependent transporter XTRP3B	<i>Slc6a20a;Slc6a20b</i>	-1.276	0.0362
ER membrane protein complex subunit 2	<i>Emc2</i>	-1.276	0.0001
Mitochondrial genome maintenance exonuclease 1	<i>Mgme1</i>	-1.277	0.0005
	<i>Btnl2</i>	-1.277	0.0157
Condensin complex subunit 1	<i>Ncapd2</i>	-1.278	0.0125
Dolichyl-diphosphooligosaccharide--protein glycosyltransferase subunit 1	<i>Rpn1</i>	-1.278	0.0061
Volume-regulated anion channel subunit LRRC8D	<i>Lrrc8d</i>	-1.278	0.0003
Lysine-specific histone demethylase 1A	<i>Kdm1a</i>	-1.278	0.0017
Ubiquitin carboxyl-terminal hydrolase isozyme L5	<i>Uchl5</i>	-1.279	0.0014
Cadherin-related family member 5	<i>Cdhr5</i>	-1.279	0.017
EF-hand calcium-binding domain-containing protein 14	<i>Efcab14</i>	-1.279	0.0317
Sortilin	<i>Sort1</i>	-1.279	0.0079
Methyltransferase-like protein 13	<i>Mettl13</i>	-1.279	0.0015
Chromodomain-helicase-DNA-binding protein 4	<i>Chd4</i>	-1.279	0.0022
Peroxisomal trans-2-enoyl-CoA reductase	<i>Pecr</i>	-1.28	0.0034
CB1 cannabinoid receptor-interacting protein 1	<i>Cnrip1</i>	-1.281	0.0428
Uroporphyrinogen decarboxylase	<i>Urod</i>	-1.281	0.0001
Zinc finger protein 512	<i>Znf512</i>	-1.282	0.0049
ADP-ribosyl cyclase/cyclic ADP-ribose hydrolase 2	<i>Bst1</i>	-1.282	0.0165
Negative elongation factor B	<i>Nelfb</i>	-1.282	0.0012
Basigin	<i>Bsg</i>	-1.282	0.0014
Eukaryotic translation initiation factor 2D	<i>Eif2d</i>	-1.283	0.0023
Serine/threonine-protein phosphatase 2A 56 kDa regulatory subunit epsilon isoform	<i>Ppp2r5e</i>	-1.283	0.0022
Vacuolar protein-sorting-associated protein 25	<i>Vps25</i>	-1.283	0.0006
Angiotensin-converting enzyme;Angiotensin-converting enzyme, soluble form	<i>Ace</i>	-1.283	0.004
	<i>Malrd1</i>	-1.284	0.0123
General vesicular transport factor p115	<i>Uso1</i>	-1.285	0.0002
DDRGK domain-containing protein 1	<i>Ddrgk1</i>	-1.285	0.0281
Autophagy-related protein 2 homolog B	<i>Atg2b</i>	-1.285	0.0072
55 kDa erythrocyte membrane protein	<i>Mpp1</i>	-1.285	0.0007
Clarin-3	<i>Clrn3</i>	-1.285	0.0045
Torsin-1A-interacting protein 2	<i>Tor1aip2</i>	-1.285	0.0019
Extended synaptotagmin-2	<i>Esyt2</i>	-1.286	0.0005

Inner nuclear membrane protein Man1	<i>Lemd3</i>	-1.286	0.0253
Supervillin	<i>Svil</i>	-1.286	0.0139
DNA replication licensing factor MCM4	<i>Mcm4</i>	-1.286	0.0069
COMM domain-containing protein 3	<i>Commd3</i>	-1.287	0.022
Plexin-B2	<i>Plxnb2</i>	-1.287	0.0014
NADH dehydrogenase [ubiquinone] 1 beta subcomplex subunit 6	<i>Ndufb6</i>	-1.287	0.0003
Rho GTPase-activating protein 12	<i>Arhgap12</i>	-1.287	0.0037
Mitochondrial glutamate carrier 1	<i>Slc25a22</i>	-1.287	0.0224
Protein FAM83B	<i>Fam83b</i>	-1.288	0.0022
Serum paraoxonase/arylesterase 2	<i>Pon2</i>	-1.288	0.0084
Ribosomal protein S6 kinase alpha-5	<i>Rps6ka5</i>	-1.288	0.0078
Protein FAM73B	<i>Fam73b</i>	-1.288	0.0123
Switch-associated protein 70	<i>Swap70</i>	-1.288	0.0037
Ubiquitin-protein ligase E3C	<i>Ube3c</i>	-1.288	0.0012
Interferon-induced very large GTPase 1	<i>Gvin1</i>	-1.289	0.0012
Tyrosine-protein kinase STYK1	<i>Styk1</i>	-1.289	0.004
Ubiquitin-fold modifier 1	<i>Ufm1</i>	-1.289	0.0327
ADP-ribosylation factor-like protein 2	<i>Arl2</i>	-1.289	0.0113
ADP-ribosylation factor 5	<i>Arf5</i>	-1.289	0.0094
Serine/threonine-protein kinase 17B	<i>Stk17b</i>	-1.29	0.0039
FYVE, RhoGEF and PH domain-containing protein 4	<i>Fgd4</i>	-1.29	0.0092
Eukaryotic translation initiation factor 3 subunit F	<i>Eif3f</i>	-1.29	0.0005
Adaptin ear-binding coat-associated protein 1	<i>Necap1</i>	-1.292	0.0015
Exocyst complex component 3	<i>Exoc3</i>	-1.292	0.0006
Ras-related protein Rab-24	<i>Rab24</i>	-1.292	0.0006
Guanine nucleotide exchange factor VAV2	<i>Vav2</i>	-1.292	0.0011
GRAM domain-containing protein 1C	<i>Gramd1c</i>	-1.292	0.0004
Magnesium transporter protein 1	<i>Magt1</i>	-1.292	0.0264
Apoptosis regulator BAX	<i>Bax</i>	-1.293	0.0002
Dimethylaniline monooxygenase [N-oxide-forming] 4	<i>Fmo4</i>	-1.293	0.0044
G protein-coupled receptor kinase 6	<i>Grk6</i>	-1.294	0.0326
	<i>Pdzd8</i>	-1.294	0.009
Translocation protein SEC62	<i>Sec62</i>	-1.294	0.0032
Leucine-rich repeat protein SHOC-2	<i>Shoc2</i>	-1.294	0.004
Sister chromatid cohesion protein PDS5 homolog A	<i>Pds5a</i>	-1.295	0.0012
Cytochrome c oxidase assembly factor 3 homolog, mitochondrial	<i>Coa3</i>	-1.295	0.002
Eukaryotic translation initiation factor 4 gamma 2	<i>Eif4g2</i>	-1.296	0.0002
Pleckstrin homology domain-containing family G member 6	<i>Plekhg6</i>	-1.296	0.0001
ATP synthase protein 8	<i>Mtatp8</i>	-1.296	0.0043
Alpha-(1,6)-fucosyltransferase	<i>Fut8</i>	-1.296	0.0008
Tyrosine-protein kinase FRK	<i>Frk</i>	-1.297	0.0028
Transcription initiation factor IIB	<i>Gtf2b</i>	-1.297	0.0017
RAC-alpha serine/threonine-protein kinase	<i>Akt1</i>	-1.297	0.0092
Golgi phosphoprotein 3	<i>Golph3</i>	-1.297	0.0003
	<i>Fmn1</i>	-1.298	0.0292
SH3 domain-binding protein 1	<i>Sh3bp1</i>	-1.298	0.0374
Metal transporter CNNM4	<i>Cnm4</i>	-1.298	0.0001

ATP-binding cassette sub-family B member 10, mitochondrial	<i>Abcb10</i>	-1.298	0.0094
ER membrane protein complex subunit 6	<i>Emc6</i>	-1.299	0.002
Atlastin-3	<i>Atl3</i>	-1.299	0.0027
Zinc finger protein 622	<i>Znf622</i>	-1.299	0.0002
OTU domain-containing protein 4	<i>Otud4</i>	-1.299	0.0124
NADH dehydrogenase [ubiquinone] 1 alpha subcomplex subunit 2	<i>Ndufa2</i>	-1.3	0.0037
Mitochondrial import receptor subunit TOM40 homolog	<i>Tomm40</i>	-1.3	0.0408
Bcl 10-interacting CARD protein		-1.3	0.0006
Nuclear RNA export factor 1	<i>Nxf1</i>	-1.3	0.0031
Ras GTPase-activating-like protein IQGAP2	<i>Iqgap2</i>	-1.301	0.001
Brain-specific angiogenesis inhibitor 1-associated protein 2-like protein 2	<i>Baiap2l2</i>	-1.301	0.0315
Oxysterol-binding protein;Oxysterol-binding protein-related protein 6	<i>Osbp16</i>	-1.301	0.0184
Glycerophosphodiester phosphodiesterase domain-containing protein 1	<i>Gdpd1</i>	-1.301	0.0231
Ubiquitin-conjugating enzyme E2 R2	<i>Ube2r2</i>	-1.301	0.0375
CDGSH iron-sulfur domain-containing protein 3, mitochondrial	<i>Cisd3</i>	-1.302	0.0062
RNA-binding protein 39	<i>Rbm39</i>	-1.302	0.0025
C1GALT1-specific chaperone 1	<i>C1galt1c1</i>	-1.303	0.0014
	<i>Chn2</i>	-1.303	0.0001
Long-chain-fatty-acid--CoA ligase 3	<i>Acs13</i>	-1.303	0.0012
WD and tetratricopeptide repeats protein 1	<i>Wdtdc1</i>	-1.303	0.0277
Upstream-binding protein 1	<i>Ubp1</i>	-1.304	0.0059
Transcription intermediary factor 1-alpha	<i>Trim24</i>	-1.304	0.0308
Rho-associated protein kinase;Rho-associated protein kinase 2	<i>Rock2</i>	-1.304	0.0001
Serine/threonine-protein kinase MRCK gamma	<i>Cdc42bpg</i>	-1.304	0.0182
Chromobox protein homolog 5	<i>Cbx5</i>	-1.304	0.007
Mothers against decapentaplegic homolog;Mothers against decapentaplegic homolog 2	<i>Smad2</i>	-1.304	0.001
GTPase KRas;GTPase KRas, N-terminally processed	<i>Kras</i>	-1.305	0.0001
Lethal(2) giant larvae protein homolog 2	<i>Lgl2</i>	-1.305	0.0009
Proteasome-associated protein ECM29 homolog	<i>Ecm29;AI314180</i>	-1.306	0.0053
Cytosolic 5-nucleotidase 3A	<i>Nt5c3a</i>	-1.306	0.0019
Trafficking protein particle complex subunit 12	<i>Trappc12</i>	-1.307	0.0008
Cytochrome b-c1 complex subunit 1, mitochondrial	<i>Uqcrc1</i>	-1.307	0.0021
Transmembrane protein 165	<i>Tmem165</i>	-1.307	0.0037
cGMP-dependent protein kinase;cGMP-dependent protein kinase 2	<i>Prkg2</i>	-1.308	0.0014
COP9 signalosome complex subunit 7a	<i>Cops7a</i>	-1.308	0.0052
Cytochrome b-c1 complex subunit 8	<i>Uqcrcq</i>	-1.308	0.0051
Angiotensin-converting enzyme 2;Processed angiotensin-converting enzyme 2	<i>Ace2</i>	-1.308	0.0254
Phosphatidylinositol 5-phosphate 4-kinase type-2 gamma	<i>Pip4k2c</i>	-1.309	0.0001

Arylacetylamide deacetylase	<i>Aadac</i>	-1.309	0.0166
Copine-2	<i>Cpne2</i>	-1.31	0.0083
Thioredoxin-related transmembrane protein 1	<i>Tmx1</i>	-1.31	0.0028
Vacuolar protein sorting-associated protein 4A	<i>Vps4a</i>	-1.31	0.0092
Ras-related protein Rab-10	<i>Rab10</i>	-1.311	0.0047
Endoplasmic reticulum-Golgi intermediate compartment protein 2	<i>Ergic2</i>	-1.311	0.0003
PC4 and SFRS1-interacting protein	<i>Psip1</i>	-1.312	0.0478
		-1.312	0.0028
Ubiquitin carboxyl-terminal hydrolase;Ubiquitin carboxyl-terminal hydrolase 3	<i>Usp3</i>	-1.312	0.0108
Histone deacetylase complex subunit SAP18	<i>Gm10094;Sap18</i>	-1.313	0.0002
Unconventional myosin-IXb	<i>Myo9b</i>	-1.313	0.0164
Ataxin-10	<i>Atxn10</i>	-1.313	0.0008
Signal recognition particle receptor subunit alpha	<i>Srpr</i>	-1.314	0.0014
Retinol dehydrogenase 13	<i>Rdh13</i>	-1.314	0.0044
GH3 domain-containing protein	<i>Ghdc</i>	-1.314	0.0021
Protein SCO2 homolog, mitochondrial	<i>Sco2</i>	-1.314	0.0019
DnaJ homolog subfamily C member 10	<i>Dnajc10</i>	-1.315	0.0059
RWD domain-containing protein 1	<i>Rwdd1</i>	-1.316	0.0311
MOB kinase activator 1A;MOB kinase activator 1B	<i>Mob1b;Mob1a</i>	-1.316	0.0075
Probable N-acetyltransferase CML5	<i>Cml5</i>	-1.316	0.0402
Mitochondrial import receptor subunit TOM22 homolog	<i>Tomm22</i>	-1.317	0.0008
Large neutral amino acids transporter small subunit 4	<i>Slc43a2</i>	-1.317	0.0129
Guanine nucleotide-binding protein G(i) subunit alpha-2	<i>Gnai2</i>	-1.317	0.0001
5-AMP-activated protein kinase subunit gamma-1	<i>Prkag1</i>	-1.317	0.0116
Growth factor receptor-bound protein 7	<i>Grb7</i>	-1.317	0.015
Ras GTPase-activating-like protein IQGAP1	<i>Iqgap1</i>	-1.318	0.0005
Calcium and integrin-binding protein 1	<i>Cib1</i>	-1.319	0.0249
Cytochrome c oxidase subunit NDUFA4	<i>Ndufa4</i>	-1.319	0.0033
Probable rRNA-processing protein EBP2	<i>Ebna1bp2</i>	-1.319	0.0201
Coxsackievirus and adenovirus receptor homolog	<i>Cxadr</i>	-1.32	0.0041
	<i>Gcn1l1</i>	-1.32	0.0061
Serine incorporator 3	<i>Serinc3</i>	-1.32	0.0482
Tubulin beta-5 chain	<i>Tubb5</i>	-1.321	0.0025
Secretory carrier-associated membrane protein 1	<i>Scamp1</i>	-1.321	0.0001
Nicotinamide/nicotinic acid mononucleotide adenylyltransferase 3	<i>Nmnat3</i>	-1.321	0.0022
Mitochondrial calcium uniporter regulator 1	<i>Mcur1</i>	-1.321	0.0029
Sodium/hydrogen exchanger	<i>Slc9a2</i>	-1.321	0.0065
Integrin alpha-V;Integrin alpha-V heavy chain;Integrin alpha-V light chain	<i>Itgav</i>	-1.322	0.0018
Optic atrophy 3 protein homolog	<i>Opa3</i>	-1.322	0.0045
Insulin-like growth factor 2 mRNA-binding protein 2	<i>Igf2bp2</i>	-1.322	0.0016
Programmed cell death protein 2	<i>Pdcd2</i>	-1.322	0.0083
Cyclin-dependent kinase 2	<i>Cdk2</i>	-1.323	0.0123
Bifunctional apoptosis regulator	<i>Bfar</i>	-1.323	0.0098

NADH dehydrogenase [ubiquinone] flavoprotein 1, mitochondrial	<i>Ndufv1</i>	-1.323	0.0065
	<i>Dnajc13</i>	-1.324	0.0001
Oxysterol-binding protein;Oxysterol-binding protein-related protein 11	<i>Osbpl11</i>	-1.324	0.043
Motile sperm domain-containing protein 2	<i>Mospd2</i>	-1.325	0.0026
Type 2 lactosamine alpha-2,3-sialyltransferase	<i>St3gal6</i>	-1.327	0.0002
Very long-chain specific acyl-CoA dehydrogenase, mitochondrial	<i>Acadvl</i>	-1.327	0.0082
O-acetyl-ADP-ribose deacetylase MACROD1	<i>Macrod1</i>	-1.327	0.0075
Partitioning defective 6 homolog beta	<i>Pard6b</i>	-1.328	0.0032
CAAX prenyl protease 1 homolog	<i>Zmpste24</i>	-1.328	0.0136
Cytochrome P450 3A25	<i>Cyp3a25;Cyp3a59</i>	-1.328	0.0395
NADH dehydrogenase [ubiquinone] iron-sulfur protein 2, mitochondrial	<i>Ndufs2</i>	-1.328	0.0011
MARVEL domain-containing protein 2	<i>Marveld2</i>	-1.329	0.0018
Cytoskeleton-associated protein 5	<i>Ckap5</i>	-1.329	0.0034
Leukocyte surface antigen CD47	<i>Cd47</i>	-1.33	0.0005
Advillin	<i>Avil</i>	-1.33	0.0186
Charged multivesicular body protein 7	<i>Chmp7</i>	-1.33	0.0111
UPF0668 protein C10orf76 homolog		-1.33	0.0026
Cytochrome P450 20A1	<i>Cyp20a1</i>	-1.331	0.0041
	<i>Numa1</i>	-1.331	0.0108
Calcium uptake protein 1, mitochondrial	<i>Micu1</i>	-1.331	0.0026
Multivesicular body subunit 12A	<i>Mvb12a</i>	-1.331	0.007
Translocon-associated protein subunit alpha	<i>Ssr1</i>	-1.332	0.0004
N-alpha-acetyltransferase 20	<i>Naa20</i>	-1.332	0.0001
Carbonyl reductase [NADPH] 3	<i>Cbr3</i>	-1.332	0.0262
NADH dehydrogenase [ubiquinone] 1 alpha subcomplex assembly factor 4	<i>Ndufaf4</i>	-1.333	0.001
	<i>Ppp2r5d</i>	-1.333	0.0007
Vacuolar protein sorting-associated protein 51 homolog	<i>Vps51</i>	-1.333	0.0011
Dnaj homolog subfamily B member 6	<i>Dnajb6</i>	-1.333	0.0012
	<i>Slc2a9</i>	-1.334	0.0058
ATP-binding cassette sub-family F member 2	<i>Abcf2</i>	-1.334	0.0068
Tetratricopeptide repeat protein 9C	<i>Ttc9c</i>	-1.334	0.0017
Transmembrane emp24 domain-containing protein 5	<i>Tmed5</i>	-1.334	0.0012
NACHT, LRR and PYD domains-containing protein 6	<i>Nlrp6</i>	-1.334	0.0111
Sideroflexin-1	<i>Sfxn1</i>	-1.335	0.0124
ADP-ribosylation factor 4	<i>Arf4</i>	-1.335	0.006
	<i>Pigg</i>	-1.336	0.0009
Dynammin-3	<i>Dnm3</i>	-1.336	0.002
Glucocorticoid receptor	<i>Nr3c1</i>	-1.336	0.0111
Probable arginine--tRNA ligase, mitochondrial	<i>Rars2</i>	-1.336	0.0019
Epidermal growth factor receptor kinase substrate 8-like protein 3	<i>Eps8l3</i>	-1.336	0.0316
Cytosolic phospholipase A2;Phospholipase A2;Lysophospholipase	<i>Pla2g4a</i>	-1.336	0.0089
Tight junction protein ZO-3	<i>Tjp3</i>	-1.336	0.0001

PDZ domain-containing protein GIPC2	<i>Gipc2</i>	-1.337	0.0066
Glutamyl aminopeptidase	<i>Enpep</i>	-1.338	0.0239
Cell surface A33 antigen	<i>Gpa33</i>	-1.338	0.002
Mitochondrial import receptor subunit TOM6 homolog	<i>Tomm6</i>	-1.338	0.002
Eyes absent homolog;Eyes absent homolog 3	<i>Eya3</i>	-1.338	0.0169
UBX domain-containing protein 6	<i>Ubxn6</i>	-1.339	0.0011
Transmembrane protein 109	<i>Tmem109</i>	-1.339	0.0011
Oxysterol-binding protein;Oxysterol-binding protein-related protein 3	<i>Osbp13</i>	-1.339	0.004
Aldehyde dehydrogenase;Fatty aldehyde dehydrogenase	<i>Aldh3a2</i>	-1.34	0.0197
Fermitin family homolog 2	<i>Fermt2</i>	-1.34	0.0284
Formin-binding protein 1-like	<i>Fnbp1l</i>	-1.34	0.0107
Syntaxin-binding protein 1	<i>Stxbp1</i>	-1.341	0.0025
Dual specificity mitogen-activated protein kinase kinase 2	<i>Map2k2</i>	-1.341	0.0003
PRA1 family protein 3	<i>Arl6ip5</i>	-1.341	0.0417
N-alpha-acetyltransferase 11	<i>Gm16286;Naa11</i>	-1.342	0.0087
Transmembrane protein 87A	<i>Tmem87a</i>	-1.342	0.0001
PDZ domain-containing protein GIPC1	<i>Gipc1</i>	-1.342	0.0608
Ras-related protein Rab-8A	<i>Rab8a</i>	-1.342	0.0001
	<i>Cyp4f13</i>	-1.342	0.0047
Synaptosomal-associated protein;Synaptosomal-associated protein 23	<i>Snap23</i>	-1.343	0.0038
	<i>Slc35d1</i>	-1.343	0.0365
	<i>Mettl7a1</i>	-1.344	0.028
Guanine nucleotide-binding protein G(s) subunit alpha isoforms short;Guanine nucleotide-binding protein G(s) subunit alpha isoforms XLas	<i>Gnas</i>	-1.344	0.0018
Transient receptor potential cation channel subfamily M member 4	<i>Trpm4</i>	-1.344	0.0001
Membrane magnesium transporter 1	<i>Mmgt1</i>	-1.345	0.0019
Prenylcysteine oxidase	<i>Pcyox1</i>	-1.345	0.0014
DNA mismatch repair protein Msh2	<i>Msh2</i>	-1.345	0.0052
Methylsterol monooxygenase 1	<i>Msmo1</i>	-1.345	0.0413
Leucine-rich repeat-containing protein 57	<i>Lrrc57</i>	-1.347	0.0133
NADH dehydrogenase [ubiquinone] 1 alpha subcomplex subunit 10, mitochondrial	<i>Ndufa10</i>	-1.348	0.0007
Ras-related protein Rab-35	<i>Rab35</i>	-1.348	0.0011
BTB/POZ domain-containing protein KCTD12	<i>Kctd12</i>	-1.348	0.0023
Mitofusin-2	<i>Mfn2</i>	-1.348	0.0002
Mitogen-activated protein kinase 3;Mitogen-activated protein kinase	<i>Mapk3</i>	-1.348	0.0002
NADH-cytochrome b5 reductase 3;NADH-cytochrome b5 reductase 3 membrane-bound form;NADH-cytochrome b5 reductase 3 soluble form;NADH-cytochrome b5 reductase	<i>Cyb5r3</i>	-1.349	0.023
Interleukin-18	<i>Il18</i>	-1.349	0.022
GTP-binding protein Rheb	<i>Rheb</i>	-1.349	0.0002
Rho-related GTP-binding protein RhoG	<i>Rhog</i>	-1.349	0.0037

E3 ubiquitin-protein ligase NEDD4-like	<i>Nedd4l</i>	-1.35	0.0002
Mitochondrial Rho GTPase 2	<i>Rhot2</i>	-1.35	0.0013
Cyclin-dependent kinase 11B	<i>Cdk11b</i>	-1.35	0.0041
Integrin alpha-6;Integrin alpha-6 heavy chain;Integrin alpha-6 light chain	<i>Itga6</i>	-1.351	0.0001
Leucine-rich repeat-containing protein 47	<i>Lrrc47</i>	-1.351	0.0006
Nostrin	<i>Nostrin</i>	-1.351	0.0164
Lamin-B2	<i>Lmnb2</i>	-1.351	0.0045
Transmembrane protein 209	<i>Tmem209</i>	-1.351	0.0108
Glutamine-rich protein 1	<i>Qrich1</i>	-1.352	0.0051
Engulfment and cell motility protein 3	<i>Elmo3</i>	-1.352	0.0032
	<i>Sis</i>	-1.353	0.0037
Dynamin-like 120 kDa protein, mitochondrial;Dynamin-like 120 kDa protein, form S1	<i>Opa1</i>	-1.353	0.0013
Probable lysosomal cobalamin transporter	<i>Lmbrd1</i>	-1.353	0.007
TBC1 domain family member 9B	<i>Tbc1d9b</i>	-1.355	0.0011
Bifunctional polynucleotide phosphatase/kinase;Polynucleotide 3-phosphatase;Polynucleotide 5-hydroxyl-kinase	<i>Pnkp</i>	-1.355	0.0119
SWI/SNF-related matrix-associated actin-dependent regulator of chromatin subfamily B member 1	<i>Smarchb1</i>	-1.355	0.0004
Annexin A7	<i>Anxa7</i>	-1.356	0.0006
Caseinolytic peptidase B protein homolog	<i>Clpb</i>	-1.357	0.0005
NADH dehydrogenase [ubiquinone] 1 beta subcomplex subunit 3	<i>Ndufb3</i>	-1.358	0.0108
Synaptobrevin homolog YKT6	<i>Ykt6</i>	-1.358	0.0117
DNA ligase;DNA ligase 1	<i>Lig1</i>	-1.358	0.02
Protein numb homolog	<i>Numb</i>	-1.359	0.0001
E3 SUMO-protein ligase PIAS1;E3 SUMO-protein ligase PIAS2	<i>Pias1;Pias2</i>	-1.359	0.0085
Protein phosphatase methylesterase 1	<i>Ppme1</i>	-1.359	0.0004
Dystrophin	<i>Dmd</i>	-1.359	0.0119
Galectin;Galectin-3	<i>Lgals3</i>	-1.359	0.0043
Transcription initiation factor TFIID subunit 9B;Transcription initiation factor TFIID subunit 9	<i>Taf9;Taf9b</i>	-1.359	0.001
Bone marrow stromal antigen 2	<i>Bst2</i>	-1.36	0.0053
Unconventional myosin-Vb	<i>Myo5b</i>	-1.36	0.0001
SOSS complex subunit C	<i>Inip</i>	-1.361	0.0075
Calcium-binding mitochondrial carrier protein Aralar1	<i>Slc25a12</i>	-1.361	0.0006
	<i>Ugt2b34</i>	-1.361	0.0218
Syntaxin-4	<i>Stx4</i>	-1.363	0.0001
Cytochrome b-c1 complex subunit 2, mitochondrial	<i>Uqcrc2</i>	-1.364	0.0004
Unconventional myosin-Ic	<i>Myo1c</i>	-1.364	0.0038
Transcriptional regulator ATRX	<i>Atrx</i>	-1.365	0.0064
UDP-glucuronosyltransferase 1-7C	<i>Ugt1a7c</i>	-1.365	0.0469
Phospholipid-transporting ATPase IC	<i>Atp8b1</i>	-1.365	0.0001
Peroxisomal membrane protein 11B	<i>Pex11b</i>	-1.366	0.0117
Coiled-coil domain-containing protein 127	<i>Ccdc127</i>	-1.366	0.0022

Protein scribble homolog	<i>Scrib</i>	-1.366	0.0015
Coiled-coil and C2 domain-containing protein 1A	<i>Cc2d1a</i>	-1.366	0.0018
Probable glutamate--tRNA ligase, mitochondrial	<i>Ears2</i>	-1.368	0.0001
Ras GTPase-activating protein-binding protein 1	<i>G3bp1</i>	-1.368	0.0005
Phosphoinositide phospholipase C;1-phosphatidylinositol 4,5-bisphosphate phosphodiesterase delta-1	<i>Plcd1</i>	-1.368	0.0001
Normal mucosa of esophagus-specific gene 1 protein	<i>AA467197;Nmes1</i>	-1.369	0.0029
Protein lin-7 homolog C	<i>Lin7c</i>	-1.37	0.0006
Solute carrier family 25 member 45	<i>Slc25a45</i>	-1.371	0.0459
Dedicator of cytokinesis protein 1	<i>Dock1</i>	-1.371	0.0003
Tubulin alpha chain-like 3	<i>Tubal3</i>	-1.372	0.0046
Sulfotransferase family cytosolic 1B member 1	<i>Sult1b1</i>	-1.372	0.0004
Proline-serine-threonine phosphatase-interacting protein 2	<i>Pstpip2</i>	-1.372	0.011
Arf-GAP with dual PH domain-containing protein 2	<i>Adap2</i>	-1.373	0.0028
L-seryl-tRNA(Sec) kinase	<i>Pstk</i>	-1.373	0.0002
	<i>Gstt3</i>	-1.373	0.0012
Ras-related C3 botulinum toxin substrate 1;Ras-related C3 botulinum toxin substrate 3	<i>Rac1;Rac3</i>	-1.374	0.0134
Protein FAM210A	<i>Fam210a</i>	-1.375	0.0025
Signal recognition particle subunit SRP68	<i>Srp68</i>	-1.375	0.0007
ADP-ribosylation factor GTPase-activating protein 1	<i>Arfgap1</i>	-1.375	0.0331
	<i>Arhgef11</i>	-1.375	0.001
Poly(A) RNA polymerase, mitochondrial	<i>Mtpap</i>	-1.377	0.0022
Adiponectin receptor protein 2	<i>Adipor2</i>	-1.377	0.0092
Peripheral plasma membrane protein CASK	<i>Cask</i>	-1.377	0.0001
Pyridoxal-dependent decarboxylase domain-containing protein 1	<i>Pdxdc1</i>	-1.377	0.0023
Band 4.1-like protein 2	<i>Epb412</i>	-1.378	0.0085
LIM domain kinase 2	<i>Limk2</i>	-1.378	0.0047
Death-associated protein kinase 3	<i>Dapk3</i>	-1.378	0.0058
Chromosome transmission fidelity protein 18 homolog	<i>Chtf18</i>	-1.378	0.0099
Dual specificity mitogen-activated protein kinase kinase 1	<i>Map2k1</i>	-1.379	0.0002
NADH-ubiquinone oxidoreductase 75 kDa subunit, mitochondrial	<i>Ndufs1</i>	-1.379	0.0013
NADH dehydrogenase [ubiquinone] 1 alpha subcomplex subunit 5	<i>Ndufa5</i>	-1.379	0.0001
Endoplasmic reticulum-Golgi intermediate compartment protein 3	<i>Ergic3</i>	-1.38	0.0057
Mitofusin-1	<i>Mfn1</i>	-1.38	0.0001
N-alpha-acetyltransferase 40	<i>Naa40</i>	-1.381	0.0242
Protein kinase C and casein kinase substrate in neurons protein 2	<i>Pacsin2</i>	-1.381	0.002
DENN domain-containing protein 2D	<i>Dennd2d</i>	-1.381	0.0047
Zinc transporter SLC39A7	<i>Slc39a7</i>	-1.382	0.0045
Ras-related protein Ral-A	<i>Rala</i>	-1.382	0.0002

Coiled-coil domain-containing protein 90B, mitochondrial	<i>Ccdc90b</i>	-1.382	0.0103
ATP-binding cassette sub-family G member 8	<i>Abcg8</i>	-1.383	0.0022
Conserved oligomeric Golgi complex subunit 5	<i>Cog5</i>	-1.383	0.0049
Dnal homolog subfamily C member 5	<i>Dnajc5</i>	-1.383	0.0001
General transcription factor II-I	<i>Gtf2i</i>	-1.384	0.0017
Activating signal cointegrator 1 complex subunit 1	<i>Ascc1</i>	-1.384	0.0042
	<i>Baz2b</i>	-1.384	0.0295
Monocarboxylate transporter 1	<i>Slc16a1</i>	-1.384	0.0052
Glycosaminoglycan xylosylkinase	<i>Fam20b</i>	-1.384	0.0001
Putative ATP-dependent RNA helicase DHX30	<i>Dhx30</i>	-1.384	0.0054
UDP-glucuronosyltransferase 2A3	<i>Ugt2a3</i>	-1.386	0.001
MAGUK p55 subfamily member 7	<i>Mpp7</i>	-1.386	0.0041
Eukaryotic peptide chain release factor subunit 1	<i>Etf1</i>	-1.386	0.0091
Signal recognition particle 54 kDa protein	<i>Srp54;Srp54c</i>	-1.387	0.0003
Prostaglandin E synthase 2;Prostaglandin E synthase 2 truncated form	<i>Ptges2</i>	-1.388	0.001
Plakophilin-3	<i>Pkp3</i>	-1.388	0.0015
Sorting nexin-2	<i>Snx2</i>	-1.388	0.0005
TNF receptor-associated factor 4	<i>Traf4</i>	-1.389	0.0049
Complement component receptor 1-like protein	<i>Cr1l</i>	-1.389	0.0008
RNA polymerase-associated protein RTF1 homolog	<i>Rtf1</i>	-1.389	0.0225
Catechol O-methyltransferase domain-containing protein 1	<i>Comtd1</i>	-1.389	0.0022
Methylmalonate-semialdehyde dehydrogenase [acylating], mitochondrial	<i>Aldh6a1</i>	-1.389	0.0003
Unconventional myosin-VIIb	<i>Myo7b</i>	-1.39	0.0059
WW domain-binding protein 2	<i>Wbp2</i>	-1.39	0.0152
Transmembrane emp24 domain-containing protein 2	<i>Tmed2</i>	-1.39	0.0031
Sphingomyelin phosphodiesterase 3	<i>Smpd3</i>	-1.391	0.0001
N-acetylgalactosaminyltransferase 7	<i>Galnt7</i>	-1.391	0.0003
Ribonuclease H2 subunit A;Ribonuclease	<i>Rnaseh2a</i>	-1.391	0.0017
Vasodilator-stimulated phosphoprotein	<i>Vasp</i>	-1.391	0.0043
Membrane-associated progesterone receptor component 1	<i>Pgrmc1</i>	-1.392	0.0012
Protein disulfide-isomerase A5	<i>Pdia5</i>	-1.392	0.0165
Lysophosphatidic acid receptor 1	<i>Lpar1</i>	-1.392	0.0026
Retinol dehydrogenase 7	<i>Rdh7</i>	-1.392	0.0187
Transmembrane protein 186	<i>Tmem186</i>	-1.393	0.0273
Vasoactive intestinal polypeptide receptor 1	<i>Vipr1</i>	-1.394	0.0018
Phospholipase D1	<i>Pld1</i>	-1.394	0.0001
Presenilins-associated rhomboid-like protein, mitochondrial;P-beta	<i>Parl</i>	-1.395	0.0113
Guanine nucleotide-binding protein subunit alpha-13	<i>Gna13</i>	-1.396	0.0001
Chromodomain-helicase-DNA-binding protein 8;Chromodomain-helicase-DNA-binding protein 9	<i>Chd8;Chd9</i>	-1.396	0.0097
Methyltransferase-like protein;Methyltransferase-like protein 16	<i>Mettl16</i>	-1.396	0.0098
Delta(24)-sterol reductase	<i>Dhcr24</i>	-1.397	0.0048

Solute carrier family 25 member 51	<i>Slc25a51</i>	-1.397	0.0151
TLD domain-containing protein 1	<i>Tldc1</i>	-1.398	0.0051
Ras-responsive element-binding protein 1	<i>Rreb1</i>	-1.399	0.0031
T-box transcription factor TBX3	<i>Tbx3</i>	-1.4	0.0115
FERM, RhoGEF and pleckstrin domain-containing protein 2	<i>Farp2</i>	-1.4	0.0016
Growth hormone-regulated TBC protein 1	<i>Grtp1</i>	-1.401	0.0023
Neutral and basic amino acid transport protein rBAT	<i>Slc3a1</i>	-1.401	0.0028
Probable ATP-dependent RNA helicase DDX6	<i>Ddx6</i>	-1.401	0.0025
Alpha-actinin-1	<i>Actn1</i>	-1.401	0.0033
Insulin receptor;Insulin receptor subunit alpha;Insulin receptor subunit beta	<i>Insr</i>	-1.401	0.0001
Sorting nexin-6;Sorting nexin-6, N-terminally processed	<i>Snx6</i>	-1.402	0.0019
Cytoskeleton-associated protein 4	<i>Ckap4</i>	-1.402	0.0024
Rho GTPase-activating protein 27	<i>Arhgap27</i>	-1.403	0.0002
Up-regulated during skeletal muscle growth protein 5	<i>Usmg5</i>	-1.404	0.0007
Immediate early response 3-interacting protein 1	<i>Hdhd2;Ier3ip1;Gm10784</i>	-1.404	0.0027
STE20-like serine/threonine-protein kinase	<i>Slk</i>	-1.405	0.0004
Developmentally-regulated GTP-binding protein 1	<i>Drg1</i>	-1.406	0.0025
Mitochondrial dicarboxylate carrier	<i>Slc25a10</i>	-1.407	0.0099
Heterogeneous nuclear ribonucleoprotein M	<i>Hnrnpm</i>	-1.407	0.0095
NADH dehydrogenase [ubiquinone] 1 beta subcomplex subunit 9	<i>Ndufb9</i>	-1.407	0.0011
Abhydrolase domain-containing protein 4	<i>Abhd4</i>	-1.407	0.0042
Prohibitin	<i>Phb</i>	-1.408	0.001
Sulfotransferase 1 family member D1	<i>Sult1d1</i>	-1.409	0.0042
Peroxisomal biogenesis factor 3	<i>Pex3</i>	-1.41	0.003
ADP-ribosylation factor GTPase-activating protein 3	<i>Arfgap3</i>	-1.41	0.0005
Ribosomal protein S6 kinase;Ribosomal protein S6 kinase alpha-1	<i>Rps6ka1</i>	-1.411	0.0007
Interferon regulatory factor 2-binding protein 1	<i>Irf2bp1</i>	-1.411	0.0001
	<i>Myo6</i>	-1.412	0.0002
Pre-mRNA-splicing factor CWC22 homolog	<i>Cwc22;Gm13695;Gm13697</i>	-1.412	0.0084
RPA-interacting protein	<i>Rpain</i>	-1.412	0.0005
Serine/threonine-protein kinase TAO3	<i>Taok3</i>	-1.412	0.0005
Mortality factor 4-like protein 1	<i>Morf4l1</i>	-1.412	0.0003
DnaJ homolog subfamily C member 9	<i>Dnajc9</i>	-1.413	0.001
Alpha/beta hydrolase domain-containing protein 11	<i>Abhd11</i>	-1.414	0.0001
Mortality factor 4-like protein 2	<i>Morf4l2</i>	-1.415	0.0014
NADH dehydrogenase [ubiquinone] 1 beta subcomplex subunit 5, mitochondrial	<i>Ndufb5</i>	-1.416	0.0059
Apoptosis facilitator Bcl-2-like protein 14	<i>Bcl2l14</i>	-1.416	0.0008
NADH dehydrogenase [ubiquinone] 1 alpha subcomplex subunit 12	<i>Ndufa12</i>	-1.417	0.0006

DCC-interacting protein 13-alpha	<i>Appl1</i>	-1.418	0.0001
Galectin-4	<i>Lgals4</i>	-1.418	0.0045
Cell cycle control protein 50B	<i>Tmem30b</i>	-1.418	0.0002
NADH dehydrogenase [ubiquinone] 1 alpha subcomplex subunit 1	<i>Ndufa1</i>	-1.418	0.0024
RNA-binding protein 10	<i>Rbm10</i>	-1.42	0.0257
Gastric intrinsic factor	<i>Gif</i>	-1.42	0.0103
Band 4.1-like protein 5	<i>Epb415</i>	-1.42	0.0001
Phospholipase DDHD1	<i>Ddhd1</i>	-1.422	0.0041
SWI/SNF-related matrix-associated actin-dependent regulator of chromatin subfamily A member 5	<i>Smarca5</i>	-1.422	0.0059
SH2 domain-containing protein 4A	<i>Sh2d4a</i>	-1.422	0.002
DNA helicase INO80	<i>Ino80</i>	-1.422	0.0282
Paraplegin	<i>Spg7</i>	-1.422	0.0001
Erlin-1	<i>Erlin1</i>	-1.422	0.0042
[3-methyl-2-oxobutanoate dehydrogenase [lipoamide]] kinase, mitochondrial	<i>Bckdk</i>	-1.422	0.0001
NAD-dependent protein deacetylase sirtuin-3	<i>Sirt3</i>	-1.423	0.001
NADH dehydrogenase [ubiquinone] iron-sulfur protein 3, mitochondrial	<i>Ndufs3</i>	-1.424	0.0001
ATP-binding cassette sub-family A member 3	<i>Abca3</i>	-1.424	0.0061
Protein LSM14 homolog A	<i>Lsm14a</i>	-1.424	0.0001
Ras-related protein Ral-B	<i>Ralb</i>	-1.425	0.0015
SH3 domain-containing protein 21	<i>Sh3d21</i>	-1.426	0.0116
StAR-related lipid transfer protein 4	<i>Stard4</i>	-1.427	0.0018
Selenoprotein T	<i>Selt</i>	-1.427	0.0035
MOB kinase activator 2	<i>Mob2</i>	-1.427	0.0015
Programmed cell death protein 4	<i>Pdcd4</i>	-1.428	0.0076
Bcl-2 homologous antagonist/killer	<i>Bak1</i>	-1.429	0.001
Aspartyl/asparaginyl beta-hydroxylase	<i>Asph</i>	-1.429	0.0001
Prostamide/prostaglandin F synthase	<i>Fam213b</i>	-1.429	0.0051
Nucleoporin NDC1	<i>Ndc1</i>	-1.431	0.0149
Hypermethylated in cancer 2 protein	<i>Hic2</i>	-1.432	0.002
DNA mismatch repair protein Msh6	<i>Msh6</i>	-1.432	0.0008
Sortilin-related receptor	<i>Sorl1</i>	-1.432	0.0011
Flotillin-2	<i>Flot2</i>	-1.432	0.0442
NADH dehydrogenase [ubiquinone] flavoprotein 2, mitochondrial	<i>Ndufv2</i>	-1.435	0.0031
Pyrroline-5-carboxylate reductase 2	<i>Pycr2</i>	-1.435	0.0001
Dihydroorotate dehydrogenase (quinone), mitochondrial	<i>Dhodh</i>	-1.436	0.0003
Golgi integral membrane protein 4	<i>Golim4</i>	-1.437	0.0002
Nuclear prelamin A recognition factor	<i>Narf</i>	-1.437	0.001
Transmembrane emp24 domain-containing protein 3	<i>Tmed3</i>	-1.437	0.033
Multifunctional protein ADE2;Phosphoribosylaminoimidazole-succinocarboxamide synthase;Phosphoribosylaminoimidazole carboxylase	<i>Paics</i>	-1.438	0.006

Rho GTPase-activating protein 1	<i>Arhgap1</i>	-1.438	0.0005
ATP synthase F(0) complex subunit B1, mitochondrial	<i>Atp5f1</i>	-1.439	0.0031
NADH dehydrogenase [ubiquinone] iron-sulfur protein 6, mitochondrial	<i>Ndufs6</i>	-1.439	0.0085
NADH dehydrogenase [ubiquinone] 1 alpha subcomplex subunit 7	<i>Ndufa7</i>	-1.439	0.0011
Coiled-coil domain-containing protein 47	<i>Ccdc47</i>	-1.44	0.0001
Protein 4.1	<i>Epb4.1;Epb41</i>	-1.441	0.0006
AP-3 complex subunit beta-1	<i>Ap3b1</i>	-1.441	0.0147
Solute carrier family 12 member 7	<i>Slc12a7</i>	-1.442	0.0001
Laminin subunit beta-1	<i>Lamb1</i>	-1.443	0.0016
Probable ATP-dependent RNA helicase DDX17	<i>Ddx17</i>	-1.443	0.0013
MICOS complex subunit Mic27	<i>Apool</i>	-1.443	0.0007
Malignant T-cell-amplified sequence 1	<i>Mcts1</i>	-1.443	0.0299
Carboxypeptidase E	<i>Cpe</i>	-1.443	0.0046
Rho GTPase-activating protein 17	<i>Arhgap17</i>	-1.444	0.0022
Ephexin-1	<i>Ngef</i>	-1.446	0.0005
Nuclease EXOG, mitochondrial	<i>Exog</i>	-1.446	0.0001
Choline transporter-like protein 4	<i>Slc44a4</i>	-1.447	0.0024
Transmembrane emp24 domain-containing protein 9	<i>Tmed9</i>	-1.448	0.0011
Helicase-like transcription factor	<i>Hltf</i>	-1.449	0.0093
CDGSH iron-sulfur domain-containing protein 2	<i>Cisd2</i>	-1.449	0.0038
Fatty-acid amide hydrolase 1	<i>Faah</i>	-1.449	0.0051
Cytoplasmic FMR1-interacting protein 2	<i>Cyfi2</i>	-1.45	0.0039
GEM-interacting protein	<i>Gmip</i>	-1.45	0.0004
Solute carrier family 2, facilitated glucose transporter member 7	<i>Slc2a7</i>	-1.452	0.0269
Cytochrome c oxidase subunit 7A-related protein, mitochondrial	<i>Cox7a2l</i>	-1.452	0.001
Cytochrome P450 4B1	<i>Cyp4b1</i>	-1.456	0.0202
Coiled-coil and C2 domain-containing protein 1B	<i>Cc2d1b</i>	-1.458	0.0009
Vacuolar protein sorting-associated protein 33B	<i>Vps33b</i>	-1.461	0.0035
Uncharacterized protein C19orf43 homolog		-1.461	0.004
Gamma-glutamyltranspeptidase 1;Gamma-glutamyltranspeptidase 1 heavy chain;Gamma-glutamyltranspeptidase 1 light chain	<i>Ggt1</i>	-1.462	0.0027
	<i>Lct</i>	-1.464	0.0011
N-terminal Xaa-Pro-Lys N-methyltransferase 1	<i>Ntmt1</i>	-1.465	0.0029
Extended synaptotagmin-1	<i>Esyt1</i>	-1.465	0.0013
Adseverin	<i>Scin</i>	-1.465	0.0001
Bromodomain adjacent to zinc finger domain protein 2A	<i>Baz2a</i>	-1.465	0.0081
Syntaxin-binding protein 5	<i>Stxbp5</i>	-1.465	0.0003
Cysteine-rich and transmembrane domain-containing protein 1	<i>Cystm1</i>	-1.467	0.0025
StAR-related lipid transfer protein 5	<i>Stard5</i>	-1.468	0.0034
Kinesin-like protein;Kinesin-like protein KIF21A	<i>Kif21a</i>	-1.47	0.0013
Unconventional myosin-Ia	<i>Myo1a</i>	-1.47	0.0006
Tetraspanin-8	<i>Tspan8</i>	-1.47	0.0024

Nuclear pore membrane glycoprotein 210	<i>Nup210</i>	-1.471	0.0022
Glutaminase kidney isoform, mitochondrial	<i>Gls</i>	-1.472	0.0003
Bromodomain adjacent to zinc finger domain protein 1A	<i>Baz1a</i>	-1.473	0.0248
Transmembrane protein 126A	<i>Tmem126a</i>	-1.474	0.0007
Canalicular multispecific organic anion transporter 1	<i>Abcc2</i>	-1.474	0.0039
Complex I intermediate-associated protein 30, mitochondrial	<i>Ndutfaf1</i>	-1.475	0.0001
Prohibitin-2	<i>Phb2</i>	-1.476	0.0151
ATPase family AAA domain-containing protein 1	<i>Atad1</i>	-1.476	0.0017
		-1.477	0.0008
Methyltransferase-like protein 17, mitochondrial	<i>Mettl17</i>	-1.478	0.0002
Golgin subfamily A member 7	<i>Golga7</i>	-1.478	0.0001
Uncharacterized protein C18orf8 homolog	<i>Mic1</i>	-1.478	0.0002
Ribonucleoside-diphosphate reductase large subunit	<i>Rrm1</i>	-1.479	0.0089
Integrin-linked protein kinase	<i>Ilk</i>	-1.479	0.0005
IST1 homolog	<i>Ist1</i>	-1.479	0.0001
Lymphocyte-specific helicase	<i>Hells</i>	-1.48	0.0362
ATP-dependent RNA helicase DDX3Y	<i>Ddx3y</i>	-1.481	0.0008
E3 ubiquitin-protein ligase UHRF1	<i>Uhrf1</i>	-1.481	0.0144
Cysteine-rich with EGF-like domain protein 1	<i>Creld1</i>	-1.484	0.0002
Very long-chain acyl-CoA synthetase	<i>Slc27a2</i>	-1.485	0.0042
Nucleolar GTP-binding protein 2	<i>Gnl2</i>	-1.486	0.0001
Single Ig IL-1-related receptor	<i>Sigirr</i>	-1.487	0.0011
AFG3-like protein 2	<i>Afg3l2</i>	-1.488	0.0003
Numb-like protein	<i>Numbl</i>	-1.49	0.0003
Cytochrome c oxidase subunit 4 isoform 1, mitochondrial	<i>Cox4i1</i>	-1.491	0.0001
Rhotekin	<i>Rtkn</i>	-1.491	0.0004
NADH dehydrogenase [ubiquinone] iron-sulfur protein 8, mitochondrial	<i>Ndufs8</i>	-1.491	0.0003
DENN domain-containing protein 1B	<i>Dennd1b</i>	-1.492	0.0021
NADH dehydrogenase [ubiquinone] 1 alpha subcomplex subunit 9, mitochondrial	<i>Ndufa9</i>	-1.492	0.0044
Metalloendopeptidase OMA1, mitochondrial	<i>Oma1</i>	-1.493	0.0005
Probable tRNA N6-adenosine threonylcarbamoyltransferase	<i>Osgep</i>	-1.494	0.0003
Zinc finger CCCH domain-containing protein 18	<i>Zc3h18</i>	-1.494	0.0054
Sorting nexin-27	<i>Snx27</i>	-1.494	0.0047
Required for meiotic nuclear division protein 1 homolog	<i>Rmnd1</i>	-1.495	0.0012
Iodotyrosine dehalogenase 1	<i>lyd</i>	-1.496	0.0124
Glycoprotein-N-acetylgalactosamine 3-beta-galactosyltransferase 1	<i>C1galt1</i>	-1.496	0.0001
X-ray repair cross-complementing protein 5	<i>Xrcc5</i>	-1.496	0.0003
Guanine nucleotide-binding protein subunit alpha-11	<i>Gna11</i>	-1.497	0.001
Deleted in malignant brain tumors 1 protein	<i>Dmbt1</i>	-1.498	0.0044
Tricarboxylate transport protein, mitochondrial	<i>Slc25a1</i>	-1.498	0.024

Anoctamin-10	<i>Ano10</i>	-1.499	0.0005
LEM domain-containing protein 2	<i>Lemd2</i>	-1.499	0.0001
Cytochrome c oxidase subunit 5A, mitochondrial	<i>Cox5a</i>	-1.5	0.0478
Mediator of RNA polymerase II transcription subunit 25	<i>Med25</i>	-1.5	0.0025
Tyrosyl-DNA phosphodiesterase 2	<i>Tdp2</i>	-1.502	0.0009
Anoctamin-6	<i>Ano6</i>	-1.503	0.0025
Pericentriolar material 1 protein	<i>Pcm1</i>	-1.505	0.0012
Cyclin-dependent kinase 18;Cyclin-dependent kinase 17	<i>Cdk18;Cdk17</i>	-1.506	0.001
Plasminogen receptor (KT)	<i>Plgrkt</i>	-1.506	0.0164
NADH dehydrogenase [ubiquinone] iron-sulfur protein 4, mitochondrial	<i>Ndufs4</i>	-1.506	0.0007
Replication factor C subunit 1	<i>Rfc1</i>	-1.506	0.0022
Secretory carrier-associated membrane protein 2	<i>Scamp2</i>	-1.507	0.0014
Solute carrier family 15 member 1	<i>Slc15a1</i>	-1.507	0.0024
Cdc42-interacting protein 4	<i>Trip10</i>	-1.508	0.0048
Mitogen-activated protein kinase 13	<i>Mapk13</i>	-1.509	0.0008
Mitochondrial fission 1 protein	<i>Fis1</i>	-1.51	0.0001
DNA-directed RNA polymerase III subunit RPC3	<i>Polr3c</i>	-1.514	0.0184
Mitochondrial import inner membrane translocase subunit TIM14	<i>Dnajc19</i>	-1.515	0.0001
Dephospho-CoA kinase domain-containing protein	<i>Dcakd</i>	-1.515	0.0037
Signal peptidase complex subunit 2	<i>Spcs2</i>	-1.516	0.0054
Coiled-coil domain-containing protein 134	<i>Ccdc134</i>	-1.516	0.0008
Solute carrier family 2, facilitated glucose transporter member 2	<i>Slc2a2</i>	-1.517	0.0001
Glutathione S-transferase theta-1	<i>Gstt1</i>	-1.518	0.0015
Phosphatidylserine decarboxylase proenzyme	<i>Pisd;Gm20671</i>	-1.519	0.0066
Aminoacylase-1	<i>Acy1</i>	-1.52	0.0177
Zinc transporter 9	<i>Slc30a9</i>	-1.522	0.0025
Choline-phosphate cytidyltransferase A	<i>Pcyt1a</i>	-1.523	0.0032
N-terminal kinase-like protein	<i>Scyl1</i>	-1.524	0.0013
Sorting nexin-7	<i>Snx7</i>	-1.524	0.0018
Sphingomyelin phosphodiesterase 4	<i>Smpd4</i>	-1.524	0.0017
Erlin-2	<i>Erlin2</i>	-1.525	0.0013
Casein kinase I isoform alpha	<i>Csnk1a1</i>	-1.526	0.0036
Solute carrier family 12 member 6	<i>Slc12a6</i>	-1.526	0.0001
Mitochondrial import inner membrane translocase subunit TIM50	<i>Timm50</i>	-1.527	0.0009
Casein kinase I isoform delta;Casein kinase I isoform epsilon	<i>Csnk1d;Csnk1e</i>	-1.531	0.0014
Unconventional myosin-1e	<i>Myo1e</i>	-1.531	0.0019
Sodium/potassium-transporting ATPase subunit alpha-1	<i>Atp1a1</i>	-1.531	0.0004
GPI-anchor transamidase	<i>Pigk</i>	-1.532	0.0001
ATP synthase subunit d, mitochondrial	<i>Gm10250;Atp5h</i>	-1.534	0.0005
Protein ITFG3	<i>Itfg3</i>	-1.534	0.0008
Serine/threonine-protein kinase MARK2	<i>Mark2</i>	-1.535	0.0046
Methyl-CpG-binding protein 2	<i>Mecp2</i>	-1.536	0.0162
E3 ubiquitin-protein ligase RLIM	<i>Rlim</i>	-1.536	0.0131

Cytochrome c oxidase subunit 5B, mitochondrial	<i>Cox5b</i>	-1.538	0.0181
YTH domain-containing protein 1	<i>Ythdc1</i>	-1.538	0.0304
Chromodomain-helicase-DNA-binding protein 1	<i>Chd1</i>	-1.539	0.0193
THO complex subunit 4	<i>Alyref</i>	-1.539	0.002
Cytochrome b5 type B	<i>Cyb5b</i>	-1.54	0.0006
All-trans-retinol 13,14-reductase	<i>Retsat</i>	-1.541	0.0029
AFG3-like protein 1	<i>Afg3l1</i>	-1.542	0.0017
Sorting nexin-4	<i>Snx4</i>	-1.544	0.0008
Dual specificity mitogen-activated protein kinase kinase 6	<i>Map2k6</i>	-1.546	0.0001
ATP synthase subunit epsilon, mitochondrial	<i>Atp5e</i>	-1.549	0.0129
ATP synthase subunit gamma;ATP synthase subunit gamma, mitochondrial	<i>Atp5c1</i>	-1.55	0.0023
Transcriptional repressor CTCF	<i>Ctcf</i>	-1.552	0.008
Integrin beta;Integrin beta-5	<i>Itgb5</i>	-1.553	0.0004
Protein FAM162A	<i>Fam162a</i>	-1.556	0.0003
Gastric inhibitory polypeptide	<i>Gip</i>	-1.556	0.0404
Pantetheinase	<i>Vnn1</i>	-1.557	0.0034
Butyrophilin-like protein 2	<i>Btnl2</i>	-1.557	0.0004
Carnitine O-palmitoyltransferase 1, liver isoform	<i>Cpt1a</i>	-1.56	0.0028
	<i>Slc5a4b</i>	-1.56	0.0091
Calcium-binding mitochondrial carrier protein SCaMC-1	<i>Slc25a24</i>	-1.562	0.0005
Protein ERGIC-53	<i>Lman1</i>	-1.563	0.0004
Integrin alpha-2	<i>Itga2</i>	-1.563	0.0001
Niemann-Pick C1-like protein 1	<i>Npc1l1</i>	-1.565	0.0007
Plasma membrane calcium-transporting ATPase 1	<i>Atp2b1</i>	-1.566	0.0024
N-acylneuraminate cytidyltransferase	<i>Cmas</i>	-1.566	0.0148
	<i>Tor1aip1</i>	-1.567	0.0004
CDGSH iron-sulfur domain-containing protein 1	<i>Cisd1</i>	-1.567	0.0014
ATP synthase subunit f, mitochondrial	<i>Atp5j2</i>	-1.569	0.0012
Tropomodulin-3	<i>Tmod3</i>	-1.569	0.0065
Mitochondrial carrier homolog 2	<i>Mtch2</i>	-1.571	0.0387
4F2 cell-surface antigen heavy chain	<i>Slc3a2</i>	-1.572	0.002
Sodium/potassium-transporting ATPase subunit beta-1	<i>Atp1b1</i>	-1.573	0.0001
Guanine nucleotide-binding protein G(q) subunit alpha	<i>Gnaq</i>	-1.575	0.0001
YTH domain-containing family protein 2	<i>Ythdf2</i>	-1.575	0.002
DEP domain-containing mTOR-interacting protein	<i>Deptor</i>	-1.576	0.0001
	<i>Myl12a</i>	-1.576	0.0012
ATP-binding cassette sub-family B member 8, mitochondrial	<i>Abcb8</i>	-1.577	0.0003
Replication factor C subunit 4	<i>Rfc4</i>	-1.578	0.0005
Cytochrome b-c1 complex subunit 7	<i>Uqcrb</i>	-1.578	0.0003
Mitochondrial ubiquitin ligase activator of NFKB 1	<i>Mul1</i>	-1.578	0.0009
b(0,+)-type amino acid transporter 1	<i>Slc7a9</i>	-1.579	0.0068
Feline leukemia virus subgroup C receptor-related protein 1	<i>Flvcr1</i>	-1.579	0.0001
Importin subunit alpha-1	<i>Kpna2</i>	-1.581	0.0002
Inositol monophosphatase 3	<i>Impad1</i>	-1.581	0.0001

Syntaxin-16	<i>Stx16</i>	-1.584	0.0001
ATP-dependent RNA helicase DDX3X;Putative ATP-dependent RNA helicase PI10	<i>Ddx3x;D1Pas1</i>	-1.589	0.001
Peptidyl-prolyl cis-trans isomerase FKBP5;Peptidyl-prolyl cis-trans isomerase FKBP5, N-terminally processed	<i>Fkbp5</i>	-1.589	0.0035
Tripartite motif-containing protein 26	<i>Trim26</i>	-1.589	0.0008
	<i>Pkp2</i>	-1.59	0.0001
Serpin H1	<i>Serpinh1</i>	-1.59	0.0123
Fibronectin;Anastellin	<i fn1<="" i=""></i>	-1.591	0.0175
UPF0585 protein C16orf13 homolog	<i>0610011F06Rik</i>	-1.591	0.0001
DnaJ homolog subfamily C member 1	<i>Dnajc1</i>	-1.594	0.0001
Ras-related protein Rab-22A	<i>Rab22a</i>	-1.595	0.0021
Circadian locomotor output cycles protein kaput	<i>Clock</i>	-1.595	0.0013
Mitochondrial import receptor subunit TOM5 homolog	<i>Tomm5</i>	-1.595	0.0004
Peptidyl-tRNA hydrolase 2, mitochondrial	<i>Pthr2</i>	-1.597	0.0002
EH domain-containing protein 4	<i>Ehd4</i>	-1.598	0.0017
Calcium uniporter protein, mitochondrial	<i>Mcu</i>	-1.599	0.0013
Poly [ADP-ribose] polymerase 1	<i>Parp1</i>	-1.599	0.0004
Transcription factor MafK;Transcription factor MafG	<i>Mafk;Mafg</i>	-1.599	0.0138
Non-histone chromosomal protein HMG-17	<i>Hmgn2;Gm16494</i>	-1.603	0.1837
Stomatin-like protein 2, mitochondrial	<i>Stoml2</i>	-1.604	0.0001
ATP synthase subunit O, mitochondrial	<i>Atp5o</i>	-1.605	0.0001
N-acetylneuraminase lyase	<i>Npl</i>	-1.605	0.0145
	<i>Secisbp2</i>	-1.606	0.0066
Bcl-2-like protein 1	<i>Bcl2l1</i>	-1.607	0.0001
Flap endonuclease 1	<i>Fen1</i>	-1.607	0.0025
	<i>Myo5c</i>	-1.609	0.0002
Cytochrome b-c1 complex subunit 10	<i>Uqcrc11</i>	-1.609	0.0167
Platelet glycoprotein 4	<i>Cd36</i>	-1.61	0.0028
Diacylglycerol kinase;Diacylglycerol kinase zeta	<i>Dgkz</i>	-1.612	0.0002
DNA topoisomerase 1	<i>Top1</i>	-1.62	0.0042
Histone H1.1	<i>Hist1h1a</i>	-1.622	0.01
ATP-binding cassette sub-family G member 5	<i>Abcg5</i>	-1.624	0.0001
Voltage-dependent anion-selective channel protein 1	<i>Vdac1</i>	-1.625	0.0106
DnaJ homolog subfamily A member 3, mitochondrial	<i>Dnaja3</i>	-1.633	0.0001
Protein kinase C delta-binding protein	<i>Prkcdbp</i>	-1.638	0.0115
Mitochondrial import inner membrane translocase subunit Tim23	<i>Timm23</i>	-1.64	0.0002
	<i>Dlg3</i>	-1.642	0.002
	<i>Gm20498</i>	-1.644	0.0001
NADH dehydrogenase [ubiquinone] 1 alpha subcomplex subunit 6	<i>Ndufa6</i>	-1.645	0.0003
Opioid growth factor receptor	<i>Ogfr</i>	-1.648	0.0182
Replication factor C subunit 5	<i>Rfc5</i>	-1.649	0.0016
Oxysterol-binding protein-related protein 2	<i>Osbp12</i>	-1.649	0.0056

NADH dehydrogenase [ubiquinone] 1 alpha subcomplex subunit 13	<i>Ndufa13</i>	-1.65	0.0001
Signal peptidase complex catalytic subunit SEC11;Signal peptidase complex catalytic subunit SEC11A	<i>Sec11a</i>	-1.652	0.0196
Neutral cholesterol ester hydrolase 1	<i>Nceh1</i>	-1.654	0.0005
Sorting nexin-3	<i>Snx3</i>	-1.655	0.0003
Histone H1.0;Histone H1.0, N-terminally processed	<i>H1f0</i>	-1.656	0.004
	<i>Inpp5a</i>	-1.658	0.0001
Protein KTI12 homolog	<i>Kti12</i>	-1.658	0.001
Coiled-coil domain-containing protein 51	<i>Ccdc51</i>	-1.659	0.0003
Serine/threonine-protein kinase VRK1	<i>Vrk1</i>	-1.659	0.0009
Annexin A13;Annexin	<i>Anxa13</i>	-1.663	0.0041
Phosphofurin acidic cluster sorting protein 2	<i>Pacs2</i>	-1.665	0.0004
Myosin light chain 1/3, skeletal muscle isoform;Myosin light chain 3	<i>Myl1;Myl3</i>	-1.665	0.0377
Carboxypeptidase D	<i>Cpd</i>	-1.669	0.0001
Cytochrome P450 3A11	<i>Cyp3a11</i>	-1.67	0.0352
	<i>Akr1c14</i>	-1.675	0.001
Succinate dehydrogenase cytochrome b560 subunit, mitochondrial	<i>Sdhc</i>	-1.675	0.0078
GTP-binding protein 8	<i>Gtpbp8</i>	-1.68	0.0014
GTP-binding protein SAR1b	<i>Sar1b</i>	-1.681	0.0002
Multidrug resistance protein 1A	<i>Abcb1a</i>	-1.684	0.0035
	<i>Myo6</i>	-1.685	0.0019
Signal peptidase complex subunit 1	<i>Spcs1</i>	-1.686	0.0002
Tyrosine-protein kinase BAZ1B	<i>Baz1b</i>	-1.686	0.001
Endophilin-A1	<i>Sh3gl2</i>	-1.687	0.0042
	<i>Ak2</i>	-1.694	0.0007
Calmodulin-regulated spectrin-associated protein 3	<i>Camsap3</i>	-1.701	0.0013
Annexin A1	<i>Anxa1</i>	-1.707	0.0001
Inactive serine/threonine-protein kinase VRK3	<i>Vrk3</i>	-1.707	0.0001
Mucin-2	<i>Muc2</i>	-1.709	0.0021
Krueppel-like factor 5	<i>Klf5</i>	-1.711	0.0054
PX domain-containing protein kinase-like protein	<i>Pxk</i>	-1.712	0.0018
EH domain-containing protein 1	<i>Ehd1</i>	-1.713	0.0006
Pinin	<i>Pnn</i>	-1.714	0.0003
Long-chain-fatty-acid--CoA ligase 1	<i>Acsl1</i>	-1.716	0.0001
Trinucleotide repeat-containing gene 6B protein	<i>Tnrc6b</i>	-1.717	0.0007
Protein XRP2	<i>Rp2</i>	-1.718	0.0001
Phosphatidylcholine transfer protein	<i>Pctp</i>	-1.719	0.0013
Barrier-to-autointegration factor;Barrier-to-autointegration factor, N-terminally processed	<i>Banf1</i>	-1.719	0.0131
Syntaxin-3	<i>Stx3</i>	-1.721	0.0001
	<i>Cpb1</i>	-1.722	0.17
Putative hexokinase HKDC1	<i>Hkdc1</i>	-1.725	0.0003
Unconventional myosin-IId	<i>Myo1d</i>	-1.726	0.0001
ATP synthase F(0) complex subunit C1, mitochondrial;ATP synthase F(0) complex subunit C3, mitochondrial;ATP synthase F(0) complex subunit C2, mitochondrial	<i>Atp5g2;Atp5g1;At p5g3</i>	-1.731	0.0071

A-kinase anchor protein 7 isoform alpha;A-kinase anchor protein 7 isoform gamma	<i>Akap7</i>	-1.734	0.0055
X-ray repair cross-complementing protein 6	<i>Xrcc6</i>	-1.737	0.0001
SH2B adapter protein 1	<i>Sh2b1</i>	-1.74	0.0033
Sorting and assembly machinery component 50 homolog	<i>Samm50</i>	-1.743	0.0014
Synaptic vesicle membrane protein VAT-1 homolog	<i>Vat1</i>	-1.75	0.0002
Amine oxidase [flavin-containing] B	<i>Maob</i>	-1.752	0.0048
Consortin	<i>Cnst</i>	-1.753	0.0046
15-hydroxyprostaglandin dehydrogenase [NAD(+)]	<i>Hpgd</i>	-1.755	0.0006
	<i>Cyp2c65</i>	-1.769	0.0065
Amine oxidase [flavin-containing] A	<i>Maoa</i>	-1.769	0.0062
Cytochrome P450 2C40	<i>Cyp2c68;Cyp2c67;Cyp2c40;Cyp2c69</i>	-1.771	0.0001
Apolipoprotein O	<i>ApoO</i>	-1.771	0.0004
Lamina-associated polypeptide 2, isoforms beta/delta/epsilon/gamma	<i>Tmpo</i>	-1.774	0.0287
Glypican-4;Secreted glypican-4	<i>Gpc4</i>	-1.776	0.0001
Kinesin-like protein KIF3B;Kinesin-like protein KIF3B, N-terminally processed	<i>Kif3b</i>	-1.778	0.0123
ADP-ribosylation factor 6	<i>Arf6</i>	-1.778	0.0031
	<i>Zfp780b</i>	-1.778	0.0022
Sodium/hydrogen exchanger 1	<i>Slc9a1</i>	-1.778	0.0004
Non-syndromic hearing impairment protein 5 homolog	<i>Dfna5</i>	-1.78	0.0002
Amino acid transporter;Neutral amino acid transporter B(0)	<i>Slc1a5</i>	-1.781	0.0003
Transmembrane protein 65	<i>Tmem65</i>	-1.781	0.0002
Syndecan-1	<i>Sdc1</i>	-1.781	0.0002
Mitochondrial pyruvate carrier 1	<i>Mpc1</i>	-1.782	0.0002
Uncharacterized aarF domain-containing protein kinase 5	<i>Adck5</i>	-1.783	0.0001
ATPase family AAA domain-containing protein 3	<i>Atad3</i>	-1.787	0.0001
EH domain-containing protein 2	<i>Ehd2</i>	-1.791	0.0022
Cyclin-dependent kinase 1	<i>Cdk1</i>	-1.792	0.0004
	<i>Xpnpep2</i>	-1.796	0.008
DNA primase large subunit	<i>Prim2</i>	-1.8	0.0003
Sarcolemmal membrane-associated protein	<i>Slmap</i>	-1.8	0.015
Transmembrane protein 9B	<i>Tmem9b</i>	-1.805	0.0002
Serine/threonine-protein kinase Nek3	<i>Nek3</i>	-1.807	0.0033
Guanine nucleotide-binding protein-like 3-like protein	<i>Gnl3l</i>	-1.808	0.0197
Spermatogenesis-defective protein 39 homolog	<i>Vipas39</i>	-1.809	0.0003
Transcriptional repressor protein YY1	<i>Yy1</i>	-1.81	0.0001
E3 ubiquitin-protein ligase NEDD4	<i>Nedd4</i>	-1.811	0.0003
Phospholipid scramblase 1	<i>Plscr1</i>	-1.82	0.0022
MICOS complex subunit Mic60	<i>Immt</i>	-1.827	0.0001
Probable ATP-dependent RNA helicase DDX5	<i>Ddx5</i>	-1.828	0.0014
	<i>Rsf1</i>	-1.828	0.0003
	<i>Apol9a;Apol9b</i>	-1.837	0.0091
MICOS complex subunit Mic19	<i>Chchd3</i>	-1.84	0.0004

Sorting nexin-9	<i>Snx9</i>	-1.841	0.0001
Peroxisomal acyl-coenzyme A oxidase 2	<i>Acox2</i>	-1.842	0.0036
Meprin A subunit alpha	<i>Mep1a</i>	-1.846	0.0005
Centromere protein V	<i>Cenpv</i>	-1.846	0.0107
Sulfate transporter	<i>Slc26a2</i>	-1.85	0.0001
Decorin	<i>Dcn</i>	-1.857	0.0008
NADH-cytochrome b5 reductase 1	<i>Cyb5r1</i>	-1.863	0.0005
Synemin	<i>Synm</i>	-1.865	0.243
Redox-regulatory protein FAM213A	<i>Fam213a</i>	-1.868	0.0011
CKLF-like MARVEL transmembrane domain-containing protein 6	<i>Cmtm6</i>	-1.87	0.0001
Metaxin-2	<i>Mtx2</i>	-1.883	0.0001
Bile salt export pump	<i>Abcb11</i>	-1.888	0.0079
Metaxin-1	<i>Mtx1</i>	-1.901	0.0001
	<i>Spcs3</i>	-1.902	0.0027
N-acetylated-alpha-linked acidic dipeptidase-like protein	<i>Naaladl1</i>	-1.909	0.0012
Myosin light polypeptide 6	<i>Myl6</i>	-1.924	0.0094
Diacylglycerol O-acyltransferase 1	<i>Dgat1</i>	-1.926	0.0025
Sterol 26-hydroxylase, mitochondrial	<i>Cyp27a1</i>	-1.929	0.0016
	<i>Actn1</i>	-1.954	0.0143
Cubilin	<i>Cubn</i>	-1.955	0.0019
	<i>Slfn9</i>	-1.96	0.0003
	<i>Sar1a</i>	-1.967	0.0001
Ras suppressor protein 1	<i>Rsu1</i>	-1.969	0.0002
MAU2 chromatid cohesion factor homolog	<i>Mau2</i>	-1.98	0.0011
Lumican	<i>Lum</i>	-1.983	0.0009
High mobility group protein 20A	<i>Hmg20a</i>	-1.985	0.0003
Protein NDRG1	<i>Ndr1</i>	-1.991	0.0001
Acylglycerol kinase, mitochondrial	<i>Agk</i>	-1.994	0.0003
Histone H3.2	<i>Hist1h3b</i>	-1.997	0.0711
Epoxide hydrolase 1	<i>Ephx1</i>	-2.009	0.0005
	<i>Bptf</i>	-2.009	0.0002
FACT complex subunit SSRP1	<i>Ssrp1</i>	-2.012	0.0008
Atypical kinase ADCK3, mitochondrial	<i>Adck3</i>	-2.014	0.0001
Lipoamide acyltransferase component of branched-chain alpha-keto acid dehydrogenase complex, mitochondrial	<i>Dbt</i>	-2.014	0.0001
Regulator of chromosome condensation	<i>Rcc1</i>	-2.016	0.0018
Receptor expression-enhancing protein; Receptor expression-enhancing protein 5	<i>Reep5</i>	-2.022	0.0001
Histone H2B type 3-B; Histone H2B type 3-A; Histone H2B type 2-E	<i>Hist3h2bb; Hist3h2ba; Hist2h2be</i>	-2.033	0.013
MLV-related proviral Env polyprotein; Surface protein; Transmembrane protein		-2.048	0.0002
Anterior gradient protein 2 homolog	<i>Agr2</i>	-2.051	0.0004
Alpha-parvin	<i>Parva</i>	-2.051	0.0004
Cell division cycle protein 27 homolog	<i>Cdc27</i>	-2.072	0.0004
Secretin	<i>Sct</i>	-2.073	0.0282
Leiomodin-1	<i>Lmod1</i>	-2.078	0.0422

Transforming growth factor-beta-induced protein ig-h3	<i>Tgfb1</i>	-2.079	0.0028
Protein QIL1	<i>Qil1</i>	-2.081	0.0001
Histidine triad nucleotide-binding protein 3	<i>Hint3</i>	-2.09	0.0007
Nuclear factor 1;Nuclear factor 1 A-type	<i>Nfia</i>	-2.106	0.0004
Estradiol 17-beta-dehydrogenase 2	<i>Hsd17b2</i>	-2.151	0.0001
E3 ubiquitin-protein ligase TRIM23	<i>Trim23</i>	-2.171	0.0062
Sterol O-acyltransferase 1	<i>Soat1</i>	-2.174	0.0004
Nucleolar transcription factor 1	<i>Ubtf</i>	-2.184	0.001
ETS-related transcription factor Elf-3	<i>Elf3</i>	-2.197	0.0007
Endoplasmic reticulum-Golgi intermediate compartment protein 1	<i>Ergic1</i>	-2.199	0.0001
Solute carrier family 12 member 2	<i>Slc12a2</i>	-2.229	0.0001
Integrin alpha-1	<i>Itga1</i>	-2.238	0.0011
Alpha-defensin 23	<i>Defa23</i>	-2.247	0.0248
Cytochrome P450 2J6	<i>Cyp2j6</i>	-2.256	0.0004
FACT complex subunit SPT16	<i>Supt16;Supt16h</i>	-2.258	0.0004
SUN domain-containing protein 1	<i>Sun1</i>	-2.261	0.0005
Myosin regulatory light chain 12B	<i>Myl12b</i>	-2.266	0.0043
Calcium-activated chloride channel regulator 1	<i>Clca1</i>	-2.269	0.0001
UDP-glucuronosyltransferase 2B17	<i>Ugt2b5;Ugt2b17;Ugt2b38</i>	-2.272	0.0444
BRI3-binding protein	<i>Bri3bp</i>	-2.274	0.0118
Endoplasmic reticulum resident protein 27	<i>Erp27</i>	-2.278	0.0089
Calcium-transporting ATPase;Sarcoplasmic/endoplasmic reticulum calcium ATPase 3	<i>Atp2a3</i>	-2.284	0.0001
Polymerase I and transcript release factor	<i>Ptrf</i>	-2.315	0.0086
Core histone macro-H2A.1	<i>H2afy</i>	-2.32	0.0012
40S ribosomal protein S30	<i>Fau</i>	-2.346	0.0138
Sodium/potassium-transporting ATPase subunit alpha-4	<i>Atp1a4</i>	-2.363	0.0006
Sorting nexin;Sorting nexin-18	<i>Snx18</i>	-2.363	0.0005
Unconventional myosin-XVIIIa	<i>Myo18a</i>	-2.382	0.0011
Chymotrypsin-like elastase family member 2A	<i>Cela2a</i>	-2.384	0.0011
Basement membrane-specific heparan sulfate proteoglycan core protein	<i>Hspg2</i>	-2.391	0.0006
Pancreatic alpha-amylase;Alpha-amylase	<i>Amy2;Amy2a1</i>	-2.406	0.0248
Thymidylate synthase	<i>Tyms</i>	-2.411	0.0005
Fatty acid-binding protein, adipocyte	<i>Fabp4</i>	-2.427	0.036
RNA-binding protein with serine-rich domain 1	<i>Rnps1</i>	-2.43	0.0035
	<i>Ctrl</i>	-2.448	0.0012
	<i>1700123L14Rik</i>	-2.452	0.0194
Adenylate cyclase type 6	<i>Adcy6</i>	-2.456	0.0002
Histone H3.1	<i>Hist1h3a</i>	-2.538	0.0034
	<i>Syne2</i>	-2.618	0.0002
Sideroflexin-3	<i>Sfxn3</i>	-2.618	0.0005
DNA topoisomerase 2-beta	<i>Top2b</i>	-2.632	0.0002
	<i>Mptx2</i>	-2.66	0.0057
	<i>Tns1</i>	-2.679	0.0074
Bile salt-activated lipase	<i>Cel</i>	-2.691	0.0056

Syndecan-4	<i>Sdc4</i>	-2.725	0.0001
Chromodomain-helicase-DNA-binding protein 2	<i>Chd2</i>	-2.868	0.0006
	<i>Myl10</i>	-2.873	0.0009
	<i>Cyp2c66</i>	-2.93	0.0013
Histone H2AX	<i>H2afx</i>	-2.962	0.0015
Colipase	<i>Clps</i>	-3.039	0.0042
DNA topoisomerase 2-alpha	<i>Top2a</i>	-3.067	0.0002
Myosin-9	<i>Myh9</i>	-3.075	0.0004
ADP/ATP translocase 1	<i>Slc25a4</i>	-3.08	0.0269
Myosin-14	<i>Myh14</i>	-3.083	0.0006
Pancreatic lipase-related protein 2	<i>Pnliprp2</i>	-3.144	0.0005
Histone H2B type 1-F/J/L;Histone H2B;Histone H2B type 1-P;Histone H2B type 1-K;Histone H2B type 1-B;Histone H2B type 1-A	<i>Hist1h2bf;Hist1h2br;Hist1h2bp;Hist1h2bk;Hist1h2bb;Hist1h2ba</i>	-3.153	0.0004
	<i>Muc3</i>	-3.27	0.0005
Histone H4	<i>Hist1h4a</i>	-3.324	0.0012
Histone H2A type 2-B	<i>Hist2h2ab</i>	-3.34	0.0008
Cytochrome P450 2C55	<i>Cyp2c55</i>	-3.424	0.0001
Caveolin-1;Caveolin	<i>Cav1</i>	-3.551	0.0005
Histone H2A type 1-F	<i>Hist1h2af</i>	-3.674	0.0004
Alpha-defensin 21;Alpha-defensin 22	<i>Defa22;Defa21</i>	-3.777	0.006
Histone H3.3;Histone H3.3C;Histone H3	<i>H3f3a;H3f3c</i>	-3.796	0.0021
Peptidyl-prolyl cis-trans isomerase FKBP11	<i>Fkbp11</i>	-3.896	0.0005
Histone H2A;Histone H2A type 2-A;Histone H2A type 2-C	<i>Hist1h2al;Hist2h2aa1;Hist2h2ac</i>	-4.019	0.0004
Collagen alpha-1(VI) chain	<i>Col6a1</i>	-4.254	0.0022
Lactase-like protein	<i>Lct1</i>	-4.285	0.033
	<i>Col6a3</i>	-4.316	0.001
Intellectin-1a	<i>Itln1</i>	-4.367	0.0002
Histone H2A type 1-K	<i>Hist1h2ak</i>	-4.386	0.0004
Histone H2A.V;Histone H2A.Z;Histone H2A	<i>H2afv;H2afz</i>	-4.546	0.0035
Myosin regulatory light polypeptide 9	<i>Myl9</i>	-4.614	0.0333
Chymotrypsinogen B;Chymotrypsin B chain A;Chymotrypsin B chain B;Chymotrypsin B chain C	<i>Ctrb1</i>	-4.645	0.0173
	<i>Myh11</i>	-4.855	0.0165
	<i>Gm15299</i>	-4.982	0.0003
Alpha-defensin 24	<i>Defa24</i>	-5.1	0.0001
Zymogen granule membrane protein 16	<i>Zg16</i>	-5.125	0.0005
Alpha-defensin-related sequence 1	<i>Gm14851;Defars1</i>	-5.286	0.001
Proteasome subunit beta type-5	<i>Psmb5</i>	-5.379	0.0004
Histone H2B type 1-C/E/G;Histone H2B type 1-M;Histone H2B type 2-B;Histone H2B type 1-H	<i>Hist1h2bc;Hist1h2bm;Hist2h2bb;Hist1h2bh</i>	-5.554	0.001
	<i>Gm7849</i>	-5.596	0.0011
Lysozyme C-1;Lysozyme C-2	<i>Lyz1;Lyz2</i>	-5.614	0.0014
Protein disulfide-isomerase A2	<i>Pdia2</i>	-6.4	0.001
Alpha-defensin 20	<i>Defcr20;Defa20</i>	-6.753	0.0049
Ig kappa chain C region	<i>Igkc</i>	-7.942	0.0007
Ig alpha chain C region	<i>Igha</i>	-11.05	0.0007

**Appendix 3: significant proteomic changes in *c-Rel*<sup>-/-</sup> small intestinal mucosa in comparison to C57BL/6J mice**

Protein names	Gene names	Regulation fold change	P value
Solute carrier family 35 member A4	<i>Slc35a4</i>	16.79	0.0001
Glutathione peroxidase 2	<i>Gpx2</i>	4.246	0.0002
Unconventional myosin-IXb	<i>Myo9b</i>	2.89	0.0001
Transformation/transcription domain-associated protein	<i>Trrap</i>	2.793	0.0065
MAU2 chromatid cohesion factor homolog	<i>Mau2</i>	2.42	0.0119
Dual oxidase 2	<i>Duox2</i>	2.293	0.029
Mucosal pentraxin 2	<i>Mptx2</i>	2.154	0.0237
Lactase-like protein	<i>Lctf</i>	2.126	0.0037
Uncharacterized protein KIAA0556	<i>D430042O09Rik;Kiaa0556</i>	2.079	0.0289
1,4-alpha-glucan-branching enzyme	<i>Gbe1</i>	2.074	0.0022
Peripherin	<i>Prph</i>	2.048	0.0154
Regenerating islet-derived protein 3-gamma;Regenerating islet-derived protein 3-gamma 16.5 kDa form;Regenerating islet-derived protein 3-gamma 15 kDa form	<i>Reg3g</i>	1.995	0.022
Sorting nexin-3	<i>Snx3</i>	1.986	0.0082
Polymeric immunoglobulin receptor;Secretory component	<i>Pigr</i>	1.972	0.002
Palmitoyl-protein thioesterase 1	<i>Ppt1</i>	1.97	0.0314
Cathepsin L1;Cathepsin L1 heavy chain;Cathepsin L1 light chain	<i>Ctsl</i>	1.96	0.0006
Thymidylate synthase	<i>Tyms</i>	1.96	0.0484
MLV-related proviral Env polyprotein;Surface protein;Transmembrane protein		1.959	0.0357
Dystrophin	<i>Dmd</i>	1.954	0.0453
Beta-galactosidase	<i>Glb1</i>	1.927	0.0062
Regenerating islet-derived protein 3-beta	<i>Reg3b</i>	1.912	0.0004
Mitochondrial pyruvate carrier 1	<i>Mpc1</i>	1.899	0.0421
Uroporphyrinogen decarboxylase	<i>Urod</i>	1.875	0.007
Transcriptional repressor protein YY1	<i>Yy1</i>	1.867	0.0239
Fatty acid-binding protein, epidermal	<i>Fabp5</i>	1.863	0.0474
Sideroflexin-3	<i>Sfxn3</i>	1.859	0.0081
Glycerol-3-phosphate dehydrogenase 1-like protein	<i>Gpd1l</i>	1.858	0.003
	<i>Parp3</i>	1.855	0.0337
	<i>Chn2</i>	1.849	0.0126
Molybdenum cofactor biosynthesis protein 1	<i>Mocs1</i>	1.847	0.0112
Sodium/hydrogen exchanger 1	<i>Slc9a1</i>	1.844	0.0109
Serum paraoxonase/lactonase 3	<i>Pon3</i>	1.832	0.0002
Protein NDRG1	<i>Ndr1</i>	1.799	0.0092
Protein-tyrosine kinase 6	<i>Ptk6</i>	1.798	0.0119
	<i>Syne2</i>	1.792	0.0276
O-phosphoserine-tRNA(Sec) selenium transferase	<i>Sepsecs</i>	1.792	0.0112

SH3 domain-containing protein 21	<i>Sh3d21</i>	1.79	0.0097
Transmembrane protein 260	<i>Tmem260</i>	1.781	0.0032
Adiponectin receptor protein 2	<i>Adipor2</i>	1.779	0.0233
Conserved oligomeric Golgi complex subunit 5	<i>Cog5</i>	1.779	0.0059
Histone H2A type 1-K	<i>Hist1h2ak</i>	1.77	0.0163
Aminoacylase-1	<i>Acy1</i>	1.754	0.0544
S-methyl-5-thioadenosine phosphorylase	<i>Mtap</i>	1.75	0.0259
Serine/threonine-protein phosphatase 6 catalytic subunit;Serine/threonine-protein phosphatase 6 catalytic subunit, N-terminally processed	<i>Ppp6c</i>	1.735	0.0022
Succinyl-CoA:3-ketoacid coenzyme A transferase 1, mitochondrial;Succinyl-CoA:3-ketoacid-coenzyme A transferase	<i>Oxct1</i>	1.732	0.0021
Purine nucleoside phosphorylase	<i>Pnp2</i>	1.73	0.0035
UPF0585 protein C16orf13 homolog	<i>0610011F06Rik</i>	1.728	0.0145
Transmembrane protein 9B	<i>Tmem9b</i>	1.726	0.0004
b(0,+)-type amino acid transporter 1	<i>Slc7a9</i>	1.722	0.0403
Proteasome subunit beta type-2	<i>Psmb2</i>	1.72	0.0045
Peroxisomal 2,4-dienoyl-CoA reductase	<i>Decr2</i>	1.714	0.022
Arf-GAP domain and FG repeat-containing protein 1	<i>Agfg1</i>	1.71	0.0029
Protein FAM134A	<i>Fam134a</i>	1.71	0.0058
	<i>Tns1</i>	1.708	0.0395
	<i>Rabgap1l</i>	1.703	0.0207
Zinc finger protein 512	<i>Znf512</i>	1.699	0.0463
Ketohexokinase	<i>Khk</i>	1.697	0.0479
Probable RNA-binding protein 19	<i>Rbm19</i>	1.697	0.0189
	<i>Acy1</i>	1.69	0.0093
Long-chain specific acyl-CoA dehydrogenase, mitochondrial	<i>Acadl</i>	1.689	0.0313
Protein disulfide-isomerase A4	<i>Pdia4</i>	1.688	0.0111
Acylamino-acid-releasing enzyme	<i>Apeh</i>	1.687	0.0208
Proteasome subunit beta type-9	<i>Psmb9</i>	1.684	0.001
Eukaryotic translation initiation factor 2D	<i>Eif2d</i>	1.682	0.0098
		1.682	0.011
Transaldolase	<i>Taldo1</i>	1.678	0.02
E3 ubiquitin-protein ligase RNF170	<i>Rnf170</i>	1.677	0.0082
L-lactate dehydrogenase;L-lactate dehydrogenase A chain	<i>Ldha</i>	1.673	0.001
	<i>Actn1</i>	1.673	0.0244
SH3 domain-binding protein 1	<i>Sh3bp1</i>	1.672	0.0009
Nardilysin	<i>Nrd1</i>	1.671	0.0001
Phosphatidate cytidyltransferase;Phosphatidate cytidyltransferase 2	<i>Cds2</i>	1.669	0.0076
	<i>Neb</i>	1.667	0.0156
Hemoglobin subunit beta-1;Hemoglobin subunit beta-2	<i>Hbbt1;Hbb-bs;Hbb-b1;Hbb-b2</i>	1.66	0.0091
CDGSH iron-sulfur domain-containing protein 3, mitochondrial	<i>Cisd3</i>	1.654	0.0065

Clathrin light chain A	<i>Clta</i>	1.653	0.0222
Probable ATP-dependent RNA helicase YTHDC2	<i>Ythdc2</i>	1.651	0.0328
TATA element modulatory factor	<i>Tmf1</i>	1.65	0.0076
Heterogeneous nuclear ribonucleoprotein D-like	<i>Hnrnpdl</i>	1.649	0.0031
Mth938 domain-containing protein	<i>Aamdc</i>	1.649	0.0147
THO complex subunit 6 homolog	<i>Thoc6</i>	1.643	0.0062
Uncharacterized aarF domain-containing protein kinase 5	<i>Adck5</i>	1.641	0.0257
	<i>Gm20498</i>	1.64	0.0025
Helicase-like transcription factor	<i>Hltf</i>	1.628	0.014
Bola-like protein 3	<i>Bola3</i>	1.628	0.022
Proto-oncogene vav	<i>Vav1</i>	1.628	0.0105
Cytosolic acyl coenzyme A thioester hydrolase	<i>Acot7</i>	1.626	0.0275
Alpha-mannosidase;Alpha-mannosidase 2C1	<i>Man2c1</i>	1.622	0.0043
	<i>Nbeal1</i>	1.619	0.0078
Nucleoside diphosphate kinase;Nucleoside diphosphate kinase B	<i>Gm20390;Nme2</i>	1.618	0.0295
Sulfatase-modifying factor 1	<i>Sumf1</i>	1.617	0.0058
	<i>Zfp780b</i>	1.611	0.0274
Bromodomain adjacent to zinc finger domain protein 2A	<i>Baz2a</i>	1.609	0.0138
Major vault protein	<i>Mvp</i>	1.608	0.0048
	<i>Adh6a</i>	1.603	0.0005
Calmodulin-regulated spectrin-associated protein 3	<i>Camsap3</i>	1.603	0.0165
Prefoldin subunit 4	<i>Pfdn4</i>	1.6	0.0419
	<i>Arhgef5</i>	1.599	0.0239
Acylphosphatase;Acylphosphatase-1	<i>Acyp1</i>	1.599	0.0045
	<i>Myh11</i>	1.598	0.0054
	<i>Gm15299</i>	1.598	0.0082
	<i>Ak2</i>	1.597	0.0063
Leiomodin-1	<i>Lmod1</i>	1.594	0.0458
Adenylate cyclase type 6	<i>Adcy6</i>	1.594	0.0024
Serine/threonine-protein kinase Nek3	<i>Nek3</i>	1.593	0.0462
Adenosylhomocysteinase;Putative adenosylhomocysteinase 3	<i>Ahcyl2</i>	1.592	0.011
Serpin B6	<i>Serpinb6a;Serpinb6</i>	1.591	0.0376
Coiled-coil domain-containing protein 58	<i>Ccdc58</i>	1.589	0.0124
Protein PRRC2A	<i>Prrc2a</i>	1.584	0.0137
	<i>Gm20441</i>	1.58	0.0354
Serine hydroxymethyltransferase;Serine hydroxymethyltransferase, cytosolic	<i>Shmt1</i>	1.58	0.0252
Carboxypeptidase;Lysosomal protective protein;Lysosomal protective protein 32 kDa chain;Lysosomal protective protein 20 kDa chain	<i>Ctsa</i>	1.578	0.0451
S-formylglutathione hydrolase	<i>Esd</i>	1.576	0.0378
Copper transport protein ATOX1	<i>Atox1</i>	1.575	0.0059
Proteasome subunit beta type-1	<i>Psmb1</i>	1.574	0.0214
Glutathione S-transferase omega-1	<i>Gsto1</i>	1.573	0.0072

D-dopachrome decarboxylase	<i>Ddt</i>	1.573	0.0318
Acidic leucine-rich nuclear phosphoprotein 32 family member A	<i>Anp32a</i>	1.571	0.0201
Annexin A3;Annexin	<i>Anxa3</i>	1.568	0.0025
Polymerase I and transcript release factor	<i>Ptrf</i>	1.566	0.001
Death-associated protein kinase 3	<i>Dapk3</i>	1.563	0.0024
Proteasome subunit alpha type-3	<i>Psm3</i>	1.56	0.0135
Prefoldin subunit 2	<i>Pfdn2</i>	1.557	0.0056
Craniofacial development protein 1	<i>Cfdp1</i>	1.557	0.0435
WD repeat-containing protein 1	<i>Wdr1</i>	1.556	0.0038
Aromatic-L-amino-acid decarboxylase	<i>Ddc</i>	1.554	0.0247
Glucosamine-6-phosphate isomerase 1	<i>Gnpda1</i>	1.551	0.0072
Aspartate aminotransferase, cytoplasmic	<i>Got1</i>	1.551	0.0253
Tubulin alpha-3 chain	<i>Tuba3a</i>	1.55	0.0396
Glucose-6-phosphate isomerase	<i>Gpi</i>	1.549	0.0096
Serum albumin	<i>Alb</i>	1.549	0.0067
Superoxide dismutase [Cu-Zn]	<i>Sod1</i>	1.548	0.016
Nucleolin	<i>Ncl</i>	1.544	0.0075
Phosphoglycerate kinase 1;Phosphoglycerate kinase	<i>Pgk1</i>	1.543	0.0117
Delta-aminolevulinic acid dehydratase	<i>Alad</i>	1.541	0.0299
Transcription elongation factor A protein 1	<i>Tcea1</i>	1.541	0.0001
Beta-glucuronidase	<i>Gusb</i>	1.538	0.0386
Malate dehydrogenase, cytoplasmic	<i>Mdh1</i>	1.536	0.0361
Calreticulin	<i>Calr</i>	1.535	0.0122
Nucleoside diphosphate kinase A;Nucleoside diphosphate kinase	<i>Nme1</i>	1.534	0.0219
Peptidyl-prolyl cis-trans isomerase A;Peptidyl-prolyl cis-trans isomerase A, N-terminally processed;Peptidyl-prolyl cis-trans isomerase	<i>Ppia;Gm5160</i>	1.533	0.0012
Triosephosphate isomerase	<i>Tpi1</i>	1.529	0.0257
Cofilin-1	<i>Cfl1</i>	1.524	0.0142
Serpin H1	<i>Serpinh1</i>	1.524	0.0377
Aldose reductase-related protein 1	<i>Akr1b7</i>	1.521	0.0251
Protein-glutamine gamma-glutamyltransferase 2	<i>Tgm2</i>	1.516	0.0156
Leukotriene A-4 hydrolase	<i>Lta4h</i>	1.513	0.0028
Protein disulfide-isomerase A3	<i>Pdia3</i>	1.511	0.0125
Proteasome subunit beta type-8;Proteasome subunit beta type	<i>Psm8</i>	1.505	0.0224
Cytoplasmic aconitate hydratase	<i>Aco1</i>	1.505	0.0234
DNA-(apurinic or apyrimidinic site) lyase;DNA-(apurinic or apyrimidinic site) lyase, mitochondrial	<i>Apex1</i>	1.504	0.0144
Alcohol dehydrogenase class-3	<i>Adh5</i>	1.504	0.0011
Acyl-CoA-binding protein	<i>Dbi</i>	1.503	0.0024
Ran-specific GTPase-activating protein	<i>Ranbp1</i>	1.5	0.0052
Protein phosphatase 1B	<i>Ppm1b</i>	1.5	0.0011
Transketolase	<i>Tkt</i>	1.5	0.0007
Vacuolar protein sorting-associated protein 26A	<i>Vps26a</i>	1.491	0.0231

Glutathione reductase, mitochondrial	<i>Gsr</i>	1.491	0.0256
Fos-related antigen 2	<i>Fosl2</i>	1.49	0.0086
Proteasome subunit alpha type-2	<i>Psm2</i>	1.487	0.0062
Caveolin-1;Caveolin	<i>Cav1</i>	1.481	0.0058
Adenosylhomocysteinase	<i>Ahcy</i>	1.481	0.0057
Arylamine N-acetyltransferase 2	<i>Nat2</i>	1.478	0.0073
Estradiol 17-beta-dehydrogenase 2	<i>Hsd17b2</i>	1.476	0.0006
Ubiquitin-conjugating enzyme E2 E3;Ubiquitin-conjugating enzyme E2 E2	<i>Ube2e3;Ube2e2</i>	1.476	0.0064
Uridine phosphorylase 1	<i>Upp1</i>	1.472	0.0084
Cellular nucleic acid-binding protein	<i>Cnbp</i>	1.466	0.0066
Programmed cell death protein 5	<i>Pdcd5</i>	1.466	0.0049
Elongation factor 2	<i>Eef2</i>	1.465	0.0108
Telomerase-binding protein EST1A	<i>Smg6</i>	1.463	0.0233
DDB1- and CUL4-associated factor 7	<i>Dcaf7</i>	1.46	0.0013
Mitochondrial import inner membrane translocase subunit Tim10	<i>Timm10</i>	1.459	0.016
40S ribosomal protein S29	<i>Rps29</i>	1.456	0.0025
U6 snRNA-associated Sm-like protein LSM3	<i>Lsm3</i>	1.455	0.0201
Serine/threonine-protein phosphatase 2A catalytic subunit beta isoform	<i>Ppp2cb</i>	1.454	0.0084
Myotrophin	<i>Mtpn</i>	1.453	0.001
Transcription elongation factor B polypeptide 2	<i>Tceb2</i>	1.453	0.0155
Cytochrome c, somatic	<i>Cycc</i>	1.449	0.0036
Platelet-activating factor acetylhydrolase IB subunit alpha	<i>Pafah1b1</i>	1.446	0.0028
40S ribosomal protein S10	<i>Rps10</i>	1.444	0.0167
Serine/threonine-protein phosphatase 2A catalytic subunit alpha isoform	<i>Ppp2ca</i>	1.442	0.0074
Actin, alpha cardiac muscle 1;Actin, alpha skeletal muscle	<i>Actc1;Acta1</i>	1.439	0.0033
Guanine nucleotide-binding protein subunit beta-2-like 1;Guanine nucleotide-binding protein subunit beta-2-like 1, N-terminally processed	<i>Gnb2l1</i>	1.436	0.0007
Histone H3.1	<i>Hist1h3a</i>	1.434	0.0024
Acid sphingomyelinase-like phosphodiesterase 3a	<i>Smpdl3a</i>	1.431	0.0126
Proteasome subunit beta type-7	<i>Psm7</i>	1.427	0.0054
Phosphatidylethanolamine-binding protein 1;Hippocampal cholinergic neurostimulating peptide	<i>Pebp1</i>	1.423	0.0001
T-box transcription factor TBX3	<i>Tbx3</i>	1.422	0.002
Fructose-1,6-bisphosphatase isozyme 2	<i>Fbp2</i>	1.416	0.0009
Rho-related GTP-binding protein RhoG	<i>Rhog</i>	1.412	0.0039
Cysteine and glycine-rich protein 2	<i>Csrp2</i>	1.41	0.0122
Serine/threonine-protein phosphatase 4 catalytic subunit	<i>Ppp4c</i>	1.405	0.0084
Dipeptidyl peptidase 1;Dipeptidyl peptidase 1 exclusion domain chain;Dipeptidyl peptidase 1 heavy chain;Dipeptidyl peptidase 1 light chain	<i>Ctsc</i>	1.405	0.0021

Acidic leucine-rich nuclear phosphoprotein 32 family member E	<i>Anp32e</i>	1.404	0.0042
Xanthine dehydrogenase/oxidase;Xanthine dehydrogenase;Xanthine oxidase	<i>Xdh</i>	1.403	0.0033
Epithelial discoidin domain-containing receptor 1	<i>Ddr1</i>	1.395	0.0055
Creatine kinase B-type	<i>Ckb</i>	1.392	0.0011
Collagen alpha-1(VI) chain	<i>Col6a1</i>	1.388	0.0044
Cyclin-dependent kinase 18;Cyclin-dependent kinase 17	<i>Cdk18;Cdk17</i>	1.384	0.001
Retinol-binding protein 2	<i>Rbp2</i>	1.379	0.0094
Bcl-2-like protein 15	<i>Bcl2l15</i>	1.368	0.0101
Puromycin-sensitive aminopeptidase	<i>Npepps</i>	1.367	0.0008
Xaa-Pro dipeptidase	<i>Pepd</i>	1.366	0.0002
Zinc transporter SLC39A7	<i>Slc39a7</i>	1.366	0.0095
S-adenosylmethionine synthase isoform type-2	<i>Mat2a</i>	1.364	0.0017
PDZ and LIM domain protein 7	<i>Pdlim7</i>	1.362	0.0076
Peptidyl-prolyl cis-trans isomerase CWC27 homolog	<i>Cwc27</i>	1.36	0.0073
PEST proteolytic signal-containing nuclear protein	<i>Pcnp</i>	1.357	0.0028
Mesencephalic astrocyte-derived neurotrophic factor	<i>Manf</i>	1.35	0.0044
Heat shock 70 kDa protein 4	<i>Hspa4</i>	1.344	0.0066
Abhydrolase domain-containing protein 4	<i>Abhd4</i>	1.344	0.0065
MOB kinase activator 1A;MOB kinase activator 1B	<i>Mob1b;Mob1a</i>	1.321	0.0005
DAZ-associated protein 1	<i>Dazap1</i>	1.315	0.0012
28 kDa heat- and acid-stable phosphoprotein	<i>Pdap1</i>	1.29	0.0004
MAP kinase-activated protein kinase 3	<i>Mapkapk3</i>	-1.28	0.0006
	<i>1700123L14Rik</i>	-1.28	0.0004
Phosphatase and actin regulator 4	<i>Phactr4</i>	-1.29	0.0008
Purine nucleoside phosphorylase	<i>Pnp</i>	-1.3	0.0004
Alpha-defensin 23	<i>Defa23</i>	-1.3	0.0001
Insulin-like growth factor 2 mRNA-binding protein 2	<i>Igf2bp2</i>	-1.32	0.0003
RNA-binding protein EWS	<i>Ewsr1</i>	-1.32	0.0014
Presenilins-associated rhomboid-like protein, mitochondrial;P-beta	<i>Parl</i>	-1.33	0.003
Growth factor receptor-bound protein 2	<i>Grb2</i>	-1.33	0.0036
Heterogeneous nuclear ribonucleoprotein D0	<i>Hnrnpd</i>	-1.33	0.0009
Proteasome subunit beta type-6	<i>Psm6</i>	-1.33	0.0033
Stress-induced-phosphoprotein 1	<i>Stip1</i>	-1.33	0.0042
Caprin-1	<i>Caprin1</i>	-1.33	0.0023
Lamina-associated polypeptide 2, isoforms beta/delta/epsilon/gamma	<i>Tmpo</i>	-1.35	0.0045
Kinase suppressor of Ras 1	<i>Ksr1</i>	-1.35	0.003
Receptor tyrosine-protein kinase erbB-3	<i>Erb3</i>	-1.35	0.0049
Heat shock protein 105 kDa	<i>Hsp105</i>	-1.35	0.0039
Nucleophosmin	<i>Npm1</i>	-1.36	0.0055
U1 small nuclear ribonucleoprotein C	<i>Snrpc</i>	-1.36	0.009
Sulfate transporter	<i>Slc26a2</i>	-1.37	0.0053

Cystatin-B	<i>Cstb</i>	-1.37	0.0073
Bile salt-activated lipase	<i>Cel</i>	-1.37	0.0105
Peroxiredoxin-6	<i>Prdx6</i>	-1.37	0.0007
Clathrin light chain B	<i>Cltb</i>	-1.37	0.0054
ATP-binding cassette sub-family F member 1	<i>Abcf1</i>	-1.38	0.0009
Synemin	<i>Synm</i>	-1.38	0.0031
Ubiquitin domain-containing protein Ubfd1	<i>Ubfd1</i>	-1.38	0.0003
UPF0587 protein C1orf123 homolog	<i>0610037L13Rik</i>	-1.39	0.0048
Neutral alpha-glucosidase AB	<i>Ganab</i>	-1.39	0.0041
Protein RCC2	<i>Rcc2</i>	-1.39	0.0091
F-box only protein 38	<i>Fbxo38</i>	-1.39	0.0008
Eukaryotic translation initiation factor 1A, X-chromosomal;Eukaryotic translation initiation factor 1A	<i>Eif1ax;Eif1a;Gm5039;Gm5662;Gm8300;Gm2016;Gm21936;Gm2056;Gm6803;Gm2035;Gm2075</i>	-1.39	0.0117
Golgi pH regulator	<i>Gpr89a</i>	-1.4	0.0063
Mannose-1-phosphate guanyltransferase beta	<i>Gmppb</i>	-1.4	0.0104
KN motif and ankyrin repeat domain-containing protein 2	<i>Kank2</i>	-1.4	0.0068
Phosphoglucomutase-like protein 5	<i>Pgm5</i>	-1.4	0.0052
	<i>Mettl7a1</i>	-1.4	0.0158
Rhotekin	<i>Rtkn</i>	-1.4	0.0158
NHL repeat-containing protein 3	<i>Nhlrc3</i>	-1.4	0.0039
Transmembrane protein 230	<i>Tmem230</i>	-1.4	0.0104
AFG3-like protein 2	<i>Afg3l2</i>	-1.4	0.0148
GDP-mannose 4,6 dehydratase	<i>Gmds</i>	-1.4	0.0034
Sodium/myo-inositol cotransporter 2	<i>Slc5a11</i>	-1.4	0.0105
Aldose 1-epimerase	<i>Galm</i>	-1.4	0.0006
Protein farnesyltransferase subunit beta	<i>Fntb</i>	-1.41	0.0002
NAD(P)H-hydrate epimerase	<i>Apoa1bp</i>	-1.42	0.0018
Sulfite oxidase, mitochondrial	<i>Suox</i>	-1.42	0.0041
Uncharacterized protein C1orf43 homolog	<i>4933434E20Rik</i>	-1.42	0.0065
Cytosolic 10-formyltetrahydrofolate dehydrogenase	<i>Aldh1l1</i>	-1.42	0.0035
Fucose mutarotase	<i>Fuom</i>	-1.42	0.0046
Diphosphoinositol polyphosphate phosphohydrolase 2	<i>Nudt4</i>	-1.42	0.0183
Aspartoacylase	<i>Aspa</i>	-1.43	0.0003
Interferon regulatory factor 2-binding protein 1	<i>Irf2bp1</i>	-1.44	0.0218
Protein QIL1	<i>Qil1</i>	-1.44	0.0007
Glycosaminoglycan xylosylkinase	<i>Fam20b</i>	-1.45	0.005
Aminopeptidase B	<i>Rnpep</i>	-1.45	0.0012
Heterogeneous nuclear ribonucleoprotein U-like protein 1	<i>Hnrnpul1</i>	-1.45	0.0042
Filamin-C	<i>Flnc</i>	-1.45	0.0033
40S ribosomal protein S5;40S ribosomal protein S5, N-terminally processed	<i>Rps5</i>	-1.46	0.0005

Hemoglobin subunit alpha	<i>haemaglobin alpha 2;Hba</i>	-1.46	0.0066
Protein MEMO1	<i>Memo1</i>	-1.46	0.0039
FERM, RhoGEF and pleckstrin domain-containing protein 2	<i>Farp2</i>	-1.46	0.0013
Stromal membrane-associated protein 1	<i>Smap1</i>	-1.47	0.0027
Activating signal cointegrator 1 complex subunit 2	<i>Ascc2</i>	-1.47	0.0055
Uncharacterized protein KIAA2013	<i>Kiaa2013</i>	-1.47	0.0142
Pyridoxine-5-phosphate oxidase	<i>Pnpo</i>	-1.48	0.0196
Cytochrome c oxidase assembly factor 7	<i>Coa7</i>	-1.48	0.0212
Heterogeneous nuclear ribonucleoprotein A/B	<i>Hnrnpab</i>	-1.48	0.0291
Cyclin-dependent kinase 9	<i>Cdk9</i>	-1.48	0.0119
Nicotinamide/nicotinic acid mononucleotide adenylyltransferase 3	<i>Nmnat3</i>	-1.48	0.0112
	<i>Sar1a</i>	-1.49	0.0154
RNA-binding protein 10	<i>Rbm10</i>	-1.49	0.0094
Lipolysis-stimulated lipoprotein receptor	<i>Lsr</i>	-1.5	0.0146
Dipeptidyl peptidase 3	<i>Dpp3</i>	-1.5	0.0064
Lambda-crystallin homolog	<i>Cryl1</i>	-1.5	0.0204
Peptidyl-prolyl cis-trans isomerase F, mitochondrial	<i>Ppif</i>	-1.5	0.0064
Nucleolar GTP-binding protein 2	<i>Gnl2</i>	-1.51	0.0101
Lysine--tRNA ligase	<i>Kars</i>	-1.51	0.0139
	<i>Cyp4f13</i>	-1.52	0.0045
Breast cancer metastasis-suppressor 1 homolog	<i>Brms1</i>	-1.52	0.0045
Myeloid-derived growth factor	<i>Mydgf</i>	-1.53	0.011
Lactoylglutathione lyase	<i>Glo1</i>	-1.54	0.0196
Ribonuclease T2	<i>Rnaset2</i>	-1.54	0.01
Myosin regulatory light polypeptide 9	<i>Myl9</i>	-1.55	0.0362
GTP-binding protein SAR1b	<i>Sar1b</i>	-1.55	0.0297
Protein NipSnap homolog 3B	<i>Nipsnap3b</i>	-1.56	0.0428
Endoplasmic reticulum-Golgi intermediate compartment protein 3	<i>Ergic3</i>	-1.56	0.0194
Thioredoxin domain-containing protein 17	<i>Txndc17</i>	-1.56	0.0175
U6 snRNA-associated Sm-like protein LSM7	<i>Lsm7</i>	-1.57	0.0435
40S ribosomal protein S21	<i>Rps21</i>	-1.57	0.0215
Thioredoxin domain-containing protein 12	<i>Txndc12</i>	-1.58	0.0071
Adaptin ear-binding coat-associated protein 1	<i>Necap1</i>	-1.58	0.009
Protein FAM136A	<i>Fam136a</i>	-1.58	0.0196
OCIA domain-containing protein 1	<i>Ociad1</i>	-1.58	0.0002
Bifunctional purine biosynthesis protein PURH;Phosphoribosylaminoimidazolecarboxamide formyltransferase;IMP cyclohydrolase	<i>Atic</i>	-1.59	0.0163
U6 snRNA-associated Sm-like protein LSM4	<i>Lsm4</i>	-1.6	0.0334
Cysteine-rich with EGF-like domain protein 2	<i>Creld2</i>	-1.6	0.0117
5-methylcytosine rRNA methyltransferase NSUN4	<i>Nsun4</i>	-1.61	0.0353
Threonine--tRNA ligase, cytoplasmic	<i>Tars</i>	-1.62	0.0065
Peptidyl-prolyl cis-trans isomerase-like 1	<i>Ppil1</i>	-1.62	0.0109
Peptidyl-prolyl cis-trans isomerase FKBP11	<i>Fkbp11</i>	-1.64	0.0236

Dolichol-phosphate mannosyltransferase subunit 3	<i>Dpm3</i>	-1.64	0.0106
Low molecular weight phosphotyrosine protein phosphatase	<i>Acp1</i>	-1.65	0.0068
3-oxoacyl-[acyl-carrier-protein] synthase, mitochondrial	<i>Oxsm</i>	-1.69	0.0338
SUN domain-containing protein 1	<i>Sun1</i>	-1.69	0.0009
Mitochondrial glutamate carrier 1	<i>Slc25a22</i>	-1.69	0.0461
Phospholysine phosphohistidine inorganic pyrophosphate phosphatase	<i>Lhpp</i>	-1.69	0.05
	<i>2200002D01Rik</i>	-1.69	0.0026
Mitochondrial import inner membrane translocase subunit TIM50	<i>Timm50</i>	-1.7	0.0317
N-acetyl-D-glucosamine kinase	<i>Nagk</i>	-1.7	0.0405
Abcission/NoCut checkpoint regulator	<i>Zfyve19</i>	-1.72	0.0077
Peroxisomal carnitine O-octanoyltransferase	<i>Crot</i>	-1.73	0.0122
Ribosome biogenesis protein BRX1 homolog	<i>Brix1</i>	-1.74	0.0379
6-phosphogluconate dehydrogenase, decarboxylating	<i>Pgd</i>	-1.74	0.0042
Apoptosis-associated speck-like protein containing a CARD	<i>Pycard</i>	-1.75	0.0001
ADP-ribosylation factor GTPase-activating protein 1	<i>Arfgap1</i>	-1.77	0.0242
Protein SET	<i>Set</i>	-1.77	0.0478
LIM domain and actin-binding protein 1	<i>Lima1</i>	-1.79	0.0238
Inositol-3-phosphate synthase 1	<i>Isyna1</i>	-1.85	0.0387
Transcription and mRNA export factor ENY2	<i>Eny2</i>	-1.86	0.0251
Signal peptide peptidase-like 2A	<i>Sppl2a</i>	-1.87	0.0359
SH3 domain-binding glutamic acid-rich-like protein	<i>Sh3bgrl</i>	-1.88	0.0278
Tyrosyl-DNA phosphodiesterase 2	<i>Tdp2</i>	-1.9	0.0085
UPF0160 protein MYG1, mitochondrial	<i>Myg1</i>	-1.91	0.0004
BUB3-interacting and GLEBS motif-containing protein ZNF207	<i>Znf207;Zfp207</i>	-1.93	0.0146
Thioredoxin reductase 1, cytoplasmic	<i>Txnrd1</i>	-1.93	0.0051
Proteasome subunit alpha type-6	<i>PsmA6</i>	-1.96	0.0081
Prolyl endopeptidase	<i>Prep</i>	-1.97	0.0005
Peptidyl-prolyl cis-trans isomerase NIMA-interacting 1	<i>Pin1;Pin1rt1</i>	-2.02	0.0243
Protein canopy homolog 2	<i>Cnpy2</i>	-2.12	0.0025
E3 ubiquitin-protein ligase AMFR	<i>Amfr</i>	-2.17	0.0227
Galactokinase	<i>Galk1</i>	-2.31	0.0302
Guanine deaminase	<i>Gda</i>	-2.33	0.0369
Proteasome subunit alpha type-1	<i>PsmA1</i>	-2.4	0.0014
6-pyruvoyl tetrahydrobiopterin synthase	<i>Pts</i>	-2.45	0.0012
Semaphorin-4G	<i>Sema4g</i>	-2.49	0.0113
Mitochondrial import inner membrane translocase subunit Tim8 A	<i>Timm8a1</i>	-2.67	0.011
Proteasome subunit alpha type-7	<i>PsmA7</i>	-2.82	0.0132
Proteasome subunit alpha type-5	<i>PsmA5</i>	-3.23	0.0427
Serine/threonine-protein kinase 25	<i>Stk25</i>	-10.9	0.0106

**Appendix 4: significantly up- and downregulated proteins in C57BL/6J small intestinal mucosa post administration of 0.125mg/kg LPS**

Protein names	Gene names	Regulation fold change	P value
PHD finger protein 10	<i>Phf10</i>	10.67	0.0017
THAP domain-containing protein 4	<i>Thap4</i>	5.444	0.0004
Lactase-like protein	<i>Lctf</i>	5.103	0.0354
Nucleolar protein 9	<i>Nop9</i>	5.018	0.0181
Reticulon;Reticulon-1	<i>Rtn1</i>	2.785	0.0189
Metastasis-associated protein MTA1	<i>Mta1</i>	2.602	0.0057
Catenin alpha-3	<i>Ctnna3</i>	2.396	0.0041
Proto-oncogene c-Fos	<i>Fos</i>	2.192	0.0009
Acyl-CoA-binding protein	<i>Dbi</i>	1.967	0.0207
Clathrin light chain B	<i>Cltb</i>	1.914	0.0354
	<i>2200002D01Rik</i>	1.843	0.0266
Sorbitol dehydrogenase	<i>Sord</i>	1.815	0.0438
Small ubiquitin-related modifier;Small ubiquitin-related modifier 3	<i>Sumo3</i>	1.81	0.0023
Small acidic protein	<i>Smap;1110004F1ORik</i>	1.799	0.0003
Ran-specific GTPase-activating protein	<i>Ranbp1</i>	1.791	0.0297
Caspase-3;Caspase-3 subunit p17;Caspase-3 subunit p12	<i>Casp3</i>	1.791	0.0058
Copper transport protein ATOX1	<i>Atox1</i>	1.791	0.0451
	<i>Gm20441</i>	1.787	0.0451
39S ribosomal protein L21, mitochondrial	<i>Mrpl21</i>	1.782	0.0077
Guanine deaminase	<i>Gda</i>	1.77	0.0239
GDP-L-fucose synthase	<i>Tsta3</i>	1.764	0.0065
Isocitrate dehydrogenase [NADP] cytoplasmic	<i>Idh1</i>	1.746	0.0379
Cysteine-rich protein 1	<i>Crip1</i>	1.742	0.028
Vacuolar protein sorting-associated protein 29	<i>Vps29</i>	1.732	0.0015
Superoxide dismutase [Cu-Zn]	<i>Sod1</i>	1.731	0.0466
Cytochrome c, somatic	<i>Cycc</i>	1.731	0.0225
	<i>Adh6a</i>	1.697	0.0211
Glucose-6-phosphate isomerase	<i>Gpi</i>	1.693	0.009
Prostaglandin reductase 1	<i>Ptgr1</i>	1.691	0.0254
Mesencephalic astrocyte-derived neurotrophic factor	<i>Manf</i>	1.683	0.0202
Epididymal secretory protein E1	<i>Npc2</i>	1.681	0.0177
Guanylate cyclase activator 2B;Uroguanylin	<i>Guca2b</i>	1.671	0.026
28 kDa heat- and acid-stable phosphoprotein	<i>Pdap1</i>	1.666	0.0178
Transaldolase	<i>Taldo1</i>	1.663	0.0377
Superoxide dismutase [Mn], mitochondrial	<i>Sod2</i>	1.657	0.0057
Malate dehydrogenase, cytoplasmic	<i>Mdh1</i>	1.654	0.0128
Hydroxyacylglutathione hydrolase, mitochondrial	<i>Hagh</i>	1.639	0.0104
L-lactate dehydrogenase;L-lactate dehydrogenase A chain	<i>Ldha</i>	1.638	0.0297
Xaa-Pro aminopeptidase 1	<i>Xpnpep1</i>	1.638	0.011

Ensconsin	<i>Map7</i>	1.623	0.0024
Protein LZIC	<i>Lzic</i>	1.616	0.0341
SH3 domain-binding glutamic acid-rich-like protein	<i>Sh3bgrl</i>	1.615	0.0157
Eukaryotic translation initiation factor 4H	<i>Eif4h</i>	1.612	0.0017
Lambda-crystallin homolog	<i>Cryl1</i>	1.606	0.0184
Creatine kinase B-type	<i>Ckb</i>	1.599	0.0399
Phosphoglycerate kinase 1;Phosphoglycerate kinase	<i>Pgk1</i>	1.594	0.0312
Phenazine biosynthesis-like domain-containing protein 2	<i>Pbld2</i>	1.592	0.0399
Creatine kinase U-type, mitochondrial	<i>Ckmt1</i>	1.59	0.0196
Acidic leucine-rich nuclear phosphoprotein 32 family member B	<i>Anp32b</i>	1.58	0.0332
	<i>Tfg</i>	1.578	0.022
Peptidyl-prolyl cis-trans isomerase A	<i>Ppia;Gm5160</i>	1.576	0.0349
Myeloid-derived growth factor	<i>Mydgf</i>	1.574	0.0297
Thioredoxin reductase 1, cytoplasmic	<i>Txnrd1</i>	1.574	0.0212
Protein disulfide-isomerase	<i>P4hb</i>	1.571	0.033
Glutathione S-transferase omega-1	<i>Gsto1</i>	1.563	0.0305
Beta-hexosaminidase subunit alpha	<i>Hexa</i>	1.561	0.0007
Protein atonal homolog 7	<i>Atoh7</i>	1.559	0.0002
Acylamino-acid-releasing enzyme	<i>Apeh</i>	1.558	0.0224
Hyaluronan-binding protein 2	<i>Habp2</i>	1.557	0.0492
Alcohol dehydrogenase class-3	<i>Adh5</i>	1.551	0.0201
Transgelin-2	<i>Tagln2</i>	1.549	0.0007
Translationally-controlled tumor protein	<i>Tpt1</i>	1.549	0.0465
Essential MCU regulator, mitochondrial	<i>Smdt1</i>	1.548	0.0168
Fos-related antigen 2	<i>Fosl2</i>	1.547	0.0069
Thioredoxin domain-containing protein 12	<i>Txndc12</i>	1.546	0.0165
Cytidine deaminase	<i>Cda</i>	1.544	0.0156
Glycerol-3-phosphate dehydrogenase	<i>Gpd1</i>	1.544	0.0134
Triosephosphate isomerase	<i>Tpi1</i>	1.542	0.0288
WD repeat-containing protein 1	<i>Wdr1</i>	1.541	0.0177
GDP-mannose 4,6 dehydratase	<i>Gmds</i>	1.535	0.0429
Protein FAM136A	<i>Fam136a</i>	1.534	0.0345
Alcohol dehydrogenase [NADP(+)]	<i>Akr1a1</i>	1.53	0.0338
Serine/arginine-rich splicing factor 3	<i>Srsf3;Gm12355</i>	1.528	0.0078
D-dopachrome decarboxylase	<i>Ddt</i>	1.527	0.0372
Mth938 domain-containing protein	<i>Aamdc</i>	1.525	0.026
Alpha-2-macroglobulin receptor-associated protein	<i>Lrpap1</i>	1.515	0.0476
Fatty acid-binding protein, liver	<i>Fabp1</i>	1.507	0.036
Stress-induced-phosphoprotein 1	<i>Stip1</i>	1.507	0.0386
Alanine aminotransferase 1	<i>Gpt</i>	1.507	0.0483
Src substrate cortactin	<i>Ctnn</i>	1.506	0.0008
Clathrin light chain A	<i>Clta</i>	1.496	0.0219
Xanthine dehydrogenase/oxidase;Xanthine dehydrogenase;Xanthine oxidase	<i>Xdh</i>	1.488	0.0191
Taperin	<i>Tprn</i>	1.484	0.0032

Ubiquitin-fold modifier 1	<i>Ufm1</i>	1.484	0.012
Major vault protein	<i>Mvp</i>	1.478	0.0268
Xaa-Pro dipeptidase	<i>Pepd</i>	1.474	0.0218
Adrenodoxin, mitochondrial	<i>Fdx1</i>	1.474	0.0162
Serine/arginine-rich splicing factor 6	<i>Srsf6</i>	1.469	0.0188
Beta-lactamase-like protein 2	<i>Lactb2</i>	1.469	0.0073
Glutathione synthetase	<i>Gss</i>	1.464	0.0445
Nicotinamide phosphoribosyltransferase	<i>Nampt</i>	1.464	0.0442
Serine/arginine-rich splicing factor 1	<i>Srsf1</i>	1.463	0.0237
Retinol-binding protein 2	<i>Rbp2</i>	1.463	0.0306
	<i>Fcgbp</i>	1.462	0.0214
V-type proton ATPase subunit G 1	<i>Atp6v1g1</i>	1.462	0.0035
Aldose 1-epimerase	<i>Galm</i>	1.459	0.0426
Caspase-6;Caspase-6 subunit p18;Caspase-6 subunit p11	<i>Casp6</i>	1.455	0.0165
Peroxiredoxin-6	<i>Prdx6</i>	1.455	0.0479
Hypermethylated in cancer 2 protein	<i>Hic2</i>	1.45	0.007
Protein deglycase DJ-1	<i>Park7</i>	1.447	0.0115
Na(+)/H(+) exchange regulatory cofactor NHE-RF1	<i>Slc9a3r1</i>	1.447	0.0082
Calreticulin	<i>Calr</i>	1.443	0.0388
Cathepsin Z	<i>Ctsz</i>	1.44	0.0221
Peroxisomal carnitine O-octanoyltransferase	<i>Crot</i>	1.44	0.0295
Pterin-4-alpha-carbinolamine dehydratase	<i>Pcbd1</i>	1.439	0.0121
6-phosphogluconate dehydrogenase, decarboxylating	<i>Pgd</i>	1.438	0.0346
Acid sphingomyelinase-like phosphodiesterase 3a	<i>Smpdl3a</i>	1.437	0.0104
Serine/arginine-rich splicing factor 7	<i>Srsf7</i>	1.437	0.0204
Cytochrome c oxidase assembly factor 7	<i>Coa7</i>	1.436	0.0457
Cytoplasmic aconitate hydratase	<i>Aco1</i>	1.435	0.0478
Vacuolar protein sorting-associated protein 26A	<i>Vps26a</i>	1.434	0.0237
Prefoldin subunit 6	<i>Pfdn6</i>	1.432	0.0383
Espin	<i>Espin</i>	1.432	0.0255
Aspartate aminotransferase, cytoplasmic	<i>Got1</i>	1.429	0.0328
Cofilin-1	<i>Cfl1</i>	1.428	0.0131
DAZ-associated protein 1	<i>Dazap1</i>	1.423	0.0085
Leukotriene A-4 hydrolase	<i>Lta4h</i>	1.421	0.0436
SRA stem-loop-interacting RNA-binding protein, mitochondrial	<i>Slirp</i>	1.421	0.0061
N-acetylglucosamine-6-sulfatase	<i>Gns</i>	1.419	0.0161
WAS/WASL-interacting protein family member 3	<i>Wipf3</i>	1.412	0.0442
Phosphatidylethanolamine-binding protein 1;Hippocampal cholinergic neurostimulating peptide	<i>Pebp1</i>	1.406	0.0441
Far upstream element-binding protein 2	<i>Khsrp</i>	1.401	0.038
Calmodulin-like protein 4	<i>Calml4</i>	1.397	0.0122
High mobility group protein B3	<i>Hmgb3</i>	1.396	0.0299
Cytosolic acyl coenzyme A thioester hydrolase	<i>Acot7</i>	1.387	0.0421
Cingulin	<i>Cgn</i>	1.386	0.0106

RNA-binding protein EWS	<i>Ewsr1</i>	1.384	0.0258
Guanine nucleotide-binding protein subunit beta-2-like 1	<i>Gnb2l1</i>	1.384	0.0353
40S ribosomal protein S28	<i>Rps28;Gm10263</i>	1.382	0.0006
14 kDa phosphohistidine phosphatase	<i>Phpt1</i>	1.382	0.0168
Microsomal triglyceride transfer protein large subunit	<i>Mttp</i>	1.381	0.0293
Protein phosphatase 1 regulatory subunit 12C	<i>Ppp1r12c</i>	1.381	0.0003
E3 ubiquitin-protein ligase MYCBP2	<i>Mycbp2</i>	1.38	0.0411
Ladinin-1	<i>Lad1</i>	1.378	0.0039
Pyridoxine-5-phosphate oxidase	<i>Pnpo</i>	1.377	0.026
39S ribosomal protein L12, mitochondrial	<i>Mrpl12</i>	1.377	0.0374
Fructose-1,6-bisphosphatase isozyme 2	<i>Fbp2</i>	1.376	0.0368
Aldose reductase-related protein 1	<i>Akr1b7</i>	1.372	0.0235
Isochorismatase domain-containing protein 1	<i>Isoc1</i>	1.369	0.0002
Delta(3,5)-Delta(2,4)-dienoyl-CoA isomerase, mitochondrial	<i>Ech1</i>	1.366	0.0384
Cystatin-B	<i>Cstb</i>	1.365	0.0365
Acetyl-CoA acetyltransferase, cytosolic	<i>Acat2;Acat3</i>	1.364	0.0367
Dynactin subunit 2	<i>Dctn2</i>	1.363	0.0293
Nuclear transport factor 2	<i>Nutf2</i>	1.363	0.0024
Peroxisome oxidoreductin-5, mitochondrial	<i>Prdx5</i>	1.362	0.0269
Nucleoside diphosphate kinase;Nucleoside diphosphate kinase B	<i>Gm20390;Nme2</i>	1.362	0.043
<i>Ester hydrolase C11orf54 homolog</i>		1.362	0.0459
Protein disulfide-isomerase A4	<i>Pdia4</i>	1.36	0.0325
Cathepsin S	<i>Ctss</i>	1.358	0.0279
Sulfiredoxin-1	<i>Srxn1</i>	1.354	0.0109
Coiled-coil domain-containing protein 9	<i>Ccdc9</i>	1.35	0.0387
PDZ and LIM domain protein 2	<i>Pdlim2</i>	1.347	0.0056
Ankyrin repeat and SAM domain-containing protein 4B	<i>Anks4b</i>	1.346	0.0329
Alpha-enolase	<i>Eno1</i>	1.346	0.028
Serpin B6	<i>Serpinb6a;Serpinb6</i>	1.346	0.0213
b(0,+)-type amino acid transporter 1	<i>Slc7a9</i>	1.344	0.0391
UDP-glucose 4-epimerase	<i>Gale</i>	1.344	0.0319
Galectin-2	<i>Lgals2</i>	1.343	0.0365
Prostaglandin reductase 2	<i>Ptgr2</i>	1.341	0.0282
Putative adenosylhomocysteinase 2	<i>Ahcyl1</i>	1.339	0.0049
Trehalase	<i>Treh</i>	1.339	0.0377
Osteoclast-stimulating factor 1	<i>Ostf1</i>	1.337	0.0026
Heat shock 70 kDa protein 4	<i>Hspa4</i>	1.335	0.0222
Four and a half LIM domains protein 2	<i>Fhl2</i>	1.334	0.0046
Uridine phosphorylase 1	<i>Upp1</i>	1.334	0.027
Isocitrate dehydrogenase [NAD] subunit alpha, mitochondrial	<i>Idh3a</i>	1.329	0.0224
Spectrin alpha chain, non-erythrocytic 1	<i>Sptan1</i>	1.329	0.0157
EF-hand domain-containing protein D2	<i>Efhd2</i>	1.328	0.0085

Serine/arginine repetitive matrix protein 1	<i>Srrm1</i>	1.328	0.0197
	<i>Sptan1</i>	1.327	0.0364
Polyglutamine-binding protein 1	<i>Pqbp1</i>	1.326	0.0269
Thioredoxin	<i>Txn</i>	1.326	0.0286
Sulfite oxidase, mitochondrial	<i>Suox</i>	1.325	0.0149
14-3-3 protein sigma	<i>Sfn</i>	1.325	0.009
Ubiquitin-conjugating enzyme E2 L3	<i>Ube2l3</i>	1.324	0.0344
Proteasome subunit alpha type-4;Proteasome subunit alpha type	<i>Psm4</i>	1.322	0.0269
Transcription and mRNA export factor ENY2	<i>Eny2</i>	1.32	0.0395
PDZ and LIM domain protein 1	<i>Pdlim1</i>	1.318	0.0215
	<i>Lmo7</i>	1.318	0.0136
Caspase-7;Caspase-7 subunit p20;Caspase-7 subunit p11	<i>Casp7</i>	1.318	0.0164
Xenotropic and polytropic retrovirus receptor 1	<i>Xpr1</i>	1.316	0.0225
TBC1 domain family member 4	<i>Tbc1d4</i>	1.315	0.014
N-acetylglucosamine-1-phosphotransferase subunits alpha/beta	<i>Gnptab</i>	1.312	0.0274
Epsin-1	<i>Epn1</i>	1.308	0.0095
Syntaxin-3	<i>Stx3</i>	1.307	0.0001
UV excision repair protein RAD23 homolog B	<i>Rad23b</i>	1.307	0.0083
Protein lin-7 homolog C	<i>Lin7c</i>	1.303	0.0028
Cytosol aminopeptidase	<i>Lap3</i>	1.302	0.0129
Leucine zipper protein 1	<i>Luzp1</i>	1.299	0.0276
UMP-CMP kinase	<i>Cmpk1</i>	1.296	0.0231
Calcium-regulated heat stable protein 1	<i>Carhsp1</i>	1.295	0.0298
Uncharacterized protein KIAA1211	<i>C530008M17Rik; Kiaa1211</i>	1.294	0.0252
Endoplasmic reticulum resident protein 29	<i>Erp29</i>	1.294	0.0266
UV excision repair protein RAD23 homolog A	<i>Rad23a</i>	1.291	0.0295
Glyceraldehyde-3-phosphate dehydrogenase	<i>Gapdh;Gm3839</i>	1.287	0.0096
Synaptosomal-associated protein 29	<i>Snap29</i>	1.284	0.0037
Chloride intracellular channel protein 1	<i>Clic1</i>	1.282	0.0106
Gamma-glutamyltranspeptidase 1	<i>Ggt1</i>	1.282	0.0096
Adenosylhomocysteinase;Putative adenosylhomocysteinase 3	<i>Ahcyl2</i>	1.281	0.0088
Aspartyl aminopeptidase	<i>Dnpep</i>	1.28	0.0157
Heterogeneous nuclear ribonucleoproteins A2/B1	<i>Hnrnpa2b1</i>	1.279	0.0106
Protein MAL2	<i>Mal2</i>	1.276	0.0283
Putative N-acetylglucosamine-6-phosphate deacetylase	<i>Amdhd2</i>	1.276	0.0194
Acetyl-CoA acetyltransferase, mitochondrial	<i>Acat1</i>	1.276	0.0183
Platelet-activating factor acetylhydrolase IB subunit gamma	<i>Pafah1b3</i>	1.275	0.0142
Heterogeneous nuclear ribonucleoprotein F;Heterogeneous nuclear ribonucleoprotein F, N-terminally processed	<i>Hnrnpf</i>	1.275	0.0175
FGFR1 oncogene partner 2 homolog	<i>Fgfr1op2</i>	1.271	0.0193
Pyruvate kinase PKM	<i>Pkm</i>	1.269	0.0006

Serine/threonine-protein phosphatase CPPED1	<i>Cpped1</i>	1.268	0.0258
Heterogeneous nuclear ribonucleoproteins C1/C2	<i>Hnrnpc</i>	1.267	0.0209
Phosphomannomutase 2	<i>Pmm2</i>	1.265	0.0197
Endoplasmic reticulum resident protein 44	<i>Erp44</i>	1.263	0.0099
N-acetylgalactosamine-6-sulfatase	<i>Galns</i>	1.261	0.0083
Cathepsin D	<i>Ctsd</i>	1.26	0.0236
Peptidyl-prolyl cis-trans isomerase B	<i>Ppib</i>	1.257	0.0167
Hephaestin	<i>Heph</i>	1.257	0.0154
Sorting nexin-3	<i>Snx3</i>	1.256	0.0028
40S ribosomal protein S12	<i>Rps12</i>	1.251	0.01
Scaffold attachment factor B1	<i>Safb</i>	1.25	0.005
Semaphorin-4G	<i>Sema4g</i>	1.248	0.004
Gamma-soluble NSF attachment protein	<i>Napg</i>	1.244	0.0057
E3 ubiquitin-protein ligase UBR2	<i>Ubr2</i>	1.239	0.0154
Ig alpha chain C region	<i>Igha</i>	1.238	0.0174
Plasma alpha-L-fucosidase	<i>Fuca2</i>	1.236	0.0051
Sorcin	<i>Sri</i>	1.234	0.0036
Clathrin interactor 1	<i>Clint1</i>	1.23	0.0153
	<i>Srsf11</i>	1.227	0.0142
UBX domain-containing protein 1	<i>Ubxn1</i>	1.22	0.001
Protein cordon-bleu	<i>Cobl</i>	1.22	0.0044
Heterogeneous nuclear ribonucleoprotein A1	<i>Hnrnpa1</i>	1.218	0.0021
E3 SUMO-protein ligase PIAS1;E3 SUMO-protein ligase PIAS2	<i>Pias1;Pias2</i>	1.215	0.0108
	<i>Ppm1b</i>	1.214	0.0019
Arpin	<i>Arpin</i>	1.212	0.0009
Acyl-coenzyme A thioesterase 8	<i>Acot8</i>	1.209	0.0015
Catenin delta-1	<i>Ctnnd1</i>	1.207	0.0006
General transcription factor 3C polypeptide 4	<i>Gtf3c4</i>	1.204	0.0003
Mannose-6-phosphate isomerase	<i>Mpi</i>	1.2	0.0029
U6 snRNA-associated Sm-like protein LSM2	<i>Lsm2</i>	1.19	0.0022
ATP-dependent 6-phosphofructokinase;ATP-dependent 6-phosphofructokinase, platelet type	<i>Pfkp</i>	1.166	0.0001
HEAT repeat-containing protein 5A	<i>Heatr5a</i>	-1.15	0.0003
Vacuolar protein sorting-associated protein 33B	<i>Vps33b</i>	-1.15	0.0003
Importin-11	<i>Ipo11</i>	-1.16	0.0004
Helicase with zinc finger domain 2	<i>Helz2</i>	-1.16	0.0001
Serine/threonine-protein phosphatase 2A 56 kDa regulatory subunit alpha isoform	<i>Ppp2r5a</i>	-1.16	0.0001
Pannexin-1	<i>Panx1</i>	-1.16	0.0013
Mitogen-activated protein kinase 1	<i>Mapk1</i>	-1.17	0.0001
5-AMP-activated protein kinase catalytic subunit alpha-1	<i>Prkaa1</i>	-1.17	0.0001
Selenoprotein O	<i>Selo</i>	-1.17	0.001
Histone-lysine N-methyltransferase EZH2	<i>Ezh2</i>	-1.17	0.0011
E3 ubiquitin-protein ligase RNF31	<i>Rnf31</i>	-1.17	0.0016
WD repeat-containing protein 13	<i>Wdr13</i>	-1.17	0.0006
DNA-directed RNA polymerase II subunit RPB7	<i>Polr2g</i>	-1.17	0.0012

Protein FAM98B	<i>Fam98b</i>	-1.17	0.0004
Type 2 lactosamine alpha-2,3-sialyltransferase	<i>St3gal6</i>	-1.17	0.0012
Cytosolic Fe-S cluster assembly factor NUBP2	<i>Nubp2</i>	-1.17	0.0001
Signal transducer and transcription activator 6	<i>Stat6</i>	-1.17	0.0019
TBC1 domain family member 10B	<i>Tbc1d10b</i>	-1.17	0.0021
Mitogen-activated protein kinase kinase kinase 2	<i>Map3k2</i>	-1.17	0.0014
Palmitoyltransferase ZDHHC13;Palmitoyltransferase	<i>Zdhhc13</i>	-1.17	0.0014
NLR family CARD domain-containing protein 4	<i>Nlrc4</i>	-1.17	0.0021
Zinc finger protein 622	<i>Znf622</i>	-1.18	0.0018
Conserved oligomeric Golgi complex subunit 7	<i>Cog7</i>	-1.18	0.0004
APOBEC1 complementation factor	<i>A1cf</i>	-1.18	0.0003
Polypeptide N-acetylgalactosaminyltransferase 6	<i>Galnt6</i>	-1.18	0.0021
Exocyst complex component 2	<i>Exoc2</i>	-1.18	0.0015
Conserved oligomeric Golgi complex subunit 4	<i>Cog4</i>	-1.18	0.0026
Vacuolar protein sorting-associated protein 53 homolog	<i>Vps53</i>	-1.18	0.0007
Serine/threonine-protein kinase mTOR	<i>Mtor</i>	-1.18	0.0009
Cytoplasmic tRNA 2-thiolation protein 2	<i>Ctu2</i>	-1.18	0.0008
Vacuolar protein sorting-associated protein 51 homolog	<i>Vps51</i>	-1.18	0.0036
X-ray repair cross-complementing protein 5	<i>Xrcc5</i>	-1.18	0.0017
Anaphase-promoting complex subunit 2	<i>Anapc2</i>	-1.18	0.0024
Ras-related GTP-binding protein C	<i>Rragc</i>	-1.18	0.0006
Translocation protein SEC63 homolog	<i>Sec63</i>	-1.18	0.0004
THUMP domain-containing protein 3	<i>Thumpd3</i>	-1.19	0.0038
39S ribosomal protein L23, mitochondrial	<i>Mrpl23</i>	-1.19	0.0017
Ketosamine-3-kinase	<i>Fn3krp</i>	-1.19	0.0027
Inositol polyphosphate 1-phosphatase	<i>Inpp1</i>	-1.19	0.0033
GH3 domain-containing protein	<i>Ghdc</i>	-1.19	0.0022
Protein phosphatase 1H	<i>Ppm1h</i>	-1.19	0.0002
Interleukin enhancer-binding factor 3	<i>Ilf3</i>	-1.19	0.001
Apoptosis-inducing factor 2	<i>Aifm2</i>	-1.19	0.0029
Protein O-glycosyltransferase 1	<i>Poglut1</i>	-1.19	0.0014
Nuclear factor NF-kappa-B p105 subunit;Nuclear factor NF-kappa-B p50 subunit	<i>Nfkb1</i>	-1.19	0.0008
E3 ubiquitin-protein ligase listerin	<i>Ltn1</i>	-1.19	0.0038
Kelch-like ECH-associated protein 1	<i>Keap1</i>	-1.19	0.0021
	<i>Brd1</i>	-1.19	0.0041
Patatin-like phospholipase domain-containing protein 2	<i>Pnpla2</i>	-1.19	0.001
Mitochondrial intermediate peptidase	<i>Mipep</i>	-1.19	0.0007
Spermatogenesis-associated protein 5	<i>Spata5</i>	-1.2	0.0027
Tubulin-tyrosine ligase-like protein 12	<i>Ttl12</i>	-1.2	0.0024
3-keto-steroid reductase	<i>Hsd17b7</i>	-1.2	0.0002
Glycoprotein-N-acetylgalactosamine 3-beta- galactosyltransferase 1	<i>C1galt1</i>	-1.2	0.0014
Myc-associated zinc finger protein	<i>Vezf1;Maz;Patz1</i>	-1.2	0.0042

Protein-tyrosine kinase 2-beta	<i>Ptk2b</i>	-1.2	0.0013
WD repeat and HMG-box DNA-binding protein 1	<i>Wdhd1</i>	-1.2	0.0031
SWI/SNF-related matrix-associated actin-dependent regulator of chromatin subfamily D member 1	<i>Smarcd1</i>	-1.2	0.0002
Ubiquitin carboxyl-terminal hydrolase;Ubiquitin carboxyl-terminal hydrolase 19	<i>Usp19</i>	-1.2	0.0043
Mitochondrial ribonuclease P protein 1	<i>Trmt10c</i>	-1.2	0.0006
Rhotekin	<i>Rtkn</i>	-1.2	0.0049
TRMT1-like protein	<i>Trmt1l</i>	-1.2	0.007
E2/E3 hybrid ubiquitin-protein ligase UBE2O	<i>Ube2o</i>	-1.2	0.0057
Insulin-like growth factor 2 mRNA-binding protein 2	<i>Igf2bp2</i>	-1.2	0.0025
N-alpha-acetyltransferase 25, NatB auxiliary subunit	<i>Naa25</i>	-1.2	0.0034
Sorting nexin-14	<i>Snx14</i>	-1.2	0.0044
L-seryl-tRNA(Sec) kinase	<i>Pstk</i>	-1.2	0.0076
Phosphatidylinositol 3-kinase;Phosphatidylinositol 3-kinase catalytic subunit type 3	<i>Pik3c3</i>	-1.2	0.0005
Thioredoxin-interacting protein	<i>Txnip</i>	-1.2	0.0017
Phosphatidylinositol transfer protein beta isoform	<i>Pitpnb</i>	-1.2	0.0009
Uncharacterized protein C18orf8 homolog	<i>Mic1</i>	-1.2	0.0008
Unconventional myosin-VIIa	<i>Myo7a</i>	-1.2	0.0008
Dynammin-1	<i>Dnm1</i>	-1.21	0.001
Crooked neck-like protein 1	<i>Crnkl1</i>	-1.21	0.0006
Probable ATP-dependent RNA helicase DDX47	<i>Ddx47</i>	-1.21	0.0012
[Pyruvate dehydrogenase (acetyl-transferring)] kinase isozyme 1, mitochondrial	<i>Pdk1</i>	-1.21	0.0067
Serine/threonine-protein kinase SMG1	<i>Smg1</i>	-1.21	0.003
Kinesin-like protein KIF3B;Kinesin-like protein KIF3B, N-terminally processed	<i>Kif3b</i>	-1.21	0.0022
Myotubularin-related protein 12	<i>Mtmr12</i>	-1.21	0.0008
Pentatricopeptide repeat-containing protein 2, mitochondrial	<i>Ptcd2</i>	-1.21	0.0012
Ubiquitin-conjugating enzyme E2 E3;Ubiquitin-conjugating enzyme E2 E2	<i>Ube2e3;Ube2e2</i>	-1.21	0.0077
Protein FAM45A	<i>Fam45a</i>	-1.21	0.0032
SHC-transforming protein 1	<i>Shc1</i>	-1.21	0.0026
N-acetylglutamate synthase, mitochondrial;N-acetylglutamate synthase long form;N-acetylglutamate synthase short form;N-acetylglutamate synthase conserved domain form	<i>Nags</i>	-1.21	0.0011
Activity-dependent neuroprotector homeobox protein	<i>Adnp</i>	-1.21	0.0089
Intron-binding protein aquarius	<i>Aqr</i>	-1.21	0.0012
Probable proline--tRNA ligase, mitochondrial	<i>Pars2</i>	-1.21	0.0004
DnaJ homolog subfamily B member 14	<i>Dnajb14</i>	-1.21	0.0042
Signal transducer and activator of transcription 5B;Signal transducer and activator of transcription;Signal transducer and activator of transcription 5A	<i>Stat5b;Stat5a</i>	-1.21	0.0075

Mitogen-activated protein kinase;Mitogen-activated protein kinase 8	<i>Mapk8</i>	-1.21	0.0054
Inhibitor of nuclear factor kappa-B kinase subunit alpha	<i>Chuk</i>	-1.21	0.0055
Translocation protein SEC62	<i>Sec62</i>	-1.21	0.0032
Choline/ethanolamine kinase	<i>Chkb</i>	-1.21	0.0026
Selenoprotein H	<i>2700094K13Rik;Selh</i>	-1.21	0.0005
Cell cycle progression protein 1	<i>Ccpg1</i>	-1.21	0.0081
Mimitin, mitochondrial	<i>Ndufaf2</i>	-1.21	0.0097
Importin-4	<i>Ipo4</i>	-1.21	0.0027
	<i>Fryl</i>	-1.21	0.0058
<i>Uncharacterized protein C7orf26 homolog</i>		-1.21	0.003
Serine/threonine-protein phosphatase PGAM5, mitochondrial	<i>Pgam5</i>	-1.21	0.0084
Poly(A) polymerase alpha	<i>Papola</i>	-1.21	0.0051
Elongator complex protein 4	<i>Elp4</i>	-1.21	0.0002
MAGUK p55 subfamily member 6	<i>Mpp6</i>	-1.21	0.0033
GTP-binding protein Rheb	<i>Rheb</i>	-1.22	0.007
UPF0505 protein C16orf62 homolog	<i>9030624J02Rik</i>	-1.22	0.0051
	<i>Ttc37</i>	-1.22	0.008
Phospholipase DDHD1	<i>Ddhd1</i>	-1.22	0.0036
Macrophage erythroblast attacher	<i>Maea</i>	-1.22	0.0006
Mitochondrial ubiquitin ligase activator of NFKB 1	<i>Mul1</i>	-1.22	0.0065
Large subunit GTPase 1 homolog	<i>Lsg1</i>	-1.22	0.0079
Nucleolysin TIAR	<i>Tial1</i>	-1.22	0.0061
Ubiquitin carboxyl-terminal hydrolase;Ubiquitin carboxyl-terminal hydrolase 24	<i>Usp24</i>	-1.22	0.0006
Dual specificity mitogen-activated protein kinase kinase 4	<i>Map2k4</i>	-1.22	0.002
Tudor domain-containing protein 7	<i>Tdrd7</i>	-1.22	0.0029
Tyrosine-protein phosphatase non-receptor type 11	<i>Ptpn11</i>	-1.22	0.0049
Exosome complex exonuclease RRP44	<i>Dis3</i>	-1.22	0.0075
Fermitin family homolog 1	<i>Fermt1</i>	-1.22	0.0029
RNA-binding protein 39	<i>Rbm39</i>	-1.22	0.0103
Coiled-coil and C2 domain-containing protein 1A	<i>Cc2d1a</i>	-1.22	0.001
Polypeptide N-acetylgalactosaminyltransferase 4	<i>Galnt4</i>	-1.22	0.002
	<i>Raph1</i>	-1.22	0.0032
Deubiquitinating protein VCIP135	<i>Vcpip1</i>	-1.22	0.0003
Reticulon-3	<i>Rtn3</i>	-1.22	0.0035
6-phosphofructo-2-kinase/fructose-2,6-bisphosphatase 4;6-phosphofructo-2-kinase;Fructose-2,6-bisphosphatase	<i>Pfkfb4</i>	-1.22	0.0029
Vacuolar protein sorting-associated protein 33A	<i>Vps33a</i>	-1.22	0.0024
Sestrin-1	<i>Sesn1</i>	-1.22	0.0115
Nucleoporin NUP188 homolog	<i>Nup188</i>	-1.22	0.01
	<i>Nbeal1</i>	-1.22	0.0076

Ubiquitin-conjugating enzyme E2 Q1	<i>Ube2q1</i>	-1.22	0.0069
26S proteasome non-ATPase regulatory subunit 5	<i>Psmc5</i>	-1.22	0.0002
LIM and cysteine-rich domains protein 1	<i>Lmcd1</i>	-1.22	0.0045
Transmembrane protein 214	<i>Tmem214</i>	-1.22	0.0006
Tyrosine-protein kinase STYK1	<i>Styk1</i>	-1.23	0.0096
Ras-related protein Ral-A	<i>Rala</i>	-1.23	0.0073
Diacylglycerol kinase alpha	<i>Dgka</i>	-1.23	0.0027
Transmembrane protein 230	<i>Tmem230</i>	-1.23	0.008
Protein-associating with the carboxyl-terminal domain of ezrin	<i>Scyl3</i>	-1.23	0.0021
SCY1-like protein 2	<i>Scyl2</i>	-1.23	0.0038
Protein Hikeshi	<i>L7rn6;l7Rn6</i>	-1.23	0.0002
ORM1-like protein 1	<i>Gm28778;Ormdl1</i>	-1.23	0.0006
Cullin-5	<i>Cul5</i>	-1.23	0.0061
Ferrochelatase;Ferrochelatase, mitochondrial	<i>Fech</i>	-1.23	0.0032
Protein FAM49B	<i>Fam49b</i>	-1.23	0.0053
Ubiquitin carboxyl-terminal hydrolase CYLD	<i>Cyld</i>	-1.23	0.0079
Cell death activator CIDE-B	<i>Cideb</i>	-1.23	0.0004
Selenocysteine-specific elongation factor	<i>Eefsec</i>	-1.23	0.0115
Serine/threonine-protein kinase TAO1	<i>Taok1</i>	-1.23	0.011
DNA primase large subunit	<i>Prim2</i>	-1.23	0.0092
Conserved oligomeric Golgi complex subunit 6	<i>Cog6</i>	-1.23	0.004
Phosphatidylinositol 4-kinase type 2-alpha	<i>Pi4k2a</i>	-1.23	0.0113
Cyclin-T1	<i>Ccnt1</i>	-1.23	0.0069
Zinc transporter 7	<i>Slc30a7</i>	-1.23	0.0008
Cullin-3	<i>Cul3</i>	-1.23	0.0069
Interferon-stimulated 20 kDa exonuclease-like 2	<i>Isg20l2</i>	-1.23	0.0064
Leucine-rich repeat protein SHOC-2	<i>Shoc2</i>	-1.23	0.0121
V-type proton ATPase subunit a;V-type proton ATPase 116 kDa subunit a isoform 1	<i>Atp6v0a1</i>	-1.23	0.0105
Galactose-3-O-sulfotransferase 2	<i>Gm6086;Gm9994;Gal3st2</i>	-1.23	0.0011
mRNA turnover protein 4 homolog	<i>Mrto4</i>	-1.23	0.0055
Glycogen synthase kinase-3 alpha	<i>Gsk3a</i>	-1.23	0.0017
Signal recognition particle subunit SRP72	<i>Srp72</i>	-1.23	0.006
Condensin-2 complex subunit D3	<i>Ncapd3</i>	-1.23	0.0093
Tubulin-specific chaperone E	<i>Tbce</i>	-1.23	0.0028
Polypeptide N-acetylgalactosaminyltransferase 12	<i>Galnt12</i>	-1.23	0.0064
ATP-binding cassette sub-family D member 4	<i>Abcd4</i>	-1.23	0.0051
Replication protein A 32 kDa subunit	<i>Rpa2</i>	-1.23	0.0098
ATP-dependent RNA helicase Dhx29	<i>Dhx29</i>	-1.23	0.0045
Cohesin subunit SA-1	<i>Stag1</i>	-1.23	0.0043
[Pyruvate dehydrogenase (acetyl-transferring)] kinase isozyme 3, mitochondrial	<i>Pdk3</i>	-1.23	0.0035
Nuclear RNA export factor 1	<i>Nxf1</i>	-1.24	0.0046
Laminin subunit beta-1	<i>Lamb1</i>	-1.24	0.0069
Choline transporter-like protein 1	<i>Slc44a1</i>	-1.24	0.0104
ADP-dependent glucokinase	<i>Adpgk</i>	-1.24	0.0002

Active breakpoint cluster region-related protein	<i>Abr</i>	-1.24	0.0053
Cytoplasmic dynein 1 light intermediate chain 2	<i>Dync1li2</i>	-1.24	0.0157
Nuclear receptor subfamily 2 group F member 6	<i>Nr2f6</i>	-1.24	0.0132
Ribosomal protein S6 kinase alpha-3	<i>Rps6ka3</i>	-1.24	0.0109
	<i>Gtf3c3</i>	-1.24	0.0006
Serine/threonine-protein kinase ULK3	<i>Ulk3</i>	-1.24	0.0116
CXXC-type zinc finger protein 1	<i>Cxxc1</i>	-1.24	0.01
ER membrane protein complex subunit 3	<i>Emc3</i>	-1.24	0.0045
Histone acetyltransferase KAT8	<i>Kat8</i>	-1.24	0.0019
Mothers against decapentaplegic homolog;Mothers against decapentaplegic homolog 1;Mothers against decapentaplegic homolog 5	<i>Smad1;Smad5</i>	-1.24	0.0058
	<i>Ncapg</i>	-1.24	0.0132
CCR4-NOT transcription complex subunit 10	<i>Cnot10</i>	-1.24	0.0082
Vacuolar protein sorting-associated protein 52 homolog	<i>Vps52</i>	-1.24	0.0039
Cytochrome c oxidase subunit 7A-related protein, mitochondrial	<i>Cox7a2l</i>	-1.24	0.0102
Interferon-induced very large GTPase 1	<i>Gvin1</i>	-1.24	0.0143
FSD1-like protein	<i>Fsd1l</i>	-1.24	0.0109
Exocyst complex component 4	<i>Exoc4</i>	-1.24	0.0051
Transcriptional adapter 1	<i>Tada1</i>	-1.24	0.0019
Pyroline-5-carboxylate reductase 2	<i>Pycr2</i>	-1.24	0.004
Metastasis-associated protein MTA3	<i>Mta3</i>	-1.24	0.0079
ATP-dependent RNA helicase DDX51	<i>Ddx51</i>	-1.24	0.011
Pre-mRNA-splicing factor CWC22 homolog	<i>Cwc22;Gm13695;Gm13697</i>	-1.24	0.0022
DEP domain-containing mTOR-interacting protein	<i>Deptor</i>	-1.24	0.005
	<i>Gcn1l1</i>	-1.24	0.0113
Retinoblastoma-associated protein	<i>Rb1</i>	-1.24	0.0053
Serine/threonine-protein phosphatase;Serine/threonine-protein phosphatase 2B catalytic subunit beta isoform	<i>Ppp3cb</i>	-1.24	0.0027
Poly(rC)-binding protein 2	<i>Pcbp2</i>	-1.24	0.0053
tRNA pseudouridine synthase-like 1	<i>Pusl1</i>	-1.24	0.003
Cullin-4A	<i>Cul4a</i>	-1.24	0.0048
Prostaglandin G/H synthase 1	<i>Ptgs1</i>	-1.24	0.0021
40S ribosomal protein S27-like;40S ribosomal protein S27	<i>Rps27l</i>	-1.24	0.0136
Eukaryotic translation initiation factor 4E type 2	<i>Eif4e2</i>	-1.24	0.0002
Leukocyte surface antigen CD47	<i>Cd47</i>	-1.24	0.0057
Protein RMD5 homolog A	<i>Rmnd5a</i>	-1.24	0.0162
Signal transducer and activator of transcription 3;Signal transducer and activator of transcription	<i>Stat3</i>	-1.24	0.0033
Tripartite motif-containing protein 14	<i>Trim14</i>	-1.24	0.0031
Casein kinase I isoform gamma-1	<i>Csnk1g1</i>	-1.25	0.0021
Vacuolar protein-sorting-associated protein 36	<i>Vps36</i>	-1.25	0.0021

Phosphatidylinositol 5-phosphate 4-kinase type-2 beta	<i>Pip4k2b</i>	-1.25	0.0133
CWF19-like protein 1	<i>Cwf19l1</i>	-1.25	0.0049
Calcium/calmodulin-dependent protein kinase type II subunit delta	<i>Camk2d</i>	-1.25	0.0166
28S ribosomal protein S24, mitochondrial	<i>Mrps24</i>	-1.25	0.0021
Leucine-rich repeat-containing protein 40	<i>Lrrc40</i>	-1.25	0.0061
Guanylate-binding protein 4	<i>Gbp4</i>	-1.25	0.0039
Importin-7	<i>Ipo7</i>	-1.25	0.0022
Corticosteroid 11-beta-dehydrogenase isozyme 2	<i>Hsd11b2</i>	-1.25	0.0028
Coiled-coil domain-containing protein 167	<i>Ccdc167</i>	-1.25	0.0045
Pancreatic lipase-related protein 2	<i>Pnliprp2</i>	-1.25	0.02
Eukaryotic translation initiation factor 3 subunit L	<i>Eif3l</i>	-1.25	0.0183
Structural maintenance of chromosomes protein 2	<i>Smc2</i>	-1.25	0.0131
Methyltransferase-like protein 13	<i>Mettl13</i>	-1.25	0.0003
Serine hydrolase-like protein	<i>Serhl</i>	-1.25	0.0138
MAP kinase-activated protein kinase 3	<i>Mapkapk3</i>	-1.25	0.0115
Integrator complex subunit 5	<i>Ints5</i>	-1.25	0.0058
Mitochondrial Rho GTPase 1	<i>Rhot1</i>	-1.25	0.0136
Interferon-inducible double-stranded RNA-dependent protein kinase activator A	<i>Prkra</i>	-1.25	0.0222
E3 ubiquitin-protein ligase UBR5	<i>Ubr5</i>	-1.25	0.0045
Rho guanine nucleotide exchange factor 2	<i>Arhgef2</i>	-1.25	0.0013
Signal recognition particle subunit SRP68	<i>Srp68</i>	-1.26	0.0023
Inhibitor of nuclear factor kappa-B kinase subunit beta	<i>Ikbkb</i>	-1.26	0.0055
RWD domain-containing protein 2B	<i>Rwdd2b</i>	-1.26	0.0052
Talin-2	<i>Tln2</i>	-1.26	0.0193
Sphingomyelin phosphodiesterase 4	<i>Smpd4</i>	-1.26	0.0005
E3 ubiquitin-protein ligase MARCH5	<i>38412</i>	-1.26	0.018
Putative ribosome-binding factor A, mitochondrial	<i>Rbfa</i>	-1.26	0.0163
Membrane magnesium transporter 1	<i>Mmgt1</i>	-1.26	0.0038
DNA mismatch repair protein Msh6	<i>Msh6</i>	-1.26	0.012
Ribosomal protein S6 kinase;Ribosomal protein S6 kinase alpha-1	<i>Rps6ka1</i>	-1.26	0.0067
Breast carcinoma-amplified sequence 3 homolog	<i>Bcas3</i>	-1.26	0.0177
E3 ubiquitin-protein ligase RNF128	<i>Rnf128</i>	-1.26	0.0117
DENN domain-containing protein 3	<i>Dennd3</i>	-1.26	0.0198
Pantothenate kinase 3	<i>Pank3</i>	-1.26	0.0114
YTH domain-containing family protein 1	<i>Ythdf1</i>	-1.26	0.0136
DNA polymerase delta catalytic subunit;DNA polymerase	<i>Pold1</i>	-1.26	0.0082
Glycogen synthase kinase-3 beta	<i>Gsk3b</i>	-1.26	0.0067
Katanin p60 ATPase-containing subunit A1	<i>Katna1</i>	-1.26	0.0231
Golgi to ER traffic protein 4 homolog	<i>Get4</i>	-1.26	0.0139
AP-3 complex subunit beta-1	<i>Ap3b1</i>	-1.26	0.0083
L-aminoadipate-semialdehyde dehydrogenase-phosphopantetheinyl transferase	<i>Aasdhppt</i>	-1.26	0.0015
Glutamine-rich protein 1	<i>Qrich1</i>	-1.26	0.0032

Apoptosis-resistant E3 ubiquitin protein ligase 1	<i>Arel1</i>	-1.26	0.0099
Tensin-3	<i>Tns3</i>	-1.26	0.0003
DNA repair protein complementing XP-C cells homolog	<i>Xpc</i>	-1.26	0.0243
Peroxisomal membrane protein PEX16	<i>Pex16</i>	-1.26	0.0069
Syntaxin-binding protein 1	<i>Stxbp1</i>	-1.26	0.016
Syntaxin-binding protein 5	<i>Stxbp5</i>	-1.26	0.0049
Coatomer subunit gamma-2	<i>Copg2</i>	-1.26	0.0163
Histone deacetylase;Histone deacetylase 3	<i>Hdac3</i>	-1.26	0.0212
Serine/threonine-protein kinase N1	<i>Pkn1</i>	-1.26	0.0028
60S ribosomal export protein NMD3	<i>Nmd3</i>	-1.26	0.001
ADP-ribosylation factor 4	<i>Arf4</i>	-1.26	0.017
Activating signal cointegrator 1 complex subunit 3	<i>Ascc3</i>	-1.26	0.0028
Protein SCO2 homolog, mitochondrial	<i>Sco2</i>	-1.26	0.0098
Copine-1	<i>Cpne1</i>	-1.26	0.0087
Phospholipid-transporting ATPase	<i>Atp11b</i>	-1.26	0.0017
Probable ATP-dependent RNA helicase DDX41	<i>Ddx41</i>	-1.26	0.0019
Chloride intracellular channel protein 4	<i>Clic4</i>	-1.26	0.0008
E3 ubiquitin-protein ligase Itchy	<i>Itch</i>	-1.26	0.0126
Uridine 5-monophosphate synthase;Orotate phosphoribosyltransferase;Orotidine 5-phosphate decarboxylase	<i>Umps</i>	-1.27	0.0034
DENN domain-containing protein 1B	<i>Dennd1b</i>	-1.27	0.0166
BRO1 domain-containing protein BROX	<i>Brox</i>	-1.27	0.0028
Condensin complex subunit 1	<i>Ncapd2</i>	-1.27	0.0247
Polypeptide N-acetylgalactosaminyltransferase 2;Polypeptide N-acetylgalactosaminyltransferase 2 soluble form	<i>Galnt2</i>	-1.27	0.0006
Interleukin enhancer-binding factor 2	<i>Ilf2</i>	-1.27	0.0009
Pancreatic secretory granule membrane major glycoprotein GP2	<i>Gp2</i>	-1.27	0.0197
Nucleolar GTP-binding protein 1	<i>Gtpbp4</i>	-1.27	0.0171
ATP-binding cassette sub-family F member 3	<i>Abcf3</i>	-1.27	0.0037
Cytokine receptor-like factor 3	<i>Crlf3</i>	-1.27	0.0084
DENN domain-containing protein 2D	<i>Dennd2d</i>	-1.27	0.0052
Exocyst complex component 3	<i>Exoc3</i>	-1.27	0.0004
Required for meiotic nuclear division protein 1 homolog	<i>Rmnd1</i>	-1.27	0.0162
N-alpha-acetyltransferase 16, NatA auxiliary subunit	<i>Naa16</i>	-1.27	0.0097
	<i>Trim12c;Trim5</i>	-1.27	0.0032
Elongation factor 1-alpha 1	<i>Eef1a1</i>	-1.27	0.0144
Putative glutathione-specific gamma-glutamylcyclotransferase 2	<i>Chac2</i>	-1.27	0.0074
Hepatocyte nuclear factor 4-alpha	<i>Hnf4a</i>	-1.27	0.008
Elongator complex protein 3	<i>Elp3</i>	-1.27	0.0116
E3 ubiquitin-protein ligase AMFR	<i>Amfr</i>	-1.27	0.0005
ADP-ribosylation factor-like protein 2	<i>Arl2</i>	-1.27	0.0117
GPI-anchor transamidase	<i>Pigk</i>	-1.27	0.006

Tyrosine-protein phosphatase non-receptor type 6	<i>Ptpn6</i>	-1.27	0.0124
ATP-binding cassette sub-family E member 1	<i>Abce1</i>	-1.28	0.017
	<i>Bcl2l15</i>	-1.28	0.0165
Protein misato homolog 1	<i>Msto1</i>	-1.28	0.0072
	<i>Arhgef5</i>	-1.28	0.0162
Eukaryotic initiation factor 4A-I	<i>Eif4a1</i>	-1.28	0.0103
Protein diaphanous homolog 2	<i>Diap2;Diaph2</i>	-1.28	0.0079
Putative pre-mRNA-splicing factor ATP-dependent RNA helicase DHX32	<i>Dhx32</i>	-1.28	0.007
Protein DENND6A	<i>Dennd6a</i>	-1.28	0.002
X-ray repair cross-complementing protein 6	<i>Xrcc6</i>	-1.28	0.0128
Dual specificity mitogen-activated protein kinase kinase 6	<i>Map2k6</i>	-1.28	0.0131
Rhophilin-2	<i>Rhpn2</i>	-1.28	0.0126
Complement C3	<i>C3</i>	-1.28	0.0258
PAB-dependent poly(A)-specific ribonuclease subunit PAN3	<i>Pan3</i>	-1.28	0.0113
Dimethylaniline monooxygenase [N-oxide-forming] 2	<i>Fmo2</i>	-1.28	0.0134
Protein lifeguard 3	<i>Tmbim1</i>	-1.28	0.0213
Methyltransferase-like protein 17, mitochondrial	<i>Mettl17</i>	-1.28	0.0162
Myotubularin-related protein 9	<i>Mtmr9</i>	-1.28	0.0238
Uncharacterized protein KIAA2013	<i>Kiaa2013</i>	-1.28	0.0007
Beta-adrenergic receptor kinase 1	<i>Adrbk1</i>	-1.28	0.0019
Integrin-linked protein kinase	<i>Ilk</i>	-1.28	0.0204
Transmembrane protein 126A	<i>Tmem126a</i>	-1.28	0.0157
TraB domain-containing protein	<i>Trabd</i>	-1.28	0.0005
Mini-chromosome maintenance complex-binding protein	<i>Mcmbp</i>	-1.28	0.0018
GPN-loop GTPase 3	<i>Gpn3</i>	-1.28	0.0099
WASH complex subunit 7	<i>Kiaa1033</i>	-1.28	0.005
Endoplasmic reticulum-Golgi intermediate compartment protein 1	<i>Ergic1</i>	-1.28	0.0162
RAF proto-oncogene serine/threonine-protein kinase	<i>Raf1</i>	-1.28	0.0149
ADP-ribosylation factor-like protein 1	<i>Arl1</i>	-1.28	0.0084
Glucocorticoid receptor	<i>Nr3c1</i>	-1.28	0.0069
Developmentally-regulated GTP-binding protein 2	<i>Drg2</i>	-1.28	0.0189
LIM domain kinase 2	<i>Limk2</i>	-1.29	0.0186
Translation initiation factor eIF-2B subunit alpha	<i>Eif2b1</i>	-1.29	0.0007
Casein kinase I isoform delta;Casein kinase I isoform epsilon	<i>Csnk1d;Csnk1e</i>	-1.29	0.0118
Probable ergosterol biosynthetic protein 28	<i>ORF11;0610007P14Rik</i>	-1.29	0.0236
Complex I assembly factor TIMMDC1, mitochondrial	<i>Timmdc1</i>	-1.29	0.0255
Vacuolar protein sorting-associated protein 16 homolog	<i>Vps16</i>	-1.29	0.0079
Activating signal cointegrator 1 complex subunit 1	<i>Ascc1</i>	-1.29	0.0033

Replication protein A 70 kDa DNA-binding subunit;Replication protein A 70 kDa DNA-binding subunit, N-terminally processed	<i>Rpa1</i>	-1.29	0.004
39S ribosomal protein L16, mitochondrial	<i>Mrpl16</i>	-1.29	0.0024
Transmembrane protein 70, mitochondrial	<i>Tmem70</i>	-1.29	0.0067
Uridine-cytidine kinase 2	<i>Uck2</i>	-1.29	0.0083
Inter-alpha-trypsin inhibitor heavy chain H5	<i>Itih5</i>	-1.29	0.0092
DNA replication licensing factor MCM3	<i>Mcm3</i>	-1.29	0.0267
Poly [ADP-ribose] polymerase 12	<i>Parp12</i>	-1.29	0.0158
Junction-mediating and -regulatory protein	<i>Jmy</i>	-1.29	0.0096
Cell division cycle protein 16 homolog	<i>Cdc16</i>	-1.29	0.001
	<i>Dhx37</i>	-1.29	0.0211
Death-associated protein kinase 3	<i>Dapk3</i>	-1.29	0.0038
Histone-lysine N-methyltransferase setd3	<i>Setd3</i>	-1.29	0.005
C-Maf-inducing protein	<i>Cmip</i>	-1.29	0.0004
Serine/threonine-protein kinase Chk2	<i>Chek2</i>	-1.29	0.02
Mitogen-activated protein kinase 13	<i>Mapk13</i>	-1.29	0.0006
Rho guanine nucleotide exchange factor 1	<i>Arhgef1</i>	-1.29	0.0052
AP2-associated protein kinase 1	<i>Aak1</i>	-1.29	0.0003
Transmembrane protein 258	<i>Tmem258</i>	-1.29	0.0022
Structural maintenance of chromosomes protein;Structural maintenance of chromosomes protein 4	<i>Smc4</i>	-1.29	0.0192
	<i>Gbp7</i>	-1.29	0.0272
Proteasome inhibitor PI31 subunit	<i>Psmf1</i>	-1.3	0.026
Cytochrome c oxidase assembly protein COX15 homolog	<i>Cox15</i>	-1.3	0.0026
Importin-9	<i>Ipo9</i>	-1.3	0.0063
Kinesin-like protein;Kinesin-like protein KIF2A	<i>Kif2a</i>	-1.3	0.0032
ADP-ribosylation factor-like protein 8A	<i>Arl8a</i>	-1.3	0.003
Helicase-like transcription factor	<i>Hltf</i>	-1.3	0.0022
Mitochondrial fission 1 protein	<i>Fis1</i>	-1.3	0.0019
Hexokinase;Hexokinase-1	<i>Hk1</i>	-1.3	0.0279
Exportin-2	<i>Cse1l</i>	-1.3	0.0025
Growth factor receptor-bound protein 7	<i>Grb7</i>	-1.3	0.0159
Protein O-linked-mannose beta-1,4-N-acetylglucosaminyltransferase 2	<i>Pomgnt2</i>	-1.3	0.0124
Myosin-9	<i>Myh9</i>	-1.3	0.0182
Inactive phospholipase C-like protein 2	<i>Plcl2</i>	-1.3	0.0007
Mitogen-activated protein kinase kinase kinase 4	<i>Map3k4</i>	-1.3	0.0019
Golgin-45	<i>Blzf1</i>	-1.3	0.0174
Rap guanine nucleotide exchange factor 2	<i>Rapgef2</i>	-1.3	0.0024
DNA replication licensing factor MCM4	<i>Mcm4</i>	-1.31	0.0118
Bromodomain adjacent to zinc finger domain protein 2A	<i>Baz2a</i>	-1.31	0.006
Protein FAM83F	<i>Fam83f</i>	-1.31	0.0238
Oxysterol-binding protein-related protein 2	<i>Osbpl2</i>	-1.31	0.0019
DNA-dependent protein kinase catalytic subunit	<i>Prkdc</i>	-1.31	0.0234

Golgi integral membrane protein 4	<i>Golim4</i>	-1.31	0.0065
Amino acid transporter;Neutral amino acid transporter B(0)	<i>Slc1a5</i>	-1.31	0.0244
Cyclin-dependent kinase 7	<i>Cdk7</i>	-1.31	0.0182
Peroxisomal membrane protein PEX13	<i>Pex13</i>	-1.31	0.0062
Serine/threonine-protein kinase WNK2	<i>Wnk2</i>	-1.31	0.0011
Inositol-trisphosphate 3-kinase C	<i>Itpkc</i>	-1.31	0.0085
60S ribosomal protein L10;60S ribosomal protein L10-like	<i>Rpl10;Rpl10l</i>	-1.31	0.0335
Calpain-2 catalytic subunit	<i>Capn2</i>	-1.31	0.0033
DNA replication licensing factor MCM2	<i>Mcm2</i>	-1.31	0.0214
Zinc finger MYND domain-containing protein 11	<i>Zmynd11</i>	-1.31	0.0371
Transient receptor potential cation channel subfamily M member 7	<i>Trpm7</i>	-1.31	0.0128
60S ribosomal protein L23	<i>Rpl23</i>	-1.31	0.0113
Ubiquitin-protein ligase E3C	<i>Ube3c</i>	-1.31	0.0015
rRNA methyltransferase 3, mitochondrial	<i>Rnmt1l</i>	-1.31	0.0181
TAF5-like RNA polymerase II p300/CBP-associated factor-associated factor 65 kDa subunit 5L	<i>Taf5l</i>	-1.31	0.0154
Heterochromatin protein 1-binding protein 3	<i>Hp1bp3</i>	-1.31	0.0254
Protein spinster homolog 1	<i>Spns1</i>	-1.31	0.0364
Unconventional myosin-1e	<i>Myo1e</i>	-1.32	0.009
Rab-like protein 6	<i>Rabl6</i>	-1.32	0.0005
	<i>Hp1bp3</i>	-1.32	0.024
Vesicle transport protein GOT1B	<i>Golt1b</i>	-1.32	0.0261
Myotubularin-related protein 7	<i>Mtmr7</i>	-1.32	0.0002
Replication factor C subunit 2	<i>Rfc2</i>	-1.32	0.0033
Ribosomal protein L19;60S ribosomal protein L19	<i>Rpl19</i>	-1.32	0.015
Nucleolar GTP-binding protein 2	<i>Gnl2</i>	-1.32	0.015
Sorting nexin;Sorting nexin-18	<i>Snx18</i>	-1.32	0.0191
Inositol polyphosphate multikinase	<i>Ipmk</i>	-1.32	0.0015
DNA primase small subunit;DNA primase	<i>Prim1</i>	-1.32	0.0163
Asparagine synthetase [glutamine-hydrolyzing]	<i>Asns</i>	-1.32	0.027
Coiled-coil domain-containing protein 61	<i>Ccdc61</i>	-1.32	0.0006
Septin-1	<i>37135</i>	-1.32	0.0062
ATP-dependent RNA helicase DDX19A	<i>Ddx19a</i>	-1.32	0.0126
Sigma non-opioid intracellular receptor 1	<i>Sigmar1</i>	-1.32	0.0124
Cleft lip and palate transmembrane protein 1 homolog	<i>Clptm1</i>	-1.32	0.0221
NEDD4-like E3 ubiquitin-protein ligase WWP1	<i>Wwp1</i>	-1.32	0.0012
NADH dehydrogenase [ubiquinone] 1 alpha subcomplex subunit 6	<i>Ndufa6</i>	-1.33	0.0222
Phosphatidylinositol glycan anchor biosynthesis class U protein	<i>Pigu</i>	-1.33	0.0319
Band 4.1-like protein 5	<i>Epb41l5</i>	-1.33	0.0002
DNA mismatch repair protein Msh2	<i>Msh2</i>	-1.33	0.0109
Nuclear factor 1;Nuclear factor 1 B-type	<i>Nfib</i>	-1.33	0.0158
N-alpha-acetyltransferase 40	<i>Naa40</i>	-1.33	0.016
Aurora kinase A-interacting protein	<i>Aurkaip1</i>	-1.33	0.0041

Cyclin-dependent kinase 2	<i>Cdk2</i>	-1.33	0.0023
Phosphoinositide 3-kinase regulatory subunit 4	<i>Pik3r4</i>	-1.33	0.0143
Surfeit locus protein 1	<i>Surf1</i>	-1.33	0.0141
Protein PAT1 homolog 1	<i>Pat1</i>	-1.33	0.0006
Zinc transporter 5	<i>Slc30a5</i>	-1.33	0.0406
Serine/threonine-protein kinase STK11	<i>Stk11</i>	-1.33	0.0164
Vesicle-associated membrane protein 7	<i>Vamp7</i>	-1.33	0.0395
Phosphatidate cytidyltransferase 1	<i>Cds1</i>	-1.33	0.0168
Annexin A6	<i>Anxa6</i>	-1.33	0.0133
Thioredoxin-related transmembrane protein 2	<i>Tmx2</i>	-1.34	0.0041
NADH dehydrogenase [ubiquinone] 1 beta subcomplex subunit 4	<i>Ndufb4</i>	-1.34	0.0404
Mitochondrial ribosome-associated GTPase 1	<i>Mtg1</i>	-1.34	0.0026
Putative RNA polymerase II subunit B1 CTD phosphatase Rpap2	<i>Rpap2</i>	-1.34	0.0073
Signal transducer and activator of transcription	<i>Stat1</i>	-1.34	0.0285
CAD protein;Glutamine-dependent carbamoyl-phosphate synthase;Aspartate carbamoyltransferase;Dihydroorotase	<i>Cad</i>	-1.34	0.0448
Zinc finger protein 512	<i>Znf512</i>	-1.34	0.005
Lanosterol 14-alpha demethylase	<i>Cyp51a1</i>	-1.34	0.0023
HEAT repeat-containing protein 3	<i>Heatr3</i>	-1.34	0.0163
Serine/threonine-protein kinase 38	<i>Stk38</i>	-1.34	0.0075
15-hydroxyprostaglandin dehydrogenase [NAD(+)]	<i>Hpgd</i>	-1.34	0.0298
Methylsterol monooxygenase 1	<i>Msmo1</i>	-1.34	0.0259
40S ribosomal protein S9	<i>Rps9</i>	-1.35	0.0162
Probable ATP-dependent RNA helicase DDX17	<i>Ddx17</i>	-1.35	0.0048
Vitamin K epoxide reductase complex subunit 1-like protein 1	<i>Vkorc1l1</i>	-1.35	0.042
DNA ligase;DNA ligase 1	<i>Lig1</i>	-1.35	0.0205
Metalloendopeptidase OMA1, mitochondrial	<i>Oma1</i>	-1.35	0.0174
Extended synaptotagmin-1	<i>Esyt1</i>	-1.35	0.0056
	<i>Dab1</i>	-1.35	0.0003
	<i>Serpib9</i>	-1.35	0.0441
Probable U3 small nucleolar RNA-associated protein 11	<i>Utp11l</i>	-1.35	0.0236
Protein zwilch homolog	<i>Zwilch</i>	-1.35	0.0124
Prohibitin-2	<i>Phb2</i>	-1.35	0.0434
Transmembrane protein 135	<i>Tmem135</i>	-1.35	0.0177
Eosinophil peroxidase;Eosinophil peroxidase light chain;Eosinophil peroxidase heavy chain	<i>Epx</i>	-1.35	0.043
Polynucleotide 5-hydroxyl-kinase NOL9	<i>Nol9</i>	-1.35	0.0006
Peroxisomal biogenesis factor 3	<i>Pex3</i>	-1.35	0.0323
Diphthamide biosynthesis protein 2	<i>Dph2</i>	-1.36	0.0069
SPATS2-like protein	<i>Spats2l</i>	-1.36	0.0093
Fermitin family homolog 2	<i>Fermt2</i>	-1.36	0.0412
Solute carrier family 52, riboflavin transporter, member 3	<i>Slc52a3</i>	-1.36	0.0204
DNA polymerase alpha catalytic subunit	<i>Pola1</i>	-1.36	0.016

ATP-binding cassette sub-family F member 2	<i>Abcf2</i>	-1.36	0.0076
Mitochondrial import inner membrane translocase subunit Tim23	<i>Timm23</i>	-1.36	0.0115
Importin-8	<i>Ipo8</i>	-1.36	0.0029
Exportin-5	<i>Xpo5</i>	-1.36	0.0046
Chromodomain-helicase-DNA-binding protein 8;Chromodomain-helicase-DNA-binding protein 9	<i>Chd8;Chd9</i>	-1.36	0.009
Fibronectin;Anastellin	<i fn1<="" i=""></i>	-1.36	0.0296
CDP-diacylglycerol--inositol 3-phosphatidyltransferase	<i>Cdipt</i>	-1.36	0.0422
CAAX prenyl protease 1 homolog	<i>Zmpste24</i>	-1.36	0.037
Protein Niban	<i>Fam129a</i>	-1.36	0.0006
Ubiquitin-conjugating enzyme E2 J2	<i>Ube2j2</i>	-1.36	0.036
Anoctamin-10	<i>Ano10</i>	-1.36	0.0286
Protein RER1	<i>Rer1</i>	-1.36	0.0345
Oxysterol-binding protein;Oxysterol-binding protein-related protein 11	<i>Osbpl11</i>	-1.37	0.0099
Serine/threonine-protein kinase MRCK gamma	<i>Cdc42bpg</i>	-1.37	0.0051
	<i>Inpp5a</i>	-1.37	0.0018
	<i>Mettl7a1</i>	-1.37	0.0253
Uncharacterized protein C1orf43 homolog	<i>4933434E20Rik</i>	-1.37	0.0015
Mitochondrial import receptor subunit TOM40 homolog	<i>Tomm40</i>	-1.37	0.0269
	<i>Myl10</i>	-1.37	0.0302
GTPase IMAP family member 8	<i>Gimap8</i>	-1.37	0.023
Serine/threonine-protein kinase 17B	<i>Stk17b</i>	-1.37	0.0234
Cytochrome P450 20A1	<i>Cyp20a1</i>	-1.37	0.0033
DNA replication licensing factor MCM7	<i>Mcm7</i>	-1.37	0.0133
Histidine triad nucleotide-binding protein 3	<i>Hint3</i>	-1.38	0.0286
Ras-related protein Rab-19	<i>Rab19</i>	-1.38	0.0103
Antigen peptide transporter 1	<i>Tap1</i>	-1.38	0.0317
60S ribosomal protein L13a	<i>Rpl13a</i>	-1.38	0.0045
WW domain-binding protein 2	<i>Wbp2</i>	-1.38	0.0234
Rho GTPase-activating protein 35	<i>Arhgap35</i>	-1.38	0.0245
Neutrophil cytosol factor 1	<i>Ncf1</i>	-1.38	0.0274
Cyclin-dependent kinase 1	<i>Cdk1</i>	-1.38	0.0051
Peroxisomal membrane protein 11B	<i>Pex11b</i>	-1.38	0.0146
Mimecan	<i>Ogn</i>	-1.38	0.0121
Eukaryotic initiation factor 4A-II;	<i>Eif4a2</i>	-1.39	0.0158
Methyltransferase-like protein 16	<i>Mettl16</i>	-1.39	0.0012
Kinetochores-associated protein 1	<i>Kntc1</i>	-1.39	0.0348
Probable 18S rRNA (guanine-N(7))-methyltransferase	<i>Wbscr22</i>	-1.39	0.0066
Exportin-1	<i>Xpo1</i>	-1.39	0.0109
Protein jagunal homolog 1	<i>Jagn1</i>	-1.39	0.0016
Tyrosine-protein phosphatase non-receptor type 2	<i>Ptpn2</i>	-1.39	0.0428
DnaJ homolog subfamily C member 11	<i>Dnajc11</i>	-1.39	0.0119
Lymphokine-activated killer T-cell-originated protein kinase	<i>Pbk</i>	-1.39	0.006

Twinfilin-2	<i>Twf2</i>	-1.39	0.0325
PX domain-containing protein kinase-like protein	<i>Pxk</i>	-1.39	0.0029
	<i>Slfn9</i>	-1.39	0.0254
Collagen alpha-1(XIV) chain	<i>Col14a1</i>	-1.39	0.0083
	<i>Mkrn2os</i>	-1.39	0.0043
Translocating chain-associated membrane protein 1	<i>Tram1</i>	-1.4	0.049
Ceramide synthase 5	<i>Cers5</i>	-1.4	0.0027
Dynamin-2	<i>Dnm2</i>	-1.4	0.0073
L-lactate dehydrogenase;L-lactate dehydrogenase B chain	<i>Ldhb</i>	-1.41	0.0101
Protein FAM210B	<i>Fam210b</i>	-1.41	0.0215
Glomulin	<i>Glmn</i>	-1.41	0.0037
Lymphocyte-specific helicase	<i>Hells</i>	-1.41	0.0089
DNA polymerase alpha subunit B	<i>Pola2</i>	-1.41	0.0051
Developmentally-regulated GTP-binding protein 1	<i>Drg1</i>	-1.41	0.0048
Transmembrane protein 194A	<i>Tmem194;Tmem194a</i>	-1.41	0.04
Dolichyl-diphosphooligosaccharide--protein glycosyltransferase subunit STT3B	<i>Stt3b</i>	-1.41	0.0283
B-cell receptor-associated protein 29	<i>Bcap29</i>	-1.41	0.044
Tenascin	<i>Tnc</i>	-1.42	0.0077
Zinc finger FYVE domain-containing protein 16	<i>Zfyve16</i>	-1.42	0.0043
Ribosome production factor 2 homolog	<i>Rpf2</i>	-1.42	0.0471
Interferon regulatory factor 8	<i>Irf8</i>	-1.43	0.0277
Histone acetyltransferase type B catalytic subunit	<i>Hat1</i>	-1.43	0.0051
Nucleoporin NDC1	<i>Ndc1</i>	-1.43	0.0157
Peroxisomal membrane protein 11C	<i>Pex11g</i>	-1.43	0.0422
E3 ubiquitin-protein ligase NEDD4	<i>Nedd4</i>	-1.43	0.006
Transmembrane protein 165	<i>Tmem165</i>	-1.43	0.0038
Alpha-1,6-mannosyl-glycoprotein 2-beta-N-acetylglucosaminyltransferase	<i>Mgat2</i>	-1.43	0.0276
GTPase IMAP family member 1	<i>Gimap1</i>	-1.44	0.0158
Ribonucleoside-diphosphate reductase large subunit	<i>Rrm1</i>	-1.44	0.0176
Acylglycerol kinase, mitochondrial	<i>Agk</i>	-1.44	0.0135
Chromodomain-helicase-DNA-binding protein 5	<i>Chd5</i>	-1.45	0.0129
	<i>2010107G12Rik</i>	-1.45	0.0494
Sorting and assembly machinery component 50 homolog	<i>Samm50</i>	-1.45	0.0217
ATP-dependent RNA helicase DDX3Y	<i>Ddx3y</i>	-1.46	0.0044
Myosin-10	<i>Myh10</i>	-1.46	0.0138
N-acylneuraminate-9-phosphatase	<i>Nanp</i>	-1.47	0.0063
Transmembrane emp24 domain-containing protein 11	<i>Tmed11</i>	-1.47	0.0143
Transmembrane protein 161B	<i>Tmem161b</i>	-1.47	0.0253
Glutamyl-tRNA(Gln) amidotransferase subunit C, mitochondrial	<i>Gatc</i>	-1.47	0.0007
	<i>Pank2</i>	-1.47	0.0001

Transforming growth factor-beta-induced protein ig-h3	<i>Tgfb1</i>	-1.47	0.0359
G protein-coupled receptor kinase 6	<i>Grk6</i>	-1.48	0.0044
Protein crumbs homolog 3	<i>Crb3</i>	-1.48	0.0098
Biglycan	<i>Bgn</i>	-1.48	0.0001
Transmembrane protein 205	<i>Tmem205</i>	-1.49	0.0413
Fermitin family homolog 3	<i>Fermt3</i>	-1.49	0.0076
Myristoylated alanine-rich C-kinase substrate	<i>Marcks</i>	-1.5	0.0301
Phosphatidate cytidyltransferase;Phosphatidate cytidyltransferase 2	<i>Cds2</i>	-1.5	0.0222
Collagen alpha-1(XII) chain	<i>Col12a1</i>	-1.5	0.0177
Ras association domain-containing protein 2	<i>Rassf2</i>	-1.5	0.009
Plasminogen receptor (KT)	<i>Plgrkt</i>	-1.51	0.0192
2-phosphoxylose phosphatase 1	<i>Pxylp1</i>	-1.51	0.0234
	<i>Urb2</i>	-1.52	0.0206
Sterol O-acyltransferase 2	<i>Soat2</i>	-1.52	0.0356
Phospholipid scramblase 3	<i>Plscr3</i>	-1.53	0.0038
Dynein heavy chain 17, axonemal	<i>Dnah17</i>	-1.55	0.0278
Sterol O-acyltransferase 1	<i>Soat1</i>	-1.55	0.0267
Laminin subunit gamma-1	<i>Lamc1</i>	-1.55	0.0419
GDP-fucose transporter 1	<i>Slc35c1</i>	-1.55	0.0305
Transmembrane protein 143	<i>Tmem143</i>	-1.55	0.0277
	<i>Ctrl</i>	-1.56	0.0117
RNA-binding protein PNO1	<i>Pno1</i>	-1.56	0.0323
Mitotic spindle assembly checkpoint protein MAD2A	<i>Mad2l1</i>	-1.57	0.0232
Calcium/calmodulin-dependent protein kinase type II subunit gamma	<i>Camk2g</i>	-1.57	0.0116
Interferon-induced guanylate-binding protein 2	<i>Gbp2</i>	-1.58	0.0304
Thymidine kinase, cytosolic	<i>Tk1</i>	-1.58	0.007
Very-long-chain (3R)-3-hydroxyacyl-CoA dehydratase 2	<i>Hacd2</i>	-1.58	0.0214
5-phosphohydroxy-L-lysine phospho-lyase	<i>Phytpl</i>	-1.59	0.0293
Basement membrane-specific heparan sulfate proteoglycan core protein;Endorepellin;LG3 peptide	<i>Hspg2</i>	-1.59	0.0007
Guanine nucleotide-binding protein G(o) subunit alpha	<i>Gnao1</i>	-1.59	0.0033
Pancreatic triacylglycerol lipase	<i>Pnlip</i>	-1.62	0.0488
CMP-sialic acid transporter	<i>Slc35a1</i>	-1.62	0.041
Leiomodin-1	<i>Lmod1</i>	-1.62	0.0451
Non-specific serine/threonine protein kinase;Serine/threonine-protein kinase MRCK alpha	<i>Cdc42bpa</i>	-1.62	0.0198
Ubiquitin-protein ligase E3B	<i>Ube3b</i>	-1.63	0.0044
Colipase	<i>Clps</i>	-1.65	0.0063
Organic solute transporter subunit beta	<i>Slc51b</i>	-1.65	0.0074
Brain acid soluble protein 1	<i>Basp1</i>	-1.66	0.0114
Microfibril-associated glycoprotein 4	<i>Mfap4</i>	-1.67	0.0367

	<i>2210010C04Rik</i>	-1.69	0.0045
ATP synthase subunit e, mitochondrial	<i>Atp5i;Atp5k</i>	-1.7	0.0077
NUAK family SNF1-like kinase 2	<i>Nuak2</i>	-1.7	0.0188
Poly(A) RNA polymerase GLD2	<i>Papd4</i>	-1.7	0.0004
Laminin subunit alpha-5	<i>Lama5</i>	-1.7	0.0421
5-nucleotidase	<i>Nt5e</i>	-1.73	0.0222
Adenosine 3-phospho 5-phosphosulfate transporter 1	<i>Slc35b2</i>	-1.74	0.046
Sodium-dependent phosphate transport protein 2B	<i>Slc34a2</i>	-1.74	0.0336
Interferon-induced guanylate-binding protein 1	<i>Gbp1;Gbp2b</i>	-1.76	0.0131
	<i>Gimap7</i>	-1.76	0.0497
Collagen alpha-2(VI) chain	<i>Col6a2</i>	-1.8	0.0266
Collagen alpha-4(VI) chain	<i>Col6a4</i>	-1.83	0.0058
	<i>Actn1</i>	-1.87	0.0404
Chymotrypsin-like elastase family member 1	<i>Cela1</i>	-1.9	0.0468
	<i>Tns1</i>	-1.91	0.0185
Bile salt-activated lipase	<i>Cel</i>	-1.96	0.0017
Endoplasmic reticulum resident protein 27	<i>Erp27</i>	-2.05	0.0209
Cystathionine beta-synthase	<i>Cbs</i>	-2.11	0.0139
Collagen alpha-1(VI) chain	<i>Col6a1</i>	-2.15	0.0359
Peptidyl-prolyl cis-trans isomerase FKBP11	<i>Fkbp11</i>	-2.16	0.0001
carboxypeptidase B1	<i>Cpb1</i>	-2.17	0.0204
Tropomyosin alpha-1 chain	<i>Tpm1</i>	-2.22	0.0309
Protein disulfide-isomerase A2	<i>Pdia2</i>	-2.29	0.0133
Tubulointerstitial nephritis antigen-like	<i>Tinagl1</i>	-2.4	0.0418
collagen type VI alpha 3 chain	<i>Col6a3</i>	-2.55	0.007
Tropomodulin-1	<i>Tmod1</i>	-2.55	0.0198
Myosin heavy chain 11	<i>Myh11</i>	-2.58	0.005
Carboxypeptidase A1	<i>Cpa1</i>	-3.4	0.0141
Otolin-1	<i>Otol1</i>	-4.16	0.0162

**Appendix 5: Proteins that are exclusively changed in regulation in LPS-treated *Nfκb1*<sup>-/-</sup> compared with LPS-treated C57BL/6J small intestinal mucosa (excluding significant changes between *Nfκb1*<sup>-/-</sup> and C57BL/6J at baseline)**

Protein names	Gene names	Regulation fold changes	P value
Solute carrier family 35 member B1	<i>Slc35b1</i>	7.642	0.0034
NADH-ubiquinone oxidoreductase chain 5	<i>Mtnd5</i>	3.766	0.0301
NADH:ubiquinone oxidoreductase core subunit S1	<i>Ndufs1</i>	3.546	0.0005
85/88 kDa calcium-independent phospholipase A2	<i>Pla2g6</i>	3.246	0.0002
Protein transport protein Sec61 subunit gamma	<i>Sec61g</i>	3.158	0.0007
Oligosaccharyltransferase complex subunit OSTC	<i>Ostc</i>	3.012	0.0442
Apolipoprotein C-I;Truncated apolipoprotein C-I	<i>Apoc1</i>	2.749	0.0042
ATP synthase subunit e, mitochondrial	<i>Atp5i;Atp5k</i>	2.615	0.0005
interferon gamma induced GTPase	<i>Igtp</i>	2.526	0.0014
DNA-dependent protein kinase catalytic subunit	<i>Prkdc</i>	2.488	0.0005
Keratin, type II cytoskeletal 2 oral	<i>Krt76</i>	2.456	0.0384
	<i>Cpb1</i>	2.415	0.048
	<i>Irgm2</i>	2.308	0.0039
Dynein light chain 1, cytoplasmic	<i>Dynll1;BC048507</i>	2.304	0.0002
NADH-ubiquinone oxidoreductase chain 2	<i>Mtnd2</i>	2.286	0.0228
Krueppel-like factor 5	<i>Klf5</i>	2.273	0.0029
Hydroxymethylglutaryl-CoA synthase, cytoplasmic	<i>Hmgcs1</i>	2.258	0.0028
Transmembrane emp24 domain-containing protein 3	<i>Tmed3</i>	2.236	0.0022
E3 ubiquitin-protein ligase RNF213	<i>Rnf213</i>	2.159	0.0012
H-2 class II histocompatibility antigen, E-B beta chain	<i>H2-Eb1</i>	2.155	0.0494
	<i>Ptbp1</i>	2.152	0.0296
Dynein heavy chain 17, axonemal	<i>Dnah17</i>	2.13	0.0155
Anionic trypsin-2	<i>Prss2</i>	2.13	0.0248
GDP-fucose transporter 1	<i>Slc35c1</i>	2.128	0.0356
2-5-oligoadenylate synthase 3	<i>Oas3</i>	2.086	0.0013
CTTNBP2 N-terminal-like protein	<i>Cttnbp2nl</i>	2.074	0.0003
E3 ubiquitin-protein ligase RBX1;E3 ubiquitin-protein ligase RBX1, N-terminally processed	<i>Rbx1</i>	2.057	0.0006
	<i>Ddx60</i>	2.055	0.0017
Exosome complex component CSL4	<i>Exosc1</i>	2.045	0.0041
60S ribosomal protein L34	<i>Rpl34</i>	2.023	0.0002
Zinc finger HIT domain-containing protein 2	<i>Znhit2</i>	2.004	0.0011
40S ribosomal protein S16	<i>Rps16</i>	1.995	0.0005
Signal transducer and activator of transcription;Signal transducer and activator of transcription 1	<i>Stat1</i>	1.983	0.0008
60S ribosomal protein L13a	<i>Rpl13a</i>	1.973	0.0014
UMP-CMP kinase 2, mitochondrial	<i>Cmpk2</i>	1.967	0.0013
ATP-dependent RNA helicase DDX18	<i>Ddx18</i>	1.95	0.0055
H/ACA ribonucleoprotein complex subunit 3	<i>Nop10</i>	1.943	0.0066
V-type proton ATPase subunit a	<i>Tcirg1</i>	1.929	0.0056
Immunity-related GTPase family M protein 1	<i>Irgm1</i>	1.901	0.0017
Annexin A5	<i>Anxa5</i>	1.898	0.0803
	<i>Gsn</i>	1.889	0.003
	<i>Gbp6;Gbp10</i>	1.857	0.0044

60S ribosomal protein L4	<i>Rpl4</i>	1.839	0.0064
S-methyl-5-thioadenosine phosphorylase	<i>Mtap</i>	1.837	0.0007
Annexin A6	<i>Anxa6</i>	1.829	0.1031
CD151 antigen	<i>Cd151</i>	1.828	0.0051
Fibrous sheath-interacting protein 2	<i>Fsip2</i>	1.826	0.001
Mixed lineage kinase domain-like protein	<i>Mlkl</i>	1.803	0.0017
Protein unc-93 homolog B1	<i>Unc93b1</i>	1.8	0.0091
Charged multivesicular body protein 6	<i>Chmp6</i>	1.784	0.0037
Serine/threonine-protein phosphatase PP1-gamma catalytic subunit	<i>Ppp1cc</i>	1.774	0.0001
Nucleoside diphosphate-linked moiety X motif 19, mitochondrial	<i>Nudt19</i>	1.768	0.0009
Antigen peptide transporter 2	<i>Tap2</i>	1.767	0.0063
Activated RNA polymerase II transcriptional coactivator p15	<i>Sub1</i>	1.756	0.0002
Gamma-aminobutyric acid receptor-associated protein;Gamma-aminobutyric acid receptor-associated protein-like 1	<i>Gabarap;Gabarapl1</i>	1.755	0.0121
14-3-3 protein gamma;14-3-3 protein gamma, N-terminally processed	<i>Ywhag</i>	1.753	0.0006
Prolyl endopeptidase-like	<i>Prepl</i>	1.736	0.0017
40S ribosomal protein S15	<i>Rps15</i>	1.736	0.0085
60S ribosomal protein L37a	<i>Rpl37a</i>	1.731	0.0001
Elongation of very long chain fatty acids protein 7	<i>Elovl7</i>	1.724	0.0485
2-5-oligoadenylate synthase-like protein 1	<i>Oasl1</i>	1.724	0.0005
Antigen peptide transporter 1	<i>Tap1</i>	1.724	0.0177
Ubiquitin-like protein ISG15	<i>Isg15</i>	1.718	0.0032
Casein kinase I isoform delta;Casein kinase I isoform epsilon	<i>Csnk1d;Csnk1e</i>	1.712	0.0207
40S ribosomal protein S11	<i>Rps11</i>	1.711	0.0002
	<i>Immt</i>	1.703	0.0188
	<i>Gm5431;9930111J21 Rik2;9930111J21Rik1</i>	1.703	0.0012
60S ribosomal protein L12	<i>Rpl12</i>	1.69	0.0047
Kinetochores-associated protein 1	<i>Kntc1</i>	1.675	0.0051
Eukaryotic translation initiation factor 2 subunit 3, X-linked;Eukaryotic translation initiation factor 2 subunit 3, Y-linked	<i>Eif2s3x;Eif2s3y</i>	1.672	0.0029
60S ribosomal protein L35a	<i>Rpl35a</i>	1.669	0.0002
Activator of 90 kDa heat shock protein ATPase homolog 1	<i>Ahsa1</i>	1.668	0.0025
Acetoacetyl-CoA synthetase	<i>Aacs</i>	1.662	0.0008
5-AMP-activated protein kinase catalytic subunit alpha-1	<i>Prkaa1</i>	1.659	0.0019
Heterogeneous nuclear ribonucleoprotein A0	<i>Hnrnpa0</i>	1.658	0.0006
Mitotic spindle assembly checkpoint protein MAD2A	<i>Mad2l1</i>	1.658	0.0008
60S ribosomal protein L9	<i>Rpl9</i>	1.658	0.0005
Ribonuclease P protein subunit p30	<i>Rpp30</i>	1.655	0.0052
Spermatogenesis-associated protein 5	<i>Spata5</i>	1.651	0.0017
60S ribosomal protein L28	<i>Rpl28</i>	1.649	0.0012
Tubulin-folding cofactor B	<i>Tbcb</i>	1.642	0.0002
Ribosomal protein L19;60S ribosomal protein L19	<i>Rpl19</i>	1.638	0.0056
Thioredoxin-related transmembrane protein 2	<i>Tmx2</i>	1.637	0.0127

N-acetyllactosaminide beta-1,3-N-acetylglucosaminyltransferase 3	<i>B3gnt3</i>	1.633	0.0034
Poly(rC)-binding protein 2	<i>Pcbp2</i>	1.631	0.002
Cat eye syndrome critical region protein 5 homolog	<i>Cecr5</i>	1.625	0.0008
S-adenosylmethionine synthase isoform type-2	<i>Mat2a</i>	1.624	0.0012
Interferon-induced, double-stranded RNA-activated protein kinase	<i>Eif2ak2</i>	1.621	0.0049
	<i>Nans</i>	1.62	0.0002
AP-1 complex subunit gamma-1	<i>Ap1g1</i>	1.6	0.0021
28S ribosomal protein S11, mitochondrial	<i>Mrps11</i>	1.594	0.0028
60S ribosomal protein L30	<i>Rpl30</i>	1.587	0.0004
Ribose-phosphate pyrophosphokinase 1	<i>Prps1l3;Prps1</i>	1.585	0.0002
Phosphoribosyl pyrophosphate synthase-associated protein 2	<i>Prpsap2</i>	1.569	0.0002
Peptidyl-prolyl cis-trans isomerase FKBP4;Peptidyl-prolyl cis-trans isomerase FKBP4, N-terminally processed;Peptidyl-prolyl cis-trans isomerase	<i>Fkbp4</i>	1.563	0.0004
Phosphoribosyl pyrophosphate synthase-associated protein 1	<i>Prpsap1</i>	1.547	0.0005
Bis(5-nucleosyl)-tetraphosphatase [asymmetrical]	<i>Nudt2</i>	1.535	0.0002
Bcl-2-like protein 15	<i>Bcl2l15</i>	1.19	0.0114
5-oxoprolinase	<i>Oplah</i>	-1.55	0.0004
Transmembrane protein 9B	<i>Tmem9b</i>	-1.57	0.0007
UPF0585 protein C16orf13 homolog	<i>0610011F06Rik</i>	-1.58	0.0009
Pre-mRNA-processing factor 40 homolog A	<i>Prpf40a</i>	-1.6	0.0019
Protein C19orf12 homolog	<i>1600014C10Rik</i>	-1.61	0.0003
Gastric inhibitory polypeptide	<i>Gip</i>	-1.61	0.0074
	<i>Slc2a9</i>	-1.62	0.0019
Ubiquitin-fold modifier 1	<i>Ufm1</i>	-1.62	0.0015
Cubilin	<i>Cubn</i>	-1.64	0.0103
MAGUK p55 subfamily member 5	<i>Mpp5</i>	-1.66	0.0001
Phospholipid scramblase 1	<i>Plscr1</i>	-1.66	0.0087
Glutamyl aminopeptidase	<i>Enpep</i>	-1.66	0.0121
[3-methyl-2-oxobutanoate dehydrogenase [lipoamide]] kinase, mitochondrial	<i>Bckdk</i>	-1.67	0.0079
Solute carrier family 2, facilitated glucose transporter member 5	<i>Slc2a5</i>	-1.67	0.0078
Chromosome transmission fidelity protein 18 homolog	<i>Chtf18</i>	-1.67	0.0086
Annexin A13;Annexin	<i>Anxa13</i>	-1.67	0.001
Retinol dehydrogenase 7	<i>Rdh7</i>	-1.68	0.0171
Ankyrin repeat and SAM domain-containing protein 4B	<i>Anks4b</i>	-1.72	0.0126
	<i>Mgam</i>	-1.73	0.0258
Zinc transporter 10	<i>Slc30a10</i>	-1.74	0.0297
Transporter;Sodium- and chloride-dependent transporter XTRP3A;Sodium- and chloride-dependent transporter XTRP3B	<i>Slc6a20a;Slc6a20b</i>	-1.76	0.0062
E3 SUMO-protein ligase PIAS1;E3 SUMO-protein ligase PIAS2	<i>Pias1;Pias2</i>	-1.76	0.0004
Solute carrier family 26 member 6	<i>Slc26a6</i>	-1.76	0.0139
Anoctamin-6	<i>Ano6</i>	-1.77	0.001
Calcium-activated chloride channel regulator 1	<i>Clca1</i>	-1.78	0.0009
3-ketoacyl-CoA thiolase B, peroxisomal	<i>Acaa1b</i>	-1.79	0.0384
39S ribosomal protein L21, mitochondrial	<i>Mrpl21</i>	-1.79	0.0011

Pancreatic lipase-related protein 2	<i>Pnliprp2</i>	-1.81	0.0044
Bile salt export pump	<i>Abcb11</i>	-1.82	0.0412
Sodium/myo-inositol cotransporter 2	<i>Slc5a11</i>	-1.84	0.0062
N-acetylneuraminase lyase	<i>Npl</i>	-1.86	0.0182
Enscosin	<i>Map7</i>	-1.87	0.0177
	<i>2010106E10Rik</i>	-1.88	0.0191
Meprin A subunit alpha	<i>Mep1a</i>	-1.88	0.0022
Hepatoma-derived growth factor-related protein 2	<i>Hdgfrp2</i>	-1.89	0.0039
Epidermal growth factor receptor kinase substrate 8-like protein 3	<i>Eps8l3</i>	-1.89	0.0084
Choline transporter-like protein 4	<i>Slc44a4</i>	-1.89	0.001
Peroxisomal acyl-coenzyme A oxidase 2	<i>Acox2</i>	-1.9	0.0022
Alkaline phosphatase	<i>Alpi</i>	-1.92	0.0039
Niemann-Pick C1-like protein 1	<i>Npc1l1</i>	-1.94	0.004
Uncharacterized protein KIAA1211	<i>C530008M17Rik;Kiaa1211</i>	-1.94	0.0133
Solute carrier family 2, facilitated glucose transporter member 7	<i>Slc2a7</i>	-1.98	0.0114
Gastric intrinsic factor	<i>Gif</i>	-2.01	0.0025
Neutral ceramidase;Neutral ceramidase soluble form	<i>Asah2</i>	-2.04	0.0076
Sodium-dependent neutral amino acid transporter B(0)AT1	<i>Slc6a19</i>	-2.06	0.004
Canalicular multispecific organic anion transporter 1	<i>Abcc2</i>	-2.06	0.0025
Thymidylate synthase	<i>Tyms</i>	-2.06	0.0006
Neutral and basic amino acid transport protein rBAT	<i>Slc3a1</i>	-2.07	0.0023
Cysteine-rich and transmembrane domain-containing protein 1	<i>Cystm1</i>	-2.07	0.0198
Pantetheinase	<i>Vnn1</i>	-2.08	0.0005
Multidrug resistance protein 1A	<i>Abcb1a</i>	-2.1	0.0132
Angiotensin-converting enzyme;Angiotensin-converting enzyme, soluble form	<i>Ace</i>	-2.11	0.0054
A-kinase anchor protein 7 isoform alpha;A-kinase anchor protein 7 isoform gamma	<i>Akap7</i>	-2.12	0.0052
Gamma-glutamyltranspeptidase 1;Gamma-glutamyltranspeptidase 1 heavy chain;Gamma-glutamyltranspeptidase 1 light chain	<i>Ggt1</i>	-2.13	0.0003
		-2.2	0.0085
Acid sphingomyelinase-like phosphodiesterase 3b	<i>Smpdl3b</i>	-2.27	0.0014
Cytochrome c oxidase subunit 5A, mitochondrial	<i>Cox5a</i>	-2.28	0.0001
b(0,+)-type amino acid transporter 1	<i>Slc7a9</i>	-2.28	0.0001
	<i>Enpp7</i>	-2.29	0.0039
	<i>Adh6a</i>	-2.3	0.008
Clarín-3	<i>Clrn3</i>	-2.31	0.0031
N-acetylated-alpha-linked acidic dipeptidase-like protein	<i>Naaladl1</i>	-2.32	0.0003
Superoxide dismutase [Mn], mitochondrial	<i>Sod2</i>	-2.33	0.0265
Glutathione S-transferase A4	<i>Gsta4</i>	-2.34	0.0013
Secretin	<i>Sct</i>	-2.38	0.0002
Trehalase	<i>Treh</i>	-2.4	0.0016
Carboxylesterase 1D	<i>Ces1d</i>	-2.46	0.0031
	<i>Lct</i>	-2.52	0.0011

Angiotensin-converting enzyme 2;Processed angiotensin-converting enzyme 2	<i>Ace2</i>	-2.52	0.0006
Proteasome subunit beta type-5	<i>Psmb5</i>	-2.53	0.0079
Neprilysin	<i>Mme</i>	-2.54	0.001
ADP-ribosyl cyclase/cyclic ADP-ribose hydrolase 2	<i>Bst1</i>	-2.55	0.0008
Ectonucleotide pyrophosphatase/phosphodiesterase 3	<i>Enpp3</i>	-2.61	0.0078
Solute carrier family 15 member 1	<i>Slc15a1</i>	-2.68	0.0006
Syntaxin-3	<i>Stx3</i>	-2.77	0.0003
Liver carboxylesterase 1	<i>Ces1</i>	-2.99	0.0016
Reticulon;Reticulon-1	<i>Rtn1</i>	-3.36	0.0022
Aminoacylase-1	<i>Acy1</i>	-3.39	0.0401
Serine (or cysteine) peptidase inhibitor, clade B, member 9b and 9c	<i>Serpib9b;Serpib9c</i>	-3.5	0.001
THAP domain-containing protein 4	<i>Thap4</i>	-7.04	0.0003
PHD finger protein 10	<i>Phf10</i>	-7.91	0.0005

**Appendix 6: Proteins that are exclusively changed in regulation in LPS-treated *Nfkb2*<sup>-/-</sup> compared with LPS-treated C57BL/6J small intestinal mucosa (excluding significant changes between *Nfkb2*<sup>-/-</sup> and C57BL/6J at baseline)**

Protein names	Gene names	Regulation fold change	P value
NADH dehydrogenase [ubiquinone] 1 alpha subcomplex assembly factor 5	<i>Ndufaf5</i>	2.962	0.0019
Peripherin	<i>Prph</i>	2.149	0.0033
Interferon-induced guanylate-binding protein 2	<i>Gbp2</i>	1.809	0.0065
Ras-related protein Rab-8B	<i>Rab8b</i>	1.795	0.0004
Volume-regulated anion channel subunit LRRC8A	<i>Lrrc8a</i>	1.672	0.0003
Translation factor Guf1, mitochondrial	<i>Guf1</i>	1.596	0.0016
Annexin	<i>Anxa6</i>	1.595	0.0161
Serine/threonine-protein kinase MRCK alpha	<i>Cdc42bpa</i>	1.586	0.0019
Disheveled-associated activator of morphogenesis 1	<i>Daam1</i>	1.582	0.0112
Ufm1-specific protease 2	<i>Ufsp2</i>	1.566	0.0012
cAMP-dependent protein kinase catalytic subunit beta	<i>Prkacb</i>	1.546	0.01
Receptor-interacting serine/threonine-protein kinase 3	<i>Ripk3</i>	1.512	0.0002
Hexokinase;Hexokinase-1	<i>Hk1</i>	1.495	0.0141
Vacuole membrane protein 1	<i>Vmp1</i>	1.485	0.0018
Zinc finger matrin-type protein 2	<i>Zmat2</i>	1.476	0.0007
Calcium-activated chloride channel regulator 4A	<i>Clca4a</i>	1.46	0.0325
Kininogen-1;Kininogen-1 heavy chain;Bradykinin;Kininogen-1 light chain	<i>Kng1</i>	1.454	0.0416
40S ribosomal protein S14	<i>Rps14</i>	1.432	0.006
Cytochrome b5	<i>Cyb5a</i>	1.416	0.021
Selenide, water dikinase 2	<i>Sephs2</i>	1.412	0.008
1-acyl-sn-glycerol-3-phosphate acyltransferase beta	<i>Agpat2</i>	1.404	0.0027
Radixin	<i>Rdx</i>	1.395	0.1441

Ena/VASP-like protein	<i>Evl</i>	1.384	0.1202
Chloride intracellular channel protein 4	<i>Clic4</i>	1.383	0.0043
Serine hydrolase-like protein	<i>Serhl</i>	1.379	0.0007
Phosphatidylinositol 3,4,5-trisphosphate 5-phosphatase 1	<i>Inpp5d</i>	1.377	0.0229
Spermatogenesis-associated protein 5	<i>Spata5</i>	1.376	0.0029
Protein-L-isoaspartate O-methyltransferase;Protein-L-isoaspartate(D-aspartate) O-methyltransferase	<i>Pcmt1</i>	1.372	0.0004
AP-1 complex subunit sigma-1A	<i>Ap1s1</i>	1.361	0.0046
Oxidoreductase NAD-binding domain-containing protein 1	<i>Oxnad1</i>	1.355	0.0021
Zinc finger protein 800	<i>Znf800;Zfp800</i>	1.345	0.0225
BRO1 domain-containing protein BROX	<i>Brox</i>	1.344	0.0015
Cytochrome b-c1 complex subunit 9	<i>Uqcr10</i>	1.343	0.0164
HRAS-like suppressor 3	<i>Pla2g16</i>	1.333	0.0087
Fibrous sheath-interacting protein 2	<i>Fsip2</i>	1.331	0.0042
DNA-directed RNA polymerase II subunit RPB11	<i>Polr2j</i>	1.324	0.0015
Trafficking protein particle complex subunit 2-like protein	<i>Trappc2l</i>	1.323	0.0005
Reticulon-3	<i>Rtn3</i>	1.322	0.0006
Ras-related GTP-binding protein C	<i>Rragc</i>	1.321	0.0004
UBX domain-containing protein 1	<i>Ubxn1</i>	-1.321	0.0001
Vacuolar protein sorting-associated protein VTA1 homolog	<i>Vta1</i>	-1.324	0.0002
Beta-catenin-like protein 1	<i>Ctnnbl1</i>	-1.325	0.0026
Iron-sulfur cluster assembly 1 homolog, mitochondrial	<i>AK157302;Isca1</i>	-1.34	0.0084
	<i>Tjp1</i>	-1.344	0.0002
Nucleoplasmin-3	<i>Npm3</i>	-1.344	0.0223
Receptor-type tyrosine-protein phosphatase kappa	<i>Ptprk</i>	-1.345	0.0226
Neutral ceramidase;Neutral ceramidase soluble form	<i>Asah2</i>	-1.347	0.008
Ran GTPase-activating protein 1	<i>Rangap1</i>	-1.349	0.001
Bromodomain-containing protein 3	<i>Brd3</i>	-1.353	0.02
Dystroglycan;Alpha-dystroglycan;Beta-dystroglycan	<i>Dag1</i>	-1.353	0.0008
Glycosylphosphatidylinositol anchor attachment 1 protein	<i>Gpaa1</i>	-1.357	0.0196
Constitutive coactivator of PPAR-gamma-like protein 2	<i>Fam120c</i>	-1.359	0.0086
Aminopeptidase N	<i>Anpep</i>	-1.362	0.0018
Actin-related protein 2/3 complex subunit 5-like protein	<i>Arpc5l</i>	-1.363	0.0013
	<i>Tfg</i>	-1.363	0.0284
Lysosome membrane protein 2	<i>Scarb2</i>	-1.364	0.0046
ORM1-like protein 2;ORM1-like protein 3	<i>Ormdl2;Ormdl3</i>	-1.365	0.04
Calcium homeostasis endoplasmic reticulum protein	<i>Cherp</i>	-1.365	0.0065
Protein odr-4 homolog	<i>Odr4;BC003331</i>	-1.374	0.0067
Selenoprotein M	<i>Selm</i>	-1.383	0.0095
Interleukin-10 receptor subunit beta	<i>Il10rb;Gm21970</i>	-1.386	0.0157
Protein DEK	<i>Dek</i>	-1.388	0.0475
Inositol 1,4,5-trisphosphate receptor type 2	<i>Itpr2</i>	-1.39	0.0019

Ubiquinone biosynthesis protein COQ9, mitochondrial	<i>Coq9</i>	-1.39	0.0003
Pterin-4-alpha-carbinolamine dehydratase	<i>Pcbd1</i>	-1.393	0.0116
Glutathione S-transferase Mu 2	<i>Gstm2</i>	-1.395	0.0427
Prenylated Rab acceptor protein 1	<i>Rbac1</i>	-1.395	0.0002
Protein NDRG2	<i>Ndrg2</i>	-1.404	0.0003
Transmembrane channel-like protein;Transmembrane channel-like protein 4	<i>Tmc4</i>	-1.41	0.0054
Dehydrogenase/reductase SDR family member 4	<i>Dhrs4</i>	-1.415	0.0022
Epithelial splicing regulatory protein 2	<i>Esrp2</i>	-1.42	0.0048
Neprilysin	<i>Mme</i>	-1.422	0.0137
DNA damage-regulated autophagy modulator protein 2	<i>Dram2</i>	-1.435	0.0053
Splicing factor U2AF 35 kDa subunit	<i>U2af1</i>	-1.437	0.0013
Thiosulfate sulfurtransferase	<i>Tst</i>	-1.438	0.0028
Dynactin subunit 5	<i>Dctn5</i>	-1.438	0.0163
Putative RNA-binding protein Luc7-like 1	<i>Luc7l</i>	-1.44	0.0008
Epsin-1	<i>Epn1</i>	-1.442	0.0005
Pumilio domain-containing protein KIAA0020	<i>Kiaa0020</i>	-1.449	0.0228
	<i>2010106E10Rik</i>	-1.453	0.0156
Zinc finger Ran-binding domain-containing protein 2	<i>Zranb2</i>	-1.465	0.0022
General transcription factor 3C polypeptide 4	<i>Gtf3c4</i>	-1.465	0.0006
Sulfiredoxin-1	<i>Srxn1</i>	-1.47	0.008
RNA binding motif protein, X-linked-like-1	<i>Rbmxl1</i>	-1.473	0.004
Copper-transporting ATPase 2	<i>Atp7b</i>	-1.479	0.0102
Sulfite oxidase, mitochondrial	<i>Suox</i>	-1.483	0.0044
Enscosin	<i>Map7</i>	-1.487	0.0017
Transmembrane protease serine 4	<i>Tmprss4</i>	-1.489	0.0079
Pre-mRNA-processing factor 40 homolog A	<i>Prpf40a</i>	-1.494	0.0018
Ankyrin repeat and SAM domain-containing protein 4B	<i>Anks4b</i>	-1.545	0.0106
	<i>Dnm1l</i>	-1.546	0.026
Proteasome subunit beta type-6	<i>Psmb6</i>	-1.559	0.0015
	<i>Srsf11</i>	-1.573	0.0004
BET1-like protein	<i>Bet1l</i>	-1.601	0.0041
Beta-hexosaminidase subunit alpha	<i>Hexa</i>	-1.619	0.0006
Ribosome biogenesis protein BRX1 homolog	<i>Brix1</i>	-1.631	0.0068
Cell division cycle protein 23 homolog	<i>Cdc23</i>	-1.638	0.0076
Essential MCU regulator, mitochondrial	<i>Smdt1</i>	-1.658	0.0067
Kinesin-like protein KIF11	<i>Kif11</i>	-1.661	0.0003
ER lumen protein-retaining receptor 1;ER lumen protein-retaining receptor 2;ER lumen protein-retaining receptor 3	<i>Kdelr1;Kdelr2;Kdelr3</i>	-1.674	0.0353
Bcl-2-like protein 15	<i>Bcl2l15</i>	-1.674	0.0314
Protein phosphatase 1 regulatory subunit 12C	<i>Ppp1r12c</i>	-1.675	0.0001
Hepatoma-derived growth factor-related protein 2	<i>Hdgfrp2</i>	-1.689	0.0025
39S ribosomal protein L21, mitochondrial	<i>Mrpl21</i>	-1.747	0.0016
Ly6/PLAUR domain-containing protein 8	<i>Lypd8</i>	-1.838	0.0122
PHD finger protein 10	<i>Phf10</i>	-9.489	0.0004

**Appendix 7: Proteins that are exclusively changed in regulation in LPS-treated *c-Rel*<sup>-/-</sup> compared with LPS-treated C57BL/6J small intestinal mucosa (excluding significant changes between *c-Rel*<sup>-/-</sup> and C57BL/6J at baseline)**

Protein names	Gene names	Regulation fold change	P value
Unconventional myosin-IXb	<i>Myo9b</i>	3.989	0.0018
Transformation/transcription domain-associated protein	<i>Trrap</i>	3.884	0.0495
	<i>Mptx2</i>	3.254	0.0493
Uncharacterized protein KIAA0556	<i>D430042O09Rik;Kiaa0556</i>	3.001	0.019
1,4-alpha-glucan-branching enzyme	<i>Gbe1</i>	2.711	0.0387
Regenerating islet-derived protein 3-gamma	<i>Reg3g</i>	2.487	0.0003
Sorting nexin-3	<i>Snx3</i>	2.222	0.0002
Polymeric immunoglobulin receptor;Secretory component	<i>Pigr</i>	2.201	0.0003
MLV-related proviral Env polyprotein;Surface protein;Transmembrane protein		1.971	0.0102
Nectin-2	<i>Pvrl2</i>	1.853	0.0007
Ribose-5-phosphate isomerase	<i>Rpia</i>	1.81	0.003
Mitochondrial pyruvate carrier 1	<i>Mpc1</i>	1.806	0.0002
Dynein light chain 1, cytoplasmic	<i>Dynll1;BC048507</i>	1.77	0.0023
Uroporphyrinogen decarboxylase	<i>Urod</i>	1.769	0.0075
Transcriptional repressor protein YY1	<i>Yy1</i>	1.747	0.0089
Fatty acid-binding protein, epidermal	<i>Fabp5</i>	1.705	0.0075
Sideroflexin-3	<i>Sfxn3</i>	1.698	0.0005
Glycerol-3-phosphate dehydrogenase 1-like protein	<i>Gpd1l</i>	1.68	0.0039
	<i>Parp3</i>	1.673	0.0007
	<i>Chn2</i>	1.666	0.013
Molybdenum cofactor biosynthesis protein 1;Cyclic pyranopterin monophosphate synthase;Cyclic pyranopterin monophosphate synthase accessory protein	<i>Mocs1</i>	1.654	0.0068
Sodium/hydrogen exchanger 1	<i>Slc9a1</i>	1.647	0.0017
Serum paraoxonase/lactonase 3	<i>Pon3</i>	1.646	0.0181
Protein-tyrosine kinase 6	<i>Ptk6</i>	1.638	0.0157
	<i>Syne2</i>	1.611	0.0011
O-phosphoserine-tRNA(Sec) selenium transferase	<i>Sepsecs</i>	1.59	0.005
SH3 domain-containing protein 21	<i>Sh3d21</i>	1.588	0.0069
Trinucleotide repeat-containing gene 6B protein	<i>Tnrc6b</i>	1.587	0.0029
Transmembrane protein 260	<i>Tmem260</i>	1.582	0.0058
Adiponectin receptor protein 2	<i>Adipor2</i>	1.569	0.0009
S-methyl-5-thioadenosine phosphorylase	<i>Mtap</i>	1.549	0.0094
Serine/threonine-protein phosphatase 6 catalytic subunit;Serine/threonine-protein phosphatase 6 catalytic subunit, N-terminally processed	<i>Ppp6c</i>	1.546	0.0008

Succinyl-CoA:3-ketoacid coenzyme A transferase 1, mitochondrial	<i>Oxct1</i>	1.543	0.0112
Purine nucleoside phosphorylase	<i>Pnp2</i>	1.537	0.0117
Transmembrane protein 9B	<i>Tmem9b</i>	1.514	0.0023
Proteasome subunit beta type-2	<i>Psmb2</i>	1.503	0.0149
Peroxisomal 2,4-dienoyl-CoA reductase	<i>Decr2</i>	1.502	0.0132
Ig kappa chain C region	<i>Igkc</i>	1.494	0.0083
UDP-GlcNAc:betaGal beta-1,3-N-acetylglucosaminyltransferase 7	<i>B3gnt7</i>	1.482	0.0071
THAP domain-containing protein 4	<i>Thap4</i>	1.457	0.0009
LIM and senescent cell antigen-like-containing domain protein 1	<i>Lims1</i>	1.456	0.0075
Kininogen-1;Kininogen-1 heavy chain;Bradykinin;Kininogen-1 light chain	<i>Kng1</i>	1.449	0.0092
ADP-ribosyl cyclase/cyclic ADP-ribose hydrolase 2	<i>Bst1</i>	1.44	0.0046
OTU domain-containing protein 4	<i>Otud4</i>	1.44	0.0013
[3-methyl-2-oxobutanoate dehydrogenase [lipoamide]] kinase, mitochondrial	<i>Bckdk</i>	1.428	0.0061
Signal peptidase complex subunit 2	<i>Spcs2</i>	1.423	0.0011
Choline transporter-like protein 1	<i>Slc44a1</i>	1.414	0.0002
Reticulon;Reticulon-1	<i>Rtn1</i>	1.412	0.0022
Host cell factor 1	<i>Hcfc1</i>	1.396	0.0014
Integrin beta;Integrin beta-6	<i>Itgb6</i>	1.381	0.0019
Cysteine-rich and transmembrane domain-containing protein 1	<i>Cystm1</i>	1.373	0.002
Ubiquitin-fold modifier 1	<i>Ufm1</i>	1.373	0.0003
Enscosin	<i>Map7</i>	1.37	0.0005
Vacuolar protein sorting-associated protein 29	<i>Vps29</i>	1.369	0.0003
E3 ubiquitin-protein ligase MYCBP2	<i>Mycbp2</i>	1.366	0.0002
	<i>Muc3</i>	1.364	0.0008
Cytochrome c oxidase subunit 7A-related protein, mitochondrial	<i>Cox7a2l</i>	1.332	0.0001
Alpha/beta hydrolase domain-containing protein 14B	<i>Abhd14b</i>	-1.34	0.0005
Insulin-degrading enzyme	<i>Ide</i>	-1.35	0.0011
	<i>Lmo7</i>	-1.35	0.001
CB1 cannabinoid receptor-interacting protein 1	<i>Cnrip1</i>	-1.36	0.0004
Serine/threonine-protein kinase N2	<i>Pkn2</i>	-1.38	0.0021
	<i>Akr1c19</i>	-1.39	0.0022
Hydroxyacylglutathione hydrolase, mitochondrial	<i>Hagh</i>	-1.39	0.0008
	<i>Pde4dip</i>	-1.39	0.0004
PHD finger protein 10	<i>Phf10</i>	-1.4	0.0019
Arginase-2, mitochondrial	<i>Arg2</i>	-1.41	0.0005
Disintegrin and metalloproteinase domain-containing protein 10	<i>Adam10</i>	-1.41	0.0034
Epididymis-specific alpha-mannosidase	<i>Man2b2</i>	-1.41	0.0013
Membrane-associated progesterone receptor component 1	<i>Pgrmc1</i>	-1.44	0.002

A-kinase anchor protein 7 isoform alpha;A-kinase anchor protein 7 isoform gamma	<i>Akap7</i>	-1.44	0.0014
H-2 class II histocompatibility antigen, E-B beta chain	<i>H2-Eb1</i>	-1.44	0.0005
H-2 class II histocompatibility antigen gamma chain	<i>Cd74</i>	-1.45	0.0004
H-2 class II histocompatibility antigen, A beta chain	<i>H2-Ab1</i>	-1.46	0.0085
UDP-glucuronosyltransferase 2B17	<i>Ugt2b5;Ugt2b17;Ugt2b38</i>	-1.48	0.0006
CD63 antigen	<i>Cd63</i>	-1.48	0.0091
Enoyl-CoA delta isomerase 1, mitochondrial	<i>Eci1</i>	-1.48	0.0099
Adrenodoxin, mitochondrial	<i>Fdx1</i>	-1.49	0.0047
Dynein light chain Tctex-type 1	<i>Dynlt1</i>	-1.49	0.0109
Acyl-coenzyme A thioesterase 8	<i>Acot8</i>	-1.51	0.0002
Serine/threonine-protein phosphatase PP1-gamma catalytic subunit	<i>Ppp1cc</i>	-1.52	0.0163
Cholinesterase	<i>Bche</i>	-1.53	0.0108
ATP synthase subunit e, mitochondrial	<i>Atp5i;Atp5k</i>	-1.53	0.002
Secretin	<i>Sct</i>	-1.53	0.0166
Protein phosphatase 1 regulatory subunit 12C	<i>Ppp1r12c</i>	-1.53	0.0092
Mimitin, mitochondrial	<i>Ndufaf2</i>	-1.54	0.0034
Alpha-defensin 24	<i>Defa24</i>	-1.54	0.0094
	<i>Cyp2c66</i>	-1.54	0.0128
Asparagine synthetase [glutamine-hydrolyzing]	<i>Asns</i>	-1.55	0.0029
Leukocyte surface antigen CD47	<i>Cd47</i>	-1.56	0.0158
Histone H2A type 2-B	<i>Hist2h2ab</i>	-1.57	0.0006
Syntaxin-3	<i>Stx3</i>	-1.57	0.0051
N-acetylglucosamine-1-phosphotransferase subunits alpha/beta	<i>Gnptab</i>	-1.59	0.0003
E3 ubiquitin-protein ligase UBR2	<i>Ubr2</i>	-1.61	0.0019
Up-regulated during skeletal muscle growth protein 5	<i>Usmg5</i>	-1.61	0.0115
StAR-related lipid transfer protein 4	<i>Stard4</i>	-1.61	0.0153
Serine/threonine-protein kinase VRK1	<i>Vrk1</i>	-1.64	0.0014
Disheveled-associated activator of morphogenesis 1	<i>Daam1</i>	-1.64	0.003
Consortin	<i>Cnst</i>	-1.66	0.0001
Dynactin subunit 4	<i>Dctn4</i>	-1.66	0.0039
Riboflavin kinase	<i>Rfk</i>	-1.66	0.001
Histone H2B type 3-B;Histone H2B type 3-A;Histone H2B type 2-E	<i>Hist3h2bb;Hist3h2ba;Hist2h2be</i>	-1.66	0.0004
CCA tRNA nucleotidyltransferase 1, mitochondrial	<i>Trnt1</i>	-1.68	0.0011
BRO1 domain-containing protein BROX	<i>Brox</i>	-1.68	0.0009
Ankyrin repeat and SAM domain-containing protein 4B	<i>Anks4b</i>	-1.69	0.0005
Liver carboxylesterase 1	<i>Ces1</i>	-1.7	0.0119
Polymerase delta-interacting protein 2	<i>Poldip2</i>	-1.72	0.0064
Probable ATP-dependent RNA helicase DDX41	<i>Ddx41</i>	-1.74	0.0003
Atlastin-3	<i>Atl3</i>	-1.76	0.0042

ER lumen protein-retaining receptor 1;ER lumen protein-retaining receptor 2;ER lumen protein-retaining receptor 3	<i>Kdelr1;Kdelr2;Kdelr3</i>	-1.82	0.002
Dehydrogenase/reductase SDR family member 4	<i>Dhrs4</i>	-1.82	0.0046
Trafficking protein particle complex subunit 5	<i>Trappc5</i>	-1.85	0.0283
H/ACA ribonucleoprotein complex subunit 2	<i>Nhp2</i>	-1.87	0.0281
39S ribosomal protein L21, mitochondrial	<i>Mrpl21</i>	-1.93	0.0002
39S ribosomal protein L17, mitochondrial	<i>Mrpl17</i>	-2	0.0004
Acyl-coenzyme A thioesterase 2, mitochondrial	<i>Acot2</i>	-2.24	0.0005
Replication factor C subunit 2	<i>Rfc2</i>	-3.26	0.0013
Sodium/potassium-transporting ATPase subunit alpha-4	<i>Atp1a4</i>	-3.79	0.0019
Solute carrier family 2, facilitated glucose transporter member 5	<i>Slc2a5</i>	-4.38	0.0006
Krueppel-like factor 5	<i>Klf5</i>	-8.69	0.0005